

**Driving Simulator Motion Cueing Assessment:
A Platform Design Perspective**

Ehsan Sadraei

Submitted in accordance with the requirements for the degree of
Doctor of Philosophy (PhD)

The University of Leeds
Institute for Transport Studies

May 2019

The candidate confirms that the work submitted is his own, except where work which has formed part of jointly-authored publications has been included. The contribution of the candidate and the other authors to this work has been explicitly indicated below. The candidate confirms that appropriate credit has been given within the thesis where reference has been made to the work of others.

1) Chapter 5, tuning of classic algorithm partly based on the publication: “Understanding Cue Utility in Controlled Evasive Driving Manoeuvres: Optimizing Vestibular Cues for Simulator & Human Abilities” Sadraei, E., Romano, R., Advani, S., Jamson, AH., Chappell, P., Markkula, G., Bean, A., Boer, ER (2016) IFAC-PapersOnLine, 49(19), pp.414-419.

2) Chapter 3 and 8, fidelity criteria, and motion platform sizing using classic algorithm based on the publication: “Driving simulator motion base right sizing” Sadraei, E., Romano, R., Jamson, S., Markkula, G., Jamson, H, (2018) Driving Simulation Conference (DSC), Antibes, France.

The contributions of the co-authors consisted of supervision, critique and advice during the whole process, proof-reading and commenting.

This copy has been supplied on the understanding that it is copyright material and that no quotation from the thesis may be published without proper acknowledgement.

© 2019 The University of Leeds, and Ehsan Sadraei

Acknowledgements

I would like to thank my supervisors Samantha Jamson and Richard Romano. They have always been supportive throughout my study. At any point in time that I was lost in thoughts and the feeling of doubt was winning, they enlightened me with the right path and encouraged me further. Richard's inspirational experience in area of simulator motion cueing truly guided and enthused me.

I would like to express my gratitude to my co-supervisor Erwin Boer for his beautiful in-depth advisory insights in different stages of the project that nurtured my creativity. Thanks to Gustav Markkula for leading the project and getting the pieces of jigsaw together and delivered on time. His expertise in driver behaviour modelling was exemplary. To Hamish Jamson who initialised the project and led me and other PhD colleagues at the beginning.

I need to acknowledge my family for being the backbone wholeheartedly in any time during years while I was studying abroad. I am really grateful to my lifetime love Atefeh, during last months of my study she provided me of serene energy to focus and get the words of this thesis together. Their support has been precious in completion of this thesis.

This research has been sponsored by Jaguar Land Rover and the UK-EPSC, as part of the jointly funded Programme for Simulation Innovation (PSi) project. I would like to state my thanks to the JLR PSi Project manager Ian Knight, and industrial advisors Paul Chappell and Alex Bean.

Abstract

The overall aim of this thesis was to study the effects of a simulator's motion system on vestibular motion cueing fidelity in different contexts, evaluated in terms of drivers' perception and behaviour, in low and high road friction conditions. The effects of manipulating the motion cueing algorithm (MCA), was found to be a function of the vehicle motion in a manoeuvre, and significant effects were observed.

The applicability of simulators for the assessment of vehicle driven attribute qualities such as ride, steering and handling were studied by manipulating vehicle ride height (RH). The differences between the RHs were subjectively distinguishable by the drivers in the simulator. Incongruities between the subjective preferences and objective performances were observed in both of the independent comparisons of the MCAs and RHs.

The effects of motion platform (MP) workspace size were found to be dependent on the manoeuvres and road friction level. In the low-friction condition, with the increase of MP size, two opposite effects were observed on drivers' preferences and their performances, depending on the manoeuvre. In high-friction, in most of the handling and steering qualities, a direct relation was found between the MP size and appropriate vehicle RH.

Furthermore, the optimal tuning of the MCAs and optimisation of the MP workspace size was introduced. A conservative motion cueing fidelity criteria was defined. A multi-layered optimisation method was developed that uses the optimal setting of the MCA, to address the MP translational workspace size, and to meet the fidelity criteria; applicable for different manoeuvres. This method was tested on the drivers' performance data collected from the experiments in the simulator.

Table of Contents

Acknowledgements	ii
Abstract	iii
Table of Contents	iv
List of Tables	viii
List of Figures	xi
Abbreviations	xix
1 Introduction	1
1.1 Background	1
1.2 Thesis aim and objective	3
1.3 Thesis structure	5
2 Driver Perception and Performance	6
2.1 Introduction.....	6
2.2 Perception of self-motion	8
2.2.1 Visual perception	9
2.2.2 Vestibular perception	11
2.2.2.1 Otolith.....	11
2.2.2.2 Semicircular canal	16
2.3 Driver performance in vehicle	20
3 Motion Cueing in High-Performance Simulators	33
3.1 Driving simulator subsystems	33
3.2 Motion platforms.....	37
3.2.1 Hexapod and sliding rail platforms	39
3.2.2 High bandwidth platforms.....	42
3.2.3 Alternative platforms	43
3.3 Motion cueing algorithms.....	46
3.3.1 Introduction.....	46
3.3.2 Nonlinear scaling of vehicle motion	48
3.3.3 Classic algorithm	49
3.3.4 Model predictive control algorithm.....	52
3.3.4.1 Plant model	54
3.3.4.2 Quadratic Programming.....	56
3.3.4.3 Cost function	58
3.3.4.4 Reference input	61
3.3.4.5 Constraints	61

3.3.5 Adaptive algorithm	64
3.3.6 Optimal algorithm.....	65
3.4 Fidelity definitions and assessment methods.....	67
4 Motion Cueing in University of Leeds Driving Simulator	77
4.1 Classic algorithm for UoLDS.....	77
4.1.1 Coordinate transformation.....	77
4.1.2 Tilt coordination	79
4.1.3 Complete plant model	80
4.2 MPC algorithm for UoLDS	82
4.2.1 Coordinate transformation.....	83
4.2.2 State-space realisation of the vestibular model	83
4.2.3 Tilt coordination	86
4.2.4 Complete plant model	87
5 Assessment of Low-Friction Motion Cueing.....	91
5.1 Introduction.....	91
5.2 Experimental design	92
5.3 Dependent variables.....	93
5.3.1 Subjective measures.....	93
5.3.2 Objective measures	95
5.4 Experiment configurations	97
5.4.1 Motion platforms	97
5.4.2 Motion cueing algorithms	98
5.5 Research questions and hypotheses	101
5.6 Driving tasks.....	102
5.6.1 Land Rover Handling Track (LHT)	102
5.6.2 Slalom (SLM)	103
5.7 Drivers.....	104
5.8 Test vehicle	104
5.9 Experiment procedure	105
5.10 Analyses and results	107
5.10.1 Overview and general approach.....	107
5.10.1.1 Hypothesis testing	107
5.10.1.2 Effect size and statistical power	107
5.10.1.3 Repeated Measure ANOVA.....	109
5.10.2 Subjective evaluations.....	110

5.10.2.1	Land Rover Land Rover Handling Track (LHT)	110
5.10.2.2	Slalom (SLM).....	119
5.10.3	Objective evaluations	126
5.10.3.1	Land Rover Handling Track (LHT)	126
5.10.3.2	Slalom (SLM).....	147
5.11	Discussion and conclusions.....	160
6	Assessment of High-Friction Motion Cueing	170
6.1	Introduction.....	170
6.2	Experimental design	172
6.3	Dependent variables.....	173
6.3.1	Subjective measures.....	173
6.3.2	Objective measures	176
6.4	Experiment configurations	176
6.4.1	Motion platform	176
6.4.2	Air suspension ride height.....	179
6.5	Research questions and hypotheses	179
6.6	Driving task.....	180
6.7	Drivers.....	181
6.8	Test vehicle	182
6.9	Experiment procedure	183
6.10	Analyses and results	185
6.10.1	Overview and general approach.....	185
6.10.2	Subjective evaluations.....	186
6.10.3	Objective evaluations	199
6.11	Discussion and conclusions.....	214
7	Tuning Optimisation of Motion Cueing Algorithms	221
7.1	Introduction.....	221
7.2	Tuning of classic motion cueing algorithm	225
7.2.1	Translational motions.....	232
7.2.1.1	First order high-pass filter	232
7.2.1.2	Second order high-pass filter	235
7.2.1.3	Third order high-pass filter	238
7.2.2	Tilt motion	241
7.2.2.1	Second order low-pass filter	241
7.2.3	Translational and tilt motions	242

7.3	Tuning of MPC motion cueing algorithm	245
7.3.1	Translational motion.....	256
7.3.2	Tilt motion	258
7.3.3	Translational and tilt motions	260
7.4	Discussion and conclusions.....	264
7.4.1	Classic parameters	266
7.4.2	MPC parameters.....	267
8	Workspace Optimisation of Motion Platforms	269
8.1	Introduction.....	269
8.2	Optimisation analysis and results	272
8.3	Conclusions and suggestions	280
9	Conclusion and Recommendations.....	283
9.1	Summary of results.....	285
9.1.1	Assessment of low-friction motion cueing	285
9.1.2	Assessment of high-friction motion cueing	288
9.1.3	Comparison of low and high friction effects.....	292
9.1.4	Optimisation of motion cueing algorithm and motion platform ...	294
9.2	Contributions to knowledge	295
9.3	Study Limitations	297
9.4	Potential for future work.....	297
	References	299
	Appendices	311
A	Motion platform characteristics of simulators	311
B	Assessment of Low-Friction Motion Cueing Experiment Documents	315
	Briefing	315
	Questionnaire	318
	Counter balancing table.....	327
	MCA tuning parameter values	327
C	Assessment of High-Friction Motion Cueing Experiment Documents	331
	Briefing	331
	Questionnaire	334
	Counter balancing table.....	343
	MCA tuning parameter values	343
D	List of tilt settings used throughout the thesis	344

List of Tables

Table 2-1. Otolith model parameters	15
Table 2-2. Semicircular canal model parameters, roll direction	19
Table 3-1. UoLDS motion characteristics, (Jamson, 2010)	41
Table 4-1. Classic MCA parameters for surge/pitch and sway/roll channels	81
Table 4-2. Classic MCA parameters for heave/yaw channel	82
Table 4-3. Vestibular parameters used in models, from.....	85
Table 4-4. MPC parameters for heave/yaw channel.....	89
Table 4-5. MPC parameters for surge/pitch and sway/roll channels.....	89
Table 5-1. Simulator subjective questions	94
Table 5-2. Utility triplet used for objective behaviour analysis.....	97
Table 5-3. Motion platform specifications configured in this experiment.....	98
Table 5-4. Motion configurations acceleration and excursion differences.....	99
Table 5-5. Tilt rotational parameters used in this study.....	101
Table 5-6. Statistical power table.....	109
Table 5-7 Repeated measure ANOVA results for grouped question ratings, LHT task. F and P values are shown on each box corresponds to a factor and an output measure. Black highlighted boxes show where the p-value is less than 0.1	112
Table 5-8. Results of subjective ratings for MCA comparison in each MP size, LHT task.....	116
Table 5-9. Results of subjective ratings for MP size comparison in each MCA (all compared to small), LHT task	118
Table 5-10. Repeated measure ANOVA results for grouped question ratings, SLM task. F and P values are shown on each box corresponds to a factor and an output measure. Black highlighted boxes show where the p-value is less than 0.1.....	120
Table 5-11. Results of subjective ratings for MCA comparison in each MP size, SLM task	123
Table 5-12. Results of subjective ratings for MP size comparison in each MCA (all compared to large), SLM task	125
Table 5-13. Group sections, LHT task	127
Table 5-14. Repeated measure ANOVA time series metrics results of curve greater than 180° grouped sections, LHT task.	131
Table 5-15. Repeated measure ANOVA time series metrics results of curve smaller than 180° grouped sections, LHT task.....	136
Table 5-16. Repeated measure ANOVA time series metrics results of straight line grouped sections, LHT task.	140

Table 5-17. Repeated measure ANOVA time series metrics results of inflection zones grouped sections, LHT task.....	143
Table 5-18. Repeated measure ANOVA time series metrics results of whole track, LHT task.	145
Table 5-19. Group sections, SLM task.....	148
Table 5-20. Repeated measure ANOVA time series metrics results of straight lines grouped sections, SLM task.....	150
Table 5-21. Repeated measure ANOVA time series metrics results of peak zone grouped sections, SLM task.....	151
Table 5-22. Repeated measure ANOVA time series metrics results of inflection zone grouped sections, SLM task.	155
Table 5-23. Repeated measure ANOVA time series metrics results of whole track, SLM task.....	157
Table 5-24. Summary of results, research question 1 (highest values), LHT task.....	163
Table 5-25. Summary of results, research question 1 (highest values), SLM task	164
Table 5-26. Summary of results, research question 2 (highest values), LHT task.....	168
Table 5-27. Summary of results, research question 2 (highest values), SLM task	169
Table 6-1. Driven attribute questions	175
Table 6-2. Simulator realism questions.....	176
Table 6-3. Motion platform specifications configured in this experiment.....	177
Table 6-4. Motion configurations acceleration and excursion differences...	178
Table 6-5. Statistical power table.....	185
Table 6-6. Repeated measure ANOVA results for grouped question ratings. F and P values are shown on each point corresponding to a factor and an output measure. Black highlighted boxes shows where the p-value is less than 0.1.....	189
Table 6-7. Results of the driven attribute questionnaire for RH comparison in each MP. Most near to appropriate for this vehicle (0.5 line)	195
Table 6-8. Results of the driven attribute questionnaire for RH comparison in each MP. Most distant from appropriate for this vehicle (0.5 line)	196
Table 6-9. Results of the driven attribute questionnaire for MP comparison in each RH. Most near to appropriate for this vehicle (0.5 line)	198
Table 6-10. Results of the driven attribute questionnaire for MP comparison in each RH. Most distant from appropriate for this vehicle (0.5 line)	199

Table 6-11. Group sections, LHT task	200
Table 6-12. Repeated measure ANOVA time series metrics results of curve grouped sections.....	204
Table 6-13. Repeated measure ANOVA time series metrics results of straight line grouped sections	208
Table 6-14. Repeated measure ANOVA time series metrics, whole track.....	212
Table 6-15. Summary of results, research question 1 (most appropriate for this vehicle in subjective and highest values in objective).....	217
Table 6-16. Summary of results, research question 2 (most appropriate for this vehicle in subjective and highest values in objective).....	220
Table 7-1. Motion platform maximum excursion, using different order high-pass filters and inputs	228
Table 8-1. Tilt parameters used for optimisations	275
Table 0-1. Daimler-Benz driving simulators motion characteristics (Zeeb, 2010).....	311
Table 0-2. VTI IV simulator motion characteristics (Fischer et al., 2011)	311
Table 0-3. PSA Peugeot-Citroën motion characteristics (Chapron and Colinot 2007)	312
Table 0-4. NADS1 simulator motion characteristics (Clark, A.J. et al., 2001).....	312
Table 0-5. Toyota Research Driving Simulator (TRDS) motion characteristics (Greenberg and Blommer, 2011)	313
Table 0-6. DESDEMONA simulator motion characteristics.....	313
Table 0-7. MPI CyberMotion simulator motion characteristics (Nieuwenhuizen and Bülthoff, 2013).....	314

List of Figures

Figure 2-1. Model of tasks carried out while driving, (Nash et al., 2016)	7
Figure 2-2. Vestibular system, semicircular canals (left), and utricle and saccule of the otolith (right), from Encyclopaedia Britannica	11
Figure 2-3. Bode frequency response of otolith models.....	15
Figure 2-4. Bode frequency response of semicircular canal models.....	19
Figure 2-5. Kondo's shaft model and basic driver control loop, (Kondo, 1953) cited in (Plöchl and Edelman, 2007)	22
Figure 2-6. Driver model scheme proposed by (Sharp et al., 2000).....	24
Figure 2-7. The overall structure of the driver model, (Nash and Cole, 2018).....	27
Figure 2-8. Schematic representation of the driver steering model, (Markkula et al., 2018c).	31
Figure 3-1. Dynamic driving simulator subsystems (driver in the loop).....	33
Figure 3-2. UoLDS simulator subsystem communications, (Markkula et al., 2016).....	35
Figure 3-3. IKK driving simulator (left), VTI II (right) (Nordmark et al., 1984).....	38
Figure 3-4. Daimler-Benz driving simulators 1985 (left) (Drosdol and Panik, 1985), 2010 (right) (Zeeb, 2010).....	39
Figure 3-5. Iowa Driving Simulator 1992 (left) (Freeman et al., 1995) and, National Advanced Driving Simulator 2001 (right) (Clark, A. et al., 2001).....	40
Figure 3-6. University of Leeds Driving Simulator (UoLDS) 2007 (top left) (Jamson, 2010), Toyota Driving simulator (TDS) 2007 (top right) (Greenberg and Blommer, 2011), VTI IV 2011 (bottom left) (Fischer et al., 2011), Renault Ultimate (bottom right) (Dagdelen et al., 2004).....	41
Figure 3-7. Vehicle Dynamics Simulator (VDS) of McLaren Applied Technologies (MTS), 2017	42
Figure 3-8. Advanced Vehicle Driving Simulator (aVDS) of AB Dynamics	43
Figure 3-9. DESDEMONA 2007 flight and driving simulator (Mayrhofer, 2009).....	43
Figure 3-10. MPI CyberMotion Simulator (left) and its 8 axes (right) (Nieuwenhuizen and Bulthoff, 2013)	44
Figure 3-11. Atlas Motion System (ATMOS) driving simulator 2009 (Hassan, 2014).....	45
Figure 3-12. Assembled motion system (left), rotational mechanism (right) (Slob, 2008).....	45
Figure 3-13. Classic motion cueing algorithm, (Jamson, 2010).....	50

Figure 3-14. MCA step response, time domain (top) and frequency domain (bottom).....	51
Figure 3-15. Schematic representation of MPC principle, Wikipedia.	54
Figure 3-16. Flight simulator fidelity evaluated at mechanical, perceptual and behavioural levels, (Pool, 2012).....	69
Figure 3-17. Sinacori (dashed line) and Schroeder (solid line) fidelity corridors for translational motion at 1 rad/s, (Schroeder, 1999).....	72
Figure 3-18. Signal-to-noise-ratio (SNR) contour for the VIRTEX simulator, (Grant et al., 2001)	73
Figure 3-19. Fidelity corridors for longitudinal (top) and lateral (bottom) directions, (Hosman and Advani, 2016).....	74
Figure 3-20. Coherence zones represented for sway motion. The horizontal black lines span different measurements made at the same visual amplitude (Valente Pais, 2013).	75
Figure 4-1. Schematic representation of the classic model structure for surge/pitch and sway/roll motion cueing channels.....	77
Figure 4-2. Overview of reference frames, side view	78
Figure 4-3. Frequency response of the classic algorithm, hexapod translation $khex, tr = 0.5, \omega_{hp1} = 1.51, \omega_{hp2} = 2.35$, rail translation $krail, tr = 0.5, \omega_{hp1} = 0.26, \omega_{hp2} = 0.35, \omega_{lp2} = 11$, Tilt $\omega_{lp2} = 3$	82
Figure 4-4. Schematic representation of MPC model structure for surge/pitch motion cueing channel	83
Figure 5-1. The JLR Revi test centre	102
Figure 5-2. Simulated LHT course	103
Figure 5-3. Simulated Slalom Layout.....	104
Figure 5-4. Graphical representation of the SimPack multi-body model of the Jaguar XF vehicle dynamics	105
Figure 5-5. Example of subjective question and ratings. The drivers did mark each new test with A, B, C, ..., in the order they experienced them	106
Figure 5-6. Subjective rating boxplot, and effect size r-value bar graphs for grouped questions, LHT task. Red flat lines show median and black stars shows mean.	111
Figure 5-7. Overall assessment grouped question ratings, LHT task.....	113
Figure 5-8. Motion cueing grouped question ratings, LHT task	114
Figure 5-9. Vehicle assessment grouped question ratings, LHT task.....	115
Figure 5-10. Subjective ratings for grouped questions, MCA comparison for three MP sizes. Effect size r-value bar graphs are shown for each MP, comparing MCAs, LHT task	116

Figure 5-11. Subjective ratings for group questions, MP comparison for two MCAs. Effect size r-value bar graphs are shown for each MCA, comparing MPs, LHT task	118
Figure 5-12. Subjective rating boxplot, and effect size r-value bar graphs for grouped questions, SLM task. Red flat lines show median and black stars shows mean.....	120
Figure 5-13. Overall assessment grouped question ratings, SLM task	121
Figure 5-14. Vehicle assessment grouped question ratings, SLM task	122
Figure 5-15. Subjective ratings for grouped questions, MCA comparison for three MP sizes, SLM task. Effect size r-value bar graphs are shown for each MP, comparing MCAs, SLM task.....	123
Figure 5-16. Subjective ratings for group questions, MP comparison for two MCAs. Effect size r-value bar graphs are shown for each MCA, comparing MPs, SLM task.....	125
Figure 5-17. Land Rover Handling Track (LHT) course and sections	127
Figure 5-18. Lap time, LHT	128
Figure 5-19. Spin/skid outs, LHT.....	129
Figure 5-20. Speed variations, LHT	129
Figure 5-21. Lateral position deviation, LHT	130
Figure 5-22. Maximum longitudinal velocity, curves greater than 180°	131
Figure 5-23. Maximum lateral velocity, curves greater than 180°	132
Figure 5-24. Steering reversal rate 1°, curves greater than 180°	133
Figure 5-25. Steering reversal rate 10°, curves greater than 180°	133
Figure 5-26. Driver model steering gain, curves greater than 180°	134
Figure 5-27. Longitudinal acceleration, LHT task.....	135
Figure 5-28. Maximum longitudinal acceleration, curves smaller than 180°	136
Figure 5-29. Driver model steering gain, curves smaller than 180°	137
Figure 5-30. Steering reversal rate 1°, curves smaller than 180°	138
Figure 5-31. Steering reversal rate 10°, curves smaller than 180°	138
Figure 5-32. Maximum lateral velocity, curves smaller than 180°	139
Figure 5-33. Maximum yaw rate, curves smaller than 180°	139
Figure 5-34. Maximum longitudinal acceleration, straight line.....	141
Figure 5-35. Driver model steering gain, straight line	141
Figure 5-36. Steering reversal rate 10°, straight line	142
Figure 5-37. Longitudinal acceleration, inflection zone	143
Figure 5-38. Steering reversal rate 1°, inflection zone	144
Figure 5-39. Driver model delay time, inflection zone	145

Figure 5-40. Driver model gain, whole track	146
Figure 5-41. Maximum yaw rate, whole track.....	146
Figure 5-42. Slalom course and sections.....	147
Figure 5-43. Lap time, SLM.....	148
Figure 5-44. Spin/skid outs and cone hits, SLM	149
Figure 5-45. Speed variations, SLM	149
Figure 5-46. Maximum longitudinal velocity, peak zones	151
Figure 5-47. Maximum lateral velocity, peak zones.....	152
Figure 5-48. Maximum yaw rate, peak zones	153
Figure 5-49. Driver model delay time, peak zone.....	153
Figure 5-50. Steering reversal rate 1°, peak zone	154
Figure 5-51. Maximum longitudinal acceleration, inflection zone	155
Figure 5-52. Driver model gain, inflection zone	156
Figure 5-53. Driver model delay time, inflection zone	157
Figure 5-54. Longitudinal velocity, whole track.....	158
Figure 5-55. Driver model steering gain, whole track.....	159
Figure 5-56. Maximum lateral velocity, whole track	159
Figure 6-1. Nonlinear scaling of the vehicle lateral motion	178
Figure 6-2. Map view of Gosport Lane. A still from the video logs of the real vehicle driving on Gosport Lane	181
Figure 6-3. A snapshot of the UoLDS graphical representation of Gosport Lane.....	181
Figure 6-4. Graphical representation of the SimPack multi-body model of the Range Rover Velar vehicle dynamics.....	182
Figure 6-5. Example of driven attribute question and ratings. The drivers did mark each new test with A, B, ..., H, in the order they experienced them.....	184
Figure 6-6. Example of simulator realism question and ratings. The drivers did mark each new session with 1, 2, 3 in the order they experienced them.....	185
Figure 6-7. Subjective rating boxplot, and effect size r-value bar graphs for driven attribute grouped questions. Red flat lines show median and black stars show mean.....	188
Figure 6-8. Subjective rating boxplot, and effect size r-value bar graphs for realism questions.....	189
Figure 6-9. Ride grouped questions ratings	190
Figure 6-10. Steering gain linearity away from centre ratings	191
Figure 6-11. Handling roll (lateral) acceleration/deceleration ratings	192

Figure 6-12. Handling under/oversteering ratings.....	193
Figure 6-13. Subjective ratings for grouped questions, RH comparison for three MP sizes. Effect size r-value bar graphs are shown for each MP, comparing RHs	194
Figure 6-14. Subjective ratings for grouped questions, MP comparison for three RHs. Effect size r-value bar graphs are shown for each RH, comparing MPs	197
Figure 6-15. Gosport lane course and sections.....	200
Figure 6-16. Lap time	201
Figure 6-17. Number of failures	202
Figure 6-18. Speed variations	202
Figure 6-19. Lateral position deviation.....	203
Figure 6-20. Driver model preview time, curves	205
Figure 6-21. Maximum longitudinal velocity, curves.....	205
Figure 6-22. Steering wheel reversal rate 1°, curves	206
Figure 6-23. Steering wheel reversal rate 10°, curves	206
Figure 6-24. Longitudinal acceleration, curves	207
Figure 6-25. Maximum yaw rate, straight lines	208
Figure 6-26. Maximum body slip angle, straight lines.....	209
Figure 6-27. Maximum longitudinal acceleration, straight lines.....	209
Figure 6-28. Maximum lateral acceleration, straight lines	210
Figure 6-29. Steering wheel reversal rate 10°, straight lines	211
Figure 6-30. Steering wheel reversal rate 1°, straight lines	211
Figure 6-31. Driver model steering gain, whole track.....	213
Figure 6-32. Steering wheel reversal rate 1°, whole track.....	213
Figure 7-1. Time response of second order high-pass filter with parameters of $k = 0.8$, $\zeta = 1$, $\omega_{hp} = 1 \text{ radsec}$, and the measurement metrics	224
Figure 7-2. Bode plot of second order high-pass filter with parameters of $k = 1$, $\zeta = 1$, $\omega_{hp} = 1.5 \text{ radsec}$, and frequencies of interest highlighted in green.....	225
Figure 7-3. Acceleration and position response of high-pass and low-pass filters to step, square, triangle-square, sinusoid and vehicle lateral acceleration inputs, $k = 0.5$, $\zeta = 1$, $\omega_{hp1} = 0.4$, $\omega_{hp2} = 0.4 \text{ rad/sec}$ are the filter parameters	231
Figure 7-4. Bode frequency response of the high-pass and low-pass filters.....	232
Figure 7-5. The time domain true and false output accelerations in a range of filter parameters, first order high-pass filter	233

Figure 7-6. The time domain true, false accelerations and position excursions in a range of filter parameters (top), and cropped out settings with excursions smaller than 2.5 (m) (bottom), first order high-pass filter	234
Figure 7-7. The frequency domain gain, phase errors and position excursions in a range of filter parameters (top), and cropped out settings with excursions smaller than 2.5 (m) (bottom), first order high-pass filter	235
Figure 7-8. The time domain true and false output accelerations in a range of filter parameters, second order high-pass filter	236
Figure 7-9. The time domain true, false accelerations and position excursions in a range filter parameters (top), and cropped out settings with excursions smaller than 2.5 (m) (bottom), second order high-pass filter	237
Figure 7-10. The frequency domain gain, phase errors and position excursions in a range of filter parameters (top), and cropped out settings with excursions smaller than 2.5 (m) (bottom), second order high-pass filter	238
Figure 7-11. The time domain true and false output accelerations in a range of filter parameters (top), cropped out settings with excursions smaller than 2.5 (m) (bottom), third order high-pass filter	239
Figure 7-12. The frequency domain gain, phase errors in a range of filter parameters (top), cropped out settings with excursions greater than 2.5 (m) and errors greater than normalised value of 0.5 (middle) and both in the same plot (bottom), third order high-pass filter	240
Figure 7-13. The time domain true and false output accelerations by tilting in a range of filter parameters (left) maximum angular velocity and accelerations (right), second order low-pass filter	241
Figure 7-14. The frequency domain gain, phase errors in a range of filter parameters, second order low-pass filter.....	242
Figure 7-15. The time domain true and false output accelerations in a range of filter parameters (top), cropped out settings with excursions greater than 2.5 (m) (bottom), high-pass and low-pass filter	243
Figure 7-16. The frequency domain gain, phase errors in a range of filter parameters (top), cropped out settings with excursions greater than 2.5 (m) and errors greater than normalised value of 0.4 (middle) and both in same plot (bottom), high-pass and low-pass	244
Figure 7-17. Acceleration and position response of the MPC model, to step, square, triangle-square, sinusoid and vehicle lateral acceleration inputs, fixed look-ahead reference input	248
Figure 7-18. Bode frequency response of the MPC model	248

Figure 7-19. Time response of the MPC model to step input in various prediction H_p and control horizons H_u in both constant (left) and variable reference look-ahead inputs (right)	251
Figure 7-20. Time response of the MPC model to triangle-square input in various prediction H_p and control horizons H_u in both constant (left) and variable reference look-ahead inputs (right)	253
Figure 7-21. Time response of the MPC model to sinusoid input in various prediction H_p and control horizons H_u in both constant (left) and variable reference look-ahead inputs (right)	254
Figure 7-22. Time response of the MPC model to vehicle lateral acceleration input in various prediction H_p and control horizons H_u in both constant (left) and variable reference look-ahead inputs (right)	255
Figure 7-23. The time domain true and false output accelerations in a range of weight factors (top), cropped out settings $Tr > 0.6$ and $Fs < 0.2$ (bottom), MPC translational motion.....	257
Figure 7-24. The frequency domain gain, phase errors in a range of weight factors (top), cropped out settings $G_n < 0.2$ and $Ph < 0.3$ (middle), and both in the same plot (bottom), MPC translational motion.....	258
Figure 7-25. The time domain true and false output tilt acceleration felt through tilting in a range of weight factors, MPC tit motion	259
Figure 7-26. The frequency domain gain, phase errors in a range of weight factors, MPC tit motion.....	260
Figure 7-27. The time domain true and false output accelerations in a range of weight factors (top), cropped out settings $Tr > 0.7$ and $Fs < 0.5$ (middle) and both in the same plot (bottom), MPC translational and tilt motion	261
Figure 7-28. The frequency domain gain, phase errors in a range wright factors (top), cropped out settings $G_n < 0.2$ and $Ph < 0.2$ (middle), and both in same plot (bottom), MPC translational and tilt motion.....	262
Figure 7-29. The time domain true and false output accelerations in a range of weight factors (top), cropped out settings $Tr > 0.6$ and $Fs < 0.2$ (bottom), MPC translational and tilt motion	263
Figure 7-30. The frequency domain gain, phase errors in a range wright factors (top), cropped out settings with $G_n < 0.4$ and $Ph < 0.2$ (middle), and both in the same plot (bottom), MPC translational and tilt motion	264
Figure 8-1. Vehicle model lateral acceleration, time series profile of an example run (left), and maximum amplitude of all runs with 95 percent confidence interval (right), for both LHT and SLM tasks.....	271
Figure 8-2. Perceived vehicle model lateral acceleration, power spectral density (left) of an example run, and maximum frequency of interest of all runs with 95 percent confidence interval (right), for both LHT and SLM tasks.	271

Figure 8-3. Fidelity corridors defined by OMCT, Sinacori, coherent zone and the one used in optimisations for LHT task	272
Figure 8-4. Optimisation process	274
Figure 8-5. Optimisation results for the LHT task with tilt setting high (left) and low (right). The bars show number of recorded runs that would require a given rail size.	276
Figure 8-6. Optimisation results for the slalom task with tilt limits high (left) and low (right). The bars show the number of recorded runs that would require a given rail size.	276
Figure 8-7. Optimisation results for frequency ω_{hp} (left) and gain k_{hp} (right) range, for both driving tasks.	276
Figure 8-8. Sinusoid input used to estimate the frequency response of the models	277
Figure 8-9. The classic algorithm estimated frequency response, requiring ± 16 (m) of MP workspace	279
Figure 8-10. The MPC algorithm estimated frequency response, requiring ± 14 (m) of MP workspace	28
0	

Abbreviations

Abbreviation	Meaning	Comments
MP	Motion platform	Mechanical system of which the physical actuators generate motions
MCA	Motion cueing algorithm	Control method to fit the vehicle motion within the motion platform limitations
MPC	Model predictive control	Optimal control method with moving horizon, respects the plant constraints
SCC	Semicircular canals	Inner ear vestibular system, sensor of rotational motions
OTO	Otoliths	Inner ear vestibular system, sensor of translational motions
LHT	Land Rover Handling Track	Vehicle testing track, include multiple turns and straight lines sections
SLM	Slalom	Driving task, negotiating between cones that are spaced at certain distances
GSP	Gosport lane	A public road for vehicle testing, include multiple turns and straight lines sections
DPYRE	Desired path yaw rate error	Driver model that characterises the driver as a controller through changes of parameters
OMCT	Objective motion cueing test	An objective motion system performance assessment method
RMS	Root mean square	The square root of mean square
PSD	Power spectral density	A measure of signal's power content versus frequency
DoF	Degrees of freedom	In a mechanical context, defined as modes in which a mechanical system can move

1 Introduction

1.1 Background

Driving simulators have been used for research on driver behaviour, impairment, road safety and infrastructure design, and vehicle design purposes. Compared to real driving, simulators facilitate a safer, repeatable, more versatile and less costly environment. They provide safe and repeatable measurements of driver behaviour in potentially risky conditions that are unethical and illegal to assess in the real world e.g. fatigue, subordinate or incidental secondary tasks, near-miss car crashes or alcohol and drug intake. Besides, they can be used in clinical research with patients with performance decline, neurodegenerative disorders and chronic effects of medications (Fisher, D.L. et al., 2011). However, the training contribution of driving simulators is lower compared to aviation, rail and maritime transports where the vehicles are more costly than simulators.

The advantage of easy manipulation of driving scenarios and environmental variables such as road surface, signage, traffic, weather for a particular behaviour investigation or road and traffic design, are listed for the transport research applications (Carsten and Jamson, 2011). In general, among the advantages of simulators are controllability, reproducibility, and standardization, ease of data collection, encountering dangerous driving conditions without risk, and opportunity for feedback and instruction and among the disadvantages are limited physical, perceptual, and behavioural fidelity, shortage of research validity of simulation, and simulator discomfort (De Winter et al., 2012).

Driving involves a wide range of activity in the human body often classified as sensation, perception of self-motion followed by decision making and behaviour. Various internal sensory modalities of eyes (visual motion), vestibular (inertial motion), ears (aural), joints, muscles, haptic (proprioceptive receptors) receive signals (cues), which then are integrated through a neural multisensory combination process that contributes to motion perception (Hosman et al., 2011). Next, human decision making takes place based on the acquired perception and results in behavioural performance. Simulator subsystems including the visual, vestibular, auditory and proprioceptive (haptic) sensory generator and display devices together with vehicle model, computers and electronics, cabs and controls are designed to replicate the real world cues in a virtual environment (Allen et al., 2011).

One-to-one replication of the real world cues is not feasible in simulators, because of practical, technological and financial hindrances, and reportedly not always

necessary. The extent of similarity between the real and virtual environments has been referred to as simulator fidelity. Fidelity is typically evaluated subjectively at the perceptual level and objectively at the sensory and behavioural levels. To elicit a realistic driving experience, i.e. high fidelity, cues similar to real the world need to be represented in simulators, in addition to the similarity of driver's performance in both environments.

Although simulators provide most of the visual cues available in real driving, representation of vestibular cues has always been challenging (Kemeny and Panerai, 2003). Moreover, studies done in large simulators have shown that vestibular motion cues that are objectively closer to the actual vehicle motion (one to one) in a given driving task are not always perceived as more realistic (Berthoz et al., 2013). From a motion perspective, simulators are divided into static and dynamic types. Static simulators represent motion through a visual cueing system, whereas in a dynamic simulator both visual and vestibular (inertial) motion cues are available.

Preliminary studies indicating the importance of vestibular motion cueing in simulators began by comparing the effect of static and dynamic motion configurations on drivers' perception and performance. Repa et al. (1981) reported that the presence of motion tends to reduce path keeping errors and driver control activity; roll and yaw motions influence driver vehicle performance; and they emphasized the need for motion in more extreme manoeuvres. Reymond et al. (1999) showed lateral acceleration has a significant effect on drivers' speed choice strategy on curved roads. Evaluating two driving tasks, Siegler et al. (2001) showed in a stopping task that the presence of motion in a simulator helps to avoid reaching too high and unrealistic decelerations and decrease in behaviour adaptation. In a cornering task, the availability of lateral motion influences the driver's choice of trajectory; and longitudinal motion cue decreases linear velocity.

The representation of vestibular motion cues in dynamic driving simulators is a function of four main components. These are the vehicle model, motion platform dynamics, motion cueing algorithm (MCA) and data transport time delay (computations, digital/analogue conversions, transmissions). Having an accurate vehicle model in hand leaves the motion platform and motion cueing algorithm characteristics as remaining variables affecting the motion cueing fidelity of a driving simulator, while the transport delay is usually dependent on both of the variables.

The motion platform typically is the costliest component of simulators. It is a mechanical system (robot manipulator) of which the physical actuators generate motions. These are available in various shapes and characteristics, among them

the synergistic 6 degrees of freedom (DoF) hexapod-type optionally integrated with sliding rail to provide larger translational motion workspace is commonly used for research applications. There is a large variation in workspaces of both the hexapod and sliding rail used in the simulators and the lack of a general conclusion on what size is really needed to have high fidelity motion cueing in simulators.

The MCA is designed to represent the vehicle's motions in the motion platform while keeping the motion platform within its physically limited envelope; there are many approaches to achieve it. Many MCAs are developed in literature from classic, the most typical, to adaptive, optimal and more recently model predictive control (MPC) models with mixed results about which one provides higher fidelity. Other than the diversity in model types, there is a challenge of tuning (selecting parameters) the MCAs which has a major impact on their performance, as another source affecting the fidelity.

Driven attributes of a vehicle include properties such as steering feel, handling, and ride qualities. The current main approach to test these qualities require costly physical prototypes, and the testing itself is time-consuming, with associated risks of less accurate evaluations since drivers are not comparing alternative designs in close temporal proximity. Tests in the simulator do not require physical prototypes, and arbitrary changes to vehicle designs can be applied without time delays. However, the applicability of the simulators for evaluation of the vehicle qualities is sparsely investigated, and the effect that motion cueing of the simulator might have on these tests is not known.

1.2 Thesis aim and objective

The perception of self-motion and behaviour of a driver in a simulator is affected by a simulator's subsystems and their limited capability to stimulate drivers' sensory modules which has the potential to influence the fidelity of the simulators. The required characteristics of each of the subsystems to achieve a desired level of fidelity is an extensively broad question and often there is no clear answer. Thus, the scope of this research focuses only on the subsystems that affect vestibular motion cueing.

The overall aim of the effect of simulator motion system on motion cueing fidelity has been pursued throughout this thesis in different contexts and evaluated in terms of drivers' perception, and behaviour performance. Typically, higher capabilities of the motion system present higher fidelity in simulators, however bearing in mind that one could optimally cut costs of purchasing a motion platform considerably by not building it too large and using a more sophisticated MCA.

In this regard, the effects of manipulating the two most influential motion cueing components of the simulators are studied in this thesis, those are the motion cueing algorithm, and motion platform workspace size. The probable effect that the MP size might have on the MCA performance, is also evaluated. The evaluations are done specifically for vehicle testing in low-friction winter conditions, and low and high motion demanding manoeuvres.

Furthermore, to evaluate the applicability of simulators for assessments of the vehicle driven attribute properties, a variation to the vehicle ride height is studied. The probable effect that the motion platform size might have on the assessments, is also evaluated. The evaluations are done for a high-friction public road routinely used for testing vehicle prototypes.

In the conventional vehicle design process, prototypes need to meet certain design criteria in both high-friction and low-friction road conditions. This is essential for car manufacturers, who export their products to countries of different climates. Similarly, the routinely carried out testing of vehicle designs by Jaguar Land Rover (JLR) includes both of the road friction conditions.

Hence, as an overarching aim of Programme for Simulation Innovation (PSi) Theme 3 projects, throughout this thesis, two experiments were designed and conducted in the simulator to study the effects of the simulator motion system in a low road friction condition, and aspects of vehicle design in a high road friction condition, to find out if professional drivers find the driving simulator to be a realistic and reliable tool for the evaluations.

Although the road friction effect is not the main focus in this thesis, and separate main aims of the effect of motion cueing algorithm and vehicle driven attributes are studied respectively in low and high road friction conditions, there is a mutual aim of motion platform workspace size in both of the experiments, which is evaluated and compared in both friction conditions.

The assessments are based on the subjective perception and performance of professional drivers who typically evaluate the vehicle designs and often have higher demands. Hence, the conclusions from the experiments are more applicable for the vehicle design process, and requirements for the simulator motion system might be lower for other research applications with normal drivers.

Due to the significant effect of MCA parameters on the motion cueing, optimal tuning of the MCA parameters is introduced that minimises motion errors and exploits the motion platform capability. These optimal settings are further used, together with appropriate fidelity criteria, and a multi-layered optimisation method to

address the motion platform translational workspace requirement, to achieve a certain level of perceptual fidelity, and lowering the costs of procurement.

1.3 Thesis structure

Following the research challenges identified in this chapter, in Chapter 2 human perception and performance during driving and attempts to model them are reviewed, mainly to select the appropriate models for MCA development and drivers' objective performance analysis. In Chapter 3, simulator subsystems are introduced, including the motion cueing system employed in the experiments. Moreover, various fidelity criteria available in the literature are reviewed with an emphasis on motion cueing fidelity. In Chapter 4 the MCAs of reportedly higher fidelity are developed and adapted specifically for the motion platform and following experiments. In Chapter 5 an experiment is reported which evaluates the MCA and motion platform size effects, while in Chapter 6 an experiment is reported to evaluate vehicle ride height and motion platform size effects; both are based on measurements of perception and performance of drivers. In Chapter 7 the effect of the MCA tuning parameters is introduced, and optimal settings of the algorithms are extracted. In Chapter 8 using the obtained tuning parameters, fidelity criteria, and optimisation method, the motion platform workspace is optimised to achieve an acceptable level of perceptual fidelity. In Chapter 9 summary of all findings is represented followed by conclusions.

2 Driver Perception and Performance

2.1 Introduction

Driving is one of the human sensorimotor activities that involve the perception of stimuli from environment and response with physical behaviour. Knowledge of the human sensory systems in addition to that of the vehicle dynamics is necessary for a complete understanding of human-vehicle interactions. Vehicle development process still relies on expensive and time-consuming pilot/driver subjective evaluations of a prototype. Through a deeper understanding of human-vehicle interaction, driver models have been developed to help the process of design and evaluations of vehicle systems (Nash et al., 2016).

The human sensory systems (modules) have a significant role in self-motion perception and performance, and the visual and vestibular signals are the two most influential cues in the perception process. Fetsch et al. (2009) showed that rapid and unpredictable change of sensory information, affects its reliability; considering this uncertainty, the integration of multiple sensory signals in the brain is still unclear. They considered a psychophysical approach together with Bayesian probability theory that the integration of the cues was done by weighting them in proportion to their reliability. They found that monkeys similar to human, also “dynamically reweight visual and vestibular cues in proportion to their reliability”. However, some of the subjects tended to overweight vestibular cues.

Nash et al. (2016) described the process of sensory, perceptual and control behaviour of a human to the input stimulus. Briefly, when a sensory module is excited by a stimulus, it produces chemical signals, which are then transmitted through nerves as electrical impulses by neuron firing. The physical and biochemical limitations accompanying the process are listed to be time delays of sensorimotor systems, noises in receptor and neuromuscular systems, errors in the internal model of the brain and spontaneous firing of neurons, in addition to the certain threshold of perception of stimuli. All reflecting that the accurate measurement of stimuli and execution of an ideal response is not always performed by a human (Fernandez and Goldberg, 1971). The sensory signals are processed in the sensory cortex of the brain, where the information is extracted from encoded signals. The information from different sensors are integrated, forming a representation of the surrounding environment and leading to perception; then using an internal model of the body and the surrounding environment, the physical response is planned. Signals are then generated in the motor cortex to activate the muscles, which are further tuned using feedback signals from the sensory modules (Kandel et al., 2000). Finally, signals are transmitted through motor neurons to

activate muscle fibres to contract; this process is a function of the dynamic properties of the muscle.

Although the complete human sensory, perceptual and behaviour is a complex process, “for purpose of driver/pilot modelling it is not necessary or feasible to model all aspects” (Nash et al., 2016). The driver uses the sensory information to infer the state of the vehicle and its environment. While driving, the visual cues are used by the driver in detecting the upcoming road geometry and objects, and relative motion of the vehicle to the surroundings. This information is then combined with the vestibular motion cues, which sense the angular velocities and translation linear accelerations of the driver’s head. These, in addition to information from other sensory modules, lead to the perception and behaviour of the driver.

A hypothetical block diagram of a model of driver controlling vehicle direction and speed is shown in Figure 2-1, which is inspired by (Donges, 1978). It is explained that the upcoming road geometry is previewed through the driver’s visual system, and using an ‘internal model of the vehicle dynamics’, the driver plans the desired trajectory and speed profile to generate the required feedforward control actions (steering wheel angle and pedal forces). At the same time, the vehicle motion relative to the planned profiles is sensed by the driver, who generates the feedback control actions to reduce the effect of disturbances. However, in this model, the vehicle motion feedback is not directly used for generating the feedforward control actions, but rather it helps to correct the imperfections such as disturbances.

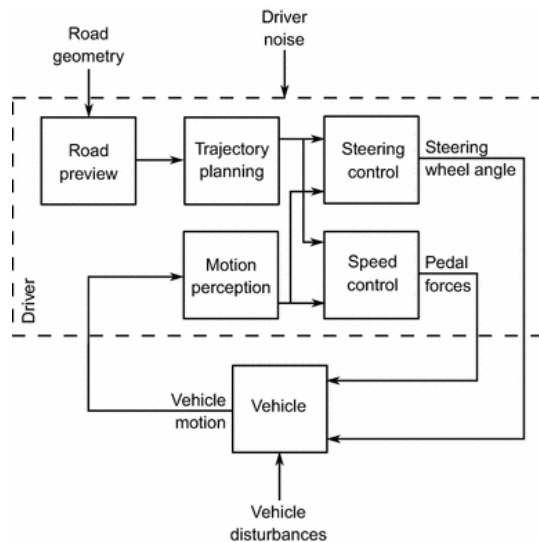


Figure 2-1. Model of tasks carried out while driving, (Nash et al., 2016)

The overall goal of drivers in steering control is to follow a target path and not surpass the road boundaries, with the choice of trajectory and speed depending on the situation. In normal driving, the driver compromise between factors such as journey time, safety, comfort, and control effort (Odhams and Cole, 2004), minimise

the lateral acceleration in corners (Reymond et al., 2001), anticipation in entering and cutting through the inside of a curve to keep maximum curvature of the car as low as possible (Boer, 1996). However, in motor racing, drivers aim to maximise the lateral acceleration by higher speeds to minimise the lap time (Timings and Cole, 2014). In traffic situations, the steering and pedal controls might be affected by other cars, to maintain a safe distance with the front car (Boer, 1999).

The first attempts at modelling human control behaviour of longitudinal, lateral, heading of vehicles began in the early years of human-machine and aircraft pilot studies. Those often considered the human-vehicle interactions as a driver/pilot a controller of car/aeroplane a dynamic plant. A review on control aspects of a human driver in path-following, obstacle avoidance, headway control and related models is available in (Macadam, 2003).

In the majority of driver models, drivers aim to minimise a tracking error within a finite interval of the future path ahead. Tracking errors can be due to a single or combination of different variables such as lateral deviation, heading angle and are usually the result of the difference between previewed and desired path using a prediction of vehicle motion. Optimal control models suggest that humans act to minimise a cost function, consisting of tracking and steering control errors. It is still not fully understood whether the nervous system has such internal models, or uses other mechanisms to achieve the optimality (Markkula et al., 2014). In the next sections a review of the efforts in understanding and modelling the human sensory dynamics, and human-vehicle interactions is presented.

2.2 Perception of self-motion

Self-motion perception is the process of inferring the movements of one's body in space, normally through movements of the eyes relative to fixed surroundings or illusory by moving surroundings relative to fixed eyes known asvection. It involves a relative body motion e.g. moving hands or feet relative to body, mostly supported by the proprioceptive and visual systems; as well as motion of the complete body (posture control) that includes the head, e.g. movement of the whole body in a dark room where there is no visual cue, supported by the proprioceptive and vestibular modules. Due to the different characteristics of the visual and vestibular systems, motion perception using the visual system is a slower process compared to the vestibular system (Zacharias and Young, 1981). Besides, vestibular cues dominate the sensation of cues at higher frequencies and visual system at lower frequencies, and both are augmented to provide a wideband sensation system.

Vehicle displacement, velocity and acceleration motion in space could be described in three translational surge (longitudinal), sway (lateral), heave (vertical) and three rotational (angular) roll, pitch, yaw local coordinate directions. Motion perception regarding position and velocity takes place by the visual system, while acceleration via the vestibular system (Gordon, D.A., 1965; Mark et al., 2006). Through the vestibulo-ocular reflex (an eye movement that compensates for head movement using vestibular information) the vestibular motion cues also have an impact on the visual motion perception. However, the focus of this thesis is only on the motion cueing subsystems in the simulator that affects vestibular motion perception.

In case of absence or disagreement of either the visual and vestibular cues, there might arise conflict introducing illusions or motion sickness. An example is circularvection, where the subject sits upright, fixed to the earth and visual field rotates inducing conflict. In this case, the visual system perceives the rotation while the vestibular system does not. Although there is no vestibular motion, the subject eventually feels himself rotating at a constant speed. This type of motion perception, takes longer than normal where both visual and vestibular cues are available (Brandt et al., 1973; Zacharias and Young, 1981). Similar conflicts happen in simulators when the visual and vestibular motion cues do not match, and in extreme cases, motion sickness may occur with symptoms of dizziness, fatigue and nausea.

2.2.1 Visual perception

The contribution of the visual sensory system to motion perception has been the subject of research in different fields of biology, neuroscience and psychology. The visual system works by measuring the movement of objects relative to the environment and movement of the environment relative to the eye; this measurement is derived from the displacement of the image on the retina. During driving, the visual system detects upcoming road geometry and assesses vehicle motion relative to the surrounding environment. There is still much to learn about how neural signals received by the retina from a visual scene are interpreted; however, as mentioned earlier not all aspects need to be modelled to study visual perception while driving (Nash et al., 2016).

In order to perceive depth and construct a 3D interpretation of the environment (together called stereopsis), the human brain uses the information obtained from two eyes; this is referred to as binocular vision. Optic flow and disparity were suggested to have the main effect on visual perception (Gibson, 1950). Binocular disparity is the difference in the retinal image location of an object seen by the left and right eyes. Each eye has a slightly different view of the world, and the visual cortex of the brain uses the binocular disparity to extract depth information from the

2D retinal images. The disparity has been shown to have an effect over distances of up to 30 metres (Knapp, 2003). Optic flow refers to the dynamic patterns of motion of points in a visual scene (e.g. objects, surfaces, and edges flowing over the retina) caused by relative movement between observer and scene.

In straight road driving, the driver uses patterns from a point directly in front, called the focus of radial outflow (FRO). In rotational motion, the patterns are curved, and there is no FRO; however, the point in front may still be used to determine the heading. Both have been found to have a role in the control of vehicle heading (Gibson, 1950) and collision detection (Reymond et al., 2001). Gordon, D.A. (1965) proposed that humans measure the rate of changes of the vectors between the observer and scene. Moreover, it was found that contrary to the motion parallax, these velocity vector patterns in curved trajectories did not reveal distance, and angular acceleration is not directly sensed by the visual system. Through measurements of visual sensory thresholds at different frequencies of stimulus, a low-pass characteristic was observed for the visual sensory dynamics for both surge and sway motions (Riemersma, 1981; Bigler, 2013).

The driver previews the road geometry ahead to control the vehicle. To pinpoint where drivers look, many studies have been conducted on drivers' eye behaviour, and various points on the road reported to be used by drivers. For instance, it has been shown that drivers use the 'tangent point' on the inside of the road (Boer, 1996), where the distance to the 'tangent point' and the car's heading relative to the tangent point vector are intermittently used to update the steering angle. Sharp et al. (2000); Sharp and Valtetsiotis (2001) used a multi-point preview controller, based on the idea that the drivers figure a 'multi-point image of the road geometry' ahead of the vehicle in their memory. In a review of two-point and multi-point visual models, Steen et al. (2011) showed that the Donges (1978) two-point preview model was the most realistic visual behaviour model. They also reported that the two-point model outperformed in the parameter identification process.

Donges (1978) introduced, modelled and identified the two levels of control in a steering task. In feedforward control (anticipatory), the visual system assesses the instantaneous and future course of the road to allow the driver to generate the feedforward open-loop control inputs to the vehicle. This information is called 'guidance information' because the driver uses it for guiding the vehicle along its desired path (e.g., in a target-following task). In feedback control (compensatory), the instantaneous deviations between the vehicle's actual path and its desired path are detected using static and dynamic cues in the visual field to allow the driver to perform closed-loop feedback control of the vehicle. This subset of information is called 'stabilisation information' because the driver uses the visual cues to stabilise

vehicle motions (e.g., in a disturbance rejection task). Disturbances might originate from wind gusts, road surface undulations, nonlinearities in vehicle dynamics or the driver's constraints and nonlinearities.

Driving simulators provide “most, but not all, of the real world visual cues” (Kemeny and Panerai, 2003). It is explained that in simulators, the speed evaluation is acquired by self-motion perception from the direction of an object in space relative to observer rather than the eyes i.e. egocentric direction and optic flow. The optic flow from the movement of images of objects in the scene is available. However, binocular cues and motion parallax (the distance and difference in the observable position of an object from two different lines of sight) are often absent. Providing these cues increases the cost and complexity of image generation and display equipment and requires integration of head-tracking devices.

2.2.2 Vestibular perception

The vestibular sensory organ located in the inner ear is considered to be the body's motion sensor. It is embedded in the temporal bone alongside the cochlea (which is responsible for hearing). It provides information about the maintenance of visual and postural stability and perception of motion and orientation. The inner ear vestibular organ contains otoliths (OTO) that sense translational motions and semicircular canals (SCC) that sense rotational motions, as illustrated in Figure 2-2. The vestibular systems of humans and primates have been investigated to discover their response to different stimuli, through different methods such as measuring vestibulo-ocular reflex, and electrical signals in the brain.

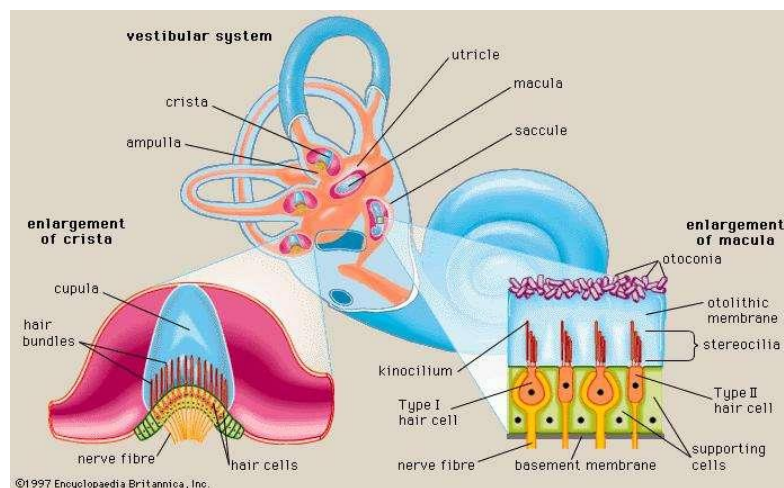


Figure 2-2. Vestibular system, semicircular canals (left), and utricle and saccule of the otolith (right), from Encyclopaedia Britannica

2.2.2.1 Otolith

Otoliths consist of a set of two sensory receptors known as maculae. They lie at the point where the three semicircular canal ducts converge, within bulb-shaped

expansions called the utricle and saccule. The macula in the utricle is oriented horizontally and is sensitive to the planar longitudinal and lateral motions, while the macula in the saccule is oriented vertically and is sensitive to vertical motion. At the base of the macula, hair cells project into a gelatinous substrate on top of which sits a blanket of granular crystal particles referred to as statoconia. During translational motions in the plane of the macula, the inertia of these particles and the substrate cause the hair cells to be deflected in the direction opposite to the movement and excitation of the sensory cells.

Experiments have been conducted to measure the ability of subjects to perceive a variety of linear motions, and mathematical models have been developed relating the subjective perception of motion to their objective values. Meiry (1966) showed that humans perceive velocity in translational motions, and in experiments, subjective responses to the perception of the direction of longitudinal motion were measured. The input stimulus was sinusoidal acceleration, which allowed the researchers to study the phase dependency on the frequency of the stimulus. A linear transfer function model was developed, shown here as Eq. 2.1. The long time T_L and short time T_S constants had values of 10 and 0.66 s, respectively. There was no amplitude measurement, so K was unspecified.

$$G(s) = \frac{v_p}{a_a} = \frac{K}{(1 + T_L s)(1 + T_S s)} \quad 2.1$$

Three years later, Peters (1969) suggested that in the Meiry's (1968) experiment subjects had perceived acceleration, not velocity. Research by other authors indicated that subjective perception of acceleration does not diminish with time but has a steady-state component. This argument was supported by the equivalence between the perceived acceleration due to linear motion or tilting. In the response of the Meiry's (1968) model to step input acceleration decayed to zero; however, there is no decay to zero in perceived tilt for a step input tilt angle. Thus, the model was updated so that the output was the perceived acceleration a_p rather than velocity v_p .

Young and Meiry (1968) introduced a revised model later. A neural processing (lead) term was added to the afferent output to describe the displacement of statoconia, and the long time constant T_L was shortened to 5.33 s. Therefore, the model was able to consider both perceived linear acceleration and tilt angle to input linear acceleration. Moreover, the authors mentioned that the model could be applied to specific force sensation, and noted that over typical normal head motions (i.e., a frequency range of 0.19 to 1.5 rad/s), the model acts as a velocity transducer and has a static sensitivity gain K of 0.4 (see Eq. 2.2). In this model, time constants T_a , T_L and T_S had values of 13.2, 5.33 and 0.66 s, and gain K had a

value of 0.4. This model, with the identified parameters, is essentially a low-pass filter.

$$G_{(s)} = \frac{f_p}{f_a} = K \frac{(1 + T_a s)}{(1 + T_L s)(1 + T_S s)} \quad 2.2$$

Considering the difference between the transduction and sensation in the otolith, Ormsby (1974) developed a linear perceptual model. The otolith dynamics model used cascaded transducer and estimator models that combined the mechanical and afferent firing rate (AFR) dynamics of otoliths to input specific force. Then, a steady-state optimal processor linked the AFR to the perceived specific force. This is shown in simplified form in Eq. 2.3. The model parameters of BK° , A , B , $(B + C) \frac{A}{B}$, F , and G had values of 0.911, 0.2, 91.1, 0.0988, 0.133, and 1.95 respectively.

$$G_{(s)} = \frac{f_p}{f_a} = BK^\circ \frac{\left(s + \frac{(B + C)A}{B} \right)}{(s + F)(s + G)} \quad 2.3$$

Regardless of the more descriptive nature of the model in Eq. 2.3, it yielded results similar to those of the Young and Meiry (1968) model in Eq. 2.2 with the interchangeable time constants T_a , T_L and T_S having values of 10.13, 7.52 and 0.51 s and gain K having a value of 0.35. Ormsby's (1974) model was reported to differ by about 30% from the values proposed by Young and Meiry; however, it resolved the inconsistency between high bandwidth transducer dynamics and low bandwidth perceptual dynamics and also showed that transduction and estimation were best treated as two separate processes (Asadi et al., 2016).

Fernandez and Goldberg (1976) measured the afferent firing rate of both regular and irregular otolith neurons in squirrel monkeys' brains at various amplitudes and frequencies of sinusoidal input accelerations. The response of regular units proved to be more tonic (adapting slowly to a stimulus and producing action over the duration of the stimulus) with mostly less than two times gain increase when the frequency was increased; a small phase lead and lag was observed at low and high frequencies respectively. Irregular units' response was more phasic (with rapid adaptation to a stimulus and action diminishing very quickly), with 20 times gain increase and a 20 to 40 degree phase lead, in the same frequency spectrum.

The authors fit a transfer function (Eq. 2.4) to the results that included three terms. a velocity sensitive operator G_V with a fractional exponent that provides most of the phase lead and the gain increase in irregular units. A low frequency adaptation operator G_A contributing to the phase leads and gain increase at low frequencies. Finally, a first order lag operator G_M that reflects the mechanics of otolith of high frequency phase lag in regular units and attenuates phase lead of irregular units from velocity-sensitive operators at high frequencies. All of the parameters of the

proposed transfer function— k_v , k_A , τ_M , τ_A , and τ_M —were identified for both regular and irregular units, with values of 0.188-0.44, 1.2-1.9, 40, 69-101 s, and 16-9 ms respectively.

$$G_{(s)} = \frac{AFR}{f_a} = G_V G_A G_M = \frac{(1 + k_A \tau_A S)(1 + k_v (\tau_v S)^{k_v})}{(1 + \tau_A S)(1 + \tau_M S)} \quad 2.4$$

$$G_V = 1 + k_v (\tau_v S)^{k_v}, \quad G_A = \frac{(1 + k_A \tau_A S)}{(1 + \tau_A S)}, \quad G_M = \frac{1}{(1 + \tau_M S)}$$

The fractional exponent term in the transfer function of Eq. 2.4, made it practically difficult to implement it in motion cueing algorithm (MCA) development. Therefore, Hosman (1996) provided a model (Eq. 2.5) that was a simplification of the model Hosman and van der Vaart (1978) originally proposed. It was similar to the models of Young and Meiry (1968) and Ormsby (1974) but with different parameters relating the perceived specific force to actual input specific force. Hosman (1996) chose the time T_S to be equal to τ_M the time constant of otolith mechanics for regular units (Fernandez and Goldberg, 1976). The model parameter time constants T_a , T_L and T_S had values of 1, 0.5 and 0.016 s, and gain K had a value of 0.4.

$$G_{(s)} = \frac{f_p}{f_a} = 0.4 \frac{(1 + S)}{(1 + 0.5S)(1 + 0.016S)} \quad 2.5$$

In a review of otolith models, Telban and Cardullo (2005) used the lead T_a and long T_L time constants reported by Ormsby (1974); Jones et al. (1964) with values of 10 and 5 s and the short time constant T_S reported by Hosman (1996) with a value of 0.016, which resulted in the transfer function in Eq. 2.6. The time domain step response (onset time, steady-state response) of this model is shown to fit between the step responses of otolith models of regular and irregular unit parameters by Fernandez and Goldberg (1976).

$$G_{(s)} = \frac{f_p}{f_a} = 0.4 \frac{(1 + 10S)}{(1 + 5S)(1 + 0.016S)} \quad 2.6$$

The parameters of otolith models reviewed in this section are presented in Table 2-1, and the Bode¹ plot of frequency response of the models is shown in Figure 2-3. The midrange frequencies between 0.1 and 10 *rad/s* are the most important in driving, and it can be observed that the otoliths have a proportional response to accelerations in this frequency range (Nash et al., 2016). Moreover, there is a perception threshold of the otolith system that is a function of input frequency and

¹ A graph of the frequency response of a system. It is usually a combination of Bode magnitude and phase plots, expressing the magnitude and phase shift of the frequency response respectively

amplitude, and varies between the passive (open-loop) and active (close-loop) driving. It is usually modelled as a nonlinear dead-zone block cascaded between the transfer functions, makes it unappropriated for direct use in MCAs with linear plant models.

Table 2-1. Otolith model parameters

Otolith model by	K	T_a	T_L	T_S
Young and Meiry	0.4	13.2	5.33	0.66
Ormsby	0.35	10.12	7.52	0.51
Hosman	0.4	1	0.5	0.016
Telban and Cardullo	0.4	10	5	0.016

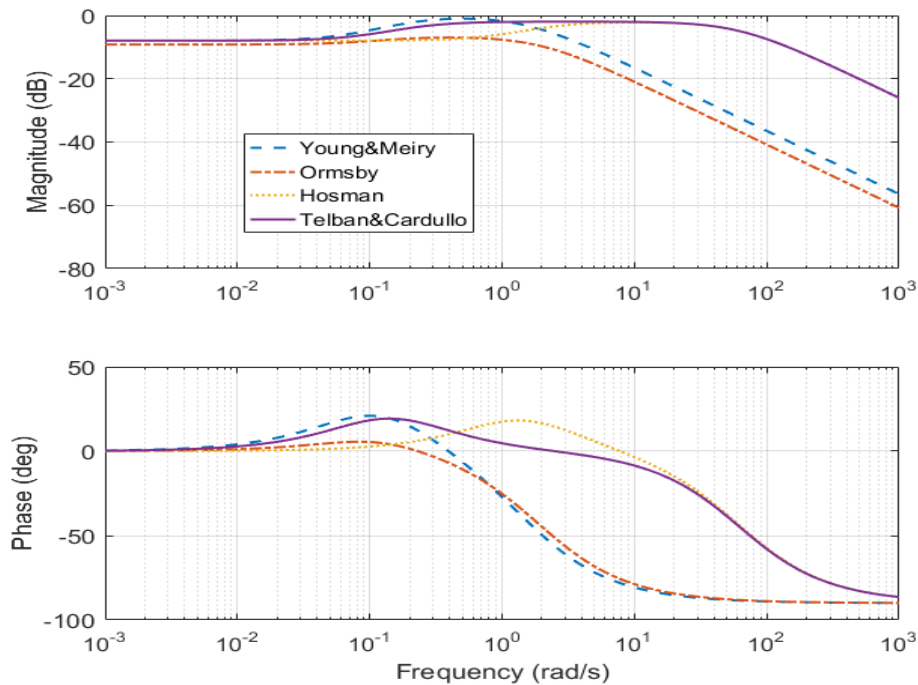


Figure 2-3. Bode frequency response of otolith models

Asadi et al. (2016) reviewed otolith models and showed that the Telban and Cardullo (2005) model acts as a reliable specific force sensor in the range of normal head movements. Telban and Cardullo (2005) used a combination of model parameters from other authors (long and lead time constants from (Ormsby, 1974) and gain from (Hosman, 1996)) and has shown the model to be suitable for use in MCA models. In Chapter 4, the otolith model used in the development of the model predictive control MCA is based on the model of Telban and Cardullo (2005) presented in Eq. 2.6.

2.2.2.2 Semicircular canal

Semicircular canals consist of a set of three perpendicular elliptical cavities (canals) that are filled with a viscous endolymph fluid (see Figure 2-2). At the endpoint of each canal, there is a bulb-shaped expansion called an ampulla, which contains the crista. The crista contains sensory hair bundles extending into a gelatinous mass called the cupula. The cupula forms a seal in the ampulla that resists circulation of endolymph fluid. When the head undergoes angular motion in the plane axis of the canals, the inertia force of fluid causes deflection of the cupula in the opposite direction of head movement, which causes displacement of hair bundles and excitation of sensory cells (Telban and Cardullo, 2005).

In early attempts to characterise the dynamics of semicircular canals, Steinhausen (1933) observed vestibular induced eye movements in the pike fish, and developed a linear second-order model and selected appropriate parameters to explain cupula dynamics. He showed that following a step angular velocity input, the cupula deflects by a rapid rise and then gradually decays back to its rest position, which was reflected in his model. A more formulised model was introduced by van Egmond et al. (1949) as a torsion-pendulum with a high degree of damping, which related the cupula-endolymph deflection δ to head angular velocity using Eq. 2.7. It was explained that there is always a slight leaking between the cupula and ampulla that causes the deviation between the actual and model SCC responses.

$$G(s) = \frac{\delta}{\omega} = \frac{KS}{(1 + T_L S)(1 + T_S S)} \quad 2.7$$

Based on a psychophysical testing method, they measured the verbal response of subjects regarding the duration of sensation after various input stimuli. Subjects were placed on a rotating chair and torsion swing in darkness. The researchers identified the time constants T_L and T_S to be 10 and 0.1s, respectively, also included a long time constant T_L as a gain; that introduced the first angular velocity sensation model in the form of Eq. 2.8.

$$G(s) = \frac{\omega_p}{\omega_a} = \frac{T_L S}{(1 + T_L S)(1 + T_S S)} \quad 2.8$$

For several years, researchers conducted studies to verify and expand this model. Meiry (1966) showed that his data was consistent with the model for yaw axis rotation and proposed a long time T_L of 7 s. In another study, Jones et al. (1964) evaluated the model parameter long time T_L in three rotational axes using two methods: a) subjective sensation, using a velocity step input stimulus and elapsed time to sensation decay as the measured response; and b) nystagmus slow phase velocity, measuring vestibular induced eye movement. Values for T_L for a and b

tests for different rotational axes were reported as follows: roll, 6.1 ± 1.2 and 4 ± 0.4 ; pitch, 5.3 ± 0.7 and 6.6 ± 0.7 ; and yaw, 10.2 ± 1.8 and 15.6 ± 1.2 s.

The response of the torsion-pendulum model (Eq. 2.8) to step angular velocity decays to zero, and the response to step angular acceleration is a steady sensation of rotation. This contradicted the actual measurements by Young (1969), in which the sensation of step velocity includes an overshoot, and step acceleration eventually decays to zero sensation. Young (1969) proposed an adaptation term to be added to the model to include the washout of human response to steady-state rotational acceleration, which was cascaded to the torsion-pendulum model in its linearized form as shown in Eq. 2.9. Parameter values of T_a , T_L and T_S were 30, 16 and 0.04 s, respectively. They also proposed a dual channel model that took into consideration the reported inconsistency between nystagmus and subjective response measures.

$$G_{(s)} = \frac{\omega_p}{\omega_a} = \frac{T_a S}{(1 + T_a S)} \frac{T_L S}{(1 + T_L S)(1 + T_S S)} \quad 2.9$$

Using direct measurements of the response of the afferent nerves in the semicircular canals of squirrel monkeys to angular acceleration inputs, Fernandez and Goldberg (1971) developed a model that consisted of the dynamic characteristics of Steinhausen (1933), an adaptation and lead terms. The lead term was found to be needed to generate the high-frequency deviation from the torsion-pendulum model and to including the gain and phase lead. According to Zacharias (1978), who reported from other studies, there is evidence of lead sensitivity in processing angular velocity information that was observed from gain rise at high frequencies; requiring the addition of lead term $(1 + T_{Ld}S)$, with T_{Ld} having the values from 17 to 50 ms (Fernandez and Goldberg, 1976) and 60 ms (Ormsby, 1974). Using the experimental data on AFR of squirrel monkeys, the parameters T_a , T_L , T_S , and T_{Ld} for Eq. 2.10 were determined to be 80, 5.7, 0.003 and 0.049 s, respectively. The parameter T_S was determined from properties of the endolymph and was noted to be 0.005 s for humans.

$$G_{(s)} = \frac{AFR}{a_a} = \frac{T_a S}{(1 + T_a S)} \frac{(1 + T_{Ld}S)}{(1 + T_L S)(1 + T_S S)} \quad 2.10$$

A more detailed model was proposed by Ormsby (1974), consisting of the transfer functions for transduction, filtering and cross-coupling. The most important part of the model was the transduction; other parts could be omitted in normal conditions or did not have a significant effect. In the transduction part of the model, the adaptation and lead terms were cascaded to the torsion-pendulum model of Young (1969), as in Eq. 2.11. The perceived angular velocity was proportional to the AFR.

Values for the parameters T_a , T_L , T_S , and T_{Ld} were 30, 18, 0.005, and 0.01 s. respectively.

$$G_{(s)} = \frac{AFR}{\omega_a} = (1 + T_{Ld}S) \frac{T_a S}{(1 + T_a S)} \frac{(1 + T_L S)}{(1 + T_L S)(1 + T_S S)} \quad 2.11$$

This model was simplified by removing the adaptation and gain sensitivity terms, resulting in Eq. 2.12 (Hosman and van der Vaart, 1978). It was argued that the adaptation term is important for low frequency stimulus, and it is outside the frequency range of a pilot tracking task (Hosman, 1996). Also, if neglecting the high frequency vibrations of the motion platform, the lead term could be omitted for MCA modelling purposes. The parameters of the model were identified through measurements of pilots' of angular acceleration threshold on a dynamic simulator motion platform. The model parameters of T_L , T_S , and T_{Ld} were 5.9, 0.005, 0.1 s.

$$G_{(s)} = \frac{\omega_p}{\omega_a} = \frac{(1 + T_{Ld}S)}{(1 + T_L S)(1 + T_S S)} \quad 2.12$$

In a review of the models in the literature, Telban and Cardullo (2005) suggested a transfer function that was noted to be suitable for angular velocity perception of input stimulus, and applicable to MCA models. The transfer function Eq. 2.13 resulted from cascading the torsion-pendulum model with the adaptation and lead terms. The model parameter values of T_a , T_L , T_S , and T_{Ld} for the roll, pitch and yaw rotational directions were determined to be 80, 5.73, 0.005, and 0.06 s.

$$G_{(s)} = \frac{\omega_p}{\omega_a} = \frac{T_L T_a S^2 (1 + T_{Ld} S)}{(1 + T_a S)(1 + T_L S)(1 + T_S S)} \quad 2.13$$

It was reported that the short time T_S caused instability of the transfer function model. Moreover, it was noted that if the MCA time step is equal to the lead time, then both the lead and short time constants could be omitted to avoid the instability, resulting in a reduced order model as shown in Eq. 2.14. However, because the numerator and denominator are of the same order, this model is not a strictly proper transfer function and therefore, is not appropriate for MCA development, as discussed in Chapter 4.

$$G_{(s)} = \frac{\omega_p}{\omega_a} = \frac{T_L T_a S^2}{(1 + T_a S)(1 + T_L S)} \quad 2.14$$

In another study, Zacharias (1978) removed the lead term from the model of Young (1969); the model was a cascade of an overdamped torsion-pendulum model together with a threshold of perceiving the velocity and an adaptation term that reflected the washout of human response to steady-state rotational acceleration input Eq.2.15. Parameter values of T_a , T_L , and T_S were determined to be 30, 30, and 30 s for roll; 6.1, 5.3, and 10.2 s for pitch; and 0.1, 0.1, and 0.1 s for yaw, respectively.

$$G(s) = \frac{\omega_p}{\omega_a} = \frac{T_a S}{(1 + T_a S)} \frac{T_L S}{(1 + T_L S)(1 + T_S S)} \quad 2.15$$

The parameters of SCC models reviewed in this section are presented in Table 2-2, and the Bode plot of frequency response of the models is shown in Figure 2-4. In the midrange frequencies between 0.1 and 10 *rad/sec* are the most important (Nash et al., 2016). It is observable in Figure 2-4 that the SCC transfer functions have characteristics of an integrator; for this reason, Telban and Cardullo (2005) suggested that the SCC is a sensor of velocity rather than acceleration. Similar to otoliths, there is a perception threshold of the semicircular canals which is a function of input frequency and amplitude, and it varies between the passive (open-loop) and active (close-loop) driving. It is usually modelled as a nonlinear dead-zone block cascaded between the transfer functions, that makes it unappropriated for direct use in MCAs with linear plant models.

Table 2-2. Semicircular canal model parameters, roll direction

Semicircular canal model	T_a	T_L	T_S	T_{Ld}
Egmond	-	10	0.1	-
Young and Meiry	30	16	0.04	-
Fernandez and Goldberg	80	5.7	0.003	0.049
Ormsby	30	18	0.005	0.01
Zacharias	30	6.1	0.1	-
Hosman	80	5.9	0.005	(0.11)
Telban and Cardullo	80	5.73	(0.005)	(0.06)

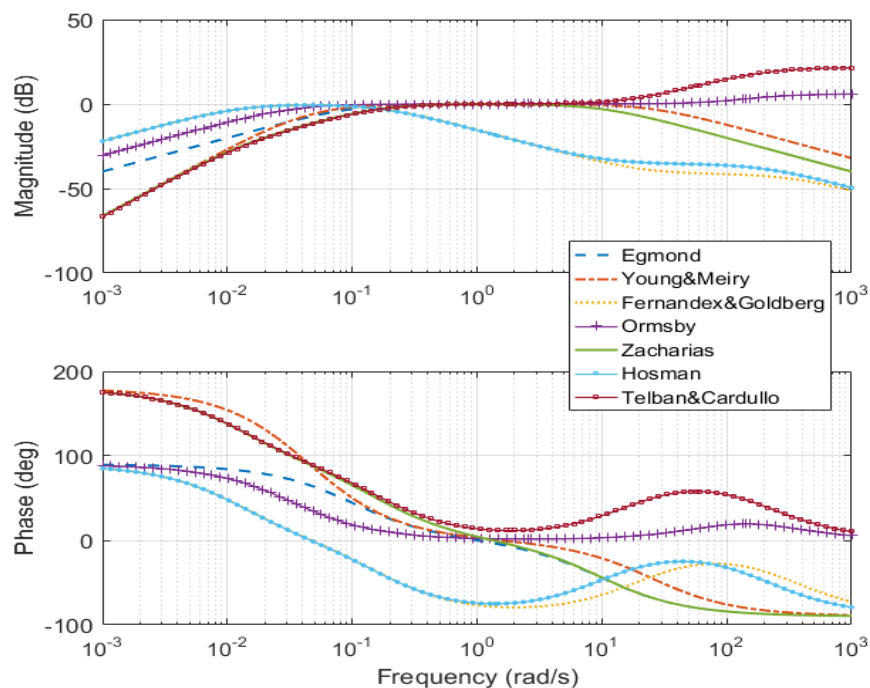


Figure 2-4. Bode frequency response of semicircular canal models

Asadi et al. (2017) reviewed the SCC models and showed that the Telban and Cardullo (2005) model acts as a reliable angular velocity sensor in the range of normal head movements. However, because their transfer function is not strictly proper, it was not possible to use it for the formulation of the model predictive control MCA in Chapter 4. The SCC model of Zacharias (1978) was an appropriate candidate that included the torsion-pendulum model, an adaptation and a lead term (see Eq. 2.15). This model has been used in MCA models in many studies, such as (Reid and Nahon, 1985; Augusto and Loureiro, 2009; Garrett and Best, 2013). Consequently, this semicircular canal model is used in the development of the MCA in Chapter 4.

2.3 Driver performance in vehicle

Blending engineering, psychological and physiological views about driver behaviour, and its analysis and modelling, McRuer et al. (1977) explained the driving task to be a “hierarchy of navigation, guidance and control phases conducted simultaneously with visual search, recognition and monitoring operations”. Navigation is the overall selection of a route, guidance is the selection, decision and path definition, and control is the process of affecting the guidance by actuating the steering wheel to follow the desired path.

To better understand, analyse and improve the man-machine system of driver and automobile, driver models have been developing in the literature. The introduction of more advanced systems controlling the dynamics and stability of the vehicle, and driver assistance systems, have led to greater demand for a sophisticated driver model. To mimic the drivers' performance, the driver models required to include general driver skill as well as characteristics such as information sensation, perception and processing of various cues, preview, prediction/anticipation, and adaptation/learning (Plöchl and Edelman, 2007). Furthermore, characteristics of drivers such as experience and age are needed to be included, as well as factors such as concentration and fatigue. Similarities and differences between models stem from various mathematical approaches used to realise demands, and emphasis on different aspects depending on an application.

It is possible to categorise the models based on the mathematical methods used, including control theory (e.g., optimal, adaptive control, identification theory), fuzzy logic, and neural network. These mathematical methods also have been used to describe the pilot control behaviour. The driver models could also be categorised based on their application; however, this gets complicated because a model might have several applications. Categorising driver models based on their applications usually involves investigating either the vehicle (e.g., design of vehicle components

and dynamics); the driver (e.g., driver behaviour, path and speed planning); both driver and vehicle; accident analysis/prevention, learning, and active safety; or the environment/traffic (e.g., traffic flow, influence of driver in simulator or traffic) (Plöchl and Edelmann, 2007). Some of the well-known models that are reviewed in that survey are represented here.

Driver models have also been incorporated into advanced driver assistance systems (ADAS) in vehicles. Some examples include coupling sensing information with accurate lane changing prediction models, preventing accidents by warning the driver of potential danger ahead of time or determining the driver's state such as attention level and driving competence. Furthermore, the information gained from driver models about drivers' objectives such as destination and road preferences, helps in the development of travel assistance systems and services (AbuAli and Abou-zeid, 2016).

The preliminary models were developed to control lateral vehicle dynamics. The longitudinal dynamics were often simple, such as following a given speed profile independent of the driver's steering task (Hoffmann, 1976). Among the first efforts, Kondo (1953) proposed a model based on the idea that drivers steer in such a way that a point a certain distance along the vehicle centre axis ahead coincides with the sight point, which is the preview distance L ahead on the reference course (see Figure 2-5). On the actual road, surroundings and traffic conditions are changing and the driver's sight point moves constantly. Many studies have been conducted to measure the driver's sight point, its distance, direction, and other variables.

The model can be illustrated by a cascaded control loop where the steering strategy is the driver's attempt to reduce the Δy_p at a distance L ahead of the vehicle with current lateral deviation of y_p . The equation $P(s) = e^{T_p s}$ represents the preview strategy of the driver for the desired path y_d with input path y_0 , preview time $T_p = L/v$, vehicle longitudinal speed v , and yaw angle ψ , where $H(s) = K$ is the control character of the driver, $G(s)$ the vehicle and $B(s) = e^{T_p s}$ the feedback function. With some simplifications in the transfer functions, this yields the steering angle model in Eq. 2.16. Kondo and Ajimine (1968) developed the model further to include linear feedback on the deviation of the yaw angle, course angle and lateral position deviation, and this became a baseline for the enhancements of later models.

$$\delta_s = K e^{T_p s} y \quad \text{for desired } y_0 = 0 \quad 2.16$$

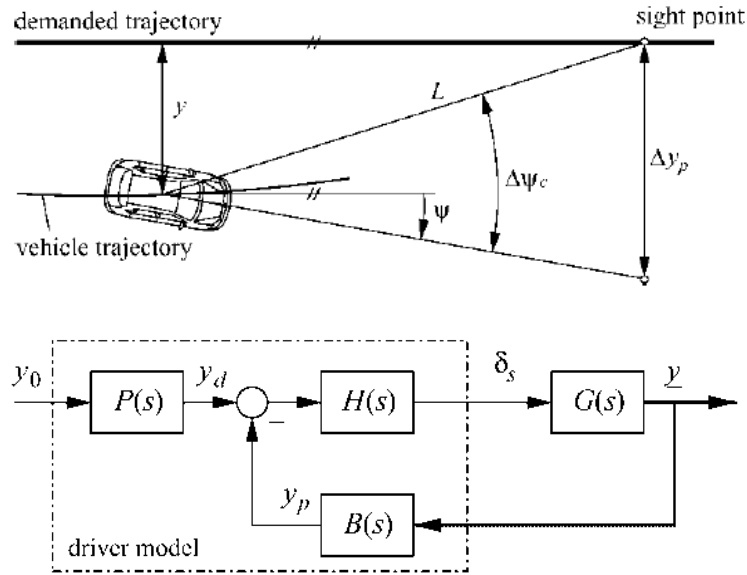


Figure 2-5. Kondo's shaft model and basic driver control loop, (Kondo, 1953) cited in (Plöchl and Edelmann, 2007)

The studies on pilot behaviour in controlling the aircraft have also been used in modelling driver behaviour in different tasks. The quasi-linear models known as 'cross-over model' by McRuer and Graham (1965) was successfully applied to model the human driver; however, it was limited, and parameters may depend on the type of input signal. For instance, when this model is used for driver-vehicle assessments at low frequencies, an increased gain and phase shift must be considered (Weir and DiMarco, 1978). The foundation of this model is in regulatory tasks, such as travelling in a straight line under cross-wind disturbance, and efforts to refine the model for more general applications seem to have been marginally effective (Sharp et al., 2000).

According to McRuer et al. (1977), for each specific driving manoeuvre, various compensatory, pursuit and precognitive levels of human behaviour are involved and need to be considered to model the driver as a controller. Pursuit structure describes the steering control with preview task, such as in lane change manoeuvre. Precognitive structure is present at the most skilled tasks, such as rapid lane change and obstacle avoidance. In these models, compensatory feedback from the lateral position deviation Δy with respect to a reference position, yaw angle error $\Delta\psi$, road curvature ρ_r^* , vehicle speed u , and filtered white noise n were available. T_L is the preview time. The pursuit model was formulated as follow:

$$\delta_s = Y_y Y_\psi \Delta y + Y_\psi \Delta\psi + \frac{K_c}{K_\psi} Y_\psi r_c + n \quad 2.17$$

$$Y_\psi = K_\psi (T_L s + 1) e^{-\tau_r s}, Y_y = K_y, r_c = \rho_r^* u$$

This model is often referred to as the System Technology Inc. (STI) pursuit or compensatory driver model. It was further refined by integrating the preview and choosing different points on the road as well as redefining some of the parameters above to be applicable to the assessment of potential roadway accident scenarios (Reid, 1983). In this context, he laid out criteria for a successful driver model:

- a. It needs to model a potentially dangerous driving scenario
- b. It has sufficient detail to acquire meaningful results
- c. Its structure should not be too difficult to implement
- d. There should be a set of parameter selection rules covering the model parameters
- e. It should have been validated against other results

Donges (1978) proposed another model for lateral vehicle control based on the duality of information presented to the driver by the forward view of the road. It included two layers of open-loop anticipatory and closed-loop compensatory control. The open-loop control represents guidance and involves the perception of current and future courses provided by the forward view of the road, and the anticipatory response to it. The closed-loop control represents stability for a successful feedforward anticipatory layer that compensates for deviations from the forcing function. This model compares the actual and desired path curvature using path curve error, heading error and lateral deviation. The parameters of these layers were estimated using measured data about road curvature and driver steering wheel angle by minimising a quadratic criterion, and they could be chosen to meet the requirements of a crossover model.

This model was further extended to include a third level that takes local deviations into account (Plöchl and Lugner, 1999). Local control is activated in critical situations when other levels fail, replacing them for a short period to reduce the local deviation directly. In another modification, the essential nonlinearities of vehicle handling behaviour were brought into the model by changes to the driver's internal model of the vehicle. This model could handle higher lateral acceleration with good tracking behaviour (Edelmann et al., 2007).

A so-called preview/prediction driver model was developed based on optimal control theory utilising a preview control strategy for regulation or tracking tasks. This type of control strategy is used during a path-following task in which drivers look ahead to follow the desired path and to stabilise and control the vehicle. Humans are capable of controlling and adapting to various dynamic systems (e.g., bicycles, cars), but some training is required to give the operator an understanding of vehicle response to control inputs. A certain amount of this is usually learned through open-loop responses for repeated scenarios, and the remainder comes from strengthening the operator's feel of vehicle response to control input in a

closed-loop for regulation/pursuit needs. The model had a state-space formulation including the input steering angle δ_s constant input over preview interval, and output lateral displacement of vehicle centre of mass. The objective cost function included the path error between the desired and actual lateral positions (Macadam, 1981).

The main weakness of this model was the need to presume a constant control input over preview time (Guo and Guan, 1993). Markkula et al. (2014) in a comparison of few models in low-friction collision avoidance scenarios listed the 'vehicle-independent parameters' and 'reasonable fit of collision avoidance steering' among the advantageous of this model; whereas its reliance on 'the desired path to achieve fit of collision avoidance steering' and rather 'poor fit of stabilisation steering' (behaviour after unexpected or expected near-collision) as the drawbacks of this model.

Sharp et al. (2000) introduced the multi-point preview model. The structure of this model was a nonlinear derivation from discrete linear optimal preview control theory and was shown to be robust against changes in the vehicle dynamics. The control law was obtained from multiple points defined along the actual trajectory of the vehicle. From a current point s , the driver monitors the path ahead by projecting an optical lever L forward up to a distance allowed by preview time T_p . A set of n points l_1, l_2, \dots, l_n is then fixed on the optical lever. Corresponding points r_1, r_2, \dots, r_n are available on the desired path, and the driver experiences the deviation angle e between points on both paths. The length of the optical lever is $L = T_p v_x$ that is, preview time multiplied by vehicle longitudinal velocity, see Figure 2-6.

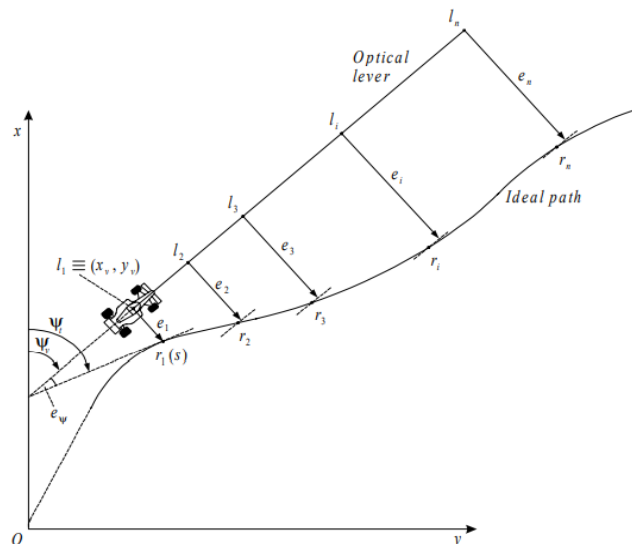


Figure 2-6. Driver model scheme proposed by (Sharp et al., 2000)

The distances between the points on each of the paths are equal to corresponding differences in the other path (i.e., $\overline{l_i l_{i+1}} = \overline{r_i r_{i+1}}$) because the points on the desired

path are not perpendicular to the points on the optical lever. The first point coincides with the current position of the vehicle's centre of gravity, and e_1 represents the vehicle's lateral offset from the current intended position on the path. In addition to e_1 , the difference between the vehicle yaw angle and the tangent angle of the intended path at r_1 , $e_\psi = (\psi - \theta_d)$ is another state feedback used for steering control. The steering angle then is calculated as the combination of the errors and control gains K_ψ, K_1, \dots, K_n .

$$\delta_s = K_\psi e_\psi + K_1 e_1 + \sum_{i=2}^n K_i e_i \quad 2.18$$

There were separate uncoupled controllers for longitudinal and lateral vehicle motions. Besides, human specifications were not included, as is common among velocity tracking controllers. The lateral model was further developed to identify the preview control parameters using a linear quadratic regulator (LQR) (Sharp and Valtetsiotis, 2001). The researchers also transformed the reference frame of the preview control from a fixed frame to the moving frame of the driver, which is the case in reality. The models using the optimal control theory are quite similar to each other, differing in the performance criterion used (e.g., absolute or relative lateral path, yaw angle information, preview horizon, and the duration that steering angle can change within the preview horizon) (Plöchl and Edelmann, 2007).

In a comparison between the driver models for the problem of path-following control with preview, the two approaches of predictive control theory and LQ control theory were tested using the same state-space model of vehicle dynamics (Cole et al., 2006). It was found that two transformations were needed to convert preview information from the ground to the vehicle frame, and another to combine the lateral and yaw preview information. Using long preview and control horizons, it was found that the state and preview gains were identical for the predictive controls, receding horizon LQ control and infinite horizon LQ control. In another comparison in a collision-avoidance scenario, Markkula et al. (2014) found that Macadam's predictive controller and Sharp's LQR controller yield different control gains in the same condition. The benefits of Sharp's model are reasonable fits for both collision avoidance steering and stabilisation steering, while reliance on the desired path construct and a large number of parameters are drawbacks.

Nonlinear control methods have been used for driver modelling. The nonlinear dynamics of the vehicle was taken into account in an effective path control driver model (Mayr and Freund, 1992). In another study, using the two-layer driver model, in the anticipatory level a nonlinear optimal control problem for a reduced vehicle dynamic was solved to find near optimal setpoint for the full model. In the stabilisation level, a nonlinear poison controller was available to track the setpoints

with full vehicle dynamics (Bulirsch et al., 2003). Nash and Cole (2018) also used the nonlinear control model to include the nonlinearity of tyre model in extreme manoeuvres. Fuzzy logic control (FLC) Zadeh (1965) is another nonlinear method that is said to be similar to human thinking and compromise in the process of decision making, that has been used for driver modelling (Ghazi Zadeh et al., 1997). A fuzzy rule-based neural network model was used to obtain individuals' driving rules from their trajectories (Chong et al., 2013). It included driver behaviour in longitudinal and lateral actions and in car-following and critical safety events.

In other studies, to develop behavioural models during car following manoeuvre for applications in the simulator and real world, (Naseri et al., 2015) emphasised on the importance of psychological than control-engineering point of view. They gathered data of drivers' behaviour in different scenarios and estimated the parameters of the proposed model. (Naseri et al., 2017) presented model for virtual vehicle during lane changing and line changing manoeuvres. Their algorithm included two steps of decision making and manoeuvre. It consecutively considered, deciding on when to initiate the lane change, choosing a target lane and if there is sufficient gap to do the manoeuvre, creating a desired path using a path-following algorithm, and including a collision avoidance algorithm to avoid crashed as the path is followed. They validated their model with drivers' behaviour in few lane change scenarios.

Although a large amount of research has been dedicated to understanding human perception, cognition and behaviour in various control tasks from biological and neuroscience perspectives, most of the described models did not take into account human sensory dynamics (Nash et al., 2016). During most sensorimotor tasks, a human develops an internal model of their surroundings that integrates the information from different sensory modules in a statistically optimal fashion to plan an appropriate control action. The cognitive processing of these sensory signals is delayed due to the latency of sensors, nerve conduction and neural processes. There is also a sensory perception threshold, and stimuli with amplitudes or frequencies below this threshold are not perceived. The thresholds have been found to be higher during an active control task involving multi-sensory input compared to passive unimodal control tasks (Nash and Cole, 2018).

Nash and Cole (2016) developed a model that incorporated the limitations of sensory dynamics and used the common assumption of the optimal models that the driver steers close to optimally based on his or her sensory limitations. He noted that pitch tracking tasks for pilots are very similar to drivers' steering tasks, and therefore the model was validated by the data in a study of pilot control behaviour in a flight simulator (Zaal et al., 2009). Reportedly, the model can predict human control behaviour accurately during a target-following and disturbance-rejection

task. The linear models are applicable for normal driving conditions, but in extreme manoeuvres in which the operating point of the vehicle changes rapidly and the friction limits of the tyres are reached, a different model was needed to cope with nonlinear vehicle dynamics (Nash and Cole, 2018). To this end, they further developed steering control model to include human sensory dynamics together with control of a vehicle with nonlinear tyres.

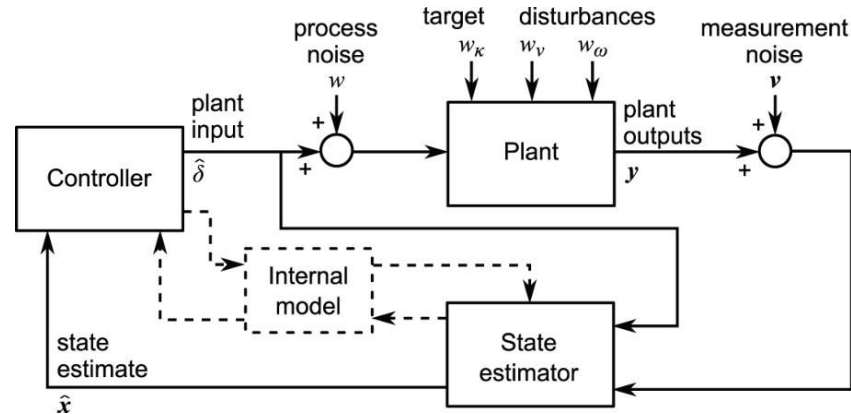


Figure 2-7. The overall structure of the driver model, (Nash and Cole, 2018)

The model of Nash and Cole (2018) was based on an idea introduced by Donges (1978), that vehicle steering control can be represented by combining target-following and disturbance-rejection tasks. In the target-following task, the driver must follow a target path while responding to disturbances on lateral and angular velocities of the vehicle. Because the driver previews the upcoming target path to plan the steering control, it is usually a feedforward control. The disturbance-rejection task is feedback control because the driver cannot perceive the disturbance until after it has occurred. The linear part of the model uses the optimal control theory (LQR) to represent the driver's steering behaviour.

It consisted of three components: a plant, a controller and a state estimator, as illustrated in Figure 2-7. The dynamics of vehicle and driver are described in the plant, which is perturbed by the target and disturbance white noise w_k, w_v, w_ω and process noise w . The plant output y represents the output of the driver's sensory modules, which are perturbed by measurement noise v . The state estimator calculates an estimate of plant states \hat{x} using the internal model of the plant. Finally, the controller uses the estimated states and the internal model to calculate the optimal plant input $\hat{\delta}$. The cost function includes the tracking error e and plant input $\hat{\delta}$ terms to minimise. The described components were further extended to control a vehicle with nonlinear tyres, albeit with many simplifications. Sensory dynamics reportedly affected the control performance and stability of the driver-vehicle system, especially when there is disturbance or driver noise.

Markkula et al. (2018d) explained that this model seems sophisticated because it considers different aspects of human perception and behaviour; however, further experiments are needed for validation. Moreover, behaviour adaptation and a mechanism for identifying the reliability of the sensory signals were missing. In another experiment involving a vehicle steering task, an identification method was used to find the parameters of the model, using the data from driving simulator experiment with no motion scaling. Results supported the hypothesis that driver steering control can be predicted using driver models. The identified parameters were said to be physically plausible compared with values from the literature, and identified delays were longer for vestibular than visual delays, supporting the literature (Nash and Cole, 2019).

For modelling the driver's steering, it has been shown to be more appropriate to use the steering rate or individual steering adjustments than the steering angle (Markkula et al., 2014). Moreover, the concept of the internal vehicle model may be less useful in non-routine situations such as near-crashes, where the driver's behaviour can better be described as a direct response to salient perceptual cues. The latter idea has been further supported by modelling the steering rates or adjustments as delayed linearly scaled version of the yaw rate error (Markkula, 2015). The desired path yaw rate error (DPYRE) model was developed by him based on these ideas, and the concept of the desired path (similarly used in some of the models introduced earlier in this section). This model is a few-parameter driver model that maps vehicle world states to driver control actions. It uses three parameters of delay time, preview time and gain and the desired path to predict driver behaviour (steering rate):

$$\dot{\delta}_s(t) = -K\omega_{err}(t - T_R) \quad 2.19$$

Where $\dot{\delta}_s$ is the rate of change of the steering wheel angle, K is a gain constant, the yaw rate error $\omega_{err} = \omega - \omega^*$ is the deviation between current yaw rate ω and desired yaw rate ω^* , and T_R is a response delay. In Eq. 2.19, $\dot{\delta}_s$ is obtained by looking ahead a preview time T_p on the desired path to determine a desired vehicle position at that point in time, and then determine the desired yaw rate ω^* as the yaw rate that would take the vehicle to that desired vehicle position in the time T_p , if starting from the current vehicle position and heading.

The first parameter to fit is the preview time T_p ; however, it has been shown that using a task-dependent fixed preview time did not affect the model fits much (Markkula et al., 2016). To fit the model parameters, a brute force grid search was used for all nonlinear parameters (e.g. T_R), and for each tested combination of these nonlinear parameters, all linear parameters (e.g. K) were estimated using least squares fitting. The goodness of fit of the best-fitting parameterisations was

expressed as R^2 ($R^2 = 1$ means that the model explains 100% of the variance in the data, $R^2 = 0$ means that the model is no better than approximating the data by using its observed average).

This type of model is neutral on whether or not drivers directly perceive or mentally represent actual and desired yaw rates. It is compatible with the idea that drivers simply have access to sensory cues and neural pathways that allow them to act as if they directly perceived and represented these kinds of quantities (Markkula, 2015). In the same review, the validity of driver models for evaluation of driver behaviour is studied. Different levels of behaviour validity were defined, and it was shown that the DPYRE model could be employed as a task-general driver model for evaluations. This model was compared to a modified model of Gordon, T. and Magnuski (2006) and performed much better. It does not explicitly represent the sensory or neuromuscular dynamics but has proved to be sufficient for behaviour evaluations; moreover, its parameters are easily identified in an open-loop fitting method. It is shown that how steering torque and motion cues affect the DPYRE model's parameters (Markkula et al., 2016; Markkula et al., 2018b).

Another type of model has been developed with an emphasis on the intermittency of human control. A brief review of this method is presented in (Markkula et al., 2018a). It is based on the idea that humans make use of intermittent adjustments and are not always continuously active in sensorimotor control, and it originated from observations of operator handle position in a gun aiming task (Tustin, 1947). Other examples are human behaviour tests from saccadic eye movements and inverted pendulum balancing. The control intermittency arises due to the minimum 'refractory time' that must pass between consecutive control activities and/or the minimum control error threshold that must be reached before control is applied. Using these assumptions, task-specific intermittent control models have been proposed (Meyer et al., 1988; Gawthrop et al., 2014).

Markkula et al. (2018a) provided an alternative computational framework for intermittent control by using the basic concepts developed earlier by the same author (Markkula, 2014; Markkula, 2015). This alternative framework differed from other intermittent control models, because it included a classical control theory rather than the typically used optimal control. It also connected three well-established concepts of neuroscience: implementation of intermittent control by the nervous system using a combination of motor primitives, prediction of sensory outcomes of motor actions, and evidence accumulation of prediction errors. These had not been reported before.

In this framework, Markkula et al. (2018c) showed that an estimate of currently needed control adjustment $\Delta\delta$ is continuously calculated and is compared to the

prediction of the same control adjustment to find a prediction error. This error is then fed with a gain k into an evidence accumulation step where it is integrated over time to a certain threshold; this step mimics the neurobiological decision-making mechanism to decide when a control adjustment is required. When the decision threshold is reached, a steering adjustment is initiated, a prediction is made of how the control adjustment $\Delta\delta$ will be affected, and the evidence accumulation integrator resets to zero. The steering adjustment is applied in form of a motor primitive, with a fixed-duration stepwise movement and total amplitude from current $\Delta\delta$ prediction error. The prediction is also applied in the form of a primitive stereotyped response, mimicking the neurobiological collar discharge.

$$\Delta\delta = -K\hat{\omega}_{err} = -K(\hat{\omega} - \hat{\omega}^*) \quad 2.20$$

$\hat{\omega}^*$ and $\hat{\omega}$ are the desired and actual vehicle yaw rate perceived by the driver, and K is response gain. $\hat{\omega}^*$ is defined as the yaw rate that would take the vehicle to the desired path in a preview time T_p . The preview time for the slalom task was found to be between 1.4 and 2.2 s.

The above model was further developed to include multi-sensory integration and behavioural adaptation (Markkula et al., 2018d). In this model, the dynamics of the vestibular system are not explicitly modelled, and multi-sensory integration is modelled as operating directly on external stimulus, where the estimate of yaw rate is the summation of the otolith and SCC models.

$$\begin{aligned} \hat{\omega} &= W_{vis}\hat{\omega}_{vis} + W_{ves}\hat{\omega}_{ves} \\ \hat{\omega} &= W_{vis}(\omega_{vis} + v_{vis}) + W_{ves}(\omega_{ves} + v_{ves}) \end{aligned} \quad 2.21$$

Here, $\omega_{vis} = \omega$, $\omega_{ves} = \omega_{body} = \alpha\omega$, the ω_{body} is the actual rotation of the driver's body, α is the motion scaling, ω is the yaw rate of the simulated vehicle, and v_{vis} and v_{ves} are the Gaussian white noise. Then the weights are calculated with optimal cue integration theory cited in (Fetsch et al., 2013), where r_{vis} and r_{ves} are the sensory reliabilities.

$$W_{vis} = \frac{r_{vis}}{r_{vis} + r_{ves}}, \quad W_{ves} = \frac{r_{ves}}{r_{ves} + r_{vis}} \quad 2.22$$

Overall, as can be observed in the blue dashed lines of Figure 2-8 the driver's behaviour is the neural outputs from their sensory modules that are transformed into an estimate of yaw rate, considering the predictions of past steering input. Then integrated the yaw rate as estimated in Eq. 2.21 and 2.22, compared to a visually estimated desired yaw rate, and the required steering adjustment is calculated by Eq 2.20.

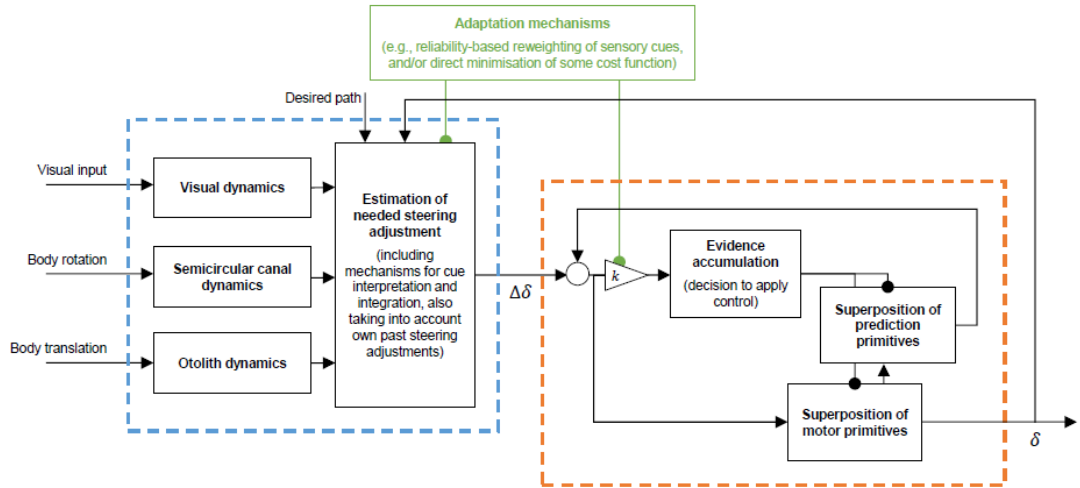


Figure 2-8. Schematic representation of the diver steering model, (Markkula et al., 2018c).

Behaviour adaptation was also available in this model that considers, adapting steering gain K , adapting effort by changing the gain k in the evidence accumulation, sensory cue reweighting and reinterpreting down-scaled vestibular cues. These four adaptations take place separately or together in the form of a cost function in Eq. 2.23 to be minimised.

$$J_{tot} = k_{path}J_{path} + k_{steer}J_{steer}$$

$$J_{tot} = k_{path} \frac{1}{N} \sum_{k=1}^N (y_k - y_k^*)^2 + k_{steer} \frac{1}{T} \sum_{i=1}^n g_i^2 \quad 2.23$$

T is simulation time, with N discrete samples, that n discrete steering adjustments with amplitude g_i are applied. y_k and y_k^* are the lateral position of the vehicle and the desired path.

The empirical data on driver behaviour was applied to the down-scaled motion of a slalom driving task to validate this model (Markkula et al., 2018c). Reportedly, removing motion cues resulted in a decrease in task performance and an increase in steering effort; however, after adaptation, performance and effort improved and decreased, respectively. They explained that drivers make direct use of the motion information to shape their steering to reach an intended target, inferred from the fact that drivers underestimate the yaw rate due to the down-scaled vestibular motion cue, and used this underestimation in shaping their behaviour. Driver adaptation to repeated task exposures was shown to be a single gain or combination of increased gains in evidence accumulation, steering response, or sensory cue reweighting.

Moreover, the model showed a local sub-unity optimum motion for task performance, and it was concluded that a full reinterpretation of the vestibular cues

may not have occurred. The optimal performance for a sub-unity gain was explained by the driver benefitting from slightly underestimating the yaw rate, which allowed the phase of the vehicle trajectory to align better with the desired path. In similar findings, the reasons are explained to be related to imperfections and false cues of the motion system at large scales, inability to maintain the coherence between the visual and vestibular cues (Berthoz et al., 2013), or difficulty in exerting accurate steering control in higher and more uncomfortable accelerations (Savona et al., 2014).

The optimum motion scaling was also observed in the subjective ratings of various motion scaling, and not necessarily matched the same scaling of optimal performance; Berthoz et al. (2013) also made a similar subjective observation. Moreover, as the yaw rate underestimation does not rely on control intermittency, the analysis was done using the DPYRE model and reportedly found that most of the results were reproduced. Differences in the steering effort were due to missing components in the simpler model. Among the reviewed driver models it was shown that the DPYRE model could be employed as a task-general driver model for evaluations. Although, it does not explicitly represent the sensory or neuromuscular dynamics but has been validated to be sufficient for behaviour evaluations. Moreover, its parameters are easily identified in an open-loop fitting method. Therefore, for the analysis of the drivers' performance in the experiments described in Chapter 5 and 6, the DPYRE model is used.

3 Motion Cueing in High-Performance Simulators

3.1 Driving simulator subsystems

Driving simulator development started in the late 1950s and has been supported for over five decades by advances in mechanics, electronics, computers and display technologies. The major elements of a dynamic driving simulator include visual, motion, auditory and proprioceptive cueing systems, in addition to the vehicle dynamics model, cab and control, electronics, measurement, data processing and storage. Cueing systems stimulate the driver sensory modalities as a consequence of driver's control input in a closed-loop form i.e. steering wheel, accelerator and brake pedals, and gear. Vestibular motion and proprioceptive steering and pedal cues are the results of vehicle dynamic response to driver's control inputs and environmental disturbance inputs e.g. wind gust. Visual and auditory cues result from the same driver-vehicle interaction in addition to the information in the driving scenario e.g. traffic, pedestrians. Figure 3-1 shows the main subsystems of simulators and how drivers interact with them. In the following sections, the role of each of the components is described based on (Jamson, 2010).

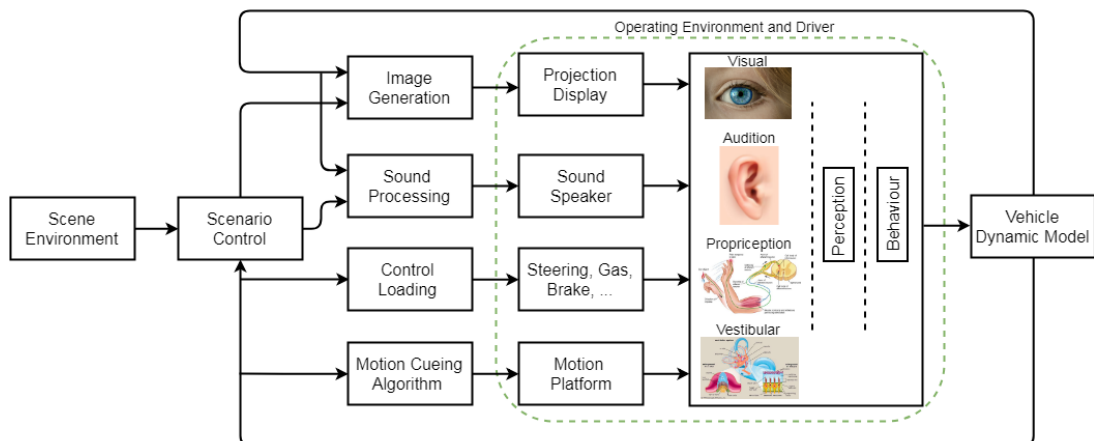


Figure 3-1. Dynamic driving simulator subsystems (driver in the loop)

Scene environment, is the structured database of the virtual scene that includes the model of the roadway and roadside objects e.g. buildings, trees, traffic, pedestrians. It consists of descriptions of objects regarding their geometry and graphics, as well as spatial and temporal information about their coordinates.

Scenario control, is defined as the process of choreographing an event within the virtual environment, such as a traffic scenario. It modifies the scene environment to add all the items such as other cars, pedestrians based on a model of their behaviour. According to Bailey et al. (1999) the Logical Road Network (LRN) is usually used in scenario control to make decisions about prioritising and overtaking of the vehicles.

Image generation and projection display, is the computational process of rendering the visual cues with respect to the driver eye point. It uses the data from the scene environment including the static items stored in the database and moving items updated by the scenario control to process concerning the driver's eye point. Other visual effects such as lighting and weather condition can also be added in this module. These are then sent to the projection displays where the images are "blended and colour balanced to create a wide field of view". This is done either in a single channel projected on a flat surface that often provides a narrow field of view or by using multi visual channels that have a wider field of view, using the cylindrical or spherical screens. In recent years the application of virtual reality (VR) in driving simulators have emerged, using head mounted displays (HMD) which eliminates the need for projectors. However, they still have problems with graphic resolution and narrow field of view (FOV) that might be solved in the near future.

Sound processing and speakers, sounds from inside the vehicle e.g. aerodynamic noise, engine noise, and outside e.g. traffic are recorded and synthesised in advance of the simulation. Those are then modified considering the current vehicle state e.g. vehicle and engine speed with respect to the acoustic field of the vehicle cab. The tuned sounds are then played to the driver through a surround sound system.

Control loading and equipment, the steering feedback to the driver in the simulator or real world, gives the sense of force (torque) during the touch (haptic), that also includes high frequency vibrations. It is a rich source of information and together with the feedback from the pedals and gear helps the driver in lateral control of the vehicle, and to understand various qualities of the vehicle such as steering and handling. In the simulator, the control feedback through the steering and foot pedals is calculated by the vehicle dynamic model from the tyre-road interface and vehicle state.

Motion cueing algorithm and motion platform, the physical apparatus representing the vehicle motions, to help provide a realistic impression and avoiding the mismatch between the visual and motion cues. Motion platforms (MP) have a limited workspace (motion envelope), hence a motion cueing algorithm (MCA) is also available to overcome this problem by maximising the usage of the motion platform while respecting its constraints. These are reviewed the next sections.

Vehicle dynamic model, analyses the vehicle's response to the driver's control inputs and simulates the dynamic response of the vehicle on the road as it is in the real world. Then the vehicle states are sent to the cueing systems and scenario control.

Operating environment, dynamic simulators often consist of a full or cut down real vehicle cockpit. Dashboard instruments are usually available to give drivers the indications of the vehicle status e.g. speed, and engine revs. In more expensive dynamic simulators that benefit from a motion platform, the whole cab fits within an isolated operating environment that is attached to the motion platform. The closed operating environment helps to avoid unwanted noises, also the inside of it is often used to project the images of visual cues.

The University of Leeds Driving Simulator (UoLDS) is made of a series of components shown in Figure 3-2. The central subsystem is the scenario control that reads the previously constructed offline scene environment, the position of the objects and the initial position of the vehicle. In the scenario control, the driver's control inputs are fed to the vehicle dynamics model, and it continuously calculates the vehicle motions felt by the driver which are then supplied to the visual and motion systems. Moreover, simultaneously additional feedback to the driver is supplied by updating the vehicle sounds, dashboard instruments and the torque felt through the steering wheel.

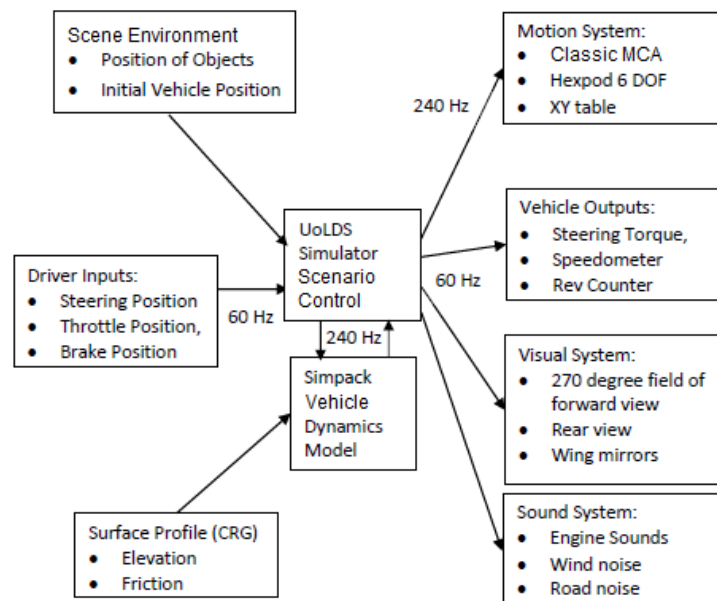


Figure 3-2. UoLDS simulator subsystem communications, (Markkula et al., 2016)

The motion system maps the motions supplied by the dynamic model to the MCA and MP. This is achieved through a designated classic MCA and 6 DoF hexapod which can supply surge, sway, heave, roll, pitch and yaw movements mounted on a sliding rail (XY table) that can replicate more of the surge and sway motions of the vehicle. Within UoLDS, the visual system is updated at the standard 60Hz to ensure a flicker-free display, with the state of the vehicle updated at a similar rate. The vehicle model (SimPack) is updated four times faster than this at 240Hz.

UoLDS supplies the steering wheel position, read from the vehicle cab via a CAN Bus, to the vehicle model, which in turn returns a steering wheel torque value based on the combination of steering wheel position, road wheel angle, vehicle speed and wheel/surface friction and elevation change. The raw steering torque value is corrected internally for torque phasing due to a universal joint introduced into the mechanical linkage of steering system on UoLDS and scaled to adjust for transmission losses in the torque motor itself. The system can deliver a closed-loop torque of up to 8 Nm (effectively 5 Nm after losses) and an open-loop torque of up to 35 Nm and can switch between these two modes depending upon the torque demanded. For scenarios within this study, the torque was supplied solely through the closed-loop system (Markkula et al., 2016).

Visual and motion cueing system

Visual cues have a major contribution to the perception of the environment, and with driving being primarily a visual task it has always been the primary focus of developments in the simulators. The presence of visual cues is crucial for drivers to estimate vehicle speed, distance to objects, to control heading and lateral motion of the vehicle. Challenges such as field of view (FOV), perceived resolution, transport delays, frequency of update, and depth perception are the main reasons for a degraded visual cue. Degraded quality of motion cues might be due to MP envelope and velocity constraints, small signal bandwidth and roughness. In control characteristics, those include the steering torque and damping, and brake pedal stiffness.

Early driving simulators used analogue electronics and the visual cues was represented through calligraphic displays, model boards or films. The introduction of the digital electronics provided a big step forward to developments of primitive low count flat-coloured polygons in early graphic cards, to shaded polygons in graphic cards with gariox shading, into today's technology of texturing the high-count polygons of common graphic cards. With those analogue electronics, the processing delay was not an issue but became a problem with early digital computers and graphic systems that provide a complex visual field for car driving and resulted in artefacts in operators control tasks. The delay problem led to developments of compensation techniques in digital processors and image generators to minimise the delay. More recently the increase in the capability of PC-based CPUs and GPUs have proliferated the development and application of driving simulation. The graphics processing units (GPU) have made real-time fast graphic rendering at a reasonable price. First single-chip GPU started with Texas Instruments Graphics Architecture (TIGA), then developed to 3DFX standard continued to the today's NVIDIA, ATI and Intel chips. Simultaneously the display

system and projectors' colour, pixel resolution, contrast and brightness were also being improved (Allen et al., 2011).

The motivation for investigations in motion cueing was to improve the realism and avoid the mismatch between the visual and vestibular cues, that in extreme cases were reported to cause motion sickness. Moreover, the sensation of forces in driving experience also provides critical information to drivers to improve their control. In the experiments comparing the static no motion and dynamic motion simulators, it has been consistently shown that the presence of motion increases the driving experience realism. Moreover, it affects the drivers' performance, such as decreasing the steering rates with an increase of the motion feedback to drivers (Berthoz et al., 2013).

The devolvement of the motion systems for driving simulators was originally inspired by the ones developed for the flight simulation. However, more varieties of MP designs have been used in driving simulators due to the differences in vehicle motions between the flight and ground vehicles. In the next section, those are briefly introduced.

3.2 Motion platforms

Simulators motion platform (MP) is a mechanical device (a robot manipulator) that has actuators to generate motions in different directions. The dependency of motion cueing fidelity to the motion platform characteristics has shaped simulators from a simple set of pedals to simulators using actual car cabs strapped to a moving motion system (Allen et al., 2011). Hundreds of simulators in various designs have been developed, however there is still no solid conclusion available on which motion platform design and characteristics suit best for the demands of a realistic driving experience; "every proud owner of a motion simulator claims to have the best simulator suitable for its purpose" (Slob, 2008).

Although for high motion demanding driving manoeuvres one to one representation of the motion cue is not feasible in most of the available motion platforms, the studies of restricted small demanding manoeuvres have reported that the one to one motion does not necessarily elicit a realistic driving experience (Berthoz et al., 2013). The problem originates from many sources, among the prominent ones are the

- Diversity of motion cueing characteristics of simulators and absence of a comprehensive database to compare them
- Lack of a general measurement tool, and benchmark for assessment of the simulator fidelity

Blana (1996) reviewed and categorised the available simulators in that period of time. Simulators were classified according to their manufacturing costs to three low, medium and high cost driving simulators. Low cost simulators term was used due to arrival and usage of PCs and inexpensive graphic displays that can provide reasonable cueing of visual, auditory and control feelings. Medium cost simulators had advanced imaging techniques, large projection screens and complete vehicle cab and its normal controls. Both low and medium simulators had either no or trivial motion system available for users. High cost simulators included high degree (e.g. 360) of the visual field of view and motion systems of a hexapod with or without small translational base motion. In another study characteristics, functionality, limitations and application of 20 contemporary simulators were reviewed and discussed (Weir and Clark, 1995). The mid-level simulators defined to have a large display with computer graphics, with vehicle cab and interactive control (e.g. steering) either with or without motion system.

The first driving simulator with dynamic motion platform in Europe was developed in 1970 by Volkswagen. It had a single screen in front of the driver without vehicle cab with 3 rotational DoF (roll, pitch and yaw) motion platform with limited movements. In 1984 Institut für Kraftfahrvehsen und Kolbenmaschinen (IKK) in Hamburg mounted Volkswagen Golf cabin on a sliding rail allowing a lateral motion for driver see Figure 3-3. Throughout 90's many car manufacturers and research institutes started using simulators with motion systems, such as Ford, General Motors, Mazda, Nissan, BMW, Renault, Modular Automobile Road Simulator (MARS), Swedish National Road and Transport Research Institute (VTI), U.K.'s Transport Research Laboratory (TRL), Japan Automobile Research Institute (JARI), University of Iowa Driving Simulator (IDS) (Slob, 2008; Jamson, 2010).

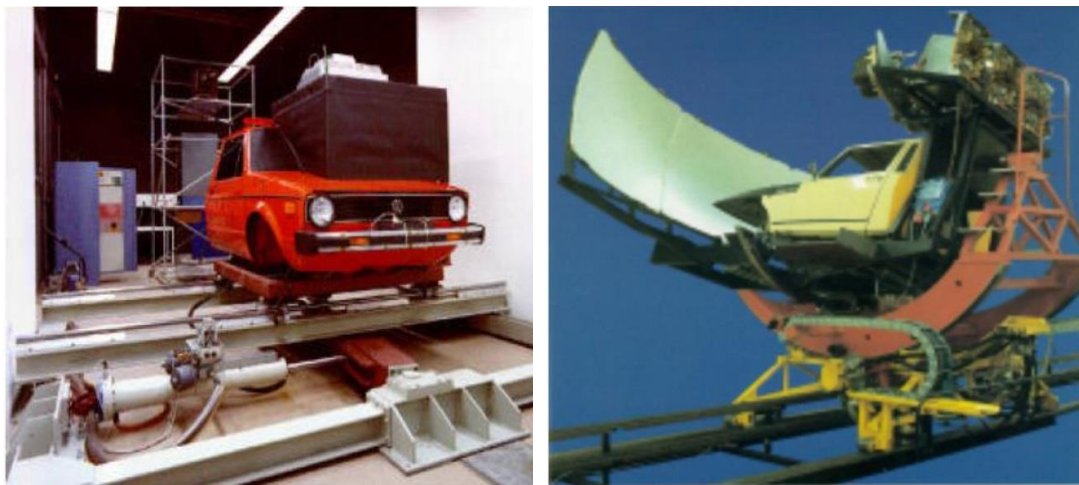


Figure 3-3. IKK driving simulator (left), VTI II (right) (Nordmark et al., 1984)

3.2.1 Hexapod and sliding rail platforms

A very commonly used type of MPs is a parallel robot manipulator that is called Hexapod or Stewart platform. This mechanism was first developed by Eric Gough in 1948 for the purpose of testing tires. Later, Stewart (1965) reintroduced the parallel 6 degrees of freedom (DoF) system that included upper and lower plates and 6 actuators. He explained its design capability to carry large payloads which drew attention in flight simulation for pilot training purposes. The Stewart platform benefits from the fact that the moving mass of the platform itself is contained within the actuators that allows room for more weight on the payload. However, it has very limited displacement and complex workspace due to the cross-coupling of its DoFs. Other low payload and large displacement designs tried to overcome this problem by decoupling the longitudinal and lateral motions, although the low payload limits the availability of full car cab. Large payload and large displacement designs make for the least compromise but also the highest costs (Greenberg and Blommer, 2011).

It was from 1985 that Daimler-Benz employed the Stewart platform and introduced the 6 DoF motion platform in driving simulators (Drosdol and Panik, 1985), see Figure 3-4. Later in 1994 they added a sliding rail to the platform for lateral motion cueing (Käding and Hoffmeyer, 1995a). They revealed their latest driving simulator in 2010 that claimed: “with this configuration we are confident to reach nearly 90 % of the requirements needed for car and truck development with acceptable technical and financial efforts” (Zeeb, 2010).



Figure 3-4. Daimler-Benz driving simulators 1985 (left) (Drosdol and Panik, 1985), 2010 (right) (Zeeb, 2010)

Nevertheless, the presence of the hexapod platform had brought a big improvement in motion cueing of simulators, but due to limited workspace of the mechanism, not much of real vehicle’s translational accelerations could be represented. It was toward the end of 90’s that the performance capability of electrically driven

actuators in manipulators became equivalent to previously used hydraulic actuators, and MPs with higher capabilities were introduced. A major development was the sliding rails that produced the large translational motions in both X and Y (Surge and Sway) directions, which was optionally integrated by the hexapod.

In 1998 National Advanced Driving Simulator (NADS1) was released at University of Iowa, that was most advanced driving simulator (Clark, A. et al., 2001), see Figure 3-5. In this simulator, a hexapod was mounted on the sliding rails giving more flexibility in representing X, Y translational motions, a turntable that was placed on top plate of hexapod that brought more freedom in yaw direction since the yaw motion in hexapods is restricted due to cross-coupling of actuator links.



Figure 3-5. Iowa Driving Simulator 1992 (left) (Freeman et al., 1995) and, National Advanced Driving Simulator 2001 (right) (Clark, A. et al., 2001)

Using the hexapod mounted on the sliding rail became a common reliable design of motion platforms in 2000's, and different size and characteristics of them were employed; such as the, Renault's (Ultimate), University of Leeds Driving Simulator (UoLDS), Toyota driving simulator (TDS), Swedish Road and Transport Research Institute (VTI), see Figure 3-6. The UoLDS motion platform characteristics is presented in Table 3-1.



Figure 3-6. University of Leeds Driving Simulator (UoLDS) 2007 (top left) (Jamson, 2010), Toyota Driving simulator (TDS) 2007 (top right) (Greenberg and Blommer, 2011), VTI IV 2011 (bottom left) (Fischer et al., 2011), Renault Ultimate (bottom right) (Dagdelen et al., 2004)

Table 3-1. UoLDS motion characteristics, (Jamson, 2010)

		Excursion m, deg°	Velocity $m/s, deg^{\circ}/s$	Acceleration $m/s^2, deg^{\circ}/s^2$	Bandwidth (Hz)	
					-3 dB Magnitude	90 Phase lag
Hexapod	Surge	-0.40/+0.30	-0.82/+0.82	-6.6/+6.6	5.9	7.8
	Sway	-0.32/+0.32	-0.82/+0.82	-6.9/+6.9	5.3	7.2
	Heave	-0.26/+0.24	-0.82/+0.82	-6.2/+6.2	9.0	9.5
	Roll	-21/+21	-41.3/+41.3	-321/+321	7.8	5.7
	Pitch	-20/+22	-40.7/+40.7	-310/+310	9.5	6.1
	Yaw	-23/+23	-53.3/+53.3	-362/+362	8.1	6.2
Rail	Surge	-2.61/+2.59	-2.1/+2.1	-5.1/+5.1	5.6	5.3
	Sway	-2.5/+2.5	-3.1/+3.1	-5.4/+5.4	5.2	7.1

3.2.2 High bandwidth platforms

There are other types of driving simulators that does have limited workspace however very high bandwidth and low latency due to their lightweight. The Vehicle Dynamics Simulator (VDS) of McLaren Applied Technologies (MTS) featured a compact, lightweight and low-friction 6 DoF MP with linear electric motors. Their motion platform design does not include a hexapod that eliminates its cross-coupling problem. Although its motion envelope is small to medium, the bandwidth is very high that has made it favourable to the race drivers. It is claimed the fidelity is very high and the ride and handling aspects of the car are easily evaluated, high enough that 95% of car setup in F1 can be done before the real car goes to a real track. Moreover, it is integrated with the driver in the loop (DIL) technology that allows drivers to give subjective feedback about the vehicle components and systems in advance of physical prototyping. Its design makes integration of the Hardware-in-the-Loop (HIL) and Advanced Driver Assistance Systems (ADAS) technologies easier, see Figure 3-7.



Figure 3-7. Vehicle Dynamics Simulator (VDS) of McLaren Applied Technologies (MTS), 2017

The Advanced Vehicle Driving Simulator (aVDS) of AB Dynamics, developed by Williams Advanced Engineering, featured a low-friction 6 DoF MP with linear electric motors. They employed wedge actuator modules mounted on two parallel rails, replacing the conventional hexapod and providing larger workspace. The latency of their system is low ranging from 4 to 10 ms, and the bandwidth is quite high ranging from 15 to 50 Hz, in various direction. It is also able to carry designed to carry a nearly large payload of 500 Kg capacity. It is also integrated with the driver in the loop (DIL) and applicable for the Advanced Driver Assistance Systems (ADAS) testing technologies, see Figure 3-8.



Figure 3-8. Advanced Vehicle Driving Simulator (aVDS) of AB Dynamics

3.2.3 Alternative platforms

In meanwhile, few alternative mechanisms also emerged other than the regular usage of the hexapod and the sliding rail. DESorientatie DEMONstrator Amst (DESDEMONA) is a serial manipulator that has the ability of unlimited roll, pitch and yaw rotations. Its design inherited from centrifugal flight simulators (mainly used for High-G² training of pilots), which made the simulator more applicable for military fight jet simulations, however it is also used for driving simulation. The rotational mechanism is placed on a 2 metre vertical (heave) linear track. The whole structure moves horizontally (translational motion) on a 4 metre radius centrifuge arm, which this arm rotates around a fixed yaw axis. From unique capabilities of this motion system is its ability to generate sustained accelerations up to 3g, applicable for evasive manoeuvres (Mayrhofer, 2009), see Figure 3-9.

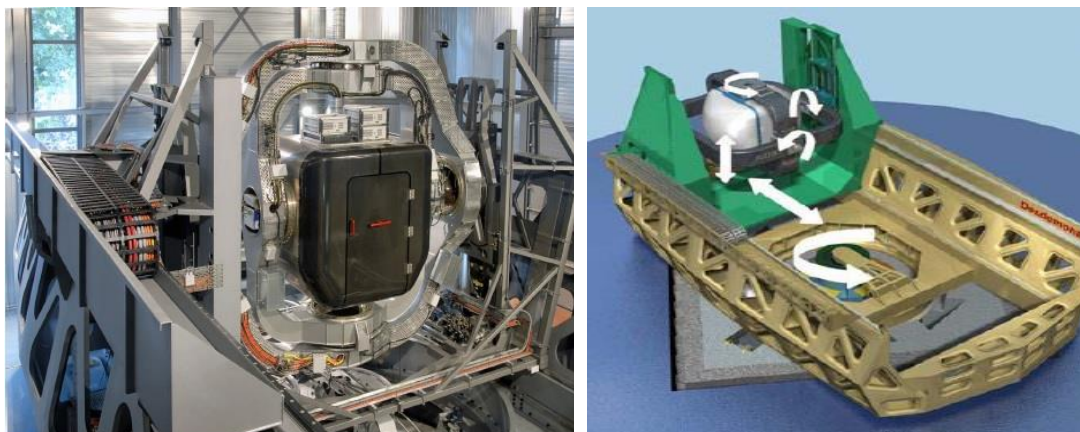


Figure 3-9. DESDEMONA 2007 flight and driving simulator (Mayrhofer, 2009)

² High-G training is for aviators and astronauts who are subject to high levels of acceleration (G). It is designed to prevent a g-induced loss of consciousness, a situation when g-force (the g-force acceleration is the cause of an object's acceleration in relation to free-fall due to weight of the object) moves the blood away from the brain to the extent that consciousness is lost

Another mechanism, employed in flight and driving simulations is a six-joint serial robot, which was originally designed for use in industries, e.g. to pick and place items in an assembly. Max Planck Institute (MPI) introduced their simulator using this mechanism called CyberMotion simulator. They added a single direction sliding rail to for more translational motion, and an extra rotational joint motion to its end effector (cabin). The latter was added for the motions in both backward and forward directions. In comparison to Stewart platform (without rail) this mechanism has advantages of larger workspace specially in yaw direction, higher dexterity and ability to render centrifugal accelerations (Nieuwenhuizen and Bulthoff, 2013).

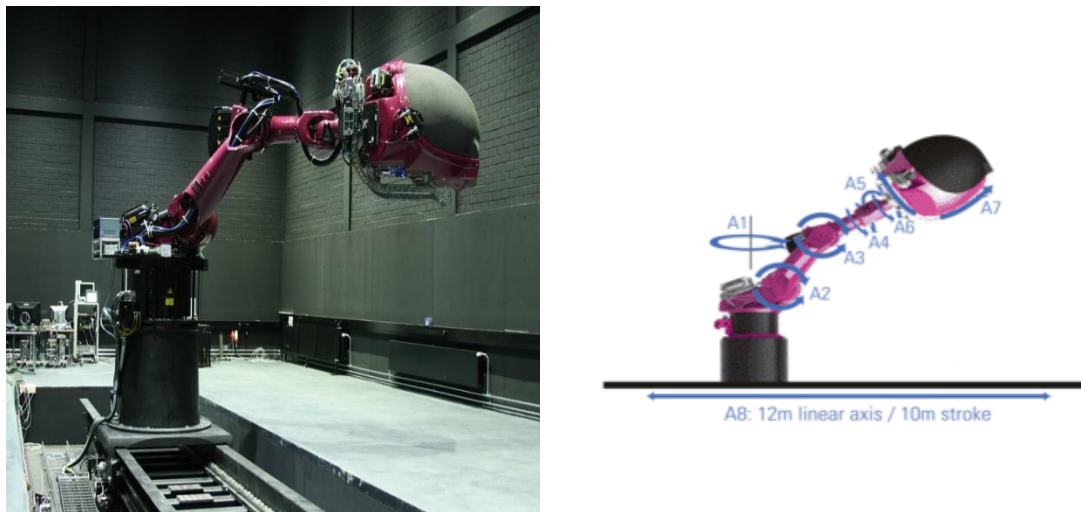


Figure 3-10. MPI CyberMotion Simulator (left) and its 8 axes (right) (Nieuwenhuizen and Bulthoff, 2013)

Another exotic driving simulator is Atlas Motion System (ATMOS) represented by Heinz Nixdorf Institute of the University of Paderborn which was developed by Rheinmetall Defence Electronics GmbH in 2009 (Hassan, 2014). This was designed with the aim of a task-based reconfigurable driving simulator. The motion platform has 5 DoF with that consists of two dynamical parts. The first part has 2 DoF and is used to simulate the horizontal translational motions. It has the 10 and 13.5 degrees of roll and pitch available to be used for tilts motion. Four linear actuators are used to generate the motions in the longitudinal and lateral directions. The second part is the shaker system, which has 3 DoF to simulate the roll and pitch and heave motions of the vehicle. The shaker is driven by a three crank mechanism and using three electrical motors.



Figure 3-11. Atlas Motion System (ATMOS) driving simulator 2009 (Hassan, 2014)

There are also conceptual driving simulator designs. Drive and control company Bosch – Rexroth has been manufacturing simulators since 1989. They started with flight simulators and their work extended to cabin crew trainers and the more advanced and sophisticated driving simulators. In a project sponsored by this company Slob et al. (2009) tried to mechanically design a motion system with the aim of higher fidelity of motion cueing. In this design of simulator motion platform is driven and supported by wheels for planar surge and sway translational and yaw rotational motions and driven by three crank mechanisms for roll and pitch rotational motions and heave translational motion (Slob, 2008), see Figure 3-12.

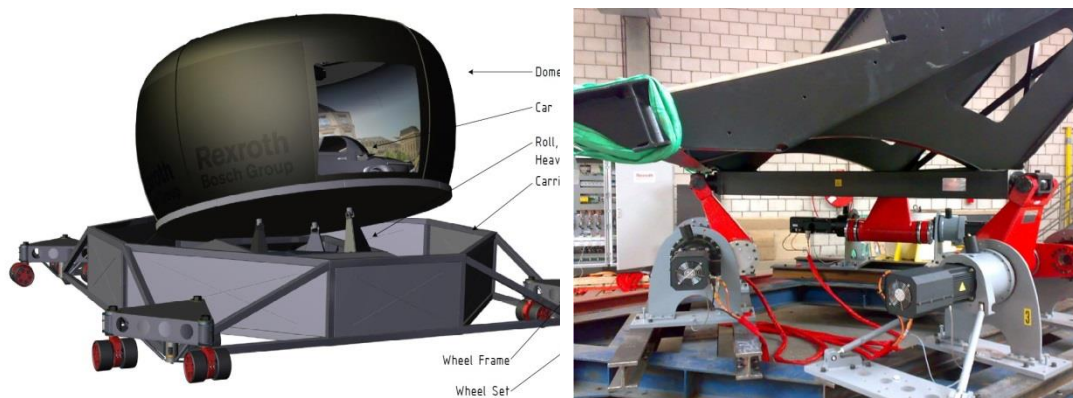


Figure 3-12. Assembled motion system (left), rotational mechanism (right) (Slob, 2008)

Various types of motion platforms that have been used in flight and driving simulators are presented in this section, it was tried to gather information about characteristic of all, which are presented in tables in Appendix A. A commonly used is the hexapod with or without base motion (sliding rail); among of all, it is not clear what size of sliding rail is sufficient to generate acceptable fidelity of motion cueing.

Moreover, recently the small workspace motion platforms are employed that reportedly are applicable for vehicle design purposes. Although, clearly this type of simulators only produces very high frequencies of vehicle motion, this range of high frequencies might be of importance to professional drivers in the vehicle design process. In this thesis due to proven research reliability and availability of the apparatus, the focus is on the commonly used hexapod mounted on sliding rail, and exploration of its characteristics and requirements.

There are other factors such as platform performance latency, smoothness and vibrations that have impact on the fidelity, but there is no information available to compare among simulators. In addition to ambiguity of motion platform characteristics and their fidelities, varieties of MCAs and custom tunings makes it even more complicated to draw a conclusion on adequate characteristics of a motion platform. In the next chapters, it is attempted to some extent enlightening the ambiguity by experimenting the differences between the MCAs, illustrating the effect of tuning MCA parameters and the optimal way of tuning them, and finally addressing the requirements for the sliding rail workspace size.

3.3 Motion cueing algorithms

3.3.1 Introduction

Several subsystems are designated in the simulators to generate the vestibular motion cues. It is the motion system task to mimic the real world vehicle motion cues to the user to help elicit a realistic impression of driving. However due to limited physical capabilities of a motion platform (MP), another subsystem is designed in the motion system named as Motion Cueing Algorithm (MCA), Motion Driving Algorithms (MDA) or Motion Cueing Strategy (MCS) in the literature. The MCA is designed for representing the displacements, velocity and mainly accelerations of the real vehicle to drivers while keeping the MP within its physically limited envelope (also named excursion and workspace). These objectives have motivated researchers to use various approaches utilising various control methods from Linear, Adaptive to Optimal and Predictive strategies. Here most commonly used types of MCAs are introduced and discussed. Moreover, the various characteristics and structures of MP make it more complicated to decide what are the requirements of MCA and MP with an acceptable level of fidelity.

The vehicle accelerations in each direction in space can be divided into transient (short-lived) and sustained (long-lived). Transient accelerations occur and disappear in a short period of time thus have higher frequencies. These can be reproduced quite accurately in most of the dynamic simulators at the onset of a

manoeuvre, due to their limited required MP excursions. The main issue in simulators is the representation of sustained accelerations that remain for longer periods of time, include lower frequencies and require large MP excursions. The sustained motions are mainly supported in surge, sway and yaw directions, however driving a car with variable speed uphill or downhill produces sustained heave acceleration as well. Unlike flight simulators, there is no sustain roll and pitch accelerations in driving simulators.

Almost no motion platform translational workspace can handle the long-lived translational accelerations of a vehicle due to great demand of motion envelop that far exceeds a conventional one. Therefore, another technique called tilt-coordination is often used to represent low frequency accelerations. In this technique, the whole human body including the head is rotated that aligns the gravity vector on the vestibular system and produces an impression of a translational acceleration, without letting the driver perceive the rotation. This is feasible by rotating under SCC rotation perception threshold, in addition to simultaneous coordination of other visual, haptic and aural cues.

The lower tilt angle, angular velocity and acceleration limits the build-up of tilt acceleration at the expense of more motion error, and vice versa. Although it is desirable to have less restricted tilt settings to achieve lower motion error, at the same time, the tilt rotations need to be limited to avoid to be noticed by the driver. In other words, there is a trade-off between “the prompt/over-tilt response against the lagged/correct-tilt” (Jamson, 2010). Hence, the selection of an appropriate tilt setting requires considerations about the rotational motion perception through the semicircular canals (SCC). In the SCC model of Meiry (1966), the rotational acceleration threshold was of 8 deg/s^2 for 0.2 seconds, and 0.3 deg/s^2 for 10 seconds of excitations. There have been many studies aiming to address an appropriate trade-off, reviewed in the next chapters.

The tilting point or motion reference point is the centre of rotation around which the simulator is tilted. Depending on whether the location of the tilt point is located above or below the driver’s head, during the tilt, additional velocity and acceleration are generated respectively in same or opposite (false cue) direction of the desired tilt acceleration. Ideally this point needs to be located on the driver’s head vestibular system positions to avoid any of the additional motions, however it requires greater actuator strokes of a hexapod MP. Therefore, in a conventional hexapods MP, this point is often located at the upper plane below the cabin to allow more workspace for motions in other direction.

In studies comparing the tilt point location, in longitudinal braking and lateral steering control driving tasks, drivers were unable to distinguish the change of tilt

point location from drivers head to a lower point, although the higher position did result smoother braking (Jamson, 2010). In another study by the subjective evaluations, the change of tilt point location was found to have a minor effect, with slight improvement when it was located higher than drivers head (Fischer and Werneke, 2008).

3.3.2 Nonlinear scaling of vehicle motion

The limitations of the MP usually require the vehicle motions to be scaled down either before or within the MCA structure. Linear scaling is often used in classic algorithms that attenuates the acceleration signal with the same amplitude to bringing the max/min of the signal within the working range of motion platform. This might make the signal in situations of low amplitudes not perceivable any more, where the motion platforms are usually capable of cueing. On the other hand, in situations of the signals of high amplitude, the scaling might still be high and cause large excursions. The solution over this was introduced by using nonlinear scaling (Telban and Cardullo, 2005). In this method, the signal of low amplitude is represented nearly one to one and a higher amplitude is more scaled down to fit within the limits of MP.

A commonly used nonlinear method is the third order polynomial scaling, however selecting its coefficient parameters is a complicated process and the wrong choice may cause perceptible distortion and a local minimum during large-range monotonic signal scaling (Chao et al., 2014). In the same paper, few of the nonlinear methods are reviewed, and they introduced a modified third order polynomial scaling that addresses selecting optimal parameters that guarantee the stability and avoiding the local minimum, described below. The third-order polynomial equation is

$$y = c_3x^3 + c_2x^2 + c_1x^1 + c_0 \quad 3.1$$

Defining the x_m and y_m as expected maximum input and output are known in priori to simulation, the λ_0 and λ_1 are the slope of scaling at $x = 0$ and $x = x_m$ of input acceleration, the four characteristics for the nonlinear gain are

$$\begin{cases} x = 0 \rightarrow y = 0 \\ x = x_m \rightarrow y = y_m \\ \dot{y}_{x=0} = \lambda_0 \\ \dot{y}_{x=x_m} = \lambda_1 \end{cases}$$

The coefficients of the third order polynomial are calculated as

$$\begin{cases} c_0 = 0 \\ c_1 = \lambda_0 \\ c_3 = x_m^{-2}(3y_m - 2\lambda_0x_m - \lambda_1x_m) \\ c_4 = x_m^{-3}(\lambda_0x_m - 2y_m + \lambda_1x_m) \end{cases} \quad 3.2$$

Choosing the λ_0 and λ_1 are usually based on subjective discrimination during the simulations and there are no solid guidelines for selecting them, and wrong choice of them may lead to local minima. In the introduced third order polynomial equation the scaling scope C is defined as x_m/y_m and when it is in a stable region the local minima is avoided. To be within the stability region it is proven that the parameters λ_0 and λ_1 needs to be chosen to ensure the scaling scope C lies within the stable region. The choice of maximum scaling scope C_m and the choice of λ_0 and λ_1 as Eq. 3.3 guarantees and maximises the stable region, which is called the optimal parameter configuration scaling (OPCS).

$$C = \frac{x_m}{y_m}$$

$$C_m = \frac{3}{(\sqrt{\lambda_1} - \sqrt{\lambda_1}/2)^2 + 3\lambda_0/4}$$

To make $C \leq C_m$ the λ is selected as

3.3

$$\begin{cases} \lambda_0 = \frac{4}{C} \\ \lambda_1 = \frac{\lambda_0}{4} \end{cases}$$

The nonlinear scaling is used for the MPC model in the experiment designed in Chapter 6, and the classic and MPC models in Chapter 5 used linear scaling.

3.3.3 Classic algorithm

The most commonly used MCA in dynamic simulators is the classical algorithm that also called washout filters, originated back to outspread works toward the end of the 1960s in flight simulations as a solution for compromising between one to one acceleration representation and MP constraints. It was initially developed by considering which motion cues are more important to pilots and which are attainable by motion system, and finally addressing mathematical model for motion cueing (Conrad and Schmidt, 1969; Conrad and Schmidt, 1970; Conrad et al., 1973). They extended their model to multi DoF which became the baseline for the motion cueing in flight simulators called the classic MCAs. Their method was about the onset of a cue, plus the representing the acceleration feeling though tilt co-ordination. Reid and Nahon (1985) further updated the model and made a comparison among MCAs which became the definition of the classical MCA, which is the most widely used today. A review of its concept and parameters is available in (Grant and Reid, 1997), and (Romano et al., 2017) introduced an updated layout of the MCA for the driving simulators.

Model structure

A general simplified schematic structure of the classic algorithm is presented in Figure 3-13. It is often a combination of scale-factors, high and low-pass filters, limiters and coordinate transformation. The input to the MCA is vehicle motions, while the output of it is the desired motion platform set points. The scale-factors reduce the acceleration output magnitude represented in comparison to the input from the vehicle motions. While the input vehicle acceleration passes through the high-pass filter the transient part of acceleration is separated to be represented by MP translational movements (linear motion). The sustained is separated by low-pass filter which is transformed to tilt coordination and is added to the rotational channel to be represented by MP rotational movements. Unlike the flight simulators in driving simulators due to limited degrees of rotations in manoeuvres, the rotational channel could be replaced by simple direct feeding of vehicle rotations.

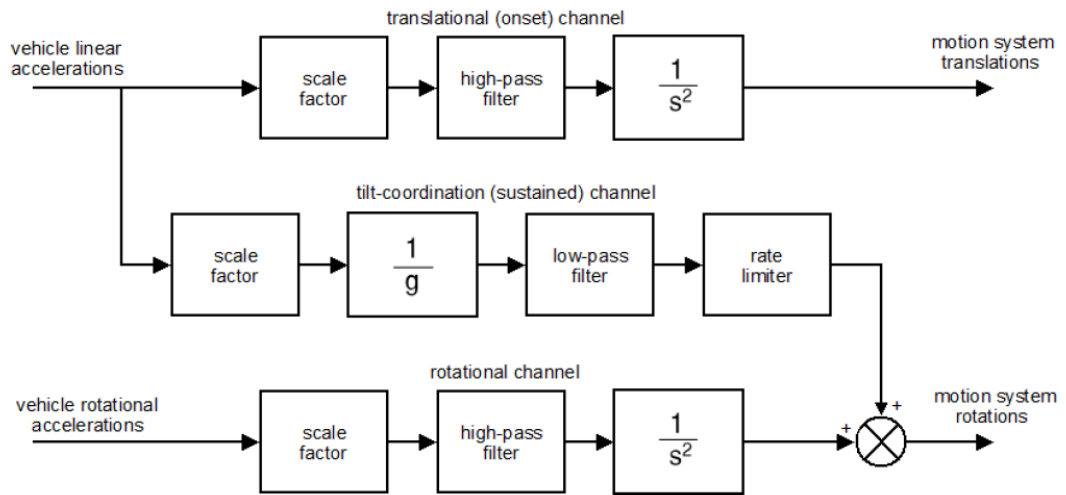


Figure 3-13. Classic motion cueing algorithm, (Jamson, 2010)

The MCA response is usually evaluated in the time and frequency domain, see Figure 3-14. The top picture is the time domain response, considering a step acceleration input, the transient motion is separated by high-pass filtering, due to limited MP translational envelope, not all the acceleration could be generated through this onset cue (blue line). The scale-factor and the filter cut-off frequency(s) are selected considering the MP constraints before the start of the simulation. The tilt coordination through the low-pass filtering separates the sustained motion (red line) and compensates for the remainder of motion that was not represented by the onset cue. The slow build-up of tilt acceleration is due to rotating under SCC angular velocity and acceleration perception thresholds, requiring a longer time to compensate. The scale-factor and the filter cut-off frequency(s) of the low-pass filter define the tilting constraints. The black line is the total motion that the driver experiences that is the summation of both translational and tilting acceleration.

Clearly, there is missing acceleration compared to input because of the mentioned MP and tilting limitations.

Similarly, in the bottom picture, the response of low and high-pass filters and their combination is shown in the frequency domain. In the phase and gain plots, the black lines show the summation of both filters, as it is observable that is not flat zero line, reflecting the phase and magnitude distortion between the input and output accelerations. The distortion can be improved by decreasing the high-pass filter or increasing the low-pass filter's cut-off frequencies, that results in larger MP excursion and rapid tilt angular velocity and acceleration, respectively.

Consequently, the limited motion envelope of the MP and under threshold tilting causes the time domain amplitude or frequency domain phase and gain distortions between the vehicle motion in the simulator and real world.

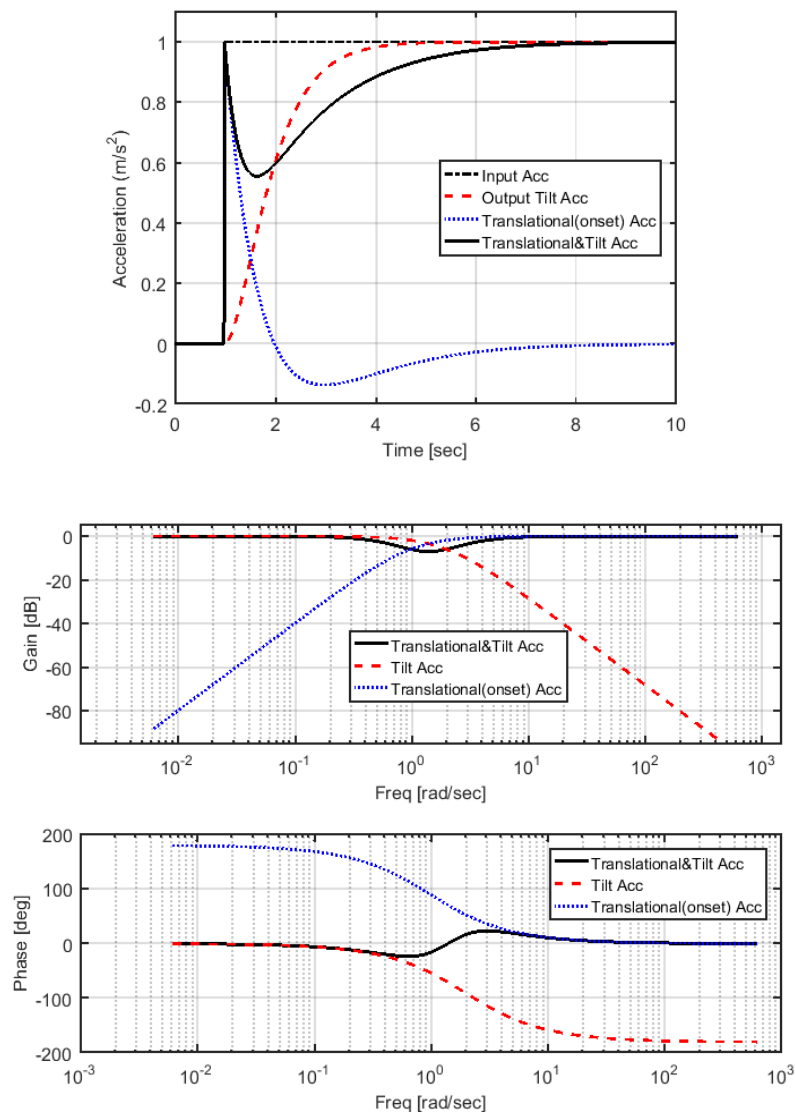


Figure 3-14. MCA step response, time domain (top) and frequency domain (bottom)

Selecting the MCA parameters (tuning it) has significant impact on the motion cueing fidelity of the simulator, those should be picked to have minimum errors between the MCA input (real vehicle motions) and MCA output (simulator motion platform set-points), while at the same time respecting the motion platform envelope and tilting constraints. The errors are usually minimised in the time domain i.e. amplitude error, and/or frequency domain i.e. gain and phase errors. The inevitable errors cause the discrepancy between the visual and motion cues which is undesirable. The question rises here that 'what is the maximum discrepancy to have acceptable fidelity?', that has been the subject of studies to address the maximum undetectable distortions between the visual and motion cues in flight and driving simulators, and to find out how it affects the drivers' perception and behaviour, this is further discussed in sections 3.4. Later in Chapter 8 the effect of the MCA parameters is thoroughly reviewed.

The classic MCA is always tuned for the worst-case scenario of vehicle motion inputs and considering the MP limits. This results in minimum exploitation of MP workspace during low to average amplitudes of vehicle motion inputs, that is being considered as the biggest disadvantage of this algorithm. However, it is possible to slightly improve the performance of the classic MCA per case by pre-tuning its parameters for a specific vehicle motion in a manoeuvre. In addition to above, the tuning is always a complicated procedure because several criteria (described earlier in this section) need to be met at the same time that takes loads of effort to find precise parameters manually. The explained issues were the motivation for developing an automated approach to finding the best classic MCA tuning parameter settings for a specific MP and manoeuvre that minimises motion discrepancy and meets the fidelity requirements, as well as considering the motion platform constraints, that is introduced in Chapter 5 and further used in Chapter 8.

3.3.4 Model predictive control algorithm

Over the past few decades, the model predictive control (MPC) has been receiving increasing attention from researchers in a variety of industries and academic communities. Richalet et al. (1978) first developed it, and its effectiveness when applied to large scale chemical process industry was proven. Furthermore, since then it has been used in various control engineering applications such as chemical plants, power systems, electronics, robotics oil refineries, supply chain management, stochastic control, problems in economic and finances. Wang, L. (2009) has mentioned four aspects that make this control method more attractive

- Design formulation that provides the intuitive understanding and parameter tuning of a multivariable control system framework
- Ability to handle soft and hard constraints on control variables
- Online optimisation process

- The simplicity of the design framework in handling complex problems.

In industrial process control applications, the MPC is more advanced control technique than standard proportional–integral–derivative (PID) control mainly because it can deal routinely with equipment and safety constraints, intuitive understanding and tuning makes it superior to conventional advance linear control (Maciejowski, 2002).

Using long enough prediction horizon, the predictive control is similar to the linear quadratic regulator (LQR) in both continues and discrete time models. The difference between them is that predictive control uses a moving time horizon window whilst LQR uses a fixed window. The moving horizon window adds the ability of real-time optimisation with hard constraints on plant variables to predict the control inputs. Having a large prediction horizon raise the numerical complexity problem, that also requires either the plant model to be asymptotically stable or using exponential weights in the cost function for transformation from unstable to stable; using the later also guarantees the closed-loop stability (Wang, L., 2009).

Dagdelen et al. (2004); Dagdelen et al. (2009); Augusto and Loureiro (2009) first successfully employed the model predictive control as MCA in simulators. Which further extended on its mathematical implicit/explicit solution techniques (Fang and Kemeny, 2012a) and stability analysis (Fang and Kemeny, 2016). Using this method as MCA, in addition to its common advantage of respecting the constraints on both inputs and outputs in a real-time optimisation problem, brought the capability of integrating human perception and motion platform models to calculate the optimal solutions. As a result, in this method, the motion platform constraints and human perception are always respected, and exploitation of workspace is maximised during simulations.

Due to the parallel architecture of the hexapod platform and strong coupling between one DoF and others, the motion workspace is a complex function of all six Cartesian DoF. In actuator space, however, the workspace is completely uncoupled; the six actuator limits are independent of each other that eases applying the constraints on actuator physical limits and avoids actuator limiting. Garrett and Best (2013) used this approach, that integrated a plant kinematic model of hexapod represented in actuator space system.

Model structure

The general objective of model predictive control is to compute future manipulated control variable u to optimise the future plant output behaviour y within a limited time window. Discrete-time output reference tracking is a common framework of MPC, an optimisation problem is solved over the prediction horizon H_p to optimally

calculate a control input action u over a control horizon H_u ($H_u \leq H_p$) by minimising a cost function and satisfying constraints. There are different variables known as output or measured, input or manipulated and state variables, and all could be constrained. The plant output variable needs to track a given reference input signal, the manipulated variables are the plant control inputs, and the latter is the plant model states.

At time k a measure of current plant output $y(k)$ and reference input $r(t|k)$ where $t \geq k$ is available. A predictive controller has an internal state estimator model of the plant which predicts the behaviour of plant states from current time k over the prediction horizon $y(k+i|k)$, $i = 0, 1, \dots, H_p$. The predicted output behaviour depends on the control input trajectory $u(k+i|k)$ $i = 0, 1, \dots, H_p - 1$ which is calculated by minimising a cost function that includes the tracking error Eq. 3.4 and control input, while respecting constraints. Once the optimal input sequence $\hat{u}(k+i|k)$ is computed, the control input at the current time step is selected as its first value $u(k) = \hat{u}(k|k)$. At the next time step $k+1$, a new output $y(k+1)$ is measured and the process is iterated similarly. Since at each time step, the prediction horizon is shifted to look H_p time steps ahead, this procedure is known as ‘receding horizon’. The principles are graphically shown in Figure 3-15.

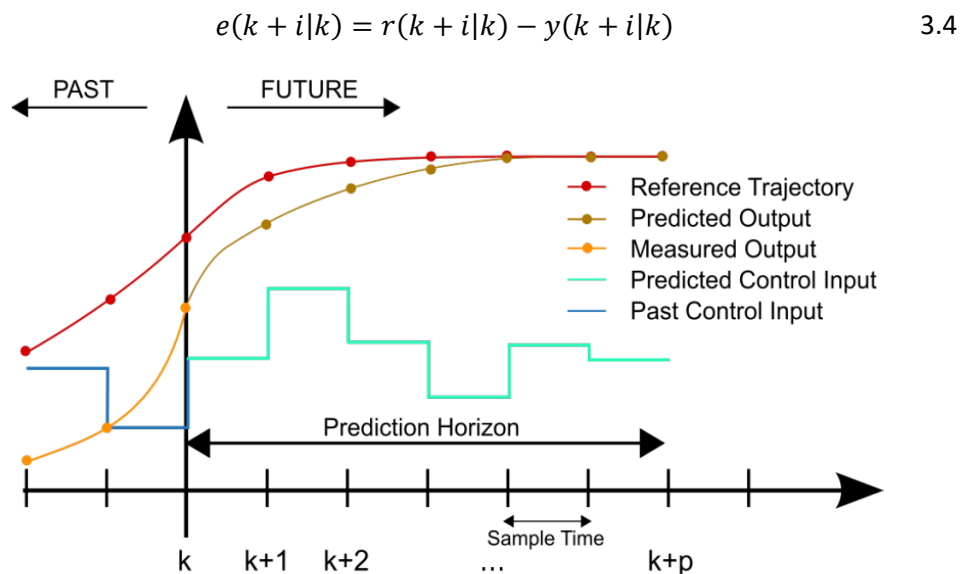


Figure 3-15. Schematic representation of MPC principle, Wikipedia.

3.3.4.1 Plant model

Different approaches have been proposed for MPC model structures in the literature. During the years finite impulse response (FIR), step-response, transfer function and state-space models have been used to represent the plant. The first three type models are usable only for stable systems and require large model orders (Wang, L., 2009). The FIR models were appealing to process engineers

because they give a description of process time delay, response time and gain. Transfer functions are a better tool and give a clearer description of process dynamics but gets tangled for the large MIMO systems. The simplicity of the design framework of state-space models specially to represent MIMO systems, direct link to linear quadratic regulators and accessible state variables, have given growing popularity to it in control theory applications. Therefore, the state-space model was chosen to be used in this thesis.

Provided formulation of the MPC for the remainder of the sections is based on (Wang, L., 2009), and MCA formulations are mainly inspired by (Augusto and Loureiro, 2009; Maran, 2013; Garrett and Best, 2013). A linear discrete state-space model of a strictly proper MIMO system is in the form of Eq. 3.5. In the 'receding horizon' control, current information of the plant is used for prediction and control. Hence the control inputs do not have a direct effect on the plant outputs, that requires the plant model to be strictly proper ($D_m = 0$). In this equation there are m number of control input or manipulated variables (u), q number of plant outputs variables (y), and n number of state variables vector (x_m).

$$\begin{aligned}x_m(k+1) &= A_m x_m(k) + B_m u(k) \\y(k) &= C_m x_m(k)\end{aligned}\tag{3.5}$$

The MPC formulation used here considers optimisation of input difference $\Delta u_m(k) = u_m(k) - u_m(k-1)$, which also gives the advantage of the flexibility of adjusting the maximum changes of the control input in a time step. Taking the difference of the above equation new state-space equation can be written

$$\begin{aligned}\Delta x_m(k+1) &= A_m \Delta x_m(k) + B_m \Delta u(k) \\ \Delta y(k) &= C_m \Delta x_m(k) \text{ or} \\ \Delta y(k+1) &= C_m \Delta x_m(k+1)\end{aligned}$$

Where

$$\begin{aligned}\Delta x_m(k+1) &= x_m(k+1) - x_m(k) \\ \Delta x_m(k) &= x_m(k) - x_m(k-1) \\ \Delta u_m(k) &= u_m(k) - u_m(k-1) \\ \Delta y(k) &= y_m(k) - y_m(k-1)\end{aligned}$$

To relate the states $\Delta x_m(k)$ to output $y(k)$, the substitution of the above equations is needed

$$y(k+1) - y(k) = C_m A_m \Delta x_m(k) + C_m B_m \Delta u(k)$$

A new augmented state variable vector is defined

$$x(k) = [\Delta x_m(k)^T \ y(k)^T]^T$$

Obtaining the augmented state-space model of

$$\begin{aligned} x(k+1) &= \begin{bmatrix} A_m & o_m^T \\ C_m A_m & I_{q \times q} \end{bmatrix} x(k) + \begin{bmatrix} B_m \\ C_m B_m \end{bmatrix} \Delta u_m(k) \\ y(k) &= [o_m \ I_{q \times q}] x(k) \end{aligned} \quad 3.6$$

Where the $I_{q \times q}$ is the identity matrix with $q \times q$ dimension, o_m is $q \times n$ zero matrices. The dimensions of A_m , B_m and C_m are $n \times n$, $n \times m$ and $q \times n$ respectively.

3.3.4.2 Quadratic Programming

Quadratic programming (QP) is a method of solving mathematical optimisation problems where the quadratic function of variables has to be minimised with linear constraints on those variables. QP in its standard form has been widely studied, and various solution methods have been developed with cons and pros considering the characteristics of the optimisation problem (Wang, Y. and Boyd, 2010). In this thesis since the MPC problem has quadratic cost function, and constraints are linear, thus was feasible to convert it to a QP one.

A classic formulation of QP optimisation problem that has a quadratic function to be minimised, and constraints are linear, is usually as

$$\begin{aligned} \min f(x) &= \frac{1}{2} x^T H x + x^T c \\ Ax &\leq b \end{aligned} \quad 3.7$$

$x, c, b \in \mathbb{R}^n$ and $H, A \in \mathbb{R}^{n \times n}$. H is Hessian symmetric matrix. If H is positive semidefinite then function f is convex, then if there exists a feasible solution x^* and f has a lower bound in the feasible region, there exists a global solution. If H is positive definite and there exists a feasible solution x^* then it is the global minimum, according to Boyd and Vandenberghe (2004) cited in (Maran, 2013). It is conventional and useful to reformulate the cost function to use ΔU as the solution vector x to be minimised.

Introducing the constraints increases the complexity of finding the solution and cannot be solved analytically, hence numerical solutions have to be used to a QP problem, and appropriate solver is required. Moreover, in real-time applications, the high control frequency update (usually between 50 and 150 Hz) requires the solver to be fast and efficient. The solvers are mainly divided into offline and online algorithms. There have been many techniques introduced to decrease the computational efforts and solve the QP problem at higher rates. It has been shown that by reordering the variables, the complexity of MPC becomes linear rather than

cubic. Another method of reducing the complexity is by reformulating it in terms of control input, together with a move blocking strategy where the input is assumed to be constant or fixed portion of the horizon. The hot-start is another strategy, that uses the results solved in previous steps to find the better starting points for current step (Wang, Y. and Boyd, 2010).

In offline solvers, the control law is precomputed considering all possible instances of the problem, and in during online process controller works similar to picking up from a lookup table. The explicit MPC is a widely used example (Bemporad et al., 2002), where the optimisation step is computed offline before the online process. In this method, the constraints are used to partition the model in polyhedral critical regions, and in these regions, the optimal control law is an affine function of the states. In the offline process these are calculated, and related parameters are stored, and during the online process the region which current state belongs to is evaluated, and corresponding affine control law is applied. Thus, there is a lower online computational process. The problem with this method is that the computational burden grows exponentially with the size of the problem and number of constraints hence it is efficient only in low dimension problems, few constraints and short time horizon. Moreover, this method does not allow the time-varying systems, constraints and cost function, that makes the online tuning difficult, which is applicable in driver in the loop tuning of the MCA parameters (Maran, 2013).

The online QP solvers mainly divided into main categories of 'Interior Point' and 'Active Set' methods. In the Interior Point method, the convexity of the cost function is exploited, and the complexity is polynomial. They lack the 'hot-start strategy' that reduces the computational burden. The primal barrier interior point method was updated using a collection of methods to find the high quality control using the sub-optimal solution for each step, that is claimed to increase the calculation speed up to 100 times faster than a general optimisation method (Wang, Y. and Boyd, 2010). The Active Set method is inspired by the explicit approach, to find the current critical region however without pre-computations. Similar to the explicit method inside the critical regions the solutions are an affine function of the states. In this method, the polynomial complexity (worst case) is not always achieved and a hot start strategy is available.

In the MPC model used here the default QP solver designated in MATLAB 2016a, MPC Toolbox, which is a modified version of Active Set method. This decision was made base on the tens of offline motion cueing simulations in worse-case scenarios. Testing for input/output signal rate transition, surge/pitch, sway/roll and heave/yaw controllers separately executing on 4 cores of a dual Xeon CPU 16-core Concurrent iHawk hardware platform running the real-time derivative of the RedHat

Linux operating system, that could afford the calculation efforts. After many test runs and time measurements, it was observed that using the originally designated QP solver of the KWIK algorithm provides satisfactory performance for real-time motion cueing.

The formulation of the objective function and the inequality and equality constraints used in Matlab MPC quadratic programming solver based on the KWIK algorithm (Schmid and Biegler, 1994) has the form of

$$\begin{aligned} \min f(x) &= \frac{1}{2}x^T Hx + x^T c \\ Ax &\leq b \\ A_{eq}x &= b_{eq} \end{aligned} \tag{3.8}$$

This solver algorithm uses the reduced hessian successive quadratic programming (SQP), which is shown to be suitable for large scale optimisation problems. In the pre-processing phase, linear feasibility of the nonlinear programming formulation is being solved, which is then served to determine an initial consistency to select a non-singular set of basic variables and to identify dependency between the equality constraints. This algorithm QPKWIK was an improvement to the dual active set method of Goldfarb and Idrani (1983). It uses the inverse Cholesky factor of the Hessian matrix at each time step that reduces the computational complexity. It has the ability to determine a search direction when infeasible QP subproblems are encountered by relaxing the quality constraints (Schmid and Biegler, 1994).

“This solver requires the Hessian to be positive definite. In the first control step, KWIK uses a cold start, and the initial guess is from the unconstrained solution. If x satisfies the constraints it is the optimal solution x^* and stops. Otherwise, at least one of the linear inequalities constraints must be satisfied as equality, then an efficient, numerically robust strategy is used by the solver to determine the active constraint set satisfying the standard optimisation conditions. In the next control steps, a warm start is used. In this case, the active constraint set determined at the previous control step becomes the initial guess for the next” (MathWorks, 2016a).

3.3.4.3 Cost function

The next step of the design of a predictive control system is calculating plant output with future control input, within an optimisation window. Here the current time is k_i and length of optimisation window is N_p number of samples i.e. the prediction horizon. Assuming at sampling time k_i the state variable vector $x(k_i)$ is available from the measurement. The future control trajectory is

$$\Delta u(k_i)^T, \Delta u(k_i + 1)^T, \dots, \Delta u(k_i + N_c - 1)^T$$

Where N_c is control horizon number of samples, that defines the number of parameters to capture future control trajectory. Given the $x(k_i)$ the future state variables are predicted for the length of optimisation window N_p . The control horizon N_c is always chosen to be smaller or equal the prediction horizon N_p .

$$x(k_i + 1|k_i)^T, x(k_i + 2|k_i)^T, \dots, x(k_i + N_p|k_i)^T$$

For the state-space representation of the plant, the future state variables sequence corresponding the future control input is

$$\begin{aligned} x(k_i + 1|k_i) &= Ax(k_i) + B\Delta u(k_i) \\ x(k_i + 2|k_i) &= Ax(k_i + 1|k_i) + B\Delta u(k_i + 1) \\ &= A^2x(k_i) + AB\Delta u(k_i) + B\Delta u(k_i + 1) \\ &\vdots \\ x(k_i + N_p|k_i) &= A^{N_p}x(k_i) + A^{N_p-1}B\Delta u(k_i) + A^{N_p-2}B\Delta u(k_i + 1) + \dots \\ &\quad + A^{N_p-N_c}B\Delta u(k_i + N_c - 1) \end{aligned}$$

From the predicted state variables, the predicted output variables become

$$\begin{aligned} y(k_i + 1|k_i) &= CAx(k_i) + CB\Delta u(k_i) \\ y(k_i + 2|k_i) &= CA^2x(k_i) + CAB\Delta u(k_i) + CB\Delta u(k_i + 1) \\ &\vdots \\ y(k_i + N_p|k_i) &= CA^{N_p}x(k_i) + CA^{N_p-1}B\Delta u(k_i) + CA^{N_p-2}B\Delta u(k_i + 1) + \dots \\ &\quad + CA^{N_p-N_c}B\Delta u(k_i + N_c - 1) \end{aligned}$$

Defining new vectors in terms of current state variable $x(k_i)$ and future control parameter $\Delta u(k_i + j)$, $j = 0, 1, \dots, N_c - 1$.

$$\begin{aligned} \Delta U &= [\Delta u(k_i)^T \Delta u(k_i + 1)^T \dots \Delta u(k_i + N_c - 1)^T]^T \\ Y &= [y(k_i + 1|k_i)^T y(k_i + 2|k_i)^T \dots y(k_i + N_p|k_i)^T]^T \end{aligned} \quad 3.9$$

Representing the above equations in compact matrix form as

$$Y = Fx(k_i) + \Phi\Delta U$$

$$F = \begin{bmatrix} CA \\ CA^2 \\ CA^3 \\ \vdots \\ CA^{N_p} \end{bmatrix}, \Phi = \begin{bmatrix} CB & 0 & 0 & \dots & 0 \\ CAB & CB & 0 & \dots & 0 \\ CA^2B & CAB & CB & \dots & 0 \\ \vdots & \vdots & \vdots & \ddots & \vdots \\ CA^{N_p-1} & CA^{N_p-2}B & CA^{N_p-3}B & \dots & CA^{N_p-N_c}B \end{bmatrix} \quad 3.10$$

The objective of the predictive controller is to find the best control parameter vector ΔU to minimise the error between the predicted output and the reference signal $r(k_i)$ at sample time k_i within a prediction horizon, reflected in the cost function J . The $r(k_i)$ could be constant or variable which is discussed in next section.

$$J = (R_s - Y)^T Q (R_s - Y) + U^T S U + \Delta U^T R \Delta U$$

Where

$$R_s = N_p \begin{Bmatrix} 1 \\ 1 \\ 1 \\ \vdots \\ 1 \end{Bmatrix} r(k_i) \quad 3.11$$

The first term is to minimise the error between the reference input and predicted output, while the second and third terms reflect the consideration about the size of control variable U and its rate of change ΔU to be as small as possible. The $Q, S, R \geq 0$ are the block diagonal weight matrices, assigning zero or higher values to them comparably is interpreted as importance of minimising each term, substituting Eq. 3.10 in the Eq. 3.11 it becomes

$$J = (R_s - Fx(k_i) - \Phi \Delta U)^T Q (R_s - Fx(k_i) - \Phi \Delta U) + U^T S U + \Delta U^T R \Delta U$$

The input sequences of U is related to ΔU as

$$\begin{bmatrix} u(k_i) \\ u(k_i + 1) \\ u(k_i + 2) \\ \vdots \\ u(k_i + N_c - 1) \end{bmatrix} = \begin{bmatrix} u(k_i - 1) \\ u(k_i - 1) \\ u(k_i - 1) \\ \vdots \\ u(k_i - 1) \end{bmatrix} + \begin{bmatrix} I & 0 & 0 & \dots & 0 \\ I & I & 0 & & 0 \\ I & I & I & & 0 \\ \vdots & \vdots & \vdots & \ddots & \vdots \\ I & I & \dots & I & I \end{bmatrix} \begin{bmatrix} \Delta u(k_i) \\ \Delta u(k_i + 1) \\ \Delta u(k_i + 2) \\ \vdots \\ \Delta u(k_i + N_c - 1) \end{bmatrix}$$

or

$$U = U_i + T \Delta U \quad 3.12$$

With further simplifications on the cost function and substitution of the above results in Eq. 3.13

$$J = \Delta U^T (\Phi^T Q \Phi + R + T^T S T) \Delta U + 2 \Delta U^T (\Phi^T Q (Fx(k_i) - R_s) + T^T S U_i) \quad 3.13$$

Defining matrices of Eq. 3.14 the above equation takes the form of a QP problem cost function of 3.15 with ΔU being the variable to minimise

$$\begin{aligned} H &= 2(\Phi^T Q \Phi + R + T^T S T) \\ c &= 2(\Phi^T Q (Fx(k_i) - R_s) + T^T S U_i) \end{aligned} \quad 3.14$$

The cost function becomes

$$J(\Delta U) = \frac{1}{2} \Delta U^T H \Delta U + \Delta U^T c \quad 3.15$$

The matrix H is the Hessian matrix and is assumed to be positive definite. Since the cost function is quadratic and constraints are linear inequalities, the predictive control problem is finding an optimal solution ΔU to a standard quadratic programming problem.

3.3.4.4 Reference input

As it is shown in the Eq. 3.11 the reference input signal R_s is a data vector to the length of prediction horizon H_p that contains the set-point information required for tracking the output variables of the plant in the objective function. In a typical MPC framework, a constant look-ahead approach is used where the reference input is constant over the prediction horizon time steps. On the other hand, a variable look-ahead approach uses a variable reference input within the prediction horizon. Although using the constant reference input still is reliable for many applications with low frequencies changes of input signal, where there is high frequency of changes in signal it might lead to poor tracking performance of controller, this is explained in Chapter 7. As a result, having precise estimation of future reference input improves the performance of controller; however, a reliable prediction of reference input is not always available.

In the application of MCA, the prediction of future reference input gets more complicated in the presence of the unpredictable behaviour of the human in the loop. A simple method to overcome this is by using the recorded repetitive patterns of drivers, however only professional can keep a high level of repeatability, and low skilled drivers have more unpredictable behaviour (Bruschetta et al., 2017). A solution was proposed by them to have a switching strategy between constant and variable look-ahead strategies for drivers with different skills. In their approach when the expected behaviour of a driver is available in the database, the look-ahead is activated otherwise non-look-ahead is used. Moreover, it is mentioned that using the information of the future vehicle trajectories may lead to an effective repositioning of the motion platform.

3.3.4.5 Constraints

In control problems, there are always concerns over the physical limitation of plant e.g. actuator kinematic and dynamic. Constrained formulation of control strategy has the advantage of finding a reliable optimal control sequence during a real-time simulation. Being real-time allows calculating the optimal solution considering the current state of the problem rather than a priori to start of simulation as offline optimal control methods. The constraints are divided to hard and soft constraints, Hard constraints are the ones that QP solution must satisfy to avoid leading to an infeasible solution, and soft constraints are the one that controller may violate in case of producing an optimal value for a manipulated variable. In standard applications of MPC, there are three major types of constraints on variables, being either soft or hard constraints, those are

- Control variables $u(k)$, most commonly encountered constraints, usually are hard constraints. In case it is the only constraint it does not lead to infeasibility
- Rate of change of control variables $\Delta u(k)$, to cope with the cases where the rate of changes of control amplitude is restricted, are often soft constraints. Having constraints both on control and its rate of changes may lead to infeasibility
- Output $y(k)$ or state variable $x(k)$, specifying the range for the plant output. Usually are soft constraints, if there are constraints on control input or rate of change.

Computational complexity may lead to the infeasibility of finding a solution and relaxation of some of the hard constraints might be needed in the design process. However, the soft constraints can be violated and do not lead to infeasibility.

For multi-input multi-output models, constraints are specified for each input and output independently. The upper and lower limits for each of the control signals, rate of changes of control signals and output and state variables are defined as Eq. 3.16,

$$\begin{aligned}
 u_{min} &\leq u(t) \leq u_{max} \\
 \Delta u_{min} &\leq \Delta u(t) \leq \Delta u_{max} \\
 y_{min} &\leq y(t) \leq y_{max}
 \end{aligned}
 \tag{3.16}$$

The next step is to translate the constraints into linear inequalities and relate them to the predictive control model, that needs to parametrise the constrained variables in terms of the vector ΔU same as used in the design of predictive control model. The vector ΔU is often called the decision variable. The constraints are taken to account for each of the moving horizon window sample time, and to reduce the computations it is possible to choose smaller number of samples. For instance at the sample time k_i the rate of changes of the control signal on the first three samples are

$$\begin{aligned}
 \Delta u_{min} &\leq \Delta u(k_i) \leq \Delta u_{max} \\
 \Delta u_{min} &\leq \Delta u(k_i + 1) \leq \Delta u_{max} \\
 &\vdots
 \end{aligned}$$

To relate the constraints in the cost function J , as required by the quadratic programming formulation, the constraints need to be decomposed into two inequalities reflecting the lower and upper limits.

$$\begin{bmatrix} I & 0 & \dots & 0 \\ 0 & I & & 0 \\ \vdots & & \ddots & \vdots \\ 0 & 0 & & I \\ -I & 0 & \dots & 0 \\ 0 & -I & & 0 \\ \vdots & & \ddots & \vdots \\ 0 & 0 & \dots & -I \end{bmatrix} \begin{bmatrix} \Delta u(k_i) \\ \Delta u(k_i + 1) \\ \Delta u(k_i + 2) \\ \vdots \\ \Delta u(k_i + N_c) \end{bmatrix} \leq \begin{bmatrix} \Delta u_{max} \\ \Delta u_{max} \\ \vdots \\ \Delta u_{max} \\ -\Delta u_{min} \\ -\Delta u_{min} \\ \vdots \\ -\Delta u_{min} \end{bmatrix}$$

or

$$M_1 \Delta U \leq N_1$$

Constraints on manipulated control variable $u(t)$ in Eq. 3.16 are expressed in terms of ΔU using the Eq. 3.12.

$$\begin{bmatrix} I & 0 & \dots & 0 \\ I & I & & 0 \\ \vdots & & \ddots & \vdots \\ I & I & & I \\ -I & 0 & \dots & 0 \\ -I & -I & & 0 \\ \vdots & & \ddots & \vdots \\ -I & -I & \dots & -I \end{bmatrix} \begin{bmatrix} \Delta u(k_i) \\ \Delta u(k_i + 1) \\ \Delta u(k_i + 2) \\ \vdots \\ \Delta u(k_i + N_c) \end{bmatrix} \leq \begin{bmatrix} u_{max} - u(k_i - 1) \\ u_{max} - u(k_i - 1) \\ \vdots \\ u_{max} - u(k_i - 1) \\ -u_{min} + u(k_i - 1) \\ -u_{min} + u(k_i - 1) \\ \vdots \\ -u_{min} + u(k_i - 1) \end{bmatrix}$$

or

$$M_2 \Delta U \leq N_2$$

The output constraints are expressed in terms of ΔU using equations 3.10 and 3.16. y_{max}, y_{min} is of size $N_p \cdot n_{out}$.

$$y_{min} \leq Fx(k_i) + \Phi \Delta U \leq y_{max}$$

$$\begin{bmatrix} \Phi \\ -\Phi \end{bmatrix} \Delta U \leq \begin{bmatrix} y_{max} - Fx(k_i) \\ -y_{min} + Fx(k_i) \end{bmatrix}$$

or

$$M_3 \Delta U \leq N_3$$

Finally, the model predictive control in presence of constraints can be expressed in a Quadratic Programming problem where the sequence vector ΔU has to be calculated that minimises the cost function J and satisfying the inequality constraints for a QP problem as

$$\begin{bmatrix} M_1 \\ M_2 \\ M_3 \end{bmatrix} \Delta U \leq \begin{bmatrix} N_1 \\ N_2 \\ N_3 \end{bmatrix} \quad 3.17$$

Matrix M shows the constraints, its number of rows equals the number of constraints and columns equals the dimension of ΔU . Number of constraints when those are fully imposed is equal to $4 \times m \times N_c + 2 \times q \times N_p$. Where m is the number of inputs and q is the number of outputs.

3.3.5 Adaptive algorithm

Parrish et al. (1975) first introduced this algorithm, where adaptive filters were employed to represent the translational or rotational motions somewhat similar to the structure of the classic algorithm, and filter parameters were updated during the real-time simulations through an optimisation problem. In a quadratic cost function, angular velocity and translational acceleration errors between desired vehicle input and motion platform's motion were minimised, it also included displacement and velocity errors of motion platform from their neutral points.

Nahon et al. (1992) described that in this method, smaller inputs were attenuated less than larger ones since they are less likely to result in large simulator displacements. Thus, false cueing should be reduced, and better use made of the MP capabilities. However the issue accompanying this method was the instabilities of the model (Fang and Kemeny, 2012b), and in case of large inputs, it became under-damped leading to oscillatory response and large false cues.

Nahon et al. (1992) developed a hybrid model at the University of Toronto Institute for Aerospace Studies (UTIAS) which was a combination of classical and adaptive algorithms. They used higher-order cost function with more variables and weights to find out the adaptive filter parameters. The terms in the cost function penalise acceleration and roll rate motion errors, simulator velocity, position, roll rate and roll. Moreover, there were other terms included to return the adaptive parameters to their original reference values.

Actuator State Based Adaptive algorithm (ASBA) was developed to use MP's actuator states in the cost function instead of the Cartesian based motion states (Grant and Naseri, 2005). The ASBA algorithm works similar to the hybrid (UTIAS) algorithm in cases for a single DoF manoeuvre. For higher DoF manoeuvres, however, the ASBA avoids actuator limiting in cases where the UTIAS algorithm results in one or more actuators limiting. They found improved stability and adaptation compared to the previous UTIAS hybrid adaptive algorithm.

In a study done by Colombet et al. (2008) the results of an experiment carried out at Renault, to measure drivers' ability to follow a car in three motion system configurations of static, dynamic (Renault CARDS) with a classical motion cueing algorithm (Reid and Nahon, 1986a), and an adaptive motion cueing algorithm (Parrish et al., 1975). They concluded that drivers subjectively preferred dynamical sessions, but the effect of the algorithms on their tracking performance was not significant. In offline comparisons between the classical and adaptive and optimal

MCA, it was reported the classic choice in fare of easy tuning of the classic (Nehaoua et al., 2008). However, in both studies, the motion platforms had very small workspace that might have made the algorithms indistinguishable to drivers and in offline comparisons.

3.3.6 Optimal algorithm

This method is similar to the adaptive algorithm in terms of solving an optimisation problem to find filter parameters; however, the structure of this algorithm is not based on the classic algorithm as in the adaptive. The optimal term is used since this method is using the mathematical logics and expressions such as Linear-Quadratic Regulator (LQR) for the cost function and Riccati equation that are used in optimal control theory for controlling systems at minimum cost. This method is available in both online and offline optimisation, in offline the filter parameters are optimized and implemented once before the beginning of the simulation, and in online filter parameters are updating during the simulation that needs the Riccati equation to be solved in real-time.

The first effort of using this method for MCA in simulators could be referred to (Kurosaki, 1978). He used state-space linear optimal control theory, to the design of washout filters for NASA's vertical motion simulator and his method was restricted to be offline. The vestibular system and motion platform dynamics were not included in the optimisation. In another study, a simple model for the motion platform was included, but still offline, with no vestibular model (Sturgeon, 1981).

Most of the literature refer that optimal control approach for cueing algorithm was first introduced by Sivan et al. (1982), however it is better to say it was the first model that included human vestibular model, in a cost function to minimise of error between pilot in simulator and aeroplane, although that algorithm was still offline. They claimed that washout filters derived from the optimal control problem have the same order as the conventional filters. Moreover, the optimal filters can be tuned by to satisfy a variety of additional conditions such as different travel lengths of the simulator, flight trajectories, and emphasises on motion cues. However, Telban et al. (2002) reported that using this algorithm yields higher order filters, and reported of its poor performance in tracking changes to aircraft inputs in comparison to adaptive method.

Telban et al. (2002); Telban and Cardullo (2005) combined both adaptive and linear optimal algorithm and introduced an approach for motion cueing that would benefit from both methods resulting in nonlinear cueing filters. They included improved visual-vestibular motion perception model and a neurocomputing approach was used to solve the Riccati equation in real-time. They expressed the cost function

with a parameter called α varied with respect to input vehicle motion, to adjust for faster control action and stabilising the system. It was a nonlinear time-varying algorithm producing small cues for a longer duration and washing out larger cues more quickly.

Reid and Nahon (1985); Reid and Nahon (1986a) developed the three classic, adaptive and optimal algorithms. The four no-motion, classic, adaptive and optimal motion cases were compared among pilots in a commercial jet transport simulator (Reid and Nahon, 1986b; Reid and Nahon, 1988). Their results showed a little effect of algorithm type on the performance and control activity; however, those subjectively differed to drivers to perceive the simulation environment. The adaptive algorithm was generally preferred the best and no-motion the worst. In complementary work, Nahon and Reid (1990) showed that all the three algorithms could be adjusted to give a good performance in terms of pilots ratings, where the optimal fared the worst and adaptive method the best. The author mentioned the adaptive has the most potential for further improvement because of its nonlinear nature. Moreover, it was concluded that the classic was the best of ease of adjustment and implementation, where opposite was true for optimal and it may not worth the effort for adjustments.

In the VIRTEX simulator at Ford Motor company, few of the MCAs were compared evaluating the algorithm and parameter tuning effects (Grant et al., 2003; Grant et al., 2009). A lane position algorithm that used the lateral vehicle position to generate the motion in the simulator, a well-tuned classic and three other general-purpose classic algorithms that were not specifically tuned for the manoeuvre. Parameters of the classic for the three sets were selected to have different ratios of specific force error to roll rate error. It was found that well-tuned classic and lane position algorithm had same level of fidelity, while the general-purpose classic did not reach the same fidelity with identical scaling. No effect was found on the trade-off between the specific force and angular rate errors. They also found that drivers performed better with lane position algorithm than a well-tuned classic algorithm. Reportedly, an increase of motion scaling from 0.3 to 0.5 improved the performance and increased the subjective fidelity.

To eliminate the false cues in sustained accelerations represented by tilt coordination, and the interaction between tilt coordination and turntable motion, (Romano, 1999) developed a new algorithm that was based on the concept of Overtilt. A method of tilting that generated a negative acceleration to stop the simulator and drive it back to the centre position faster than other washout algorithms. Furthermore, to reduce the MP excursions a third order minimum time control method was developed that included a prepositioning of the motion platform,

used predicted acceleration information and dynamic adjustments to the tilt rate limiting. He showed this algorithm provides better lateral specific force and yaw angular velocity cues than the classic algorithm. Moreover, he showed both the third order minimum time controller and the LQGR controller, increased MCA performance over the classical.

Romano (2003) developed a nonlinear tilt coordination algorithm that replaced the conventional filters of the classic algorithm, and the tilt channel was controlled by a linear Gaussian regulator (LQGR) to control the tilt rate and motion platform position. Besides, nonlinear feedback was used to reduce the linear acceleration to a be controllable by the tilt channel. It was shown the improvement of performance compared to classic for deceleration manoeuvres, also compared to the classic it required much fewer filter and control parameters

An experiment conducted in the Ride Motion Simulator (RMS) of US Army Tank Automotive Research, Development and Engineering Centre (TARDEC), comparing two RideCue and OverTilt Track algorithms to a default algorithm of the motion platform and a no motion case. The comparisons were done in the context of vehicle handling of heavy off-road vehicles. The RideCue algorithm used a swing motion concept, and OverTilt Track used a pre-positioning for tilt adjustments. Their results showed that the presence of motion contributed to the performance in controlling their steering inputs. Subjectively drivers were influenced by the presence of motion and realism of control induced motions (Romano et al., 2016).

3.4 Fidelity definitions and assessment methods

Different definitions have been proposed for the fidelity of simulators, but it is most commonly described as the degree to which the real and virtual environments match from driver/pilot realism experience and behavioural performance. Due to limited knowledge about human motion perception and control behaviour, and the diversity of simulator cueing systems, introducing a benchmark for simulator visual and motion system requirements to achieve an adequate level of fidelity has been always a difficult problem. It gets even more challenging because of the dependency on vehicle specifications, driving task, and individual driver preferences.

Preliminary studies about fidelity definitions began in the flight simulation industry. Among the first efforts, the validity of the different subsystems was considered to find the areas of the deficient fidelity; this gave rise to questions about the appropriate subjective and objective metrics, the computer image generation system, visual field of view, computational delay and actuator dynamics (Sinacori,

1978). Many of these deficiencies has been reduced by technology improvements; however, the ambiguity about the fidelity level needed for specific applications of the simulator e.g. training or research, and the simulator subsystem requirements to meet the fidelity remains unaddressed.

AGARD (1980) studied the cause of deficiencies in fidelity, for training purpose. The cues were divided to equipment and environmental cues and introduced the concept of perceptual fidelity i.e. a psychological/physiological viewpoint with which the trainee subjectively perceives the simulator and objective fidelity an engineering viewpoint in which simulator equipment and environmental can reproduce the cues compared to real aircraft. They considered for each of the cues how much subjective and objective fidelity is required to achieve satisfactory training, and to provide cost versus training information for procurement purposes. It was concluded that there are four major steps in the development of simulator facilities, those were to analyse the training requirement and objectives, define methods and facilities to perform the training, develop simulator hardware and validate the simulator. Many of the deficiencies in the above steps were related to simulator technology limitations and how the cueing fidelity impacts on the training effectiveness and only a few recommendations for improvements were provided.

Pool (2012) gathered the fidelity definitions and produced a schematic representation of fidelity definitions for skill-based manual closed-loop control tasks in real and virtual flight, see Figure 3-16. In his definition, the aircraft model fidelity is considered separately, and objective fidelity is determined by the quality of the simulator cueing systems. Addressing the simulator cueing system only based on objective fidelity does not consider the limitations of human perception, and results in more expensive hardware to achieve high fidelity.

In contrast to the objective fidelity, perceptual fidelity is operator centred and high perceptual fidelity is defined as the indistinguishable perception of cue stimuli in a real and virtual environment. It is possible to use human sensory-perception models to objectively quantify the fidelity. Although the human sensory is adequately understood and modelled, there is a limited understanding of how the sensory outputs are integrated as perception in the brain, which makes using this approach debatable. Perceptual fidelity is often evaluated subjectively by pilots evaluating simulation realism, using fidelity questionnaires. Although this type of fidelity evaluation might be biased by individual preferences and expectations, and result in unrepeatable, contradictory and inconclusive results, it is still the main human centred approach used to evaluate the realism.

Error fidelity is defined as the measurement of error in vehicle response between the real-virtual environment and is the direct result of operator perception and

control performance. The issue with this method is that in various cueing conditions, the participants might adapt their behavioural control performance to them. Hence these metrics may not capture the full effect of cueing variations. Behavioural fidelity is the comparison of the behaviour performance in the simulator to real flight. It can be quantified objectively using metrics or driver/pilot behaviour models, it is also possible to have qualitative subjective assessments on drivers' behaviours. However, finding the appropriate behavioural metrics or driver models for the evaluations is a challenging task, a review of models for objective behaviours was presented in Chapter 2.

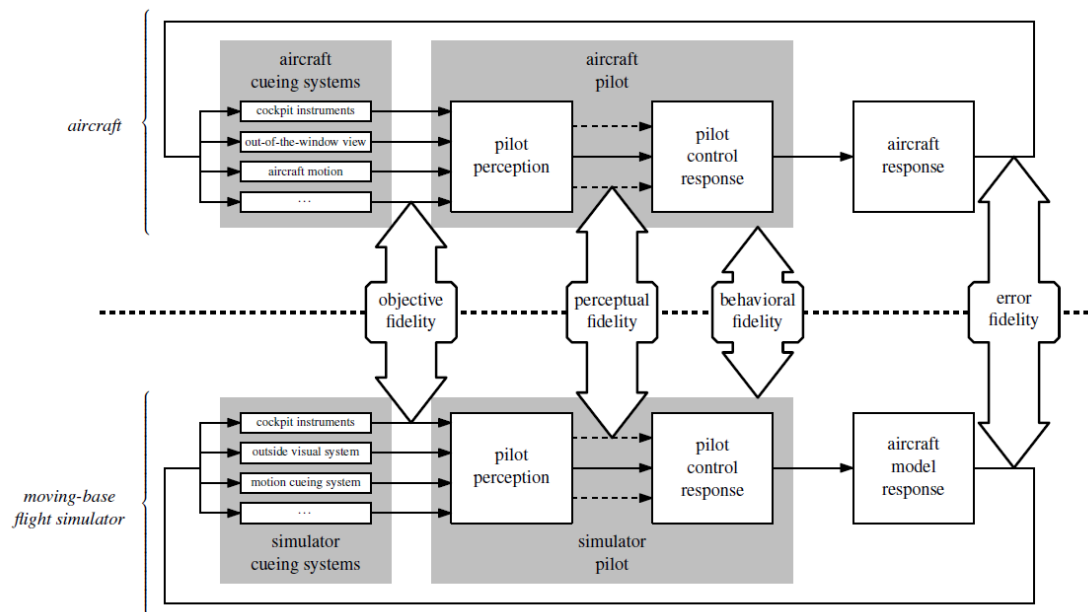


Figure 3-16. Flight simulator fidelity evaluated at mechanical, perceptual and behavioural levels, (Pool, 2012)

Greenberg and Blommer (2011) defined physical fidelity of driving simulators and introduced a four step framework that examined the type of errors and distortions that might occur at each stage of the cue representation process, those are modelling, real-time or sampling, cue generation, and presentation errors.

- Modelling errors included the powertrain and handling response of the modelled vehicle.
- Real-time or sampling error might be present in three ways of:
 - Quantification error e.g. finite precision in measuring the steering wheel angle.
 - Estimation error e.g. steering wheel velocity is usually approximated and not measured directly or the reference input to the MPC motion cueing algorithm needs predictions of future which is not usually available.
 - Temporal error e.g. the update rate and delays that are present in different components of simulator such as computational delays in visual simulations or in optimal MCAs.

- Cue-generation error, that occurs for transforming the model output to simulator specific commands. As an example, the static simulators the motion command is multiplied by zero and down-scaled in dynamic simulators.
- Presentation error, that is corresponding to the hardware constraints that may not simulate the commanded signal, such as limited bandwidth of motion platform, and resonances in the visual scene.

In addition to the above Greenberg and Blommer (2011) has also explained that there are other problems that might affect fidelity. These include the problem of extrapolation that refers to using the simulator for applications that they are not designed for e.g. simulating a specific manoeuvre that is out of the scope of simulator's operating regime. The problem of experimental artefacts may also lead to a reduction in fidelity. These are the factors occurring unwantedly and under effects the main simulation purpose, e.g. problem with vehicle model deviating the car's lateral position from centre line during a roadway design experiment. These artefacts may happen in any of the visual, motion and control cueing systems.

Although the various subsystems of a simulator as a whole affect fidelity, consideration of every single component and reviewing its effect is of the focus of many separate research studies. In this thesis, the focus is on the vestibular motion fidelity in driving simulators. Motion cueing fidelity could be explained by the extent of motion error, which is the difference in position, velocity and acceleration between the real and simulated vehicle. The position and velocity are generally perceived through the human visual system and represented by the simulator visual cueing system, and acceleration is perceived through the human vestibular and proprioceptive systems which the simulator MP reproduces.

Having a very large motion platform reduces the motion error; however, the purchase costs increase as the increases. For this reason, there is a trade-off between the MP workspace size and the resulting fidelity of motion cueing. The motion cueing fidelity criteria in the literature are often defined based on the undetectable amount of the motion errors by drivers/pilots, which is a threshold of an imperfect match between the motion and visual cues. In other words, the threshold of the discrepancy between the motion and visual cues, which is still perceived by drivers to be synchronised. These regions of synchronisation that are believed to be acceptable, and are commonly named as fidelity corridors, fidelity boundaries, coherent zones.

Fidelity corridors have been defined using both open and closed-loop methods. In the closed-loop case, drivers' subjective and objective behaviour data are measured during active driving (driver/pilot controls vehicle) and correlated to the motion error to draw the fidelity corridors. The open-loop method uses passive

driving (where the driver is not controlling the vehicle; i.e. in practice a passenger) to draw the fidelity corridors.

Moreover, motion error is usually evaluated in the time domain looking at amplitude error, or frequency domain using gain and phase errors. In the closed-loop time domain, a European collaborative project Berthoz et al. (2013) studied large driving simulators and have shown that motion that is objectively closer to the actual vehicle motion (one to one) in a given driving task is not always perceived as more realistic. They considered a slalom driving task, and prior research has consistently shown that down-scaled motion between 0.4 and 0.75 of full motion comes out as more realistic i.e. higher fidelity.

F16 pilots took part in a passive open-loop evaluation of motion scaling effect during a take-off run of a civil aircraft. The motion scaling for the surge translational and pitch tilting was systematically varied between 0 and 1, while the cut-off frequency of the filters was adjusted that keep the excursion of MP at a constant level in all cases. Their preferred scale-factor was about the 0.2, and unity scale-factor were too powerful to be realistic. It was suggested that the visual-vestibular mismatch is a result of an underestimation of visual cues that is found as an over-estimation of vestibular cues (Groen et al., 2001).

Human is proven to be sensitive not only to the acceleration but also to the jerk (derivative of acceleration) (Hosman and Stassen, 1999). The essential consistency between the visual and vestibular cues was studied considering the discrepancy between the level of the jerk and associated visual cues, that found the unity scale-factor is perceived to be too strong. A scale-factor with value around 0.7 was suggested to be acceptable for perception in a typical motion platform (Reid and Nahon, 1988).

In the early attempts of drawing the fidelity corridor in the frequency domain for research helicopter simulators, a minimum undetectable distortion between the visual and motion cues was examined in open-loop experiments. Only four phase and gain test points were examined for a tracking task with a frequency of 1 rad/s where the vestibular system has the highest perception gain (Sinacori, 1977), see the Figure 3-17 dashed line. Later, using the same approach, Schroeder (1999) postulated those results with more test points and further modified the fidelity borders, see Figure 3-17 solid line. It is observable that both authors predicted that a gain of 0.4 and a maximum phase error of 60 degrees will produce medium fidelity of motion cues. However, the accuracy of the three sections of low, medium and high fidelity is still open to debate.

In another closed-loop study of target following and disturbance rejecting tasks considering the effect of only roll motion in simulator compared to the real world, few different motion scenarios were examined on their subjective and performance effects. An optimal first order washout filter with 0.5 to 0.7 of amplitude reduction was introduced to have the acceptable motion fidelity (Jex et al., 1978).

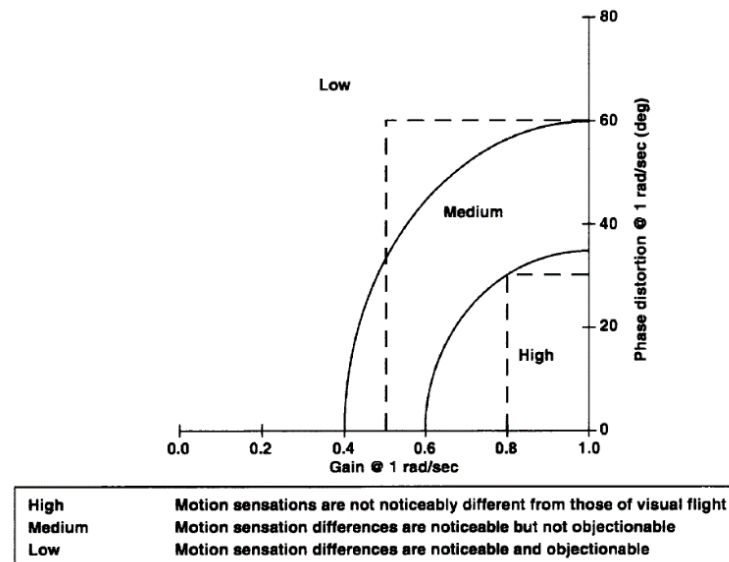


Figure 3-17. Sinacori (dashed line) and Schroeder (solid line) fidelity corridors for translational motion at 1 rad/s, (Schroeder, 1999).

It is possible to assess motion fidelity in a more objective way in order to be independent of the simulation scenario. A procedure was introduced to measure the performance of the simulator motion systems by AGARD (1977). Among all commonly used definitions for describing a motion system, they used five terms to define the motion system quality and limitations. The excursion limits, describing function, linearity and acceleration noises that were measured by the sinusoidal inputs of varying frequencies and amplitudes; the dynamic threshold measurements that were measured by input step acceleration; and the hysteresis by measurement of displacement using low frequency sinusoidal input.

This procedure was used to measure the motion performance of the VIRTTEX MP and to identify the cause of the poor performance. They found large bandwidth of the motion system, large cross-talking between the DoF, and nonlinearities in large velocities and accelerations indicating the need for further improvement to MCA to consider the observed characteristics (Grant et al., 2001). The excursion limit is among the measurement metrics that could be expressed by the signal-to-noise ratio (SNR) contours over a variety of frequencies and velocities i.e. a useful way of defining the operational and system limits of the MP. It is a diagram of velocity versus frequency plotted on a logarithmic scale, see Figure 3-18.

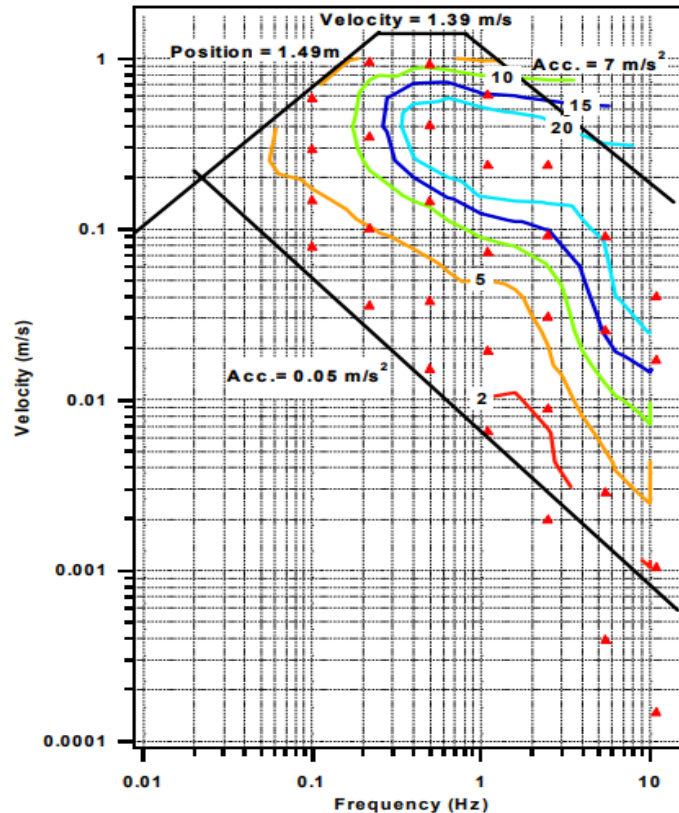


Figure 3-18. Signal-to-noise-ratio (SNR) contour for the VIRTEX simulator, (Grant et al., 2001)

In more recent studies Hosman and Advani (2016) used an objective motion cueing test (OMCT) method to evaluate the motion cueing of ten flight simulators believed to have acceptable fidelities to draw the fidelity corridors (named fidelity zones). In their method, no participants were involved and only objective measurements of the frequency response of the complete motion cueing system including the MCA and MP using a range of sinusoidal inputs were used to draw phase and gain Bode plots, as shown in Figure 3-19. The dashed lines present the fidelity corridors that are two standard deviations away from the mean value among all ten simulator tests. Fischer et al. (2016) adapted this method and tested in two driving simulators, and their performance result approximately fit in the OMCT phase and gain corridors. However, they discussed that for the method to be applicable in driving simulator evaluations, some modifications are needed such as higher input gains to raise the signal to noise ratio that allows clearer results, also higher logging frequency enhance the method for analysis of higher frequencies. Comparing the Sinacori with the OMCT it is visible that the gain of 0.4 and phase of 60 degrees is well within the OMCT fidelity zone.

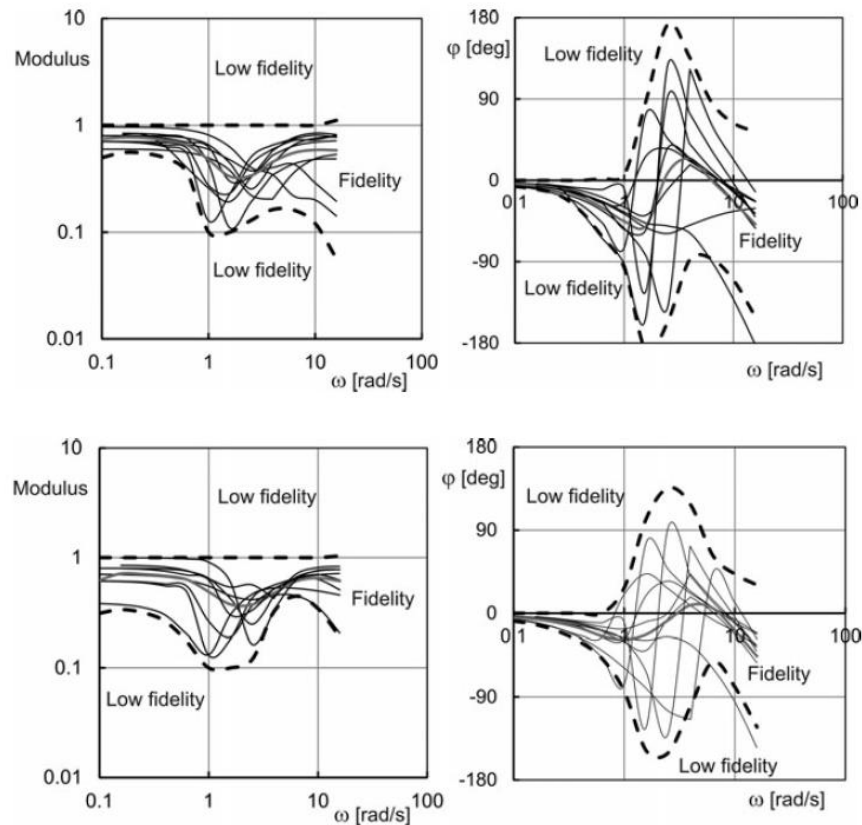


Figure 3-19. Fidelity corridors for longitudinal (top) and lateral (bottom) directions, (Hosman and Advani, 2016)

In similar research, amplitude and phase coherence zones were defined as motion cue gain and phase attenuation that although not being a perfect match to the visual cue, is still perceived by drivers to be coherent that was first introduced by van der Steen (1998) and later experimented by Valente Pais et al. (2010); Valente Pais (2013). It has been shown that amplitude coherence is a function of magnitude and frequency of a visual cue, whereas the phase coherence was argued to be not (however further investigation was needed). To define the corridors, the open-loop evaluations were used where participants were asked to determine ‘what is the strongest and weakest inertial motion amplitude that still matches the visual cue amplitude’. The experiments included flying manoeuvres and driving tasks. The ratio of vestibular amplitude to visual amplitude was defined as gain of mean coherence (GMC) and found to be decreasing with increasing stimulus amplitude, at low amplitude subjects found to be preferring larger vestibular motions than visual and vice versa in high amplitudes.

The amplitude coherence zone for the lateral (sway) motions is represented in Figure 3-20. It shows the amplitude coherence zones as coloured bars for two visual acceleration amplitudes of 0.5 and 1 m/s^2 in three frequencies of 2, 3, 5 rad/s on the horizontal axis, and motion gain on the vertical axis. The range of bars shows the zones of acceptable coherence between visual and motion cues. The

trends in the data show that both the upper and lower threshold gains decrease slightly with increasing frequency, and the gains are lower for the higher amplitude of the visual cue. It is noticeable that the mean minimum amplitude coherence zone of all frequencies is about 0.5 for 0.5 m/s^2 , and about 0.4 for 1 m/s^2 . The phase coherence was found not to be affected by either the amplitude or the frequency of the stimulus, and 19 degrees of phase-error is reported for mean yaw and pitch DoFs of all frequencies.

The accelerations available in driving tasks are usually higher than the 1 m/s^2 although that was the maximum amplitude evaluated in this study, requiring the minimum gain corridor of 0.4, which might be lower for higher acceleration demanding tasks. Moreover, the phase corridor is only available for the yaw DoF, requiring the maximum phase error of 19 degrees which might be different for other translational and rotational DoFs.

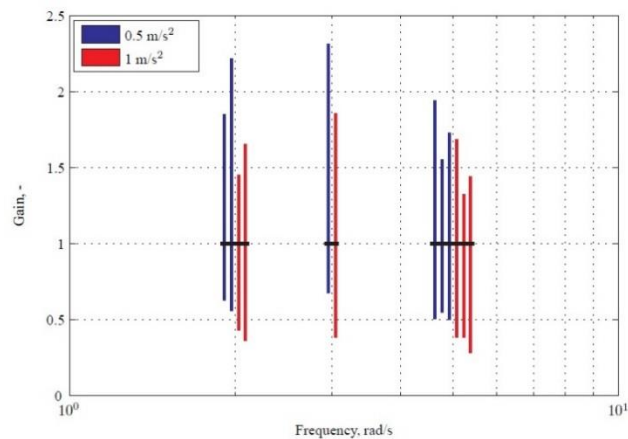


Figure 3-20. Coherence zones represented for sway motion. The horizontal black lines span different measurements made at the same visual amplitude (Valente Pais, 2013).

In similar research to the coherence zone, the participants were asked to select the appropriate vestibular motion to match the visual motion. They picked higher amplitude when reducing the vestibular motion from high to low than when increasing the motion from low to high (Correia Grácio et al., 2010). They later defined the optimal zone, an area between these upper and lower amplitudes and found that it lies within the coherence zone. Similar to the coherence zone the ratio of vestibular amplitude to visual amplitude was defined as gain of mean optimal (GMO) and found to be decreasing with the increase of amplitude and frequency, however opposed to the coherence zone the width of the optimal zone found to be not varying with the amplitude or frequency (Correia Grácio et al., 2013). Moreover, they found a strong dependency of the GMP to the quality of the visual cue (Correia Grácio et al., 2014).

A review of the studies on addressing the motion cueing fidelity corridors was presented in this section. There are many other aspects that make a general conclusion about the fidelity corridor debatable, such as being widespread around flight and driving simulators, defined for specific driving or flying manoeuvres that might be different for others, the difference in apparatus they have used including various visual and motion cueing systems. However, these are still the most reliable studies available today and many have postulated them in various applications. Later in Chapter 8, these fidelity corridors are used to address the MP workspace requirements.

In this thesis, the fidelity of a simulator is referred to the similarity between real and simulated driving in terms of drivers' subjective perception in the driving experience. It is a direct consequence of representation of visual, vestibular, proprioceptive and aural cues; however, the focus of interest is on the vestibular motion effect. The objective evaluations focus on data measurement and exploration of a phenomenon that might be a cause of motion cueing variations e.g. vehicle acceleration, steering wheel profiles and other metrics to analyse and compare.

Furthermore, the knowledge about acceptable motion fidelity corridors helps to find the best MCA tuning parameter settings for a specific MP. Since the MCA parameter values could be selected to minimise the motion discrepancy and respect the motion platform constraints. Nevertheless, available research provides the information on fidelity corridors, an automatic procedure for addressing MCA parameters was still a challenge; it was the motivation to develop an optimisation tool (Sadraei et al., 2016). The idea behind this was to find the classical MCA parameters through a mathematical optimisation method that minimises the motion error while considering both the fidelity corridor, and the constraints of the MP. On the other hand, using the fidelity corridors it is possible to address the MP workspace requirement to achieve an acceptable level of the fidelity, described in Chapter 8.

4 Motion Cueing in University of Leeds Driving Simulator

4.1 Classic algorithm for UoLDS

In this section, the classic motion cueing algorithm is developed based on the principles of the algorithm described in the previous chapter, and inspirations from the UoLDS originally designed classic MCA, to be used in the UoLDS apparatus. The main purpose is to prepare the model for the experiment described later in Chapter 5, that compares the classic and MPC algorithms. This model has two similar channels for representing the motion in surge/pitch and sway/roll and one channel for representing the motion in heave/yaw direction, see Figure 4-1. In the next sections, different components of the model are reviewed.

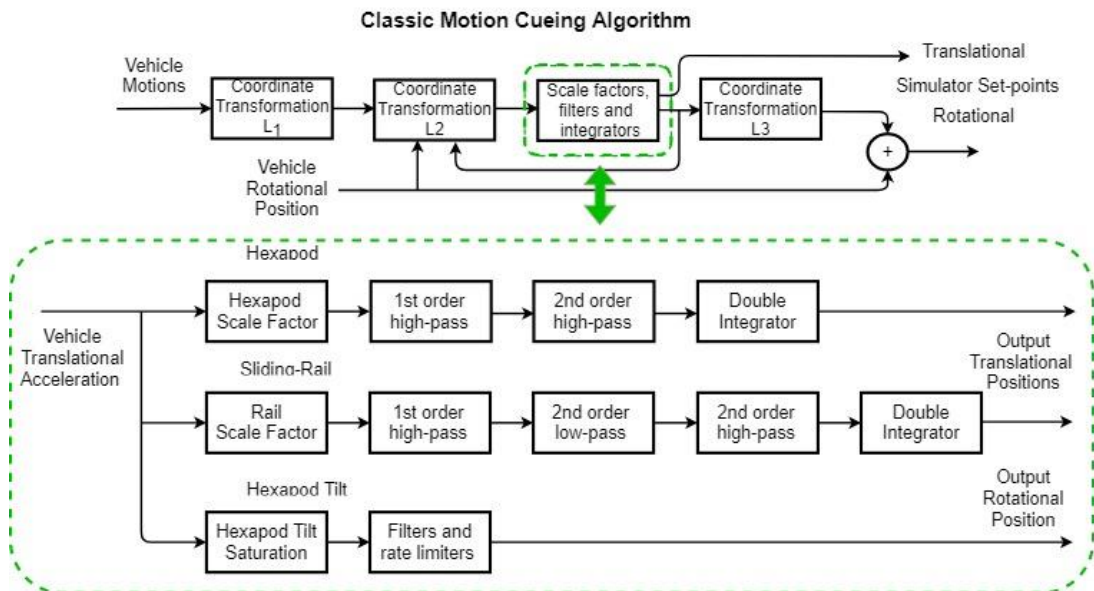


Figure 4-1. Schematic representation of the classic model structure for surge/pitch and sway/roll motion cueing channels

4.1.1 Coordinate transformation

In Figure 4-1 there are the coordinate transformations to have accurate motions with respect driver's head and then aligning the set-points in the MP coordinate system.

Coordinate transformation L_1 , transforms vehicle translational motions (vehicle model output) from driver's head frame to simulator moving frame (Eq. 4.1). Where v_h , a_h , ω_h and α_h are the translational and angular velocities and accelerations of the vehicle in driver's head frame, r_{s-h} is the constant vector from simulator moving frame to driver's head in the simulator, the v_s and a_s are the translational velocity and acceleration of the vehicle in the simulator moving frame, see Figure 4-2.

$$L_1 : \begin{cases} v_s = v_h + \omega_h \times r_{s-h} \\ a_s = a_h + \omega_h \times (\omega_h \times r_{s-h}) + \alpha_h \times r_{s-h} \end{cases} \quad 4.1$$

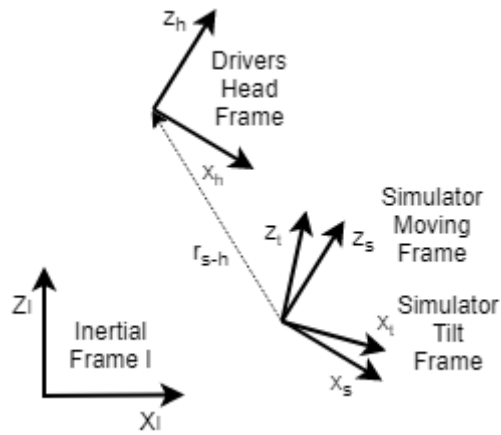


Figure 4-2. Overview of reference frames, side view

Coordinate transformation L_2 , transforms the motions from simulator moving frame to tilt coordination frame. It takes into account the current rotations of simulator moving frame (roll ϕ , pitch θ , yaw ψ) due to vehicle's roll, pitch and yaw, to rotate the translational accelerations from the moving frame to tilt frame. Having the MCA work in the tilt coordination frame brings an advantage of better control over translational motion scaling, and the tilt parameters i.e. maximum tilt angle, angular velocity and acceleration. Both guarantees the right feeling of motion to the drivers. However, it causes the output MP translational set-points of the rail and hexapod to be in the tilt frame, while those required to be in the inertial frame. This is a minor issue since the vehicle roll and pitch angles are small, and it is an acceptable approximation between the frames. Furthermore, working in tilt coordination frame keeps the model to be a second order system and avoids the need for a feedback closed-loop that is available in formulating the MCAs in the inertial frame; which changes the model to a fourth order system, and requires more care for selecting the filter parameters and stability.

An intrinsic Tait–Bryan angles with a sequence of elementary rotations of R_x , R_y and R_z was chosen for this transformation, which first rotates around the z-axis by ψ degree second rotates around new y' by θ degree and third rotates around the new x'' by ϕ degree.

$$a_t = L_2 a_s$$

$$R_x = \begin{bmatrix} 1 & 0 & 0 \\ 0 & \cos \phi & -\sin \phi \\ 0 & \sin \phi & \cos \phi \end{bmatrix} R_y = \begin{bmatrix} \cos \theta & 0 & \sin \theta \\ 0 & 1 & 0 \\ -\sin \theta & 0 & \cos \theta \end{bmatrix} R_z = \begin{bmatrix} \cos \psi & -\sin \psi & 0 \\ \sin \psi & \cos \psi & 0 \\ 0 & 0 & 1 \end{bmatrix} \quad 4.2$$

$$L_2 = R_x(\phi)R_y(\theta)R_z(\psi)$$

$$L_2 = \begin{bmatrix} \cos \theta \cos \psi & -\cos \theta \sin \psi & \sin \theta \\ \sin \phi \sin \theta \cos \psi + \cos \phi \sin \psi & -\sin \phi \sin \theta \sin \psi + \cos \phi \cos \psi & -\sin \phi \cos \theta \\ -\cos \phi \sin \theta \cos \psi + \sin \phi \sin \psi & \cos \phi \sin \theta \sin \psi + \sin \phi \cos \psi & \cos \phi \cos \theta \end{bmatrix}$$

To transfer the angular velocity of the vehicle ω to the rate of changes of Euler angles \dot{e} in simulator inertial frame. It is possible to relate them using above rotation matrices; the first Euler angle undergoes two rotations, the second angle one rotation and the third no rotation that results in Eq. 4.3.

$$\begin{aligned} \omega &= \begin{bmatrix} p \\ q \\ r \end{bmatrix}, e = \begin{bmatrix} \phi \\ \theta \\ \psi \end{bmatrix} \\ \omega &= R_x R_y \begin{bmatrix} 0 \\ 0 \\ \dot{\psi} \end{bmatrix} + R_x \begin{bmatrix} 0 \\ \dot{\theta} \\ 0 \end{bmatrix} + \begin{bmatrix} \dot{\phi} \\ 0 \\ 0 \end{bmatrix} \\ \omega &= \begin{bmatrix} 1 & 0 & \sin \theta \\ 0 & \cos \phi & -\sin \phi \cos \theta \\ 0 & \sin \phi & \cos \phi \cos \theta \end{bmatrix} \dot{e} \end{aligned} \quad 4.3$$

Taking the inverse

$$\dot{e} = \begin{bmatrix} 1 & \sin \phi \tan \theta & -\cos \phi \tan \theta \\ 0 & \cos \phi & \sin \phi \\ 0 & -\sin \phi \sec \theta & \cos \phi \sec \theta \end{bmatrix} \omega$$

Coordinate transformation L_3 , extracts the rotational angles due to simulator tilting and yaw cueing to Euler Angles of MP inertial frame (MP rotational set-points required to be in Euler Angles). It is afterwards summed with the vehicle's roll and pitch motions directly fed from vehicle model (already in Euler angles) then set points are commanded for rotational motions. Although the Euler angles cannot be simply summed up, due to the small roll and pitch it is an acceptable approximation. Using the transformation matrix L_2 and name it R (for sub indexing) where $R = L_2$ then the Euler angles are obtained as Eq. 4.4.

$$L_3 : \begin{cases} \theta = \tan^{-1} \left(\frac{R_{32}}{R_{33}} \right) \\ \phi = \tan^{-1} \left(-\frac{R_{31}}{\sqrt{R_{11}^2 + R_{21}^2}} \right) \\ \psi = \tan^{-1} \left(\frac{R_{21}}{R_{11}} \right) \end{cases} \quad 4.4$$

4.1.2 Tilt coordination

To represent the acceleration felt through the tilting the gravity vector needs to be aligned to the driver's head vestibular system reference frame. Using the rotation matrix in Eq. 4.2, the gravity vector is transformed to the simulator tilt coordination frame as

$$\vec{g} = R_x(\phi)R_y(\theta) \begin{bmatrix} 0 \\ 0 \\ g \end{bmatrix} = \begin{bmatrix} g \sin \theta \\ -g \cos \theta \sin \phi \\ g \cos \theta \cos \phi \end{bmatrix}$$

In order to do linear frequency analysis, the \vec{g} vector is linearized in small roll θ and pitch ϕ degrees, where the gravity vector becomes

$$a_{tilt} = \vec{g} = \begin{bmatrix} g\theta \\ -g\phi \\ g \end{bmatrix} \quad 4.5$$

The usual method to apply the limitations on tilt angular velocity and acceleration is by adding a second order low-pass filter and changing its cut-off frequency and damping ration to get to the desired tilt setting. However, the choices are limited to be a function of the cut-off frequency and damping ratio considering the stability of the response, further discussed in Chapter 7. To have a broad range of tilt setting it is possible to introduce nonlinearity by adding rate limiters. In the model used for the experiment in Chapter 5 the tilting channel includes is a series of a gain and saturator to limit the maximum tilt angle θ_{max} , a first order low-pass filter with cut-off frequency ω_{lp2} , a rate limiter to apply the tilting angular velocity limit $\dot{\theta}_{max}$, a first order high-pass filter, second rate limiter to apply the tilting angular acceleration limit $\ddot{\theta}_{max}$, and an integrator, all in a sequence. Cascade of the above filters and integrator (excluding the limiters) results in a second order lowpass filter, where there is a nonlinear process taking place on the signal.

4.1.3 Complete plant model

Further down in Figure 4-1 within the green dashed line, there are three rows including block diagrams of scale-factors, high-pass and low-pass filters, saturation, rate limiters and integrators, there are other gains for unit transformation and gravity vector available in the model which are not shown here. The main difference with simple classic algorithms is where the higher third order high-pass filters were used for the onset cues of the hexapod and sliding rail, and a second order low-pass filter. The first two rows are generating the transient linear motions for hexapod and sliding rail MPs, and the third row generates the sustained acceleration through tilt coordination, which is then summed with the vehicle's pitch or roll angles to send as set-points to MP. The saturator limits the maximum tilt angle and the two rate limiter is limiting both angular velocity and acceleration of tilting.

Considering longitudinal (surge) vehicle acceleration as input, the transient part of accelerations with a higher frequency is generated by rail and hexapod translational manipulations, in row one and two. It needs to be mentioned that the low-pass filter in the sliding rail row is designated to create a bandpass filter that overlaps with the high-pass filter of the hexapod in the first line, this helps to avoid representing the same range of frequencies twice by both rails and hexapod. In the third row, the

sustained acceleration that has lower frequencies and separated by low-pass filter is then represented through tilt coordination by hexapod rotational manipulation.

The sliding rail, hexapod translational position and rotational degrees are related to the input vehicle acceleration in the simulator tilt frame, by multiplication of the gain and transfer functions as Eq. 4.6.

$$\begin{aligned} \text{Hexapod} \quad \frac{x_{hex}}{a_t} &= \frac{k_1 G_{hp1} G_{hp2}}{s^2} = k_1 \frac{s}{(s + \omega_{hp1})} \frac{s^2}{(s^2 + 2\zeta\omega_{hp2}s + \omega_{hp2}^2)} \frac{1}{s^2} \\ \frac{\theta_{yaw}}{\omega_t} &= \frac{k_1 G_{hp1} G_{hp2}}{s} = k_1 \frac{s}{(s + \omega_{hp1})} \frac{s^2}{(s^2 + 2\zeta\omega_{hp2}s + \omega_{hp2}^2)} \frac{1}{s} \end{aligned} \quad 4.6$$

$$\begin{aligned} \text{Sliding rail} \quad \frac{x_{rail}}{a_t} &= \frac{k_1 G_{hp1} G_{hp2} G_{lp2}}{s^2} \\ &= k_1 \frac{s}{(s + \omega_{hp1})} \frac{s^2}{(s^2 + 2\zeta\omega_{hp2}s + \omega_{hp2}^2)} \frac{\omega_{lp2}^2}{(s^2 + 2\zeta\omega_{lp2}s + \omega_{lp2}^2)} \frac{1}{s^2} \end{aligned}$$

Summation of the accelerations in the three rows gives us the total acceleration that driver senses in the simulator. In each row, the parameters are listed in Table 4-1 and Table 4-2, as explained before the process of selecting them is mainly a trade-off between the maximum representation of motion cues in time and/or frequency domain, and considering the MP envelope and capability constraints. The frequency response of the algorithm of the separate hexapod and rail translational, tilt motions and summation of all to a set of parameters is presented in Figure 4-3.

Table 4-1. Classic MCA parameters for surge/pitch and sway/roll channels

	Parameters
Hexapod Translation	<ul style="list-style-type: none"> • Scale-factor, $k_{hex,tr}$ • First order high-pass filter, cut-off frequency ω_{hp1} • Second order high-pass filter, cut-off frequency ω_{hp2}
Sliding rail Translation	<ul style="list-style-type: none"> • Scale-factor, $k_{rail,tr}$ • First order high-pass filter, cut-off frequency ω_{hp1} • Second order high-pass filter, cut-off frequency ω_{hp2} • Second order low-pass filter, cut-off frequency ω_{lp2}
Hexapod Tilt Coordination	<ul style="list-style-type: none"> • Scale-factor, $k_{hex,tl}$ • Second order low-pass filter, cut-off frequency ω_{lp2} • Tilt angle θ_{max}, angular velocity $\dot{\theta}_{max}$, acceleration $\ddot{\theta}_{max}$

Table 4-2. Classic MCA parameters for heave/yaw channel

	Parameters
Hexapod Rotation	<ul style="list-style-type: none"> • Scale-factor gain, k_2 • First order high-pass filter, cut-off frequency ω_{hp1} • Second order high-pass filter, cut-off frequency ω_{hp2}

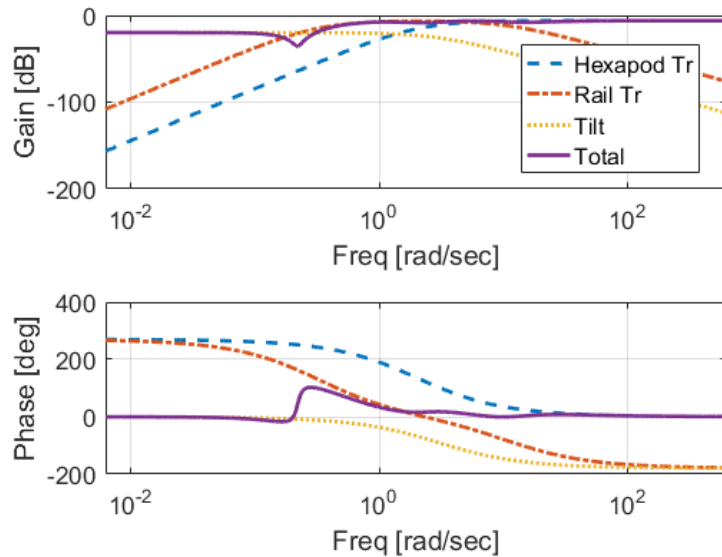


Figure 4-3. Frequency response of the classic algorithm, hexapod translation $k_{hex,tr} = 0.5$, $\omega_{hp1} = 1.51$, $\omega_{hp2} = 2.35$, rail translation $k_{rail,tr} = 0.5$, $\omega_{hp1} = 0.26$, $\omega_{hp2} = 0.35$, $\omega_{lp2} = 11$, Tilt $\omega_{lp2} = 3$

It needs to be mentioned that the classic algorithm is only used in the experiment of Chapter 5, wherein those driving manoeuvres the roll and pitch angles of vehicle do not exceed more than 4 degrees, hence there was no need for motion cueing in these directions and they were fed directly to MP. This is unlike the flight simulators where the roll, pitch and heave are always of large values and need motion control. Similarly, and the driving tasks were on the flat ground and the heave motion of vehicle always between ± 0.1 meters and fits within the UoLDS MP workspace, hence was directly fed to MP.

4.2 MPC algorithm for UoLDS

In this section, the MPC motion cueing algorithm is developed based on the principles of the algorithm described in Chapter 3, to be used in the UoLDS apparatus. The main purpose is to prepare the model for the experiments described later in Chapter 5 and 6. This model has two similar channels for representing the motion in surge/pitch and sway/roll and one channel for representing the motion in

heave/yaw direction, see Figure 4-4. The equations are derived for each of the channels separately, however, are presented only for surge/pitch in the next sections.

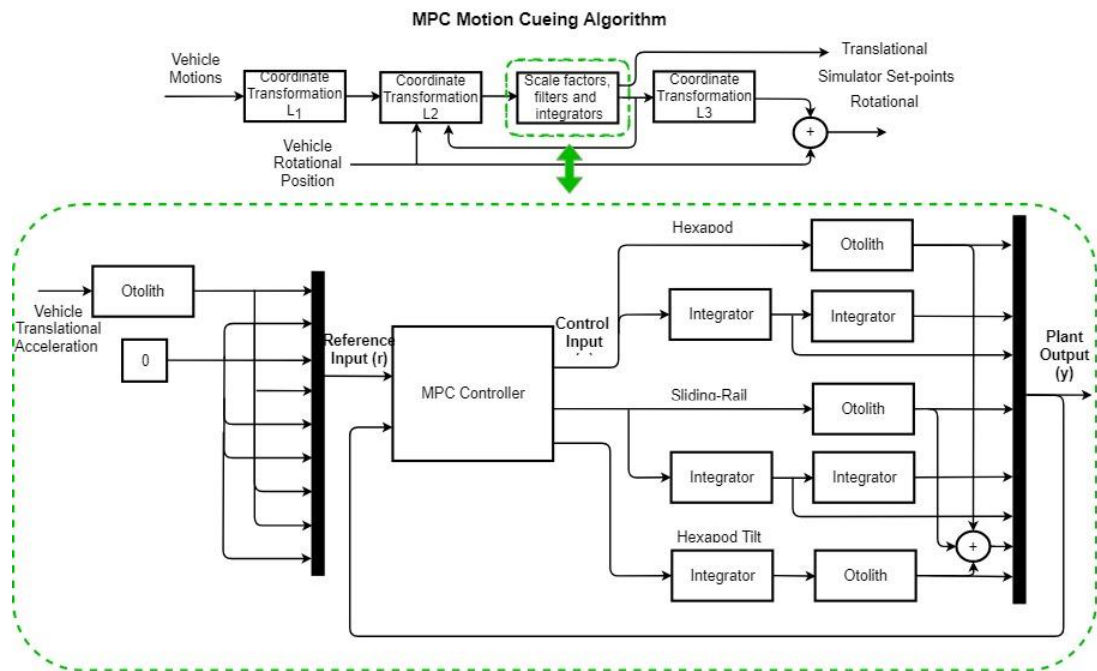


Figure 4-4. Schematic representation of MPC model structure for surge/pitch motion cueing channel

4.2.1 Coordinate transformation

On top of Figure 4-4 there are the coordinate transformations to have accurate motions with respect driver's head reference frame, and then aligning the motions in the MP coordinate system set-points. The full description is provided in section 4.1.1.

4.2.2 State-space realisation of the vestibular model

The perception models were reviewed in Chapter 2. To be able to use them in MPC formulation those needed to be converted in state-space form. The transfer function model for the otoliths is the one proposed by Telban and Cardullo (2005). They have used a combination of the model parameters from other authors i.e. long and lead time constants from (Ormsby, 1974) and gain from (Hosman, 1996) model, and have shown the model to be suitable for application in MCA models. The semicircular canals model used here were the ones being proposed by Zacharias (1978) from a review of the literature of vestibular motion sensation and to be applicable for MCA, that has been repeatedly used in many studies (Reid and Nahon, 1985; Augusto and Loureiro, 2009; Garrett and Best, 2013). The same transfer functions are used for all surge, sway and heave channels.

The semicircular canal transfer function where $\hat{\omega}$ and ω , in general, are the perceived and input vehicle angular velocities in roll (p), pitch (q), and yaw (r) directions

$$G_{scc} = \frac{\hat{\omega}}{\omega} = \frac{T_a S}{(1 + T_a S)} \frac{T_L S}{(1 + T_L S)(1 + T_S S)}$$

The state-space realisation of the transfer function is

$$x_{scc}(k+1) = A_{scc}x_{scc}(k) + B_{scc}u_{scc}(k)$$

$$y_{scc}(k) = C_{scc}x_{scc}(k)$$

Where

$$A_{scc} = \begin{bmatrix} -\left(\frac{1}{T_a} + \frac{1}{T_S} + \frac{1}{T_L}\right) & -\left(\frac{1}{T_a T_L} + \frac{1}{T_a T_S} + \frac{1}{T_S T_L}\right) & -\frac{1}{T_a T_S T_L} \\ 1 & 0 & 0 \\ 0 & 1 & 0 \end{bmatrix} \quad 4.7$$

$$B_{scc} = \begin{bmatrix} 1 \\ 0 \\ 0 \end{bmatrix}, C_{scc} = \begin{bmatrix} \frac{1}{T_S} & 0 & 0 \end{bmatrix}, D_{scc} = [0]$$

In the design of the heave/yaw channel, the reference inputs of the vehicle rotational velocities are transformed to the simulator inertial frame Euler angular rates using the Eq. 4.3. Therefore, the control input and output for yaw tracking variables are in the simulator inertial frame. However, the vehicle translational heave motion is in simulator tilt frame, as of other translational channels.

$$u_{scc} = \dot{e}_{\phi, \theta, \psi}, y_{scc} = \hat{e}_{\phi, \theta, \psi}$$

The otolith transfer function where \hat{a} and a , in general, are the perceived and input vehicle accelerations is

$$G_{oto}(s) = \frac{\hat{a}}{a} = \frac{K(1 + T_a S)}{(1 + T_L S)(1 + T_S S)}$$

The state-space realisation of the transfer function is

$$x_{oto}(k+1) = A_{oto}x_{oto}(k) + B_{oto}u_{oto}(k)$$

$$y_{oto}(k) = C_{oto}x_{oto}(k)$$

where

$$A_{oto} = \begin{bmatrix} -\left(\frac{1}{T_S} + \frac{1}{T_L}\right) & -\frac{1}{T_S T_L} \\ 1 & 0 \end{bmatrix} \quad B_{oto} = \begin{bmatrix} 1 \\ 0 \end{bmatrix} \quad 4.8$$

$$C_{oto} = \begin{bmatrix} \frac{KT_a}{T_S T_L} & \frac{K}{T_S T_L} \end{bmatrix} \quad D_{oto} = [0]$$

The reference inputs of the vehicle translational accelerations are transformed from simulator moving frame to the simulator tilt frame using the Eq. 4.2. Therefore, the control input and output tracking variables are in the simulator tilt frame.

$$u_{oto} = a_t \quad y_{oto} = \hat{a}_t$$

The vestibular model parameters are presented in Table 4-3.

Table 4-3. Vestibular parameters used in models, from

	K	T_a	T_S	T_L
Otolith (Telban and Cardullo, 2005)	0.4	10	5	0.016
Semicircular canal (Reid and Nahon, 1985)	-	30	0.1	10.2

To take advantage of imposing constraints on position and velocity of the MP and applying weights in the cost function it is required to have them explicitly available as output variables. This is possible by including the integrators in the plant model. By augmenting an integrator into the semicircular canal the state-space model updates to

$$A_{scc} = \begin{bmatrix} -\left(\frac{1}{T_a} + \frac{1}{T_S} + \frac{1}{T_L}\right) & -\left(\frac{1}{T_a T_L} + \frac{1}{T_a T_S} + \frac{1}{T_S T_L}\right) & -\frac{1}{T_a T_S T_L} & 0 \\ 1 & 0 & 0 & 0 \\ 0 & 1 & 0 & 0 \\ 0 & 0 & 0 & 0 \end{bmatrix} \quad 4.9$$

$$B_{scc} = \begin{bmatrix} 1 \\ 0 \\ 0 \\ 1 \end{bmatrix}, \quad C_{scc} = \begin{bmatrix} \frac{1}{T_S} & 0 & 0 & 0 \\ 0 & 0 & 0 & 1 \end{bmatrix}, \quad D_{scc} = \begin{bmatrix} 0 \\ 0 \end{bmatrix}$$

Recalling the fact that the vehicle angular velocity in roll and pitch directions are directly fed to motion platform, and there was no need for motion control in those directions. Therefore, the control input u_{scc} is the angular velocity \dot{e} in yaw direction; the state vector x_{scc} includes x_1, x_2 and x_3 the otolith states and output yaw degree ψ ; the output vector y_{scc} includes the \hat{e}_ψ perceived output yaw angular velocity and degree ψ .

$$u_{scc} = \dot{e}_\psi, \quad x_{scc} = \begin{bmatrix} x_1 \\ x_2 \\ x_3 \\ \psi \end{bmatrix}, \quad y_{scc} = \begin{bmatrix} \hat{e}_\psi \\ \psi \end{bmatrix}$$

By augmenting two integrators into the otolith state-space model it becomes

$$A_{oto} = \begin{bmatrix} -\left(\frac{1}{T_S} + \frac{1}{T_L}\right) & -\frac{1}{T_S T_L} & 0 & 0 \\ 1 & 0 & 0 & 0 \\ 0 & 0 & 0 & 1 \\ 0 & 0 & 0 & 0 \end{bmatrix} \quad B_{oto} = \begin{bmatrix} 1 \\ 0 \\ 0 \\ 1 \end{bmatrix} \quad 4.10$$

$$C_{oto} = \begin{bmatrix} \frac{K T_a}{T_S T_L} & \frac{K}{T_S T_L} & 0 & 0 \\ 0 & 0 & 0 & 1 \\ 0 & 0 & 1 & 0 \end{bmatrix} \quad D_{oto} = \begin{bmatrix} 0 \\ 0 \\ 0 \end{bmatrix}$$

The control input u_{oto} is the vehicle input acceleration in a single direction of x, y, z; the state vector x_{oto} includes x_1 and x_2 the otolith states and output position $p_{x,y,z}$ and velocity $v_{x,y,z}$; the output vector y_{oto} includes the $\hat{a}_{x,y,z}$ perceived acceleration, velocity $v_{x,y,z}$ and position $p_{x,y,z}$ of the motion platform in a direction.

$$u_{oto} = a_{x,y,z}, \quad x_{oto} = \begin{bmatrix} x_1 \\ x_2 \\ p_{x,y,z} \\ v_{x,y,z} \end{bmatrix}, \quad y_{oto} = \begin{bmatrix} \hat{a}_{x,y,z} \\ v_{x,y,z} \\ p_{x,y,z} \end{bmatrix}$$

4.2.3 Tilt coordination

To represent the acceleration felt through the tilting the gravity vector needs to be aligned to the driver's head vestibular system reference frame. Using the rotation matrix in Eq. 4.2, the gravity vector is transformed to the simulator tilt coordination frame as

$$\vec{g} = R_x(\phi)R_y(\theta) \begin{bmatrix} 0 \\ 0 \\ g \end{bmatrix} = \begin{bmatrix} g \sin \theta \\ -g \cos \theta \sin \phi \\ g \cos \theta \cos \phi \end{bmatrix}$$

By linearization in small roll θ and pitch ϕ degrees the gravity vector becomes

$$a_{tilt} = \vec{g} = \begin{bmatrix} g\theta \\ -g\phi \\ g \end{bmatrix}$$

Assuming the tilting as the acceleration that the driver is feeling, then similar to the linear translation acceleration it is passed to the vestibular otolith model to have the perceived tilting acceleration. It is also required for tracking of the model's reference input vehicle acceleration, which is already a perceived linear acceleration. In this regard, the state-space model is updated as

$$x_{tilt}(k+1) = A_{tilt}x_{tilt}(k) + B_{tilt}u_{tilt}(k)$$

$$y_{tilt}(k) = C_{tilt}x_{tilt}(k)$$

where

$$A_{tilt} = \begin{bmatrix} -\left(\frac{1}{T_S} + \frac{1}{T_L}\right) & -\frac{1}{T_S T_L} \\ 1 & 0 \end{bmatrix} \quad B_{tilt} = \begin{bmatrix} g \\ 0 \end{bmatrix}$$

$$C_{tilt} = \begin{bmatrix} \frac{KT_a}{T_S T_L} & \frac{K}{T_S T_L} \end{bmatrix} \quad D_{tilt} = \begin{bmatrix} 0 \\ 0 \end{bmatrix}$$

4.11

To have control over the tilting angular velocity and acceleration the MPC plant model is designed in a way that the control input u_{tilt} is an angular velocity, therefore imposing constraints on the control variable u_{tilt} and its rate of changes Δu_{tilt} is actually the constraints on the tilting angular velocity and acceleration. Moreover, there is an integrator in the tilting plant model that produces the tilting degrees as another output of the model, which prepares the ability to have the

constraints on maximum tilting degree or maximum amount of acceleration represented to drivers through tilting. The updated tilting model becomes

$$\begin{aligned}
 A_{tilt} &= \begin{bmatrix} -\left(\frac{1}{T_S} + \frac{1}{T_L}\right) & -\frac{1}{T_S T_L} & g \\ 1 & 0 & 0 \\ 0 & 0 & 0 \end{bmatrix} & B_{tilt} &= \begin{bmatrix} 0 \\ 0 \\ 1 \end{bmatrix} \\
 C_{tilt} &= \begin{bmatrix} \frac{KT_a}{T_S T_L} & \frac{K}{T_S T_L} & 0 \\ 0 & 0 & 1 \end{bmatrix} & D_{tilt} &= [0]
 \end{aligned} \tag{4.12}$$

where

$$u_{tilt} = \dot{\theta}, y_{tilt} = \begin{bmatrix} \hat{a}_{tilt} \\ \theta_{tilt} \end{bmatrix}$$

In the above equation $\dot{\theta}$ is the tilt pitch angular velocity, and \hat{a}_{tilt} is the perceived longitudinal acceleration through tilting and θ_{tilt} is the tilt pitch attitude.

4.2.4 Complete plant model

Further down in Figure 4-4 within the green dashed line, the plant model for surge/pitch channel is shown. There are three rows including block diagrams of vestibular model and integrators; there are few other gains for unit transformation and gravity vector available in the model which are not shown here. The first two rows are generating the transient linear motions by hexapod and sliding rail MPs, and the third row generates the sustained acceleration through tilt coordination. Moreover, there is a summation that adds the three perceived accelerations as another output of the plant, that is the total acceleration driver is sensing in the simulator.

$$\hat{a}_{total} = \hat{a}_{rail} + \hat{a}_{hex} + \hat{a}_{tilt} \tag{4.13}$$

Therefore, the plant model used here has three control inputs and nine outputs corresponding to the hexapod and rail translations and hexapod tilting and summation of all. The combined plant model is

$$x_{mpc}(k+1) = A_{mpc}x_{mpc}(k) + B_{mpc}u_{mpc}(k)$$

$$y_{mpc}(k) = C_{mpc}x_{mpc}(k)$$

where

$$\begin{aligned}
 A_{mpc} &= \begin{bmatrix} A_{oto} & 0 & 0 \\ 0 & A_{oto} & 0 \\ 0 & 0 & A_{tilt} \end{bmatrix}_{11 \times 11} & B_{mpc} &= \begin{bmatrix} B_{oto} & 0 & 0 \\ 0 & B_{oto} & 0 \\ 0 & 0 & B_{tilt} \end{bmatrix}_{11 \times 3} \\
 C_{mpc} &= \begin{bmatrix} C_{oto} & 0 & 0 \\ 0 & C_{oto} & 0 \\ 0 & 0 & C_{tilt} \\ C_{oto}^* & C_{oto}^* & C_{tilt}^* \end{bmatrix}_{9 \times 11} & D_{mpc} &= [0]_{9 \times 3}
 \end{aligned} \tag{4.14}$$

C_{oto}^* and C_{tilt}^* are the row vectors extracted from the first row of their belonging matrices.

$$u_{mpc} = \begin{bmatrix} u_{rail} \\ u_{hex} \\ u_{tilt} \end{bmatrix}, x_{mpc} = \begin{bmatrix} x_{oto} \\ x_{tilt} \end{bmatrix} = \begin{bmatrix} x_{1_rail} \\ x_{2_rail} \\ p_{rail} \\ v_{rail} \\ x_{1_hex} \\ x_{2_hex} \\ p_{hex} \\ v_{hex} \\ x_{1_tilt} \\ x_{2_tilt} \\ \theta_{tilt} \end{bmatrix}, y_{mpc} = \begin{bmatrix} \hat{a}_{rail} \\ v_{rail} \\ p_{rail} \\ \hat{a}_{hex} \\ v_{hex} \\ p_{hex} \\ \hat{a}_{tilt} \\ \theta_{tilt} \\ \hat{a}_{total} \end{bmatrix}$$

The state vector (manipulated variables) of the plant x_{mpc} consist of the states of the otolith model x_1, x_2 that available in the rail, hexapod and tilt; the position and velocity states of the rail p_{rail}, v_{rail} and hexapod p_{hex}, v_{hex} ; the tilt pitch angle θ_{tilt} . Output vector (tracking variables) consist of perceived acceleration, velocity and position represented by the rail $\hat{a}_{rail}, v_{rail}, p_{rail}$ and hexapod $\hat{a}_{hex}, v_{hex}, p_{hex}$; perceived acceleration represented through tilting \hat{a}_{tilt} and tilting degree θ_{tilt} ; and total perceived acceleration \hat{a}_{total} .

At every time sample, current and future reference input samples (over the prediction horizon H_p) are fed to the controller for tracking the output variables. The controller calculates a set of control inputs to minimise the error between the estimated values of all output variables and the provided references. Hence in this application, the perceived accelerations of the rail \hat{a}_{rail} , hexapod \hat{a}_{hex} , tilting \hat{a}_{tilt} all together with the \hat{a}_{total} are tracking the perceived input acceleration \hat{a}_t . Those are the errors to be minimised in the cost function. The remainder of the output variables are set to be tracking zero that helps to bring the motion platforms back to their neutral position when there is no input acceleration to be tracked; it is also possible to do this by weighting the control inputs, this is similar to washout in the classic algorithm.

The constraints could be set on u_{rail} and u_{hex} that defines the maximum acceleration that a motion platform is capable of, are soft constraints; on u_{tilt} and Δu_{tilt} that defines tilt angular velocity and acceleration, hard constraints. The constraints are being set on the output variables including maximum velocity to be within motion platform capability, soft constraint; and maximum position considering the workspace excursion limits, hard constraints for both rail v_{rail} and p_{rail} and hexapod v_{hex} and p_{hex} ; on θ_{tilt} that defines the maximum tilt degree that hexapod is allowed to rotate, hard constraint. Since there were hard constraints on output variables of rail and hexapod translational motions, their input acceleration was not

constrained to avoid any infeasibility, although those are weighted to avoid big changes. Thus, the whole vector of constrained variables is

$$[u_{tilt} \ \Delta u_{tilt} \ | \ v_{rail} \ p_{rail} \ v_{hex} \ p_{hex} \ \theta_{tilt}]$$

In the cost function Eq. 3.15, weights define the relationship between and within each of the manipulated or output tracking variables. They are applied to output variables in matrix Q , manipulates variables in matrix S and rate of changes of manipulated variables in matrix R . In this formulation the matrices $Q_{9 \times 9}$, $S_{3 \times 3}$ and $R_{3 \times 3}$ are diagonal matrices. Weighting in the matrix Q defines how the tracking of the perceived accelerations to input vehicle acceleration is important compared to MP velocity and position, or between the acceleration generated by rail \hat{a}_{rail} and by hexapod \hat{a}_{hex} . The weighting on the velocity and position variables guarantee that the platform returns to neutral states. Weights on the control input manipulated variables S and its rate of changes R prevents big changes of control input. Parameters available for tuning in each channel are listed in Table 4-5 and Table 4-4.

Table 4-4. MPC parameters for heave/yaw channel

	Parameters
Hexapod Translation	<ul style="list-style-type: none"> Acceleration tracking weight, w_{h1} Velocity tracking weight, w_{h2} Position tracking weight, w_{h3} + constraint
Hexapod Rotation	<ul style="list-style-type: none"> Velocity tracking weight, w_{h1} Position tracking weight, w_{h2} + constraint

Table 4-5. MPC parameters for surge/pitch and sway/roll channels

	Parameters
	<ul style="list-style-type: none"> Prediction horizon H_p Control horizon H_u
Hexapod Translation	<ul style="list-style-type: none"> Acceleration tracking weight, w_{h1} Velocity tracking weight, w_{h2} Position tracking weight, w_{h3} + constraint
Sliding rail Translation	<ul style="list-style-type: none"> Acceleration tracking weight, w_{r1} Velocity tracking weight, w_{r2} Position tracking weight, w_{r3} + constraint
Hexapod Tilt Coordination	<ul style="list-style-type: none"> Tilt angular velocity constraint, $\dot{\theta}_{max}$ Tilt angular acceleration constraint, $\ddot{\theta}_{max}$ Acceleration tracking weight, w_{t1} Position tracking weight, w_{t2} + constraint θ_{max}
Total	<ul style="list-style-type: none"> All acceleration tracking weight, w_a

The parameter values are selected for the experiments in Chapter 5 and 6, based on a logical concept of weighting the states and outputs which are dependent on the plant structure, all together needed tens of offline simulation trials and simulator testing to pick up best candidates. Exploration of weight effects on motion cueing response is thoroughly described in Chapter 7.

5 Assessment of Low-Friction Motion Cueing

5.1 Introduction

The emphasises on the flight and driving simulators field of research on the effect of motion cueing has developed to a state that has risen the ambiguity of how the characteristics of dynamic simulators motion cueing subsystems affect the fidelity, and sparsely there is a standardised technique available correlating them to the fidelity level. To this end in this chapter, an experiment is described where the main components of the simulator motion cueing system are manipulated as independent variables and evaluated in different driving tasks. Those are motion cueing algorithms (MCA) and motion platform (MP) size. The evaluations are based on the subjective perception of the driving experience in various motion configurations, and exploration of the effect of the changes on their performance.

The evaluations are done specifically for vehicle testing in low-friction winter conditions, such as routinely carried out by Jaguar Land Rover (JLR) in the northern parts of Sweden. Among the few driving task candidates, two tasks were selected and replicated in the driving simulator (Markkula et al., 2016). The reason was to cover the probable effect that driving manoeuvres might have in the evaluations. A more restricted, less motion demanding driving task was selected, where the lateral vehicle motion is mainly excited in a single frequency. Furthermore, a test track type manoeuvre that demands higher motion and includes a variety of frequencies for lateral motions was selected. Each of the tasks required closed-loop driver control using multiple perceptual stimuli.

It has been reported that the MCA has effects on drivers' subjective preferences. The effect might be due to the type of MCA used or their tuning setting. Among the first comparisons between the classic and model predictive control (MPC) algorithms (Dagdelen et al., 2009; Augusto and Loureiro, 2009) it was reported that drivers subjectively preferred the MPC over classic. Similar subjective preference of MPC over classic has been reported in (Fang and Kemeny, 2012b; Fang and Kemeny, 2012a; Fang and Kemeny, 2014). In driver in the loop evaluation between MCAs, drivers rated MPC higher than classic in linear and non-linear handling regimes (Garrett and Best, 2013). Although there is research available evaluating the effect of MCAs on the subjective perception of realism, there is little research available that has considered the effect on objective behaviour. Thus, as the first aim of this study, two MPC and classic type of MCAs are selected to perform a motion cueing fidelity comparison among them.

It has been reported that motion has effects on drivers' subjective preferences and objective performance. Lakerveld et al. (2016) investigated the yaw and sway motion effect on drivers' performance, they reported that the sway motion improved disturbance-rejection performance, and yaw motion reduced control activity. Moreover, in extreme scenarios such as slalom, motion feedback improved the driver's performance. Feenstra et al. (2010) showed that steering corrections i.e. number of steering wheel reversals and relatively high-frequency corrections were reduced when the magnitude of motion cue was increased.

It has been consistently shown that for specific tasks where driving simulator's MP is capable of representing the full motion to drivers, down-scaled motion between 0.4 and 0.75 of full motion is considered as more realistic i.e. higher fidelity; also vehicle control gets more demanding with larger motion scales (Berthoz et al., 2013; Savona et al., 2014). It might suggest that drivers seek to avoid a large motion to decrease their control effort. This has prompted to have the MP size as another aim of this study. Thus, as the second aim of this study three sizes of MP workspace are considered to perform a motion cueing fidelity comparison among them. The MCA comparisons (first aim) took place in each of the MP sizes, to find out probable interactions between MP sizes and MCAs.

In summary in this chapter, the variations in simulator motion cueing subsystems that have the most effect on motion cueing fidelity are assessed considering the manipulations to MCAs and MPs, and different driving tasks. For evaluations, the measurements include drivers' subjective ratings and their objective behaviour. The following sections elaborate more on, how an experiment was designed that could address comparison between the simulator motion configurations, the research questions and hypotheses are defined. Finally, the analysis of results is presented to answer the research questions followed by discussion and conclusion.

5.2 Experimental design

The two independent variables for this study were the MCA with two levels (MPC and classic) and MP size with three levels (small, medium and large). At each of the six (2x3) combinations of these independent variables, subjective ratings and drivers' objective performance were collected. To increase the power of the effect of experimental manipulations and limited availability in the number of professional drivers participating in this study, a repeated measure experiment design was used where the same participants took part in all combinations of the independent variables. It was a balanced design where there is an equal number of observations for each of the treatments. The differences between the MCAs were more subtle compared to the MP sizes, as a result, the experiment was designed in a nested

way that the comparisons between MCAs to be of primary focus for drivers and the MPs as the secondary focus. This helps the drivers to emphasise on distinguishing between the MCAs in each MP size, while next they evaluate the MP sizes.

Eight test drivers from JLR attended University of Leeds Driving Simulator (UoLDS) and drove a Jaguar XF car on low friction snow condition in both slalom task (SLM) and Land Rover handling track (LHT) and completed a questionnaire about quality of their drive on overall assessment, motion cueing and vehicle assessment, also their objective performance were collected. They were familiar with real world testing of the vehicle in similar low-friction winter condition and driving tasks.

The experiment had each of the drivers accomplish first the slalom and second the LHT driving tasks. They were consecutively presented with the six motion configurations corresponding to the permutations of three MP sizes and two MCAs. Drivers were presented with three pairs of motion configurations to make a comparison between them:

- Small-MPC (S-M) and small-classic (S-C)
- Medium-MPC (M-M) and medium-classic (M-C)
- Large-MPC (L-M) and large-classic (L-C)

This allowed examining how drivers perceived the effects of MCA and MP on fidelity and the extent to which the drivers agreed with each other's ratings. For both of the tasks, the above pairs were presented to four drivers in 1-2-3 (small-medium-large) group order and for the other four in 3-2-1 (large-medium-small) group order, drivers were randomly assigned to be in each group. The order of the MCAs within each of the above pairs was counter-balanced per driver, meaning that in each pair some drivers might start with the classic and some with the MPC. The full counterbalancing table for all drivers is provided in Appendix B.

5.3 Dependent variables

In this section, to allow the formulation of research questions and hypotheses, the subjective and objective behaviour metrics are explained. Further details about how the metrics are applied to the collected data are provided in section 5.10.

5.3.1 Subjective measures

In order to evaluate the simulator motion cueing fidelity among the motion configurations, a subjective questionnaire was designed. The participated drivers were all professionals that had the experience of driving the same car for the same driving tasks in the real world. As a result, the question anchors were selected with the range of realistic/unrealistic to have a comparison between real and virtual driving experience.

The idea behind selecting the questions originated to cover different aspects. From general impressions of realism to the ones related to simulator motion characteristics, as well as those that matter in real world vehicle evaluations. This led to prepare the questions in three categories of overall assessments, motion cueing and vehicle assessment, with each consisting of three more detailed questions, see Table 5-1.

Table 5-1. Simulator subjective questions

Question Category & Number	Question	Rating Anchors	
Overall Assessment	1	How realistic was the overall experience in the simulator compared to reality	unrealistic/realistic
	2	Do you think that these simulator configurations would be useful for testing and comparing vehicle designs	not useful/useful
	3	How easy was it to perform the task	difficult/easy
Motion Cueing	4	I felt motion in general was	unrealistic/realistic
	5	I felt longitudinal acceleration/deceleration and pitch were	unrealistic/realistic
	6	I felt lateral acceleration/deceleration and roll were	unrealistic/realistic
Vehicle Assessment	7	How confident were you in assessing the available grip and the limit of the vehicle's ability	unrealistic/realistic
	8	I felt under/oversteering was	unrealistic/realistic
	9	I felt time delay of vehicle response was	unrealistic/realistic

The overall assessment questions were designed to evaluate how the motion configurations might influence the overall driving experience between real and virtual environments, questions 1 and 3, and whether the drivers get the impression of the simulator as a reliable tool for testing vehicle designs, question 2.

The motion cueing questions were of special importance to us in this experiment. Question 4 was included to look at general realism of perception that drivers would

have at each configuration. Moreover, the different MCAs and MPs were expected to mainly affect the surge (longitudinal) and sway (lateral) motions, therefore questions 5 and 6 were included to acquire more specific ratings in each direction.

The vehicle assessment questions were chosen based on JLR test drivers' specific attribute language to describe the various characteristics of a vehicle, including the ride, steering and handling qualities (Jamson et al., 2014a). However, the main focus of this study was not to address exactly these qualities, but more of a glimpse to see whether motion configurations might influence them. In Chapter 6 these driven attribute qualities are further studied.

5.3.2 Objective measures

During the theme 3 of PSi project, the objective measurement methods have been developed for assessing the fidelity of driving simulators. The foundation of this research approach, as laid out in previous project deliverables (Jamson et al., 2013; Jamson et al., 2014a; Jamson et al., 2014b; Jamson et al., 2015) is the performance of correlation studies, using behavioural metrics in a so-called "Utility Triplet" to compare test results obtained in a real vehicle with those obtained in simulators with different capabilities. According to Markkula et al. (2016); Romano et al. (2019) the utility triplet was proven to be a useful structured approach for this type of behavioural fidelity assessment.

The utility triplet includes three major categories: aggregated performance, time series and driver model which are explained below (Boer et al., 2014), see Table 5-2.

- **Aggregate performance**
Performance in relation to the task specification. "This includes spatial and temporal proximity to constraints as well as completion time. Focus is placed on accuracy or the degree to which the task was performed".
- **Time series**
Profile of the vehicle states and driver control actions, as a function of time and distance depending on what is most meaningful for comparison per task/manoeuvre. Focus is placed on vehicle response rather than control actions.
- **Driver model**
Model that characterises the driver as a controller. The structure and coefficients of the model reflect the driver-vehicle interactions.

The aggregate performance metrics reflects the performance of a driver in terms of general qualities of driving, and it is related to the driving task definition. As it is shown in Table 5-2, the lap time is the completion time of a driving task, and interpretation of its values depend on the experiment design. The speed variability is the variation of speeds that driver has throughout the driving task.

In the driving task where the drivers are asked to adapt their speed as fast (LHT task described later), lower lap time shows improved performance in a successful attempt. In general, lower speed variation is considered to be a better performance. However, higher speed variation might be indicative of better performance if it happens together with lower lap time in a successful attempt.

In the driving task where the drivers are asked to keep a constant speed (SLM task described later), the lower lap time in a successful attempt shows improved performance; because during the experiment, they might need to reduce their speed to complete the task that results in higher lap time. The lower speed variation shows better performance since drivers were asked to keep a constant speed.

The lateral position deviation is the maximum deviation of the vehicles lateral position from a trajectory. Here average trajectory of all drivers and motion configurations is used; hence the lower value always shows a better relative performance.

Several objective metrics were candidates for the time series metrics, to account for aspects of behaviour not covered by the aggregate performance and driver model metrics. Among the time series metrics, the number of steering reversals has been emphasised to be an appropriate measure of drivers control activity (Anon, 2015), that means reduced steering reversal rate shows a more relaxed style of driving. The steering reversal rate was selected to be 1 °/s and 10 °/s to capture small and large steering adjustments (Markkula et al., 2016). The other time series metrics are related to the maximum vehicle motions in different longitudinal, lateral and yaw directions.

The driver model metrics were given by the driver model, which is the desired path yaw rate error (DPYRE) model described in section 2.3. This model uses three parameters (delay time, preview time and gain) and the desired path to predict the driver behaviour (steering rate). For the desired path, the average trajectory of all drivers was used in each of the driving tasks. It has been shown that using a task-dependent fixed preview time did not affect the model fits much (Markkula et al., 2016). After a preliminary analysis of the data collected in this experiment, no effect of preview time was found, hence a fixed value of $T_p = 1.7$ s was selected for SLM, and $T_p = 3$ s was selected for LHT.

Table 5-2. Utility triplet used for objective behaviour analysis

Land Rover Handling Track (LHT)	Slalom (SLM)
Aggregate performance	
<ul style="list-style-type: none"> • Lap time • Skid/spin outs • Speed variability • Lateral position deviation 	<ul style="list-style-type: none"> • Lap time • Skid/spin outs + Cones knocked over • Speed variability
Time series	
<ul style="list-style-type: none"> • Maximum longitudinal velocity • Maximum lateral velocity (absolute value) • Maximum longitudinal acceleration • Maximum lateral acceleration (absolute value) • Maximum yaw rate (absolute value) • Steering wheel reversal rate (1 degree) • Steering wheel reversal rate (10 degree) 	
Driver model (DRYPE)	
<ul style="list-style-type: none"> • Response delay time T_R • Steering gain K 	

5.4 Experiment configurations

Regarding the aim of this study the interest was to evaluate the drivers' subjective fidelity and objective behaviour in various MP sizes and MCAs, it was decided to select three different sizes of the MP workspace, and do the comparison between the two MPC and classic MCAs in each of the MP sizes.

5.4.1 Motion platforms

The UoLDS hexapod manipulator has relatively limited translational motion workspace which is about 0.6 meter for surge and sway directions, the reason is the availability of sliding rail that adds 5 metres to it resulting in 5.6 metres of workspace envelope in both directions. There are 23 degrees of yaw motions available, however, in simultaneous excursions in all DoFs it goes down to 15 degrees. Looking at vehicle roll and pitch motions (less than 4 degrees), assures that the hexapod workspace can sufficiently represent in them. In this study to reduce the variability between motion configurations, the MP envelope in heave, roll, pitch and yaw were identical but varied in surge and sway workspace size provided by the sliding rail, see Table 5-3. Hence, the only difference between the MP configurations are

- Hexapod & ± 0.5 (m) of rail surge and sway, i.e. small
- Hexapod & ± 1.5 (m) of rail surge and sway, i.e. medium
- Hexapod & ± 2.5 (m) of rail surge and sway, i.e. large

Table 5-3. Motion platform specifications configured in this experiment

	Hexapod						Sliding rail	
	Surge (m)	Sway (m)	Heave (m)	Roll (deg)	Pitch (deg)	Yaw (deg)	Surge (m)	Sway (m)
Small	±0.1	±0.1	±0.1	±10	±10	±15	±0.5	±0.5
Medium	±0.1	±0.1	±0.1	±10	±10	±15	±1.5	±1.5
Large	±0.1	±0.1	±0.1	±10	±10	±15	±2.5	±2.5

The hexapod's full capability is always used in all three configurations. The small motion platform was chosen to have similar total workspace envelope as the JLR Cruden simulator motion platform, which is a 6 DoF hexapod without sliding rails, and higher frequency bandwidth (Brems et al., 2015) than the UoLDS motion platform mainly due to lighter weight of the system. Another difference between the UoLDS and JLR simulator is the steering wheel force feedback. The UoLDS has a TRW electric power-assisted steering (EPAS) system, mounted at the base of the original steering column of the cockpit vehicle, whereas the JLR simulator has the Cruden control loading, providing torque directly at the handwheel.

5.4.2 Motion cueing algorithms

As it was explained in Chapter 4, the MCAs with full 6 DoFs usually includes three separate channels that each couple a rotational motion to translational motion, conventionally the channels are surge/pitch, sway/roll and heave/yaw.

The classic algorithm is tuned for the worst-case scenario of vehicle motion inputs in a manoeuvre. The tuning is always a complicated procedure because several criteria need to be met at the same time. In this regard, an automatic procedure for finding optimal parameters for the classic MCA was developed (Sadraei et al., 2016). It was an optimisation method that minimised the motion errors in time and frequency domain to meet the fidelity criteria and respect the MP workspace constraints. The MCA parameter settings in this experiment were based the on same optimisation method, although extended to include the tilt coordination, see more details in Chapter 8. The optimisation variables included only the MCA high-pass filter cut-off frequencies using the fixed scale-factors, and fixed parameters for tilting.

The tuning of the MPC algorithm is slightly simpler process compared to classic since the MP workspace constraints are always respected by the controller. However there more tuning parameters compared to classic, those are the prediction and control horizons, and depending on the model structure there are weights on the control input, states and output variables, all play a critical role in the response of the model. The tuning of the MCA parameter settings in this

experiment was based on guides about tuning process by Augusto and Loureiro (2009); Maran (2013), in addition to observations of tens of offline simulation trial and error to pick up best set of parameters.

The offline objective analysis to compare the motion cueing response between the experimental configurations was not a straight forward task; especially in manoeuvres including a variety of curves and straight lines that included a wide range of frequencies and amplitudes. Moreover, the frequency response of the MPC algorithm was not available by the time of designing this experiment. Therefore, the main comparisons were feasible and carried out only in the time domain, even though it provided limited information about the comparison between the experimental configurations.

The main measure for the comparisons was the root mean square (RMS) of the difference between the vehicle motion (before scaling) and MCA output acceleration (including scaling) and if the simulator MP workspace is exploited properly to vehicle motion input, provided in Table 5-4. As it is observable in classic, sometimes the workspace is not as exploited as MPC that might have been a reason for the RMS to be higher. Further tuning of the classic that includes the tilt coordination (introduced in Chapter 7 and 8) might result in better exploitation of workspace and reduction in RMS value, although it is also dependant on the individual performance of drivers during a manoeuvre. To validate the appropriateness of the experiment configurations, the simulator technicians, staff members, and professional drivers performed piloting and described their motion experience to approve if the tunings for both classic and MPC were comparable.

Table 5-4. Motion configurations acceleration and excursion differences

Motion Platform	Motion Cueing Algorithm	Slalom (SLM)				Land Rover Handling (LHT)			
		RMS ($a_i - a_s$)		Max excursion		RMS ($a_i - a_s$)		Max excursion	
		X	Y	X	Y	X	Y	X	Y
Small	Classic	0.40	0.76	0.48	0.43	0.93	1.38	0.36	0.39
	MPC	0.25	1.06	0.44	0.5	1.08	1.27	0.49	0.49
Medium	Classic	0.36	0.52	1.21	1.29	0.89	1.35	1.11	1.29
	MPC	0.24	0.95	1.45	1.50	0.97	1.23	1.44	1.09
Large	Classic	0.31	0.48	1.93	2.22	0.88	1.34	2.38	2.28
	MPC	0.21	0.54	2.44	2.50	0.91	1.14	2.17	1.83

In the tuning process of the MPC algorithm for lateral motion of the slalom task, it was observed of its poor performance when the constant look-ahead information is available and the prediction horizon is long. That was further investigated to the only sinusoidal inputs, and a similar response was observed. To reduce the effect the prediction horizon was decreased for the lateral motion compared to the longitudinal motion, although the horizon could not be decreased freely due to stability of the system. Despite the improvements, when it was compared to classic, the response was still worse. The response of the MPC and classic to different inputs are presented in Chapter 7. This was the main reason for hypothesising the preferences of drivers for classic over MPC in slalom manoeuvre, described in next section.

The selection of tilt setting has a major effect on the perception and performance of the drivers in simulators. The studies on the trade-off between slow/prompt build-up of tilting and corresponding high/low motion errors have shown mixed results. It has been shown that the simulation of linear self-motion became more realistic with the presence of tilt, as long as the tilt rate remained under the angular velocity perception threshold of 3 deg/s (Groen and Bles, 2004). Moreover, the choice of tilt setting has been reported to be more critical with the increase of frequency vehicle motion in a manoeuvre. Comparison between the tilt rate of 3 (limited) and 30 (unlimited) deg/s with focus on the perceived longitudinal acceleration during an emergency brake, showed the subjective preference of the unlimited tilting over the limited (Fischer and Werneke, 2008). Grant et al. (2009) observed contrary results in a study comparing a few different MCA parameter settings, including the high and low tilt rate in a lane change task. It was reported that drivers' performance and their subjective ratings were improved in the low tilt rate setting.

In a subjective comparison between ranges of tilt parameters for the slalom driving task a tilt rate of 6 deg/s and 8 deg/s^2 was found to be an acceptable set of parameters (Colombet et al., 2016). Jamson (2010), evaluated the effect of simulator motion cueing subsystems on human perception and behaviour in different driving tasks. It was concluded that the drivers' "performance varied little between sub-threshold and more rapid tilt when the sliding rail was activated". However, while the rail was inactive, the drivers' performance was better with higher tilt rate; that means the translational motion availability allows a slower tilt, which provides both improved driving task performance and perceived realism.

Considering the range of tilt-coordination parameters used in the literature, in this experiment after many trial and pilot studies the settings of the Table 5-5 were found to be appropriate, see Appendix D. The classic and MPC tuning parameter

values for the translational motion channels, for the three MP sizes and driving tasks are listed in Appendix B.

Table 5-5. Tilt rotational parameters used in this study

Angular Velocity Threshold	Rotational Acceleration Threshold
4 <i>deg/s</i>	4 <i>deg/s²</i>

5.5 Research questions and hypotheses

The overall aim of this study was to investigate how variations in simulator motion cueing components affect drivers' subjective ratings of simulator fidelity and their objective behaviour. Motion cueing configurations are selected including various MCAs and MPs and they are evaluated for different driving tasks. The fidelity assessments are based on the variations in drivers subjective ratings, and exploration of their objective behavioural performance. Two research questions are defined, as associated with these aims:

Research question 1 – How do the different MCAs affect the drivers' subjective ratings of simulator fidelity and their objective behaviour?

Within each MP configurations, pairwise comparison of MCAs takes place; the fidelity is assessed by subjective questionnaires and also objectively quantified using the utility triplet.

The hypothesis is: For the subjective ratings, in all the three MP sizes higher simulator fidelity is expected to be with MPC in LHT and classic in SLM. This is due to the poor performance of MPC in evasive manoeuvres when there is no variable look-ahead information available. It is expected to see the results in the 'overall assessment' and 'motion cueing' group of questions. For the objective evaluations, no specific hypotheses are formulated in relation to this research question.

Research question 2 – How do the different MPs affect the drivers' subjective ratings of simulator fidelity and their objective behaviour?

Within each of the MCAs, comparison between the MP configurations takes place; fidelity is assessed by subjective questionnaires and also objectively quantified using the utility triplet.

The hypothesis is: For the subjective evaluations, in both of the MCAs highest simulator fidelity is expected to be with medium MP for SLM task, this is due to the similar results in literature showing a scaled motion between 0.4 and 0.75 of full motion is considered as more realistic and it lies in the medium MP size of this experiment. It is expected to see the results in 'overall assessment' and 'motion cueing' group of questions; no hypothesis formulated for LHT. In objective

evaluations of LHT and SLM tasks, for the aggregated performance no hypothesis is formulated; for the time series with the increase of MP size a decrease in values of drivers steering reversal rate metrics is expected, as a measure of control activity; for the driver model with the increase of MP size larger control delays are expected, which might require smaller control gains in compensation.

5.6 Driving tasks

The driving tasks selected for this experiment are among the usual JLR low friction vehicle testing tasks, also the drivers participated in this experiment are all familiar with them in the real world. As part of the P*Si* Theme 3 project, the same driving tasks were replicated in the simulator virtual environment. The test tracks are at Jaguar Land Rover Revi Test Centre, formed on the frozen Lake Hornavan close to Arjeplog in Northern Sweden, shown in Figure 5-1. Revi consists of a number of prepared ice tracks, each suitable for specific driving tasks.

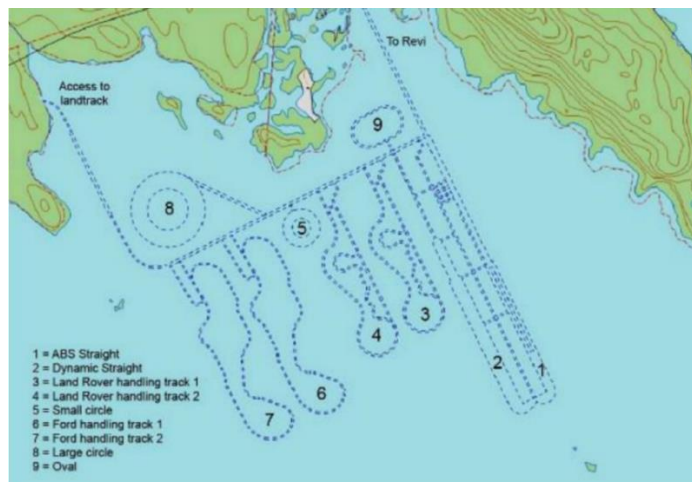


Figure 5-1. The JLR Revi test centre

The driving tasks were designed and documented during an experimental refinement stage at the Revi test centre. This period resulted in the selection of eight distinct tasks, each designed to require closed-loop driver control using multiple perceptual stimuli (Markkula et al., 2016). To the scope of this project, two tasks that had been considered in real world vehicle testing are replicated in the driving simulator and used in this study, below is the description of the tasks.

5.6.1 Land Rover Handling Track (LHT)

The LHT is the outer line of track number 3 in Figure 5-1. This track included multiple turns and straight line sections of packed snow. The drivers start driving clockwise after the entry gate (two cones on long straight line near the sharp turn) and negotiate to exit gate (two cones on the middle of the long straight line near the

sharp turn). In this task, drivers were instructed to select third gear and adapt speed so as not to lose control.

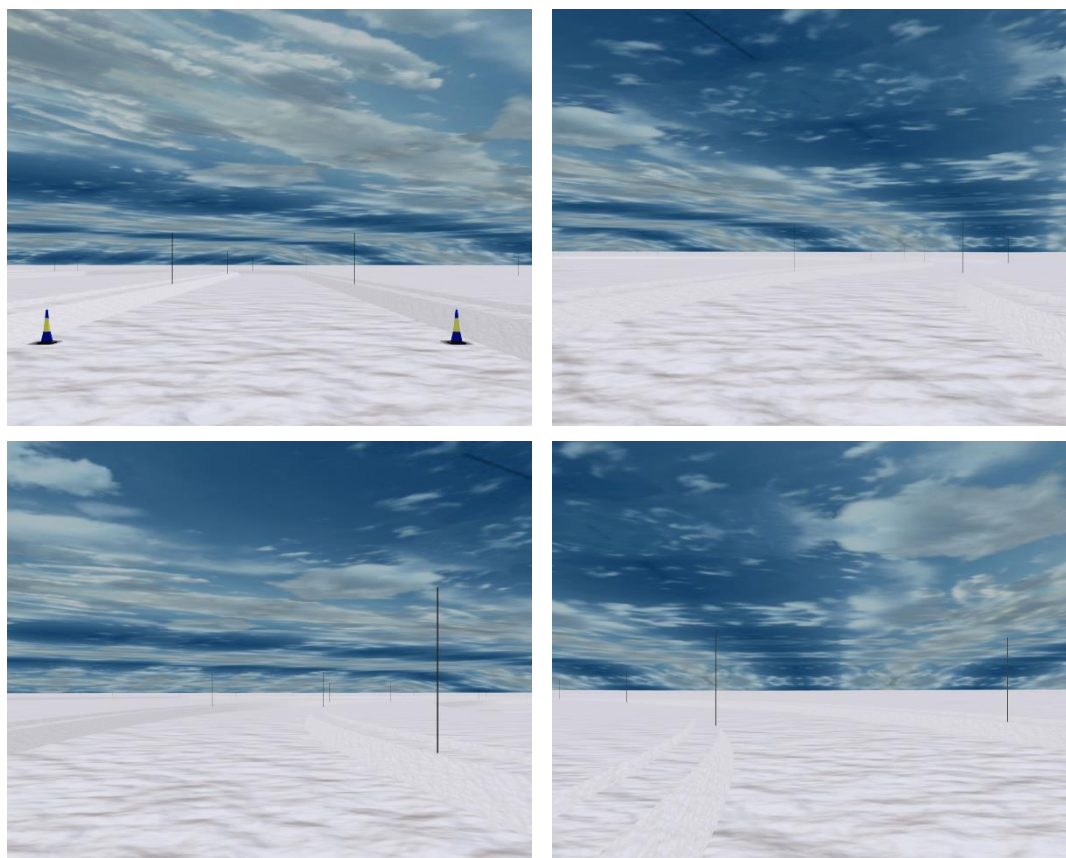


Figure 5-2. Simulated LHT course

5.6.2 Slalom (SLM)

The slalom takes place on the packed snow at the south end of the track marked 2 in Figure 5-1. After the entry gate (two cones 5m apart), there were eight cones to negotiate, each spaced by 25m which replicates a 0.2Hz sinusoidal trajectory while negotiating the cones. The task involved rapidly steering the vehicle from its initial lane to a parallel lane around each cone without striking any. The slalom required drivers to perform at 45 km/h throughout in manual transmission selected in second gear; they were also asked to always prioritise safe and successful driving as during real world vehicle evaluations.

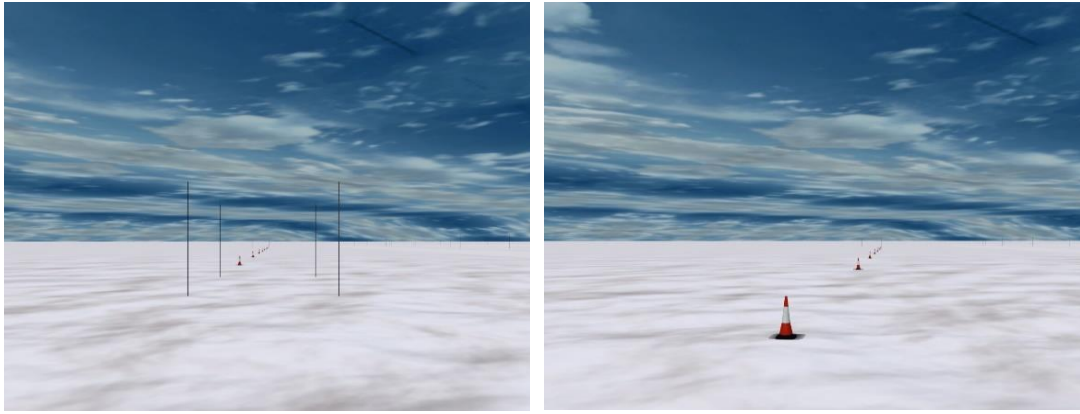


Figure 5-3. Simulated Slalom Layout

5.7 Drivers

Nine drivers were involved in the study, all JLR employees with considerable experience in winter vehicle testing. One of the drivers got motion sick after finishing the first Slalom task, consequently in total full data for eight of the drivers were used in the analysis.

The low number of participants was due to JLR personnel availability constraints. There were not as many particular drivers that could do similar tests, and these number of professional drivers are representative of the small pool of the number of drivers available that had experience in winter vehicle testing.

Moreover, the focus of the project was about the applicability of simulator for vehicle design in low-friction winter condition, and normal drivers could not be employed since the normal drivers' perception and performance might differ. Furthermore, compromise on the statistical power of the experiment was worth, to keep the samples as homogenous as possible by keeping the age band in 35-45 and use drivers with similar experience and skills.

5.8 Test vehicle

A model of the dynamics for the Jaguar XF car was executed in real-time mode using the multi-body simulation system SimPack, executing on 8 cores of a dual Xeon CPU 16-core Concurrent iHawk hardware platform running the RedHawk real-time derivative of the RedHat Linux operating system. The Jaguar XF model has been developed and extensively validated by JLR with real world data. The distribution of longitudinal speed and yaw rate to steering wheel angle, measured in the lane change, slalom and circular curve across many drivers and repetitions in both reality and simulator were compared. Despite the observed differences, the vehicle yaw rate response was well captured by the SimPack model in most of the tests. Observed differences between the real and model vehicle model response, was explained to be due to high variability of surface and unpredictability in reality

than in the simulator, and accuracy of tyre model in certain regimes (Markkula et al., 2016).

SimPack incorporates the implementation of a tyre model to represent the interaction that occurs between a vehicle's road wheels and the surface of the road. For these experiments, the well-known Delft tyre model was used. The model provides support for both non-uniform surface height and friction profiles through the use of two mesh based curve regular grids (CRG). These two grids implemented to a resolution of 50 cm in both X and Y, define values representing the surface elevation and friction (μ value) with a constant value of 0.35 friction at each point on the surface.

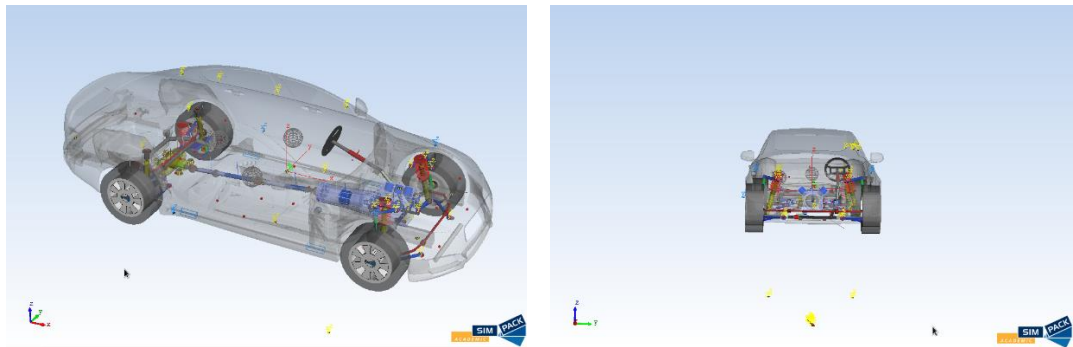


Figure 5-4. Graphical representation of the SimPack multi-body model of the Jaguar XF vehicle dynamics

5.9 Experiment procedure

The JLR test drivers attended the UoLDS in pairs per day. Drivers were sent briefing documents and the questionnaire a few days before arriving at the University of Leeds. On arrival, the drivers were talked through the briefing material on the simulator operation (safety, consent forms), see Appendix B, and they signed a consent form. In the next step, they familiarised themselves with UoLDS, driving on a simulated UK rural road to make them accustomed to the simulator vehicle cabin and the simulated motion, with default simulator motion cueing tuning introduced in (Markkula et al., 2016); they were asked to drive until they felt comfortable with the environment. Then before each of the driving tasks, the drivers familiarised themselves with the task with the MP off so that they would be familiar with the visual aspect of the tasks already on their first attempts.

The drivers completed tasks in the simulator alternatively while the other had a break. It ensured that the time in the simulator without rest time was kept to a minimum in order to reduce the risk of experiencing simulator sickness. During the experiment, for each of the driving tasks, participants were given a subjective questionnaire including the nine questions. They used the same questionnaire for all six motion configurations.

Drivers were not given any information on the nature of the motion cueing they were being provided with, they only knew there were six different motion configurations for which they were to make three pairwise comparisons. As a result, each question is repeated three times in the questionnaire corresponding to three pairs. A question example is shown in Figure 5-5; see Appendix B for the exact questionnaire used in the experiment.

Overall Assessment

1. How realistic was the overall experience in the simulator compared to reality?

For configurations A and B:

Unrealistic	<div style="display: flex; justify-content: space-between; align-items: center;"> <div style="text-align: center;">A ✕</div> <div style="flex-grow: 1; border-bottom: 1px solid black; position: relative;"> <div style="position: absolute; top: -5px; left: 50%; transform: translate(-50%, -50%);"> ----- </div> </div> <div style="text-align: center;">B ✕</div> </div>	Realistic
-------------	--	-----------

For configurations C and D:

Unrealistic	<div style="display: flex; justify-content: space-between; align-items: center;"> <div style="text-align: center;">D ✕</div> <div style="flex-grow: 1; border-bottom: 1px solid black; position: relative;"> <div style="position: absolute; top: -5px; left: 50%; transform: translate(-50%, -50%);"> ----- </div> </div> <div style="text-align: center;">C ✕</div> </div>	Realistic
-------------	--	-----------

For configurations E and F:

Unrealistic	<div style="display: flex; justify-content: space-between; align-items: center;"> <div style="text-align: center;">E ✕</div> <div style="flex-grow: 1; border-bottom: 1px solid black; position: relative;"> <div style="position: absolute; top: -5px; left: 50%; transform: translate(-50%, -50%);"> ----- </div> </div> <div style="text-align: center;">F ✕</div> </div>	Realistic
-------------	--	-----------

Figure 5-5. Example of subjective question and ratings. The drivers did mark each new test with A, B, C, ..., in the order they experienced them

The drivers made pairwise comparisons among configurations within each of the pairs and mark on the ratings, for the first configuration of the first pair they put letter A over each rating mark, and for the second configuration with B, then similarly for second and third pairs put crosses with C-D and E-F. For each configuration they had two attempts, after the first trial they fill up the questionnaire then driving the same configuration for second time complete/modify their answers. They were given a pencil and eraser that they can change the A-B or C-D or E-F positions after completing each of the trials and pairs. Moreover, after driving second and third pairs of configurations they could also modify A-B, C-D, E-F of the three pairs relative to each other. This would give them the flexibility to assess the configurations A to F all relative to each other, meaning that comparison among both the MCAs and MPs at the same time.

While the drivers were performing a pairwise comparison which included 4 trials (2 configurations * 2 trials) they stayed inside the simulator. They were allowed to have a break after each pairwise comparison, however most of the drivers were

able to do all the pairs consecutively. In total drivers had 12 trials for each of the driving tasks.

5.10 Analyses and results

5.10.1 Overview and general approach

In this section, an introduction about statistical methods required to analyse the data is presented. Most of the materials provided in this section are identical or summarised from the (Field, 2013), regarding this it is avoided to reference for the rest of this section.

5.10.1.1 Hypothesis testing

There are two hypotheses used in analysing the data. The hypothesis or prediction that comes from a theory is usually saying an effect will be present and it is called alternative or experimental hypothesis. There is another type of hypothesis opposite of alternative hypothesis that an effect is absent and it is called the null hypothesis.

In this experiment null hypothesis is that the motion cueing algorithms or motion platform sizes are similar to drivers in terms of subjective preferences and objective performances, and the alternative hypothesis is they are distinct to drivers. The statistical significance between various configurations are evaluated, if there is a statistically significant difference between them then the null hypothesis is rejected and configurations are different, and the chance of obtaining data where subjective preferences of drivers or their objective performance over various configurations to be similar is very low.

In this experiment, the type I error is finding a significant difference between motion configurations to drivers' preferences and subjective ratings while there is no difference. Type II error would be not finding any significant difference between motion cueing configurations to drivers' preferences and subjective ratings while there is a difference.

5.10.1.2 Effect size and statistical power

Just because a test statistic is significant does not mean that the effect it measures is meaningful or important. The solution to this is to measure the size of the effect it is known as effect size. An effect size is simply an objective and standardised measure of the magnitude (importance) of the observed effect. Most commonly used effect sizes are Cohen's d , Pearson's correlation coefficient r .

Effect sizes are useful because they provide an objective measure of the importance of an effect. Many of the effect sizes have been proposed, among the common ones are the Cohen's d and Pearson's correlation coefficient r . The value

of Pearson's coefficient lies between 0 (no effect) and 1 (perfect effect). Some widely used suggestions about the range of effects are:

- $r = 0.1$, small effect. The effect explains 1% of the total variance
- $r = 0.3$, medium effect. The effect explains 9% of the total variance
- $r = 0.5$, large effect. The effect explains 25% of the total variance

The effect size is linked to three statistical properties of sample size, probability level of an effect being statistically significant (p-value) that in psychology the value of 0.05 is used, and ability of a given statistical test to detect an effect assuming one exists in the population known as statistical power. The probability of a test detecting an effect if one exists is the opposite of not detecting that effect; therefore, the power of a test can be expressed as $(1-\beta)$. Cohen (1992) suggested a β value of 0.2 then the probability to detect an effect is 0.8 if one genuinely exists.

Relating four above variables of effect size, sample size, p-value and β -level it is possible to calculate the power of a test when the experiment is conducted, or calculating the sample size necessary to achieve a given level of power. In this study as there was a limited number of professional drivers available the power of the experiment is calculated using effect size, sample size and p-value.

To calculate the power of a test, often as the experiment is conducted and the value of p is already selected, the effect size can be estimated based on the sample size that how many participants are used. These values can be used to calculate the value of $1-\beta$ the power of the test. If it turns out to be greater or equals 0.8 there will be confident about the sufficient power to detect effects that might have existed.

p-value of 0.05 is usually considered as significance level threshold for outcome of test statistics, however there are references from Neyman and Pearson (1933) as well as from Fisher, R.A. (1992) that selecting the significance level has to be based on the research context and the choice on how strong the evidence needs to be. In this study due to exploratory use of ANOVA and the small number of samples the larger value of 0.1 is chosen, to be interpreted as nearly significant whilst the value of 0.05 is significant.

As explained the four variables of effect size, sample size, significance p-value and statistical power $1-\beta$ are related. To calculate the statistical power of this experiment based on the choice of p-value to be 0.05, 0.1, sample size $N = 8$, and effect sizes of $r = 0.1, 0.3, 0.58, 0.8, 1$ the statistical power for this experiment is calculated using the G*Power software. If the statistical power is equal or greater than 0.8 there will be confident that there is sufficient power to detect any effect that might have existed. It is observable in Table 5-6 with this number of samples and significance level $p = 0.05$, to have a statistically powerful $(1-\beta) \geq 0.8$ an effect size

of $r = 58$ is required, while with $p = 0.1$ to have a statistically powerful $(1-\beta) \geq 0.8$ an effect size needs to be $r \geq 0.48$.

Table 5-6. Statistical power table

	<i>Statistical Power at $r = 0.1$</i>	<i>Statistical Power at $r = 0.3$</i>	<i>Statistical Power at $r = 0.58$</i>	<i>Statistical Power at $r = 0.8$</i>	<i>Statistical Power at $r = 1$</i>
$p = 0.05$	0.08	0.19	0.80	0.97	0.997
$p = 0.1$	0.14	0.31	0.90	0.992	0.999

The range of effect sizes used in the analysis of results in the next sections is based on the widely used suggestions effect sizes of small $r = 0.1$, medium $r = 0.3$ and large $r = 0.5$, comparing this to Table 5-6, it is observable that to detect an effect with sufficient power at $p = 0.1$, a large effect size is required $r \geq 0.48$.

5.10.1.3 Repeated Measure ANOVA

Statistical procedures are usually divided into the parametric and non-parametric tests, each has assumptions to meet. Non-parametric tests also called distribution-free tests because they assume data do not follow a specific distribution, this approach is usually used when data don't meet the parametric test criteria. Parametric tests usually have assumptions that must be met for the test to be accurate. In this thesis, the parametric tests are used, after checking data to meet the criteria of the assumptions.

The repeated measure is a term when the same participants participated in all conditions of an experiment. In repeated measure experiment design the scores taken under different experimental conditions are likely to be related because they come from the same participants. Another assumption to be made that the relationship between pairs of experimental conditions is similar, which is called sphericity or circularity.

The sphericity refers to equality of variances of differences between treatment levels. It is possible to test the sphericity using the Maunchly's test to test the hypothesis that the variances of differences between conditions are equal. If its test statistic is significant (less than 0.05) it should conclude that there are significant differenced therefore the condition of sphericity is not met, and vice versa, this is the main criteria needs to be met to show that the parametric test is applicable to analyse the data.

In the repeated measure ANOVA the effect of an experiment is shown in the within-participant variance rather than in between-group variance (as of independent

ANOVA). Similar to independent ANOVA for the repeated measure the F-ratio compares the size of variation due to experimental manipulation to the size of variation due to random factors.

In this study to increase the appearance of the effect of experimental manipulations, a repeated measure design was used where the same participants were used in all conditions of an experiment. Thus, the independent variables are manipulated using the same participants. In other words, it is a within-subject or repeated measure design where the effects of experimental manipulation are more obvious than a between-subject or independent design.

5.10.2 Subjective evaluations

In this section drivers' rating on the questionnaires are presented and analysed. The cross points on the provided sheets were measured by ruler and imported as data files to MATLAB for further analysis.

As it was described in section 5.3.1, the questions targeted three different qualities of the overall assessment, motion cueing and vehicle assessment, each include few questions. Due to the high number of questions, to analyse the result it was decided to group the questions belonging to each category. Rating values for the grouped questions were calculated from the average value of all questions belonging to that group.

In order to group and report the questions, a reliability analysis was done on the ratings to find out the consistency of measures. Separate reliability analysis is done for every subscale of the overall assessment, motion cueing, and vehicle assessments. The Cronbach's α and Cronbach's α if item is deleted, showed high reliabilities thus it is was valid to group the questions, for the data of both LHT and SLM tasks.

5.10.2.1 Land Rover Land Rover Handling Track (LHT)

The results for LHT driving task of the grouped questions and six motion configurations are shown in a boxplot and bar charts in Figure 5-6. On the x-axis the characters stand for a motion configuration e.g. M-S stands for MPC algorithm and small motion platform. The effect sizes of Pearson's correlation coefficient are shown in the lower part of the figure in the bar charts. For each of the MPs i.e. (S, M, L) there are 3 bar charts representing the effect sizes. Left red and right blue bar shows the effect size between two consecutive MPs (small to medium, medium to large, and large to small) in an MCA. As an example, for the overall assessment question and small (S) MP, the red bar shows effect size between small (S) and medium (M) MPs in MPC algorithm i.e. M-S and M-M, and the third blue bar does the same but for classic algorithm i.e. the effect size between small (S) and medium

(M) MPs in classic i.e. C-S and C-M. The second (middle) green bar shows the effect size between the classic and MPC MCAs within an MP. In this example, the green bar shows the effect size between classic and MPC in small (S) MP. It is the same for next (M) and (L) MPs. The horizontal dashed lines show the small, medium and large effect sizes.

For the LHT driving task, the highest rated motion configuration in overall assessment question is the MPC MCA and large MP (M-L). It needs to be mentioned that the tuning for all the three settings of classic algorithm was done equally as it is described in section 5.4.2, It remained unclear why drivers rated C-L as low, the cause of dramatic change between the M-L and C-L in the figures, that is observable with large effect size (green bars) for all three questions. On the next figures and tables, it is tried to answer the research questions using the repeated measure ANOVA analysis, post hoc pairwise comparisons and effect sizes.

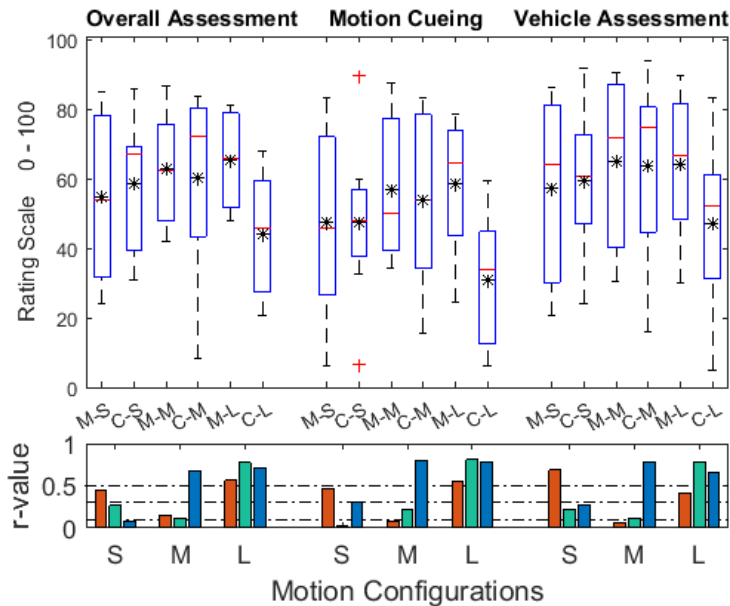


Figure 5-6. Subjective rating boxplot, and effect size r-value bar graphs for grouped questions, LHT task. Red flat lines show median and black stars shows mean.

Table 5-7 Repeated measure ANOVA results for grouped question ratings, LHT task. F and P values are shown on each box corresponds to a factor and an output measure. Black highlighted boxes show where the p-value is less than 0.1

	MP	MCA	MP*MCA	
Overall Assessment	F1.11, P0.36	F5.43, P0.05	F3.43, P0.06	P <= 0.1
Motion Cueing	F3.05, P0.08	F13.85, P0.01	F5.17, P0.02	
Vehicle Assessment	F2.27, P0.14	F3.75, P0.09	F6.82, P0.01	P > 0.1

The repeated measure ANOVA is done on the subjective ratings grouped questions. The main effect of MCAs and MPs and their interaction effect on the subjective ratings are shown in Table 5-7. First two left columns show the main effect and right column shows the interaction. The p-value and F-value of for each factor and output measure are shown in the corresponding boxes in the table. Where there is a significant effect $p \leq 0.1$ that box is highlighted black. To verify the main effects detailed ANOVA contrasts and post hoc test of Bonferroni pairwise comparison is done.

Overall assessment grouped question

Mauchly's test indicated that the assumption of sphericity is not violated for the main effects of MP $\chi^2(2) = 2.29$, $p = 0.32$, and MCA. Therefore, there was no need for degrees of freedom corrections.

There was a significant main effect of type of MCA on the overall assessment ratings, $F(1,7) = 5.43$, $p = 0.05$, $r = 0.66$. Pairwise comparison indicated significant $p = 0.05$ difference between MCAs. Contrasts revealed that ratings of MPC was significantly higher than classic.

There was a nearly significant interaction effect between the type of MP and the type of MCA used, $F(2,14) = 5.16$, $p = 0.06$. This indicates that MP had different effects on people's ratings depending on which type of MCA was used. To break down this interaction, contrasts were performed comparing all MP types to all MCA types, looking at the interaction graph Figure 5-7. These revealed nearly significant interactions when comparing classic to MPC for medium compared to large $F(1,7) = 3.53$, $p = 0.1$, $r = 0.58$. This contrast did yield a large effect size. The

remaining contrast revealed no significant interaction term when comparing classic to MPC for small compared to medium $F(1,7) = 0.28, p = 0.61, r = 0.19$.

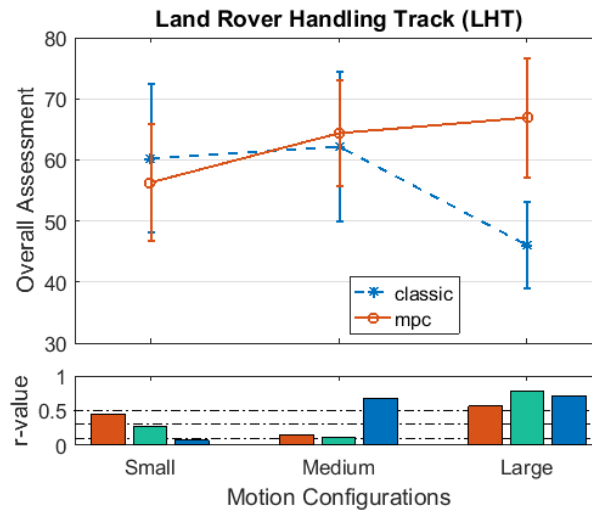


Figure 5-7. Overall assessment grouped question ratings, LHT task

Motion cueing grouped question

Mauchly's test indicated that the assumption of sphericity is not violated for the main effects of MP $\chi^2(2) = 0.79, p = 0.5$, and MCA. Therefore, there was no need for degrees of freedom corrections.

There was a nearly significant main effect of type of MP on the motion cueing ratings, $F(2,14) = 3.05, p = 0.079$. Pairwise comparison indicated nearly significant $p = 0.08$ difference of ratings between large and medium MPs. Contrasts revealed that ratings of large configuration, $F(1,7) = 6.68, p = 0.036, r = 0.70$ was significantly higher than medium.

There was a significant main effect of type of MCA on the motion cueing ratings, $F(1,7) = 13.8, p = 0.007, r = 0.81$. Pairwise comparison indicated significant $p = 0.007$ difference between MCAs. Contrasts revealed that ratings of MPC was significantly higher than classic.

There was a significant interaction effect between the type of MP and the type of MCA used, $F(2,14) = 5.16, p = 0.02$. This indicates that MP had different effects on people's ratings depending on which type of MCA was used. To break down this interaction, contrasts were performed comparing all MP types to all MCA types, looking at the interaction graph Figure 5-8. These revealed significant interactions when comparing classic to MPC for medium compared to large $F(1,7) = 5.7, p = 0.048, r = 0.67$. This contrast did yield a large effect size. The remaining contrast revealed no significant interaction term when comparing classic to MPC for small

compared to medium $F(1,7) = 0.12, p = 0.73, r = 0.13$. However, this contrast did yield a small effect size.

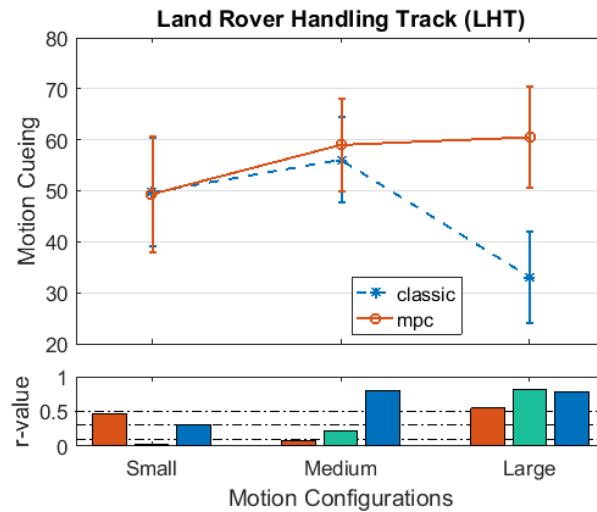


Figure 5-8. Motion cueing grouped question ratings, LHT task

Vehicle assessment grouped question

Mauchly's test indicated that the assumption of sphericity is not violated for the main effects of MP $\chi^2(2) = 0.52, p = 0.77$, and MCA. Therefore, there was no need for degrees of freedom corrections.

There was a nearly significant main effect of type of MCA on the vehicle assessment ratings, $F(1,7) = 3.75, p = 0.094, r = 0.59$. Pairwise comparison indicated nearly significant $p = 0.094$ difference between MCAs. Contrasts revealed that rating of MPC was significantly higher than classic.

There was a significant interaction effect between the type of MP and the type of MCA used, $F(2,14) = 6.82, p = 0.008$. This indicates that MP had different effects on people's ratings depending on which type of MCA was used. To break down this interaction, contrasts were performed comparing all MP types to all MCA types, looking at the interaction graph Figure 5-9. These revealed significant interactions when comparing classic to MPC for medium compared to large $F(1,7) = 11.5, p = 0.011, r = 0.79$. This contrast did yield a large effect size. The remaining contrast revealed no significant interaction term when comparing classic to MPC for small compared to medium $F(1,7) = 0.34, p = 0.57, r = 0.21$.

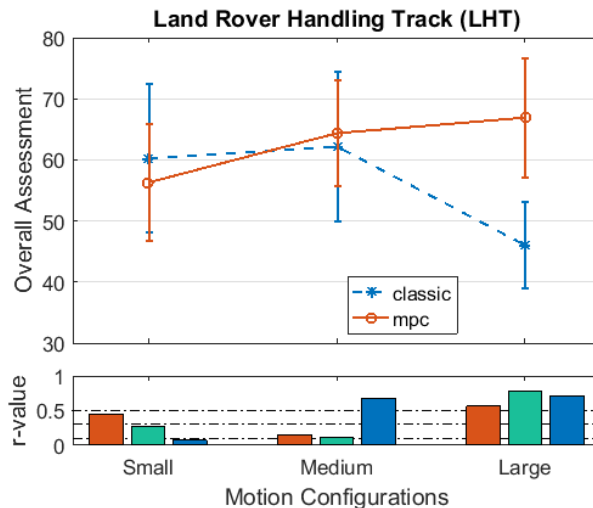


Figure 5-9. Vehicle assessment grouped question ratings, LHT task

Research question 1 – How do the different MCAs affect the drivers' subjective ratings of simulator fidelity and their objective behaviour?

The results for all three questions showed the significant or nearly significant effect of type of MCAs on subjective preferences, where overall the MPC was rated higher than classic. This is in line with the predicted hypothesis for LHT test at the beginning of the chapter. A post hoc pairwise comparison of MCAs in each MP sizes showed MPC was rated significantly $p < 0.02$ higher than classic in large motion platform size for all three questions.

The results are shown in Figure 5-10, in a way that compares the MCAs in each of the MP sizes. The r-values are calculated in each of the MPs representing the effect size of the difference between MCAs. In each of the MPs the green bar is effect size comparing classic and MPC. The outcome of the comparison between the classic and MPC in the small, medium and large MPs is presented in Table 5-8, colours show small, medium and large effect sizes in each comparison.

It is observable for all the three grouped questions the classic comes out as slightly higher fidelity in small MP, whereas the MPC shows the higher fidelity in both medium and large MPs. The effect sizes are small for both small and medium MPs, indicating that small subjective fidelity difference between the MCAs; in other words, drivers see that MCAs are quite similar (slightly different) in both small and medium MPs. For large MP the effect size is large, indicating that there is a bigger subjective fidelity difference between the MCAs to drivers.

In total it is difficult to conclude based on the effect sizes because r-values are not big enough, but it was observable that in small, medium and large MPs drivers preferred the classic, MPC and MPC respectively.

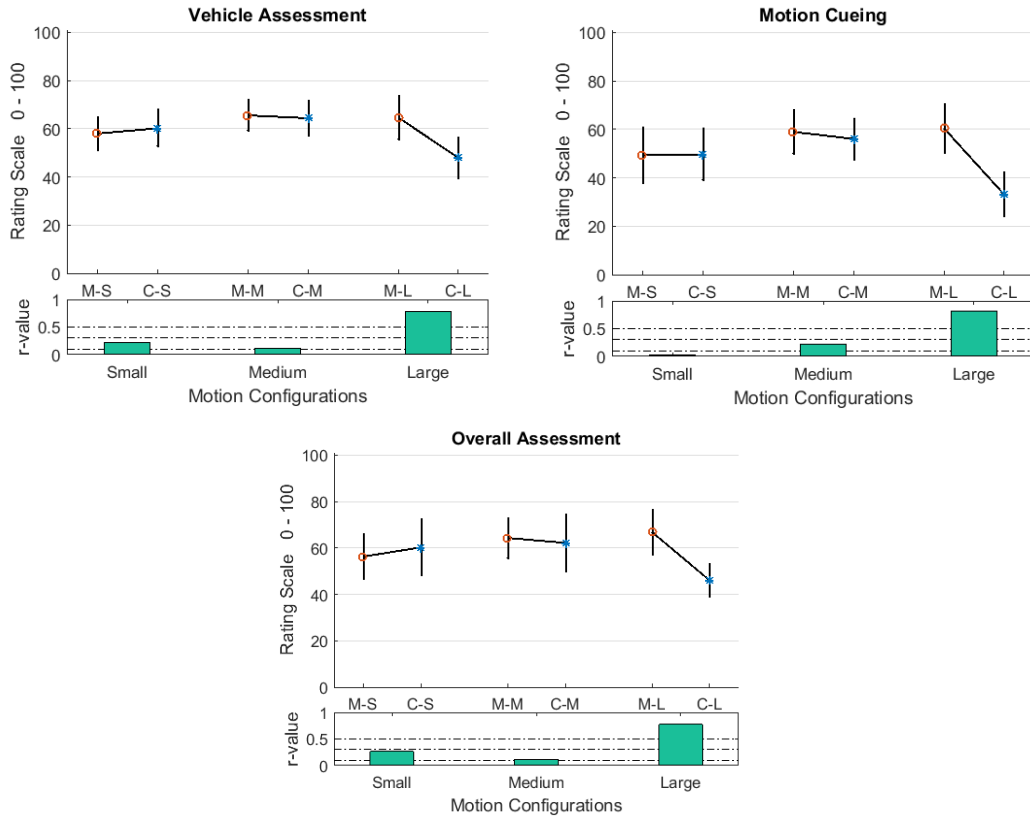


Figure 5-10. Subjective ratings for grouped questions, MCA comparison for three MP sizes. Effect size r-value bar graphs are shown for each MP, comparing MCAs, LHT task

Table 5-8. Results of subjective ratings for MCA comparison in each MP size, LHT task

	r-value < 0.3	0.3 ≤ r-value < 0.5	0.5 ≤ r-value
MP size	Small	Medium	Large
Questions			
Overall assessment	Classic	MPC	MPC
Motion cueing	Classic	MPC	MPC
Vehicle assessment	Classic	MPC	MPC

Research question 2 – How do the different MPs affect the drivers’ subjective ratings of simulator fidelity and their objective behaviour?

The results for the motion cueing question showed the nearly significant main effect of type of MPs on subjective preferences, where the large configuration was rated significantly higher than medium. This is in line with the predicted hypothesis for LHT test at the beginning of this chapter. A post hoc pairwise comparison of MPs in

each MCA showed medium was rated nearly significantly $p < 0.1$ higher than small in MPC for the vehicle assessment question.

The results are shown in Figure 5-11 in a way that compares the MPs in each of the MCAs. The r-values are calculated in each of the MCAs representing the effect size of the difference between MPs. In each of the MCAs the left red bar is effect size calculated comparing small to medium, middle green bar compares the medium to large and right blue bar compares the large to small. The outcome of the comparisons between the small, medium and large in the classic and MPC is presented in Table 5-9, colours show small, medium and large effect size in each comparison.

It is observable for the MPC algorithm, in all three questions the medium to large MP comes out as higher fidelity with large effect size. In the classic algorithm, the medium MP shows the higher fidelity for all the three groups of questions with small to medium effect sizes.

In MPC, the effect sizes are small between the medium and large MPs, indicating that small subjective fidelity difference between them, while there is large effect size between the medium and large compared to small MP. In other words, the medium and large MPs are quite similar (slightly different) to drivers and those are much different to small MP to drivers. In classic, the effect size is small between small and medium MPs, indicating that there is small subjective fidelity difference between them, while there is large effect size between the small and medium to large MP.

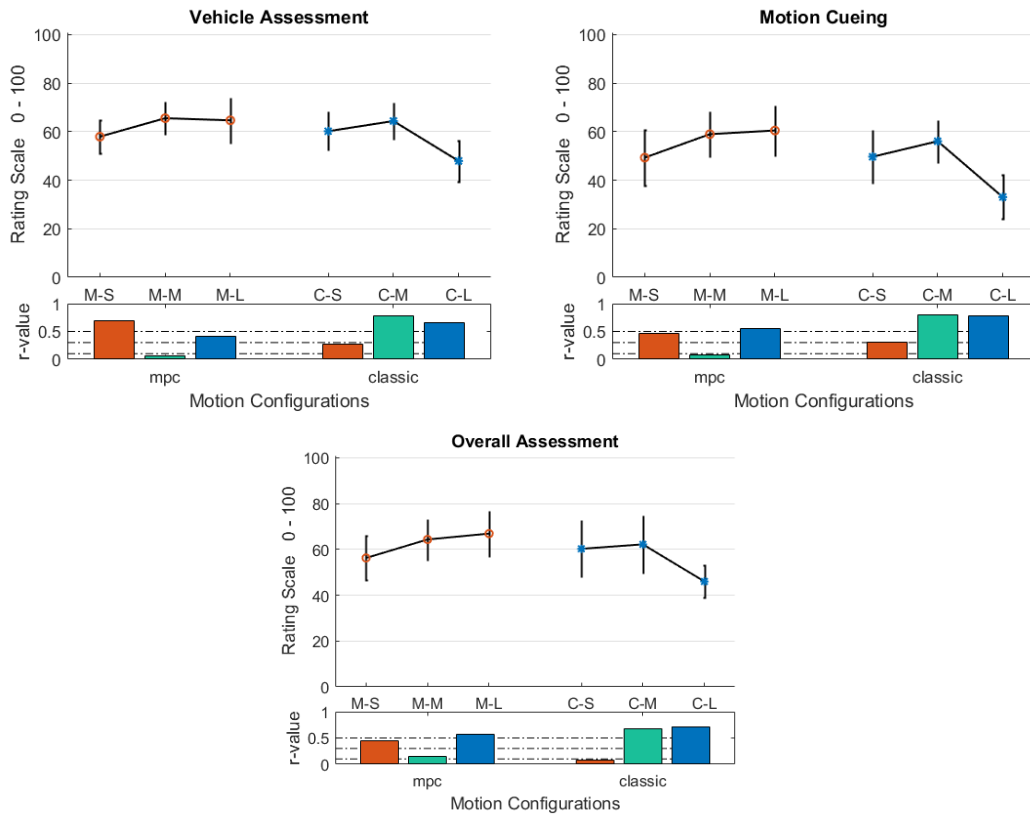


Figure 5-11. Subjective ratings for group questions, MP comparison for two MCAs. Effect size r-value bar graphs are shown for each MCA, comparing MPs, LHT task

Table 5-9. Results of subjective ratings for MP size comparison in each MCA (all compared to small), LHT task

	r-value < 0.3	0.3 ≤ r-value < 0.5	0.5 ≤ r-value
MCA		MPC	Classic
Questions			
Overall assessment		Large	Medium
Motion cueing		Large	Medium
Vehicle assessment		Medium	Medium

The results for all three questions showed the significant interaction effect between the type of MP and the type of MCA used on subjective preferences. This indicates that MP had different effects on people’s ratings depending on which type of MCA was used. To break down this interaction, contrasts were performed comparing all MP types to all MCA types for each question. These revealed nearly significant and significant interactions when comparing classic to MPC for medium compared to large for the three questions. These contrasts did yield a large effect size.

Looking at Figure 5-7 to Figure 5-9, in all the three group questions there was an increase in ratings from small to medium MPs for both classic and MPC. The

ratings increase very little from medium to large MP in MPC. Moreover, in the small the classic was always rated slightly higher, and in medium and large the MPC.

5.10.2.2 Slalom (SLM)

The results for SLM driving task of grouped questions and six motion configurations are shown in a boxplot and bar charts in Figure 5-12. On the x-axis the characters stand for a motion configuration e.g. M-S stands for MPC motion cueing algorithm and small motion platform. The effect sizes of Pearson's correlation coefficient are shown in the lower part of the figure as bar charts. For each of the MPs i.e. (S, M, L) there are 3 bar charts representing the effect sizes. Left red and right blue bar shows the effect size between two consecutive MPs (small to medium, medium to large and large to small) in an MCA. As an example, for the overall assessment question and small (S) MP, the red bar shows effect size between small (S) and medium (M) MPs in MPC MCA i.e. M-S and M-M, and the third blue bar does the same but for classic i.e. the effect size between small (S) and medium (M) MPs in classic MCA i.e. C-S and C-M. The second (middle) green bar shows the effect size between the classic and MPC MCAs within an MP. In this example, the green bar shows the effect size between classic and MPC in small (S) MP. It is the same for next (M) and (L) MPs. The horizontal dashed lines show the small, medium and large effect sizes.

For the SLM driving task, the highest rated configuration in overall assessment question is the classic MCA and small MP (C-S). On the next figures and tables, it is tried to answer the research questions using the repeated measure ANOVA analysis, post hoc pairwise comparisons and effect sizes.

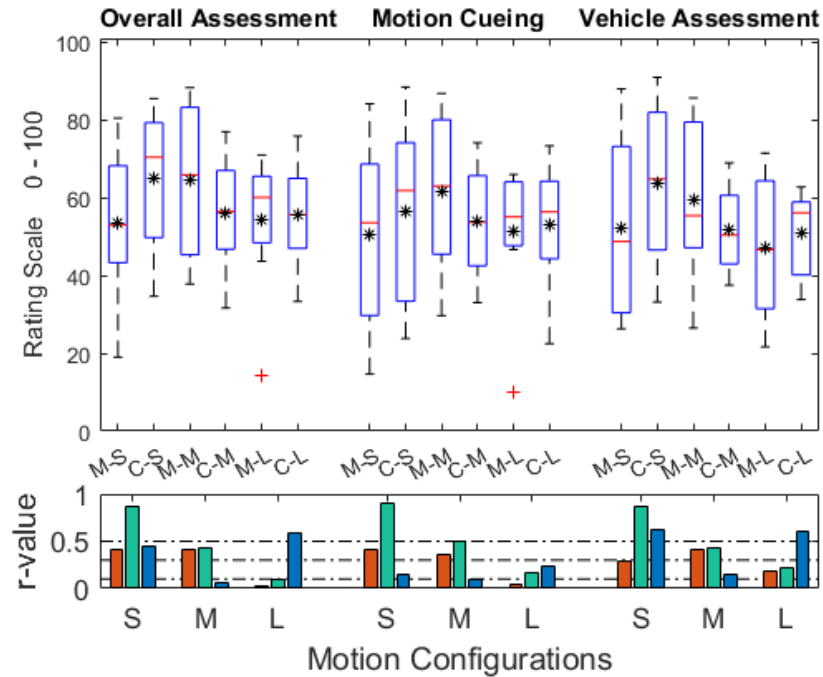


Figure 5-12. Subjective rating boxplot, and effect size r-value bar graphs for grouped questions, SLM task. Red flat lines show median and black stars shows mean.

Table 5-10. Repeated measure ANOVA results for grouped question ratings, SLM task. F and P values are shown on each box corresponds to a factor and an output measure. Black highlighted boxes show where the p-value is less than 0.1.

Overall Assessment	F0.53, P0.60	F0.36, P0.57	F3.10, P0.08	P <= 0.1
Motion Cueing	F0.38, P0.69	F0.00, P0.96	F2.61, P0.11	
Vehicle Assessment	F1.00, P0.39	F1.31, P0.29	F2.81, P0.09	P > 0.1
	MP	MCA	MP*MCA	

Similar to the analysis done for the previous task, in this task the repeated measure ANOVA is done on the subjective ratings grouped questions. The main effect of MCAs and MPs and their interaction effect on the subjective ratings are shown in Table 5-10. First two left columns show the main effect and right column shows the interaction. The p-value and F-value of for each factor and output measure is shown in the corresponding point on the table. Where there is a significant effect

$p \leq 0.1$ that box is highlighted black. To verify the main effects detailed ANOVA contrasts and post hoc test of Bonferroni pairwise comparison are done.

Overall assessment grouped question

Mauchly's test indicated that the assumption of sphericity is not violated for the main effects of MP $\chi^2(2) = 1.62$, $p = 0.44$, and MCA. Therefore, there was no need for degrees of freedom corrections.

There was a nearly significant interaction effect between the type of MP and the type of MCA used, $F(2,14) = 3.1$, $p = 0.076$. This indicates that MP had different effects on people's ratings depending on which type of MCA was used. To break down this interaction, contrasts were performed comparing all MP types to all MCA types, looking at the interaction graph Figure 5-13. These revealed significant interactions when comparing classic to MPC for small compared to medium $F(1,7) = 6$, $p = 0.04$, $r = 0.68$. This contrast did yield a large effect size. The remaining contrast revealed no significant interaction term when comparing classic to MPC for medium compared to large $F(1,7) = 1.12$, $p = 0.32$, $r = 0.37$.

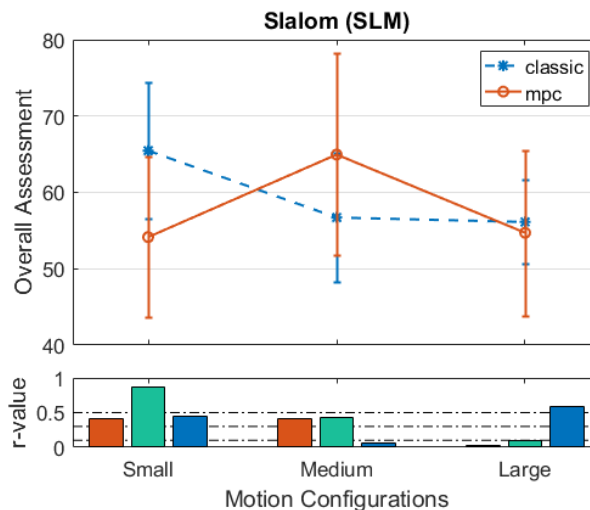


Figure 5-13. Overall assessment grouped question ratings, SLM task

Vehicle assessment grouped question

Mauchly's test indicated that the assumption of sphericity is not violated for the main effects of MP $\chi^2(2) = 0.96$, $p = 0.61$, and MCA. Therefore, there was no need for degrees of freedom corrections.

There was a nearly significant interaction effect between the type of MP and the type of MCA used, $F(2,14) = 2.81$, $p = 0.09$. This indicates that MP had different effects on people's ratings depending on which type of MCA was used. To break down this interaction, contrasts were performed comparing all MP types to all MCA types, looking at the interaction graph Figure 5-14. These revealed significant interactions when comparing classic to MPC for small compared to medium

$F(1,7) = 9.4, p = 0.018, r = 0.75$. This contrast did yield a large effect size. The remaining contrast revealed no significant interaction term when comparing classic to MPC for medium compared to large $F(1,7) = 1.17, p = 0.31, r = 0.38$.

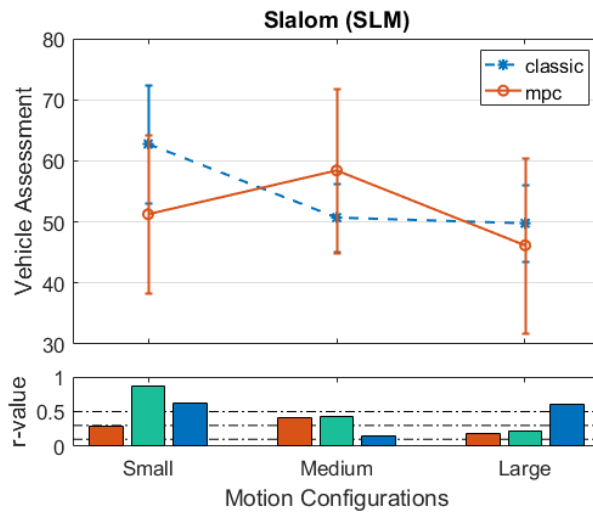


Figure 5-14. Vehicle assessment grouped question ratings, SLM task

Research question 1 - How do the different MCAs affect the drivers' subjective ratings of simulator fidelity and their objective behaviour?

The results for all three questions did not show a significant effect of type of MCAs on subjective preferences. A post hoc pairwise comparison of MCAs in each MP sizes showed classic was rated significantly $p < 0.01$ higher than MPC in small motion platform size for all three questions. This is in line with the predicted hypothesis for SLM test at the beginning of the chapter.

The results are shown in Figure 5-15, in a way that compares the MCAs in each of the MP sizes. The r-values are calculated in each of the MPs representing the effect size of the difference between MCAs. In each of the MPs, the green bar is effect size comparing classic and MPC. The outcome of the comparison between the classic and MPC in the small, medium and large MPs is presented in Table 5-11, colours show small, medium and large effect sizes in each comparison.

It is observable for all the three grouped questions the classic comes out as higher fidelity in small and large MP, whereas the MPC shows the higher fidelity in medium MP. The effect sizes are large and medium for small and medium MPs, indicating that considerable subjective fidelity difference between the MCAs. In other words, drivers see that MCAs are different in both small and medium MPs. For large MP the effect sizes are small, indicating that there is smaller subjective fidelity difference between the MCAs to drivers.

Interestingly the same table shows for all the three overall assessment, motion cueing and vehicle assessment questions the effect size is decreasing with the

increase of MP size, which means that the difference between MCAs is less distinctive with the increase of MP size. In total having big enough effect sizes, it can be concluded in small, medium and large MPs the drivers preferred the classic, MPC and classic respectively.

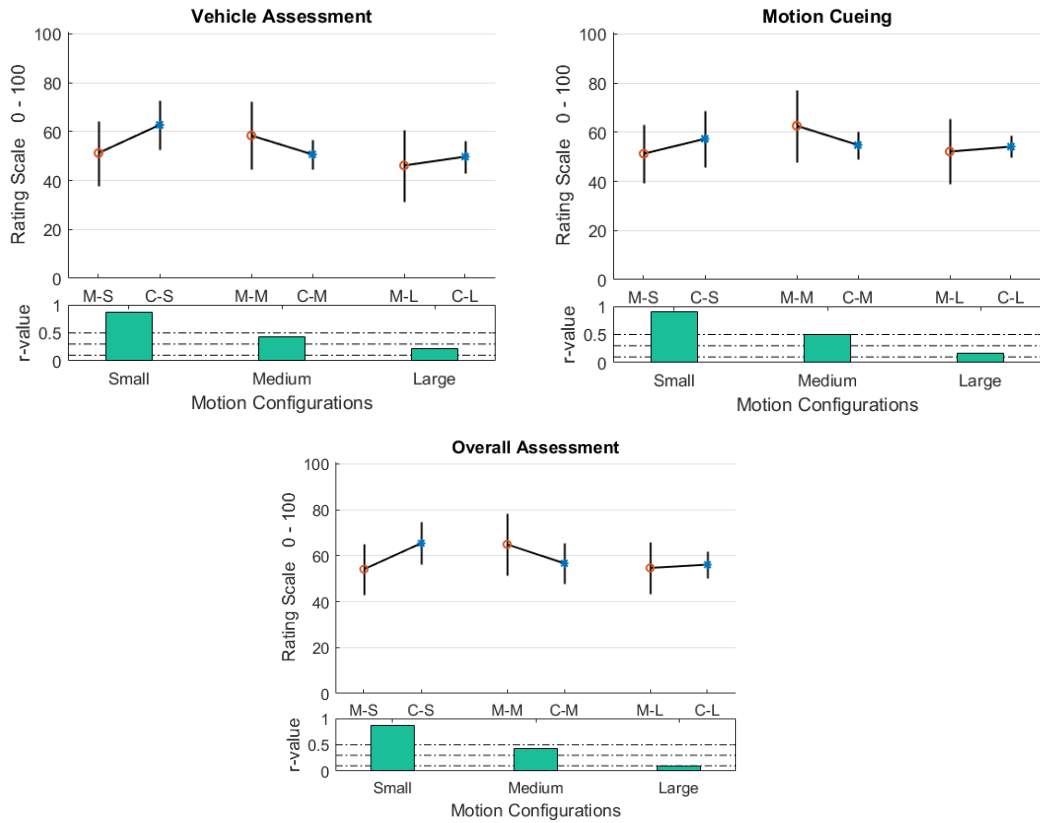


Figure 5-15. Subjective ratings for grouped questions, MCA comparison for three MP sizes, SLM task. Effect size r-value bar graphs are shown for each MP, comparing MCAs, SLM task.

Table 5-11. Results of subjective ratings for MCA comparison in each MP size, SLM task

		r-value < 0.3	0.3 ≤ r-value < 0.5	0.5 ≤ r-value
Questions	MP size	Small	Medium	Large
	Overall assessment	Classic	MPC	Classic
Motion cueing	Classic	MPC	Classic	
Vehicle assessment	Classic	MPC	Classic	

Research question 2 - How do the different MPs affect the drivers' subjective ratings of simulator fidelity and their objective behaviour?

The results for all three questions did not show a significant effect of type of MPs on subjective preferences.

The whole results are shown in Figure 5-16 in a way that compares the MPs in each of the MCAs. The r-values are calculated in each of the MCAs representing the effect size of the difference between MPs. In each of the MCAs the left red bar is effect size calculated comparing small to medium, middle green bar compares the medium to large and right blue bar compares the large to small. The outcome of the comparisons between the small, medium and large in the classic and MPC is presented in Table 5-12, colours show small, medium and large effect size in each comparison.

It is observable for the MPC algorithm, in all three questions the medium MP comes out as higher fidelity with medium effect size. In the classic algorithm, the small MP shows the higher fidelity for all three questions with small and large effect sizes.

In MPC, the effect sizes are medium between the medium to small and large MPs, indicating that considerable subjective fidelity difference between them; in other words, the medium MP is different to small and large MPs for drivers. In classic, the effect sizes are small between medium and large MPs, indicating that there is small subjective fidelity difference between them, while there is small to large effect sizes between the small to medium MP showing the preference of small to other MPs. In total having big enough effect sizes it can be concluded, in MPC the drivers preferred the medium MP and in classic they preferred the small MP.

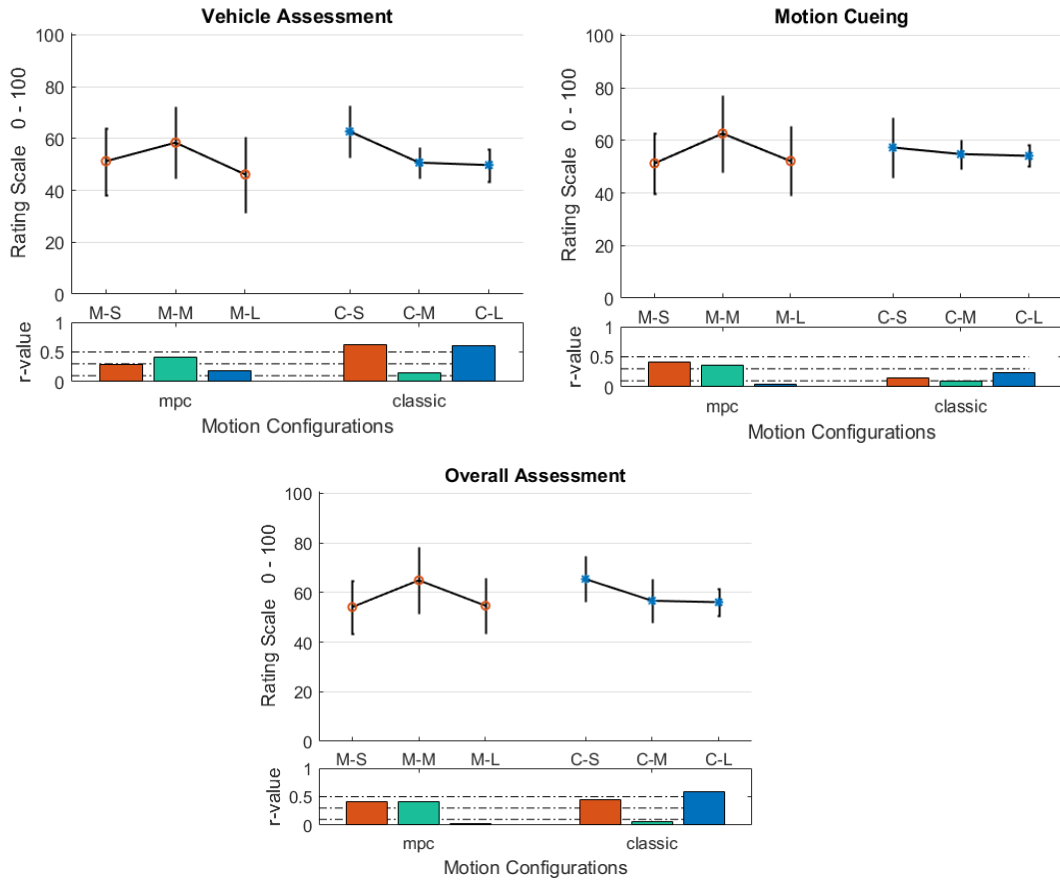


Figure 5-16. Subjective ratings for group questions, MP comparison for two MCAs. Effect size r-value bar graphs are shown for each MCA, comparing MPs, SLM task.

Table 5-12. Results of subjective ratings for MP size comparison in each MCA (all compared to large), SLM task

	r-value < 0.3	0.3 ≤ r-value < 0.5	0.5 ≤ r-value
MCA		MPC	Classic
Questions			
Overall assessment		Medium	Small
Motion cueing		Medium	Small
Vehicle assessment		Medium	Small

The results for the overall and vehicle questions showed the significant interaction effect between the type of MP and the type of MCA used on subjective preferences. This indicates that MP had different effects on people’s ratings depending on which type of MCA was used. To break down this interaction, contrasts were performed comparing all MP types to all MCA types for each question. These revealed

significant interactions when comparing classic to MPC for small compared to medium. These contrasts did yield a large effect size.

Looking at Figure 5-13 and Figure 5-14, in both of the group questions the highest ratings in small and medium MPs are for classic and MPC respectively, due to medium and large effect sizes it is a conclusion. In large MP the classic was higher however because the effect size is small it is not possible to draw a solid conclusion that classic or MPC was rated higher in large MP. In classic, decrease in rating was observable from small to medium and large MPs, whereas in MPC it has increased from small to medium and decreased to large.

5.10.3 Objective evaluations

Collected data include two runs for each of the motion configurations. This was to let the drivers acquire a full understanding of the motion characteristics of a configuration. Using both of the runs was shown to be advantageous in terms of adding power to the statistical analysis, although a check was needed to see if this introduced any noise to the analysis. To ensure the correctness of averaging both of the runs, a third time factor was added to the analysis. For all of the objective metrics described in the next sections, where there was a significant effect of MCA or MP, no significant effect of time factor was found. As a result, it was valid to average the data from both runs for further analysis.

5.10.3.1 Land Rover Handling Track (LHT)

Different sections of the driven road have different characteristics, therefore the whole track was split into sections and each section was analysed separately. Due to similarity in nature of many of the sections and to reduce the number of reporting results the sections throughout the LHT course was divided into straight lines, curves and inflection zone groups, then the curve group itself is divided into groups with smaller and greater than 180 degrees of turn. There are 10 sections in total. All the sections are shown in Figure 5-17, green dots show the entry of a section and red dots shows the exit of a section. Section 1 is the first curve where drivers start driving and it usually required lower speed to keep the safe control of the vehicle.

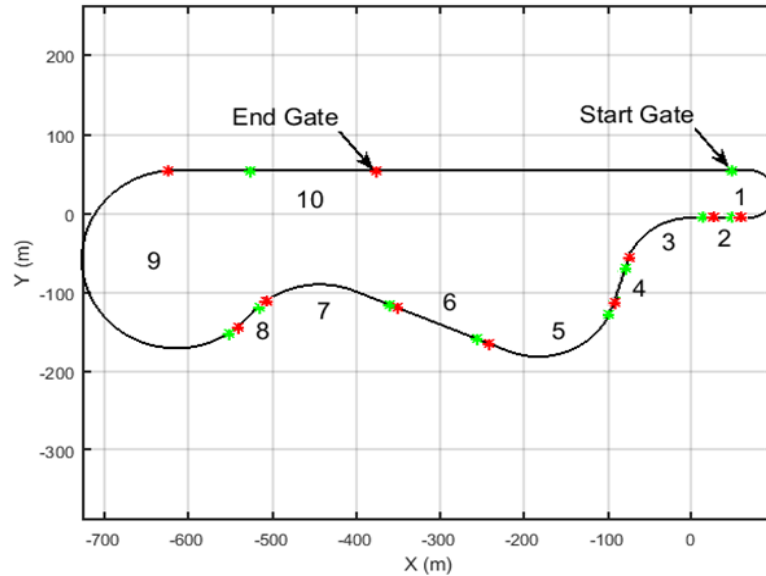


Figure 5-17. Land Rover Handling Track (LHT) course and sections

To be able to group the sections initial analysis were performed. Comparing the results of the 10 separate sections with the corresponding grouped sections, showed similarity in the values; this indicated that it was acceptable to group the sections. The objective metrics of a group section is calculated from the average value of all sections belonging to that group as Table 5-13.

Table 5-13. Group sections, LHT task

<i>Group section</i>	<i>Section Numbers</i>
Straight lines	6, 10
Curves ≥ 180 degrees of turn	1, 9
Curves < 180 degrees of turn	3, 5, 7
Inflection zones	2, 4, 8
Whole track	

Aggregated performance

The aggregated performance measures for LHT task consist of four metrics that was explained in section 5.3.2:

- Lap time, duration of time that drivers completed the task
- Spin/skid outs, number of trials that drivers spin out and exceeded the roadsides
- Speed variability, the standard deviation of drivers speed during the task
- Lateral position deviation, maximum vehicle's lateral distance from the average trajectory

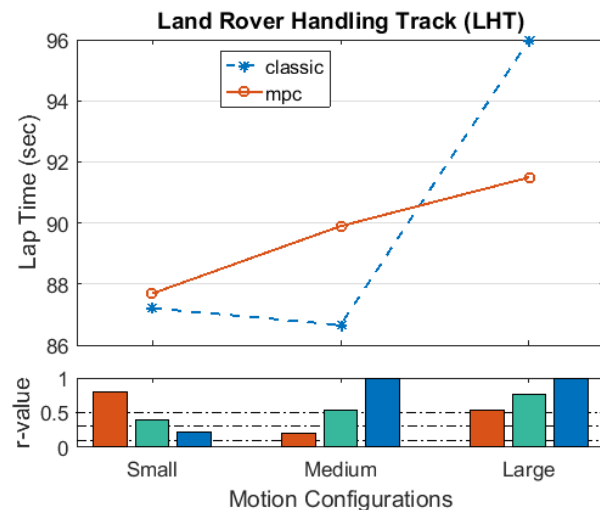


Figure 5-18. Lap time, LHT

In Figure 5-18 it is observable that the lap time has increased with the increase of MP size in both classic and MPC. In MPC the smallest MP has the shortest lap time and vice versa, in classic smallest lap time is in medium MP and it is similar to small MP. Having considerable effect sizes reveal that providing larger motion to drivers results in higher lap time to finish the driving task. However, there is no real world data available to make a comparison and decide on the best configuration.

The higher lap time with the increase of MP size, in general, is indicating the deteriorated performance when drivers are asked to adapt their speed, although considering it with the decrease in the number of failures (described next) both reflect improved performance. In other words, increasing the MP size (presenting more motion to drivers) decreased the number of failures in fare of increasing their lap time.

Comparing the MCAs in each MP size, the classic has lower lap time in small and medium MP while it is higher than MPC in large MP. Having medium to large effect sizes indicate that the drivers had mostly higher lap time driving the MPC configurations than classic.

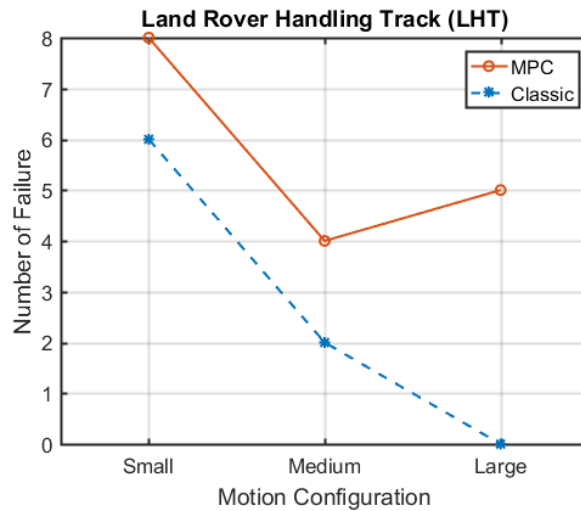


Figure 5-19. Spin/skid outs, LHT

From Figure 5-19, the number of failures decreased with increasing MP size for both MCAs, except for the medium to large in MPC, that stayed quite similar. It might be indicating that providing larger motion to drivers results in a smaller number of failures in performing the task, reflecting the improved performance of drivers. Comparing the MCAs in each MP size, the classic always has a lower number of failures than MPC in all three MPs. Considering this with lower lap time of classic both are reflecting better performance in the classic

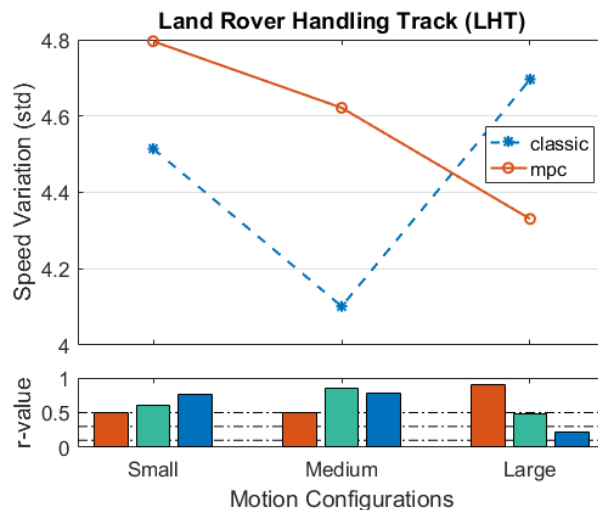


Figure 5-20. Speed variations, LHT

From Figure 5-20, the speed variation decreased with increasing MP size for both MCAs, except for the medium to large in classic MCA. Having considerable large effect sizes reveal that providing larger motion to drivers results in less speed variation during driving, reflecting improved performance of drivers.

Comparing the MCAs in each MP size, the classic has lower speed variation than MPC in small and medium MPs, and for large the classic is higher. Having large

effect sizes indicate that drivers had mostly larger speed variation driving the MPC configurations than classic, reflecting better performance in classic.

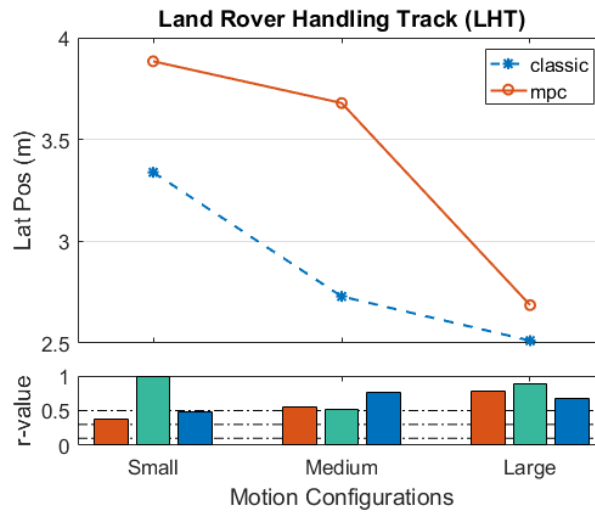


Figure 5-21. Lateral position deviation, LHT

From Figure 5-21, lateral position deviation decreased with increasing MP size for both MCAs, which means the small MP has the largest lateral position deviation and vice versa. Having considerable medium to large effect sizes reveals that providing larger motion to drivers results in less lateral position deviation during driving, reflecting the improved performance of drivers.

Comparing the MCAs in each MP size, the classic has always lower lateral position deviation than MPC in all the MPs. Having large effect sizes indicate that drivers had always larger lateral position deviation driving the MPC configurations than classic, reflecting better performance in classic.

Time series

In this section, the results of repeated measure ANOVA and post hoc analysis on the time series metrics (explained in section 5.3.2) in each of the group sections are presented, and where there are significant or near significant results those are elaborated. Looking at Table 5-14 to Table 5-18 the columns (on x-axis) belong to independent variables and their interaction and each row belongs (on y-axis) to a dependent measured variable metric. The F and p values are shown on each box corresponding to a factor and an output measure. Black highlighted boxes show where the p-value is less than 0.1 that means there is a nearly significant difference.

Curves greater than 180°

In Table 5-14 the RM ANOVA results of time series output measured metrics are shown for both MCA, MP configurations and their interactions.

Table 5-14. Repeated measure ANOVA time series metrics results of curve greater than 180° grouped sections, LHT task.

Curves Greater than 180°			
	MP	MCA	MP*MCA
Long Vel (m/s)	F4.61, P0.02	F0.15, P0.71	F0.59, P0.56
Lat Vel (m/s)	F3.80, P0.04	F0.11, P0.75	F0.03, P0.97
Yaw Rate (rad/s)	F1.80, P0.19	F0.15, P0.71	F1.07, P0.36
Long Acc (m/s ²)	F0.62, P0.54	F0.00, P0.95	F4.06, P0.03
Lat Acc (m/s ²)	F2.21, P0.13	F0.63, P0.44	F0.21, P0.81
Delay Time	F0.22, P0.80	F0.30, P0.60	F0.20, P0.82
Gain	F2.05, P0.15	F3.71, P0.08	F0.20, P0.82
StrgRevsRate 1°	F2.85, P0.08	F0.00, P0.96	F0.08, P0.92
StrgRevsRate 10°	F13.79, P0.00	F3.34, P0.09	F3.93, P0.03

P ≤ 0.1

P > 0.1

For this grouped section boxes that show significant main or interaction effects on output measures include:

For MP comparison:

- Maximum longitudinal velocity
- Maximum lateral velocity (absolute value)
- Steering wheel reversal rate (1 degree)
- Steering wheel reversal rate (10 degree)

For MCA comparison:

- Driver model gain
- Steering wheel reversal rate (10 degree)

For MCA and MP interaction:

- Maximum longitudinal acceleration
- Steering wheel reversal rate (10 degree)

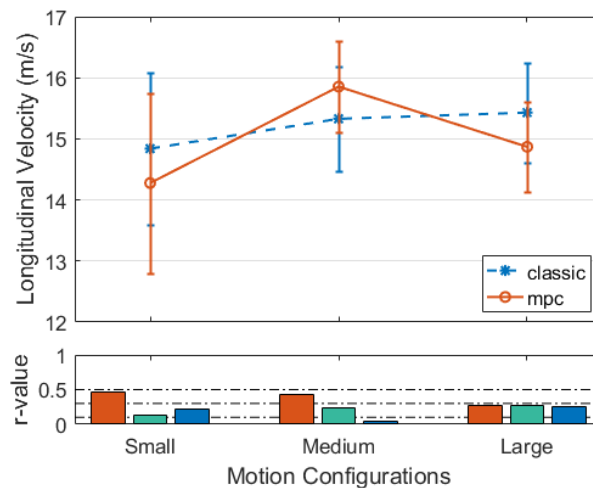


Figure 5-22. Maximum longitudinal velocity, curves greater than 180°

There was a significant main effect of type of MP on the longitudinal velocity objective metric, $F(2,12) = 4.6$, $p = 0.02$. Pairwise comparison indicated significant $p = 0.08$ difference between small and medium MPs. Contrasts revealed that longitudinal velocity in medium configuration, $F(1,6) = 9.58$, $p = 0.009$, $r = 0.66$ was significantly higher than small.

Looking at Figure 5-22 graphs and effect sizes the longitudinal velocity has increased with increasing MP size with small to medium effect size. There is a small effect size in difference between MCAs that has affected drivers' performance quite similarly.

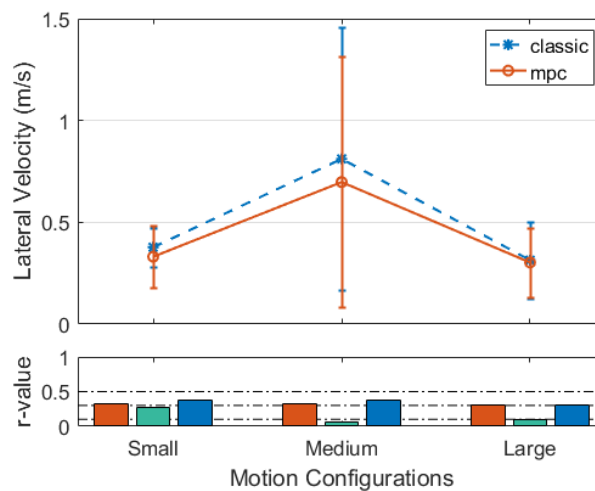


Figure 5-23. Maximum lateral velocity, curves greater than 180°

There was a significant main effect of type of MP on the lateral velocity objective metric, $F(2,12) = 3.8$, $p = 0.03$. Contrasts revealed that lateral velocity in medium configuration was significantly higher than small $F(1,6) = 3.9$, $p = 0.07$, $r = 0.49$ as well as large $F(1,6) = 3.75$, $p = 0.07$, $r = 0.48$.

Looking at Figure 5-23 graphs and effect sizes the lateral velocity has fluctuated with increasing MP size with medium effect size, where the medium has the largest values. There is a small effect size in difference between MCAs that has affected drivers' performance quite similarly.

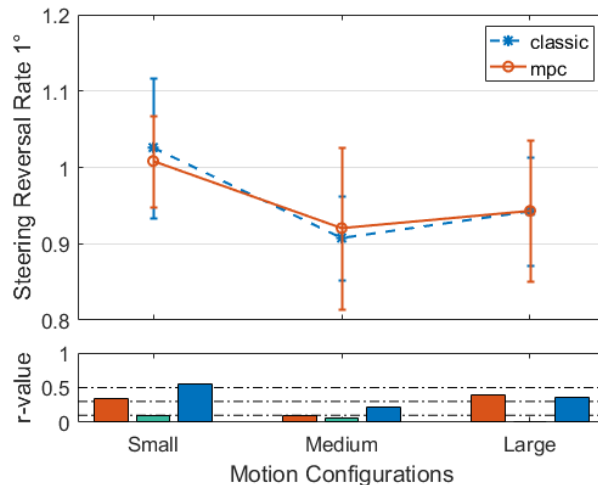


Figure 5-24. Steering reversal rate 1°, curves greater than 180°

There was a nearly significant main effect of type of MP on the steering wheel reversal rate 1° metric, $F(2,12) = 2.84$, $p = 0.078$. Contrasts revealed that steering reversal rate in medium configuration, $F(1,6) = 4.72$, $p = 0.05$, $r = 0.53$ was significantly lower than small.

Looking at Figure 5-24 graphs and effect sizes the steering wheel reversal rate has decreased with increasing MP size with small to medium effect size that shows lower control activity and more relaxed style of driving i.e. improved performance. There is a small effect size in difference between MCAs that has affected drivers' performance quite similarly.

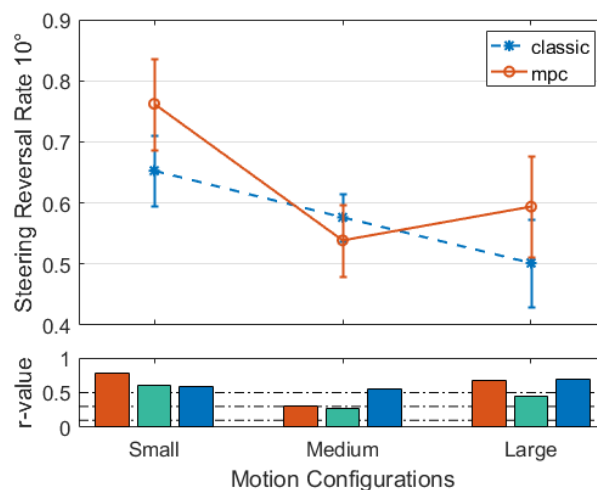


Figure 5-25. Steering reversal rate 10°, curves greater than 180°

There was a significant main effect of type of MP on the steering wheel reversal rate 10° metric, $F(2,12) = 13.79$, $p = 0.0001$. Contrasts revealed that steering reversal rate in medium configuration, $F(1,6) = 26.79$, $p = 0.0002$, $r = 0.83$ was significantly lower than small. Pairwise comparison indicated significant $p = 0.007$

difference between small and medium, and $p = 0.0006$ difference between small and large MPs.

There was a nearly significant main effect of type of MCA on the steering wheel reversal rate, $F(1,6) = 3.34$, $p = 0.09$, $r = 0.81$. Contrasts revealed that MPC was significantly higher than classic. Pairwise comparison indicated a nearly significant effect $p = 0.09$ MPC being higher than classic.

There was a significant interaction effect between the type of MP and the type of MCA used, $F(2,12) = 3.93$, $p = 0.03$. This indicates that MP had different effects on people's objective performance depending on which type of MCA was used. To break down this interaction, contrasts were performed comparing all MP types to all MCA types. These revealed significant interactions when comparing classic to MPC for small compared to medium $F(1,6) = 5.59$, $p = 0.035$, $r = 0.56$; also comparing classic to MPC for medium compared to large $F(1,6) = 4.68$, $p = 0.05$, $r = 0.53$. These contrasts did yield large effect sizes.

Looking at Figure 5-25 graphs and effect sizes the steering wheel reversal rate has decreased with increasing MP size with medium to large effect size, that shows lower control activity and more relaxed style of driving i.e. improved performance. There is small to large effect sizes in difference between MCAs that has affected drivers' performance differently, where MPC being higher than classic in small and large MPs, that shows higher control activity i.e. deteriorated performance.

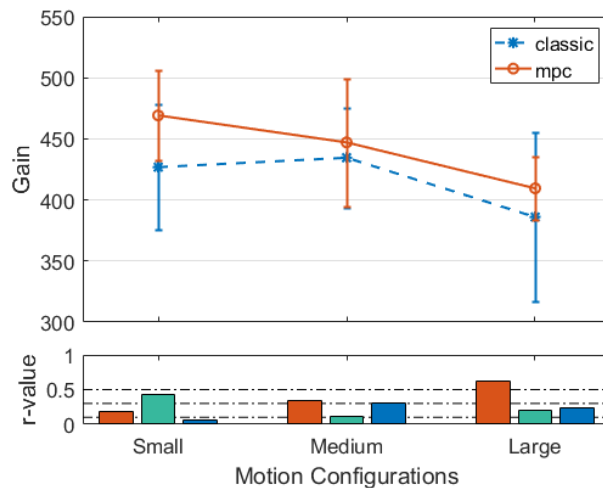


Figure 5-26. Driver model steering gain, curves greater than 180°

There was a nearly significant main effect of type of MCA on the driver model steering gain, $F(1,6) = 3.17$, $p = 0.078$, $r = 0.44$. Contrasts revealed that MPC was

significantly higher than classic. Pairwise comparison indicated a nearly significant effect $p = 0.078$, MPC being higher than classic.

Looking at Figure 5-26 graphs and effect sizes the steering gain has decreased slightly with increasing MP size with small to large effect sizes that show lower control activity and more relaxed style of driving i.e. improved performance. There is small to medium effect sizes in difference between MCAs that has affected drivers' performance differently, where MPC is higher than classic in all MPs, that shows higher control activity i.e. deteriorated performance.

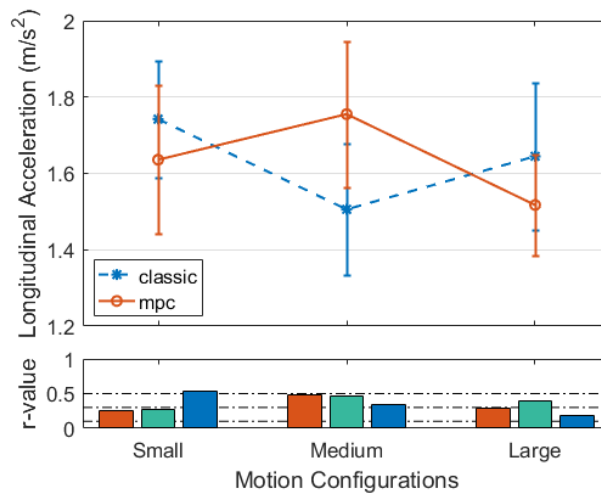


Figure 5-27. Longitudinal acceleration, LHT task

There was a significant interaction effect between the type of MP and the type of MCA used, $F(2,12) = 4.05$, $p = 0.03$. This indicates that MP had different effects on people's objective performance depending on which type of MCA was used. To break down this interaction, contrasts were performed comparing all MP types to all MCA types. These revealed significant interactions when comparing classic to MPC for small compared to medium $F(1,6) = 4.46$, $p = 0.056$, $r = 0.52$; also comparing classic to MPC for medium compared to large $F(1,6) = 6.33$, $p = 0.02$, $r = 0.58$. These contrasts did yield large effect sizes.

Curves smaller than 180°

In Table 5-15 the RM ANOVA results of time series output measured metrics are shown for both MCA, MP configurations and their interactions.

Table 5-15. Repeated measure ANOVA time series metrics results of curve smaller than 180° grouped sections, LHT task.

Curves Smaller than 180°			
	MP	MCA	MP*MCA
Long Vel (m/s)	F1.23, P0.31	F1.63, P0.23	F0.07, P0.94
Lat Vel (m/s)	F0.16, P0.85	F5.78, P0.03	F1.13, P0.34
Yaw Rate (rad/s)	F0.12, P0.88	F5.33, P0.04	F0.76, P0.48
Long Acc (m/s ²)	F2.84, P0.08	F2.23, P0.16	F0.64, P0.53
Lat Acc (m/s ²)	F1.79, P0.19	F2.77, P0.12	F0.13, P0.88
Delay Time	F0.53, P0.59	F1.78, P0.21	F1.11, P0.35
Gain	F4.17, P0.03	F1.76, P0.21	F1.61, P0.22
StrgRevsRate 1°	F2.63, P0.09	F1.03, P0.33	F1.69, P0.21
StrgRevsRate 10°	F7.42, P0.00	F1.76, P0.21	F0.15, P0.86

For this grouped section boxes that show significant main or interaction effects on output measures include:

For MP comparison:

- Maximum longitudinal acceleration
- Driver model gain
- Steering wheel reversal rate (1 degree)
- Steering wheel reversal rate (10 degree)

For MCA comparison:

- Maximum lateral velocity (absolute value)
- Maximum yaw rate (absolute value)

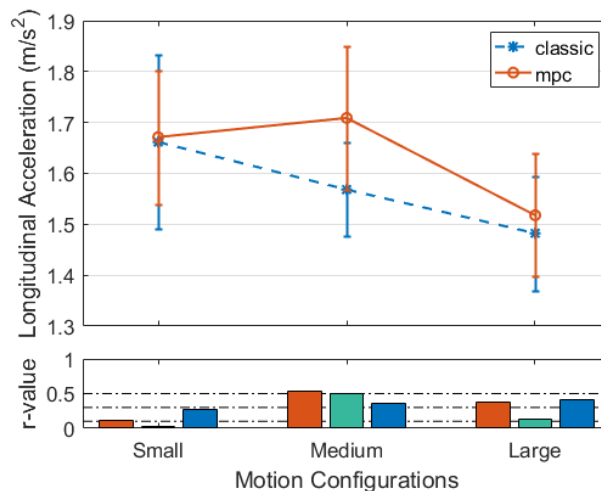


Figure 5-28. Maximum longitudinal acceleration, curves smaller than 180°

There was a significant main effect of type of MP on the longitudinal acceleration objective metric, $F(2,12) = 5.46, p = 0.037$. Pairwise comparison indicated significant $p = 0.088$ difference between medium and large MPs. Contrasts

revealed that longitudinal acceleration in medium configuration, $F(1,6) = 5.46$, $p = 0.037$, $r = 0.55$ was significantly higher than large.

Looking at Figure 5-28 graphs and effect sizes the longitudinal acceleration has slightly decreased with increasing MP size with small to medium effect size. There is a small effect size in the difference between MCAs in small and large MPs meaning they are quite similar. However, there is large effect size in medium, also pairwise comparison shows nearly significant difference $p = 0.06$ between MCAs in the medium MP.

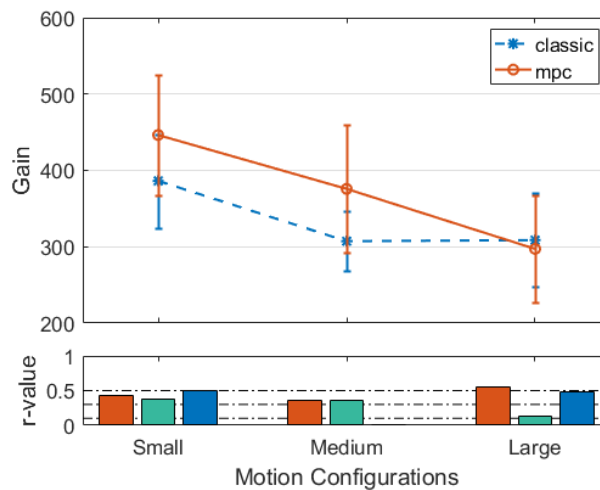


Figure 5-29. Driver model steering gain, curves smaller than 180°

There was a significant main effect of type of MP on the driver model steering gain objective metric, $F(2,12) = 4.16$, $p = 0.027$. Pairwise comparison indicated nearly significant $p = 0.08$ difference between small and medium MPs. Contrasts revealed that the steering gain in small configuration was significantly higher than medium $F(1,6) = 5.54$, $p = 0.036$, $r = 0.56$.

Looking at Figure 5-29 graphs and effect sizes the steering gain has decreased with increasing MP size with medium to large effect size, that shows lower control activity and more relaxed style of driving i.e. improved performance. There is a medium effect size in the difference between MCAs, MPC being higher than classic in small and medium MP, that shows higher control activity i.e. deteriorated performance.

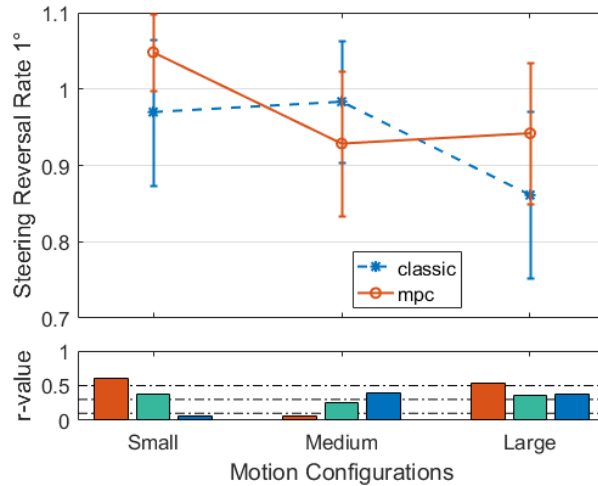


Figure 5-30. Steering reversal rate 1°, curves smaller than 180°

There was a nearly significant main effect of type of MP on the steering reversal rate, $F(2,12) = 2.63$, $p = 0.09$. Contrasts revealed that the steering reversal rate in small configuration was only higher than medium $F(1,6) = 1.85$, $p = 0.19$, $r = 0.36$.

Looking at Figure 5-30 graphs and effect sizes the steering gain has decreased with increasing MP size with medium to large effect size, that shows lower control activity and more relaxed style of driving i.e. improved performance. There is a medium effect size in difference between MCAs, MPC being higher than classic in small and large MP, that shows higher control activity i.e. deteriorated performance.

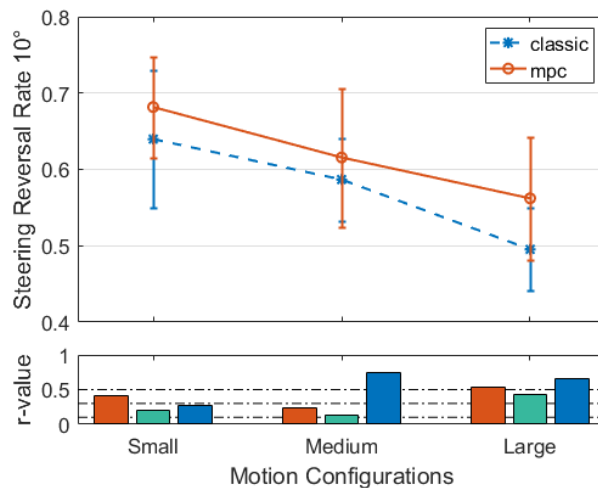


Figure 5-31. Steering reversal rate 10°, curves smaller than 180°

There was a significant main effect of type of MP on the steering reversal rate objective metric, $F(2,12) = 7.4$, $p = 0.002$. Pairwise comparison indicated a significant difference between small, medium and large MPs. Contrasts revealed that the steering reversal rate in small configuration was significantly higher than

medium $F(1,6) = 5.1, p = 0.04, r = 0.54$, also medium configuration was significantly higher than large $F(1,6) = 4.94, p = 0.046, r = 0.54$.

Looking at Figure 5-31 graphs and effect sizes the steering reversal rate has decreased with increasing MP size with medium to large effect size, that shows lower control activity and more relaxed style of driving i.e. improved performance. There is small to medium effect sizes in MCA differences, MPC being higher than classic in all MPs, that shows higher control activity i.e. deteriorated performance.

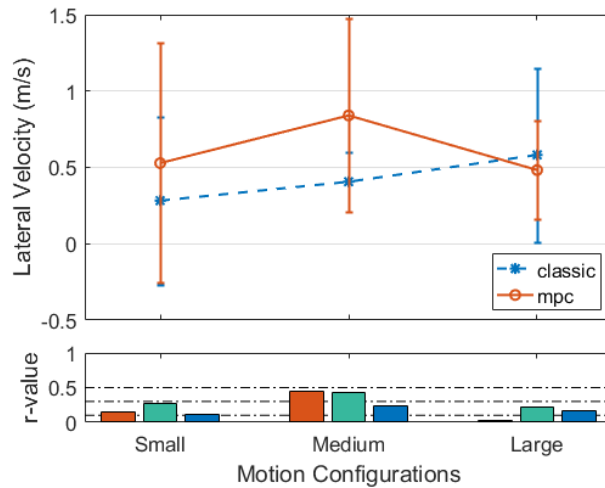


Figure 5-32. Maximum lateral velocity, curves smaller than 180°

There was a significant main effect of type of MCA on the lateral velocity, $F(1,6) = 5.78, p = 0.033, r = 0.29$. Contrasts revealed that MPC was significantly higher than classic. Pairwise comparison, $p = 0.03$ MPC being higher than classic.

Looking at Figure 5-32 graphs and effect sizes the lateral velocity has increased slightly with increasing MP size with small to medium effect sizes. There is small to medium effect sizes in difference between MCAs that has affected drivers' performance differently, where MPC is higher than classic in all MPs.

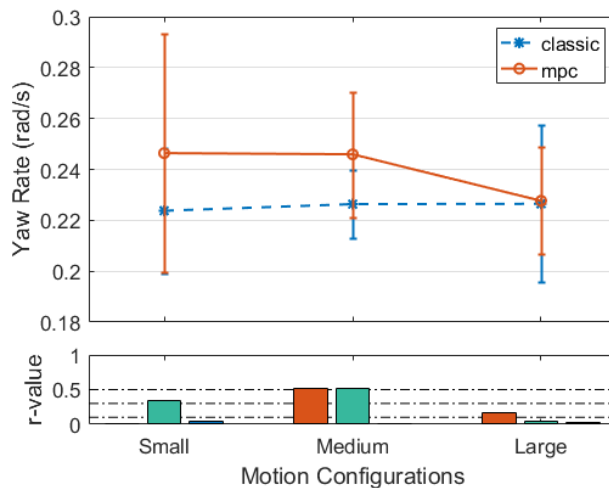


Figure 5-33. Maximum yaw rate, curves smaller than 180°

There was a significant main effect of type of MCA on the yaw rate, $F(1,6) = 5.33$, $p = 0.039$, $r = 0.55$. Contrasts revealed that MPC was significantly higher than classic. Pairwise comparison indicated significance $p = 0.039$, MPC being higher than classic.

Looking at Figure 5-33 graphs and effect sizes the yaw rate has stayed similar with increasing MP size with small effect sizes. There is small to large effect sizes in difference between MCAs that has affected drivers' performance differently, where MPC was higher than classic in all MPs.

Straight lines

In Table 5-16 the RM ANOVA results of time series output measured metrics are shown for both MCA, MP configurations and their interactions.

Table 5-16. Repeated measure ANOVA time series metrics results of straight line grouped sections, LHT task.

Straight Lines			
	MP	MCA	MP*MCA
Long Vel (m/s)	F2.52, P0.11	F0.38, P0.55	F1.74, P0.20
Lat Vel (m/s)	F0.90, P0.42	F0.67, P0.43	F1.14, P0.34
Yaw Rate (rad/s)	F0.79, P0.47	F0.28, P0.61	F1.30, P0.29
Long Acc (m/s ²)	F7.95, P0.00	F0.30, P0.59	F0.61, P0.55
Lat Acc (m/s ²)	F1.05, P0.37	F0.51, P0.49	F1.64, P0.22
Delay Time	F1.20, P0.32	F1.74, P0.22	F1.37, P0.28
Gain	F0.81, P0.46	F4.53, P0.06	F4.77, P0.02
StrgRevsRate 1°	F0.07, P0.93	F1.07, P0.32	F0.61, P0.55
StrgRevsRate 10°	F1.94, P0.17	F8.19, P0.02	F2.03, P0.16

P <= 0.1

P > 0.1

For this grouped section boxes that show significant main or interaction effects on output measures include:

For MP comparison:

- Maximum longitudinal acceleration

For MCA comparison:

- Driver model gain
- Steering wheel reversal rate (10 degree)

For MCA and MP interaction:

- Driver model gain

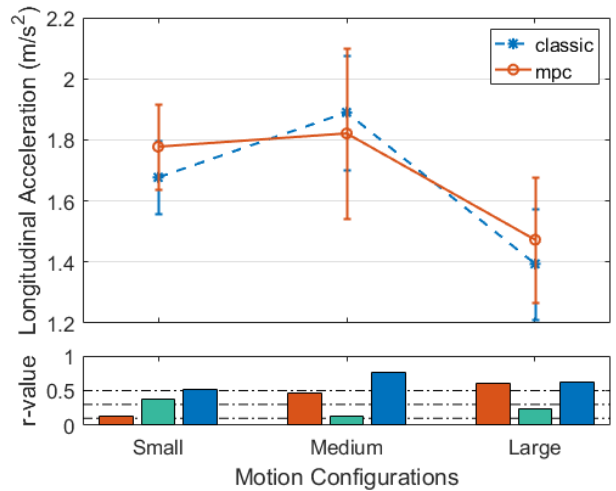


Figure 5-34. Maximum longitudinal acceleration, straight line

There was a significant main effect of type of MP on the longitudinal acceleration objective metric, $F(2,12) = 7.94, p = 0.002$. Pairwise comparison indicated significant $p = 0.088$ difference between large to medium and small MPs. Contrasts revealed that longitudinal acceleration in medium configuration, $F(1,6) = 9.62, p = 0.011, r = 0.7$ was significantly higher than large.

Looking at Figure 5-34 graphs and effect sizes the longitudinal acceleration has fluctuated but decreased with increasing MP size with small to large effect size. There is a small effect size in difference between MCAs in each MPs that has affected drivers' performance quite similarly.

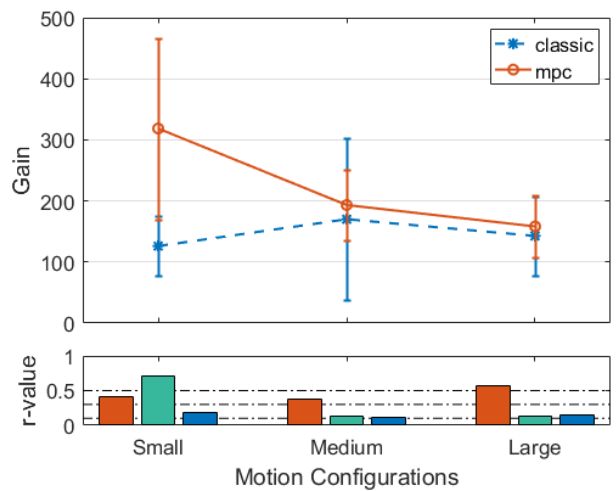


Figure 5-35. Driver model steering gain, straight line

There was a significant main effect of type of MCA on the driver model steering gain, $F(1,6) = 4.5, p = 0.05, r = 0.56$. Contrasts revealed that MPC was

significantly higher than classic. Pairwise comparison indicated significance $p = 0.05$, MPC being higher than classic.

There was a significant interaction effect between the type of MP and the type of MCA used, $F(2,12) = 4.77$, $p = 0.02$. This indicates that MP had different effects on people's objective performance depending on which type of MCA was used. To break down this interaction, contrasts were performed comparing all MP types to all MCA types. These revealed significant interactions when comparing classic to MPC for small compared to medium $F(1,6) = 5.9$, $p = 0.036$, $r = 0.61$.

Looking at Figure 5-35 graph and effect sizes driver model steering gain has slightly decreased with increasing MP size with small effect sizes, that shows lower control activity and more relaxed style of driving i.e. improved performance. There is small to large effect size in difference between MCAs that has affected drivers' performance differently, where MPC is higher than classic in all MPs, that shows higher control activity i.e. deteriorated performance.

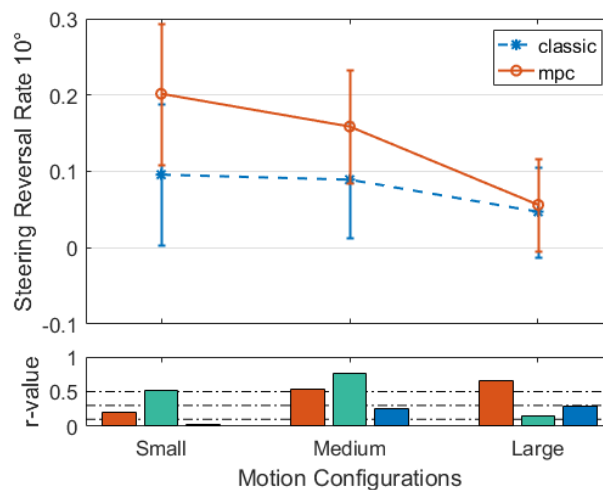


Figure 5-36. Steering reversal rate 10°, straight line

There was a significant main effect of type of MCA on the driver model steering gain, $F(1,6) = 8.19$, $p = 0.016$, $r = 0.67$. Contrasts revealed that MPC was significantly higher than classic. Pairwise comparison indicated significance $p = 0.016$, MPC being higher than classic.

Looking at Figure 5-36 graphs and effect sizes the steering reversal rate has decreased with increasing MP size with small to large effect sizes, that shows lower control activity and more relaxed style of driving i.e. improved performance. There is small to large effect sizes in difference between MCAs that has affected drivers' performance differently, where MPC is higher than classic in all MPs, that shows higher control activity i.e. deteriorated performance.

Inflection zones

In Table 5-17 the RM ANOVA results of time series output measured metrics are shown for both MCA, MP configurations and their interactions.

Table 5-17. Repeated measure ANOVA time series metrics results of inflection zones grouped sections, LHT task.

Inflection Zones				
	MP	MCA	MP*MCA	
Long Vel (m/s)	F1.19, P0.32	F0.22, P0.65	F1.74, P0.20	<div style="background-color: black; width: 100%; height: 100%;"></div> P <= 0.1 <div style="background-color: white; width: 100%; height: 100%;"></div> P > 0.1
Lat Vel (m/s)	F0.80, P0.46	F1.41, P0.26	F0.72, P0.50	
Yaw Rate (rad/s)	F0.26, P0.77	F0.13, P0.72	F0.70, P0.51	
Long Acc (m/s ²)	F4.89, P0.02	F0.22, P0.64	F0.69, P0.51	
Lat Acc (m/s ²)	F1.42, P0.26	F0.14, P0.71	F0.58, P0.57	
Delay Time	F0.06, P0.94	F1.20, P0.29	F2.98, P0.07	
Gain	F1.37, P0.27	F0.00, P0.95	F0.86, P0.44	
StrgRevsRate 1°	F6.05, P0.01	F2.63, P0.13	F0.66, P0.52	
StrgRevsRate 10°	F1.37, P0.27	F0.24, P0.63	F1.28, P0.30	

For this grouped section boxes that show significant main or interaction effects on output measures include:

For MP comparison:

- Maximum longitudinal acceleration
- Steering wheel reversal rate (1 degree)

For MCA and MP interaction:

- Driver model delay time

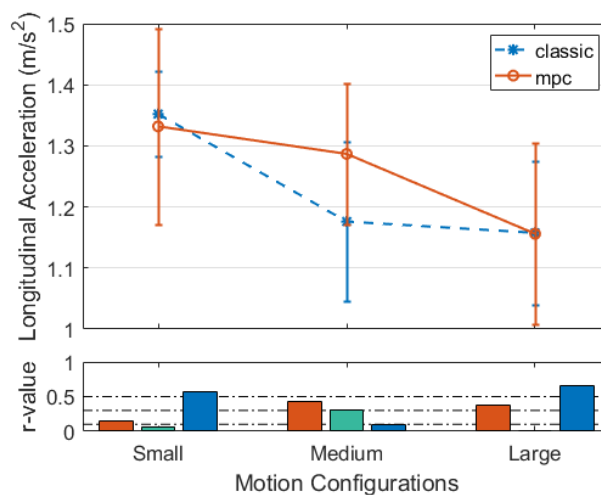


Figure 5-37. Longitudinal acceleration, inflection zone

There was a significant main effect of type of MP on the longitudinal acceleration objective metric, $F(2,12) = 4.88, p = 0.01$. Pairwise comparison indicated significant

$p = 0.07$ difference between large to medium and small MPs. Contrasts revealed that longitudinal acceleration in small configuration, $F(1,6) = 3.84$, $p = 0.07$, $r = 0.49$ was significantly higher than medium.

Looking at Figure 5-37 graphs and effect sizes the longitudinal acceleration has decreased with increasing MP size with small to large effect sizes. There are small and medium effect sizes in the difference between MCAs in each MPs that has affected drivers' performance quite similarly, where MPC is slightly higher in all MPs.

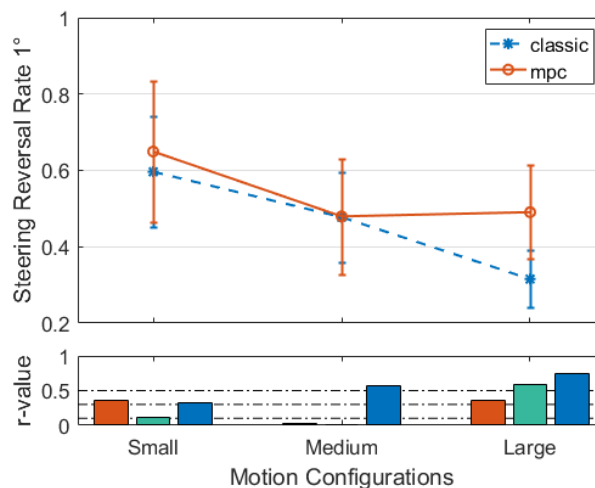


Figure 5-38. Steering reversal rate 1°, inflection zone

There was a significant main effect of type of MP on the steering reversal rate objective metric, $F(2,12) = 6.04$, $p = 0.007$. Pairwise comparison indicated significant $p = 0.012$ difference of objective performance between large to small MPs. Contrasts revealed that steering reversal rate in small configuration, $F(1,6) = 3.94$, $p = 0.07$, $r = 0.49$ was significantly higher than medium.

Looking at Figure 5-38 graph and effect sizes the steering reversal rate has decreased with increasing MP size with medium to large effect sizes, that shows lower control activity and more relaxed style of driving i.e. improved performance. There are small and large effect sizes in the difference between MCAs in each MPs that has affected drivers' performance quite similarly. However, MPC has shown higher steering reversal rate than classic in all MPs, also the detailed pair comparison showed in large the MPC is significantly higher than classic $p = 0.024$, that shows higher control activity i.e. deteriorated performance.

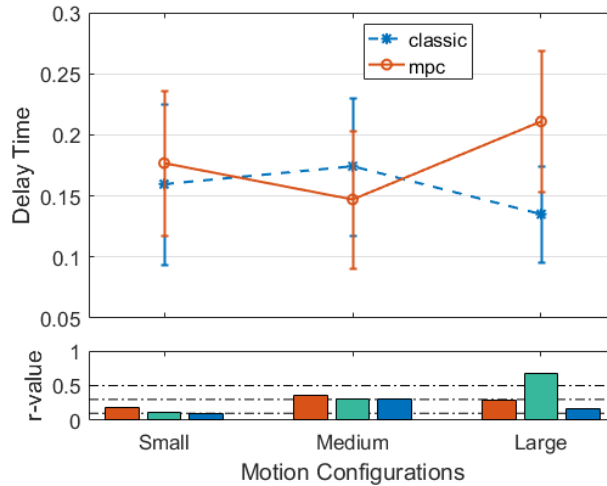


Figure 5-39. Driver model delay time, inflection zone

There was a significant interaction effect between the type of MP and the type of MCA used, $F(2,12) = 2.97, p = 0.069$. This indicates that MP had different effects on drivers' objective performance depending on which type of MCA was used. To break down this interaction, contrasts were performed comparing all MP types to all MCA types. These revealed significant interactions when comparing classic to MPC for medium compared to large $F(1,6) = 7.9, p = 0.015, r = 0.63$.

Whole track

In Table 5-18 RM ANOVA results of time series output measured metrics are shown for both MCA, MP configurations and their interactions.

Table 5-18. Repeated measure ANOVA time series metrics results of whole track, LHT task.

Whole Track				
	MP	MCA	MP*MCA	
Long Vel (m/s)	F0.35, P0.74	F1.58, P0.43	F0.21, P0.83	<div style="display: flex; align-items: center;"> <div style="width: 10px; height: 100%; background-color: black; margin-right: 5px;"></div> <div style="text-align: left; padding-left: 5px;"> <p>P <= 0.1</p> <p>P > 0.1</p> </div> </div>
Lat Vel (m/s)	F0.70, P0.59	F0.11, P0.80	F0.83, P0.55	
Yaw Rate (rad/s)	F1.95, P0.34	F0.39, P0.64	F10.73, P0.09	
Long Acc (m/s ²)	F1.01, P0.50	F3.11, P0.33	F0.31, P0.77	
Lat Acc (m/s ²)	F0.08, P0.92	F9.66, P0.20	F0.09, P0.91	
Delay Time	F1.68, P0.37	F0.10, P0.81	F1.16, P0.46	
Gain	F0.90, P0.53	F4917.26, P0.01	F0.10, P0.91	
StrgRevsRate 1°	F0.64, P0.61	F4.20, P0.29	F1.67, P0.37	
StrgRevsRate 10°	F0.19, P0.84	F0.08, P0.83	F0.16, P0.86	

For this grouped section points that show significant main or interaction effects on output measures include:

For MCA comparison:

- Driver model steering gain

For MCA and MP interaction:

- Maximum yaw rate (absolute value)

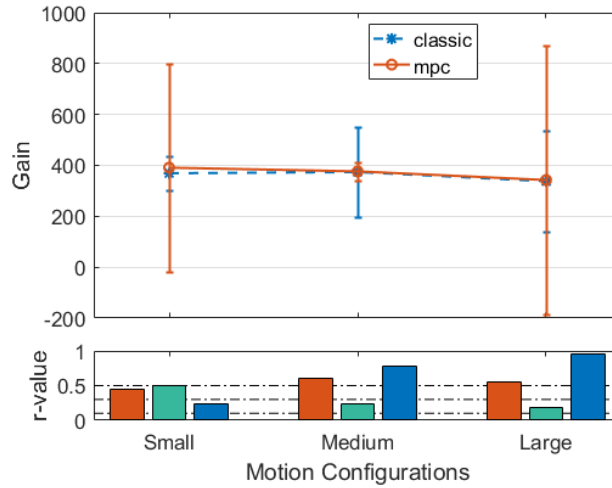


Figure 5-40. Driver model gain, whole track

There was a significant main effect of type of MCA on the driver model gain, $F(1,6) = 4917.3, p = 0.009, r = 0.99$. Contrasts revealed that MPC was significantly higher than classic. Pairwise comparison indicated significance $p = 0.009$, MPC being higher than classic.

Looking at Figure 5-40 graphs and effect sizes the driver model steering gain has slightly decreased with increasing MP size with small to large effect sizes, that shows lower control activity and more relaxed style of driving i.e. improved performance. There are small to large effect sizes in difference between MCAs that has affected drivers' performance differently, where MPC is higher than classic, that shows higher control activity i.e. deteriorated performance.

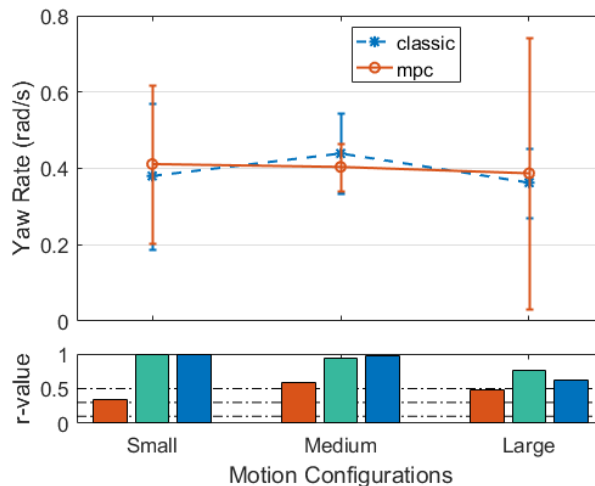


Figure 5-41. Maximum yaw rate, whole track

There was a nearly significant interaction effect between the type of MP and the type of MCA used, $F(2,4) = 10.7$, $p = 0.085$. This indicates that MP had different effects on drivers' objective performance depending on which type of MCA was used. To break down this interaction, contrasts were performed comparing all MP types to all MCA types. These revealed nearly significant interactions when comparing classic to MPC for medium compared to large $F(1,6) = 58.647$, $p = 0.082$, $r = 0.99$.

5.10.3.2 Slalom (SLM)

Different sections of negotiating a path between cones in slalom driving task have different characteristics, therefore it was split into sections and each section was analysed separately. Due to similarity in nature of many of the sections and to reduce the number of reporting results the sections throughout the SLM course was divided into straight lines, peaks and inflection zone section groups. There are 14 sections in total. All the sections are shown in Figure 5-42, green dots show the entry of a section and red dots shows the exit of a section.

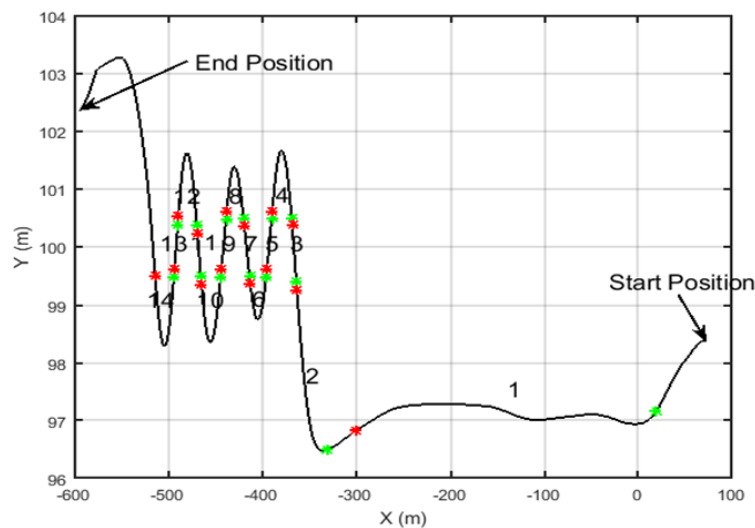


Figure 5-42. Slalom course and sections

To be able to group the sections initial analysis were performed. Comparing the results of the 14 separate sections with the corresponding grouped sections, showed similarity in the values; this indicated that it was acceptable to group the sections. The objective metrics of a group section is calculated from the average value of all sections belonging to that group as Table 5-19.

Table 5-19. Group sections, SLM task

<i>Group section</i>	<i>Section Numbers</i>
Straight lines	1
Peak zones	4, 6, 8, 10, 12, 14
Inflection zones	3, 5, 7, 9, 11, 13
Whole track	

Aggregated performance

The aggregated performance measures for SLM task consist of three metrics of:

- Lap time, duration of time that drivers completed the task
- Spin/skid outs and cone hits, trials that drivers spin out and hit the cones
- Speed variability, the standard deviation of drivers speed during the task

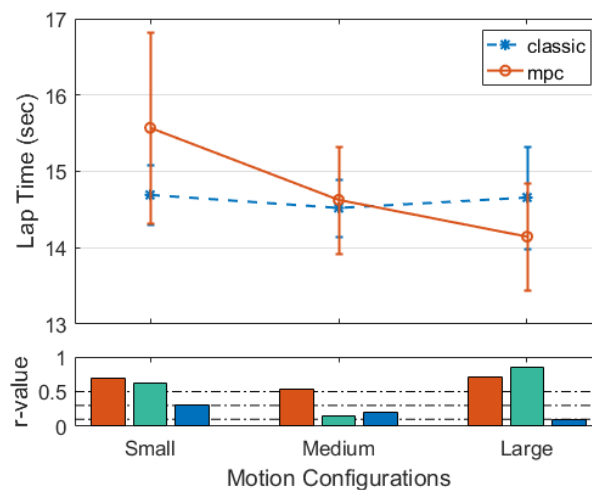


Figure 5-43. Lap time, SLM

From Figure 5-43 it is observable that the lap time has decreased with the increase of MP size. In MPC the largest MP has the smallest lap time and vice versa, in classic the lap time is similar between MPs. Having considerable effect sizes reveal that providing larger motion to drivers results in lower lap time to finish the driving task.

The lower lap time with the increase of MP size might be indicative of improved performance when drivers are asked to keep a constant speed, although the number of failures is increased as well (described next) and improved performance may not be concluded.

Comparing the MCAs in each MP size, the classic has lower lap time in small and medium MP while it is higher than MPC in large MP. Thus, drivers had mostly

higher lap time driving the MPC configurations than classic, reflecting better performance in classic.

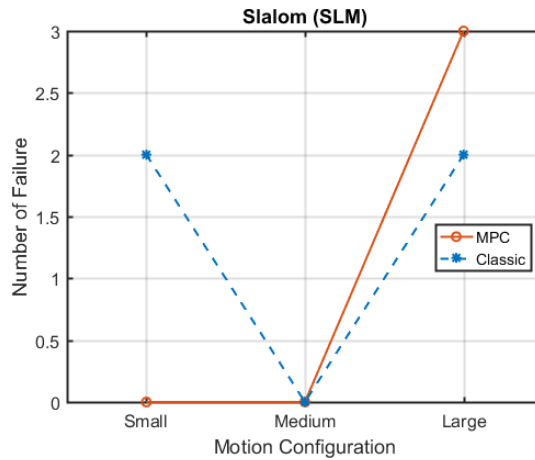


Figure 5-44. Spin/skid outs and cone hits, SLM

From Figure 5-44, despite the small total number of failures, it has increased with increasing MP size in MPC but fluctuated for the classic. It might be indicating that providing larger motion to drivers results in a greater number of failures in performing the task, reflecting the deteriorated performance of drivers.

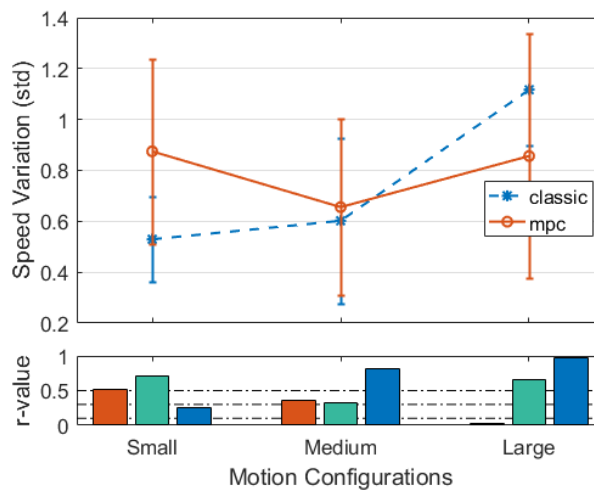


Figure 5-45. Speed variations, SLM

From Figure 5-45, the speed variation increased with increasing MP size in classic and fluctuated in MPC. Having considerable large effect sizes reveal that providing larger motion to drivers results in more speed variation during driving, reflecting the deteriorated performance of drivers.

Comparing the MCAs in each MP size, the classic has lower speed variation than MPC in small and medium MPs, for large the classic is higher. Having large effect sizes indicate that drivers had mostly larger speed variation driving the MPC configurations than classic, reflecting better performance in classic.

Time series

In this section, the results of repeated measure ANOVA and post hoc analysis on the time series metrics in each of the group sections are presented, and where there are significant or near significant results those are elaborated. Looking at Table 5-20 to Table 5-23 the columns (on x-axis) belong to independent variables and their interaction and each row (on y-axis) belong to a dependent measured variable metric. The F and p values are shown on each point corresponding to a factor and an output measure. Black highlighted point shows where the p-value is less than 0.1 that means there is a nearly significant difference.

Straight lines

In Table 5-20 the RM ANOVA results of time series output measured metrics are shown for both MCA, MP configurations and their interactions.

Table 5-20. Repeated measure ANOVA time series metrics results of straight lines grouped sections, SLM task.

Straight Lines			
	MP	MCA	MP*MCA
Long Vel (m/s)	F3.05, P0.10	F2.54, P0.19	F0.05, P0.95
Lat Vel (m/s)	F0.91, P0.44	F0.95, P0.38	F0.95, P0.43
Yaw Rate (rad/s)	F1.25, P0.34	F0.51, P0.51	F0.50, P0.62
Long Acc (m/s ²)	F0.67, P0.54	F1.76, P0.26	F1.04, P0.40
Lat Acc (m/s ²)	F1.93, P0.21	F0.23, P0.66	F0.35, P0.72
Delay Time	F1.18, P0.36	F0.00, P0.97	F1.21, P0.35
Gain	F2.72, P0.13	F1.51, P0.29	F1.79, P0.23
StrgRevsRate 1°	F1.23, P0.34	F0.97, P0.38	F0.15, P0.86
StrgRevsRate 10°	F1.06, P0.39	F0.09, P0.78	F0.07, P0.93

For this grouped section, there is no point that shows significant main or interaction effects on output measures.

Peak zone

In Table 5-21 RM ANOVA results of time series output measured metrics are shown for both MCA, MP configurations and their interactions.

Table 5-21. Repeated measure ANOVA time series metrics results of peak zone grouped sections, SLM task.

	Peak zones			
Long Vel (m/s)	F3.19, P0.10	F2.80, P0.17	F0.58, P0.58	 P <= 0.1 P > 0.1
Lat Vel (m/s)	F5.79, P0.03	F0.40, P0.56	F0.83, P0.47	
Yaw Rate (rad/s)	F6.57, P0.02	F0.29, P0.62	F1.27, P0.33	
Long Acc (m/s ²)	F0.51, P0.62	F0.03, P0.87	F2.83, P0.12	
Lat Acc (m/s ²)	F0.07, P0.93	F3.38, P0.14	F0.20, P0.83	
Delay Time	F7.45, P0.01	F7.60, P0.05	F0.15, P0.86	
Gain	F0.68, P0.53	F0.38, P0.57	F0.62, P0.56	
StrgRevsRate 1°	F2.76, P0.12	F12.34, P0.02	F3.53, P0.08	
StrgRevsRate 10°	F2.24, P0.17	F2.89, P0.16	F0.59, P0.58	
	MP	MCA	MP*MCA	

For this grouped section points that show significant main or interaction effects on output measures include:

For MP comparison:

- Maximum longitudinal velocity
- Maximum lateral velocity (absolute value)
- Maximum yaw rate (absolute value)
- Driver model delay time

For MCA comparison:

- Driver model delay time
- Steering wheel reversal rate (1 degree)

For MCA and MP interaction:

- Steering wheel reversal rate (1 degree)

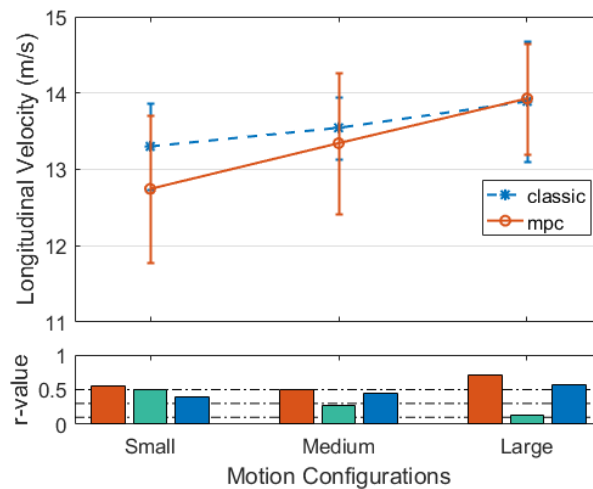


Figure 5-46. Maximum longitudinal velocity, peak zones

There was a nearly significant main effect of type of MP on the longitudinal velocity objective metric, $F(2,12) = 3.19$, $p = 0.09$. Contrasts revealed that longitudinal velocity in medium configuration, $F(1,6) = 5.03$, $p = 0.089$, $r = 0.74$ was significantly higher than small.

Looking at Figure 5-46 graphs and effect sizes the longitudinal velocity has increased with increasing MP size with medium to large effect size. There is a small to large effect size in difference between MCAs that has affected drivers' performance quite similarly.

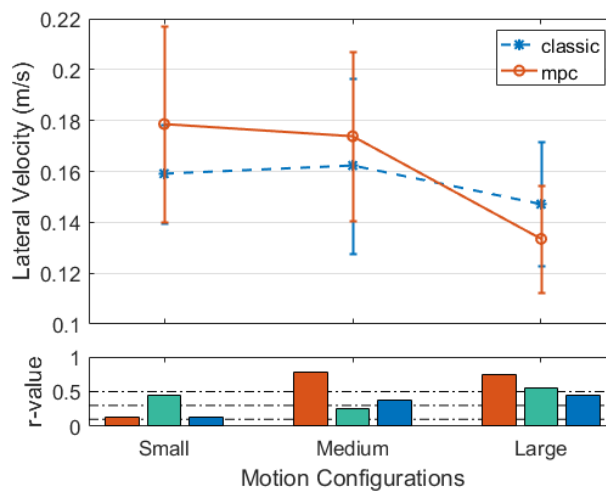


Figure 5-47. Maximum lateral velocity, peak zones

There was a significant main effect of type of MP on the lateral velocity objective metric, $F(2,12) = 5.79$, $p = 0.027$. Contrasts revealed that lateral velocity in medium configuration, $F(1,6) = 5.96$, $p = 0.07$, $r = 0.77$ was nearly significantly higher than large. Pairwise comparison indicated significant $p = 0.04$ difference in the performance between large to small MPs.

Looking at Figure 5-47 graphs and effect sizes the longitudinal velocity has decreased with increasing MP size with small to large effect size. There are small to large effect sizes in difference between MCAs that has affected drivers' performance quite similarly.

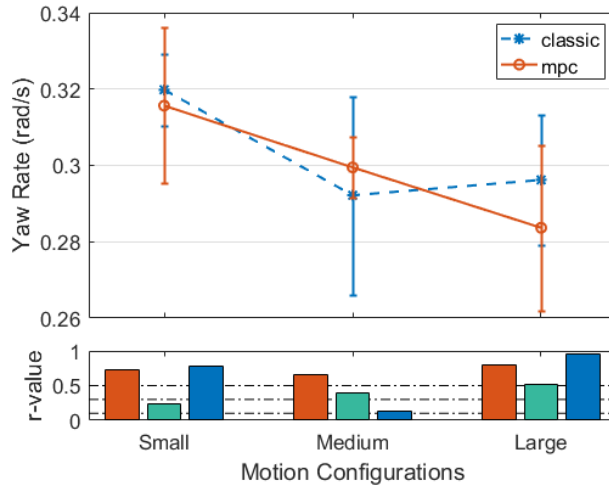


Figure 5-48. Maximum yaw rate, peak zones

There was a significant main effect of type of MP on the yaw rate objective metric, $F(2,12) = 6.57$, $p = 0.02$. Contrasts revealed that yaw rate in small configuration, $F(1,6) = 6.57$, $p = 0.062$, $r = 0.79$ was nearly significantly higher than medium. Pairwise comparison indicated significant $p = 0.017$ difference in the performance between large to small MPs.

Looking at Figure 5-48 graphs and effect sizes the yaw rate has decreased with increasing MP size with small to large effect size. There is small to large effect size in difference between MCAs that has affected drivers' performance quite similarly.

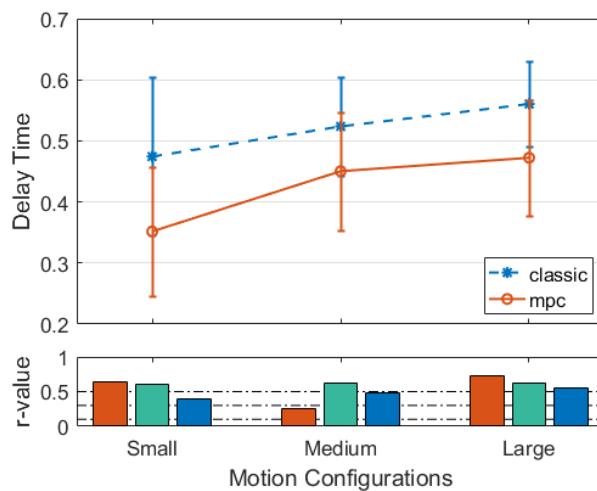


Figure 5-49. Driver model delay time, peak zone

There was a significant main effect of type of MP on the driver model delay time objective metric, $F(2,12) = 7.45$, $p = 0.014$. Contrasts revealed that the delay time in small configuration, $F(1,6) = 5.15$, $p = 0.08$, $r = 0.75$ was nearly significantly

lower than medium. Pairwise comparison indicated significant $p = 0.0017$ difference in the performance between large to small MPs.

There was a significant main effect of type of MCA on the driver model delay time, $F(1,6) = 7.6, p = 0.05, r = 0.80$. Contrasts revealed that classic was significantly higher than MPC. Pairwise comparison indicated significance $p = 0.05$, classic being higher than MPC.

Looking at Figure 5-49 graphs and effect sizes the driver model delay time has increased with increasing MP size with small to large effect sizes. There is a large effect size in difference between MCAs that has affected drivers' performance differently, where classic is higher than MPC.

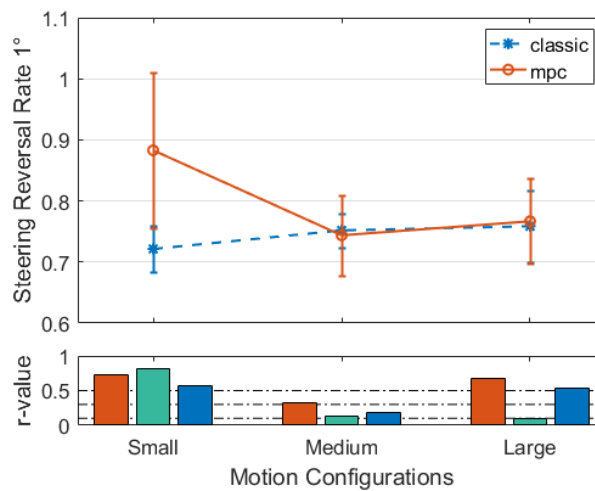


Figure 5-50. Steering reversal rate 1°, peak zone

There was a significant main effect of type of MCA on the steering wheel reversal rate, $F(1,6) = 7.6, p = 0.024, r = 0.87$. Contrasts revealed that MPC was significantly higher than classic. Pairwise comparison indicated significance $p = 0.024$, MPC being higher than classic.

There was a nearly significant interaction effect between the type of MP and the type of MCA used, $F(2,12) = 3.53, p = 0.079$. This indicates that MP had different effects on people's objective performance depending on which type of MCA was used. To break down this interaction, contrasts were performed comparing all MP types to all MCA types. These revealed nearly significant interactions when comparing classic to MPC for small compared to medium $F(1,6) = 7.9, p = 0.1, r = 0.72$.

Looking at Figure 5-50 graphs and effect sizes the steering reversal rate has fluctuated in MPC and slightly increased with increasing MP size with medium to large effect sizes. There is small to large effect size in difference between MCAs

that has affected drivers' performance differently, where MPC is higher than classic, that shows higher control activity i.e. deteriorated performance.

Inflection zone

In Table 5-22 RM ANOVA results of time series output measured metrics are shown for both MCA, MP configurations and their interactions.

Table 5-22. Repeated measure ANOVA time series metrics results of inflection zone grouped sections, SLM task.

Inflection Zones			
Metric	MP	MCA	MP*MCA
Long Vel (m/s)	F1.15, P0.36	F3.50, P0.13	F2.53, P0.14
Lat Vel (m/s)	F2.53, P0.14	F0.37, P0.58	F0.74, P0.51
Yaw Rate (rad/s)	F0.72, P0.51	F3.23, P0.15	F0.88, P0.45
Long Acc (m/s ²)	F0.27, P0.77	F4.80, P0.09	F1.95, P0.20
Lat Acc (m/s ²)	F1.43, P0.29	F1.28, P0.32	F1.23, P0.34
Delay Time	F4.43, P0.05	F0.05, P0.83	F0.51, P0.62
Gain	F1.32, P0.32	F9.25, P0.04	F0.11, P0.90
StrgRevsRate 1°	F1.00, P0.41	F1.00, P0.37	F1.00, P0.41
StrgRevsRate 10°	F1.54, P0.32	F1.38, P0.35	F1.33, P0.37

For this grouped section points that show significant main or interaction effects on output measures include:

For MP comparison:

- Driver model delay time

For MCA comparison:

- Maximum longitudinal acceleration
- Driver model gain

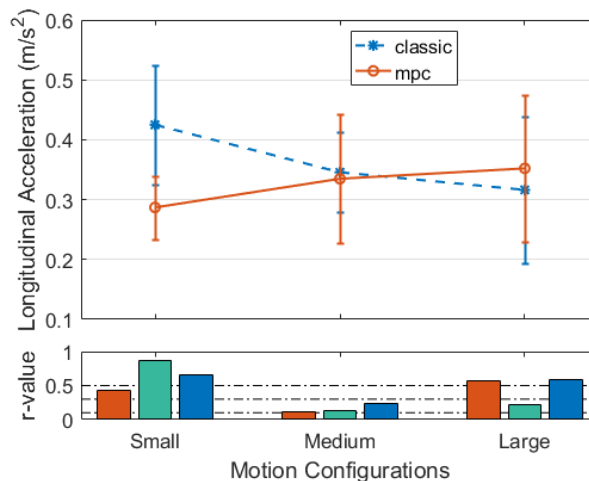


Figure 5-51. Maximum longitudinal acceleration, inflection zone

There was a nearly significant main effect of type of MCA on the longitudinal acceleration, $F(1,6) = 4.8$, $p = 0.09$, $r = 0.74$. Contrasts revealed that classic was significantly higher than MPC. Pairwise comparison indicated nearly significance $p = 0.09$, the classic being higher than MPC.

Looking at Figure 5-51 graphs and effect sizes the longitudinal acceleration has stayed similar with increasing MP size with small to large effect sizes. There are small to large effect sizes in difference between MCAs that has affected drivers' performance differently, where classic is higher than MPC.

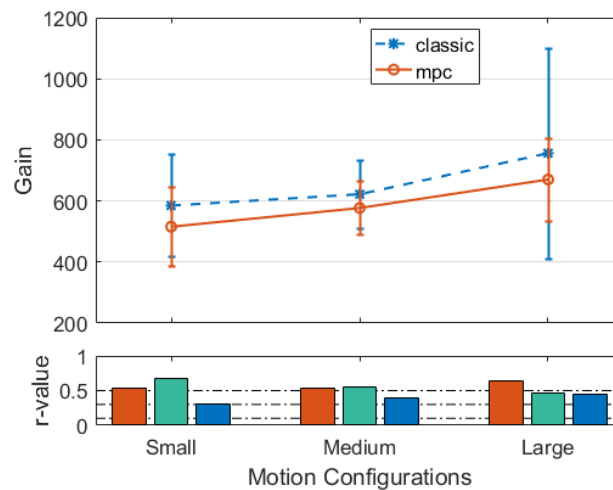


Figure 5-52. Driver model gain, inflection zone

There was a significant main effect of type of MCA on the driver model gain, $F(1,6) = 9.24$, $p = 0.038$, $r = 0.83$. Contrasts revealed that classic was significantly higher than MPC. Pairwise comparison significance also confirmed it $p = 0.038$.

Looking at Figure 5-52 graph and effect sizes the driver model gain has increased with increasing MP size with small to large effect sizes, that shows higher control activity and less relaxed style of driving i.e. deteriorate performance. There are medium to large effect sizes in difference between MCAs that has affected drivers' performance differently, where classic is higher than MPC, that shows higher control activity i.e. deteriorated performance.

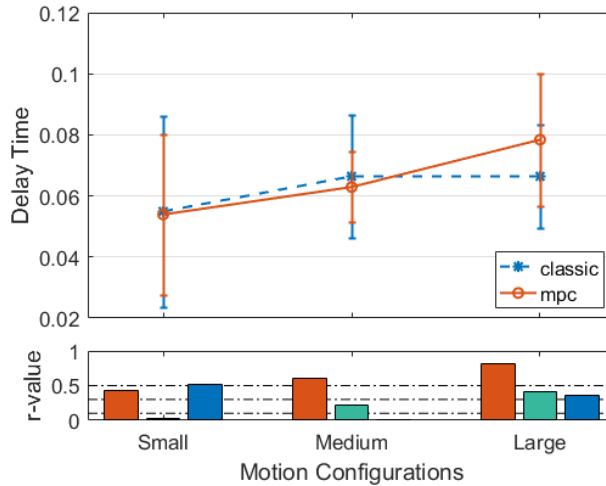


Figure 5-53. Driver model delay time, inflection zone

There was a significant main effect of type of MP on the driver model delay time objective metric, $F(2,12) = 4.42, p = 0.05$. Contrasts revealed that the delay time in small configuration, $F(1,6) = 5.15, p = 0.00003, r = 0.99$ was significantly lower than large. Pairwise comparison indicated significant $p = 0.0001$ difference in the performance between large to small MPs.

Looking at Figure 5-53 graphs and effect sizes the driver model delay has increased with increasing MP size with medium to large effect sizes. There are small to large effect sizes in difference between MCAs that has affected drivers' performance quite similarly.

Whole track

In Table 5-23 RM ANOVA results of time series output measured metrics are shown for both MCA, MP configurations and their interactions.

Table 5-23. Repeated measure ANOVA time series metrics results of whole track, SLM task.

Whole Track					
	MP	MCA	MP*MCA		
Long Vel (m/s)	F4.04, P0.06	F0.36, P0.58	F1.06, P0.39	P <= 0.1	
Lat Vel (m/s)	F0.20, P0.82	F0.00, P0.96	F5.85, P0.03		
Yaw Rate (rad/s)	F0.32, P0.73	F0.70, P0.45	F1.26, P0.33		
Long Acc (m/s ²)	F0.26, P0.78	F0.23, P0.66	F1.50, P0.28		
Lat Acc (m/s ²)	F0.18, P0.84	F3.40, P0.14	F0.59, P0.58		
Delay Time	F1.29, P0.33	F0.05, P0.84	F0.53, P0.61		
Gain	F0.80, P0.48	F5.12, P0.09	F0.99, P0.41		P > 0.1
StrgRevsRate 1°	F2.31, P0.16	F0.24, P0.65	F0.03, P0.97		
StrgRevsRate 10°	F1.87, P0.22	F2.11, P0.22	F0.62, P0.56		

For this grouped section points that show significant main or interaction effects on output measures include:

For MP comparison:

- Maximum longitudinal velocity

For MCA comparison:

- Driver model steering gain

For MCA and MP interaction:

- Maximum lateral velocity (absolute value)

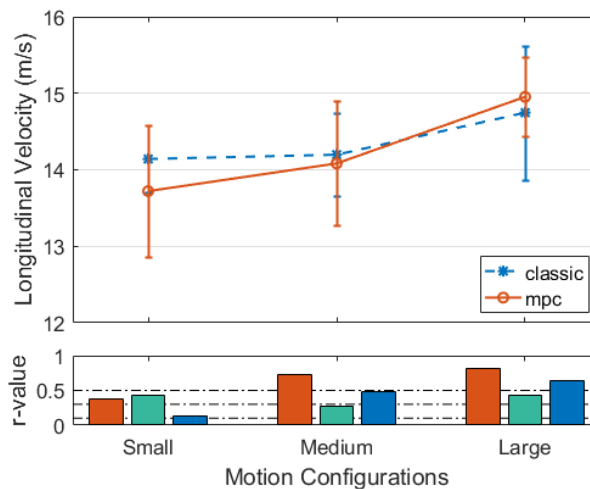


Figure 5-54. Longitudinal velocity, whole track

There was a nearly significant main effect of type of MP on the longitudinal velocity objective metric, $F(2,12) = 4.04$, $p = 0.06$. Contrasts revealed that longitudinal velocity in medium configuration, $F(1,6) = 2.6$, $p = 0.1$, $r = 0.63$ was nearly significantly lower than large. Pairwise comparison indicated significant $p = 0.09$ difference in the performance between large to small MPs.

Looking at Figure 5-54 graphs and effect sizes the longitudinal velocity has increased with increasing MP size with small to large effect sizes. There is small to medium effect size in difference between MCAs that has affected drivers' performance quite similarly.

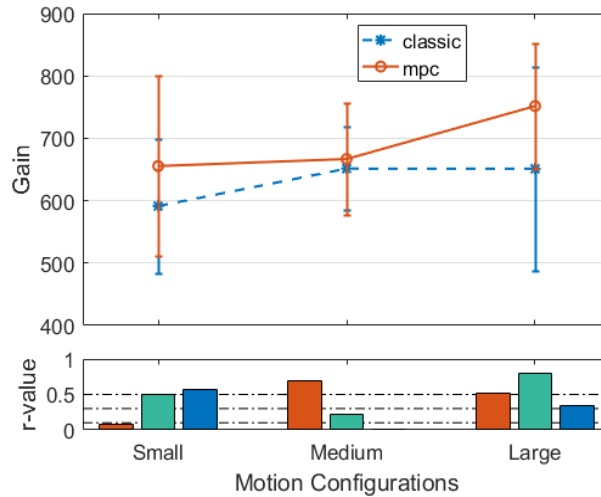


Figure 5-55. Driver model steering gain, whole track

There was a significant main effect of type of MCA on the driver model steering gain, $F(1,6) = 5.12$, $p = 0.08$, $r = 0.75$. Contrasts revealed that MPC was significantly higher than classic. Pairwise comparison indicated significance $p = 0.08$, MPC being higher than classic.

Looking at Figure 5-55 graphs and effect sizes the driver model steering gain has increased with increasing MP size with small to large effect sizes, that shows higher control activity i.e. deteriorated performance. There is small to large effect size in difference between MCAs that has affected drivers' performance differently, where MPC is higher than classic, that shows higher control activity i.e. deteriorated performance.

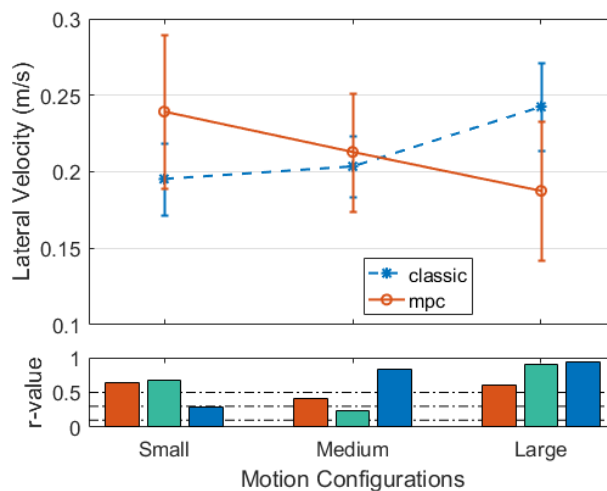


Figure 5-56. Maximum lateral velocity, whole track

There was a nearly significant interaction effect between the type of MP and the type of MCA used, $F(2,12) = 5.8$, $p = 0.027$. This indicates that MP had different effects on drivers' objective performance depending on which type of MCA was

used. To break down this interaction, contrasts were performed comparing all MP types to all MCA types. These revealed nearly significant interactions when comparing classic to MPC for medium compared to large $F(1,6) = 5.07, p = 0.08, r = 0.75$.

5.11 Discussion and conclusions

Due to the major impact of motion cueing on simulator fidelity the current study was designed to address how the variations in simulator's motion cueing subsystems affect the fidelity. To this end, the main components of the simulator motion system were chosen as variables to evaluate their effect on the simulator fidelity. Those were motion cueing algorithms (MCA) and motion platform (MP) workspace size. As the first aim of this study two MCAs with high previously reported fidelity were selected to be compared, those were classic and MPC; as the second aim of this study three sizes of MPs were considered to make comparison among them. Moreover, because of lacking previous research considering interacting effects that MP sizes might have on the MCAs fidelity assessments, the MCA comparisons (the first aim) took place in each of the MP sizes. Two driving tasks of Land Rover Handling Track (LHT) and Slalom (SLM) were selected to compare if there is relation between both aims and driving tasks. In this regard, two research questions were defined and evaluated through drivers' subjective ratings of simulator fidelity and their objective performance. The permutation of MPs and MCAs created six motion configurations of small-MPC (S-M) and small-classic (S-C), medium-MPC (M-M), medium-classic (M-C), large-MPC (L-M) and large-classic (L-C), the experiment was designed to compare between them and address the research questions. The research questions and main findings of the experiment are presented below.

Research question 1 – How do the different MCAs affect the drivers' subjective ratings of simulator fidelity and their objective behaviour?

I. Subjective fidelity results

For the LHT task, the results of the repeated measure ANOVA for all three questions showed a significant or nearly significant effect of type of MCA on subjective preferences, where mostly the MPC was rated higher than the classic. This is in line with the predicted hypothesis for LHT test at the beginning of the chapter, that was expecting MPC to be the higher fidelity configuration in all the three MPs.

Based on analysis of plots and effect sizes it was observed that for all the three grouped questions the classic was of slightly higher fidelity in small MP, whereas

the MPC was the higher fidelity in both medium and large MPs. The effect sizes were small for both small and medium MPs, indicating that small subjective fidelity difference between the MCAs. In other words, drivers see that MCAs are quite similar (slightly different) in both small and medium MPs. For large MP the effect size was large, indicative of bigger subjective fidelity difference between the MCAs to drivers, results are summarised in Table 5-24.

For the SLM task results of repeated measure, ANOVA for all three questions did not show a significant effect of type of MCAs on subjective preferences. However, a post hoc pairwise comparison of MCAs in each MP sizes showed classic was rated significantly $p < 0.01$ higher than MPC in small motion platform size for all three questions. The hypothesis was to expect classic to be the higher fidelity configuration in all the three MPs, however it was violated only for medium MP where the MPC showed higher fidelity.

Based on analysis of plots and effect sizes for all the three grouped questions it was observable the classic was of higher fidelity in small and large MPs, whereas the MPC was the higher fidelity in medium MP. The effect sizes were large and medium for small and medium MPs, indicating that considerable subjective fidelity difference between the MCAs. In other words, drivers see the MCAs different in both the small and medium MPs. For large MP the effect sizes were small, indicating that there is smaller subjective fidelity difference between the MCAs to drivers. Moreover, the MCA comparisons get less distinct to drivers from with increasing MP size, results are summarised in Table 5-25.

II. Objective behavioural results

For LHT task in each MP size comparing the classic and MPC, see Table 5-24:

Aggregated performance – for all the four lap time, number of failures, speed variation and lateral position deviation aggregated performance metrics, MPC has shown the higher values in small and medium MPs. In large MP MPC has shown higher values in lateral position deviation and number of failures, whereas classic had higher value of lap time and speed variation.

Overall, in most of the comparisons between MCAs higher lap time, number of failures, speed variation and lateral position deviation was observed in MPC compared to classic, reflecting the deteriorated performance of drivers while experiencing the MPC algorithm, although they subjectively preferred it in some of the MP sizes. Time series – In the whole track and three of the grouped road sections of curves greater than 180° , curves smaller than 180° , and inflection zones, where there was a significant main effect of type of MCAs on most of the output measured metric, the MPC has shown higher values for the objective

metrics. Those included the steering wheel reversal rates, and driver model gain, that shows higher control activity, and reflecting the deteriorated performance.

For SLM task in each MP size comparing the classic and MPC, see Table 5-25:

Aggregated performance - for the lap time and speed variation aggregated performance metrics, MPC has shown the higher values in small and medium MPs, and classic in large. In the number of failures, it is of mixed results between MPs.

Overall, in many of the comparisons between MCAs higher lap time, number of failures, speed variation was observed in MPC compared to classic, reflecting the deteriorated performance of drivers while experiencing the MPC algorithm. Time series - In the whole track and two of the grouped road sections of inflection zones and peak zones, where there was a significant main effect of type of MCAs on the output measured metric depending on the section, there were mixed results of MPC and classic. In inflection zone it is always the classic that has the highest value for the objective metrics, it is a mix of classic and MPC for the peak zones and MPC for the whole track. In total, it is more of mixed results depending on the sections.

Table 5-24. Summary of results, research question 1 (highest values), LHT task

			Significant Overall Result	Plot and effect size results			
				Small	Medium	Large	
Subjective	Overall Assessment		MPC	Classic	MPC	MPC	
	Motion Cueing		MPC	Similar	MPC	MPC	
	Vehicle Assessment		MPC	Classic	MPC	MPC	
Objective	Aggregated Performance	Lap Time		 	MPC	MPC	Classic
		Failure Number		 	MPC	MPC	MPC
		Speed Variation		 	MPC	MPC	Classic
		Lateral Deviation		 	MPC	MPC	MPC
	Time Series and driver model	Curves ≥ 180	DRYPE Gain	MPC	MPC	MPC	MPC
			Rev Rate 10	MPC	MPC	MPC	MPC
		Curves ≤ 180	Lat Velocity	MPC	MPC	MPC	Classic
			Yaw Rate	MPC	MPC	MPC	MPC
		Straight Line	DRYPE Gain	MPC	MPC	MPC	MPC
			Rev Rate 10	MPC	MPC	MPC	MPC
		Inflection Zone	-				
		Whole Track	DRYPE Gain	MPC	MPC	MPC	MPC

Table 5-25. Summary of results, research question 1 (highest values), SLM task

			Significant Overall Result	Plot and effect size results			
				Small	Medium	Large	
Subjective	Overall Assessment		-	Classic	MPC	Classic	
	Motion Cueing		-	Classic	MPC	Classic	
	Vehicle Assessment		-	Classic	MPC	Classic	
Objective	Aggregated Performance	Lap Time		MPC	MPC	Classic	
		Failure Number		Classic	Same	MPC	
		Speed Variation		MPC	MPC	Classic	
	Time Series and driver model	Straight Line	-				
		Peak Zone	DRYPE Delay	Classic	Classic	Classic	Classic
			Rev Rate 1	MPC	MPC	Classic	MPC
		Inflection Zone	Long Acc	Classic	Classic	Classic	MPC
			DRYPE Gain	Classic	Classic	Classic	Classic
	Whole Track	DRYPE Gain	MPC	MPC	MPC	MPC	

In summary, in the LHT task drivers mostly preferred the MPC over the classic, while in SLM the difference was not significant, although some preferences of the classic over MPC. Overall, in terms of aggregated performance measurements including the lap time, number of failures and speed variation, in most of the comparisons between MCAs, the deteriorated performance of drivers were observed in the MPC algorithm in both driving tasks. In the time series metrics, the differences between the MCAs were consistent in LHT and mixed in SLM task. In the LHT nearly in all of the measurement metrics, the MPC had higher values. It was comprised of the steering reversal rates and driver model steering gain i.e. the measurements over the drivers' control activity. It reflects more relaxed style of driving and improved performance in classic.

Research question 2 – How do the different MPs affect the drivers' subjective ratings of simulator fidelity and their objective behaviour?

I. Subjective fidelity results

For the LHT task the results of repeated measure ANOVA for the motion cueing questions showed a significant or nearly significant effect of type of MPs on subjective preferences, where the large configuration was rated significantly higher than medium. Other questions did not show a significant effect of type of MPs on subjective preferences. However, a post hoc pairwise comparison of MPs in each MCA showed medium was rated nearly significantly $p < 0.1$ higher than small in MPC for the vehicle assessment question.

Based on analysis of plots and effect sizes it was observable for the MPC algorithm, in all three questions the medium to large MPs comes out as higher fidelity with large effect sizes. In the classic algorithm, the medium MP shows the higher fidelity for all the three groups of questions with small to large effect sizes. It is observable for the MPC algorithm, in all three questions the medium to large MP comes out as higher fidelity with large effect size. In the classic algorithm, the medium MP shows the higher fidelity for all the three groups of questions with small to medium effect sizes.

In MPC, the effect sizes are small between the medium and large MPs, indicating that small subjective fidelity difference between them, while there is large effect size between the medium and large compared to small MP. In other words, the medium and large MPs are quite similar (slightly different) to drivers and those are much different to small MP to drivers. In classic, the effect size is small between small and medium MPs, indicating that there is small subjective fidelity difference between them, while there is large effect size between the small and medium to large MP.

This might be indicating that for the LHT task drivers preferred larger motion configuration as the ratings were increasing with increasing MP size, results are summarised in Table 5-26.

For the SLM task results of repeated measure ANOVA for all three questions did not show a significant effect of type of MPs on subjective preferences. Based on analysis of plots and effect sizes it was observable for the MPC algorithm, in all three questions the medium MP comes out as higher fidelity with medium effect size. In the classic algorithm, the small MP shows the higher fidelity for all three questions with small and large effect sizes. Having big enough effect sizes shows in MPC the drivers preferred the medium MP and in classic they preferred the small MP. This might be indicating that for the SLM task drivers preferred smaller motion

configuration as the ratings were fluctuating with increasing MP size, results are summarised in Table 5-27.

II. Objective behavioural results

For LHT task in each MCA comparing MP sizes, see Table 5-26:

Aggregated performance - For the three, number of failures, speed variation and lateral position deviation aggregated performance metrics, small MP has shown the higher values in both MPC and classic MCAs and with the increase of MP size, these metrics have decreased. In the lap time large MP has shown highest value and with the increase of MP size it has increased.

The higher lap time with the increase of MP size, in general, is indicative of deteriorated performance when drivers are asked to adapt their speed, although considering it with the decrease in number of failures, reflects improved performance. In other words, increasing the MP size (presenting more motion to drivers) decreased the number of failures in fare of increasing their lap time. At the same time, the lateral position deviation and speed variation were decreased with the increase of MP size, which shows improved performance of drivers.

Time series - In the three grouped road sections of curves greater than 180°, curves smaller than 180°, and inflection zones, where there was a significant main effect of type of MPs on the output measured metric and there were no fluctuations, the small has shown higher values for the objective metrics, and with the increase of MP size these metrics have decreased. Those metrics include the steering reversal rates and driver model steering gain that were decreased with the increase of MP size, reflecting the lower control activity and more relaxed style of driving i.e. improved performance. The hypothesis was to expect decrease in the steering wheel reversal rate metrics with the increase of MP size, and the results have approved it. The delay time did only show an interaction of MP and MCA in only in one of the sections, although in all the sections it was slightly increased with the increase of MP. Our hypothesis was to see increase in delay time and decrease in gain, which this result approved it.

For SLM task in each MCA comparing MP sizes, see Table 5-27:

Aggregated performance - For the number of failures and speed variation aggregated performance metrics, small MP has shown the higher values in both MPC and classic MCAs i.e. with the increase of MP size these metrics have increased. For the lap time small has shown higher value, and with the increase of MP size it has decreased.

The lower lap time with the increase of MP size might be indicative of improved performance when drivers were asked to keep a constant speed, although the number of failures is increased as well, and improved performance may not be concluded. At the same time, the speed variation is increased with the increase of MP size, which also shows a deteriorated performance of drivers. Time series - In the whole track and two of the grouped road sections of inflection zones and peak zones, where there was a significant main effect of type of MPs on the output measured metric depending on the section. In inflection zone and whole track, the large MP has the highest value for the objective metric i.e. with the increase of MP size these metrics have increased. In the peak zone it is mix results. In total it is more of mixed results depending on the sections. The hypothesis was to expect decrease in the steering wheel reversal rate metric with the increase of MP size, however the result did not show significant effect for the steering rate reversal rate. For the driver model metrics in some sections the result for the delay time showed significant increase effect, however no significant effect for the gain was observed, only slight increase from the plots. The hypothesis was to see increase in delay time and decrease in gain, which this result has partially approved it.

Table 5-26. Summary of results, research question 2 (highest values), LHT task

		Significant Overall Result	Plot and effect size results		Trend small to large		
			MPC	Classic			
Subjective	Overall Assessment	-	L	M	Increase		
	Motion Cueing	L	L	M	Increase		
	Vehicle Assessment	-	M	M	Increase		
Objective	Aggregated Performance	Lap Time		L	L	Increase	
		Failure Number		S	S	Decrease	
		Speed Variation		S	L	Decrease	
		Lateral Deviation		S	S	Decrease	
	Time Series and driver model	Curves ≥ 180	Long Vel	L	M	L	Increase
			Lat Vel	M	M	M	Fluctuate
			Rev Rate 1	S	S	S	Decrease
			Rev Rate 10	S	S	S	Decrease
		Curves ≤ 180	Long Acc	S	S	S	Decrease
			DRYPE Gain	S	S	S	Decrease
			Rev Rate 1	S	S	M	Decrease
			Rev Rate 10	S	S	S	Decrease
		Straight Line	Long Acc	M	M	M	Fluctuate
		Inflection Zone	Long Acc	S	S	S	Decrease
			Rev Rate 1	S	S	S	Decrease
		Whole Track		-			

Table 5-27. Summary of results, research question 2 (highest values), SLM task

		Significant Overall Result	Plot and effect size results		Trend small to large		
			MPC	Classic			
Subjective	Overall Assessment	-	M	S	Fluctuate		
	Motion Cueing	-	M	S	Fluctuate		
	Vehicle Assessment	-	M	S	Fluctuate		
Objective	Aggregated Performanc	Lap Time		S	S-L	Decrease	
		Failure Number		S	S-L	Increase	
		Speed Variation		S	L	Increase	
	Time Series and driver model	Straight Line	-				
		Peak Zone	Long Vel	L	L	L	Increase
			Lat Vel	S	S	M	Decrease
			Yaw Rate	S	S	S	Decrease
			DRYPEDelay	L	L	L	Increase
		Inflection Zone	DRYPEDelay	L	L	L	Increase
	Whole Track	Long Vel	L	L	L	Increase	

In summary, in the LHT task drivers mostly preferred the larger MP size, while in SLM they preferred smaller. Overall, in terms of aggregated performance measurements including the lap time, number of failures and speed variation; with the increase of MP size, two opposite effects were observed between the driving tasks. In LHT task the performance was improved, while in SLM it was deteriorated. In the time series metrics, the effect of the MP size was consistent in LHT and mixed in SLM task. In the LHT task nearly in all of the measurement metrics have decreased with the increase of MP size. It was comprised of the steering reversal rates and driver model steering gain i.e. the measurements over the drivers' control activity. It reflects a more relaxed style of driving and improved performance. On the other hand, in SLM no significant effect of MP size was observed on drivers' control activity other than slight increase.

6 Assessment of High-Friction Motion Cueing

6.1 Introduction

Driven attributes of a vehicle include properties such as a vehicle's steering feel, handling, and ride qualities. Currently, testing such properties is primarily performed on-road at car manufacturer companies, that is same for Jaguar Land Rover (JLR) with test drivers from the Vehicle Evaluations Team (VET) driving vehicle prototypes at various stages of development, subjectively judging their behaviour, and comparing across alternative designs. Typically, these design alternatives involve changes to the vehicle prototype that can require many hours of work at the workshop. In other words, the current main approach to driven attributes testing requires costly physical prototypes, and also the testing itself is time-consuming, with associated risks of less accurate evaluations since drivers are not comparing alternative designs in close temporal proximity (Markkula et al., 2017). Thus, there are good reasons to pursue simulator based testing of driven attributes. Tests in the simulator do not require physical prototypes, and arbitrary changes to vehicle designs can be applied without time delays.

An important question that arises was whether drivers in the simulator were able to distinguish and make subjective assessments to changes of vehicle's properties and how the changes affect their performance. At the JLR simulator, some validation tests along these lines have been carried out, confirming that test drivers are able to subjectively identify the general nature of a manipulation being applied to the simulated vehicle dynamics, and indeed have made similar judgement calls as in reality on some retrospective tuning exercises. In addition to this, in this experiment the aim was to take some steps further, to consider the effect that different motion configurations of a driving simulator might have on driven attributes assessments, by means of subjective and objective behaviour measurements.

To this end, the first independent variable was the manipulations to the ride height (RH) of the air suspension of a Range Rover Velar prototype vehicle. It was identified as a manipulation that causes changes to the driven attributes of a subjectively comparable nature and magnitude to those involved in typical on-road driven attributes testing; could be relatively quickly applied to a real vehicle; would not be discernible to the drivers before starting to drive, and was readily available in existing vehicle dynamics models from the JLR Virtual Hub could be implemented in simulator. In addition to this, the other independent variable was the manipulation of simulator motion configuration including various motion platform (MP) sizes using a single motion cueing algorithm (MCA), similar to one of the aims studied in Chapter 5.

In related prior research works, there is a relatively sizable literature on the matter of correlating subjective driver assessments of driven attributes with objective metrics; see for example (Chen and Crolla, 1998; Rothhämel et al., 2011; Nybacka et al., 2014). In this work, the typical approach has been to carry out predefined test manoeuvres, e.g., with a steering robot, to quantify the vehicle's response using various objective metrics, and then correlating these metrics against subjective ratings collected from drivers in the same vehicles. The overall impression from this literature is that the objective-subjective correlation of driven attributes is feasible in some cases but remains challenging, not least because drivers tend to differ in how they use the subjective rating scales; e.g., some drivers consistently provide higher or lower ratings than others (Chen and Crolla, 1998; Gil Gómez et al., 2015). A related set of literature focuses exclusively on objective metrics, and the study and optimisation of these, based on some criteria assumed to align with driver preferences, in purely virtual tests without any drivers involved (Rauh, 2003; Gonçalves and Ambrósio, 2005; Mohajer et al., 2017).

The work referenced above is marginally relevant here but does not address driving simulators directly. Published studies of driven attributes evaluation between reality and simulators are rare. There is a brief mention in (Käding and Hoffmeyer, 1995b) of two projects investigating an all-wheel steering system in a double lane change manoeuvre, and an active suspension roll behaviour in curve driving, respectively, where test drivers reportedly expressed the same preferences both in real driving and in the Daimler-Benz motion-based driving simulator. Furthermore, Bertolini and Hogan (1999) compared drivers' preferences of steering wheel torques between prior studies in real vehicles and their simulator based study, and found that the same general pattern occurred in both settings, of drivers preferring stiffer steering wheel response for increasing speeds. Interestingly, when they turned their simulator's motion platform off, the pattern of increasing preferred stiffness disappeared above driving speeds of 40 km/h, suggesting an interaction between perceived lateral accelerations and steering feel preference. Overall, the present study seems very timely, since there is so little in the literature on the topic of simulator based testing of driven attributes. Moreover, there is no research identified considering the effect that simulator motion cueing capability might have on the evaluations of vehicle driven attributes.

In summary, in this chapter driven attributes of a vehicle in the simulator are assessed considering the manipulations to the ride height of air suspension of a vehicle, together with manipulation to simulator motion platform size. The measurements include drivers' subjective ratings and their objective behaviour. The following sections elaborate more on, how an experiment was designed that could

address comparison between vehicle ride height and simulator motion configurations, research questions and hypotheses are defined. Finally, the analysis of results is presented to answer the research questions followed by discussion and conclusion.

6.2 Experimental design

The two independent variables for this study were the ride height (RH) of air suspension with three levels (low, medium and high) and MP sizes with three levels (small, medium and large). At each of the nine (3x3) combinations of these independent variables, subjective ratings and drivers' objective performance were collected. To increase the power of the effect of experimental manipulations, and limited availability in the number of professional drivers participating in this study, a repeated measure experiment design was used where the same participants took part in all combinations of the independent variables. It is a balanced design where there is an equal number of observations for each of the treatments. The differences between the RHs was more subtle compared to the MP sizes, as a result, the experiment was designed in a nested way that the comparisons between RHs to be of primary focus for drivers and the MPs as the secondary focus. This helps the drivers to emphasise in distinguishing between the RHs in each MP size, while next they evaluate the MP sizes.

Six test drivers from JLR attended University of Leeds Driving Simulator (UoLDS) and drove a Range Rover Velar car on Gosport Lane (GSP), a public rural road near the JLR Gaydon site with normal high friction road condition. They completed two questionnaires about the quality of the driven attributes on the ride, handling and steering, and the realism of the driving experience, moreover, their objective performance were collected. They were familiar with real world testing of the vehicle in similar high-friction condition and driving task.

The experiment had each of the drivers accomplish the Gosport lane driving task. They were consecutively presented nine motion configurations corresponding to the permutations of three RHs and three MP sizes. Drivers were presented with three sessions of motion platforms to make comparison among the ride height:

- Small-low (S-L), small-medium (S-M), small-high (S-H)
- Medium-low (M-L), medium-medium (M-M), medium-high (M-H)
- Large-low (L-L), large-medium (L-M), large-high (L-H)

This allowed examining how drivers perceived the effects of RH and MP on driven attributes quality, the fidelity and the extent to which the drivers agreed with each other's ratings. The above sessions were presented to two of drivers in small-medium-large MP group order, to two in large-medium-small order and to the other

two in medium-small-large order and drivers were randomly assigned to be in each group. The order of the RHs within each of the above MPs was counter-balanced per driver. The full counterbalancing table for all drivers is provided in Appendix C.

6.3 Dependent variables

In this section, to allow the formulation of research questions and hypotheses, the subjective and objective behaviour metrics are explained. Further details about how the metrics are applied to the collected data are provided in section 6.10.

6.3.1 Subjective measures

A questionnaire was developed in collaboration with JLR to assess the driven attributes of the Range Rover Velar vehicle. This was based on the specific attribute language used by JLR engineers to describe the properties of a vehicle (described in an appendix to (Jamson et al., 2014a)). The questionnaire items fell into three categories: i) ride, ii) steering and iii) handling. Two questions assessed the ride characteristics of the vehicle in terms of the low and high frequency movements of the vehicle. Six questions addressed the vehicle's steering characteristics across a number of dimensions. Finally, five questions assessed the vehicle handling characteristics in terms of pitch, roll and understeer/oversteer during different manoeuvres. List of questions is shown in Table 6-1.

The primary ride was the question assessing the low frequency vertical movements of the vehicle. Evaluate large amplitude (large and obvious, continuous road undulations) that cause suspension movement over a moderate range, up to the whole range of suspension travel. Similarly, the secondary ride was the vertical vibrations that are caused by the road texture and various road disturbances on flat (smooth and coarse) and/or rough roads. They are felt by the driver or passengers through the seat back and cushion, steering wheel, and floor pan. The low RH gives drivers a constrained and crashy feeling, while the high RH results in floaty and settled feeling.

Controllability refers to the steering properties around the straight ahead and cornering tasks and how these characteristics work together to allow the driver precise and confident steering control. These properties are the vehicle reactions and torque feedback to small steering corrections that are required to keep the vehicle travelling in a straight path, as well as when turning the vehicle into a corner i.e. the steering adjustments required to keep the vehicle on the intended curvature. It also includes the steering properties that help the driver return to straight-ahead when exiting a corner. The steering properties consisted of questions about:

The window at high speed (over 30 mph), the steering angle range where there seems to be no motion response. Gain linearity away from centre, the ability of the vehicle to maintain a constant level of response gain. Efforts at low speed, general level of steering torque/forces for controlling the vehicle. Efforts at high speed, general level of steering torque/forces for controlling the vehicle. Efforts at mid-corner general level of steering torque/forces for controlling the vehicle. Often low RH demands drivers of higher control activity and high RH results in more relaxed behaviour.

Stability describes the ability of the vehicle to deliver a consistent, comfortable and predictable behaviour during straight line or negotiating a cornering manoeuvre. In addition to steady-state conditions, it also includes the vehicle's ability to accelerate & decelerate without an extraneous roll, pitch, yawing and lateral motions. The handling properties consisted of questions about:

Pitch (longitudinal) acceleration/deceleration (Lift Squat), acceleration pitch/lift squat describes the degree of vehicle pitch during acceleration/deceleration phases of manoeuvre. Roll (lateral) acceleration/deceleration, acceleration roll describes the degree of vehicle roll during acceleration/deceleration in cornering phases of manoeuvre those include the transient, the degree of vehicle roll during small corrective steering inputs and the steady-state, the degree of vehicle roll for fixed-level acceleration during cornering. Under/oversteering, level of the vehicle's under/oversteer behaviour over a range of corner radii and lateral acceleration while cornering.

The weight distribution of the vehicle affects the handling. Lower RH brings the centre of gravity of the car lower that means less weight transfer during acceleration and braking, which makes the car more responsive by decreasing the body roll and pitch, while higher RH increased the body roll and pitch. If the centre of gravity is moved closer to the front axle the vehicle tends to understeer, and if the centre of gravity is toward back of the vehicle the rear axle tends to swing out that is to oversteer. The change of the RH in this experiment is done the same for the front and back axles of the vehicle, and it is not straight forward to conclude about the under/oversteer. However, the standard RH of the vehicle is usually designed to have the least under/oversteering. Furthermore, the low RH decreases the suspension travel, although maximises the downing force and tire grip.

Table 6-1. Driven attribute questions

Category		Question	Rating Anchors
Ride	1	Primary Ride	Constrained, Trapped/ Free, Floaty
	2	Secondary Ride	Crashy, Agitated, Tactile/Settled, Controlled, Calm
Steering	3	Window at High Speed (over 30 mph)	Narrow/Wide
	4	Gain Linearity Away From Centre	Linear/Nonlinear
	5	Efforts at Low Speed	Lower/Higher
	6	Efforts at High Speed	Lower/Higher
	7	Efforts at Mid-Corner	Lower/Higher
Handling	8	Pitch (Longitudinal) Acceleration/Deceleration (Lift Squat)	Less/More
	9	Roll (Lateral) Acceleration/Deceleration (Transient)	Less/More
	10	Roll (Lateral) Acceleration/Deceleration (Steady-State)	Less/More
	11	Under/Oversteering	Under/oversteer

A realism questionnaire was included in the experiment. The questionnaire assessed the realism of each simulator motion platform size configuration, a shorter version of what was evaluated in section 5.3.1. The questionnaire assessed the overall realism of the simulated driving task, how useful the drivers thought the simulator configuration would be for assessing vehicle driven attributes and how realistic the motion cueing was. List of questions is shown in Table 6-2. The full questionnaires used in the simulator data collection is provided in Appendix C.

Table 6-2. Simulator realism questions

Question Category & Number	Question	Rating Anchors	
Overall Assessment	1	How realistic was the overall experience in the simulator compared to reality?	Unrealistic/Realistic
	2	Do you think that a driving simulator, in the configuration you just experienced would be useful for testing and comparing vehicle driven attributes?	Not Useful/Useful
	3	How easy was it to perform the task	Difficult/Easy
Motion Cueing	4	I felt the motion in general was	Unrealistic/Realistic
	5	I felt longitudinal acceleration/deceleration and pitch were	Unrealistic/Realistic
	6	I felt lateral acceleration/deceleration and roll were	Unrealistic/Realistic
	7	I felt time delay of vehicle response was	Unrealistic/Realistic

6.3.2 Objective measures

The objective metrics used here is similar to what explained in the low-friction experiment in section 5.3.2 for the LHT task. The Utility Triplet behavioural metrics are used to compare test results. The utility triplet includes three major categories: aggregated performance, time series and driver model.

6.4 Experiment configurations

The aim of this study was to evaluate whether changes in the vehicle air suspension ride height and simulator motion platform size would affect the drivers' subjective assessment of vehicle driven attributes and simulator fidelity, as well as drivers' objective behaviour. Thus, three different sizes of the MP workspace was selected, and the comparison between the vehicle RHs took place in each of the MP sizes.

6.4.1 Motion platform

Three motion platform configurations for the UoLDS were selected, which varied in the workspace size in surge and sway provided by the sliding rail, and maximum rotation angle of hexapod yaw. The motion envelope in heave, roll, and pitch was the same in the three configurations similar to the low-friction experiment, see

section 5.4.1. The three motion platform configurations are shown in Table 6-3; the difference between the MP configurations are

- Hexapod $\pm 5^\circ$ of yaw & ± 0.5 (m) of rail surge and sway, i.e. small
- Hexapod $\pm 10^\circ$ of yaw & ± 1.5 (m) of rail surge and sway, i.e. medium
- Hexapod $\pm 15^\circ$ of yaw & ± 2.5 (m) of rail surge and sway, i.e. large

Table 6-3. Motion platform specifications configured in this experiment

	Hexapod						Sliding rail	
	Surge (m)	Sway (m)	Heave (m)	Roll (deg)	Pitch (deg)	Yaw (deg)	Surge (m)	Sway (m)
Small	± 0.1	± 0.1	± 0.1	± 10	± 10	± 5	± 0.5	± 0.5
Medium	± 0.1	± 0.1	± 0.1	± 10	± 10	± 10	± 1.5	± 1.5
Large	± 0.1	± 0.1	± 0.1	± 10	± 10	± 15	± 2.5	± 2.5

The results of the low-friction experiment in Chapter 5 in the comparisons between the classic and MPC algorithms for the large demanding manoeuvre of LHT showed that the model predictive control (MPC) algorithm was preferred by the drivers. Since the Gosport lane (GSP) driving task in this experiment is similar to LHT (low-friction experiment) in terms of demand for high motion and including various frequencies (curve radiuses), the MPC algorithm was selected for this study.

The model structure is similar to the model used in the previous experiment described in section 5.4.2, although there are few differences. Nonlinear scaling of vehicle input motions was used in this experiment rather linear scaling, based on the method explained in section 3.3.2. The nonlinear scaling for the lateral motion of the vehicle is shown in Figure 6-1.

It scales the input vehicle acceleration up to 8 m/s^2 nonlinearly to three different final values of 2.5, 3.5 and 4.5 m/s^2 corresponding to the small, medium and large MP workspace experiment conditions. It is observable that the low amplitude vehicle accelerations are down-scaled less than the high amplitudes. For the longitudinal vehicle motion, the final values of the scaling were set to same values of the lateral, although the maximum input acceleration was set to 9 m/s^2 , because of higher accelerations during accelerating and braking.

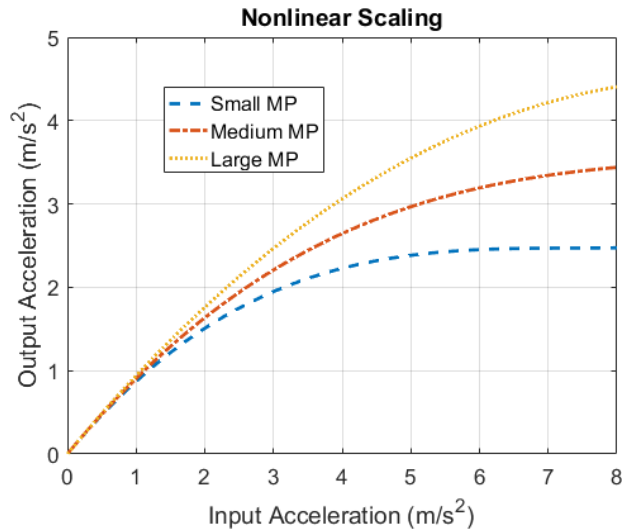


Figure 6-1. Nonlinear scaling of the vehicle lateral motion

Moreover, since the manoeuvre was not on flat ground, there was motion control in heave direction coupled with yaw in a single channel of MCA. In three MP workspace size, the MCA was tuned in time domain analysis based on substantial number of offline trial and error, and observations of avoiding extreme false cues, while exploiting the MP workspace; in addition using to some guidelines about tuning process available in the literature (Augusto and Loureiro, 2009; Maran, 2013).

The main measure for the comparisons was the root mean square (RMS) of the difference between the vehicle motion and MCA output acceleration and if the simulator MP workspace is exploited properly, the motion response of various configurations is provided in Table 6-4. Few sets of candidates were pilot tested in the simulator, to select the best set of parameters. The parameter values for all motion channels, for the three MP sizes, are listed in Appendix C.

Table 6-4. Motion configurations acceleration and excursion differences

Motion Cueing Algorithm	Motion Platform	Gosport Lane (GSP)			
		RMS ($a_i - a_s$)		Max excursion	
		X	Y	X	Y
MPC	Small	2.45	2.83	0.49	0.49
	Medium	2.38	2.78	1.45	1.46
	Large	2.12	2.71	2.48	2.50

Different tilt setting candidates were reviewed during the low-friction experiment design in sections 5.4.2. The parameters that were used in the low-friction

experiment found to be acceptable based on the drivers' comments. Moreover, to keep the variability between the low and high friction experiments to a minimum, the same set of tilt settings was used in this experiment, see Table 5-5 and Appendix D.

6.4.2 Air suspension ride height

The vehicle's air suspension ride height was selected during real world piloting. It was configured by a JLR engineer to be set at three different ride heights at 8 mm intervals. This was done in 'tight tolerance mode', in which the suspension system aims to level the car to within ± 3 mm of its target ride height. The ride heights will be referred to as Low

- -8 mm compared to a standard ride height i.e. low
- 0 mm compared to a standard ride height i.e. medium (normal)
- +8 mm compared to a standard ride height i.e. high

As mentioned in the introduction, according to a team expert from JLR who took part in the piloting of this study, the ± 8 mm ride height manipulation had impacts on the driven attributes of a subjectively comparable nature and magnitude to those involved in typical on-road driven attributes testing.

The same real world driving attributes testing person piloted the driving simulator setup and subjectively confirmed that the ride height manipulation had an impact also in the simulator. When subjected to blind testing of the Low and High ride heights, he was able to correctly identify them in 2 out of 3 pairwise comparisons.

6.5 Research questions and hypotheses

The overall aim of the present study was to investigate whether drivers can subjectively distinguish between the vehicle attributes and simulator fidelity to changes in the vehicle's ride height and how the changes affect their objective behaviour. In addition to this, the other aim was to explore the effect that the simulator motion platform size might have on the subjective and objective assessments. As outlined in previous sections, objective performance and subjective data were collected in the simulator during the public road, driving a Range Rover Velar prototype at three different air suspension ride height settings, to answer two research questions, defined below.

Research question 1 – How do the different RHs affect the drivers' subjective ratings of driven attribute qualities, simulator fidelity and their objective behaviour?

Within each MP configurations session, comparisons of RHs takes place; the driven attribute qualities and the simulator fidelity is assessed by two separate subjective

questionnaires and also drivers' behaviour objectively quantified using the utility triplet.

The hypothesis is: For the subjective evaluations, in all the three MP sizes for driven attribute qualities it is expected to see the ratings of medium RH to be closer to middle anchor i.e. appropriate for this vehicle. For the objective evaluations, no specific hypothesis is formulated in relation to this research question.

Research question 2 – How do the different MPs affect the drivers' subjective ratings of driven attribute qualities, simulator fidelity and their objective behaviour?

Within each of the RHs, comparison between the MP configurations takes place; the driven attribute qualities and the simulator fidelity is assessed by two separate subjective questionnaires and also drivers' behaviour objectively quantified using the utility triplet.

The hypothesis is: For the subjective evaluations, it is expected to see the highest simulator fidelity expected to be medium to large MP as it was observed for a large motion demanding manoeuvre in the low-friction experiment. For the objective evaluations, for the aggregated performance no hypothesis is formulated, for the time series task with the increase of MP size it is expected to see a decrease in values of drivers steering reversal rate metric, for the driver model with the increase of MP size it is expected larger control delays, which might require smaller control gains in compensation.

6.6 Driving task

Gosport Lane, shown in Figure 6-2, is a 60 mph narrow rural road including both straight segments and curves of varying radii. It is part of a public road circuit, starting and ending at the JLR Gaydon site, which is often used for assessment of vehicle driven attributes.

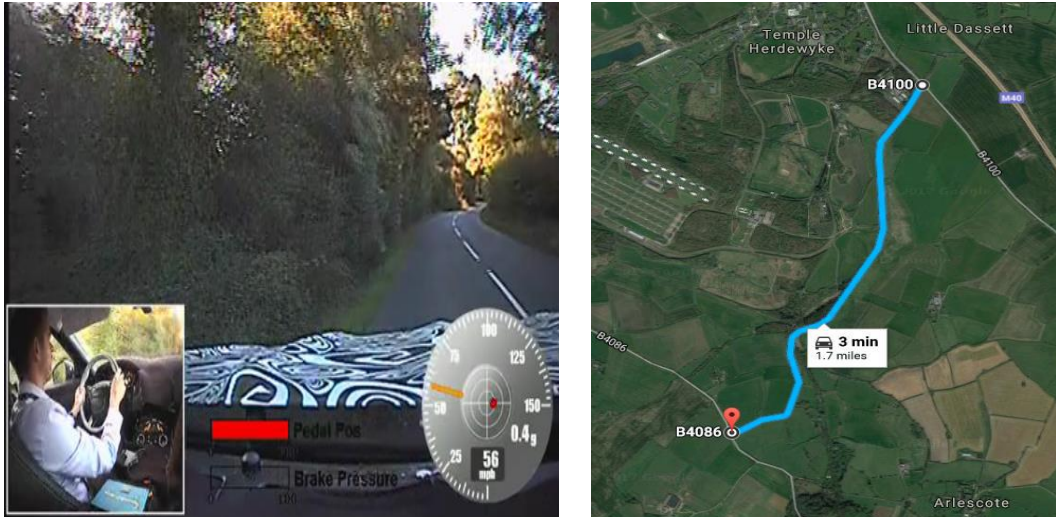


Figure 6-2. Map view of Gosport Lane. A still from the video logs of the real vehicle driving on Gosport Lane

For implementation in the simulator, a LIDAR 3D scan of the public road circuit's road surface was used, commissioned by JLR and also purchased separately by UoLDS. The UoLDS database was generated in-house at UoL and covered the Gosport Lane part of the circuit. The graphical representation, rendered within the simulator using the 3D graphics library OpenSceneGraph, was kept simple, mainly just reproducing the vision obstructions Figure 6-3.



Figure 6-3. A snapshot of the UoLDS graphical representation of Gosport Lane.

6.7 Drivers

Six drivers, all JLR employees with experience of assessing vehicle driven attributes took part in UoLDS data collections. The low number of participants was due to JLR personnel availability constraints. There were not as many particular drivers that could do similar tests, and these number of professional drivers are actually representative of the small pool of the number of drivers available from the vehicle evaluation team.

Moreover, the focus of the project was about the applicability of simulator for vehicle design in high-friction condition, and normal drivers could not be employed since the normal drivers' perception and performance might differ. Furthermore, the compromise on the statistical power of the experiment was worth, to keep the samples as homogenous as possible by keeping the age band in 35-45 and have drivers with a similar amount of experience and skills.

6.8 Test vehicle

A model of the dynamics for the Range Rover Velar prototype was implemented within the UoLDS environment. A SimPack multi-body simulation model for the dynamics of the Range Rover Velar vehicle was made available from the JLR Virtual Hub; see Figure 6-4. This model was executed on 8 cores of a dual Xeon CPU 16-core Concurrent iHawk hardware platform, running the real-time derivative of the RedHat Linux operating system. The vehicle model has been developed and extensively validated by JLR Virtual Hub Team. The yaw rate response gain of the vehicle model to steering input in 80-100 km/h speed range, for the three low/medium/high ride heights, have been validated between the reality and simulation. The observed differences were reported to be related to transient response in the simulator and were not an imperfection of the vehicle dynamics model (Markkula et al., 2017).

The air suspension configuration ride heights were modelled by changing the corresponding parameter in the SimPack model. The model incorporated an implementation of the Delft tyre model to represent the interaction between the vehicle's wheels and the LIDAR-scanned road surface, represented as a curve regular grid (CRG) at 30 cm resolution in both X and Y, with a constant 0.95 friction number.

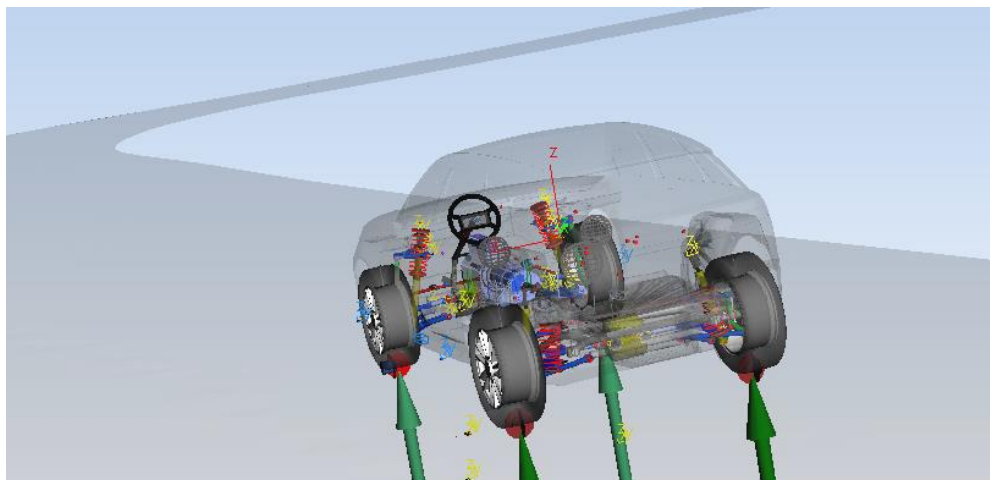


Figure 6-4. Graphical representation of the SimPack multi-body model of the Range Rover Velar vehicle dynamics

6.9 Experiment procedure

The JLR test drivers attended the UoLDS in pairs per day. Drivers were sent briefing documents, the driven attributes questionnaire and realism questionnaire a few days before arriving at the University of Leeds. On arrival, the drivers were talked through the briefing material on the simulator operation (safety, consent forms), see Appendix C, and they signed a consent form. In the next step, participants completed a familiarisation drive in the simulator. This consisted of one out and back drive of the Gosport lane simulation. The air suspension ride height was set to medium height and the simulator motion configuration was medium.

The drivers completed tasks in the simulator alternatively while the other had a break. This ensured that the time in the simulator without a rest was kept to a minimum in order to reduce the risk of experiencing simulator sickness. Each driving session took approximately 40 minutes to complete and consisted of completing the vehicle driven assessment (at Gosport Lane). Participants completed three test sessions in total, in which the simulator MP was varied small, medium and large. The drivers were instructed to "...drive through Gosport lane as you usually do for a car driver attribute quality assessment". They were also asked to keep their speed under 60mph where possible and prioritise safe driving when making the vehicle assessments.

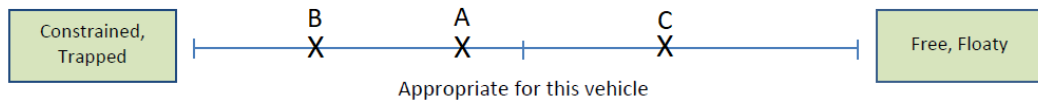
Next the participants completed the first test session. As in the real world, they drove the simulated Range Rover Velar from the North start location on Gosport Lane to the South end of the track. Upon reaching the end of the track the screen faded out and drivers were asked to fill in the vehicle driven attributes questionnaire. The vehicle was then automatically rotated to face back along the track. They then drove from the end of the track back to the start, where they continued to fill out the driven attributes questionnaire. The drivers completed the task with each of the three air suspension configurations within a single session, after which the drivers swapped over.

The questionnaire items asked participants to rate the three air suspension configurations relative to each other by placing a cross on a continuous line, with the centre point of the line representing feedback stating that the attribute in question was "appropriate for this vehicle". For example, the first question, illustrated in Figure 6-5, asked participants to rate the suspension configurations in terms of the low frequency vertical movements, on a scale from "Constrained/ Trapped" to "Free/ Floaty". Each rating was converted to a continuous score between 0 and 1. For example, a ranking of HML on the first question (i.e., if in Figure 6-5 the order of experiencing the ride heights were A=H, B=L, C=M) would

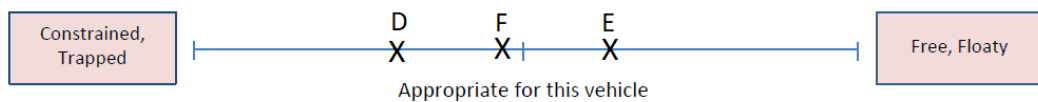
indicate that the participant considered the lowest ride height more “constrained” than the high ride height, and the high more “constrained” than the medium ride height.

Primary Ride – These are low frequency vertical movements of the vehicle. Evaluate large amplitude (large and obvious, continuous road undulations) that cause suspension movement over a moderate range, up to the whole range of suspension travel.

➤ Session 1 (A, B, C)



➤ Session 2 (D, E, F)



➤ Session 3 (G, H, I)

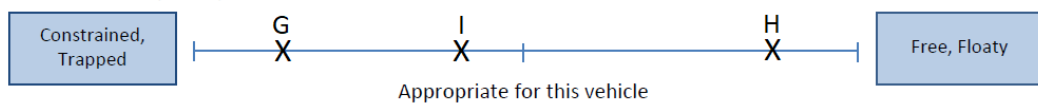


Figure 6-5. Example of driven attribute question and ratings. The drivers did mark each new test with A, B, ..., H, in the order they experienced them.

Drivers completed three sessions in total, in which the simulator motion platform configuration varied. Within each MP configuration, they tested all three air suspension configurations, giving a total of nine experimental trials. The order of the simulator motion platform configuration and ride height configuration was counterbalanced between participants, see Appendix C. Once the participants had completed each of the sessions, they filled out the realism questionnaires, see Figure 6-6.

The questionnaire items asked participants to rate the three sessions relative to each other by placing a cross on a continuous line. For example, the first question, illustrated in Figure 6-6, asked participants to rate the MP configurations in terms of the overall experience, on a scale from “Unrealistic” to “Realistic”. For example, a ranking of 123 on the first question (i.e., if in Figure 6-5 the order of experiencing the ride heights were 1=S, 2=L, 3=M) would indicate that the participant considered the medium MP more “realistic” than the large, and the large more “realistic” than the small MP size.

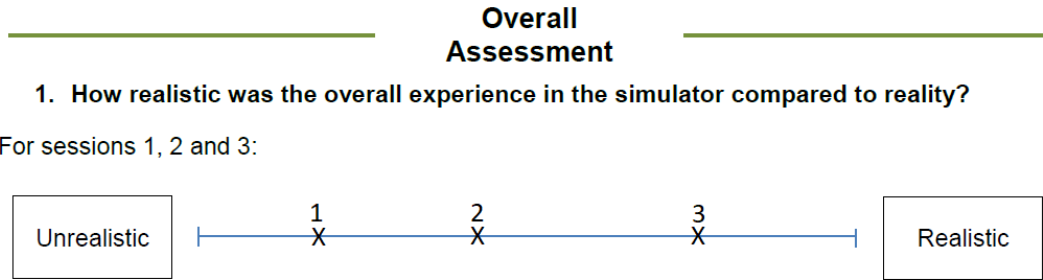


Figure 6-6. Example of simulator realism question and ratings. The drivers did mark each new session with 1, 2, 3 in the order they experienced them.

6.10 Analyses and results

6.10.1 Overview and general approach

In this section the statistical tools that are used for analysis are the same as those introduced in section 5.10 that is summarised from the (Field, 2013), hence the explanation of them are omitted from this section. Those mainly include the simple descriptive statistics, hypothesis testing, effect size and statistical power, parametric tests for comparing means such as repeated measure ANOVA.

To calculate the statistical power $1-\beta$ of this experiment based on the choice of p-value to be 0.05, 0.1, sample size $N = 6$, and effect sizes of $r = 0.1, 0.3, 0.71, 0.8, 1$ the statistical power for this experiment is calculated using the G*Power software. If the statistical power is equal or greater than 0.8 there will be confident that there is sufficient power to detect any effect that might have existed. It is observable in Table 6-6 with this number of samples and significance level $p = 0.05$, to have a statistically powerful $(1-\beta) \geq 0.8$ an effect size of $r = 0.71$ is required, while with $p = 0.1$ to have a statistically powerful $(1-\beta) \geq 0.8$ an effect size needs to be $r \geq 0.59$.

Table 6-5. Statistical power table

	<i>Statistical Power at $r = 0.1$</i>	<i>Statistical Power at $r = 0.3$</i>	<i>Statistical Power at $r = 0.71$</i>	<i>Statistical Power at $r = 0.8$</i>	<i>Statistical Power at $r = 1$</i>
$p = 0.05$	0.07	0.22	0.80	0.87	0.97
$p = 0.1$	0.13	0.36	0.91	0.95	0.99

Comparing the statistical power Table 6-6 of this experiment to Table 5-6 of the low-friction experiment it is observable that to achieve a certain level of statistical power, a higher effect size is required. This is due to lower number of participants in

this experiment (6 drivers) compared to low-friction experiment (8 drivers), that requires a higher effect size.

The range of effect sizes used in the analysis of results in the next sections is based on the widely used suggestions effect sizes of small $r = 0.1$, medium $r = 0.3$ and large $r = 0.5$, comparing this to Table 6-5, it is observable that to detect an effect with sufficient power at $p = 0.1$, higher than large effect size is required $r \geq 0.59$.

6.10.2 Subjective evaluations

In this section drivers' rating of the vehicle attribute and realism questionnaires are presented and analysed. The cross points on the provided sheets were measured by ruler and imported as data files to MATLAB for further analysis. As it was described in section 6.3.1, the questions targeted three different qualities of ride steering and handling, each includes few questions. Due to the high number of questions, to analyse the result it was decided to group the questions belonging to each category. Rating values for the grouped questions were calculated from the average value of all questions belonging to that group. There were 11 questions in the vehicle attribute questionnaire.

In order to group and report the questions, a reliability analysis was done on the ratings to find out the consistency of measures. Separate reliability analysis is done for every subscale of the ride, steering and handling of the questionnaire the Cronbach's α and Cronbach's α , if the item is deleted, indicate that:

The steering and handling subscale of the questionnaire all had high reliabilities $\alpha \sim 0.7$. However, the ride had very low reliability with negative $\alpha \sim -0.06$. Looking at the Cronbach's α if the item is deleted for each of the subscales together with keeping the significant results separated showed it is best to group the questions as Ride

- Q1 – primary ride, Q2 – secondary ride (grouped)

Steering

- Q4 – gain linearity away from centre
- Q3 – window at high speed, Q5 – efforts at low speed, Q6 – efforts at high speed, Q7 – efforts at mid-corner (grouped)

Handling

- Q9 – roll transient
- Q11 under/oversteer
- Q8 – pitch, Q10 – roll steady-state (grouped)

The results of grouped questions and nine motion configurations are shown in a boxplot and bar charts in Figure 6-7. On the x-axis the characters stand for a

motion configuration e.g. M-L stands for medium size motion platform and low ride height. The effect sizes of Pearson's correlation coefficient are shown in the lower part of the figure as bar charts.

For each of the MPs i.e. (S, M, L) there are 5 bar charts representing the effect sizes. Left red, middle black and right blue bars show the effect size between two consecutive MPs (small to medium, medium to large and large to small) in an RH. As an example, for the primary ride question and small (S) MP, the red bar shows effect size between small (S) and medium (M) MPs in low RH i.e. S-L and M-L, and the third black bar does the same but for medium RH i.e. the effect size between small (S) and medium (M) MPs in medium RH i.e. S-M and M-M, the fifth blue bar does the same but for high RH i.e. the effect size between small (S) and medium (M) MPs in High RH i.e. S-H and M-H. The second and fourth green bars show the effect size between the two consecutive RHs those are between (low to medium, medium to large) RHs in a MP. In this example, the second green bar shows the effect size between low and medium and the second between the medium and high RHs in small (S) MP. It is the same for next (M) and (L) MPs. The horizontal dashed lines show the small, medium and large effect sizes. For the remainder of this chapter, the effect sizes are presented in a similar style of bar charts.

In ride group questions the rating that is the most near to the appropriate for this vehicle anchor (closer to middle dashed line i.e.0.5) is the medium MP and high RH (M-L) and the furthest from being appropriate is the small and medium (S-L); for steering gain linearity away from centre those are the small medium (S-M) and large low (L-L); for the steering window and efforts grouped those are quite similar however those are medium medium (M-M) and large low (L-L) respectively. In handling toll transient the small low (S-L) and medium high (M-L) are respectively the nearest and furthest from being appropriate for this vehicle; for the handling under/oversteering those are large medium (L-M) and large low (L-L); for handling roll and pitch grouped questions those are small medium (S-M) and small high (S-H).

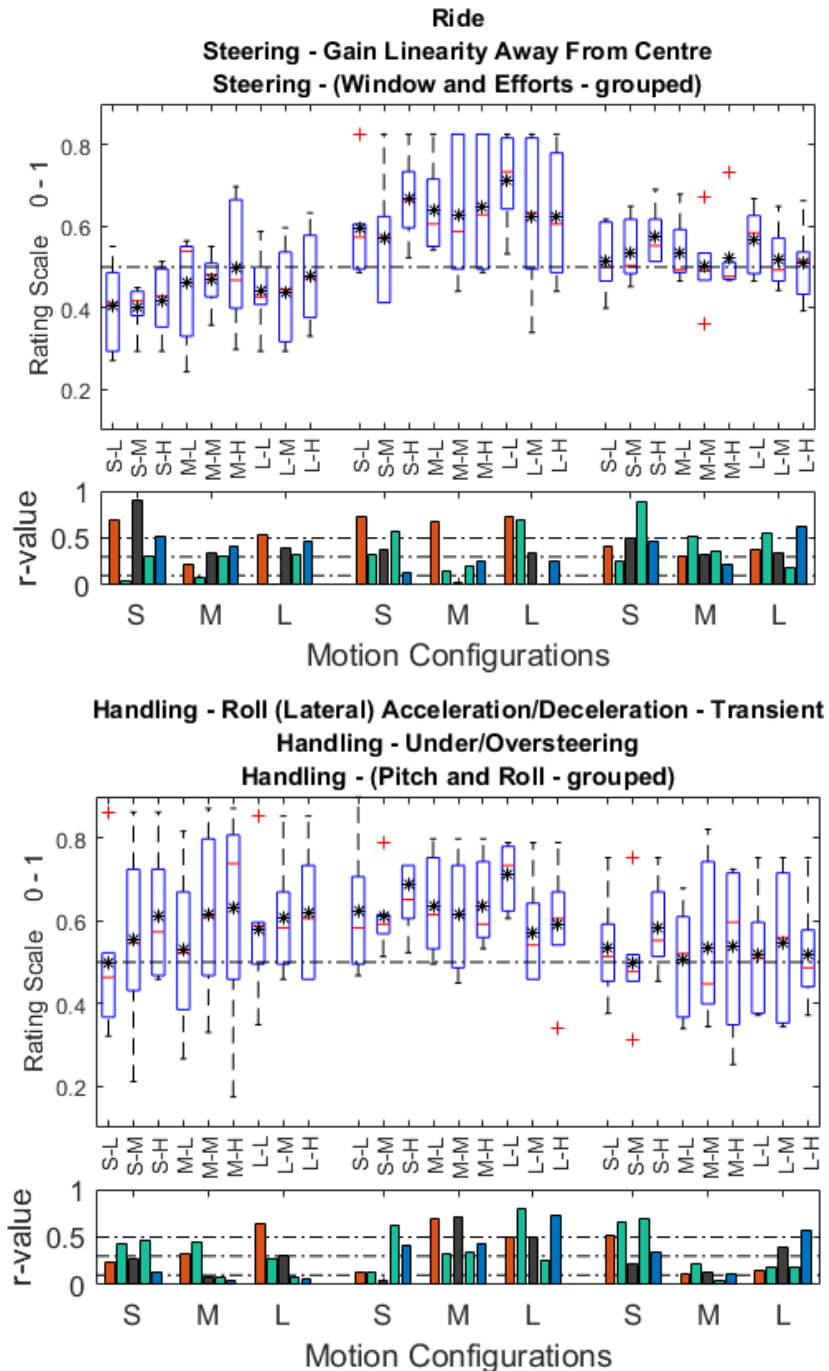


Figure 6-7. Subjective rating boxplot, and effect size r-value bar graphs for driven attribute grouped questions. Red flat lines show median and black stars show mean.

There were 7 questions in the realism questionnaire. In order to group and report the questions similarly, a reliability analysis was done on the ratings to find out the consistency of measures. Separate reliability analysis is done for every subscale of overall realism and motion cueing of the questionnaire the Cronbach's α and Cronbach's α if the item is deleted indicate that:

The overall realism and motion cueing subscale of the questionnaire all had high reliabilities $\alpha \sim 0.85$, thus it was decided to group the 7 questions into the 2

subscales to report and analyse. In both overall realism and motion cueing grouped questions the rating that has the highest value and refers to the most realistic experience for drivers is the medium MP.

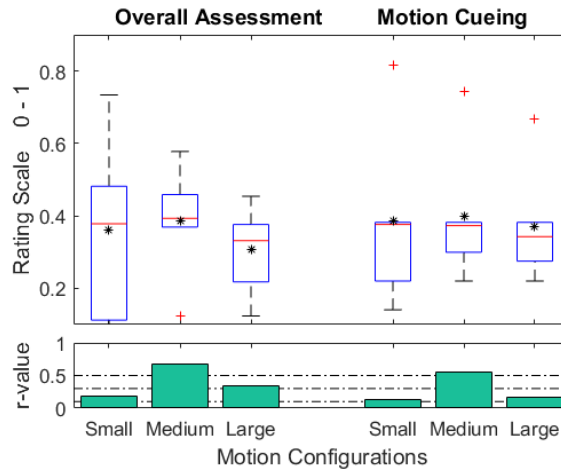


Figure 6-8. Subjective rating boxplot, and effect size r-value bar graphs for realism questions.

Table 6-6. Repeated measure ANOVA results for grouped question ratings. F and P values are shown on each point corresponding to a factor and an output measure. Black highlighted boxes shows where the p-value is less than 0.1.

	Ride	MP	Height	MP*Height	
Steering - Gain Linearity Away From Centre	F5.56, P0.02	F0.70, P0.52	F0.07, P0.99		P <= 0.1
Steering - (Window and Efforts - grouped)	F0.86, P0.45	F3.35, P0.08	F1.15, P0.36		
Handling - Roll (Lateral) Acceleration/Deceleration - Transient	F0.44, P0.66	F3.10, P0.09	F0.22, P0.92		P > 0.1
Handling - Under/Oversteering	F0.15, P0.87	F4.27, P0.05	F3.35, P0.03		
Handling - (Pitch and Roll - grouped)	F0.07, P0.93	F0.64, P0.55	F0.66, P0.62		

The repeated measure ANOVA is done on the driven attributes grouped questions. The main effect of RHs and MPs and their interaction effect on the subjective ratings are shown in Table 6-6. First, two left columns show the main effect and the right column shows the interaction. The p-value and F-value of for each factor and output measure is shown in the corresponding box on the table. Where there is a significant effect $p \leq 0.1$ that box is highlighted black. To verify the main effects detailed ANOVA contrasts and post hoc test of Bonferroni pairwise comparison are done. A similar analysis was done for the realism questionnaire considering only

effect of MP, however there wasn't any significant or nearly significant result hence the table is omitted.

Ride grouped question

Mauchly's test indicated that the assumption of sphericity is not violated for the main effect of MP $\chi^2(2) = 0.74$, $p = 0.69$. Therefore, there was no need for degrees of freedom corrections.

There was a significant main effect of type of MP on the vehicle's ride attribute quality, $F(2,10) = 5.56$, $p = 0.023$. Pairwise comparison indicated nearly significant $p = 0.08$ difference of ratings between medium and large MPs to small. Contrasts revealed that ratings of medium and large configurations, $F(1,5) = 7.77$, $p = 0.038$, $r = 0.78$; $F(1,5) = 6.63$, $p = 0.049$, $r = 0.75$ was significantly different than small, see Figure 6-9. For the interpretation of the effect sizes in the bar chart see the beginning of this section.

From Figure 6-9, the low and medium RH were quite similar to the drivers, where they found them constrained and crashy, and they found high RH settled and floaty and appropriate for the vehicle, with small effect sizes. Moreover, this trend is observable in all the three MPs, and the medium MP size was found to be more appropriate with small to large effect sizes.

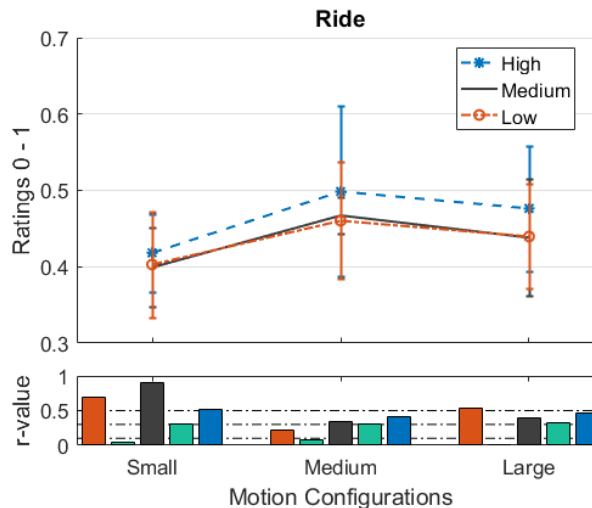


Figure 6-9. Ride grouped questions ratings

Steering – gain linearity away from centre

Mauchly's test indicated that the assumption of sphericity is not violated for the main effect of RH $\chi^2(2) = 0.57$, $p = 0.75$. Therefore, there was no need for degrees of freedom corrections.

There was a nearly significant main effect of type of RH on the vehicle's steering gain away from centre attribute quality, $F(2,10) = 3.34$, $p = 0.077$. Contrasts

revealed that ratings of low and high configurations, $F(1,5) = 4.3, p = 0.093, r = 0.68$; $F(1,5) = 4.19, p = 0.096, r = 0.67$ was nearly significant different than medium, see Figure 6-10.

From Figure 6-10, the low and high RH were more nonlinear to drivers, and the medium RH was more linear and appropriate for the vehicle, with small to large effect sizes. Moreover, an inverse relation is observable between the MP size and RH with small to large effect sizes.

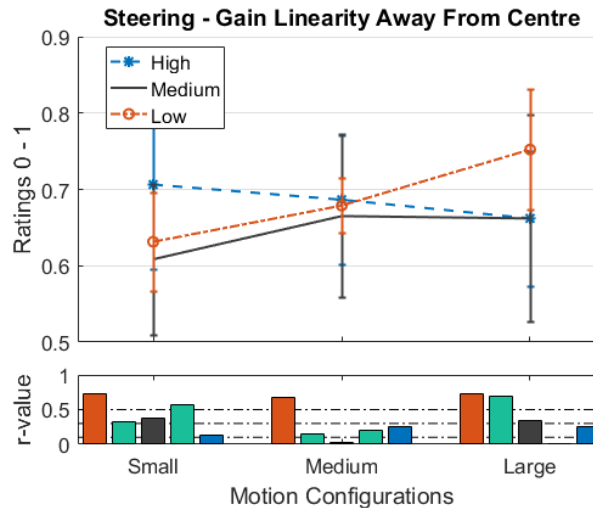


Figure 6-10. Steering gain linearity away from centre ratings

Handling - roll (lateral) acceleration/deceleration

Mauchly's test indicated that the assumption of sphericity is not violated for the main effect of RH $\chi^2(2) = 3.61, p = 0.16$. Therefore, there was no need for degrees of freedom corrections.

There was a nearly significant main effect of type of RH on the vehicle's handling roll acceleration/deceleration attribute quality, $F(2,10) = 3.09, p = 0.08$. Pairwise comparison indicated significant $p = 0.01$ difference of ratings between high and low RHs. Contrasts revealed that ratings of high configuration, $F(1,5) = 23.11, p = 0.004, r = 0.9$ was significantly different than low, see Figure 6-11.

From Figure 6-11, it is observable that the drivers have found the transient roll acceleration/deceleration to be less to more from the low to high RHs, with small to medium effect sizes, which shows they could distinguish correctly. Moreover, an increase in the value of the measurement is observable with the increase of MP size for all the three RHs, with small to medium effect sizes.

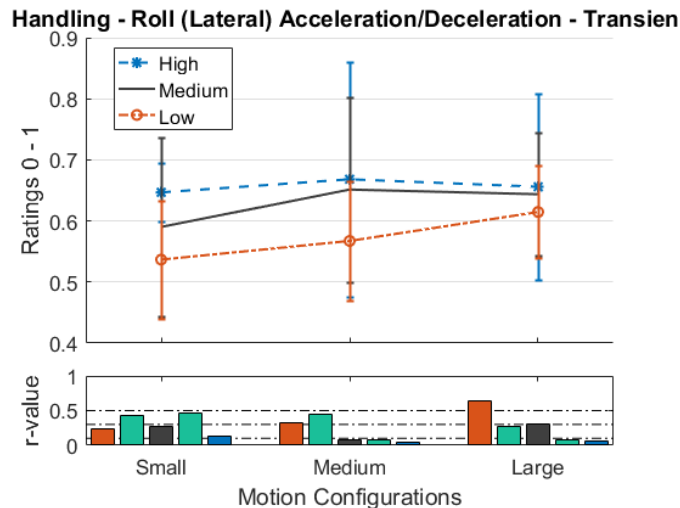


Figure 6-11. Handling roll (lateral) acceleration/deceleration ratings

Handling – under/oversteering

Mauchly's test indicated that the assumption of sphericity is not violated for the main effect of RH $\chi^2(2) = 2.01$, $p = 0.36$. Therefore, there was no need for degrees of freedom corrections.

There was a significant main effect of type of RH on the vehicle's handling under/over steering attribute quality, $F(2,10) = 4.26$, $p = 0.045$. Pairwise comparison indicated significant $p = 0.01$ difference of ratings between low and medium RHs. Contrasts revealed that ratings of low configuration, $F(1,5) = 20.7$, $p = 0.006$, $r = 0.89$ was significantly different from the medium, see Figure 6-12.

There was a significant interaction effect between the type of MP and the type of RH used, $F(4,20) = 3.35$, $p = 0.029$. This indicates that MP had different effects on people's ratings depending on which type of RH was used. To break down this interaction, contrasts were performed comparing all MP types to all RH types, looking at the interaction graph Figure 6-12. These revealed significant interactions when comparing low to medium RH for medium compared to large MP $F(1,5) = 16.11$, $p = 0.01$, $r = 0.87$. This contrast did yield a large effect size. The remaining contrasts revealed no significant interaction term.

From Figure 6-12, the low and high RH were more oversteering to drivers, and the medium RH was more understeer and appropriate for the vehicle, with small to large effect sizes. Moreover, an opposite relation is observable between the MP size and RH, with small to large effect sizes.

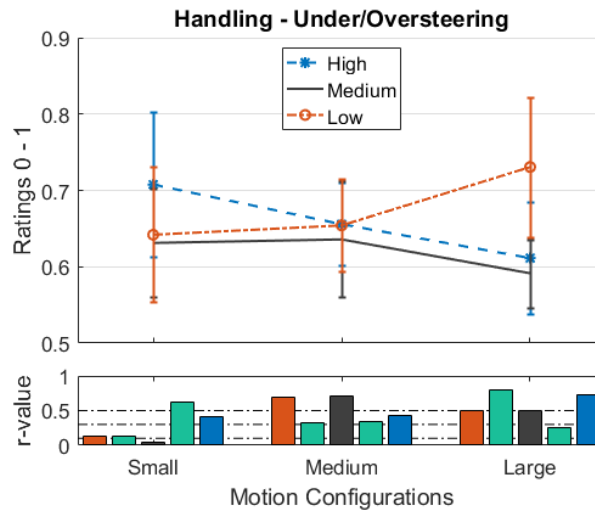


Figure 6-12. Handling under/oversteering ratings

Research question 1 – How do the different RHs affect the drivers' subjective ratings of driven attribute qualities, simulator fidelity and their objective behaviour?

The results for some of the six questions showed the significant or nearly significant effect of type of RHs on subjective ratings of driven attributes. In steering gain linearity away from centre, the low and high were nearly significant different to medium. In handling roll transient high and low were nearly significant different. In handling under/over steering the low and medium were significantly different.

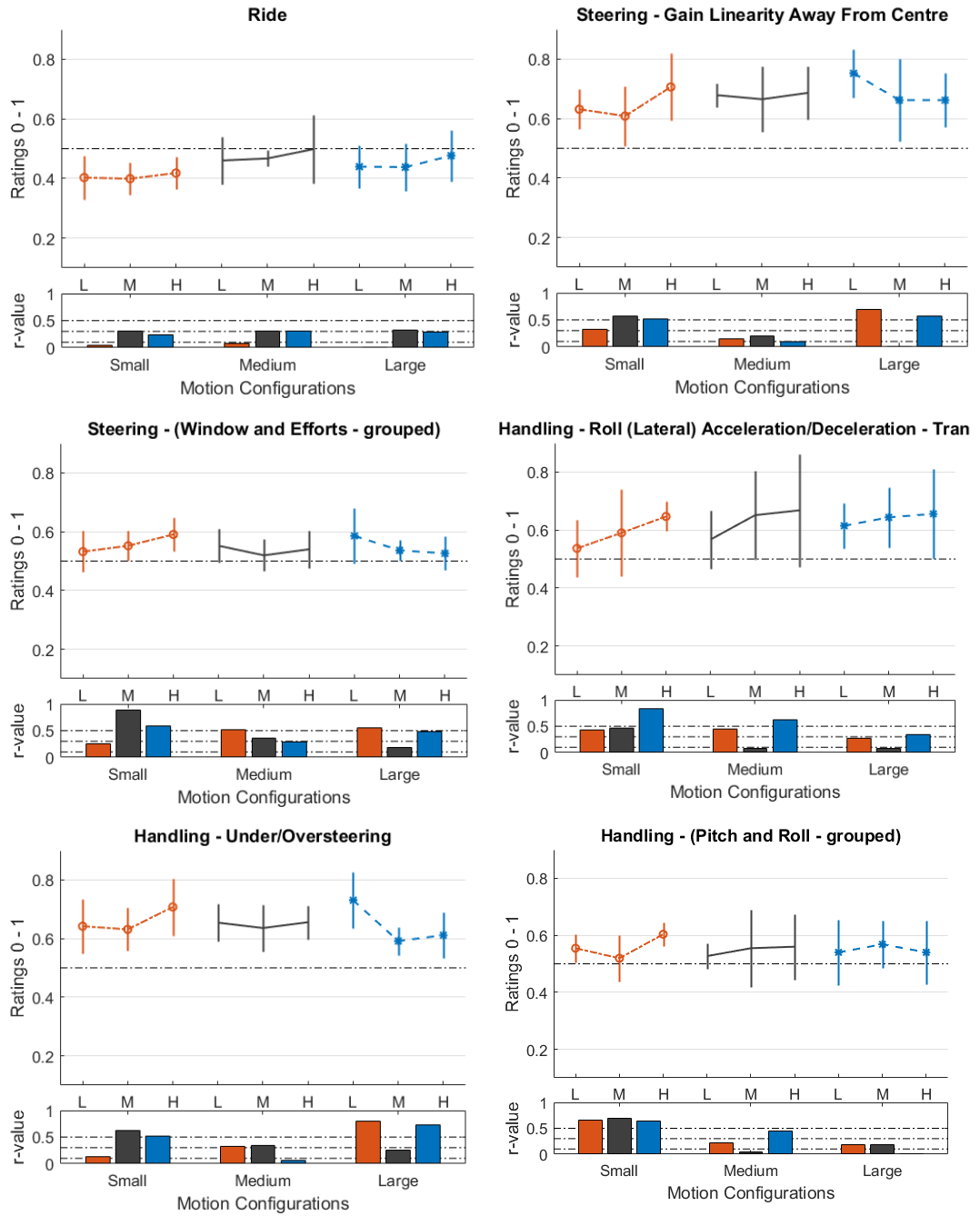


Figure 6-13. Subjective ratings for grouped questions, RH comparison for three MP sizes. Effect size r-value bar graphs are shown for each MP, comparing RHs

The results are shown in Figure 6-13, in a way that compares the RHs in each of the MP sizes. The r-values are calculated in each of the MPs representing the effect size of the difference between RHs. In each of the MPs the left red bar is effect size calculated comparing low to medium, middle black bar compares the medium to high and right blue bar compares the high to low. The outcome of the comparisons between the low, medium and high in each MP is presented in Table 6-7 and Table 6-8 where the first table looks which RH is the most appropriate for the vehicle in a MP size and second table looks which RH is the worst match for the

vehicle in a MP size. Colours show small, medium and large effect size in each comparison.

It is observable in Table 6-7 in all the three MP sizes, in the ride question, the high RH is the most appropriate for this vehicle, with small effect sizes. In steering gain linearity away from centre and handling under/over steering the medium RH is the best suited for the vehicle, with small to large effect sizes; This is in line with the predicted hypothesis. In handling roll transient question the low RH is the best suited for the vehicle, with small to large effect sizes. For the steering window and effort grouped question with increasing MP size drivers' seemed to have chosen higher RH as more appropriate i.e. low, medium and high RH respectively in small, medium and large MPs. In handling grouped questions it is of mixed results in each of the MP sizes.

Table 6-7. Results of the driven attribute questionnaire for RH comparison in each MP. Most near to appropriate for this vehicle (0.5 line)

r-value < 0.3	0.3 ≤ r-value < 0.5		0.5 ≤ r-value
MP Questions	Small	Medium	Large
Ride	High	High	High
Steering – Gain	Medium	Medium	Medium
Steering - Grouped	Low	Medium	High
Handling – Roll Tr	Low	Low	Low
Handling – U/Ostrn	Medium	Medium	Medium
Handling – Grouped	Medium	Low	Low

It is observable in Table 6-8 that in all the three MP sizes, in most of the attribute questions the high and low RH is rated the most unfitting for this vehicle (distant from 0.5) in small and large MPs with small to large effects sizes, in medium MP it is mix of both low and high RHs. This might indicate the effect that MP has on the ratings of RH. Moreover, looking at the same table, overall the unfitting RHs are mostly low and high that also indicates the drivers have selected the medium RH (the standard vehicle height) as more appropriate and were able to distinguish between the RH.

Table 6-8. Results of the driven attribute questionnaire for RH comparison in each MP. Most distant from appropriate for this vehicle (0.5 line)

r-value < 0.3	0.3 ≤ r-value < 0.5		0.5 ≤ r-value
MP Questions	Small	Medium	Large
Ride	Low	Low	Low
Steering – Gain	High	Low~high	low
Steering - Grouped	High	Low~high	low
Handling – Roll Tr	High	High	High
Handling – U/Ostrn	High	Low~high	Low
Handling – Grouped	High	medium~high	Medium

In total having big enough effect size, it is concludable that in steering and handling vehicle attribute qualities medium and rarely low RH as more appropriate for the vehicle in all three MPs. Moreover, drivers have chosen the low and high RH most of the times as the not appropriate for this vehicle (distant from 0.5) in all three MP sizes, that also indicates the medium RH is more appropriate for this vehicle in the majority of the times. That means there is an effect of MP size (i.e. the motion presented to drivers) on drivers' choice of most suitable RH.

Research question 2 – How do the different MPs affect the drivers' subjective ratings of driven attribute qualities, simulator fidelity and their objective behaviour?

The results for one of the questions showed the significant effect of type of MPs on subjective ratings of driven attributes. In the ride question, the medium and large were significantly different from small.

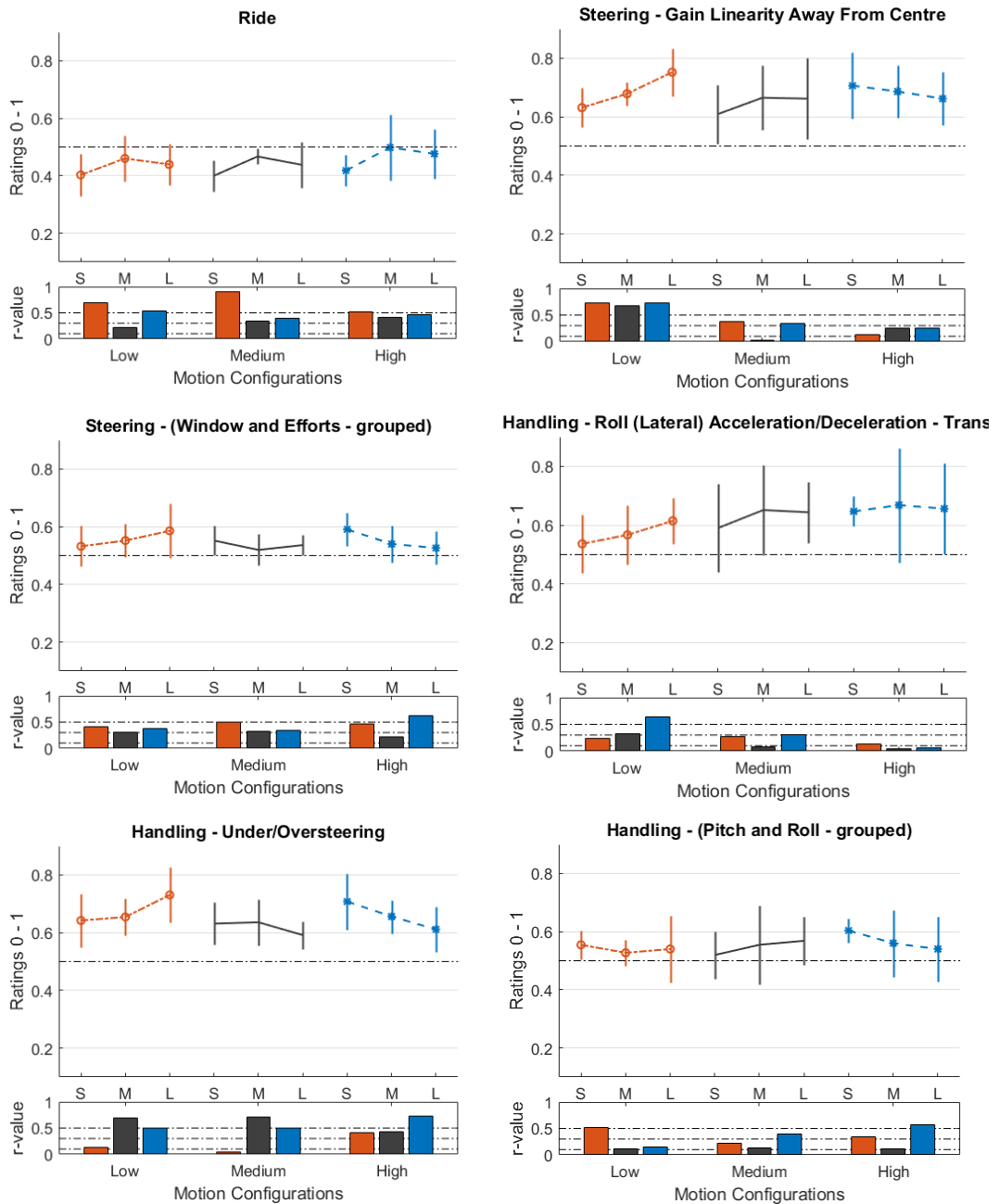


Figure 6-14. Subjective ratings for grouped questions, MP comparison for three RHs. Effect size r-value bar graphs are shown for each RH, comparing MPs

The results are shown in Figure 6-14, in a way that compares the MPs in each of the RHs. The r-values are calculated in each of the RHs representing the effect size of the difference between MP sizes. In each of the RHs the left red bar is effect size calculated comparing small to medium, middle black bar compares the medium to large and right blue bar compares the large to small. The outcome of the comparisons between the small, medium and large in each RH is presented in Table 6-9 and Table 6-10 where the first table looks which MP is the most appropriate for the vehicle in a RH and second table looks which MP is the worst

match for the vehicle in a RH. Colours show small, medium and large effect size in each comparison.

It is observable in Table 6-9 in all the three RHs, in the ride question, the medium MP is rated as the most appropriate for this vehicle with medium to large effect sizes. In steering gain linearity away from centre, handling roll transient and handling under/oversteering the small and large MP is the most suitable respectively in low and high RHs, with small to large effect sizes. For the steering window and effort grouped question drivers seemed to have chosen larger MP with increasing RH as more appropriate i.e. small, medium and large MP respectively in low, medium and high RHs. In handling grouped question it is of mixed results in each of the RHs. It is well noticeable that in most of the steering and handling group of questions, in the low RH the small MP is rates as most appropriate for this vehicle, in high RH it is the large MP, and in medium RH it is mix of the three MPs; that might indicate the higher the RH is the larger MP is selected as more appropriate, and vice versa.

Table 6-9. Results of the driven attribute questionnaire for MP comparison in each RH. Most near to appropriate for this vehicle (0.5 line)

r-value < 0.3	0.3 ≤ r-value < 0.5		0.5 ≤ r-value
RH \ Questions	Low	Medium	High
Ride	Medium	Medium	Medium
Steering – Gain	Small	Small	Large
Steering - Grouped	Small	Medium	Large
Handling – Roll Tr	Small	Small	Small~Large
Handling – U/Ostrn	Small	Large	Large
Handling – Grouped	Medium~large	Small	Large

It is observable in Table 6-10 that in all RHs, in most of the attribute qualities the small and large MPs are rated the most unfitting for this vehicle (distant from 0.5) in low and high RHs respectively with small to large effects sizes, in medium MP it is a mix of the three MPs. It might show the effect that RH has on the ratings of MP, e.g. in the smaller MP rated to be unfitting for the evaluations of higher RH.

Table 6-10. Results of the driven attribute questionnaire for MP comparison in each RH. Most distant from appropriate for this vehicle (0.5 line)

	r-value < 0.3	0.3 ≤ r-value < 0.5		0.5 ≤ r-value
RH \ Questions	Low	Medium	High	
Ride	Small	Small	Small	
Steering – Gain	Large	Medium~large	Small	
Steering - Grouped	Large	Small	Small	
Handling – Roll Tr	Large	Medium~large	Small~med~large	
Handling – U/Ostrn	Large	Small~medium	Small	
Handling – Grouped	Small~large	large	Small	

In total having big enough effect sizes, it is concludable in low and high RH drivers have chosen the small and large MP for most of the qualities as the most appropriate. Moreover, in low and high RH drivers have rated large and small MP as not fitting for this vehicle (distant from 0.5), in medium RH it is a mix of the three MPs. This shows there seems to be an effect of RH on drivers' choice of more suitable MP size (i.e. the motion presented to drivers).

The results from the realism questionnaire showed in both overall assessment and motion cueing grouped questions the medium MP had the highest rating (realistic) with small to large effect sizes. Meaning they have preferred the medium MP as being more realistic than small and large.

6.10.3 Objective evaluations

Collected data include two runs for each of the motion configurations. This was to let the drivers acquire a full understanding of the motion characteristics of a configuration. Using both of the runs was shown to be advantageous in terms of adding power to the statistical analysis, although a check was needed to see if this introduced any noise to the analysis. To ensure the correctness of averaging both of the runs, a third time factor was added to the analysis. For all of the objective metrics described in the next sections, where there was a significant effect of RH or MP, no significant effect of time factor was found. As a result, it was valid to average the data from both runs for further analysis

Different sections of the driven road have different characteristics. Therefore, the whole track was split into sections and each section was analysed separately. Due to similarity in nature of many of the sections and to reduce the number of reporting results the sections throughout the Gosport Lane was divided into straight lines and curves. There are 17 sections in total. All the sections are shown in Figure 6-15, green dots show the entry of a section and red dots shows the exit of a section.

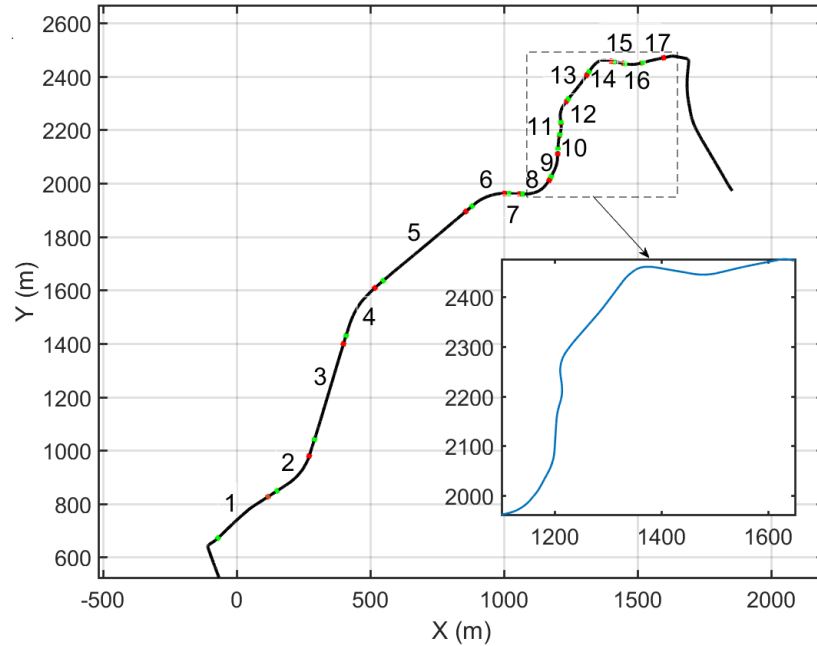


Figure 6-15. Gosport lane course and sections

To be able to group the sections initial analysis were performed. Comparing the result of the 17 separate sections with the corresponding grouped sections, showed similarity in the values; this indicated that it was acceptable to group the sections. The objective metrics of a group section is calculated from the average value of all sections belonging to that group as Table 6-11.

Table 6-11. Group sections, LHT task

<i>Group section</i>	<i>Section Numbers</i>
Straight lines	1, 3, 5, 7, 13, 15, 17
Curves	2, 4, 6, 8, 9, 10, 11, 12, 14, 16
Whole track	

Aggregated performance

The aggregated performance measures consist of four metrics of:

- Lap time, duration of time that drivers completed the task
- Spin/skid outs, number of trials that drivers span out or exceeded the roadsides
- Body slip angle that is the angle between vehicle forward orientation and direction of actual travel
- Speed variability, standard deviation of drivers speed during the task
- Lateral position deviation, maximum vehicle's lateral distance from centre of the road

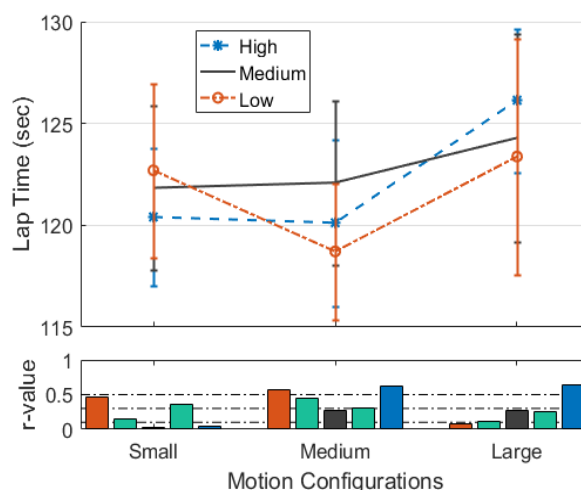


Figure 6-16. Lap time

From Figure 6-16 it is observable that the lap time has increased with the increase of MP size in both medium and high RH, although it has fluctuated in low. In low the medium MP has the smallest lap time, in medium it is the small and in high it is the medium with little difference to small. Having considerable effect sizes reveal that providing larger motion to drivers results in higher lap time to finish the driving task. Comparing the RHs in each MP size, the high has the least lap time in small and low has the least lap time in medium and large MP.

The lap time in the divided straight and curve sections showed: During straight lines there was a significant main effect of type of MP, $F(2,10) = 3.48$, $p = 0.048$. Contrasts revealed that lap time in large configuration, $F(1,5) = 5.38$, $p = 0.04$, $r = 0.57$ was significantly higher than medium. Also, there was a nearly significant interaction effect between the type of MP and the type of RH used, $F(4,20) = 2.38$, $p = 0.065$. This indicates that MP had different effects on people's performance depending on which type of RH was used. To break down this interaction, contrasts were performed comparing all MP types to all RH types. These revealed nearly significant interactions when comparing low to medium for small compared to medium $F(1,5) = 5.59$, $p = 0.09$, $r = 0.48$; significant comparing low to medium for medium compared to large $F(1,5) = 5.96$, $p = 0.03$, $r = 0.53$; significant comparing medium to high for medium compared to large $F(1,5) = 6.93$, $p = 0.023$, $r = 0.62$. During the curves, there was a significant main effect of type of MP, $F(2,10) = 3.74$, $p = 0.039$. Contrasts revealed that lap time in large configuration, $F(1,5) = 7.46$, $p = 0.019$, $r = 0.63$ was significantly higher than medium.

The higher lap time with the increase of MP size, in general, is indicating of deteriorated performance when drivers are asked to keep a constant speed, although considering it with the decrease in speed variation (described next) both reflect improved performance. In other words, increasing the MP size (presenting

more motion to drivers) decreased the speed variation in fare of increasing their lap time.

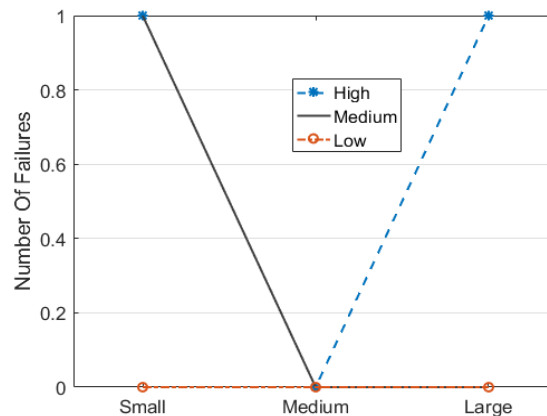


Figure 6-17. Number of failures

From Figure 6-17, the number of failures in total was too little to draw a conclusion. In medium MP size there were no failures. The high and medium had the greatest number of failures in small and large MPs.

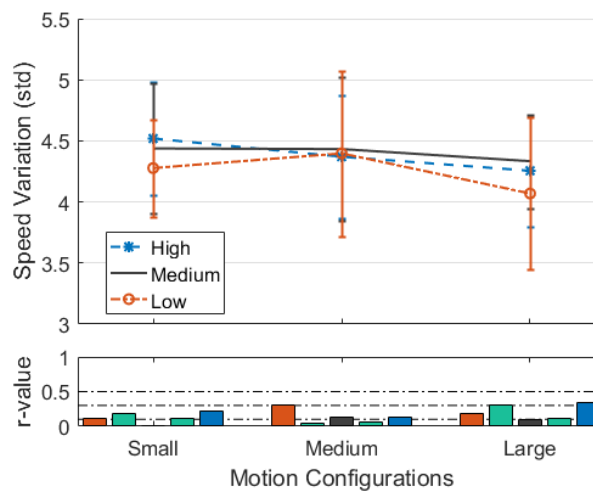


Figure 6-18. Speed variations

From Figure 6-18, the speed variation slightly decreased with increasing MP size for medium and high, except for the small to medium in low RH. Although the effect sizes are small to medium, that might indicate providing larger motion to drivers results in less speed variation during driving, that reflects the improved performance with the increase of MP size.

Comparing the RHs in each MP size, the low has slightly lower speed variation than medium and high all MPs. In medium MP all the three RHs are quite similar.

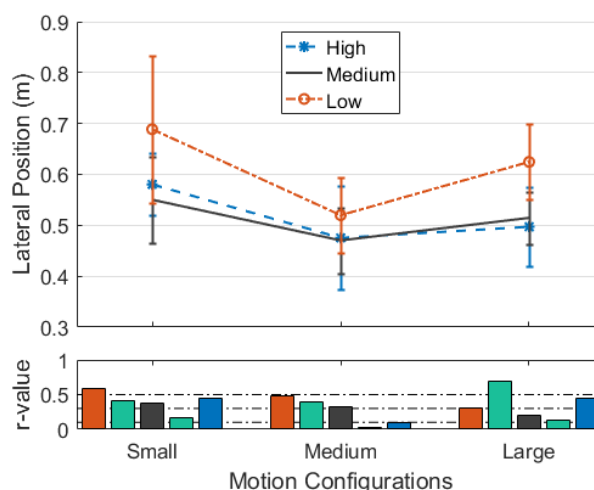


Figure 6-19. Lateral position deviation

From Figure 6-19, lateral position deviation fluctuated but decreased overall with increasing MP size for all RHs, which means the small MP has the largest lateral position deviation and vice versa. Having considerable medium to large effect sizes reveals that providing larger motion to drivers results in less lateral position deviation during driving, reflecting the improved performance of drivers.

Comparing the RHs in each MP size, the medium and high has always lower lateral position deviation than low in all the MPs. Having medium to large effect sizes indicate that drivers had always larger lateral position deviation driving the low configurations than medium and high.

The lateral position deviation in the divided straight and curve sections showed: During straight lines, there was a significant main effect of type of MP, $F(2,10) = 4.26$, $p = 0.027$. Contrasts revealed that lateral position deviation in small configuration was significantly higher than medium $F(1,5) = 6.17$, $p = 0.03$, $r = 0.59$ and large configurations, $F(1,5) = 9.4$, $p = 0.01$, $r = 0.67$. Moreover, there was a significant main effect of type of RH, $F(2,10) = 5.8$, $p = 0.009$. Contrasts revealed that lateral position deviation in low configuration was significantly higher than medium $F(1,5) = 6.67$, $p = 0.025$, $r = 0.61$ large $F(1,5) = 6.2$, $p = 0.03$, $r = 0.6$. During curves, there was a significant main effect of type of MP, $F(2,10) = 4.2$, $p = 0.02$. Contrasts revealed that lateral position deviation in small configuration was significantly higher than medium $F(1,5) = 4.47$, $p = 0.05$, $r = 0.53$ and large configurations, $F(1,5) = 10.03$, $p = 0.008$, $r = 0.69$.

Time series

In this section, the results of repeated measure ANOVA and post hoc analysis on the time series metrics in each of the group sections are presented, and where there are significant or near significant results those are elaborated. Looking at

Table 6-12, Table 6-13 and Table 6-14 the columns (on x-axis) belong to independent variables and their interaction and each row belongs (on y-axis) to a dependent measured variable metric. The F and p values are shown on each box corresponding to a factor and an output measure. Black highlighted boxes show where the p-value is less than 0.1 that means there is a significant difference.

Curves

In Table 6-12 the RM ANOVA results of time series output measured metrics are shown for both RH, MP configurations and their interactions.

Table 6-12. Repeated measure ANOVA time series metrics results of curve grouped sections

	Curves			
	MP	RH	MP*RH	
Long Vel (m/s)	F1.44, P0.26	F2.82, P0.08	F0.74, P0.57	<div style="display: flex; align-items: center;"> <div style="width: 10px; height: 100%; background-color: black; margin-right: 5px;"></div> <div style="text-align: center;">P <= 0.1</div> </div> <div style="display: flex; align-items: center; margin-top: 10px;"> <div style="width: 10px; height: 100%; background-color: white; border: 1px solid black; margin-right: 5px;"></div> <div style="text-align: center;">P > 0.1</div> </div>
Lat Vel (m/s)	F0.75, P0.48	F2.14, P0.14	F0.13, P0.97	
Yaw Rate (rad/s)	F1.77, P0.19	F1.49, P0.25	F0.43, P0.78	
Body Slip Angle	F0.70, P0.51	F2.07, P0.15	F0.25, P0.91	
Long Acc (m/s ²)	F1.63, P0.22	F1.34, P0.28	F3.49, P0.01	
Lat Acc (m/s ²)	F2.44, P0.11	F2.21, P0.13	F0.35, P0.84	
Preview Time	F8.05, P0.00	F0.76, P0.48	F0.37, P0.83	
Delay Time	F0.35, P0.71	F2.12, P0.14	F1.45, P0.23	
Gain	F0.73, P0.49	F0.28, P0.76	F1.44, P0.24	
StrgRevsRate 1°	F0.02, P0.98	F3.38, P0.05	F0.06, P0.99	
StrgRevsRate 10°	F0.23, P0.80	F2.72, P0.09	F0.38, P0.82	

For this grouped section points that show significant main or interaction effects on output measures include:

For MP comparison:

- Driver model preview time

For RH comparison:

- Maximum longitudinal velocity
- Steering wheel reversal rate (1 degree)
- Steering wheel reversal rate (10 degree)

For MP and RH interaction:

- Maximum longitudinal acceleration

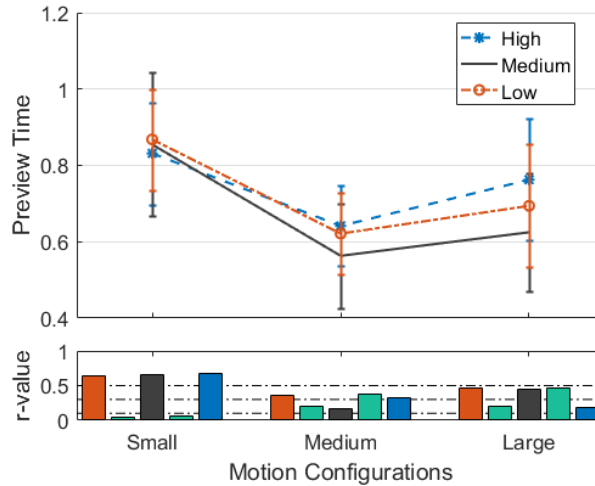


Figure 6-20. Driver model preview time, curves

There was a significant main effect of type of MP on the DRYPE preview time objective metric, $F(2,10) = 8.04, p = 0.002$. Pairwise comparison indicated significant and nearly significant $p = 0.0003, p = 0.08$ difference between small to medium and large MPs. Contrasts revealed that preview time in small configuration was significantly higher than large $F(1,5) = 5.65, p = 0.03, r = 0.58$ and medium $F(1,5) = 33.4, p = 0.0001, r = 0.86$.

Looking at Figure 6-20 graph and effect sizes the preview time has fluctuated but overall decreased with increasing MP size with medium to large effect sizes, in all the three RHs the highest value is at small MP. In small the low RH has the highest preview time although the three RHs are similar, in medium and large it is the high, with small to medium effect sizes.

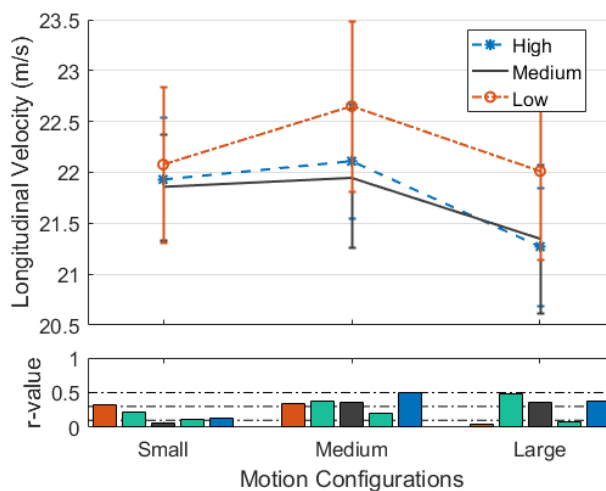


Figure 6-21. Maximum longitudinal velocity, curves

There was a significant main effect of type of RH on the longitudinal velocity objective metric, $F(2,10) = 2.81, p = 0.08$. Contrasts revealed that the velocity in

low configuration was nearly significantly higher than high $F(1,5) = 3.62, p = 0.08, r = 0.49$.

Looking at Figure 6-21 graphs and effect sizes the longitudinal velocity has fluctuated but overall decreased with increasing MP size with small to large effect sizes, in all the three RHs the lowest value is at large MP. In small, medium and large the low has the highest preview time with small to medium effect sizes.

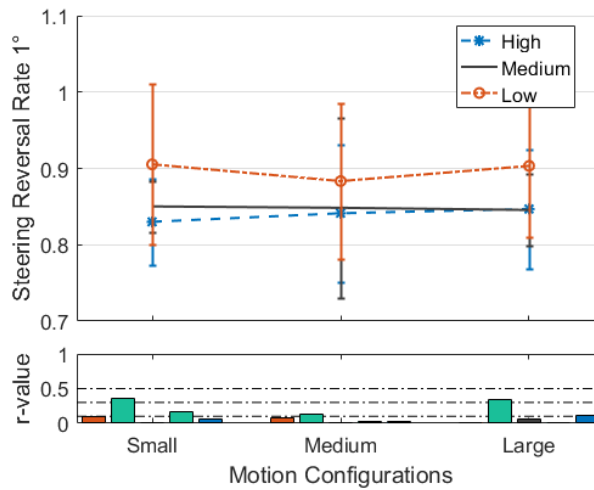


Figure 6-22. Steering wheel reversal rate 1°, curves

There was a significant main effect of type of RH on the steering wheel reversal rate 1° objective metric, $F(2,10) = 3.37, p = 0.05$. Contrasts revealed that the steering reversal rate in low configuration was significantly higher than high $F(1,5) = 9.85, p = 0.009, r = 0.68$.

Looking at Figure 6-22 graphs and effect sizes the steering wheel reversal rate has stayed similar with increasing MP size. In small, medium and large the low has the highest preview time, where the medium and high are similar with small to medium effect sizes, that shows higher control activity in low RH i.e. deteriorated performance.

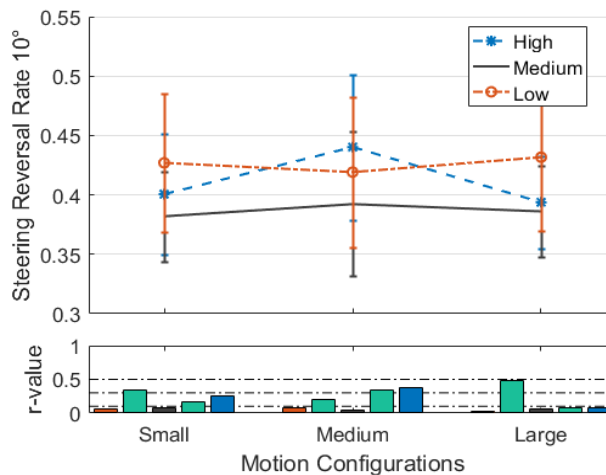


Figure 6-23. Steering wheel reversal rate 10°, curves

There was a nearly significant main effect of type of RH on the steering wheel reversal rate 10 degree objective metric, $F(2,10) = 2.725$, $p = 0.087$. Contrasts revealed that the velocity in low configuration was significantly higher than medium $F(1,5) = 5.33$, $p = 0.04$, $r = 0.57$.

Looking at Figure 6-23 graphs and effect sizes the steering wheel reversal rate has stayed similar with increasing MP size in medium and low RH, while it has fluctuated in high. In small and large the low has the highest reversal rate, in the medium it is high with small to medium effect sizes, that shows mostly higher control activity in low RH i.e. deteriorated performance.

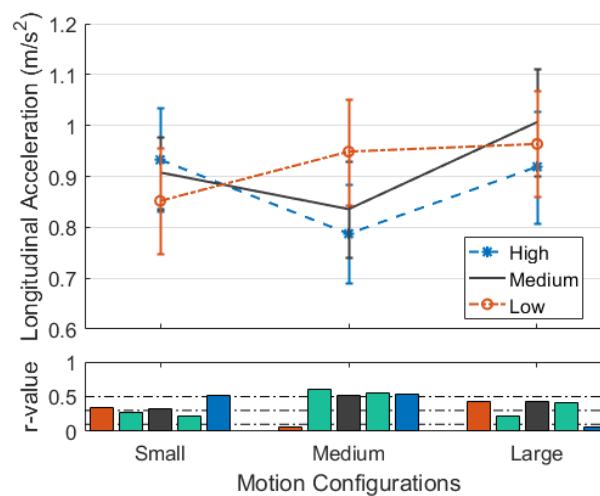


Figure 6-24. Longitudinal acceleration, curves

There was a significant interaction effect between the type of MP and the type of RH used, $F(4,20) = 3.49$, $p = 0.01$. This indicates that MP had different effects on people's performance depending on which type of RH was used. To break down this interaction, contrasts were performed comparing all MP types to all RH types. These revealed significant interactions when comparing low to medium for small compared to medium $F(1,5) = 4.64$, $p = 0.05$, $r = 0.54$; significant comparing medium to high for small compared to medium $F(1,5) = 5.04$, $p = 0.04$, $r = 0.56$; significant comparing low to medium for medium compared to large $F(1,5) = 3.81$, $p = 0.076$, $r = 0.5$.

Looking at Figure 6-24 graphs and effect sizes the longitudinal acceleration has fluctuated with increasing MP size with small to large effect sizes. In small, medium and high the highest value, is the high, low and medium with small to large effect sizes.

Straight lines

In Table 6-13 the RM ANOVA results of time series output measured metrics are shown for both RH, MP configurations and their interactions.

Table 6-13. Repeated measure ANOVA time series metrics results of straight line grouped sections

Straight Lines			
	MP	RH	MP*RH
Long Vel (m/s)	F1.99, P0.16	F2.08, P0.15	F1.20, P0.32
Lat Vel (m/s)	F0.84, P0.44	F2.37, P0.12	F1.02, P0.41
Yaw Rate (rad/s)	F1.58, P0.23	F4.75, P0.02	F0.98, P0.43
Body Slip Angle	F1.35, P0.28	F3.00, P0.07	F1.21, P0.32
Long Acc (m/s ²)	F1.89, P0.17	F3.67, P0.04	F1.02, P0.41
Lat Acc (m/s ²)	F0.76, P0.48	F4.60, P0.02	F0.86, P0.50
Preview Time	F2.36, P0.12	F0.79, P0.47	F0.90, P0.47
Delay Time	F1.00, P0.38	F0.43, P0.65	F0.96, P0.44
Gain	F1.78, P0.19	F0.84, P0.44	F1.20, P0.33
StrgRevsRate 1°	F0.15, P0.86	F0.95, P0.40	F2.94, P0.03
StrgRevsRate 10°	F0.46, P0.64	F3.42, P0.05	F0.75, P0.56

For this grouped section points that show significant main or interaction effects on output measures include:

For RH comparison:

- Maximum yaw rate
- Maximum body slip angle
- Maximum longitudinal velocity
- Maximum lateral acceleration
- Steering wheel reversal rate (10 degree)

For RH and MP interaction:

- Steering wheel reversal rate (1 degree)

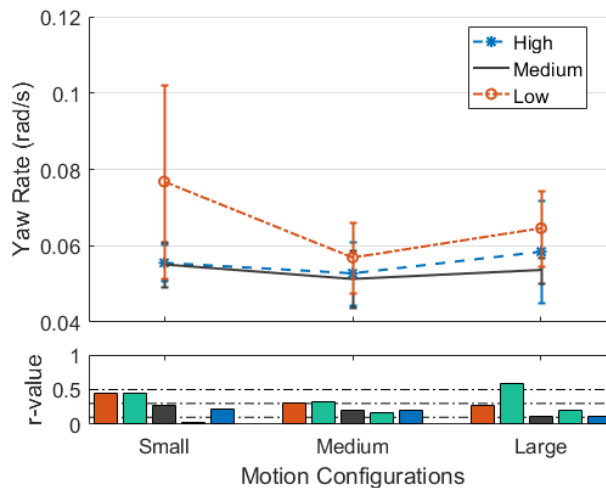


Figure 6-25. Maximum yaw rate, straight lines

There was a significant main effect of type of RH on the yaw rate objective metric, $F(2,10) = 4.75, p = 0.019$. Contrasts revealed that the yaw rate in low configuration

was significantly higher than medium $F(1,5) = 5.49, p = 0.038, r = 0.57$; nearly significantly higher than high $F(1,5) = 4.25, p = 0.06, r = 0.52$.

Looking at Figure 6-25 graphs and effect sizes the yaw rate has stayed similar or slightly decreased with increasing MP size with small to medium effect sizes, in all the three RHs the lowest value is at medium MP. In small, medium and large the low has the highest value with small to large effect sizes.

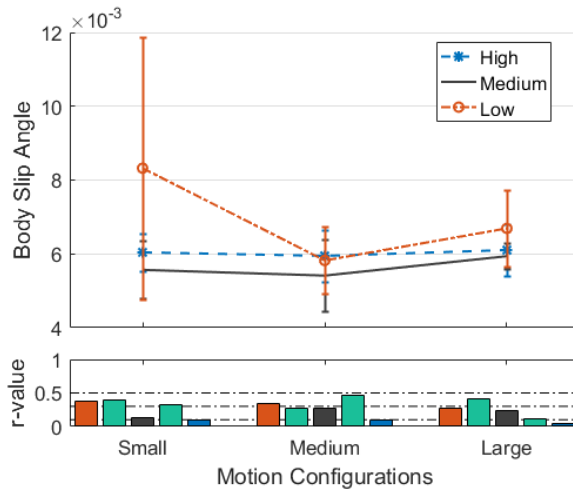


Figure 6-26. Maximum body slip angle, straight lines

There was a nearly significant main effect of type of RH on the body slip angle objective metric, $F(2,10) = 3, p = 0.07$. Contrasts revealed that the slip angle in low configuration was significantly higher than medium $F(1,5) = 3.56, p = 0.08, r = 0.49$ and high significantly higher than medium $F(1,5) = 6.05, p = 0.031, r = 0.59$.

Looking at Figure 6-26 graphs and effect sizes the slip angle has stayed similar with increasing MP size with small to medium effect sizes, in all the three RHs the lowest value is at medium MP. In small, medium and large the low has the highest value with small to medium effect sizes.

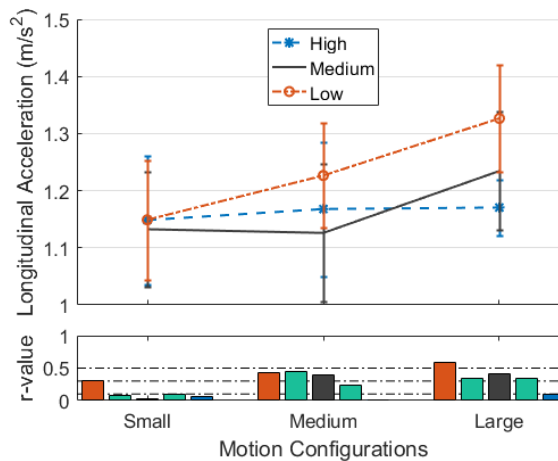


Figure 6-27. Maximum longitudinal acceleration, straight lines

There was a nearly significant main effect of type of RH on the maximum longitudinal acceleration objective metric, $F(2,10) = 3,67$, $p = 0.04$. Contrasts revealed that the acceleration in low configuration was nearly significantly higher than medium $F(1,5) = 3.64$, $p = 0.08$, $r = 0.49$ and low significantly higher than high $F(1,5) = 7.53$, $p = 0.019$, $r = 0.63$.

Looking at Figure 6-27 graphs and effect sizes the longitudinal acceleration has increased with increasing MP size with small to large effect sizes, in all the three RHs the lowest value is at small MP. In small, medium and large the low has the highest value with small to medium effect sizes.

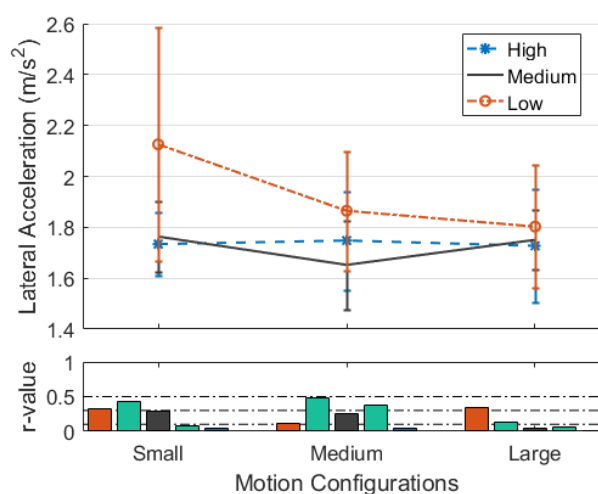


Figure 6-28. Maximum lateral acceleration, straight lines

There was a significant main effect of type of RH on the maximum lateral acceleration objective metric, $F(2,10) = 4.6$, $p = 0.02$. Contrasts revealed that the acceleration in low configuration was significantly higher than medium $F(1,5) = 5.33$, $p = 0.04$, $r = 0.57$ and low nearly significantly higher than high $F(1,5) = 4.3$, $p = 0.06$, $r = 0.53$.

Looking at Figure 6-28 graphs and effect sizes the lateral acceleration has decreased or stayed similar with increasing MP size with small to large effect sizes. In small, and large the low has the highest value with small to medium effect sizes.

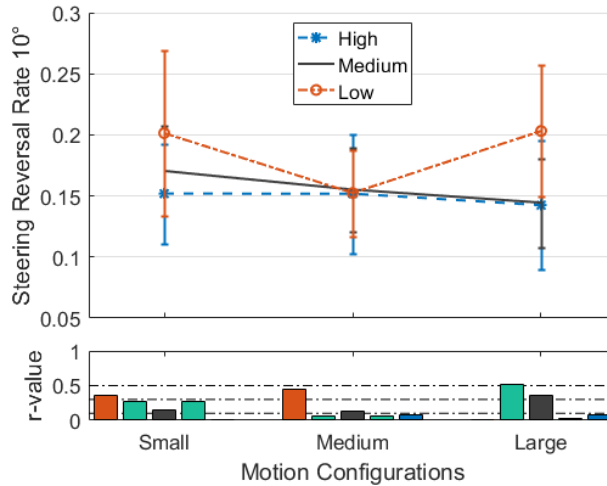


Figure 6-29. Steering wheel reversal rate 10°, straight lines

There was a significant main effect of type of RH on the steering wheel reversal rate objective metric, $F(2,10) = 3.4, p = 0.05$. Contrasts revealed that the acceleration in low configuration was nearly significantly higher than medium $F(1,5) = 4.31, p = 0.06, r = 0.53$ and low significantly higher than large $F(1,5) = 4.96, p = 0.047, r = 0.55$.

Looking at Figure 6-29 graph and effect sizes the longitudinal acceleration has slightly decreased or fluctuated with increasing MP size with small to large effect sizes, in all the three RHs the lowest value is at medium or large MP, that shows lower control activity and more relaxed style of driving with the increase of MP size i.e. improved performance. In small, medium and large the low has the highest value with small to medium effect sizes, that shows higher control activity in low RH i.e. deteriorated performance.

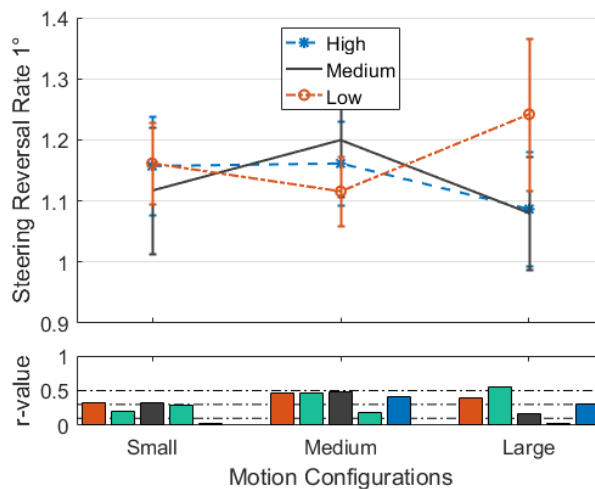


Figure 6-30. Steering wheel reversal rate 1°, straight lines

There was a significant interaction effect between the type of MP and the type of RH used, $F(4,20) = 2.93, p = 0.03$. This indicates that MP had different effects on

people’s performance depending on which type of RH was used. To break down this interaction, contrasts were performed comparing all MP types to all RH types. These revealed significant interactions when comparing low to medium for medium compared to large $F(1,5) = 5.43, p = 0.039, r = 0.57$.

Looking at Figure 6-30 graphs and effect sizes the steering wheel reversal rate 1 degree has fluctuated with increasing MP size with small to medium effect sizes. In small, medium and large the highest value, is the low, medium and low with small to large effect sizes.

Whole track

In Table 6-14 the RM ANOVA results of time series output measured metrics are shown for both RH, MP configurations and their interactions.

Table 6-14. Repeated measure ANOVA time series metrics, whole track

Whole Track			
	MP	RH	MP*RH
Long Vel (m/s)	F0.36, P0.70	F0.01, P0.99	F0.52, P0.72
Lat Vel (m/s)	F0.18, P0.83	F0.92, P0.42	F0.89, P0.48
Yaw Rate (rad/s)	F1.10, P0.36	F1.40, P0.27	F0.24, P0.91
Body Slip Angle	F1.15, P0.34	F0.92, P0.42	F1.05, P0.40
Long Acc (m/s ²)	F0.47, P0.63	F1.28, P0.31	F0.59, P0.67
Lat Acc (m/s ²)	F0.78, P0.47	F0.74, P0.49	F1.00, P0.42
Preview Time	F1.12, P0.35	F1.89, P0.18	F0.97, P0.44
Delay Time	F1.39, P0.28	F0.40, P0.68	F0.72, P0.58
Gain	F6.37, P0.01	F0.22, P0.80	F0.47, P0.76
StrgRevsRate 1°	F0.24, P0.79	F2.79, P0.09	F3.44, P0.02
StrgRevsRate 10°	F1.51, P0.25	F2.39, P0.12	F1.06, P0.39

P <= 0.1

P > 0.1

For the whole track boxes that show significant main or interaction effects on output measures include:

For MP comparison:

- Driver model gain

For RH comparison:

- Steering wheel reversal rate (1 degree)

For RH and MP interaction:

- Steering wheel reversal rate (1 degree)

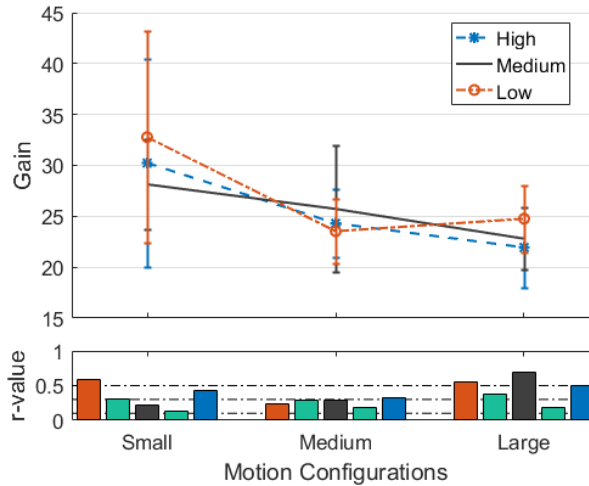


Figure 6-31. Driver model steering gain, whole track

There was a significant main effect of type of MP on the DRYPE steering gain objective metric, $F(2,10) = 6.37, p = 0.009$. Contrasts revealed that the steering gain in small configuration was significantly higher than medium $F(1,5) = 5.9, p = 0.04, r = 0.65$, and large $F(1,5) = 11.81, p = 0.008, r = 0.77$.

Looking at Figure 6-31 graphs and effect sizes the steering gain has decreased with increasing MP size with small to large effect sizes, in all the three RHs the highest value is at small MP, that shows lower control activity and more relaxed style of driving with the increase of MP size i.e. improved performance. In small, medium and large the low, medium and low has the highest values with small to medium effect sizes, that shows higher control activity in low RH i.e. deteriorated performance.

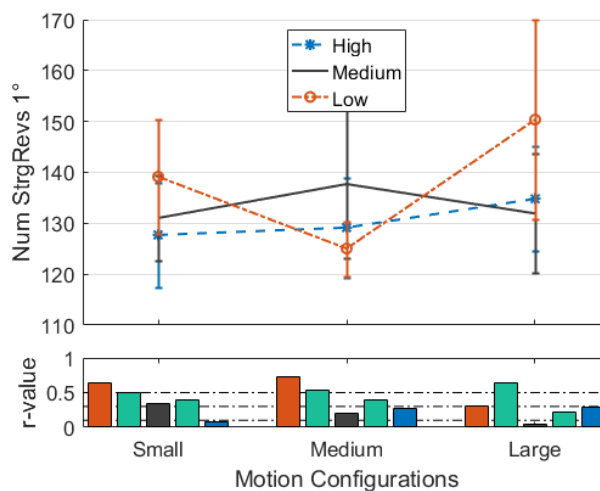


Figure 6-32. Steering wheel reversal rate 1°, whole track

There was a nearly significant main effect of type of RH on the steering wheel reversal rate objective metric, $F(2,10) = 2.69, p = 0.09$. Contrasts revealed that the

steering gain in low configuration was significantly higher than high $F(1,5) = 9.38$, $p = 0.01$, $r = 0.73$.

There was a significant interaction effect between the type of MP and the type of RH used, $F(4,20) = 4.34$, $p = 0.006$. This indicates that MP had different effects on people's performance depending on which type of RH was used. To break down this interaction, contrasts were performed comparing all MP types to all RH types. These revealed significant interactions when comparing low to medium for small compared to medium $F(1,5) = 5.43$, $p = 0.039$, $r = 0.57$; comparing low to medium for medium compared to large $F(1,8) = 8.05$, $p = 0.02$, $r = 0.57$.

Looking at Figure 6-32 graphs and effect sizes the steering wheel reversal rate 1 degree has fluctuated with increasing MP size with small to large effect sizes. In small, medium and large the highest value, is the low, medium and low with small to large effect sizes, that shows higher control activity in low RH i.e. deteriorated performance.

6.11 Discussion and conclusions

The current study was designed to assess simulator based testing of vehicle driven attribute qualities those are the ride, steering and handling. Moreover, the effect that different motion configurations of a driving simulator might have on driven attributes assessments were considered. Evaluations were done to address how variations in vehicle properties affect drivers' subjective ratings of driven attribute qualities, simulator fidelity and their objective behaviour. To this end, the first independent variable was the manipulations to the ride height (RH) of the air suspension of a Range Rover Velar prototype vehicle that was identified as a subjectively comparable manipulation that causes changes to the driven attributes. The other independent variable was the manipulation of simulator motion configuration including various motion platform (MP) workspace sizes.

As the first target of this study, three RHs were selected to be compared, those were small, medium and high; as second target of this study three sizes of MPs were selected to make a comparison, those were the small, medium and high. Moreover, because of lacking previous research considering interacting effects that MP sizes might have on the RHs the RH comparisons (first target) took place in each of the MP sizes. Gosport lane a public road circuit, starting and ending at the JLR Gaydon site were selected and replicated in the simulator for the tests. Regarding these targets two research questions were defined and evaluated through drivers' subjective ratings of driven attribute qualities, simulator fidelity and their objective behaviour performance. The permutation of MPs and RHs created

nine motion configurations of small-low (S-L), small-medium (S-M), small-high (S-H), and medium-low (M-L), medium-medium (M-M), medium-high (M-H), large-low (L-L), large-medium (L-M) and large-high (L-H), the experiment was designed to compare between them and address the research questions. The research questions and the main results of the experiment are presented below.

Research question 1 – How do the different RHs affect the drivers' subjective ratings of driven attribute qualities, simulator fidelity and their objective behaviour?

I. Subjective fidelity results

The results of repeated measure ANOVA for some of the six grouped questions of driven attributes showed the significant or nearly significant effect of type of RHs on subjective ratings of driven attributes. In steering gain linearity away from centre, the low and high were nearly significant different to medium. In handling roll transient low and high were nearly significant different. In handling under/over steering the low and medium were significantly different.

Based on analysis of plots and effect sizes it was observable that, In the ride question the low and medium RH were quite similar to drivers, where they found them constrained and crashy, and as it was expected they found high RH settled and floaty and appropriate for the vehicle. In the steering gain linearity attribute the low and high RH were more nonlinear to the drivers, and the medium RH was more linear and appropriate for the vehicle. In under/over steering quality the low and high RH were more oversteering to drivers, and the medium RH was the most appropriate for the vehicle. In the handling roll transient question the low to high RH was found to have less to more values respective, as it was expected. This shows drivers could distinguish correctly between RHs, although the low RH was selected as the most appropriate. In handling grouped questions it is of mixed results in each of the MP sizes.

Although there were mixed results for the most appropriate RH in some of the attribute qualities, in most of the attribute questions the high and low RH were rated the most unfitting for this vehicle (distant from 0.5) in small and large MPs respectively, in medium MP it was mix of both low and high RHs. This might indicate the effect that MP has on the ratings of RH. Overall, the unfitting RHs were mostly low and high, where the lack of medium RH might imply the appropriateness of the medium RH, and that they were able to distinguish between the RHs, results are summarised in Table 6-15.

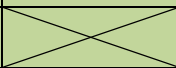
II. Objective behavioural results

In each MP size comparing the low, medium and high RHs, see Table 6-15:

Aggregated performance - for the lap time the highest value in small, medium and large MPs was mixed of with the low, medium and high RHs. For the speed variation, the differences between RHs were subtle although the medium had the highest value. In lateral position deviation metric, the low RH has shown the highest value in all MPs, reflecting the deteriorated performance of drivers while experiencing the low RH.

Time series - in the straight lines and curves there was a significant main effect of type of RHs on some of the output measured metric. The results showed that in the majority of the times the low RH has the highest values in all MPs for all of the objective measures, which is an interesting finding. This consistency might indicate the results are independent of the road sections. Looking at the plots and effect sizes from the objective metrics similarly the low RH always had the highest value and was distinct to the medium and high RHs. Those included the steering wheel reversal rates, and driver model gain, that shows higher control activity, and reflecting the deteriorated performance. However, after the low, the second highest value has fluctuated between the medium and high depending on the metric.

Table 6-15. Summary of results, research question 1 (most appropriate for this vehicle in subjective and highest values in objective)

Metrics		Significant Overall Result	Plot and effect size results				
			Small	Medium	Large		
Subjective	Ride	-	High	High	High		
	Steering – gain linearity away	Medium	Medium	Medium	Medium		
	Steering – window and effort	-	Low	Medium	High		
	Handling – roll transient	Low	Low	Low	Low		
	Handling – under/over steering	Medium	Medium	Medium	Medium		
	Handling – pitch and roll steady	-	Medium	Low	Low		
Objective	Aggregated Performance	Lap Time	-	Low	Medium	High	
		Failure Number		M=H	0	High	
		Speed variation	-	H~M	Medium	Medium	
		Lateral Deviation	Low	Low	Low	Low	
	Time Series	Curves	Long Vel	Low	Low	Low	Low
			Rev Rate 1	Low	Low	Low	Low
			Rev Rate 10	Low	Low	High	Low
		Straight Lines	Yaw Rate	Low	Low	Low	Low
			Slip Angle	Low	L~H	Low	Low
			Lat Acc	Low	Low	Low	Low
			Long Acc	Low	Low	Low	Low
			Rev Rate 10	Low	Low	L~M~H	Low
			Rev Rate 1	Low	Low	Medium	Low
Whole Track	Rev Rate 1	Low	Low	Medium	Low		

In summary, the drivers were able to distinguish between the RHs in many of the vehicle attributes and rated them correctly. In brief, they evaluated correctly that the high RH was the most settled and floaty, low and high RH were nonlinear and oversteering and the medium RH was the most appropriate for the vehicle and handling transient roll of the vehicle had increased from low to high RH.

In terms of aggregated performance measurements including the lap time, speed variation the differences between the RHs were subtle, and lateral position deviation was highest in low RH that solely indicates the deteriorated performance. In the time series metrics, the differences between the RHs were consistent. Nearly in all of the measurement metrics, the low RH had the highest values. Comprised of

the steering reversal rates and driver model steering gain i.e. the measurements over the drivers' control activity. It reflects the less relaxed style of driving and deteriorated performance in low RH.

Research question 2 – How do the different MPs affect the drivers' subjective ratings of driven attribute qualities, simulator fidelity and their objective behaviour?

I. Subjective fidelity results

The results of repeated measure ANOVA for ride question of driven attributes showed the significant effect of type of MPs on subjective ratings of driven attributes. In the ride question, the medium and large were significantly different to small.

Based on analysis of plots and effect sizes it was observable that, in the ride question the medium MP was rated as the most appropriate for this vehicle. In steering gain linearity away from centre and handling roll transient, the mostly small was the most suitable. The drivers found the transient roll of the vehicle to be increasing with the increase of MP size. In handling under/oversteering mostly the large MP was suitable. For the steering window and effort grouped question drivers seemed to have chosen larger MP with increasing RH as more appropriate.

It was noticeable that for most of the attributes especially handling under/oversteering, in the low RH, the small MP was rated as the most appropriate for this vehicle; in the high RH, it was the large MP; in the medium RH, it was a mix of the three MPs. This might indicate that for a higher RH a larger MP is more appropriate, and vice versa.

In most of the attribute questions, the small and large MPs were rated the most unfitting for this vehicle (distant from 0.5) respectively in low and high RHs, in medium RH it was a mix of the three MPs. It might show the effect that RH has on the ratings of MP, where the smaller MP was rated to be unfitting for the evaluations of higher RH, and vice versa. Results are summarised in Table 6-16.

II. Objective behavioural results

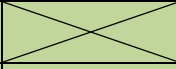
In each RH comparing MP sizes, see Table 6-16:

Aggregated performance - for the lap time the highest value was in the large MP in all RHs, and it has increased (although some time fluctuated) with the increase of MP size. In the speed variation and lateral position deviation metrics, mostly small MP has shown the highest values in all RHs, and values have decreased (although some time fluctuated) with increasing MP size. The decrease in both of the metrics reflects the improved performance of drivers with the increase of MP size.

Time series - in the curves there was a significant main effect of type of MPs on driver model preview time metric, the results showed that the small MP had the highest value in all RHs and it is decreased with increasing MP size. In the whole track, the driver model steering gain has decreased, that shows lower control activity and a more relaxed style of driving with the increase of MP size i.e. improved performance.

Looking at the plots and effect sizes from the objective metrics with increasing MP size although there were fluctuations in some of the RHs but overall: in curves maximum longitudinal velocity and preview time have decreased, 1 and 10 degrees steering wheel reversal rate have stayed similar. In straight lines maximum yaw rate and body slip angle stayed similar, 1 and 10 degrees steering wheel reversal rate has slightly decreased or fluctuated that shows lower control activity and more relaxed style of driving with the increase of MP size i.e. improved performance, longitudinal accelerations have increased. Our hypothesis was to expect a decrease in amplitude of the steering control activity with the increase of MP size that is confirmed and violated in different road sections.

Table 6-16. Summary of results, research question 2 (most appropriate for this vehicle in subjective and highest values in objective)

Metrics		Significant Overall Result	Plot and effect size results				
			Low	Medium	High		
Subjective	Ride	Medium	Medium	Medium	Medium		
	Steering – gain linearity away	-	Small	Small	Large		
	Steering – window and effort	-	Small	Medium	Large		
	Handling – roll transient	-	Small	Small	S~L		
	Handling – under/over steering	-	Small	Large	Large		
	Handling – pitch and roll steady	-	M~L	Small	Large		
	Overall assessment	-	Medium				
	Motion Cueing	-	Medium				
Objective	Aggregated Performance	Lap Time	Large	Large	Large	Large	
		Failure Number		0	Small	Large	
		Speed variation	-	Small	Small	Medium	
		Lateral Deviation	Small	Small	Small	Small	
	Time Series	Curves	Preview time	Small	Small	Small	Small
		Straight Lines	-				
		Whole Track	DRYPE Gain	Small	Small	Small	Small

In summary, drivers preferred the medium MP as more realistic. The results from attribute questions showed in ride quality the medium MP was selected as the most appropriate. In most of the steering and handling group of questions, in the low RH, the small MP was rated as the most appropriate for this vehicle, and in the high RH, it was the large MP. This might indicate the higher the RH is the larger MP is selected as more appropriate, and vice versa.

In terms of aggregated performance measurements, the speed variation and lateral position deviation were decreased with the increase of MP size, that indicates the improved performance. In the time series metrics, most of the measurements were slightly decreased or stayed similar to the increase of MP size. Consist of the steering reversal rates and driver model steering gain i.e. the measurements over the drivers' control activity. It reflects a more relaxed style of driving and improved performance with the increase of MP size.

7 Tuning Optimisation of Motion Cueing Algorithms

7.1 Introduction

The classic and model predictive control (MPC), motion cueing algorithm (MCA) models were developed and experimented in previous chapters. The selection of parameters of the MCAs is called tuning the algorithm, which is a trade-off between cue reproduction in terms of maximising correct (true) cues, and reducing false cues and missing cues, while keeping the motion commands within the envelope and capability constraints of the motion platform (MP). The significant and broad effect of the MCA parameters on the simulator motion cueing has been the subject of research to address the appropriate set of parameters.

Reymond and Kemeny (2000) proposed nonlinear filters to reduce the shortcoming of the backlash generated in the high-pass filters of the classic MCA; although there is an ongoing debate about the propriety of the backlash motion on drivers' perception. A generic algorithms (GA) optimisation method was used for tuning of the MCA with nonlinear filters (Asadi et al., 2015). In this optimisation approach, the vestibular model was included, while respecting the MP physical constraints. Based on the offline analysis it was shown the optimisation works to reduce the perceived artefacts, false cues and minimise the human perception error between vehicle and simulator.

The similar approach of the GA optimisation was used finding the MPC model parameters to replace the manual tuning (Mohammadi et al., 2018). Optimisation considered the best control and prediction horizons to minimise of the costs of sensation error, displacement and the computational burden. They found a small control horizon and much larger prediction horizon as the optimal set of parameters. Although the reported tuning parameters in the literature gives an insight on appropriate parameter selection but those are mainly applicable for a specific type and structure of MCA and characteristics of MP.

The effects of tuning of the MCAs was also observed during the design of the motion configurations of the aforementioned experiments in this thesis. The tuning settings used for the classic MCA in the experiment of Chapters 5 was based on optimisations, however only a few essential parameters of all were extracted using the optimisations, and the rest were fixed and chosen from offline trial and error observations. In the MPC model used in the experiment of Chapter 6, the parameters were selected based on offline trial and error observations and pilot tests. Hence, the question of what is the most appropriate tuning parameter setting was persistently available. It was the motivation to get a thorough understanding of

the effect of MCA parameters. In this chapter, the MCA parameters of classic and MPC and their motion cueing effect are reviewed.

The MCA parameter tuning is a process that involves the driving tasks, vehicle dynamics, MCA and MP to come up with a set of parameters that minimises the motion cueing errors between the virtual and real world, also, to take into account human perception and/or behaviour. Experimental trial and error can be used to take the drivers' subjective perception into account to find the appropriate MCA parameters. In this approach different set of parameter candidates are usually implemented in the simulator, and the drivers are asked about the realism of the settings to draw a conclusion. Although this method is still the most reliable one, it needs a lot of time and effort, and it may not lead to a solid conclusion because of individual preferences.

Alternatively, the parameter settings can be found through offline mathematical analysis. This needs to prepare models of motion system components that have a significant role on motion cueing, together with the models of drivers' perception and/or behaviour, and offline optimisation to find the appropriate MCA parameters. Although this method seems more feasible and less expensive to prepare, accurate models of the listed components are often not available. The main problem of this offline method is the lack of precise models for human perception and especially behaviour, that raise the question of how reliable the obtained parameters of this method are.

Notwithstanding the limitations, the offline analysis is essential for tuning of the algorithms to help to minimise the motion errors between the vehicle and simulator, even without the human perception and behaviour models and only relying on the response of motion cueing components of the simulator. In addition to the need for optimal tuning of the MCA to achieve the highest performance efficiency, the knowledge about the appropriate tuning also helps to address the minimum MP workspace requirements. In Chapter 8, the optimal parameters for both of the classic and model predictive control (MPC) algorithms that are introduced in this chapter are used in an iterative optimisation to address MP workspace size.

The motion errors between a real vehicle and simulators have been categorised to three types of false cues, scaling or missing cues and phase error cues (Grant and Reid, 1997). The false cues were defined to be a motion cue in the simulator in the opposite direction of vehicle, or motion in the simulator when there is none in the vehicle. Among the sources of false cues it has been listed to be from software or hardware limiting; returning to neutral position due to overshoot of high-pass filters to step-like input accelerations; tilt-coordination angular velocity, acceleration and remnant. The scaled or missing cues were the motion cues absent in simulator but

available in vehicle. It is described that the missing cues do not lead to the same reduction in perception as false cues. Among the sources of the missing cues are the missing or scaled motion cues. The phase error cues are phase lead and lag of MCA and MP response to input motion cues.

In a similar context, for the rest of this chapter, a few measurement metrics are used in the analysis of the motion errors. The effect of motion scaling is considered as a within MCA parameter because the variation to the other MCA parameters is dependant to the scaling factor. The motion cueing errors are divided into true and false acceleration cues in the time domain and phase and gain errors in the frequency domain. The true cues Tr is referred to the norm of the commanded simulator acceleration cues a_s (MCA output) that appears in the same direction of input vehicle motion a_i and having equal or smaller absolute values compared the input, Eq. 7.1. The sgn is sign function.

$$Tr = \|a_s(ind_{Tr})\|_2 \quad 7.1$$

$$ind_{Tr}: sgn(a_s) = sgn(a_i) \text{ and } |a_s| \leq |a_i|$$

The false cue is referred to the norm of the commanded simulator motion cues that appears in the opposite direction of input motion cue and/or in the same direction but have greater absolute values compared to input vehicle motion, Eq. 7.2.

$$Fs = \|a_s(ind_{Fs})\|_2 \quad 7.2$$

$$ind_{Fs}: \begin{cases} sgn(a_s) \neq sgn(a_i) \\ sgn(a_s) = sgn(a_i) \text{ and } |a_s| > |a_i| \end{cases}$$

The phase error is referred to the norm of the phase distortion (degree) in the frequency response of the MCA in a range of frequencies, i.e. called frequency of interest $\omega_{interest}$.

$$Ph_{err} = \|\text{Phase}(\omega_{interest})\|_2 \quad 7.3$$

The gain error is referred to the norm of the gain attenuation (decibels dB) in the frequency response of MCA in range of frequency of interest $\omega_{interest}$

$$Gn_{err} = \|\text{Gain}(\omega_{interest})\|_2 \quad 7.4$$

To get a better understanding of these metrics, a time response plot of a second order high-pass filter as it is used in classic MCA, is shown in Figure 7-1. The input vehicle motion is a square acceleration that resembles quick acceleration and deceleration of a vehicle. The true Tr and false Fs cues are highlighted in blue and red marks on the output acceleration response of the high-pass filter, and norm of those values is shown in the bottom of the figure in bars. It needs to be mentioned that the definitions for true and false cues are valid only when the filters are critically damped or overdamped i.e. the damping ratio of the filters is equal or greater than

one $\zeta \geq 1$, because in underdamped situations there are other false cues that this definition does not capture. Additionally, the norm of frequency response gain Gn_{err} and phase Ph_{err} errors is shown in the same bar chart. The backlash motion is highlighted in red after 15 seconds here as a false cue, although there is still a debate if it is a false cue or not.

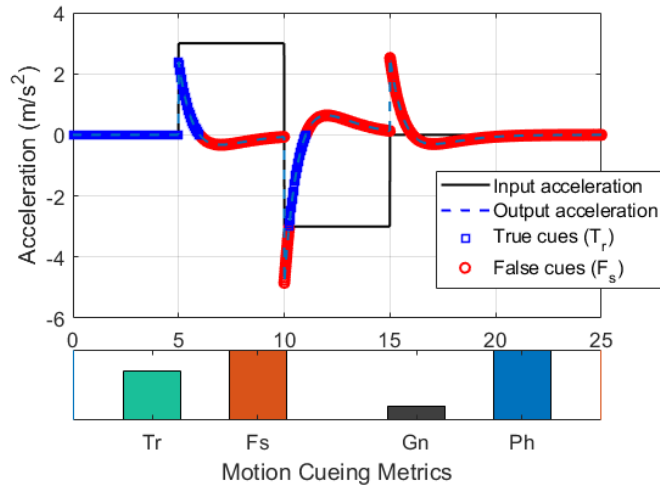


Figure 7-1. Time response of second order high-pass filter with parameters of $k = 0.8$, $\zeta = 1$, $\omega_{hp} = 1 \frac{rad}{sec}$, and the measurement metrics

The frequency of interest is the range of frequencies that is of more importance to drivers, in affecting their perception and behaviour during driving. Although, in each of the manoeuvres a certain range of frequencies may have a more significant effect but the vestibular perception of translational motions is often considered to be more sensitive in the range of $\omega_{interest} = [0.1 \ 10] \ rad/s$ (Nash et al., 2016), also observable in the bode response of the otolith models in Figure 2-3, wherein this range of frequency has the highest magnitude. A frequency response Bode plot of a second order high-pass filter as it is used in classic MCA is shown in Figure 7-2, and the frequency of interest is highlighted in green. The norm of the gain and phase responses over the frequency of interest shows the phase Ph_{err} and gain Gn_{err} .

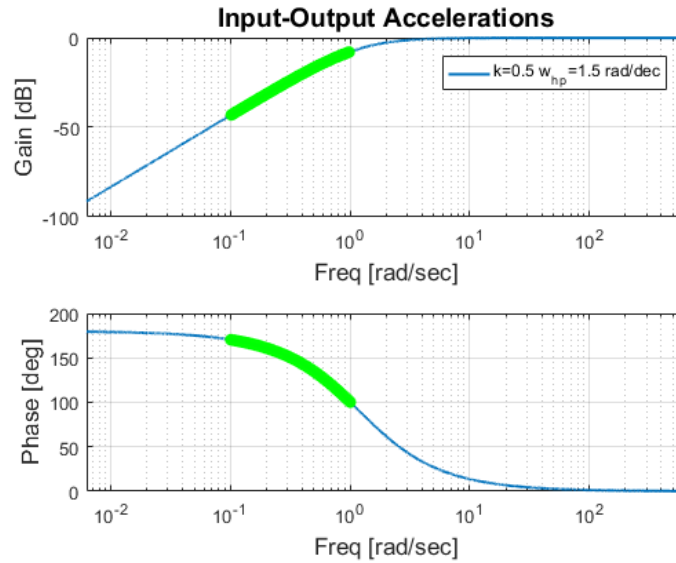


Figure 7-2. Bode plot of second order high-pass filter with parameters of $k = 1$, $\zeta = 1$, $\omega_{hp} = 1.5 \frac{rad}{sec}$, and frequencies of interest highlighted in green.

For the rest of this chapter, the classic and model predictive control (MPC) developed in Chapter 3 and 4 are used, and the alternation effect of their parameters on the motion cueing response in simulators is reviewed. In each of the MCAs, it is tried to find the optimum parameters for the tilt, translational and tilt+translations separately to have general guidelines for different applications and dynamic simulators of all characteristics. For instance, in some applications, the tilting is deactivated, and only translational motion is available, or MPs, do not have a translational workspace and only rely on tilting. Moreover, while minimising the motion cueing errors, the parameters are further refined by linking them to the MP workspace size limits.

7.2 Tuning of classic motion cueing algorithm

A general schematic structure of the classic algorithm was presented in Figure 3-13. It is often a combination of scale-factors, high and low-pass filters, limiters and coordinate transformation. The input to the MCA is vehicle motion, while the output of it is the desired motion platform set points. The scale-factors reduce the acceleration output magnitude in comparison to the input from the vehicle motions. While the input vehicle acceleration passes through the high-pass filter the transient part of acceleration is separated to be represented by MP translational movements. The sustained is separated by a low-pass filter which is transformed to tilt coordination that is added to the rotational channel to be represented by MP rotational movements.

The classic MCA is usually tuned for the worst-case scenario such that the MP does not exceed its envelope and capability while representing the maximum of vehicle motions to participants using offline analysis. The initial parameter candidates are further refined by based on the drivers' subjective comments and their performances. Beginning with the translational motions of the MP in the surge, sway and heave directions, various first, second and third order high-pass filters have been employed in flight and driving simulators depending on the application, respectively shown in Eq.7.5, 7.6 and 7.7. Depending on the filter order, the scale-factor k and the high-pass filter parameters of cut-off frequency ω and damping ratio ζ define the response of MCA to input vehicle motions.

The first order high-pass filter mostly used in flight simulators for translational or rotational motion cueing, represented in Eq.7.5. It includes the equations in Laplace and time domain, and its frequency gain and phase responses. It is observable the variables of scale-factor k and cut-off frequency of ω_{hp1} defines the output acceleration a_s rethe sponse of MCA to input vehicle acceleration a_l of the vehicle. Reducing the cut-off frequency sustains the cue for a longer duration but it increases the required motion platform excursion.

Based on the observation of longitudinal and lateral vehicle motions during in various manoeuvres, few different motion inputs were selected to find the first, second and third order high-pass filters' response to them, those include step, square, triangle-square, sinusoids input accelerations and a vehicle lateral acceleration (during LHT manoeuvre described in Chapters 5), see Figure 7-3. In each of the inputs and filters the motion cueing metrics in Eq.7.1 to 7.4 are calculated and shown in bar charts under the figures. The same filter parameters are used for all conditions. As it is observable in the plots, there are few issues accompanying the first order filter. To a step input acceleration, the position excursion diverges to infinity, and compared to higher order filters requires larger excursions. Moreover, to input sinusoid accelerations it generates a DC gain offset that might require further adjustments in the model.

$$G_{1st}(s) = \frac{a_s}{a_l} = kG_{hp1} = k \frac{s}{(s + \omega_{hp1})}$$

$$G_{1st}(t) = \frac{a_s}{a_l} = \delta(t) - \omega_{hp1} e^{-t\omega_{hp1}}$$

First
Order

$$|G_{1st}| = k \frac{\left(\frac{\omega}{\omega_{hp1}}\right)}{\left(1 + \left(\frac{\omega}{\omega_{hp1}}\right)^2\right)^{1/2}} \quad 7.5$$

$$\angle G_{1st} = \frac{\pi}{2} - \tan^{-1}\left(\frac{\omega}{\omega_{hp1}}\right)$$

The second order high-pass filter, also known as washout filter, has been widely used in both flight and driving simulators for translational and rotational motion cueing, represented in Eq. 7.6. It is designed to return the motion platform to its neutral position in a range of normal input accelerations. It is observable that the variables of scale-factor k and cut-off frequency of ω_{hp2} , and damping ratio ζ , define the time and frequency response of the MCA. Similar to the first order filter, reducing the cut-off frequency sustain the cue for a longer time, but it increases the required motion platform excursion. Decreasing the damping ratio sustains the cue for longer requiring larger excursion and reduces the effect of the washout. Since the washout moves the simulator in the opposite direction it is recommended to use lower damping ratios to avoid generating false cues. However, very low damping ratio also creates large overshoots and oscillatory response. The maximum excursion position of the second order filter to a step input goes to a fixed value of k/ω_{hp2}^2 instead of zero.

$$\begin{aligned}
 G_{2nd}(s) &= \frac{a_s}{a_I} = kG_{hp2} = k \frac{s^2}{(s^2 + 2\zeta\omega_{hp2}s + \omega_{hp2}^2)} \\
 G_{2nd}(t) &= \frac{a_s}{a_I} = \delta(t) + (t\omega_{hp2}^2 - 2\omega_{hp2})e^{-t\omega_{hp2}} \\
 \text{Second} \quad |G_{2nd}| &= -k \frac{\left(\frac{\omega}{\omega_{hp2}}\right)^2}{1 + \left(\frac{\omega}{\omega_{hp2}}\right)^2} \quad 7.6 \\
 \text{Order} \quad \angle G_{2nd} &= \pi - \tan^{-1} \left(\frac{2 \frac{\omega}{\omega_{hp2}}}{1 - \left(\frac{\omega}{\omega_{hp2}}\right)^2} \right)
 \end{aligned}$$

The third order high-pass filter has also been widely used in both flights and driving simulators for translational or rotational motion cueing, represented in Eq. 7.7. It is observable the variables of scale-factor k and two cut-off frequency of ω_{hp1} and ω_{hp2} , and damping ratio ζ , define the output acceleration a_s rethe sponse of MCA to input vehicle acceleration a_I of the vehicle. Response of this filter is the combination of the response of the first and second order filters. Similar to the first and second order filters, reducing the cut-off frequency and damping ratio sustains the cue for a longer time, and it increases the required motion platform excursion.

$$\begin{aligned}
 \text{Third} \quad G_{3rd}(s) &= \frac{a_s}{a_I} = kG_{hp1}G_{hp2} = k \frac{s}{(s + \omega_{hp1})} \frac{s^2}{(s^2 + 2\zeta\omega_{hp2}s + \omega_{hp2}^2)} \\
 \text{Order} \quad G_{3rd}(t) &= \frac{a_s}{a_I} = \delta(t) - \frac{\omega_{hp1}^3}{(\omega_{hp1} - \omega_{hp2})^2} e^{-t\omega_{hp1}} \quad 7.7
 \end{aligned}$$

$$+ \left(\frac{-2\omega_{hp2}^3 + 3\omega_{hp1}\omega_{hp2}^2}{(\omega_{hp1} - \omega_{hp2})^2} - \frac{t\omega_2^3}{\omega_{hp1} - \omega_{hp2}} \right) e^{-t\omega_{hp2}}$$

$$|G_{3rd}| = -k \frac{\frac{\omega}{\omega_{hp1}} \left(\frac{\omega}{\omega_{hp2}} \right)^2}{\left(1 + \left(\frac{\omega}{\omega_{hp1}} \right)^2 \right)^{1/2} \left(1 + \left(\frac{\omega}{\omega_{hp2}} \right)^2 \right)}$$

$$\angle G_{3rd} = \frac{3\pi}{2} - \tan^{-1} \left(\frac{\omega}{\omega_{hp1}} \right) - \tan^{-1} \left(\frac{2 \frac{\omega}{\omega_{hp2}}}{1 - \left(\frac{\omega}{\omega_{hp2}} \right)^2} \right)$$

Using the final value theorem, the steady-state response of the filters of reflecting the maximum excursion of the motion platform to various impulse, step and ramp inputs are shown in Table 7-1. The first order filter response to an impulse input reaches a steady-state value of k/ω_{hp1} , and goes to infinity in case of the step and ramp input. The second order filter to an impulse input decays to zero that explains its washout behaviour, to a step input reaches to a steady-state value of k/ω_{hp2}^2 and in a ramp to infinity. In the third order filter motion platform excursions decay to zero for impulse and step input and reaches to a steady-state value of $k/(\omega_{hp1}\omega_{hp2}^2)$.

Table 7-1. Motion platform maximum excursion, using different order high-pass filters and inputs

Input	Maximum position excursion $x_{s,max} = G_{hp}a_I$		
	G_{1st}	G_{2nd}	G_{3rd}
Impulse 1	k/ω_{hp1}	0	0
Step 1/s	∞	k/ω_{hp2}^2	0
Ramp 1/s ²	∞	∞	$k/(\omega_{hp1}\omega_{hp2}^2)$

The second order low-pass filter is a most commonly used for tilt motion cueing in surge and sway directions, represented in Eq. 7.8. It is observable the variables of scale-factor k and cut-off frequency of ω_{lp2} , and damping ratio ζ , define the output tilt feel of acceleration a_s of MCA to input vehicle acceleration a_I of the vehicle. Increasing the cut-off frequency and decreasing the damping ratio results in higher tilt angular velocity and acceleration that generates more accelerations to drivers, that might also violate tilting below the semicircular canal perception threshold.

The scale-factor is usually selected considering the maximum amplitude of the input acceleration and an intended maximum tilt degree of the MP. The latter defines the amount of acceleration to be presented through tilting. Another way of organising the tilting channel is to use a saturator in advance of the low-pass filter to apply the

restrictions on the vehicle acceleration that passes through tilting based on an intended maximum tilt degree. It allows to select higher scale-factor compared to using only a gain; however, there will be a nonlinear behaviour in accelerations above the saturation limit (max tilt degree). In both cases, the cut-off frequency and damping ratio of the second order filter define the maximum angular velocity and acceleration of the tilting.

$$G_{lp}(s) = \frac{a_s}{a_l} = kG_{lp2} = k \frac{\omega_{lp2}^2}{s^2 + 2\zeta\omega_{lp2}s + \omega_{lp2}^2}$$

$$G_{lp}(t) = \frac{a_s}{a_l} = t\omega_{lp2}^2 e^{-t\omega_{lp2}}$$

Second Order

$$|G_{lp}| = -k \frac{1}{1 + \left(\frac{\omega}{\omega_{hp2}}\right)^2} \quad 7.8$$

$$\angle G_{lp} = 1 - \tan^{-1} \left(\frac{2 \frac{\omega}{\omega_{lp2}}}{1 - \left(\frac{\omega}{\omega_{lp2}}\right)^2} \right)$$

Consequently, the acceleration generated by the tilting depends on the three variables of the maximum tilt angle θ_{max} (*deg*) which in the model used in this thesis is selected by the scale-factor and saturator parameters a_{lim} , tilt angular velocity $\dot{\theta}_{max}$ (*deg/s*), and tilt angular acceleration $\ddot{\theta}_{max}$ (*deg/s²*) both are defined by the low-pass filter cut-off frequency ω_{lp} and damping ratio ζ . To a step input acceleration and $\zeta = 1$, the maximum values of the tilting variables could be related to the cut-off frequency ω_{lp} by Eq. 7.9. Using this range of the cut-off frequency in a damping ratio $\zeta = 1$ guarantees that the tilt angular velocity and accelerations never exceed the desired values in any condition of vehicle motion, although these are conservative numbers, and usually more relaxed tilt settings are used in the literature.

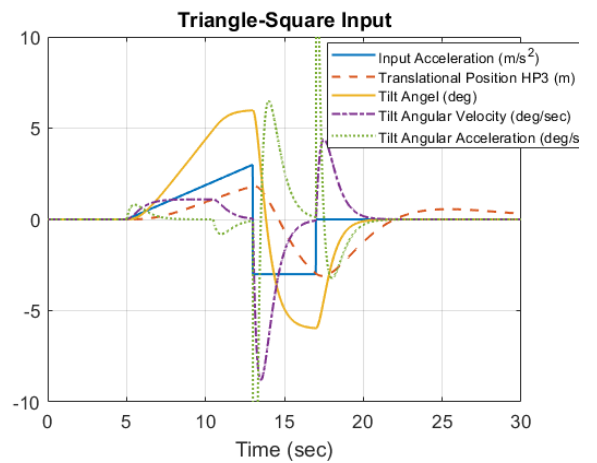
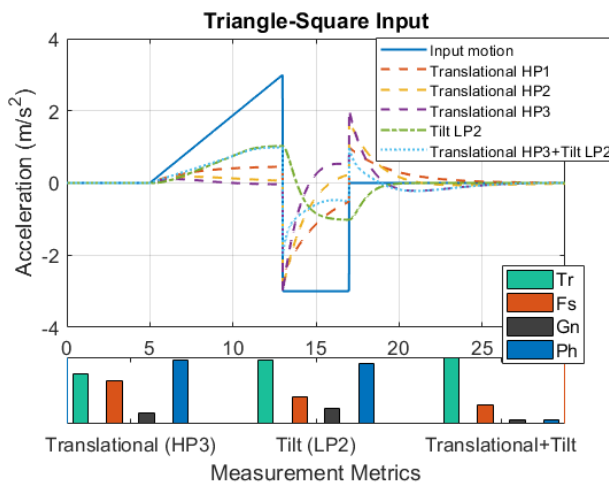
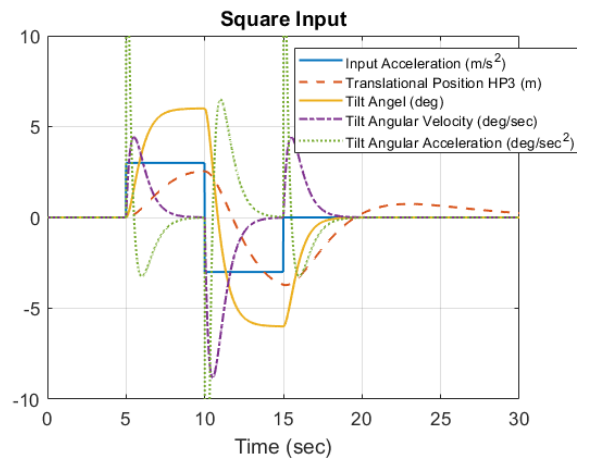
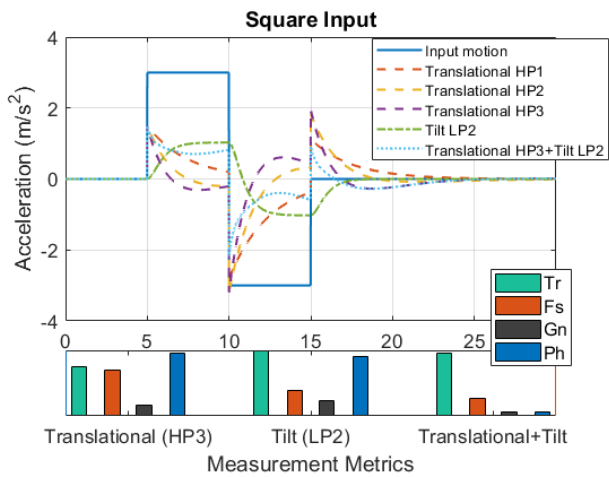
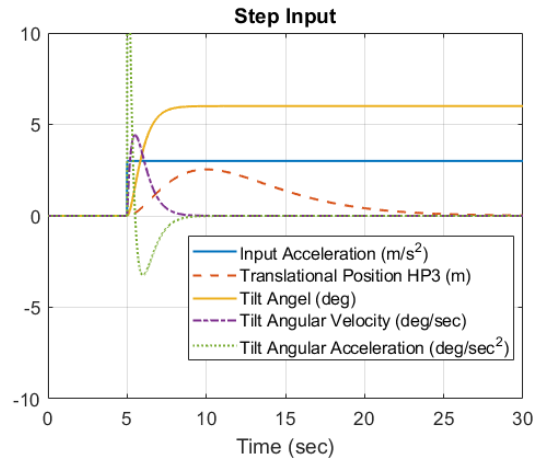
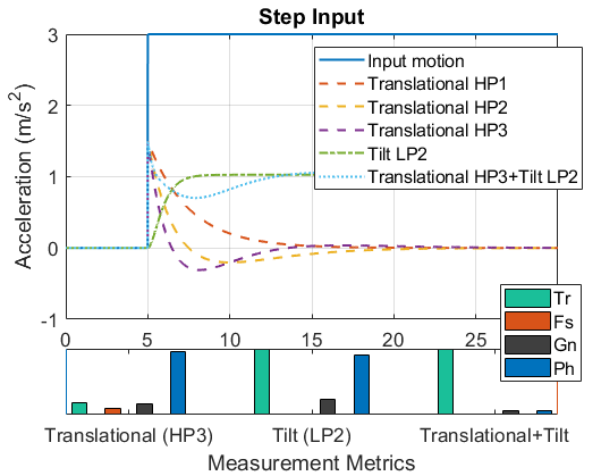
$$\frac{\theta_{max}\pi g}{180} = a_{lim} \rightarrow a_{lim} \leq \frac{\theta_{max}\pi g}{180}$$

$$\frac{\dot{\theta}_{max}\pi g}{180} = \frac{a_{lim}\omega_{lp}}{exp} \rightarrow \omega_{lp} \leq \frac{\dot{\theta}_{max}\pi g exp}{a_{lim}180} \quad 7.9$$

$$\frac{\ddot{\theta}_{max}\pi g}{180} = a_{lim}\omega_{lp}^2 \rightarrow \omega_{lp} \leq \sqrt{\frac{\ddot{\theta}_{max}\pi g}{a_{lim}180}}$$

Based on the pilot evaluations of different settings and filter orders of the classic algorithm in UTIAS flight simulator with position and acceleration limits of $\pm 1.5 \text{ m}$ and 10 m/s^2 , Nahon and Reid (1990) reported settings for translational and tilting motions. A second order high-pass filter with damping ratio of 1 and cut-off

frequency of 2.5 and 4 rad/s in x and y directions. In addition to second order low-pass filter with same damping ratio and 5 and 8 rad/s for tilt in x and y directions. These numbers have been used in many flight simulations studies later as a benchmark for comparisons, although it is valid only for a specific workspace size of MP.



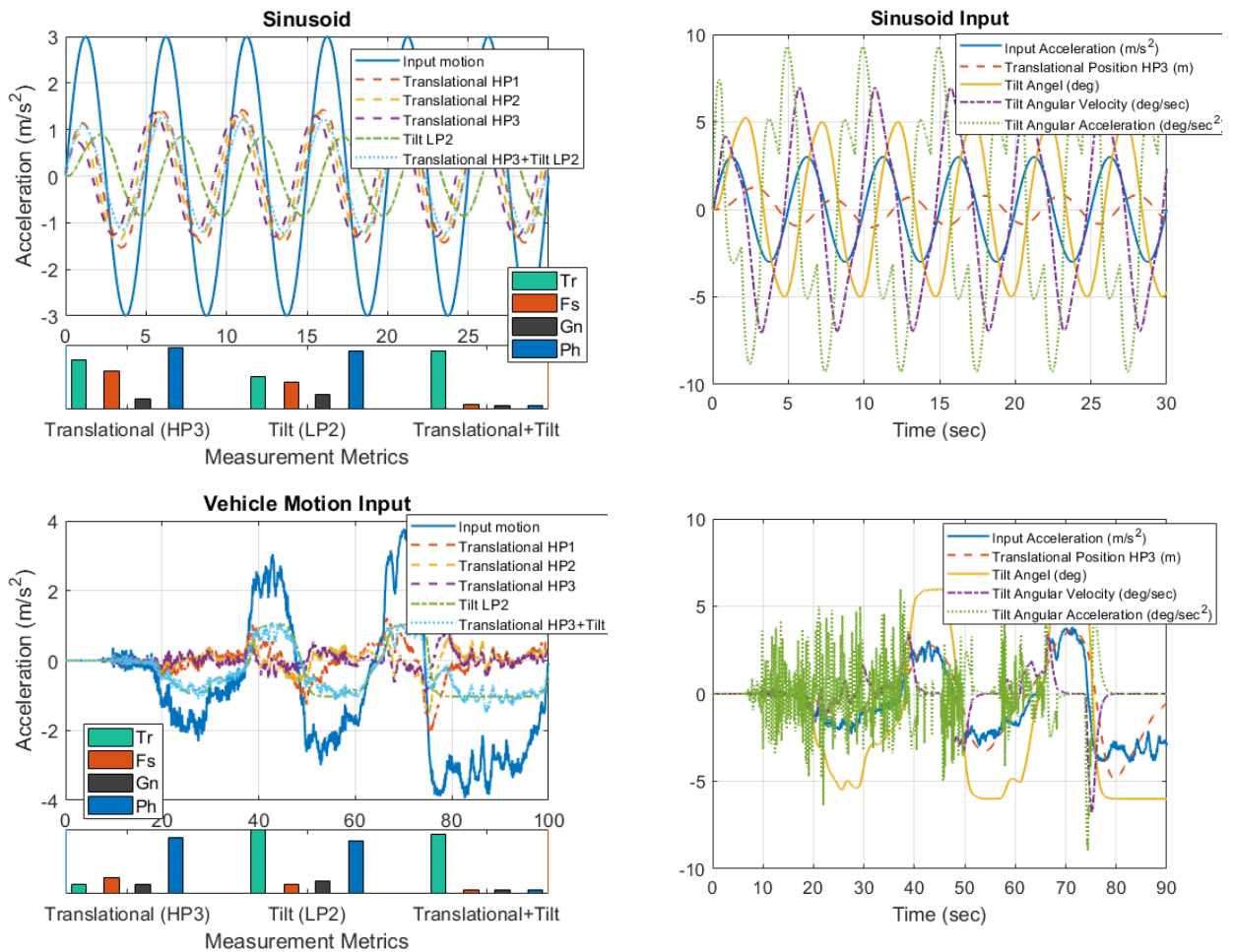


Figure 7-3. Acceleration and position response of high-pass and low-pass filters to step, square, triangle-square, sinusoid and vehicle lateral acceleration inputs, $k = 0.5$, $\zeta = 1$, $\omega_{hp1} = 0.4$, $\omega_{hp2} = 0.4 \text{ rad/sec}$ are the filter parameters

The frequency response of the high-pass, low-pass filters and summation of both is shown in the Bode plot in Figure 7-4. The main difference between a first, second and third order filters in frequency domain is that the stopband roll-off (attenuation) of second and third order filters are respectively twice or three times the first order filter at 20dB/decade, in the operating frequency below the cut-off frequency. Similarly, the phase is distorted with twice or three times the first order filter at 90 degrees. The second order low-pass filter has a similar response but attenuates the signal at higher frequencies than cut-off frequency and the phase distortion is negative. It is observable that in range of the frequency of interest $[0.1 \text{ } 10] \text{ rad/s}$ the with same cut-off frequency the higher order filters generate more magnitude attenuation and phase distortion compared to lower order. However, the combination of the low and high-pass filters and by appropriate selection of the scale-factors and cut-off frequencies the higher order filters compensate for the more phase and gain distortions, besides it adds the washout capability that prepares more workspace for excursions.

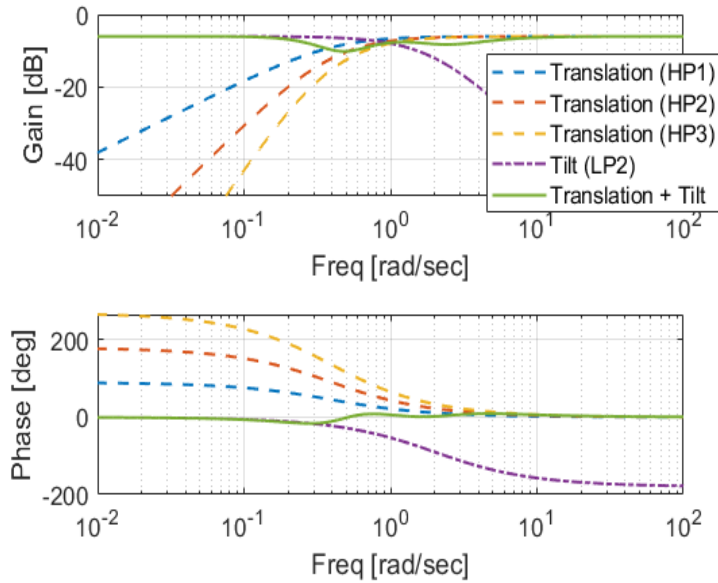


Figure 7-4. Bode frequency response of the high-pass and low-pass filters

In the previous section, the time and frequency response of the high-pass and low-pass filters for a single cut-off frequency and scale-factor parameters were presented, and the proposed measurement metrics were calculated. In a broader perspective, it is essential to find out how the variations of the filter parameters could affect the metrics and to decide on the best set of parameters as an optimum solution(s). Therefore, in the next few sections, the effect of variation of the filter parameters on the measurement metrics are reviewed for the translational, tilting and total motions of the simulator.

7.2.1 Translational motions

7.2.1.1 First order high-pass filter

The time response of the first order filter to the input vehicle lateral acceleration in LHT manoeuvre (see Figure 7-3) in different scale-factor k and cut-off frequencies ω_{hp1} is shown in Figure 7-5. Obviously, the minimum false cues and maximum true cues are at the $k = 1$, $\omega_{hp1} = 0$ where there is no effect of high-pass filtering.

Decreasing the scale-factor reduces the true and false accelerations overall and decreasing the frequency rises true cues and rises the false cues up to a certain point that falls afterwards. In most of the scale-factor and cut-off frequencies settings, the true acceleration is higher than the false acceleration, however, there is a small group of parameters where the opposite is true. The intersection of the true and false cue surfaces is shown in the right figure, the black line shows a border, where within a range of cut-off frequencies using a higher gain generates more false accelerations than true (on the top side of the borderline).

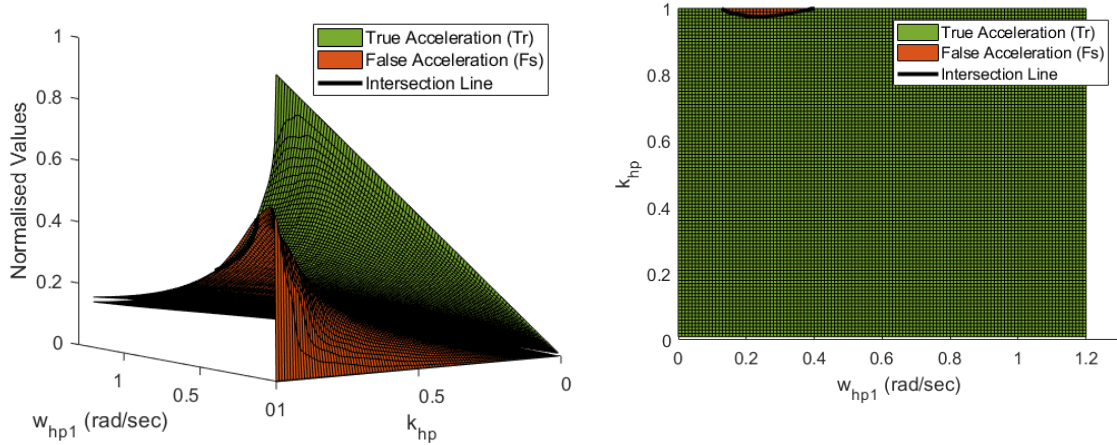


Figure 7-5. The time domain true and false output accelerations in a range of filter parameters, first order high-pass filter

It is also necessary to include the corresponding MP excursions in each of the parameter settings, see Figure 7-6 top. The excursions for such a large demanding manoeuvre for minimum discrepancy setting $k = 1$, $\omega_{hp1} = 0$ reaches to few hundreds of meters and not much of use to be presented. Therefore, a maximum excursion limit of ± 2.5 meters (UoLDS workspace limit) was chosen and settings resulting in larger values of the excursion were omitted from the plots (bottom figures). Looking at the bottom figures the true and false acceleration surfaces are nearly parallel, that indicates in any of the settings there is a similar proportion of true and false motions. Therefore, the highest scale-factor of $k_{hp} = 0.07$ and cut-off frequency of $\omega_{hp1} = 2.1 \text{ rad/s}$, produces the highest amount of motion.

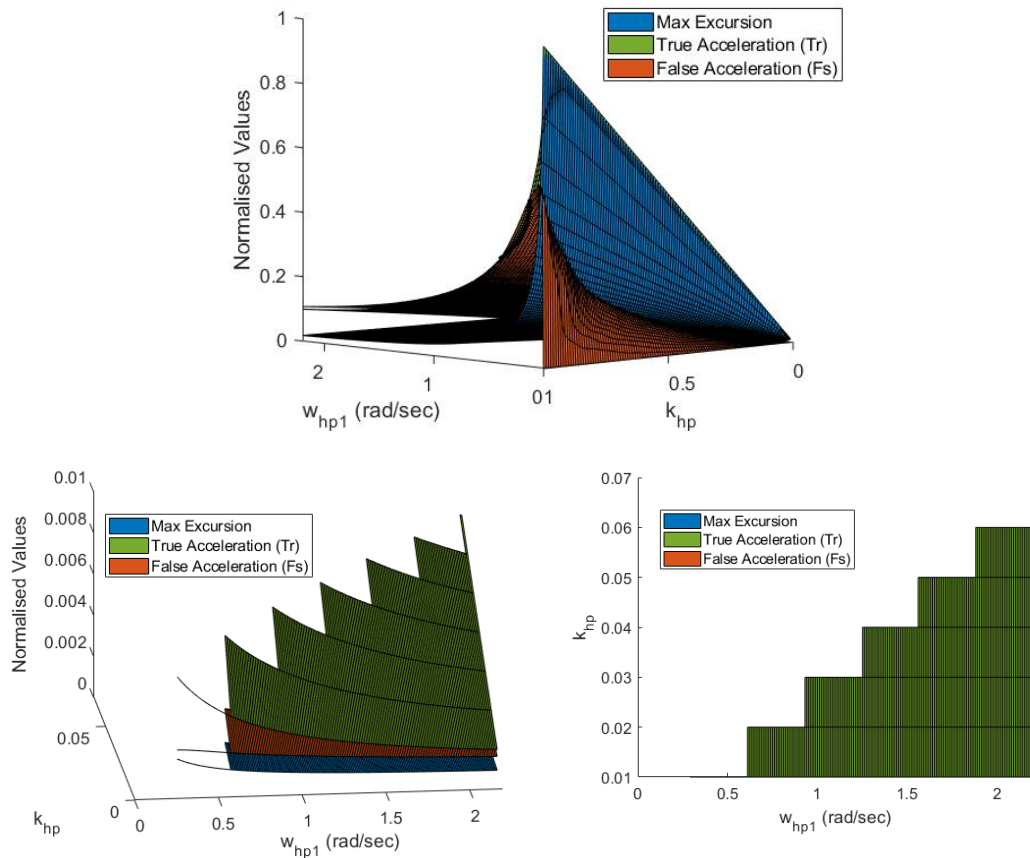


Figure 7-6. The time domain true, false accelerations and position excursions in a range of filter parameters (top), and cropped out settings with excursions smaller than 2.5 (m) (bottom), first order high-pass filter

The similar analysis was done using different motion inputs of step, triangle-square and it was observed that the surfaces of true and false motions change slightly with respect to the input acceleration profile and amplitude, hence it is difficult to find a generalised rule for an optimum set of parameters. The more reliable option is a similar analysis in the frequency domain based on the gain Gn_{err} and phase Ph_{err} error metrics. The first order filter frequency response of different gain k and cut-off frequencies ω_{hp1} , and corresponding position excursions to the same input vehicle lateral acceleration is shown in Figure 7-7.

Similarly, the minimum gain and phase errors are at the $k = 1$, $\omega_{hp1} = 0$ where there is no effect of high-pass filtering. Decreasing of the scale-factor k raises the gain error but has no effect on the phase error, and increasing the frequency raises both the gain and phase errors. The intersection of the two surfaces is shown in the same figure, the black line shows a border of parameter settings where both the gain and phase errors have the minimum values. On the sides of this border, either the phase and gain errors overweigh each other. The excursions for the manoeuvre with a maximum limit of ± 2.5 meters were used to omit the settings that cause

larger excursions from the plot (bottom figures). Comparing the top and bottom figures only small set of parameters (a little of the borderline) remains applicable to fit within the MP envelope.

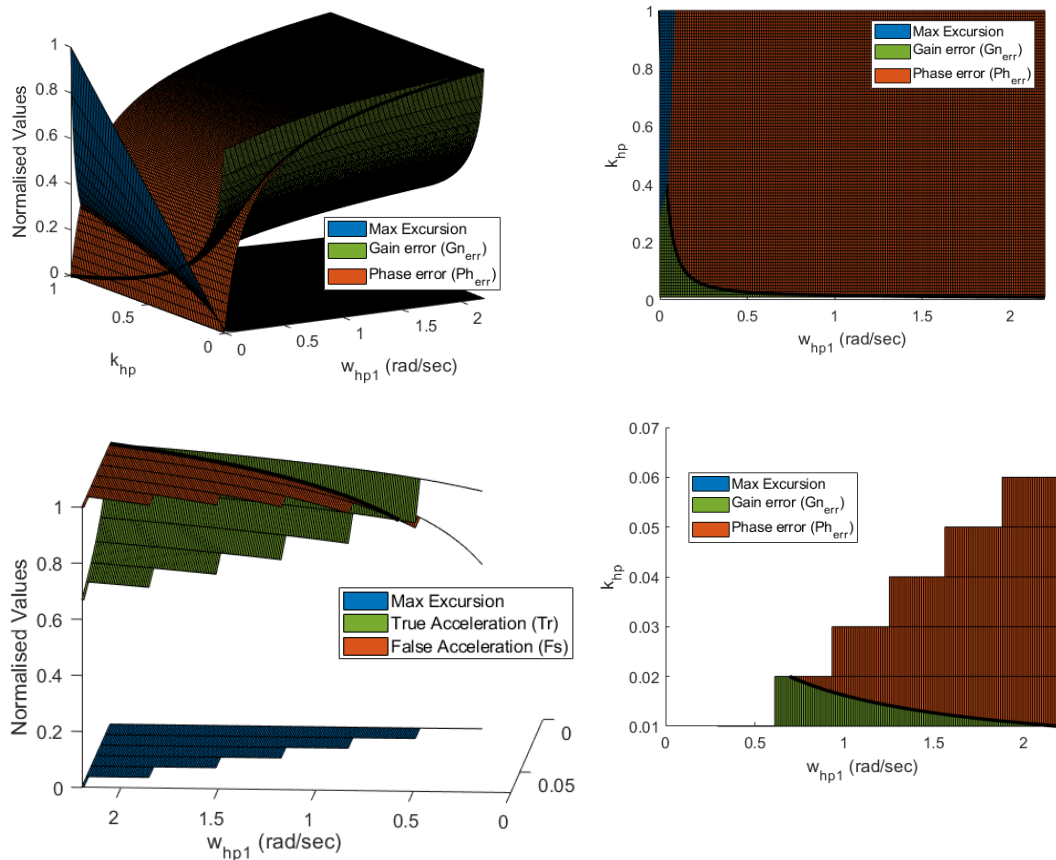


Figure 7-7. The frequency domain gain, phase errors and position excursions in a range of filter parameters (top), and cropped out settings with excursions smaller than 2.5 (m) (bottom), first order high-pass filter

The choice of an optimal setting in time and frequency domain depends on the required motion platform excursions to a vehicle input acceleration, and the workspace of a simulator motion platform. In this example of the vehicle lateral acceleration input, the time domain analysis of the first order high-pass filter showed a small scale-factor of $k = 0.07$ and cut-off frequency of $\omega_{hp1} = 2.1 \text{ rad/s}$ for optimal settings to maximise true against false cues. In the frequency domain to keep the gain and phase errors to a minimum, the small scale-factor of $k_{hp} = 0.02$ and cut-off frequency of $\omega_{hp} = 0.7 \text{ rad/s}$ was found to be an optimal setting. The small scale-factor allows selecting the lower cut-off frequency that decreases the phase error.

7.2.1.2 Second order high-pass filter

Similar to the first order filter, the time response of the second order filter to the input vehicle lateral acceleration in LHT manoeuvre in different scale-factor k and

cut-off frequencies ω_{hp2} is shown in Figure 7-8, the damping ratio $\zeta = 1$ throughout the analysis. The minimum false cues and maximum true cues are at the $k = 1$, $\omega_{hp2} = 0$ where there is no effect of high-pass filtering. Decreasing the scale-factor reduces the true and false accelerations overall and decreasing the frequency raised true cues and raises the false cues up to a certain point that decreases afterwards. The intersection of the two surfaces is shown in the same figure, the black line shows a border where the smaller scale-factor and cut-off frequencies generate more true accelerations than false (on the left side of the borderline). There is a range of settings where the amount of false cues is higher than the true cues (on the right side of the borderline).

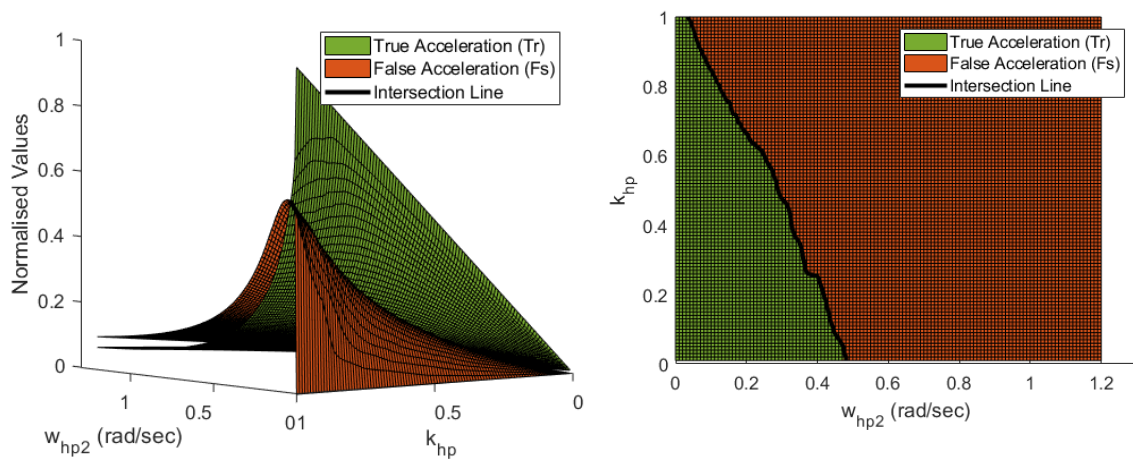


Figure 7-8. The time domain true and false output accelerations in a range of filter parameters, second order high-pass filter

Taking into the considerations the corresponding MP excursions in each of the parameters settings is shown in Figure 7-9 top, and excursions greater than 2.5 metres are omitted from the plots (bottom figures). Comparing Figure 7-8 to Figure 7-9 only a small set of parameters (a little of the borderline) remains applicable to fit within the motion platform envelop that approximately requires a gain $k = 0.15$, $\omega_{hp2} = 0.42 \text{ rad/s}$. Although in this range there is larger true compared to false cues, but the amplitude of motion is small overall. Outside this region both of the false is greater than true, however, both have larger amount, with the maximum at $k = 1$, and $\omega_{hp2} = 1.2 \text{ rad/s}$. This might need further empirical tests in simulathe tor to define better settings.

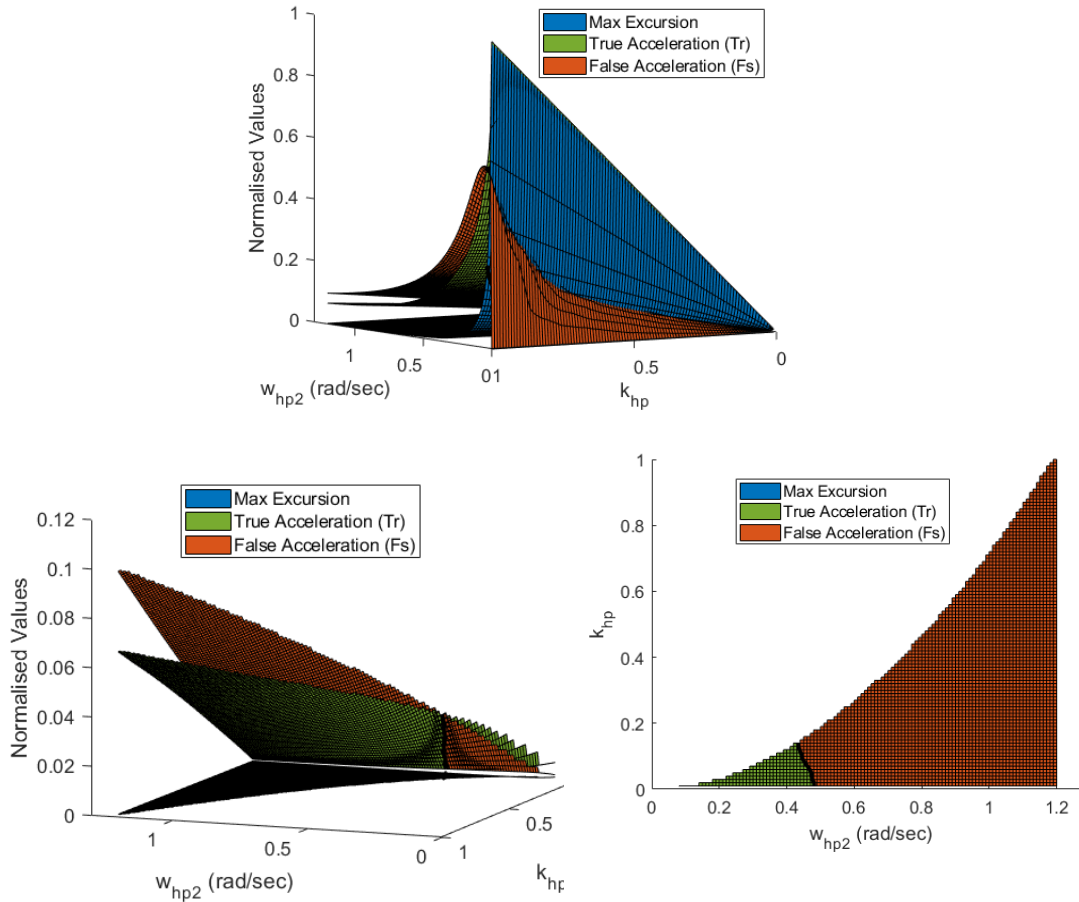


Figure 7-9. The time domain true, false accelerations and position excursions in a range filter parameters (top), and cropped out settings with excursions smaller than 2.5 (m) (bottom), second order high-pass filter

The result of the above analysis might vary slightly with respect to the input acceleration profile and amplitude. Moreover, the backlash effect introduced at the beginning of this chapter is counted as false cues, and removing that might increase the appropriate region of settings. Similar to the first order filter the analysis is carried out in the frequency domain based on the errors in the measurement metrics of gain $G_{n_{err}}$ and phase Ph_{err} . The second order filter frequency response of different scale-factor k and cut-off frequencies ω_{hp2} , and corresponding position excursions to the same input vehicle lateral acceleration is shown in Figure 7-10.

Decreasing of the gain k rises the gain error but has no effect on the phase error and increasing the frequency $\omega_{hp2} = 0$ raises both the gain and phase errors. The intersection of the two surfaces is shown in the same figure, the black line shows a border of parameter settings where both the gain and phase errors have the minimum values. On the sides of this border, either the phase and gain errors overweigh each other. The excursions for the manoeuvre with a maximum limit of

± 2.5 meters were used to omit the settings that cause larger excursions from the plot (bottom figures). Comparing the top and bottom figures only small set of parameters (a little of the borderline) remains applicable to fit within the MP envelope.

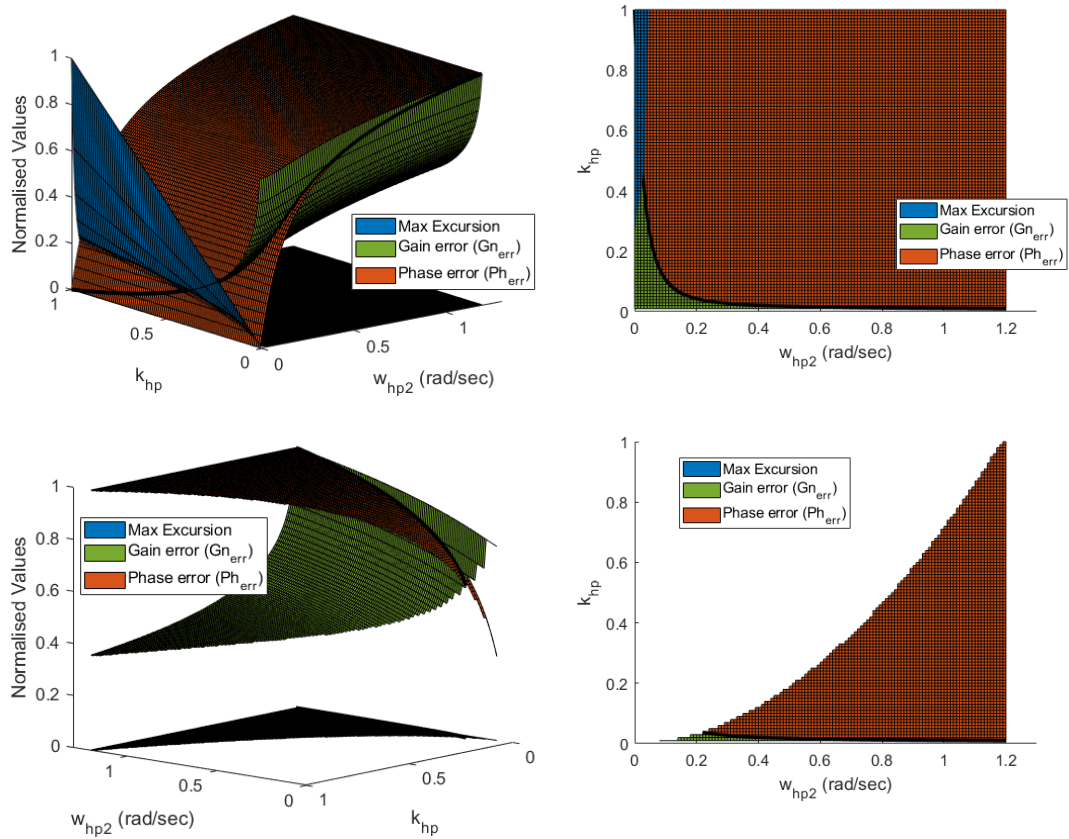


Figure 7-10. The frequency domain gain, phase errors and position excursions in a range of filter parameters (top), and cropped out settings with excursions smaller than 2.5 (m) (bottom), second order high-pass filter

The choice of an optimal setting in time and frequency domain depends on the required excursions to a vehicle input acceleration, and the workspace of a simulator motion platform. In this example of the vehicle lateral acceleration input, the time domain analysis of the second order high-pass filter showed required a scale-factor of $k = 0.15$ and cut-off frequency of $\omega_{hp2} = 0.42 \text{ rad/s}$ to maximise true against false cues in fare of a small amplitude of motion, and $k = 1$ and $\omega_{hp2} = 1.2 \text{ rad/s}$ to have a large amplitude of motion. In the frequency domain to keep the gain and phase errors to a minimum, a very small scale-factor of $k_{hp} = 0.037$ and cut-off frequency of $\omega_{hp} = 0.21 \text{ rad/s}$ found to be an optimal setting.

7.2.1.3 Third order high-pass filter

The third order filter is the combination of the first and second order filter with parameters of scale-factor k and cut-off frequencies of ω_{hp1} and ω_{hp2} , the time

response to the input vehicle lateral acceleration in the LHT manoeuvre is shown in Figure 7-11 top. The minimum false cues and maximum true cues are near the $k = 0.96$, $\omega_{hp1} = 0$, $\omega_{hp2} = 0$ where the effect of high-pass filtering is minimum.

Decreasing the scale-factor reduces the true and false accelerations overall and decreasing the frequencies raises true cues and raises the false cues up to a certain point that falls afterwards (similar to the first and second order filters).

A maximum excursion limit of ± 2.5 meters (UoLDS workspace limit) was chosen and settings resulting in larger values of excursions were omitted from the plots, Figure 7-11 bottoms. The best parameters settings are where the true acceleration is maximum, and the false acceleration is minimum. However, it is difficult to find the best set of parameters that satisfy both of the criteria. Besides, these plots might slightly vary with respect to the input acceleration profile and amplitude.

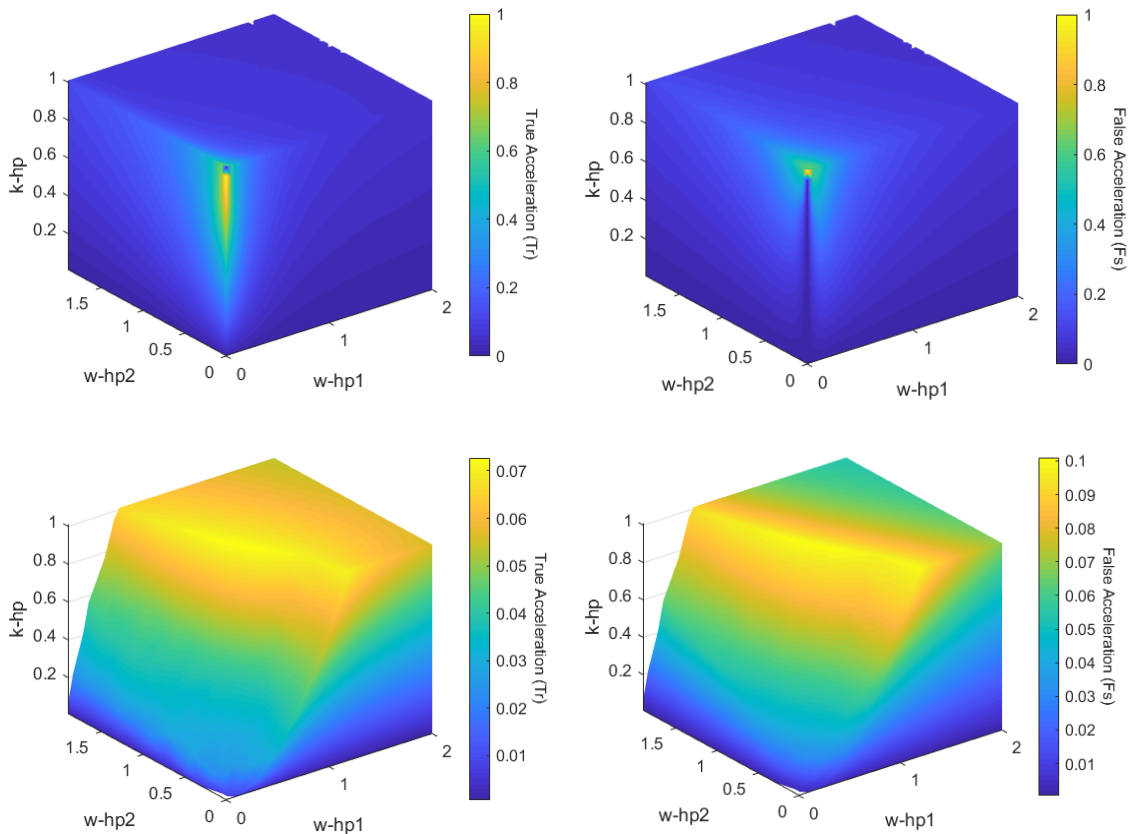


Figure 7-11. The time domain true and false output accelerations in a range of filter parameters (top), cropped out settings with excursions smaller than 2.5 (m) (bottom), third order high-pass filter

The frequency response of the model to different scale-factor k and cut-off frequencies ω_{hp1} , ω_{hp2} parameters are measured by the gain $G_{n_{err}}$ and phase Ph_{err} errors, shown in Figure 7-12. Similarly, the minimum gain and phase errors are at the $k = 1$, $\omega_{hp1} = 0$, $\omega_{hp2} = 0$ where there is no effect of high-pass filtering. Decreasing the scale-factor k raises the gain error but has no effect on the phase

error, and increasing the frequencies raises both the gain and phase errors. The parameter settings where both the normalised gain and phase errors have values greater than 0.5, and those exceed a maximum limit of ± 2.5 metres excursion was omitted from the plot (middle figures) and presented in the same plot (bottom figure). The intersection of the two volumes of phase and gain errors shows using a scale-factor of $k < 0.2$, and small cut-off frequency of $\omega_{hp1} < 0.5 \text{ rad/s}$ in a range of ω_{hp2} minimises both of the gain and phase errors and also respect the MP constraints, however small gain generates a small amount of motion overall.

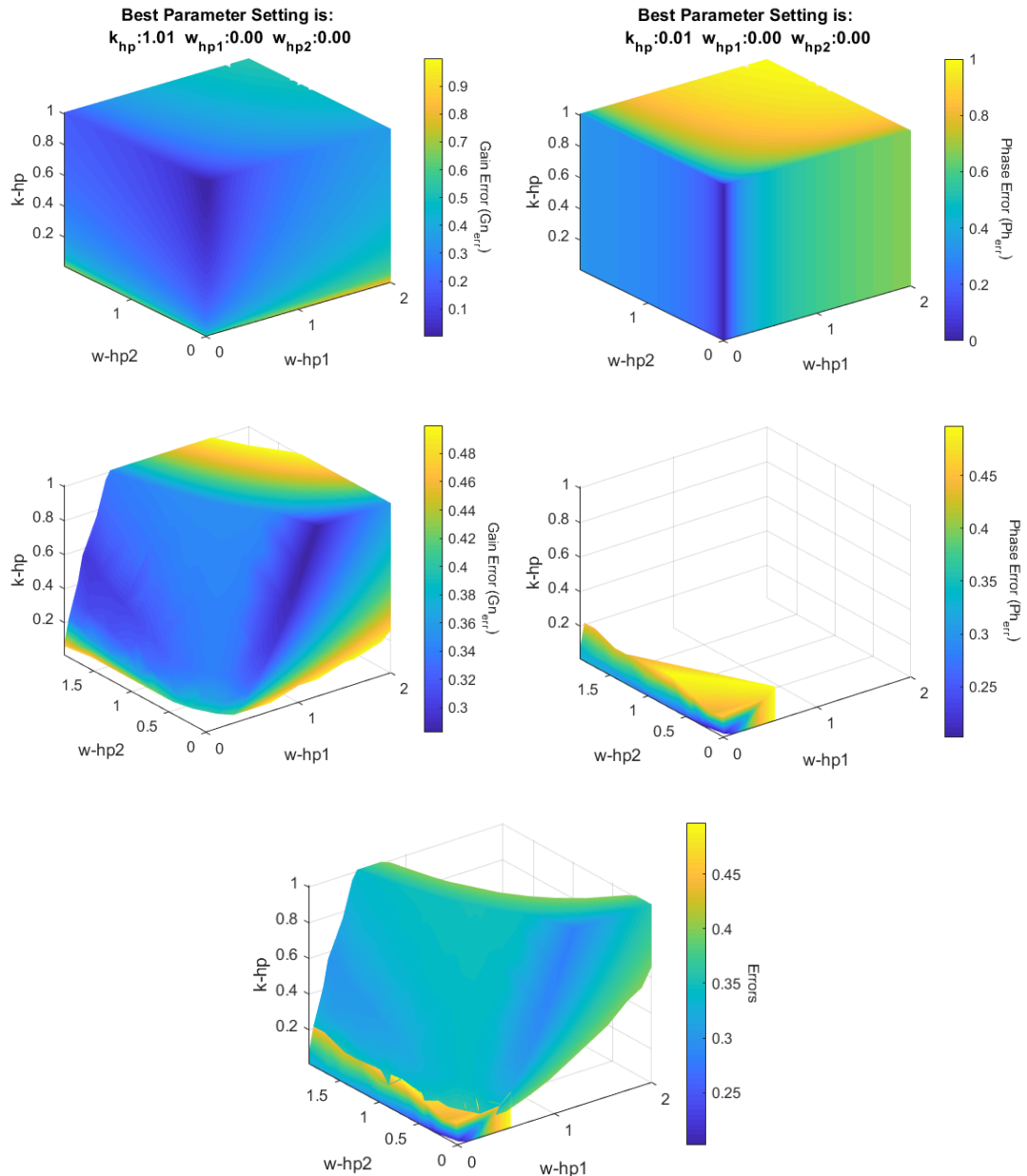


Figure 7-12. The frequency domain gain, phase errors in a range of filter parameters (top), cropped out settings with excursions greater than 2.5 (m) and errors greater than normalised value of 0.5 (middle) and both in the same plot (bottom), third order high-pass filter

7.2.2 Tilt motion

7.2.2.1 Second order low-pass filter

The low-pass filter is used to generate the sustained acceleration through tilting. The acceleration generated by the tilting depends on three variables of maximum tilt angle θ_{max} which is selected by a scale-factor and saturation parameter, tilt angular velocity $\dot{\theta}_{max}$, and tilt angular acceleration $\ddot{\theta}_{max}$ both are defined by the low-pass filter cut-off frequency ω_{lp} and damping ratio ζ . The time response of the second order low-pass filter with different cut-off frequencies ω_{lp2} and damping ratio ζ to the vehicle lateral acceleration input is shown in Figure 7-13 left. The maximum accelerations represented through tilting is limited by a scale-factor $k = 0.5$ and saturator to be 1 m/s^2 or 5.84 deg , and the free variables are the filter parameters.

The minimum false and true cues are at the $\omega_{lp2} = 0$. Increasing the cut-off frequency rise the true acceleration felt through tilting and raises false cue up to a certain point that slightly decreases afterwards. Increasing the damping ratio decreases both true and false accelerations slightly. On the right figure, increasing the cut-off frequency raises the resulting maximum tilting angular velocity and acceleration, while increasing the damping ration decreases them. By changing the two parameters the maximum tilt angular velocity and accelerations could be selected. However, it is noticeable not a full range of maximum tilt angular velocity and accelerations are achievable by the variations of the filter parameters and requires a nonlinear rate-limiting as described in Chapter 4.

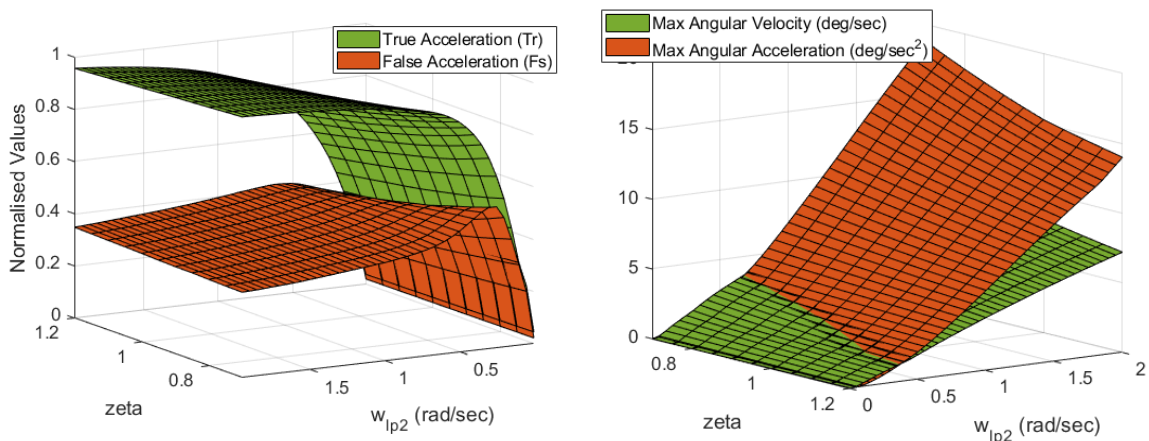


Figure 7-13. The time domain true and false output accelerations by tilting in a range of filter parameters (left) maximum angular velocity and accelerations (right), second order low-pass filter

The frequency response of the model to different parameter settings are measured by the gain Gn_{err} and phase Ph_{err} errors, see Figure 7-14. Decreasing the gain ω_{lp2} raises both the gain and phase errors, and increasing the ζ slightly increases

the gain and decreases the phase errors. The minimum gain and phase errors are at the $\omega_{lp2} = 0.01$ (nearest value to zero used here), and $\zeta = 0.7$ (min gain error, the smallest point used here) and 1.2 (min phase error, the largest point used here). To select the filter parameter values it usually needed to consider the desired angular velocity and acceleration, and often there is only a single set of parameters that meets the requirement and not much flexibility is available in compromising between the minimum phase and gain errors and the desired tilt setting.

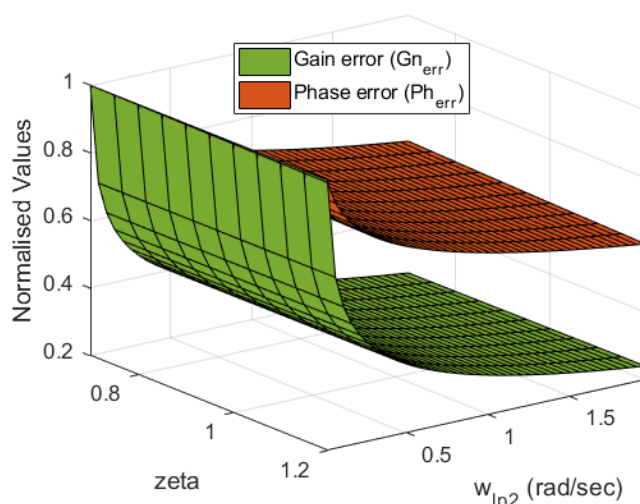


Figure 7-14. The frequency domain gain, phase errors in a range of filter parameters, second order low-pass filter

7.2.3 Translational and tilt motions

In the previous sections, the effect of variation of the filter parameters on time and frequency response of different order high-pass filters for the translational motion and low-pass filter for the tilting motion was presented. For the high-pass filters where it was possible, the best set of parameters were introduced to minimise the time and frequency response errors while respecting the MP constraints, and for the low-pass filter, the selection of parameters is based on the tilt angular velocity and acceleration.

In this section, the same time and frequency response of the combination of the third order high-pass filter and second order low-pass filter is reviewed. For the tilting motion, a single low-pass filter parameter with $\zeta = 1$ and $\omega_{lp2} = 1.5$ are chosen to keep the tilt angular velocity and accelerations below the 3.22 deg/sec and 13.14 deg/sec^2 respectively, see Appendix D. For the third order high-pass filter the three parameters of scale-factor k_{hp} and cut-off frequencies $\omega_{hp1}, \omega_{hp2}$ that are varied. The time response to the input vehicle lateral acceleration in the LHT manoeuvre is shown in Figure 7-15 top. Decreasing the scale-factor reduces the

true and false accelerations overall and decreasing the frequencies raises true and reduce the false cues. However, there is a mixed response of true and false accelerations in different area of the filter parameters.

A maximum excursion limit of ± 2.5 meters (UoLDS workspace limit) was chosen and settings resulting in larger values of excursions were omitted from the plots, Figure 7-15 bottom. The best parameters setting is where the true acceleration is maximum and the false acceleration is minimum. Although it is difficult to find the best set of parameters that satisfy both the criteria, it is observable the area with parameter setting scale-factor of $k_{hp} < 0.2$ and cut-off frequencies of $\omega_{hp1} < 0.4$, $\omega_{hp2} < 0.3$ have both the maximum true and minimum false accelerations. Besides, these plots might change with respect to the input acceleration profile and amplitude, and it is difficult to find a generalised rule for an optimum set of parameters.

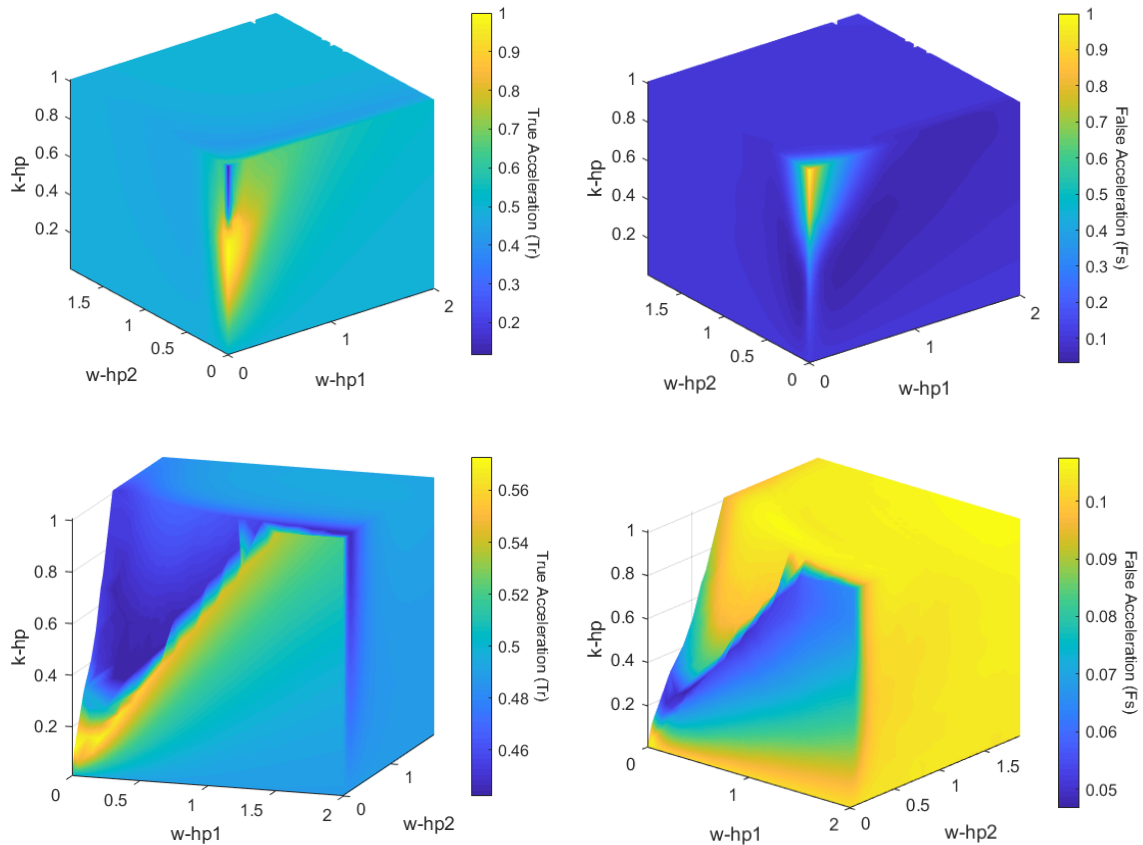


Figure 7-15. The time domain true and false output accelerations in a range of filter parameters (top), cropped out settings with excursions greater than 2.5 (m) (bottom), high-pass and low-pass filter

The frequency response of the model to different parameter settings are measured by the gain Gn_{err} and phase Ph_{err} errors, see Figure 7-16 top. Similarly, the minimum gain and phase errors are at the $k = 1$, $\omega_{hp1} = 0$, $\omega_{hp2} = 0$ where there is no effect of high-pass filtering. Decreasing the scale-factor k raises the gain error

but has no effect on the phase error, and increasing the frequencies raise both the gain and phase errors. In the phase error figure, there is a sudden change of values that is due to the low-pass filter cut-off frequency $\omega_{lp2} = 1.5$ and the high-pass filter frequency values below that generated a significant phase distortion. The parameter settings where both the normalised gain and phase errors have values greater than 0.44 and where those exceed a maximum limit of ± 2.5 meters excursion with was omitted from the plot (middle figures), and presented in the same plot (bottom figure). The intersections of the two volumes of phase and gain errors show using a $k = 0.36 - 0.61$, $\omega_{hp1} = 1.1 - 1.85$, $\omega_{hp2} = 0.2 - 0.5 \text{ rad/s}$ minimises both of the gain and phase errors respectively and also respect the MP constraints. Overall it is observable that using large ω_{hp1} and smaller ω_{hp2} results in lower gain and phase errors.

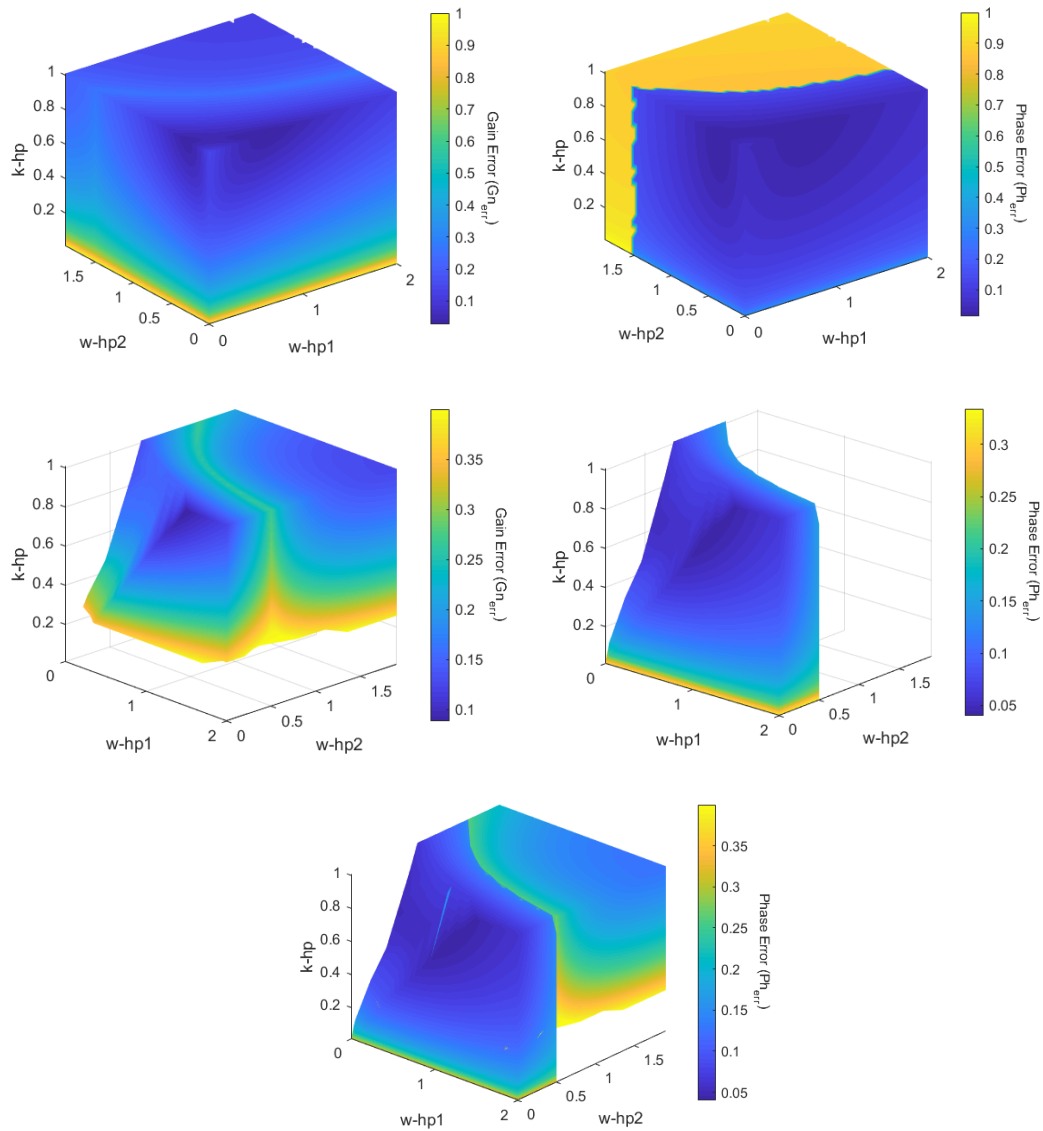


Figure 7-16. The frequency domain gain, phase errors in a range of filter parameters (top), cropped out settings with excursions greater than 2.5 (m) and errors greater than normalised value of 0.4 (middle) and both in same plot (bottom), high-pass and low-pass

7.3 Tuning of MPC motion cueing algorithm

A general schematic structure of the MPC algorithm was presented in Figure 4-4. The input to the MCA is vehicle motion, while the output is the desired MP set points. The controller tries to find optimal solutions to minimise the error between the perceived input and simulator accelerations while keeping the motion platform within its constraints. In this model, there is no filter scale-factor and cut-off frequencies to be tuned as in the classic model, but there are weights on the control inputs and plant outputs tracking variables that balances between the signals, control and prediction horizons, in addition to constant and variable reference input that defines the generated profile of motion.

There are separate channels to represent transient translational movements of MP, and the sustained motions by the tilt coordination through rotational movements. In the MPC algorithm the MP constraints e.g. the maximum envelope is always respected since those are defined explicitly in the model, however further tuning is required to choose the best set of MCA parameters to achieve optimum values of the measurement metrics, adding washout effect. These initial parameter candidates could be further refined based on the drivers' subjective comments and their performance. The model used in this section for the offline tuning considers the translational motion of an MP together with tilt in a single direction of movement. Thus, there are two control inputs u for translational and tilt motions and six plant output y corresponding to the translational, tilt and summation of both.

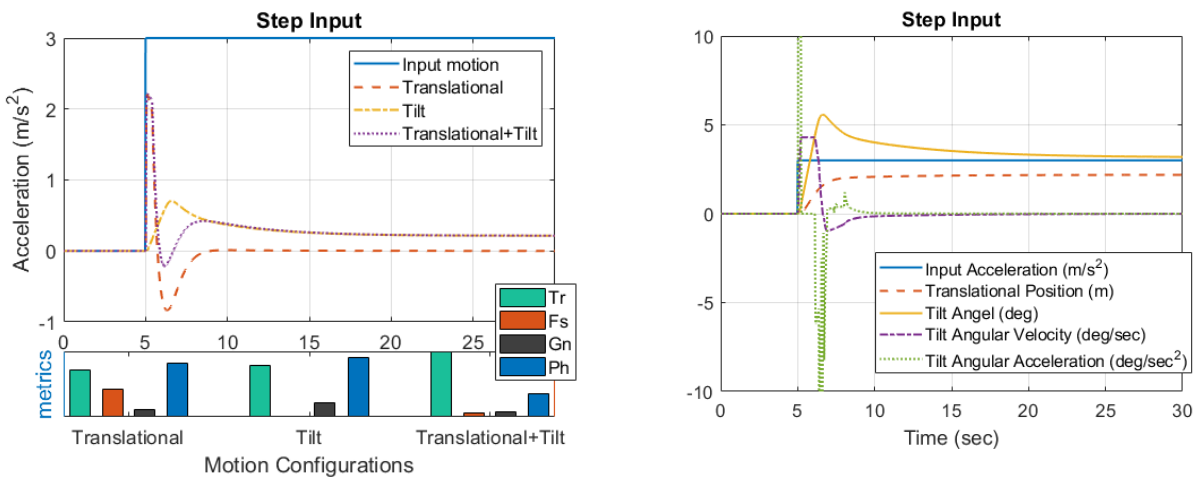
In the translational motions of the MP (e.g. sliding rail) in surge or sway directions, there are three weights on the plant output tracking variables i.e. acceleration tracking weight $w_{tr,a}$, velocity tracking weight $w_{tr,v}$ and position tracking weight $w_{tr,p}$ and a single weight on the control input $w_{u,tr}$. The acceleration is tracking the reference input perceived acceleration while the velocity and position are tracking zero reference input that helps washout of the MP to its neutral of constant input accelerations where the MP workspace constraints are met. The washout effect could be done by weighting the control input acceleration w_{ur} , however large weights on the control input cause a slow response of the controller. In the design of the MPC model used here, where there are constraints on the control input u then the weights do not have a significant effect, but in case of free constraints, the weights need to have a moderate value that keeps the controller to avoid large changes but also keeping it quick enough.

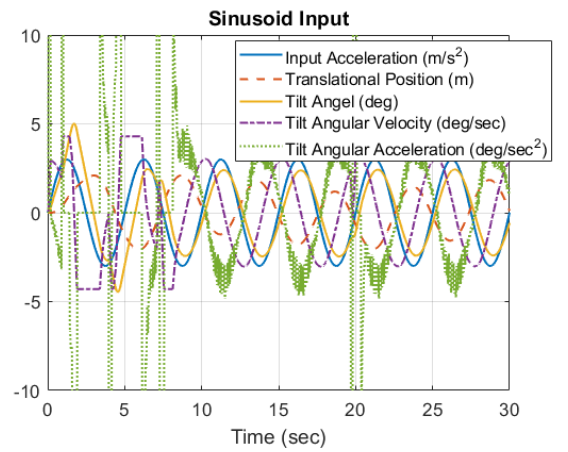
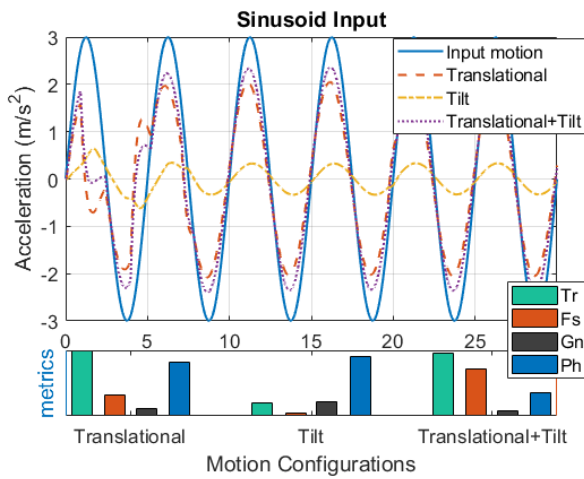
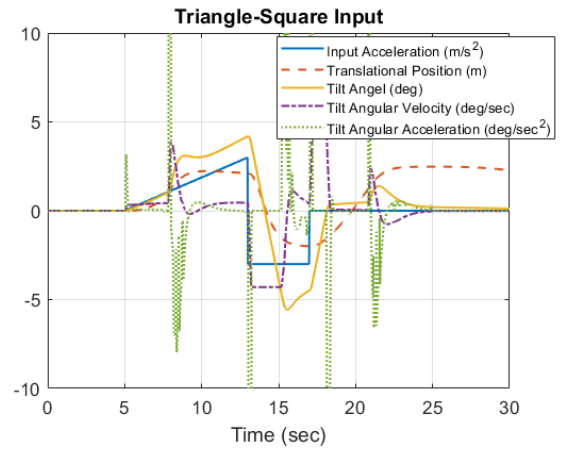
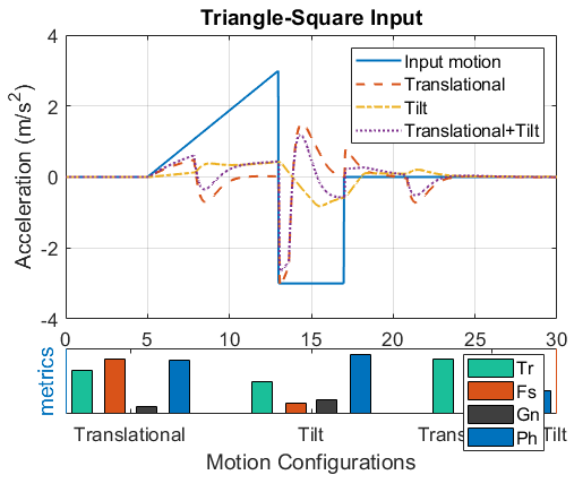
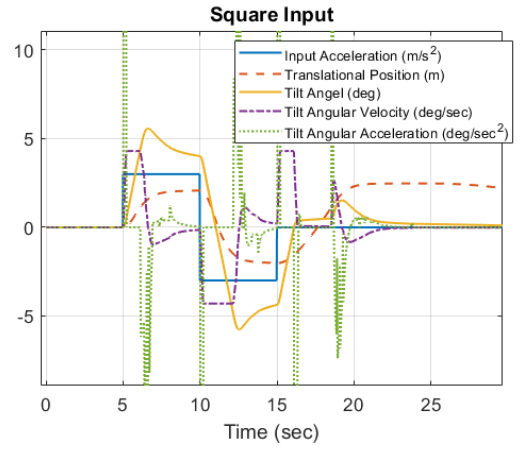
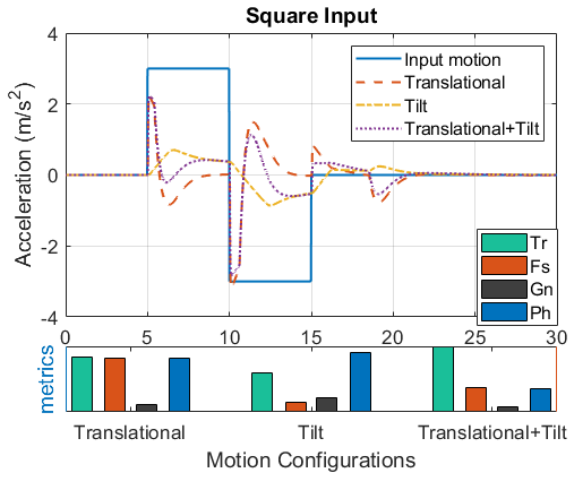
In the tilt motion, there are, two weights on the plant output tracking variables i.e. acceleration tracking weight $w_{tl,a}$, and position tracking weight $w_{tl,p}$ and a single weight on the control input $w_{u,tl}$. The acceleration is tracking the reference input

perceived acceleration while the position is tracking zero reference input that brings the MP to neutral. There is also a weight on the summation of the translational and tilting acceleration that has a significant role in tracking perceived input acceleration, and balances between the two.

Other important variables in the MPC algorithm are the prediction H_p and control horizon H_u that affect the generated motion profile remarkably. The larger values of both of the horizons lead to more optimal solutions at each time instance. However it also increases the computational efforts that might make it infeasible for real-time simulation, hence there is always a trade-off. There is another major issue in using the MPC algorithm as MCA, which is the reference input. The MPC model needs to have look-ahead information about the future of the reference input signal up to the prediction horizon. This information is often available in the MPC's original applications such as the chemical and process industry, where the changes of the reference input are steady and mostly known by the designers. During driving, the vehicle motion as the reference input changes quickly and many of the occasions it is unpredictable, that's even more complicated because it gets subjective since each driver has its own way of driving. The problem of precise look-ahead information arises from the fact that a large control and prediction horizon only lead to the optimal solution if the reference input is known up to the horizon otherwise it deteriorates the generated motion and smaller horizons are preferable.

Translational, tilt and total accelerations generated in the response of MPC algorithm to various input accelerations is shown using a single set of weights of $w_{tra} = 3$, $w_{trv} = 1.5$, $w_{trp} = 1$, $w_{tla} = 3$, $w_{tlp} = 1$, $w_{total} = 5$, and prediction $H_p = 1$ and control $H_u = 0.2$ seconds horizons are shown in Figure 7-17. The other model parameters are selected to have 1 m/s^2 or 5.84 deg of tilting, and the tilt angular velocity and accelerations below the 4.3 deg/sec and 23.5 deg/sec^2 , see Appendix D. The model sampling time is 50 Hz or 0.02 s.





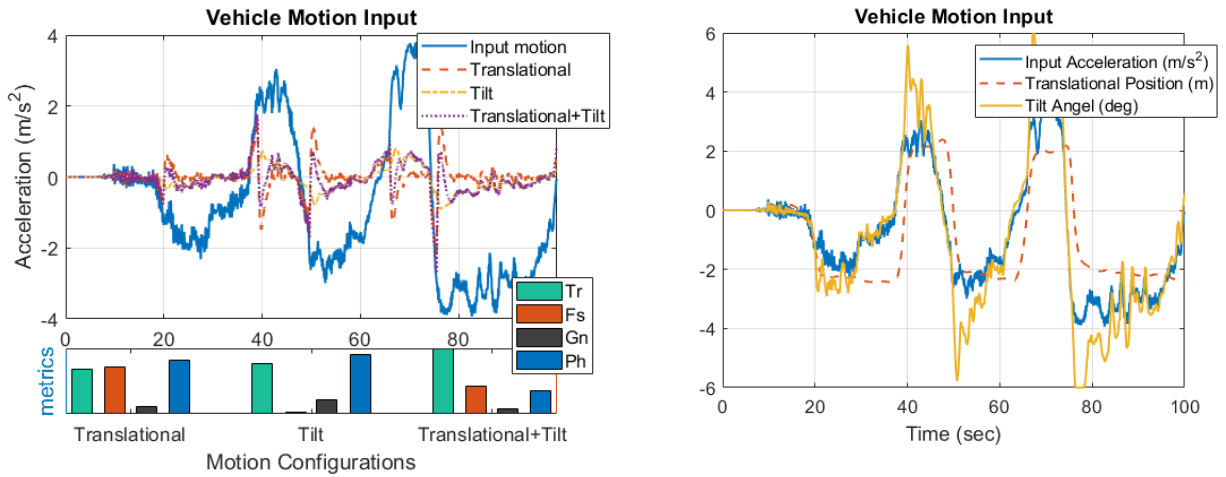


Figure 7-17. Acceleration and position response of the MPC model, to step, square, triangle-square, sinusoid and vehicle lateral acceleration inputs, fixed look-ahead reference input

Due to the nonlinear characteristics of the MPC algorithm, the calculation of exact frequency response of the model is not a straight forward task, therefore an estimation method is used to calculate the frequency response of the model and the measurement metrics. The frequency estimation considers the model's translational, tilting and total acceleration response to sinusoid input accelerations of various frequencies defined in the range of the frequency of interest, those have an amplitude value of 2 m/s^2 . It estimates the amplitude attenuation and phase shifting of output sinusoids compared to inputs and draws the frequency response. The Bode plot of the translational, tilting and total output acceleration using the same set of parameters used earlier is shown in Figure 7-18.

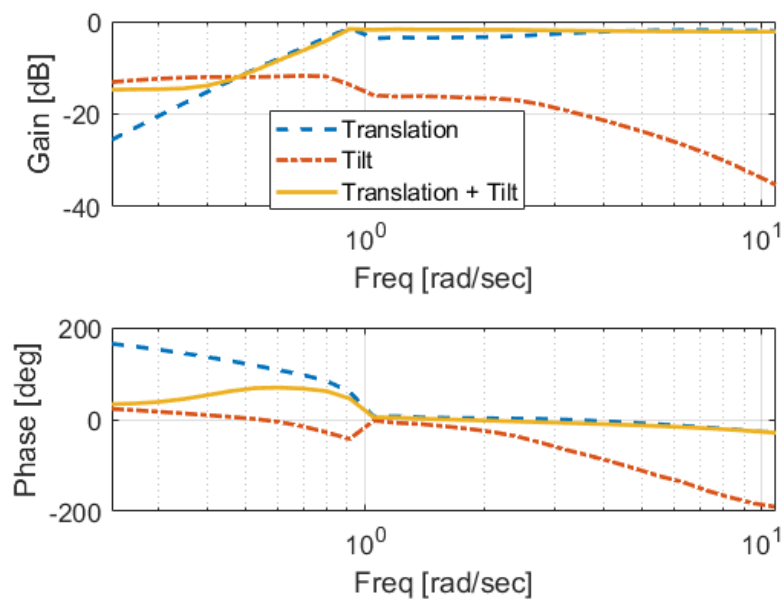


Figure 7-18. Bode frequency response of the MPC model

The other variables affecting the MPC response to vehicle motion is the prediction H_p and control H_u horizons, in addition to whether there is look-ahead information of the reference input available or it is assumed constant over the prediction horizon. The prediction and control horizons affect the optimality of the control input solution and it often needs to be selected depending on the stability of the plant model. The meaningful optimisation problem requires a well-posed condition where there is a similarity between the open and closed-loop response of the system, as opposed to ill-posed condition. Using the low prediction horizon usually leads to poor predictions and does not deal with the non-min phase, unstable and oscillatory open-loop dynamics, however as it is described later this is true only if there is look-ahead information of the reference input available.

In case of stable open-loop dynamics of the system and small control horizon, if the prediction horizon is small then emphasis of the control response is more on the transient response than the steady-state, and its considered to be ill-posed, while if the prediction horizon is large there is more emphasis on the steady-state response than transient and could be considered as well-posed. Therefore, the prediction horizon is better to be long enough beyond the open-loop steady-state settling time of the plant model, although this might be in the order of few seconds that cannot be achieved by the controller due to computational burden. This is true with the settling time of the otolith models employed here, thus a mediocre value for the prediction horizon need to be selected. For such systems, increasing the weight on the control input decreases the control activity and it requires a large control horizon to get to the steady-state response.

For the unstable open-loop dynamics, having large prediction and small control horizons results in divergent and meaningless predictions, and the same happens if the control horizon is larger than the prediction, hence for such systems both the control and prediction horizons need to be large. Therefore, it is best to start with the large prediction and control horizons and decrease them to get to the desired closed-loop response. For such systems, the weights on the control input need to be small and increasing the weight deteriorates the response.

To get a better understanding of the effect of prediction H_p and control H_u horizons, and the fixed or variable look-ahead reference inputs, the response of the MPC model to various input accelerations is shown in Figure 7-19 to Figure 7-22. The remainder of the model parameters are selected to have reasonable values of 1 m/s^2 or 5.84 deg of tilting, the tilt angular velocity and accelerations below the 4.3 deg/sec and 23.5 deg/sec^2 (see Appendix D), and the weight factors of $w_{tr_a} = 5$, $w_{tr_v} = 4$, $w_{tr_p} = 2$, $w_{tl_a} = 8$, $w_{total_a} = 10$, $w_{tl_p} = 2$. The model control sampling time is 50 Hz or 0.02 s, as a result, the horizons are multiplications of the

0.02 s e.g. $H_p = 100$ is a 2 s of the prediction horizon. After many trial and errors, it was best decided to keep the control input H_u to be 0.2 of the H_p in all settings.

The model response to step input acceleration is shown in Figure 7-19. the figures on the left show the translations, tilt and total acceleration that drivers perceive in the simulator while the look-ahead information is constant up to the prediction horizon. For the translational motion, in small horizons, there are the largest true and false accelerations where the false is greater than true cues. Increasing the horizons both of the true and false cues decrease, and true gets greater than false while having very large horizons deteriorates the response. The increase of horizons, slightly raises the gain and phase errors. A similar trend is observable for the total motion of true and false accelerations, while the gain error has fluctuated and phase is reduced, with the increase of horizons. For the tilt motion there is no significant change, where there is a slight increase in true cues and rise of phase error with the increase of horizons. The frequency analysis of other inputs described next figures is the same but repeated in the plots.

The figures on the right show where there is variable look-ahead information available, the first thing is that the controller starts generating motion in advance of initiation of the input acceleration, that is counted as false cues in the measurement metrics. For the translational motion having small horizons, there are large false cues compared to true cues, an increase of horizons causes a slight raise of true and significant reduction of false cues. A similar trend is observable for the total motion. For the tilt motion, there are no significant changes, where there is a slight increase in false cues with the increase of horizons. The frequency analysis for the variable look-ahead information is not straight forward and is omitted from figures. From the above the observations the best setting is the $H_p = 60$ and $H_u = 12$ for both fixed and variable reference inputs, where the true cue goes greater than the false cue and there is acceptable amount of phase and gain errors.

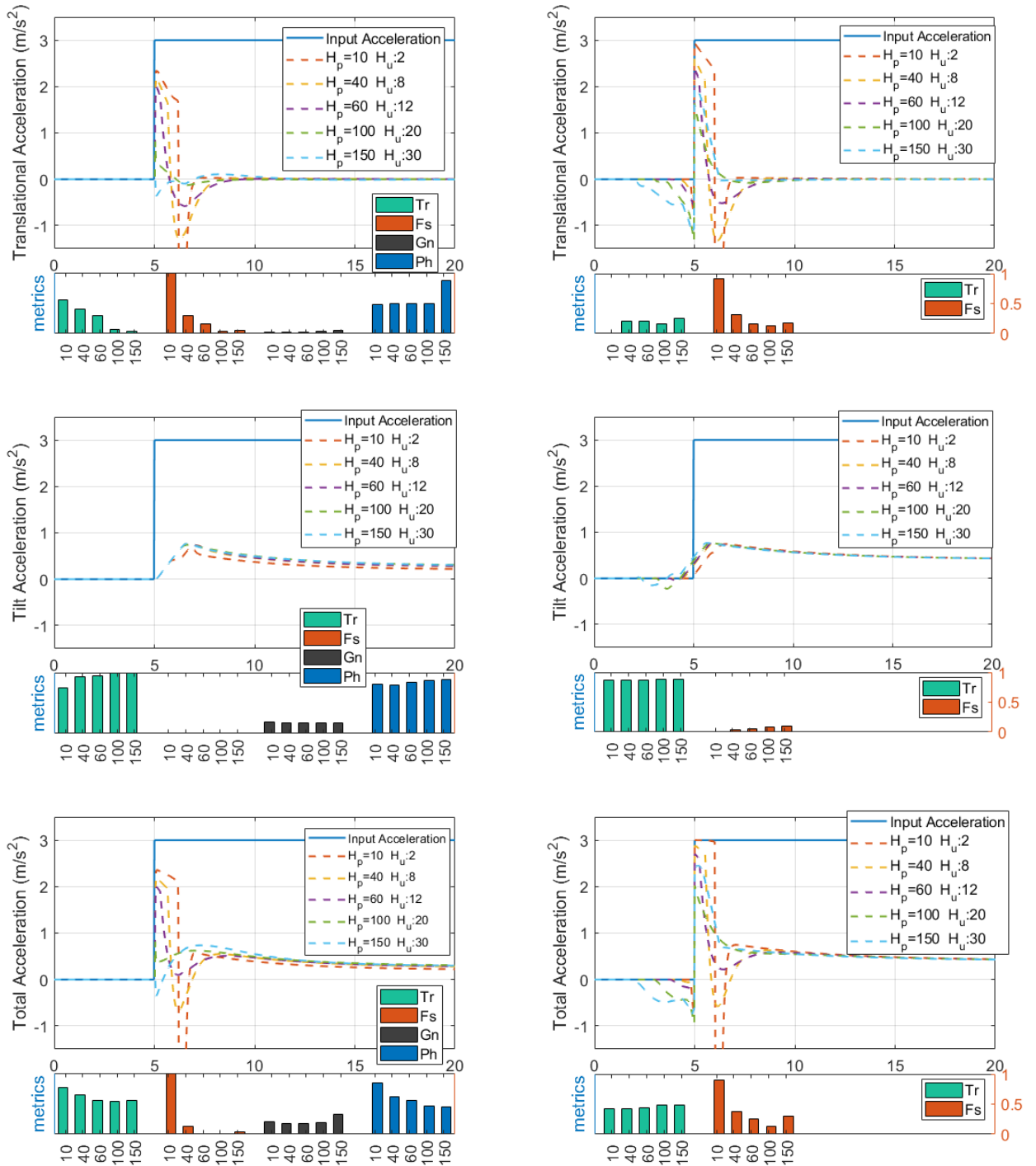


Figure 7-19. Time response of the MPC model to step input in various prediction H_p and control horizons H_u in both constant (left) and variable reference look-ahead inputs (right)

The model response to triangle-square input acceleration is shown in Figure 7-20. The figure on the left is constant look-ahead information. For the translational motion, in small horizons, the true and false accelerations are the largest where the false is greater than true cues. Increasing the horizons both of the true and false cues decrease and true gets greater than false, while having very large horizons it deteriorating the response. Similar trend is observable for the total motion. For the

tilt motion, there are no significant changes, where there is slight increase in true and false cues with the increase of horizons.

The figure on the right there is variable look-ahead information available. For the translational motion having small horizons, there are large false cues compared to true cues, as the horizons increase there is a slight rise of true and decrease of the false cues. A similar trend is observable for the total motion. For the tilt motion with the increase of horizons, there is a small improvement of true and reductions of false cues. From the above observations, the best setting is the $H_p = 60$ and $H_u = 12$ for the fixed, where the true cue goes greater than the false cue and there is acceptable amount of phase and gain errors. For the variable reference inputs also this is an acceptable setting since the improvements are minor compared to the computational burden it adds.

Similar response of the MPC model is observable to other square, sinusoid and vehicle motions inputs, where the varying extent of changes of the metrics is observable. Between the sinusoid (Figure 7-21) and vehicle motion (Figure 7-22) inputs with constant look-ahead, the large horizon worsens the translational motion to a larger extent in sinusoid compared to vehicle motion. It was the reason to reduce the horizons on the lateral motion cueing of the slalom task described in the low-friction experiment, see section 5.4.2. Moreover, comparing the MPC (Figure 7-21) and classic (Figure 7-3) models response to a sinusoid input, it is observable of better performance of classic compared to the MPC; indicative of classic to be more appropriate for more evasive manoeuvres such as slalom. Need to be mention again that the weights and filter parameters have also had a major effect on the response of the MPC and classic algorithms respectively, which could lead to further improvements.

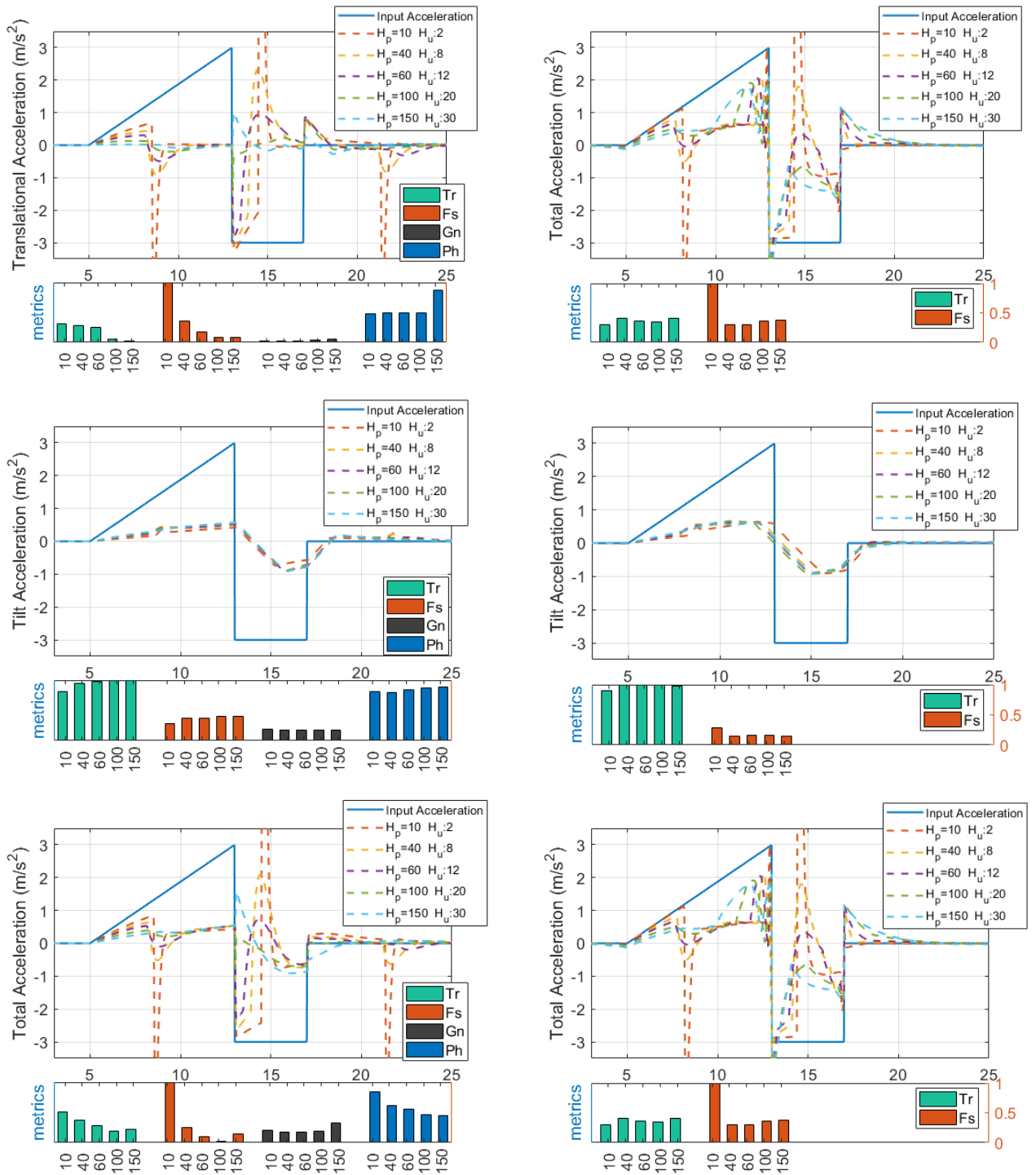


Figure 7-20. Time response of the MPC model to triangle-square input in various prediction H_p and control horizons H_u in both constant (left) and variable reference look-ahead inputs (right)

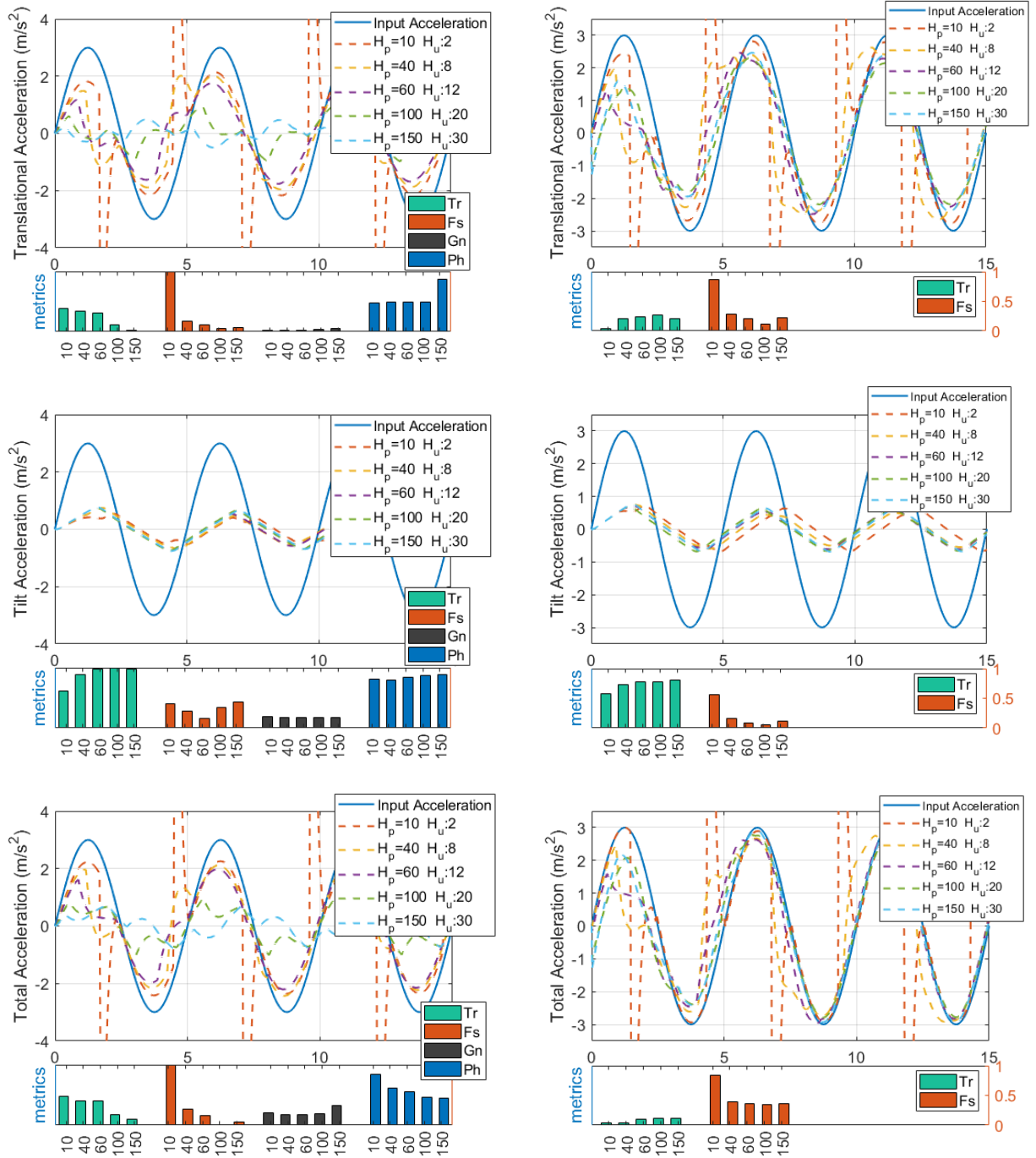


Figure 7-21. Time response of the MPC model to sinusoid input in various prediction H_p and control horizons H_u in both constant (left) and variable reference look-ahead inputs (right)

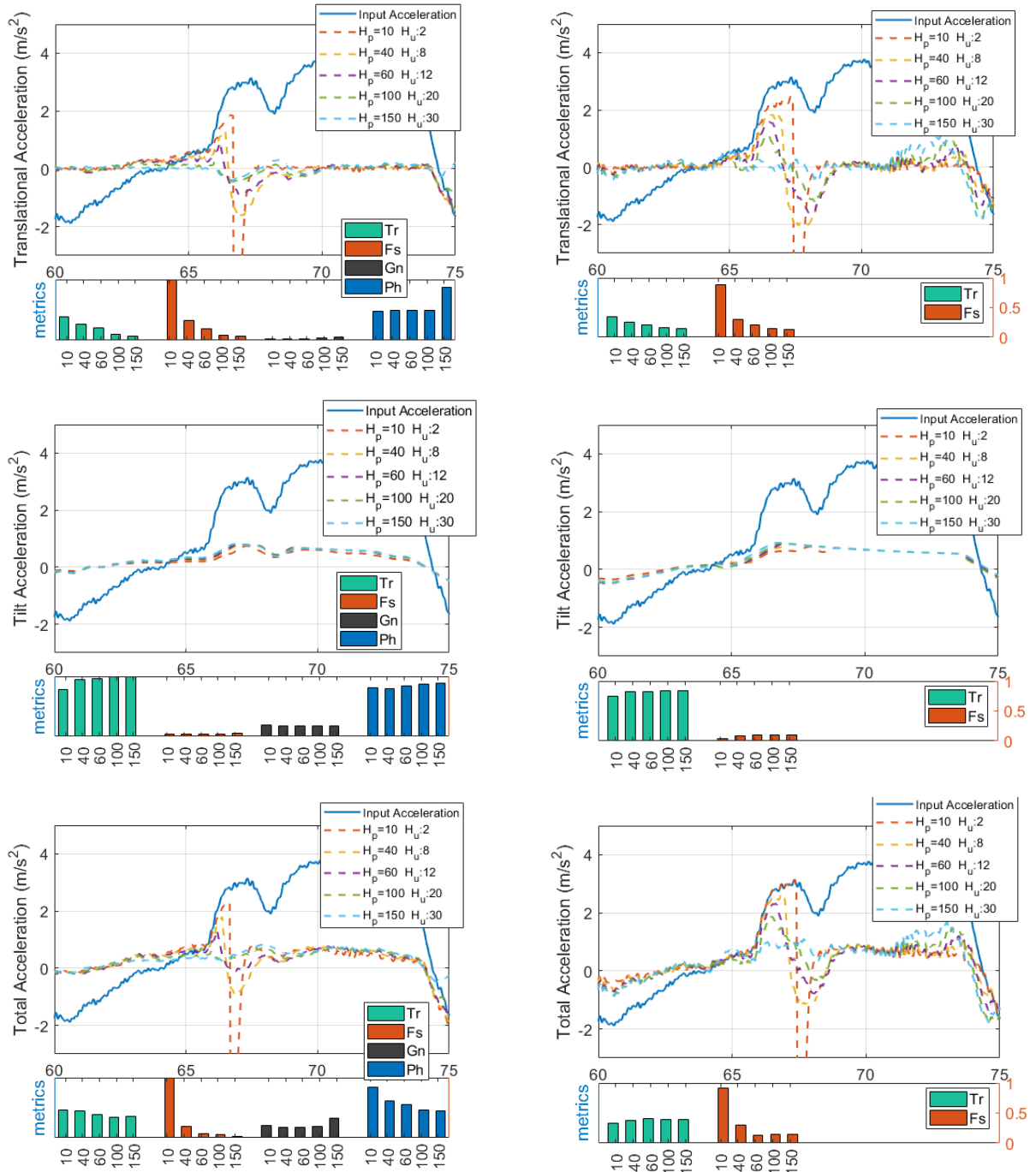


Figure 7-22. Time response of the MPC model to vehicle lateral acceleration input in various prediction H_p and control horizons H_u in both constant (left) and variable reference look-ahead inputs (right)

In summary, it is concluded that, for the translational and total motion with the constant look-ahead information, increasing the horizons up to a level improves the response that balances between the true and false cues and reduces the phase errors, but having a very large horizon deteriorates the response significantly by generating very small true cues. In the tilt motion, there is always a slight increase for both true and false cues, with the increase of horizons, all shows that when the constant look-ahead information is available a very large prediction and control

horizons need to be avoided. For the translational and total motion with the variable look-ahead information, increasing the horizons improves the response in general. However, up to a level the improvements are more significant, which slightly improves with the further increase of horizons, bearing in mind the cost of computations. In the tilt motion, there is always a slight increase for the of true and decrease of the false cues with the increase of horizons, that shows improvement for tilt motion.

The time and frequency response of the MPC model for a set of parameters were presented, and the proposed measurement metrics calculated. In a broader perspective, it is essential to find out how the variations of the parameters could affect the metrics and to decide on the best set of parameters as an optimal solution(s). Therefore, in the next few sections, the effect of variation of the model parameters on the measurement metrics are reviewed for the translational, tilting and total motions of the simulator.

7.3.1 Translational motion

The translational motion generated by the MPC model is affected by the three weights of perceived acceleration tracking $w_{tr,a}$, velocity tracking $w_{tr,v}$ and position tracking $w_{tr,p}$ and a single weight on the control input $w_{u,tr}$. In the first step, the effect of weights are reviewed using fixed prediction $H_p = 0.6$ and control horizon $H_u = 0.1$ seconds. The weight of the control input $w_{u,tr} = 1$ found to be an appropriate value that keeps the control signal not reaching too high values and not slowing down the control response.

The time response to the input vehicle lateral acceleration in the LHT manoeuvre is shown in Figure 7-23 top, and the settings of low true and high false cues are cropped out in the bottom figures. It is observable that increasing the $w_{tr,a}$ raises the true and false cues, while increasing the $w_{tr,p}$ and $w_{tr,v}$ both reduce the true and false cues. Moreover, at a constant $w_{tr,a}$ there is a trade-off between the $w_{tr,p}$ and $w_{tr,v}$, where in general having the $w_{tr,v}$ greater than $w_{tr,p}$ results in more true and less false cues. In the cropped out settings of the true cues, there seems to be a straight line describing the relation between the $w_{tr,a}$ with $w_{tr,v}$ and $w_{tr,p}$ having two different slopes, representing the fact that the $w_{tr,a}$ needs to be higher than both $w_{tr,v}$ and $w_{tr,p}$ to have high amount of true cues, although it increases the false cues as well.

The best parameters settings are where the true acceleration is maximum and the false acceleration is minimum, from the plots a setting around the $w_{tr,a} = 8$, $w_{tr,v} = 6$ and $w_{tr,p} = 2$ generates a good amount of true cues while it keeps false cues as little as possible. In the MPC model, the MP envelope is always respected, hence in

these figures the excursions are always below a maximum excursion limit of ± 2.5 meters (UoLDS workspace limit). However, these plots might slightly change to other vehicle acceleration inputs.

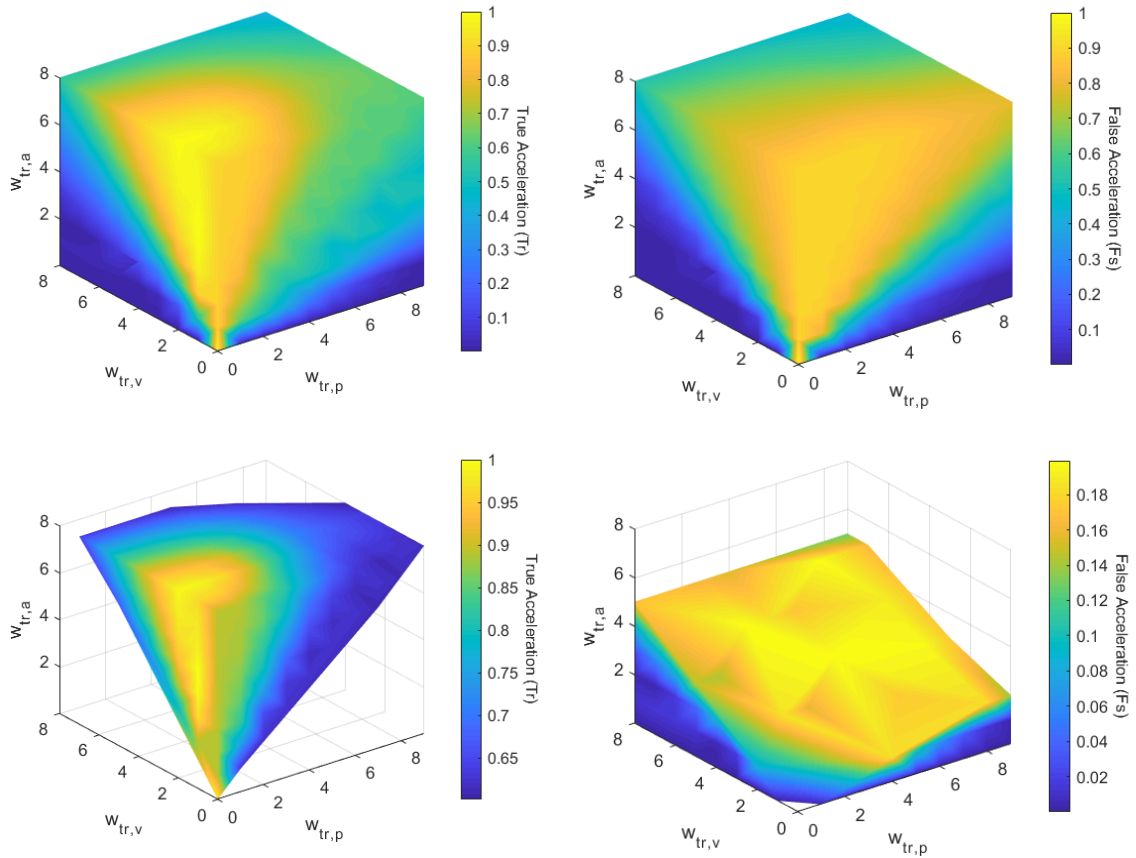


Figure 7-23. The time domain true and false output accelerations in a range of weight factors (top), cropped out settings $Tr > 0.6$ and $Fs < 0.2$ (bottom), MPC translational motion

The frequency response of the model to different parameter settings are measured by the gain Gn_{err} and phase Ph_{err} errors, see Figure 7-24 top. It is observable that increasing the $w_{tr,a}$ reduces the gain error, while increasing the $w_{tr,p}$ and $w_{tr,v}$ could raise the gain and reduce the phase errors. Depending on the $w_{tr,p}$ and $w_{tr,v}$ values, the phase error shows raise with an increase of $w_{tr,a}$, and there seems to be a border of $w_{tr,v} \geq w_{tr,a}$ where the phase error is minimum. In the cropped out settings (middle figures) the minimum gain error is where the $w_{tr,p}$ is small and the $w_{tr,v}$, $w_{tr,a}$ are relatively larger. At a particular $w_{tr,a}$, the $w_{tr,v}$ needs to have higher value than the $w_{tr,p}$ to achieve the minimum phase error. The intersection of the phase and gain error volumes is shown in the bottom figure suggests at a setting around the $w_{tr,a} = 8$, $w_{tr,v} = 6$ and $w_{tr,p} = 2$ the phase and gain errors are at a reasonable value.

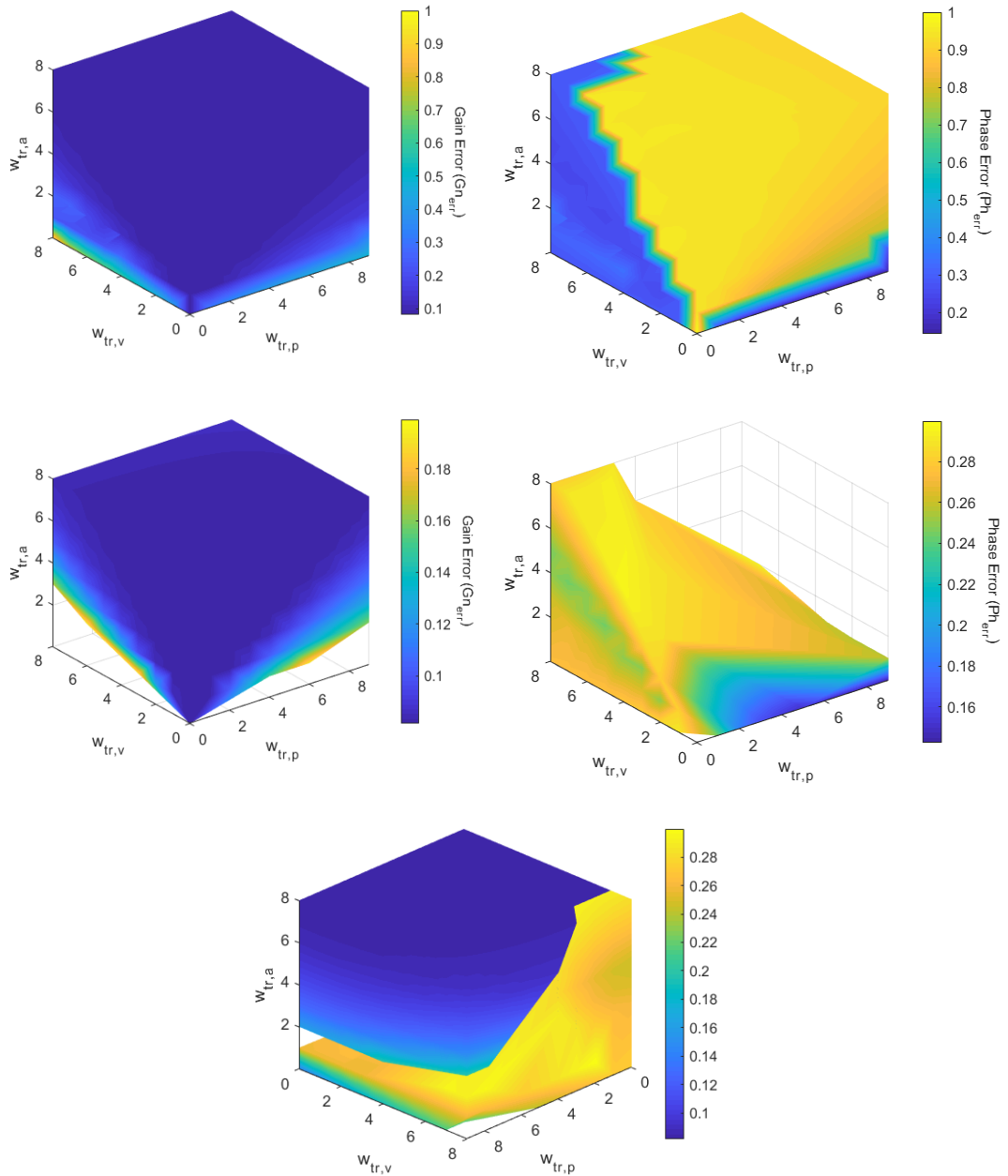


Figure 7-24. The frequency domain gain, phase errors in a range of weight factors (top), cropped out settings $G_n < 0.2$ and $Ph < 0.3$ (middle), and both in the same plot (bottom), MPC translational motion

7.3.2 Tilt motion

The tilt motion generated by the MPC model is affected by the two weights of perceived acceleration tracking $w_{tl,a}$, and position tracking $w_{tr,p}$ and a single weight on the control input $w_{u,tl}$. Same as the classic MCA the acceleration generated by the tilting depends on three variables of maximum tilt angle θ_{max} which in the MPC model is defined by a constraint on the plant output tilt degree, tilt angular velocity $\dot{\theta}_{max}$, and tilt angular acceleration $\ddot{\theta}_{max}$ both are defined by the constraints on the control input and its rate of changes. The tilt parameters are set to be same as

what was presented in the classic MCA, $\theta_{max} = 5.84 \text{ deg}$ or 1 m/s^2 , the tilt angular velocity $\dot{\theta}_{max} = 3.22 \text{ deg/sec}$ and accelerations $\ddot{\theta}_{max} = 13.14 \text{ deg/sec}^2$, see Appendix D.

The effect of weights on the output variables are reviewed using fixed prediction $H_p = 0.6$ and control horizon $H_u = 0.1$ seconds. The weight on the control input $w_{u,tr} = 1$ found to be an appropriate value. The time response to the input vehicle lateral acceleration in the LHT manoeuvre is shown in Figure 7-25. It is observable that the true and false acceleration surfaces are separated and increasing the $w_{tl,a}$ raises the true cues and slightly the false cues when the $w_{tl,p} \neq 0$, while decreasing the $w_{tl,p}$ raises the true and false cues. This indicates the $w_{tl,a}$ needs to be bigger than the $w_{tl,p}$, while the $w_{tl,p} \neq 0$ (this is required to tilting back the MP to a neutral position). In the MPC model, the tilt angular velocity and acceleration thresholds are always respected, hence in these figures, those are always below the maximum values.

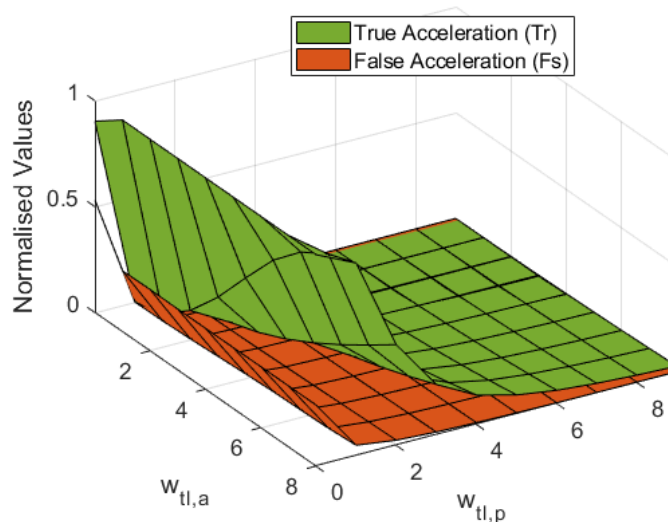


Figure 7-25. The time domain true and false output tilt acceleration felt through tilting in a range of weight factors, MPC tit motion

The frequency response of the model to different parameter settings are measured by the gain Gn_{err} and phase Ph_{err} errors, see Figure 7-26. It is observable that increasing the $w_{tl,a}$ reduces the gain and raise the phase errors, while increasing the $w_{tl,p}$ raises the gain and reduces phase errors. The intersection borderline of the two surfaces (right figure) suggests that the weight values of $w_{tl,a}$ and $w_{tl,p}$ where $w_{tl,a}$ being slightly bigger than $w_{tl,p}$ results to have minimum phase and gain errors.

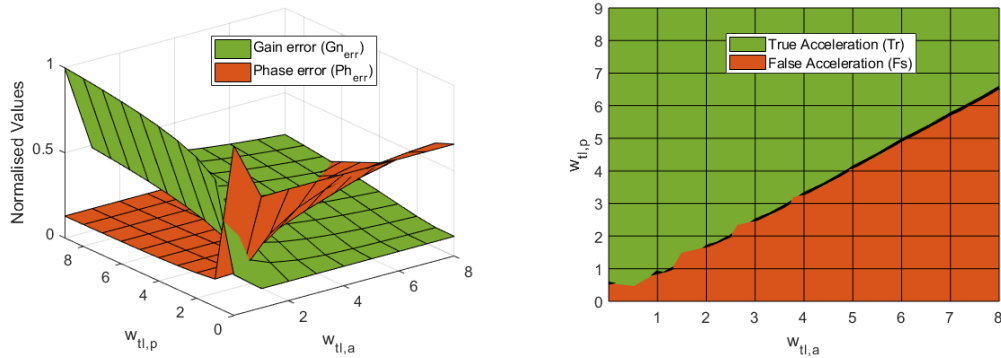


Figure 7-26. The frequency domain gain, phase errors in a range of weight factors, MPC tit motion

7.3.3 Translational and tilt motions

In the previous sections, the effect of variation of the weight factors on the time and frequency response of the translational and tilt motions were presented. For both the translational and tilt motions the best set of parameters were introduced to minimise the errors. In this section, the same time and frequency response of the combination of translational and tilt are reviewed. For the tilting motion, a single set of constraints are chosen to keep the tilt angular velocity and accelerations below the 3.22 deg/sec and 13.14 deg/sec^2 respectively, similar to what was used in tuning of the classic, see Appendix D. The weights on the control input variables are chosen to be $w_{tr,u} = 1$, $w_{tl,u} = 1$. The varying parameters, in this case, include two examinations of a) reviewing the effects of changing the weights on the acceleration tracking variables $w_{tl,a}$, $w_{tr,a}$ and $w_{total,a}$ while keeping the other $w_{tl,p} = 2$, $w_{tr,v} = 4$, $w_{tr,p} = 2$ constant values, selected based on the appropriate values found in the previous sections b) reviewing the effect of changing the weights on the translational velocity and position tracking variables $w_{tr,v}$, $w_{tr,p}$ and total acceleration tracking $w_{total,a}$ while keeping the other acceleration tracking variables $w_{tr,a} = 0$, $w_{tl,a} = 0$ to let the controller decide between the tilt and translational motions, and the tilt position tracking $w_{tl,p} = 2$ constant value.

The time response to the input vehicle lateral acceleration in the LHT manoeuvre for the first scenario is shown in Figure 7-27 top and the settings of low true and high false cues are cropped out in the bottom figures. Increasing all the three weights raises both of the true and false cues, where the $w_{total,a}$ and $w_{tl,a}$ have more significant effects on increasing the true cues, and $w_{total,a}$ and $w_{tr,a}$ on increasing the false cues. In the cropped out settings, the maximum true cues are at the highest weight $w_{total,a} = 8$ in a range of $w_{tr,a}$ being around 4 and the $w_{tl,a} = 8$. That indicates having a large value for the $w_{total,a}$ and $w_{tl,a}$, a nearly half as large value for the $w_{tr,a}$ generates most of the true accelerations. The maximum

false cues among the cropped out settings is at the $w_{total,a} = 2$, $w_{tr,a} = 3$ and $w_{tl,a} = 4$ while the tilt acceleration weight does not have a major effect. In the bottom figure, both of the cropped true and false cues are shown where that overlap shows an area of more optimal settings near the $w_{total,a} = 5$, $w_{tr,a} = 3$, $w_{tl,a} = 8$.

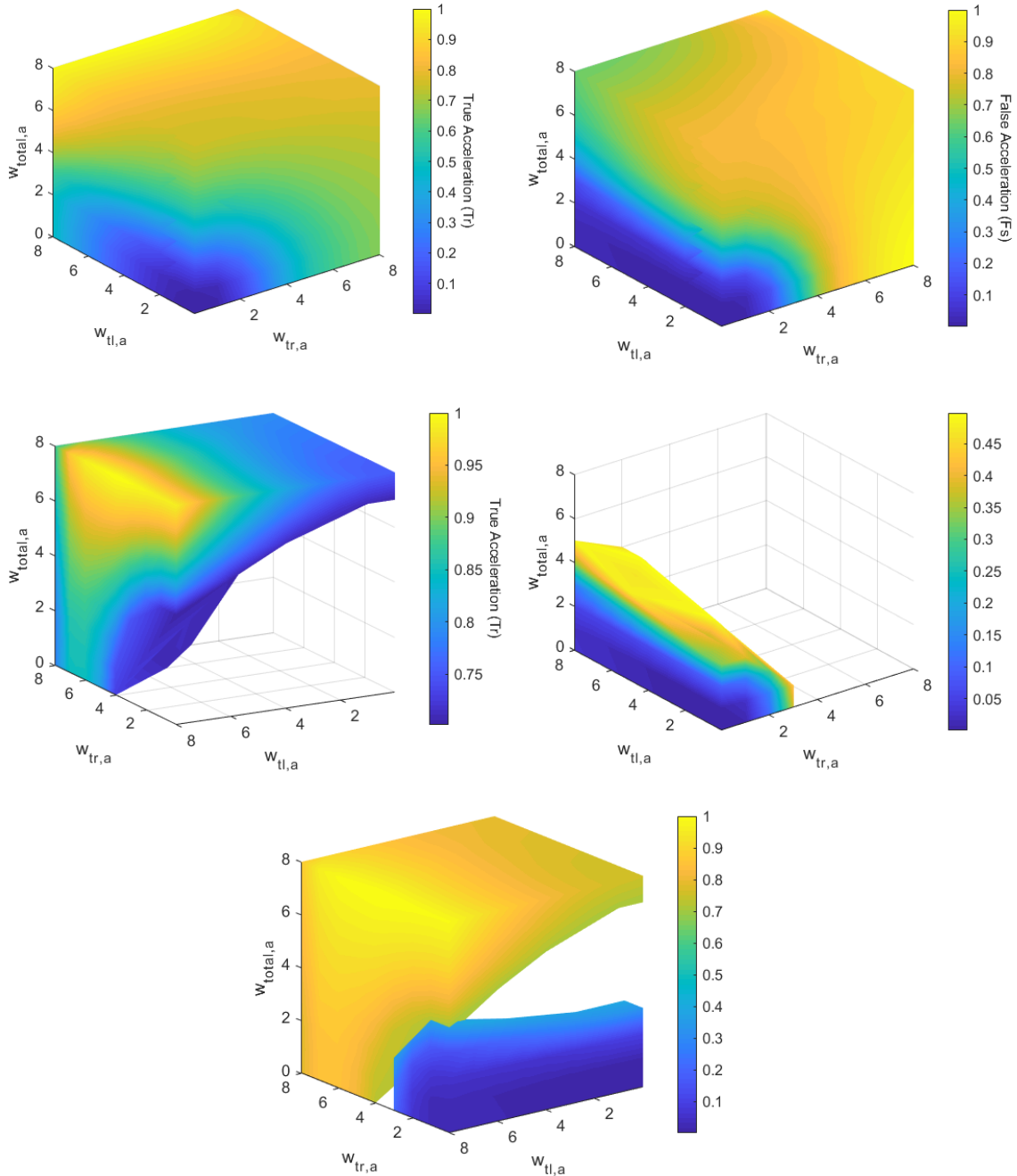


Figure 7-27. The time domain true and false output accelerations in a range of weight factors (top), cropped out settings $Tr > 0.7$ and $Fs < 0.5$ (middle) and both in the same plot (bottom), MPC translational and tilt motion

The frequency response of the model to different parameter settings are measured by the gain Gn_{err} and phase Ph_{err} errors, see Figure 7-28 top. Increasing the

$w_{total,a}$ and $w_{tl,a}$ have a major impact on reducing the gain and phase errors, while increasing the $w_{tr,a}$ reduces the gain and phase errors only when the other weights are small. In the cropped out settings (bottom figure) the minimum gain error is at the highest weight for the $w_{total,a} = 8$ and the $w_{tl,a} = 8$, being similar in a range of $w_{tr,a}$. That indicates having a large value for the total and tilt accelerations generates the least gain error. Increasing $w_{tl,a}$ have a significant effect on reducing the phase errors especially in larger $w_{total,a}$. From the cropped phase figure there are some other settings near the $w_{total,a} = w_{tl,a} = 1$ and the $w_{tr,a} = 0$ that have the lowest phase errors but in this area the gain error is no minimum. From these observations, it is concluded that having large weights on the $w_{total,a}$ and $w_{tl,a}$, and small to medium weight on the $w_{tr,a}$ minimises the gain error and results in acceptable phase error.

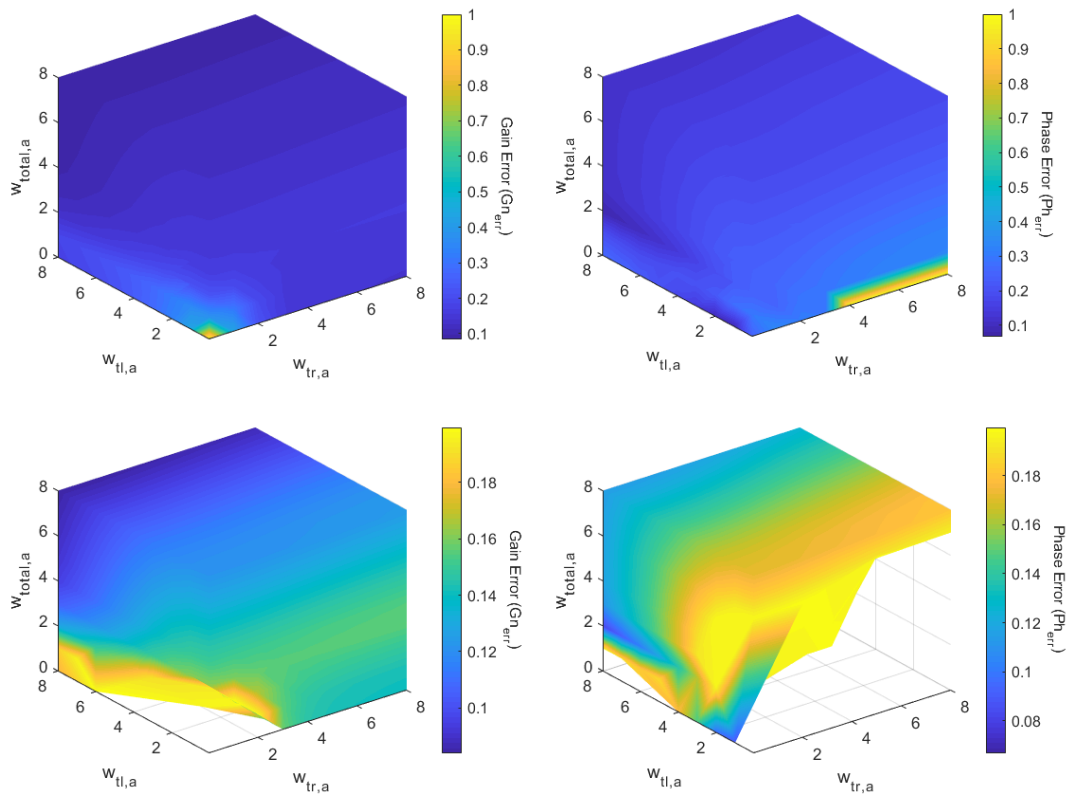


Figure 7-28. The frequency domain gain, phase errors in a range wright factors (top), cropped out settings $Gn < 0.2$ and $Ph < 0.2$ (middle), and both in same plot (bottom), MPC translational and tilt motion

The time response to the input vehicle lateral acceleration for the second scenario is shown in Figure 7-29 top and the settings of low true and high false cues are cropped out in the bottom figures, that is similar to what is described in the only translational motion section. Increasing the $w_{total,a}$ and decreasing the $w_{tr,v}$ and $w_{tr,p}$ weights raises the true and false cues. In a constant $w_{total,a}$ increase of the $w_{tr,p}$ have more significant effects on increasing the false cues than $w_{tr,v}$,

where the opposite is true for the true cues i.e. increase of the $w_{tr,v}$ have more significant effects on increasing the true cues than $w_{tr,p}$. In the cropped out settings, the maximum true cues are at the highest with weight $w_{total,a} = 8$ and $w_{tr,a} = w_{tr,v} = 0$ however this setting results in an oscillatory response of the MPC model and there is no washout to the neutral position of MP. There seems to be a straight line describing the relation between the $w_{total,a}$ with $w_{tr,v}$ and $w_{tr,p}$ having two different slopes, representing the fact that the $w_{total,a}$ needs to be higher than both $w_{tr,v}$ and $w_{tr,p}$ to have a higher amount of true cues. From both of the plots a setting around the $w_{total,a} = 8$, $w_{tr,v} = 6$ and $w_{tr,p} = 2$, generates a good amount of true cues while it keeps the false cues as little as possible.

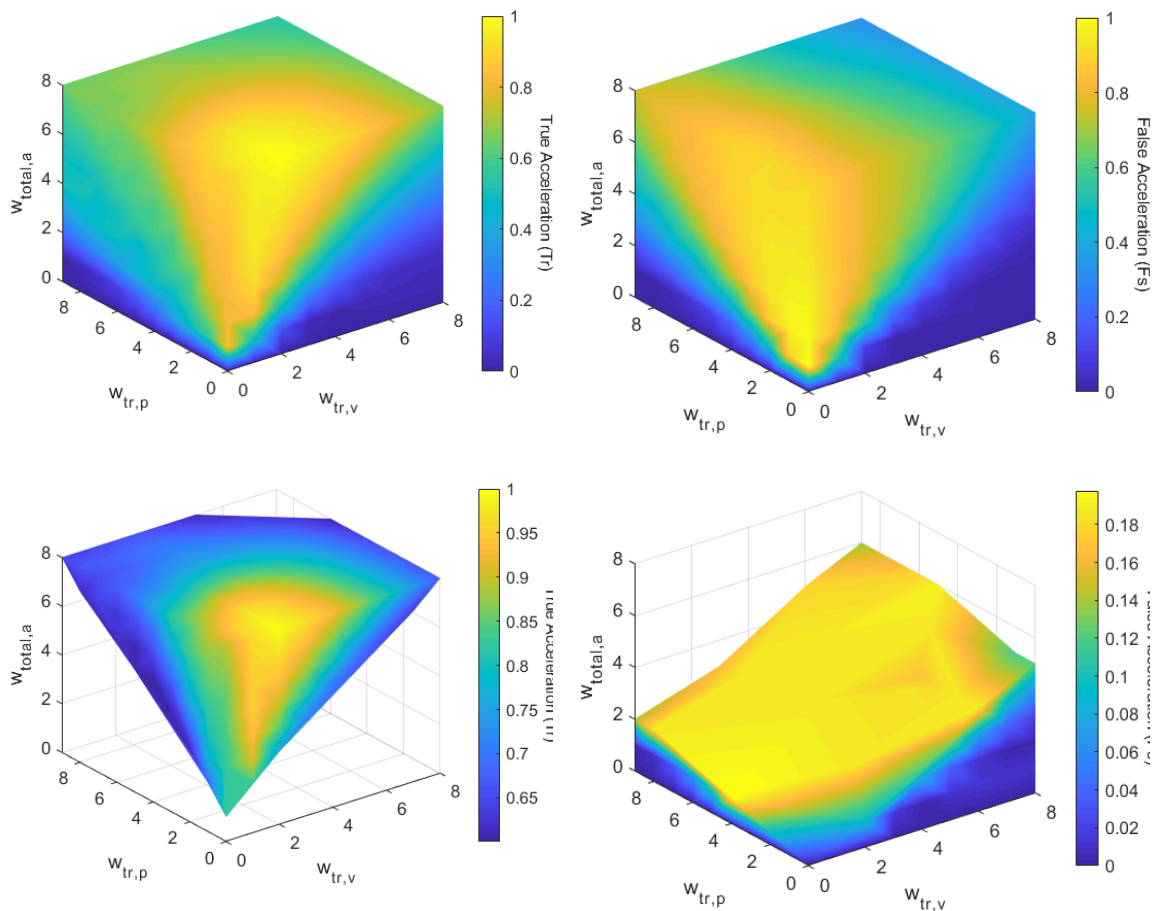


Figure 7-29. The time domain true and false output accelerations in a range of weight factors (top), cropped out settings $Tr > 0.6$ and $Fs < 0.2$ (bottom), MPC translational and tilt motion

The frequency response of the model to different parameter settings are measured by the gain Gn_{err} and phase Ph_{err} errors, see Figure 7-30 top. It is observable that increasing the $w_{total,a}$ reduces the gain error, while increasing the $w_{tr,p}$ and $w_{tr,v}$ raises the gain error. Depending on the $w_{tr,p}$ and $w_{tr,v}$ values, the phase error shows raise with the increase of the $w_{total,a}$, and decreases and fluctuates with the increase of $w_{tr,v}$, and increases with the increase of $w_{tr,p}$. In the cropped out

settings (bottom figures) having both $w_{total,a}$ and $w_{tr,p}$ large and $w_{tr,v}$ small values results in the worst phase error. Where the $w_{tr,p}$ is small (below 4) the $w_{total,a}$ could have the largest value together with medium $w_{tr,v}$. The area with both of gain errors to be minimum at expense of slightly more phase error seems to be around $w_{total,a} = 8$, $w_{tr,v} = 8$ and $w_{tr,p} = 1$. Moreover, a setting of $w_{total,a} = 4.5$, $w_{tr,v} = 2$ and $w_{tr,p} = 1$ minimises both of the gain and phase errors to an acceptable level. In total having a large value for the $w_{total,a}$, medium value for the $w_{tr,v}$ and small value for the $w_{tr,p}$ is an appropriate choice for this scenario of tuning.

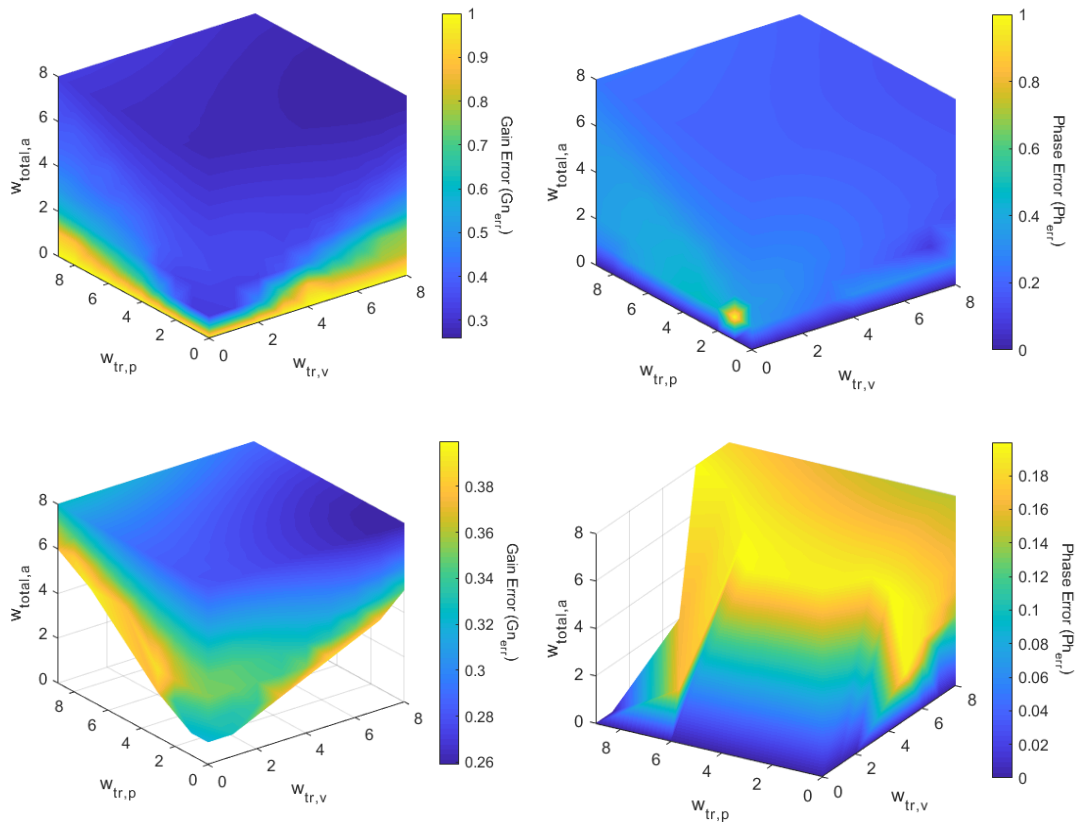


Figure 7-30. The frequency domain gain, phase errors in a range wright factors (top), cropped out settings with $Gn < 0.4$ and $Ph < 0.2$ (middle), and both in the same plot (bottom), MPC translational and tilt motion

7.4 Discussion and conclusions

In this chapter with the aim of a better understanding about the effect of MCA parameters on motion cueing, the classic and MPC models' time and frequency domain responses were analysed to the variations of their parameters. Using the measurement metrics as tools of comparison, it has been tried to figuratively address the effect of the parameters on the motion cues that in fact are the commands to the simulator motion platform.

The translational, tilt and total motions were considered separately to find out the optimal parameter settings that balance between the measurement metrics. The separate analysis of translational and tilt was to provide general guidelines for tuning the MCAs, in case each is used independently for a simulation. The analysis merely looked at the input/output of the MCA response to find the optimal parameters. However, it is possible to further optimise the parameters by including vestibular perception models and thresholds in the analysis of the translational and tilt motions.

For both classic and MPC algorithms, in the first step, the time and frequency response of models with a single set of parameters were presented, and the proposed measurement metrics were calculated to capture the effect of motion inputs such as step, square, triangle-square and sinusoid. Moreover, the choice of an optimal setting in time and frequency domain depends on the required motion platform excursions to a vehicle input acceleration. The maximum MP excursion ± 2.5 metre was included as another variable to select the best range of parameters in the classic algorithm.

In the next step, the variation to the MCA parameters was reviewed, where the lateral motion of the vehicle during a large motion demanding manoeuvre (LHT) including many curves and straight lines obtained from the experiment described in Chapter 5 was used. It is possible to use the same approach of tuning for the motion of the vehicle in more restricted manoeuvres such as double lane change and slalom, as well as longitudinal motion of the vehicle in manoeuvres such as accelerating, braking and emergency braking. This might slightly change the range of the optimal parameters.

In MPC it was concluded that, for the translational and total motion with the constant look-ahead information, increasing the horizons up to a level improves the response that balances between the true and false cues and reduces the phase errors, but having a very large horizon deteriorates the response significantly by generating very small true cues. In the tilt motion, there was always a slight increase for both true and false cues with the increase of horizons, all shows that when the constant look-ahead information is available a very large prediction and control horizons need to be avoided.

For the translational and tilt motion with the variable look-ahead information, increasing the horizons improved the response in general. However, up to a level improvement is more significant, which slightly improves with the further increase of horizons, bearing in mind the addition to the cost of computations. In the tilt motion,

there was always a slight increase for the of true and decrease of the false cues with the increase of horizons, that shows improvement for tilt motion.

7.4.1 Classic parameters

For the translational motion, the time domain analysis of the first order high-pass filter showed that a small scale-factor of $k = 0.07$ and cut-off frequency of $\omega_{hp1} = 2.1 \text{ rad/s}$ was an optimal setting to maximise true against false cues. In the frequency domain, to keep the gain and phase errors to a minimum, a small scale-factor of $k_{hp} = 0.02$ and cut-off frequency of $\omega_{hp} = 0.7 \text{ rad/s}$ was found to be an optimal setting.

The time domain analysis of the second order high-pass filter showed that a small scale-factor of $k = 0.15$ and cut-off frequency of $\omega_{hp2} = 0.42 \text{ rad/s}$ was needed to maximise true against false cues. In the frequency domain to keep the gain and phase errors to a minimum, a very small scale-factor of $k_{hp} = 0.037$ and cut-off frequency of $\omega_{hp} = 0.21 \text{ rad/s}$ was found to be an optimal setting.

The frequency domain analysis of the third order high-pass filter showed that a scale-factor of $k < 0.2$, and small cut-off frequency of $\omega_{hp1} < 0.5 \text{ rad/s}$ in a range of ω_{hp2} minimises both of the gain and phase errors.

The small scale-factor of the high-pass filters obtained in both time and frequency analysis allows the selection of lower cut-off frequencies that decrease the phase error. Hence, a wider frequency range of vehicle motions could be represented to the drivers, although the small scale-factor decreases the amplitude of the motion. This needs further experimentation to find out if the drivers prefer the smaller scale-factors, or they may find the larger scale-factor more realistic.

The second order low-pass tilt filter parameters are often limited to a single set of parameters that meet the requirement of a desired angular velocity and acceleration. Thus, not much flexibility is available in compromising between the minimum phase and gain errors.

The response of the combination of the third order high-pass filter with varying parameters and the second order low-pass filter with fixed parameters was reviewed. The low-pass filter parameters of $\zeta = 1$ and $\omega_{lp2} = 1.5$ keeps the tilt angular velocity and accelerations below the 3.22 deg/sec and 13.14 deg/sec^2 . In the time response, settings with a scale-factor of $k_{hp} < 0.2$ and cut-off frequencies of $\omega_{hp1} < 0.4$, $\omega_{hp2} < 0.3$ had the optimal true and false accelerations. The frequency response showed that a scale-factor of $k = 0.36 - 0.61$, $\omega_{hp1} = 1.1 - 1.85$, $\omega_{hp2} = 0.2 - 0.5 \text{ rad/s}$ minimises both of the gain and phase errors respectively and also respects the MP constraints. Overall it was observable that using large ω_{hp1} and smaller ω_{hp2} results in lower gain and phase errors.

7.4.2 MPC parameters

In the translational motion, the time domain analysis of the weights on acceleration $w_{tr,a}$, velocity $w_{tr,v}$ and position $w_{tr,p}$ output variables showed that in general having the $w_{tr,v}$ greater than $w_{tr,p}$ results in more true and less false cues. In the frequency domain to keep the gain and phase errors to a minimum, the $w_{tr,p}$ needs to be small and the $w_{tr,v}$, $w_{tr,a}$ relatively larger. A set of parameters of $w_{tr,a} = 8$, $w_{tr,v} = 6$ and $w_{tr,p} = 2$ found to maximise the true cues while it kept the false cues as little as possible, in this setting the phase and gain errors were at a reasonable value.

The tilt motion response is affected by the two weights on the perceived acceleration tracking $w_{tl,a}$, and position tracking $w_{tr,p}$. The output tilt degree, angular velocity and acceleration, control and prediction horizon were fixed and defined by the constraints. The review of the effects of weights in time and frequency domain showed the $w_{tl,a}$ needs to be bigger than the $w_{tl,p}$, to have maximum true cues compared to false, and to have minimum gain and phase errors.

The response of the combination of translational and tilt motions with fixed tilt angular velocity and accelerations below the 3.22 deg/sec and 13.14 deg/sec^2 , was reviewed. The varying parameters, in this case, included two scenario examinations

a) reviewing the effects of changing the weights on the acceleration tracking variables $w_{tl,a}$, $w_{tr,a}$ and $w_{total,a}$ while keeping the other velocity and position weights $w_{tl,p} = 2$, $w_{tr,v} = 4$, $w_{tr,p} = 2$ constant.

The time response of the model showed having a large value for the $w_{total,a}$ and $w_{tl,a}$, and a nearly half as large value for the $w_{tr,a}$ generates most of the true accelerations. The change of tilt acceleration weight $w_{tl,a}$ did not have a major effect. A set of optimal setting was near the $w_{total,a} = 5$, $w_{tr,a} = 3$, $w_{tl,a} = 8$. The frequency response showed, increasing the $w_{total,a}$ and $w_{tl,a}$ have a major impact on reducing the gain and phase errors, while increasing the $w_{tr,a}$ reduces the gain and phase errors only when the other weights are small. It was concluded that having large weights on the $w_{total,a}$ and $w_{tl,a}$, and small to medium weight on the $w_{tr,a}$ minimises the gain error and results in acceptable phase error.

b) reviewing the effect of changing the weights on the translational velocity and position tracking variables $w_{tr,v}$, $w_{tr,p}$ and total acceleration tracking $w_{total,a}$ while keeping the other acceleration tracking variables $w_{tr,a} = 0$, $w_{tl,a} = 0$ to let the controller decide between the tilt and translational motions, and the tilt position tracking $w_{tl,p} = 2$ constant.

The time response of the model showed the $w_{total,a}$ needs to be higher than both $w_{tr,v}$ and $w_{tr,p}$ to have a high amount of true cues. A set of optimal setting was near the $w_{total,a} = 8$, $w_{tr,v} = 6$ and $w_{tr,p} = 2$, that generates a good amount of true cues while it keeps the false cues as little as possible. The frequency response showed, increasing the $w_{total,a}$ reduces the gain error, while increasing the $w_{tr,p}$ and $w_{tr,v}$ raises the gain error. The phase error showed mixed dependency on the changes in $w_{tr,p}$, $w_{tr,v}$ and $w_{tr,a}$. It was concluded that having a large value for the $w_{total,a}$, medium value for the $w_{tr,v}$ and small value for the $w_{tr,p}$ is an appropriate choice for this scenario of tuning.

All of these guidelines provided for tuning of the MCAs are based on the offline objective analysis of the MCAs response. Often there were more than an optimal solution, that maximised the true cues against false or minimised the gain and phase errors. Thus, the optimal candidate settings need further subjective evaluations by the drivers in the simulator.

Moreover, the optimal settings were picked to have minimum errors between the MCA input (real vehicle motions) and MCA output (simulator motion platform set-points), at the same time respecting the motion platform envelope and tilting constraints. It is possible to further tune the parameters using the vestibular perception model or driver behaviour models, that might vary the range of optimal settings.

In addition to the MCA tuning effect and introducing the optimal set of parameters, these findings are used in the next chapter, together with the fidelity criteria to address the MP workspace requirement.

8 Workspace Optimisation of Motion Platforms

8.1 Introduction

A review of the available motion cueing fidelity criteria in the literature was presented in Chapter 3. Typically, small to moderate motion errors between the vestibular and visual cues that are perceived by drivers as synchronised are referred to as fidelity corridors. Despite the dependency of these fidelity criteria to specific studies in flight or driving simulators, they are the most reliable benchmarks available today. In this chapter, a combination of the fidelity criteria, together with the appropriate tuning of the MCAs described in the previous chapters are used to define the motion platform (MP) workspace requirements to achieve an acceptable level of fidelity.

There have been efforts in the literature to address and design the MP workspace. Advani (1998) specified the optimal design of the hexapod architecture to be able to represent the aircraft motions. He took few steps of mapping the six-dimension predicted simulator motion trajectories into fifteen planar surfaces, approximating the trajectory boundaries in each planar surface by two-dimensional ellipses, forming a six-dimension hyper-ellipsoid representing the shape of the desired workspace, optimising the mechanism to fit the hyper-ellipsoid by specifying its design variables and constraints. The optimisation output may have led to few candidate architectures, those needed to meet a necessary dexterity, avoid configuration singularities and leg clearance. This approach could address the 6 DoF workspace design of a hexapod by optimal positioning of its gimbal attachment points and reduce its cross-coupling problem during simultaneous excursions. However, the optimisation was only based on the aircraft motions and pilot perception and behaviour were not included.

Advani et al. (2002) included a pilot-vehicle control model into the optimisation to incorporate both the visual and vestibular feedback. In a few design steps, the pilot model was adjusted to the given dynamics of the aircraft, the MCA parameters were set to restore the pilot control behaviour, and then using flight recorded data the required MP workspace was determined using the approach explained earlier, all in a closed-loop optimisation format. Although, this approach takes into the account the pilot perception and behaviour, this type of pilot models is only valid for flight tracking manoeuvres that often have sluggish nature, and not applicable in evasive driving manoeuvres. There have been improvements in the driver models to capture the driver behaviour as it was described in section 2.3. However, there is still a need for validation of their accuracy before using them in a closed-loop optimisation in design of MP workspace. Therefore, in this chapter, the focus is on addressing the MP workspace requirement only considering the human perception.

In the frequency domain analysis of motion errors, there are two main factors a) the amount of phase and gain distortions in each frequency between the vehicle and simulator motion and b) the frequency range of interest that is most perceived by human and is of more importance to be available in the simulator. The former is limited to be within the fidelity corridor width, and the latter frequency range for translational motions where the vestibular system tends to have the highest gain of perception is about 0.1 to 10 *rad/s* (Nash et al., 2016). Furthermore, to find the frequency of interest, the input vehicle acceleration amplitude and its power spectral density (PSD) are analysed.

The data collected in the experiment described in Chapter 5 are used, where eight drivers performed a slalom (SLM) manoeuvre and drove through the so-called Land Rover handling track (LHT). In each of the tasks, the drivers were presented with six motion configurations corresponding to permutations of three small, medium, and large motion platform sizes and two classic and MPC motion cueing algorithms, in a counterbalanced order. They drove each of the configurations twice such that in total there were 8(drivers)*6(configuration)*2(repetition) equal to 96 data runs for each of the tasks.

Excluding the drivers' unsuccessful attempts, an example of simulated vehicle lateral acceleration profile and the maximum absolute amplitude of the acceleration among all runs is shown in Figure 8-1. To address the frequency of interest, the acceleration is passed through a vestibular otolith model presented in Eq. 2.6 and the power spectral density (PSD) of it is shown in Figure 8-2. The human perception threshold for translational accelerations is about 0.1 *m/s²* or $10 * \log_{10} \left(\frac{0.1}{\sqrt{2}} \right)^2 = -23$ db i.e. (the rms of a pure sine wave) shown as the black dotted line in the figure. The intersection of the perception threshold line with the perceived vehicle acceleration defines the frequency of interest, it is the point where the acceleration is not perceivable by a driver at any higher frequency. The maximum frequency of interest is calculated for all the data runs, see Figure 8-2 right. For the LHT task it is 6.35 *rad/s* and for SLM is 9.28 *rad/s*.

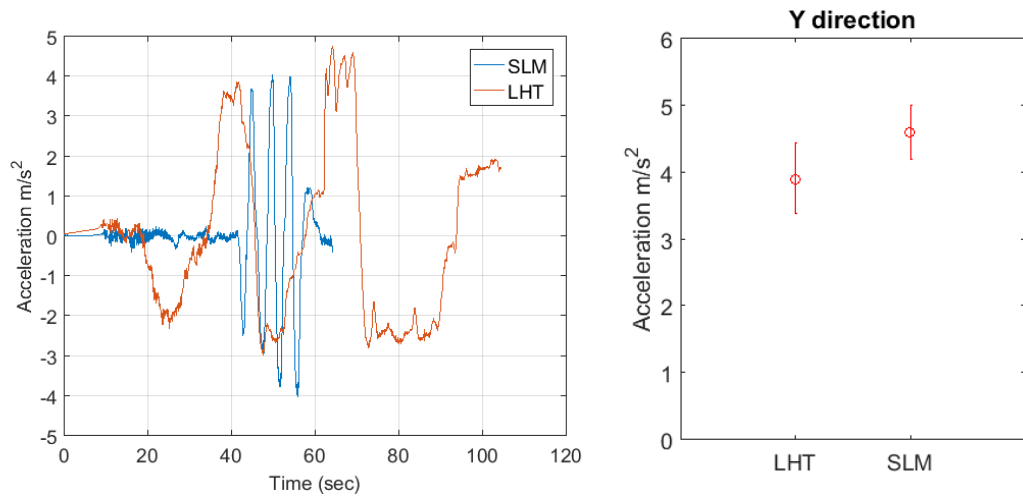


Figure 8-1. Vehicle model lateral acceleration, time series profile of an example run (left), and maximum amplitude of all runs with 95 percent confidence interval (right), for both LHT and SLM tasks

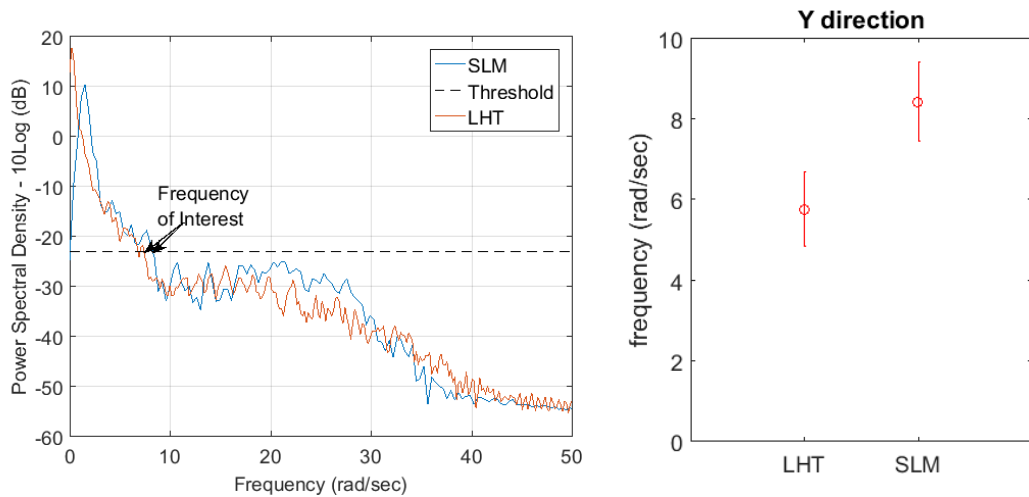


Figure 8-2. Perceived vehicle model lateral acceleration, power spectral density (left) of an example run, and maximum frequency of interest of all runs with 95 percent confidence interval (right), for both LHT and SLM tasks.

To define the fidelity corridor, the allowable gain and phase distortion is chosen based on the intersection of the represented fidelity criteria described in section 3.4, shown in Figure 8-3. Although the medium fidelity border of the Sinacori criteria (0.4 (8 dB) of gain and 60 degrees of phase error) is measured for a single frequency of 1 rad/s, here it is assumed to be the same for all frequencies as the green lines. Figure 8-3 shows that it mostly fits within the range of the OMCT fidelity zone for both gain and phase criteria and it is a more conservative corridor in the middle range of frequencies compared to OMCT. For the phase at low frequencies, it is out of the range, however as it is described later this is not a problem for the optimisation because the tilt coordination response fits within the OMCT corridor. Consequently, the optimisation corridor is selected similar to Sinacori but expanded

in frequency as shown by the yellow line and is referred to the 'Fidelity Corridor' in the remainder of this chapter.

The frequency range of interest is chosen as 0.1 to 6.35 $rad/srad/s$ for LHT task, and 0.1 to 9.28 $rad/srad/s$ for SLM task (see Figure 8-3), and outside these ranges the gain and phase requirements are relaxed considerably. This helps the optimisation problem described in the next section to focus on minimising error in the range of frequency of interest. From the optimisation fidelity corridors, it might be inferred that higher gains than 0 dB also meets the fidelity criteria, however the corridors are drawn axisymmetric around the zero y-axis only to minimise the errors to 0 dB of gain and 0 degrees of phase. This is due to the practicality to the symmetry of the exponential terms in the cost function Eq. 8.1, to have their minimum values at zero. Moreover, there is a term in the cost function to minimise the MP workspace size, hence there is no possibility to find an optimal solution to exceed the 0 dB gain, and at the same time require small MP workspace.

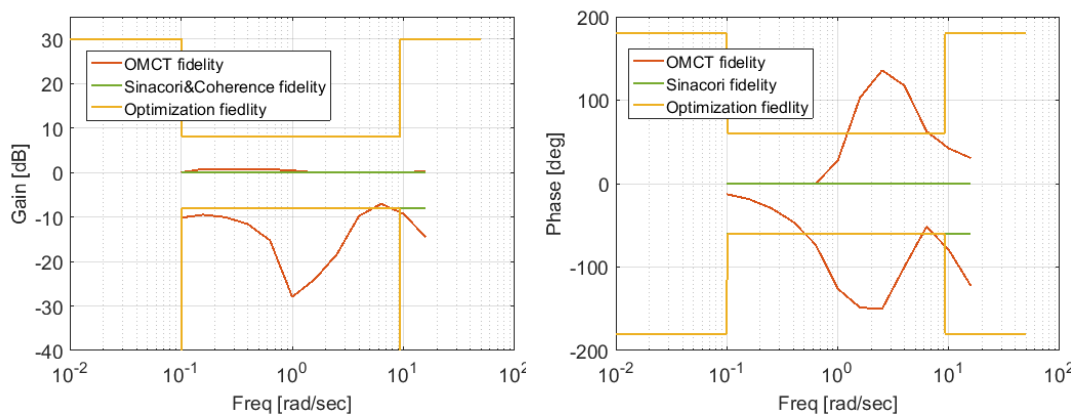


Figure 8-3. Fidelity corridors defined by OMCT, Sinacori, coherent zone and the one used in optimisations for LHT task

It is important that a motion platform be capable of representing both high and low frequency parts of the vehicle motions. The low frequency motions of the vehicle require larger MP workspace to generate the motions, which increases the costs of procurement significantly. The high frequency motions usually do not require large MP workspace but are as important especially to professional drivers to determine vehicle properties, and it is limited by the system bandwidth.

8.2 Optimisation analysis and results

The classic and MPC algorithms were introduced in Chapter 4 and their appropriate tuning parameters were extracted in Chapter 07 for tilt, translation and total motions, that minimised the frequency domain gain and phase errors and time domain true and false cues. In this chapter, the models of both MCAs for total tilt and translational motions are used in an optimisation procedure to address the

minimum workspace requirement of the MP. It is mutual between the MCAs that the low frequency large demanding motions are generated through tilting, and the high frequency smaller demanding motions are generated by the MP translational motions.

The classic MCA model is a combination of the second or third order high-pass filter for generating the translational and second order low-pass filter for tilt motions. The tilts channel might include the rate limiters to be applicable for a wider range of tilt settings, though makes the model nonlinear. The acceleration generated by the MP translational motion depends on three parameters of filter gain k_{hp} and two cut-off frequencies ω_{hp1} , ω_{hp2} . For tilt motion, the tilt maximum angle θ_{max} is selected by a saturator a_{lim} and tilt angular velocity $\dot{\theta}_{max}$ and angular acceleration $\ddot{\theta}_{max}$ are selected by the filter cut-off frequency ω_{lp} and rate limiters, see section 4.1.2.

The MPC model includes the translational, tilt and summation of both. The acceleration generated by the MP translation is affected by three weight factors on the control output tracking variables acceleration $w_{tr,a}$, velocity $w_{tr,v}$ and position $w_{tr,p}$. The tilt feel of acceleration is affected by two weights on the plant output acceleration tracking variable $w_{tl,a}$, and position $w_{tl,p}$. Another weight affecting both is total acceleration tracking $w_{total,a}$. Maximum tilt angle θ_{max} is defined by the constraint on output variable, tilt angular velocity $\dot{\theta}_{max}$ and angular acceleration $\ddot{\theta}_{max}$ by the constraints on the control input variable, see sections 4.2.3.

The selection of these parameters has a major impact on the motion cueing of the simulator, as described and reviewed in the previous chapter. Furthermore, an automatic procedure for finding optimal parameters for the classic MCA was developed (Sadraei et al., 2016). It was a mathematical optimisation method that minimised the motion errors while respecting the fidelity zones and the MP workspace constraints. In this tuning method the cost function of Eq. 8.1, minimised the acceleration error in time and frequency domain, as well as the MP excursions. W_0 to W_3 are the weights of the cost function for time domain acceleration, gain and phase frequency domain and MP position errors.

$$\begin{aligned}
 & \sum_{t=0}^{t_{sim}} w_0 (a_s - a_i)^2 \\
 & + \sum_{f \in f_{interest}} \exp^{w_1(Gain_{now} - Gain_{corridorMax})} + \exp^{-w_1(Gain_{now} - Gain_{corridorMin})} \\
 & + \sum_{f \in f_{interest}} \exp^{w_2(Phase_{now} - phase_{corridorMax})} + \exp^{-w_2(phase_{now} - phase_{corridorMin})} \\
 & + \sum_{f \in f_{interest}} \exp^{w_3(MPPos_{now} - MPPos_{Max})} + \exp^{-w_3(MPPos_{now} - MPPos_{Min})}
 \end{aligned} \tag{8.1}$$

A gradient-based method *fmincon* that is designed to work with the constrained nonlinear multivariable problems. Having the continuous cost function and constraints this method was employed in the MATLAB/Simulink. The optimisation parameters were the MCA parameters for translational motions while minimising the objective function of Eq. 8.1 and respecting the bound constraints on the parameters. This methodology was initially used to address the MCA parameters for translational motions only. It was further extended to include tilt coordination, in addition to another layer of optimisation to define the minimum MP (sliding rail) workspace size (Sadraei et al., 2018). In this optimisation, an inner-loop runs the optimisation to find if MCA parameters exist that meet the requirement for time and frequency domain fidelity corridor for an MP size, and an outer-loop adds to the MP size in meters. If the inner-loop optimisation condition is met, that size of MP is chosen, otherwise the outer-loop adds another meter until the fidelity criteria is met, see Figure 8-4.

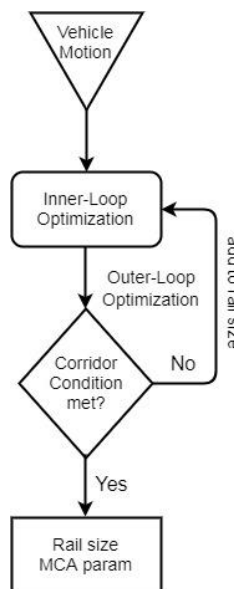


Figure 8-4. Optimisation process

This procedure was used to address the sliding rail size requirement for data of the low-friction experiment described in Chapter 5. The classic MCA model was a second order high-pass filter with inner-loop optimisation parameters of k_{hp} and ω_{hp2} for translational motion, and second order low-pass filter with fixed parameters of k_{lp} and ω_{lp2} for the tilt motion. The tilt parameters play a critical role on how large the rail size should be, because the maximum tilt angle, angular velocity and acceleration limit the build-up of tilt acceleration which results in larger translational motion of the MP to compensate. At the same time, the rotational motions of tilting needed to be limited to avoid to be noticed by the driver.

In this optimisation, the nonlinear rate limiters were not used, and the low-pass filter parameters were selected to constrain the tilt angular motions. The maximum tilt

angle that limits acceleration represented by tilting was constrained by a saturator. Various tilt settings that have been employed in the literature was reviewed in section 5.4.2. Among them two sets of parameters for tilting angular velocity and accelerations were chosen, see Table 8-1. These settings could be regarded as the range of tilt motions used in driving simulators in the literature and could be representative of the maximum and minimum of sliding rail size requirement. Moreover, linear tilting was used in the optimisations that only allows a certain choice of tilt setting, which was another reason for selecting the particular set of parameters, see section 7.2.2. In both of the settings, the maximum represented acceleration is 1 m/s^2 at unity gain due to θ_{\max} of 6 deg , see Appendix D.

Table 8-1. Tilt parameters used for optimisations

Tilting parameters	(A) : $\omega_{lp} = 2 \text{ rad/s}$	(B) : $\omega_{lp} = 1.17 \text{ rad/s}$
$\theta_{\max} \text{ (deg)}$	6	6
$\dot{\theta}_{\max} \text{ (deg/s)}$	4.3	2.51
$\ddot{\theta}_{\max} \text{ (deg/s}^2\text{)}$	23.5	8

Data of all the runs of the experiment in the low-friction condition, excluding outliers were used in the optimisation to address the minimum rail size requirement among all drivers, experimental configurations and repetitions. In the optimisation process, the high-pass filter parameters were calculated once per run and for each tilt setting; such that the fidelity criteria was met and then the MP size was recorded. The results of the optimisations for the LHT task is shown in Figure 8-5, having a higher tilt limit corresponding to $\omega_{lp} = 2 \text{ rad/s}$ a rail size of $7 (\pm 3.5)$ meters meets the fidelity requirement for most of the runs, while it goes up to $20 (\pm 10)$ meter with the more restrictive, lower tilt limit corresponding to $\omega_{lp} = 1.17 \text{ rad/s}$. Similarly for the SLM task, the rail size required is in the range of $2 (\pm 1)$ to $4 (\pm 2)$ meters for the high and low tilt limits respectively, Figure 8-6. The obtained optimisation result shows the mean high-pass filter cut-off frequency ω_{hp} is 0.57 to 0.98 rad/s and gain of 0.83 to 0.9 for the low and high tilt limits in LHT task; and for SLM task the cut-off frequency of 0.41 to 0.69 rad/s and gain of 0.68 to 0.64 for the low and high tilt limits, see Figure 8-7.

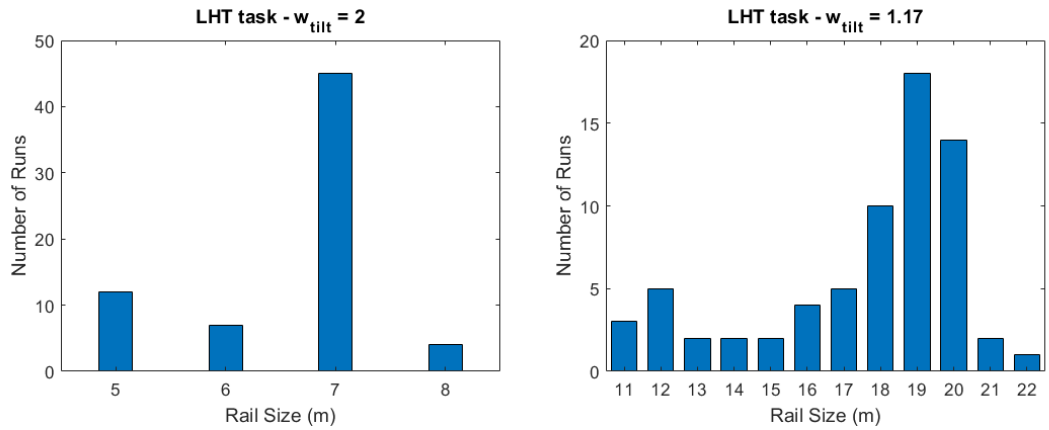


Figure 8-5. Optimisation results for the LHT task with tilt setting high (left) and low (right). The bars show number of recorded runs that would require a given rail size.

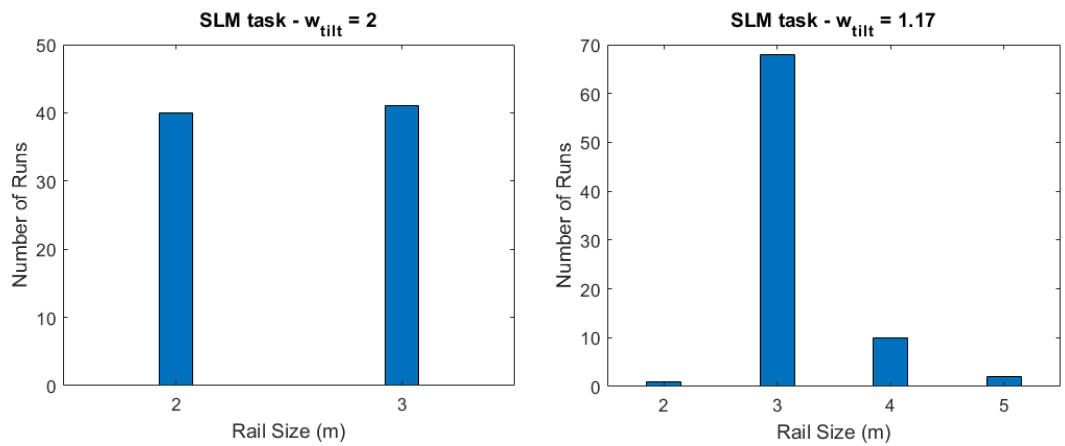


Figure 8-6. Optimisation results for the slalom task with tilt limits high (left) and low (right). The bars show the number of recorded runs that would require a given rail size.

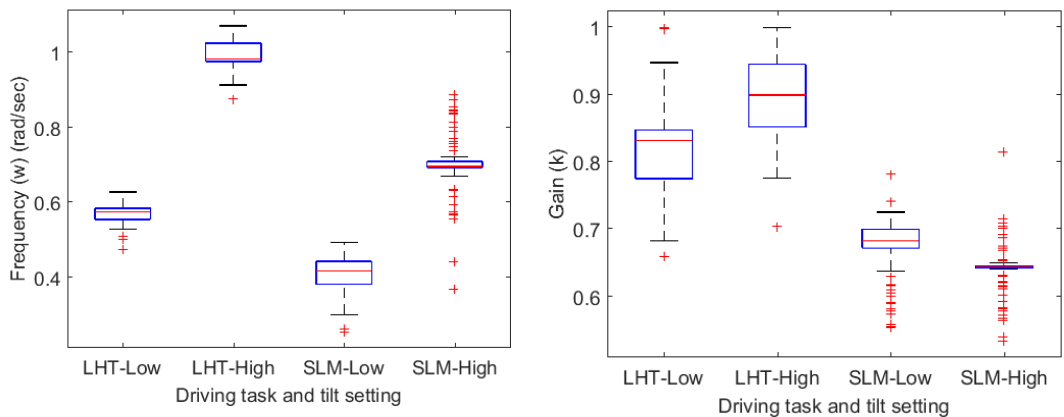


Figure 8-7. Optimisation results for frequency ω_{hp} (left) and gain k_{hp} (right) range, for both driving tasks.

In contrary to the described MP workspace optimisation considering the vehicle motion inputs (collected in the experiments) and utilising the classic MCA with linear

tilting, there are some challenges for a similar analysis using MPC algorithm and classic MCA with nonlinear tilting. Primarily, due to the nonlinearities in characteristics of the MPC algorithm and classic algorithm if the saturation, angular velocity and acceleration limiters are used for tilting; the calculation of exact linear frequency response of the models, and to respect the optimisation fidelity criteria is not possible. Therefore, an estimation method is needed to calculate the frequency response of the model. The frequency estimation used here considers the models' translational, tilting and total acceleration response to sinusoid input accelerations of 20 various frequencies defined in the range of the frequency of interest, with an amplitude of 2.5 m/s^2 , see Figure 8-8. It estimates the amplitude attenuation and phase shifting of output sinusoids compared to inputs and draws the frequency response.

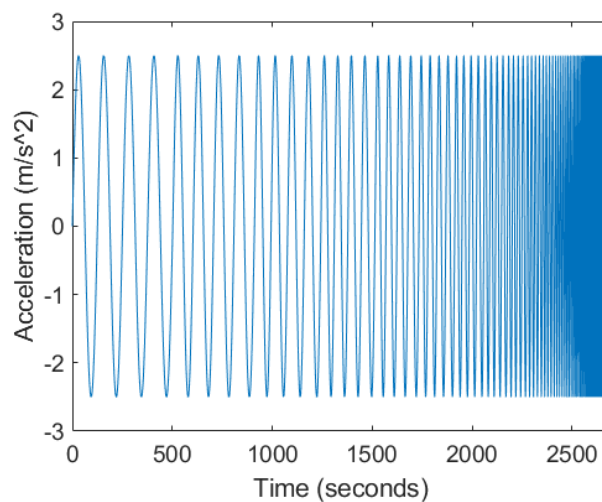


Figure 8-8. Sinusoid input used to estimate the frequency response of the models

Secondarily, using the frequency estimation makes it infeasible to simultaneously analyse the time and frequency response of the MCA, as required by the inner-loop optimisation of the workspace. This is due to the inequivalence between the time response of the MCAs to vehicle motion input and estimated frequency response to a sinusoid motion input. Principally, there is another limitation with the constrained MPC in calculating the required MP excursions in time domain to, because the maximum excursions are always respected by the controller constraints. To elaborate more about these limitations:

In the optimisation of the classic model with linear tilting, the required MP excursions to a vehicle motion input is a function of its parameters, that makes it possible to make a joint frequency and time domain analysis of the model. For instance, in the optimisation inner-loop, it is possible to minimise the gain and phase errors of the linear frequency response to fit within the fidelity corridor while

minimising the MP excursion from the time domain analysis. Introducing the nonlinear tilting, although requires the frequency estimation that raise the second limitation of inequivalence between the time and frequency response, using an appropriate approximation by a sinusoid signal reduces of its extent. In the MPC model in addition to the second limitation, the MP excursions are always constrained by the controller while calculating the time domain response to the vehicle motion. Therefore, a joint analysis of frequency and time domain is more challenging that requires modifications to the optimisation process.

To overcome these limitations and to be able to make a comparison between the frequency response and required MP excursions of the MPC and classic with nonlinear tilting algorithms. The sinusoid signal for the response estimation is used as the vehicle motion input to both the algorithms and the frequency response of the models and corresponding time domain MP excursions to the same input sinusoids are calculated. For both the models the same fixed set of tilt parameters are used in the optimisations, those are $\theta_{\max} = 6 \text{ deg}$, $\dot{\theta}_{\max} = 3 \text{ deg/sec}$, $\ddot{\theta}_{\max} = 10 \text{ deg/sec}^2$ (see Appendix D), and tilt setting gain of $k_{lp} = 1$ and cut-off frequency $\omega_{lp} = 5 \text{ rad/s}$ in the classic, and for the MPC the prediction and control horizon of $H_p = 1.2 \text{ sec}$ and $H_u = 0.2 \text{ sec}$.

Few modifications were made to the optimisations process, where the cost function Eq. 8.1 only includes the exponential terms for gain and phase errors for MPC in addition to the MP excursion term for classic. In the classic model, for a specific MP size, the inner-loop looks for the high-pass filter parameters of gain k_{hp} and two cut-off frequencies ω_{hp1} , ω_{hp2} to fit within the fidelity corridor, if it is true then that large MP workspace sufficiently meets the fidelity criteria, otherwise, the outer-loop adds to the size and looks for the parameters again.

In the MPC model in the inner-loop, a fixed set of parameters is used, those parameters are found to be optimum based on the tuning of the algorithms described in Chapter 07 and the comparisons between a number of independent optimisation runs, those variables are $w_{tr,a} = 0$, $w_{tr,v} = 3$, $w_{tr,p} = 1$, $w_{tl,a} = 0$, $w_{total,a} = 10$, $w_{tl,p} = 1$, $H_p = 60$, $H_u = 12$. The main reason for using fixed parameters was the very long runtime of the MPC models, even in a single optimisation run. Therefore, for a specific size of the MP, the MPC model frequency response is calculated and if it meets the fidelity corridor then that is the sufficient MP workspace; otherwise, the outer-loop adds to the MP size.

The required MP workspace for the classic MCA with nonlinear tilting to the input sinusoid motion with variable frequencies (see Figure 8-8) found to be of ± 16 meters with parameter values of gain $k_{hp} = 0.584$ and cut-off frequencies of $\omega_{hp1} = 0.882 \text{ rad/s}$ and $\omega_{hp2} = 0.0549 \text{ rad/sec}$. For the MPC algorithm ± 14 meters found

to be required to meet the fidelity criteria in a range of 0.15 to 10 rad/s . These indicate the MPC algorithm requires slightly smaller MP workspace compared to classic to achieve the same level of fidelity.

The frequency response of both of the algorithms is shown in Figure 8-9 and Figure 8-10. The gain and phase response of the classic algorithm is steadier and flatter over the frequencies compared to MPC. However, the MPC performs better in the lower bound of the fidelity range around 0.15 rad/s , and as a result, a smaller workspace size could meet the criteria. These results are based on the offline analysis, and the differences in the frequency response of the models may or may not be perceivable by the drivers, for instance the classic might feel better and worth the cost to build the larger simulator. Further subjective evaluations on the tuning of the parameters as it is described in Chapter 7 helps to validate the differences in model responses.

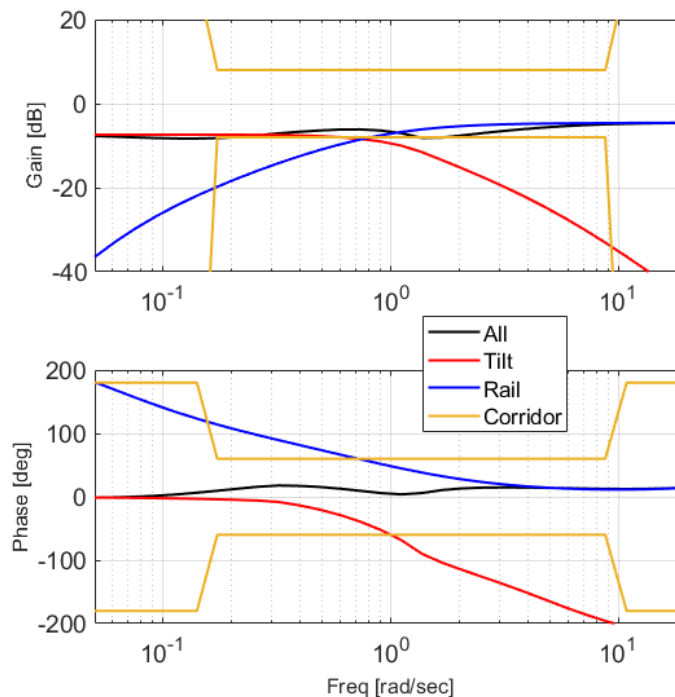


Figure 8-9. The classic algorithm estimated frequency response, requiring ± 16 (m) of MP workspace

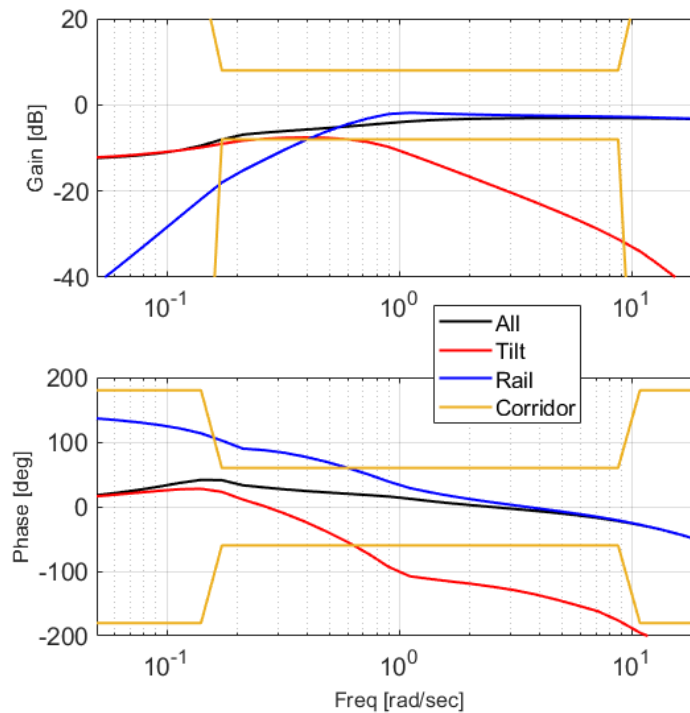


Figure 8-10. The MPC algorithm estimated frequency response, requiring ± 14 (m) of MP workspace

In order to make MP workspace optimisation between the algorithms to the vehicle motion inputs, it might be possible to use the modified optimisation process, through modifications to the input sinusoid frequency estimation signal. Considering the vehicle motion PSD as it is shown in Figure 8-2, the sinusoid signal amplitudes in the range of frequency of interest could be modified to have amplitudes same as the vehicle motions, this makes the sinusoid input to be more representative of the vehicle motion, and to reduce the inequivalence between time and frequency response of the MCAs. Despite the observations, it worth to remind that the whole optimisation is still based on estimations and not exact linear frequency response of the MCAs.

8.3 Conclusions and suggestions

A driving simulator motion platform sizing method is developed and represented in this chapter. It is a specifically designed optimisation method that searches for minimum MP workspace size while keeping the motion cueing response within the fidelity corridor. Different motion fidelity criteria are reviewed, and a reasonable fidelity corridor is selected and used in the optimisations. The reliance on tilting for motion cueing plays a significant role in rail size requirement to compensate and keep the motion cueing within the fidelity corridors.

Two possible tilt parameter sets are selected which drive a minimum and maximum sliding rail size requirement. The method is tested for lateral motion of two low friction vehicle testing manoeuvres, considered by means of a large data set of recordings from professional drivers. For the Land Rover handling track, a rail size range of 7 (± 3.5) to 20 (± 10) meters is required to meet the fidelity corridor for lateral motion cueing. For the Slalom this range is between 2 (± 1) to 3 (± 1.5) meters. This method could also be used to address the workspace requirement in high- friction condition.

To make a comparable frequency analysis between the MPC and classic algorithm with nonlinear tilting an estimation method using a sine wave of variable frequency was used that identified the models' frequency response and the time domain MP excursions. It was found that using the optimal settings of both algorithms, the MPC could meet the fidelity criteria with ± 14 meters of MP workspace, while the classic required ± 16 meters. Although a comparable MP workspace optimisation using the frequency analysis between classic and MPC algorithms for the vehicle motions is not a straight forward task, it might be possible to make a comparison by modifying the input estimation signal to assimilate the vehicle motions.

The focus here has been on lateral motion, however the motions in other DoFs that need to be generated by a simulator MP can be addressed with a similar optimisation method. Commonly, a hexapod is used to generate the rotational (roll, pitch and yaw) and vertical (heave) motions of the vehicle. In the driving simulation, roll, pitch, and heave are generally not a major concern. The collected data of various vehicle manoeuvres on the flat ground shows the roll and pitch motions of vehicle never exceed ± 5 degrees, in addition to a tilt degree of ± 8 degree for each direction, both resulting in ± 13 which can be represented one to one by a typical hexapod. The vertical (heave) motion of the vehicles is in range of 16 cm on a flat surface and could be represented one to one by a normal hexapod. However, if there is a road with slope then the slope should be added to each of the directions and a hexapod with a larger workspace is needed for one to one motion cueing.

With regards to yaw motion, depending on the driving manoeuvre 360 degrees of motion might be necessary for the one to one motion, which it is only feasible by including a turntable on top of a hexapod. However, for the yaw motion with acceptable fidelity, a similar optimisation process is then needed to find the minimum workspace requirement. This method can be used for the motion in any of the directions to fit within the fidelity corridor.

Although this method is a reliable tool to address the workspace based on a fidelity criterion, more research is needed in driving simulators to define the appropriate fidelity corridors in each DoFs and their cross-couplings effects. Moreover, by using

a reliable and experimentally validated driving model it might be possible to further extend this method to consider the workspace sizing in drivers' behaviour level.

In general recommendations about buying a simulator motion platform, it is first needed to define the application. For instance, is it for research on human factors, vehicle design, training or gaming? In this thesis, the focus has been on the tuning of MCA and addressing the MP size to meet the demands of professional drivers during vehicle design. The professional drivers sensitive to the high frequency motions, and it is a rich source of information to them. This requires the MP to have high frequency bandwidth to cover high frequency of vehicle motions. On the other hand, the high bandwidth might be of lower importance for research applications on normal drivers, that might reduce the need for a high bandwidth system and changes the procurement costs. Increasing the bandwidth of the motion system is feasible by using higher capability actuators or building a lighter weight system.

9 Conclusion and Recommendations

Driving involves a wide range of activities resulting from interactions between the driver, the surrounding environment and the vehicle. These are achieved based on sensation and perception of self-motion and translated into behaviour performance (Nash et al., 2016). In simulators, the cue generator subsystems and their associated components are designed to stimulate the human visual, vestibular, auditory and proprioceptive sensory systems, in order to replicate the real world cues and elicit a realistic driving experience in a virtual environment (Allen et al., 2011). Due to practical, technological and financial hindrances, the one to one replication of real world cues is not feasible, and reportedly not always necessary.

A compelling and realistic perceptual and performance experience of driving in simulators, i.e. high fidelity, not only requires the represented cues to be similar to the real world, but also they need to be coherent and proportionate to each other in a virtual environment (Sinacori, 1977; Valente Pais et al., 2010). Both visual and vestibular cues play a vital role in static and dynamic simulators (Hosman et al., 2011). While the visual cues are always available, the vestibular cues require dynamic motion platforms which present challenges of a physical and financial nature (Kemeny and Panerai, 2003). The presence of vestibular motion in simulators has been emphasised due to the observations of improved perception and performance of drivers (Reymond et al., 1999; Siegler et al., 2001).

The required characteristics of each of the subsystems of a simulator, to achieve a desired level of fidelity, is a broad question that involves a vast field of research (Greenberg and Blommer, 2011). In this thesis, the focus has been on vestibular motion cueing in the simulators and attempted to evaluate their effects on drivers perception and performance. In this regard, the effects of manipulating the two most influential motion cueing algorithms (MCA), and motion platform components in a simulators' motion system has been studied. Furthermore, to evaluate the applicability of the simulators for assessment of a vehicle's driven attribute properties, such as ride, steering feel and handling, the manipulation of the vehicle ride height was also studied in the simulator.

The classic MCA was originally developed for flight simulation (Conrad and Schmidt, 1969), and with the updated structure, it has been shown to be applicable for driving simulation (Colombet et al., 2008). It is easy to implement and suitable to run with a high frequency of update in real-time applications. However, it is tuned for worst-case scenarios, thus the motion platform capability might not be fully exploited for small vehicle motion inputs. The classic MCA is reported to have acceptable performance in normal manoeuvres, in comparison to other MCAs

(Grant et al., 2009). Dagdelen et al. (2004); Dagdelen et al. (2009); Augusto and Loureiro (2009) employed model predictive control (MPC) as the MCA in driving simulators. It is a sub-optimal control algorithm, runs in real-time with lower update rates compared to the classic, and is quite complicated to implement. The main advantage of this algorithm is the calculation of optimal solutions while respecting the physical constraints of the motion platform. Although tuning of this model might seem to be a more rational process compared to the classic, there are more variables involved to be carefully selected.

Motion platforms of various characteristics and workspace sizes have been employed in driving simulators. None of them can represent the one to one vehicle motions in high demanding manoeuvres. The evaluations of small demanding manoeuvres that fit one to one within the workspace consistently have shown a preference for down-scaled motion by drivers (Berthoz et al., 2013; Savona et al., 2014). The reasons were said to be related to imperfections and false cues of the motion system at large scales, inability to maintain the coherence between the visual and vestibular cues, or difficulty in exerting accurate steering control in higher and more uncomfortable accelerations. Although this seems a surprising finding, it has been reported also in flight simulation studies. Groen et al. (2001) explained this as an underestimation of visual cues that leads to an over-estimation of vestibular cues.

It was mentioned above that the visual and vestibular cues have to be coherent and proportionate and this might explain the down-scaled vestibular motion preference. Considering that the human eye sees real and virtual driving in different visual qualities, the human brain in the simulator expects to see the degraded visual cue to be proportionate to the degraded vestibular cue; this might hypothetically explain the down-scaled motion preferences. Although there is a measurement benchmark for the vestibular motion cues represented to the drivers in a simulator, the main challenge is the lack of a benchmark for the visual cue e.g. resolution.

Consequently, to evaluate the vestibular motion cueing effects in a simulator, an experiment was designed where the MCA and motion platform size were the main manipulated components. The classic and MPC algorithms were compared, in addition to three motion platform workspace sizes. Moreover, to evaluate the vehicle attributes in the simulator, a second experiment was designed. Three different vehicle ride heights were compared, in addition to three motion platform workspace sizes. The evaluations were based on the subjective perception of the driving experience in various motion and vehicle configurations, and exploration of the effects of the changes on drivers' performance. These aims were evaluated in different road friction conditions.

The significant and broad effect of MCA parameters on motion cueing has been emphasised in the literature (Reid and Nahon, 1986a; Grant and Reid, 1997), and was observed during the design of the experiments in this thesis. Therefore, the optimal tuning of the MCAs was also introduced. The time and frequency domain response of the MCAs were reviewed based on appropriate measurement metrics, and a generalised conservative fidelity criterion was defined. This information not only helps in fine tuning of the MCAs, but also it was used for the optimisation of the MP workspace. Using these extracted optimal MCA parameters, the fidelity criteria, and a multi-layered optimisation method, the required MP translational workspace was addressed for specific driving tasks.

There have been other prerequisite steps taken to prepare for the experiments and optimisations. Among the major ones, it could be mentioned that the models of vestibular sensory dynamics and their frequency response was reviewed; for the purpose of MCA development and driver's perception during driving. The latter helped for appropriate tuning of the MCAs, and optimal workspace sizing of the MP. Driver behaviour performance models was reviewed and a suitable one was selected for the analysis of drivers' performance in the experiments. Furthermore, the motion cueing fidelity criteria was reviewed and a combination of all was selected as a conservative criterion, that was used for MP optimal workspace sizing.

9.1 Summary of results

9.1.1 Assessment of low-friction motion cueing

In the evaluations of motion cueing in low-friction driving conditions, the aim of the study was to compare between the classic and model predictive control MCAs, and three sizes of motion platform (MP) workspace, in the two driving tasks of Land Rover Handling Track (LHT) and Slalom (SLM). The comparisons included the subjective evaluation of the perceived realism consisting of overall, motion cueing and vehicle assessment questions. The objective measurements for exploration of driver's performance, included metrics of aggregated performance, time series and driver model. The measurements were analysed using the descriptive and linear statistics models.

Two research questions were defined and evaluated with respect to how the different 1) MCAs and 2) MPs affect the drivers' subjective ratings of simulator fidelity and their objective behaviour. In this study the comparisons between the MCAs extended and carried out in different MP sizes, to find if there is an interaction effect between the MCA and MP size.

Motion cueing algorithm comparison

In the study carried out, regarding the MCA comparison, the subjective fidelity analysis in the LHT task showed significant or nearly significant effects of the type of MCA, whereby mostly, the MPC was rated higher (preferred by drivers) than the classic in the three groups of questions, being aligned with the hypothesis and similar studies (Fang and Kemeny, 2012b; Garrett and Best, 2013). In the SLM task, there was no significant effect of the type of MCA, although a review of the effect sizes showed that the classic was rated higher in small and large MPs. Based on the effect sizes, with the increase of MP size the differences between the MCAs became more distinct to drivers in the large motion demanding task of LHT and less distinct in the SLM.

The objective drivers' performance analysis showed the aggregated performance measurements of lap time, number of failures, and speed variation in the LHT task, the MPC was found to have higher values in most of MP sizes i.e. worse performance of drivers in MPC; as opposes to the subjective preference of MPC over classic. In the time series and driver model metrics, interestingly the MPC always had higher values in the driver model gain and steering reversal rate which indicates more control activity while driving the MPC algorithm, reflecting the worse performance. For the SLM mix results was found.

Motion platform comparison

The subjective fidelity analysis in the LHT task in only the motion cueing group of questions showed the significant or nearly significant effect of size of MPs, where the large MP was rated significantly higher (preferred by drivers) than medium and small. The review of the effect sizes indicated preferences for the larger motion since the subjective ratings improved with the increase of MP size. For the SLM task, no significant effect of MP size was found, although the effect sizes showed small to medium MP sizes were preferred depending on the MCA, reflecting the smaller motion preferences by drivers. This is in line with the literature that has shown in the SLM task drivers preferred the down-scaled motion to between 0.4 and 0.75 of full motion as more realistic (Berthoz et al., 2013; Savona et al., 2014). This range of preference could possibly be postulated to the LHT task where there is larger vehicle motion available and the larger MP size could represent the down-scaled motion, which might explain the preference for the larger MP size in this experiment.

The objective drivers' performance analysis in LHT task showed the number of failures, speed variation and lateral position deviation aggregated performance metrics decreased, while the lap time increased with the increase of MP size,

reflecting improved performance. The time series and driver model metrics such as longitudinal acceleration, steering reversal rate, and driver model gain, decreased with the increase of MP size, reflecting the more relaxed style of driving and improved performance. This is aligned with the literature that has been reported of increasing of the motion reduce the steering control effort (Reymond et al., 1999; Siegler et al., 2001; Feenstra et al., 2010; Lakerveld et al., 2016). In the SLM task, the number of failures and speed variation metrics increased, while the lap time decreased with the increase of MP size, reflecting worsened performance. In the time series and driver model metrics, longitudinal velocity and driver model delay time increased with the increase of MP size, that confirmed the hypothesis, while the yaw rate showed a reduction in value. No significant changes were observed to the steering reversal rate, although it was anticipated as reported in the literature (Berthoz et al., 2013).

In summary, the subjective evaluations showed that in the LHT task, drivers preferred the MPC algorithm and the larger MPs, whereas in the SLM task they preferred mostly the classic MCA and smaller MP. Moreover, the differences between the MCAs were more subtle in SLM than LHT, and the difference between MPs was more distinct to them. Interestingly, this inverse trend in subjective evaluations between the tasks is aligned with their results for the aggregated performance measurements, where an opposite effect of MP size was found between the two tasks i.e. the improved/worsened performance was observed with increasing MP size, respectively in LHT/SLM tasks.

In the aggregated performance metrics, the MPC mostly showed significantly higher values in both tasks, reflecting the worse performance in driving the MPC algorithm. The increase of MP size in the LHT task showed a decrease in most of the time series and driver model metrics, reflecting the lower control activities and improved performance; whereas mixed results were observed in the SLM task.

The subjective preference of the MPC over classic has been reported in the literature, although in this study it was only hypothesised to be observed only in the LHT task. Because, in the tuning process of the MPC algorithm for the SLM task, lower performance of the algorithm was observed. As it was explained in section 5.4.2 and elaborated in section 7.3, the reason was the rapid sinusoidal type of changes in the vehicle lateral motion (the dominant vehicle motion) in SLM task. In such evasive vehicle motion inputs, the MPC controller's performance is low when the prediction of the future reference signal is not available, and there are model stability concerns that limit the choice of the prediction horizon.

The preference for the larger MP size in LHT and smaller in SLM task is in line with the available literature that the one-to-one representation of vestibular motion cues

is not always perceived as more realistic. As mentioned earlier in this chapter the visual and vestibular cues have to be coherent and proportionate and this might explain the down-scaled vestibular motion preference. In the LHT task with larger motion demand the down-scaled motion could be represented with larger MP size and in SLM with smaller. However, the precise value of down-scaling may also be dependant to the driving manoeuvre characteristics.

The dependency of preference of MCAs to driving tasks, further explains the importance of tuning the algorithms. More specifically, the MPC algorithm performance could be slightly improved to the evasive vehicle motion inputs such as SLM, through optimal tuning of its parameters using the guidelines provided in Chapter 7. In such occasion, it may perform the same or better than the classic algorithm, that requires further investigations. In other words, the quality of the response of an algorithm is heavily dependent on its tuning, and an algorithm may show its eminence if and only if it is well-tuned.

The driver objective performance metrics were selected from definitions available for normal drivers' performance, although the drivers participated in this experiment were all professionals who had more racing driving style. This might explain the contradiction between their preference for a motion configuration and their worse performance. For instance, in case of a preferable motion configuration they had higher speed variability, lateral position deviations and steering control activity because they actually liked it, however it is counted as a worse performance.

These findings are based on the evaluation in the low friction conditions which by nature is a more complex situation for drivers compared to high friction since it increases their mental workload that might be affecting their performance. For instance, during the SLM or LHT tasks not only they have to accomplish a demanding manoeuvre, but also not to lose the grip of tyres and spin-out which is not available in high-friction condition. Although this effect is minimised by using the experienced professional drivers, it may still be a potential influencing factor. In other words, there are more uncertainties and variabilities available to drivers' preferences and performance in low friction testing. The experiment design of this study has the transferability to the high friction condition. Although, it is expected to obtain similar results in high friction condition, due to lower mental workload in high friction drivers' preferences and performance might vary.

9.1.2 Assessment of high-friction motion cueing

In the low-friction experiment, the evaluations were mainly focused on the effect of motion cueing components in the simulator. However, in this experiment as reported in Chapter 6, the focus of evaluations was on the motion cueing in addition

to the driven attribute qualities of the vehicle in the simulator. The aim of this study was to compare between three vehicle ride heights (RH), and three sizes of MP workspace, experimented in a high-friction driving condition in the Gosport lane (GSP), a public road circuit at JLR Gaydon site. The means for the comparisons included the subjective evaluations of the vehicle ride, steering and handling qualities, in addition to their perception of realism. The objective measures for exploration of driver's objective performance were similar to the previous study.

Regarding these aims, two research questions were defined and evaluated. How the different 1) RHs and 2) MPs affect the drivers' subjective ratings of vehicle attribute qualities, simulator fidelity and their objective behaviour. The studies available in the literature about the study of the vehicle driven attribute evaluations in simulators are rare and there is no research identified considering the effect that simulator motion cueing might have on the evaluations of the attributes.

Ride height comparison

In the study carried out, regarding the RH comparison, the subjective analysis of driven attributes showed a significant or nearly significant effect of RHs in few of the steering and handling quality attributes. Drivers found medium (standard vehicle height), and in some of the qualities the low RHs more appropriate for the vehicle.

The review of effect sizes for the most appropriated RH showed that in the ride question the low and medium RH were constrained and crashy, and high RH settled and floaty and appropriate for the vehicle. In the steering gain linearity attribute the low and high RH were more nonlinear to the drivers, and the medium RH was the most linear and appropriate for the vehicle. In under/over steering quality the low and high RH was more oversteering to drivers, and the medium RH was the most appropriate for the vehicle. In the handling roll transient question the low to high RH was found to have less to more values than appropriate, respectively. This shows drivers could distinguish correctly between RHs.

Furthermore, the review of effect sizes for the most unappropriated RH showed that the low and high RHs were mostly selected as not appropriate for this vehicle; those were observed in large and small MPs respectively which might indicate the effect of MP size on drivers' choice of more suitable RH. The absence of medium RH among them might imply the appropriateness of the medium RH, and that they were able to distinguish between the RHs.

The objective drivers' performance analysis for the aggregated performance measurements showed the difference between RHs were more subtle in speed variation. In lateral position deviation, the low RHs had the highest value in all MPs

that solely indicates the worst performance. The highest lap time in small, medium and large MPs was with the low, medium and high RHs.

In the time series and driver model metrics, where there was a significant effect of RH on measurement metrics, the low RH was consistently found to have the highest value in all the metrics, being independent of the road sections and MP sizes. Comprised of the steering wheel reversal rates, and driver model gain, that shows highest control activity and the worst performance in low RH.

Motion platform comparison

The subjective ratings of the driven attributes only in the ride group of question showed a significant effect of the size of MPs, where the medium MP was the most appropriate.

The review of effect sizes for the most appropriate MP showed that in most of the handling and steering attributes, the low RH the small MP was rated as the most appropriate for this vehicle, and in the high RH the large MP. It indicates the higher the RH is, the larger MP was selected as more appropriate, and vice versa. In detail, in the ride question, the medium MP was rated as the most floaty and settled and appropriate for this vehicle. In steering gain linearity away from centre, the small MP was the most suitable. In handling roll transient the small MP was most suitable, while with the increase of MP size drivers found the roll to be increasing. For the steering window and effort grouped question drivers seemed to have chosen larger MP with increasing RH as more appropriate.

Furthermore, the inverse trend was observed for the most unappropriated MP in different RHs, where in the low and high RHs drivers have rated large and small MP, respectively as the most unappropriated. These show there might be an effect of RH on drivers' choice of appropriate MP size. The subjective ratings of the drivers' perception of realism of overall assessment and motion cueing, showed the medium MP as the most preferred by drivers.

The objective drivers' performance analysis showed for the speed variation and lateral position deviation aggregated performance metrics, values have decreased with the increase of MP size i.e. improved performance, and the lap time increased with the increase of MP size; however, for these metrics, some fluctuations were observed. In the time series metrics, no significant changes were observed to change of MP size and most of the measurements stayed similar or slightly decreased with the increase of MP size. The driver model metrics of preview time and gain parameters showed a decrease with the increase of MP size. This confirms the hypothesis of requiring smaller steering gain with the increase of MP

size. Moreover, the decrease in driver model steering gain reflects more relaxed style of driving and improved performance with the increase of MP size.

In summary, the steering and handling subjective assessment of the driven attribute qualities by the drivers showed that the drivers found medium and low RH to be more appropriate for the vehicle. It was concluded that the small and large MPs provide more appropriate motions for the evaluations of the low and high RHs respectively. This indicates that there is an effect of MP on the RH, and the higher the RH is the larger MP is selected as more appropriate, and vice versa. The overall pattern of the aggregated performance showed in the low RH and small MP the drivers had the highest lateral position deviation, reflecting the worst performance. In all the time series and driver model metrics the low RH always had the highest value in all MP sizes and road sections, with significant effects; including the highest steering control activity, reflecting the worst performance in low RH. There were no significant changes in time series metrics observed with changes of MP size, and most of the metrics stayed similar or slightly decreased. Some of the driver model metrics showed a decrease with the increase of MP size, indicating the decrease in control activity, relaxed style of driving and improved performance with the increase of MP size.

The subjective preference of the medium RH over low and high was hypothesised to be observed, as it is the standard vehicle RH. Although the drivers have selected the medium RH to be appropriate in most of steering and handling attributes, the observed choice of the low RH in some of the attributes might be explained by professional drivers' desire for race style of driving, which is more eminent in low RH. The preference of the high RH in ride attribute might be because of drivers' expectation from driving an SUV car (e.g. to be floatier and more settled), and/or the vehicle height point of the visual cueing was better at high RH configuration.

The preference for the medium MP size means drivers found the motion in small and large MPs not to be suitable. The vehicle motion in the GSP task have high amplitudes and it was expected to see drivers mostly prefer the large MP. However, it is not straight forward to explain this as a cause of incoherence between the visual and vestibular cues, because the nonlinear scaling has been used in this study, but it is a potential cause. The other scenario might be related to the tuning of the MCA. The tunings for the three MP sizes were done identically; however, there might be a possibility for further improvement using the optimal tuning guidelines provided in Chapter 7.

Another observation was the direct relationship between the MP size and choice of appropriate RH. In the lower RH, the smaller MP was selected as more appropriate, and vice versa. This could be explained by the low/high frequency of the vehicle

motions in high/low RH; especially in roll and pitch directions that also affect the perception of lateral and longitudinal motions. The drivers have correctly selected that the roll of the vehicle have increased with the increase of RH, and correspondingly the larger lateral motion may have been expected, where the larger MP could meet the desired lateral motion cue. This is an explanation for the observed relation between the MP and RH, although this relationship was observed in most of the driven attributes.

In an effort to investigate the applicability of driving simulators for the virtual prototyping of vehicles, in this study, changes to the vehicle attributes from a single vehicle property adjustment were evaluated. The results showed drivers could distinguish between the vehicle configurations in the simulator, and their performance varied. However, the vehicle design consists of a range of components such as body shell, powertrain, transmission system, and more research is needed in each section to see if simulators are applicable for virtual prototyping. In fact, the current technology of dynamic simulators is applicable for evaluations of certain aspects of vehicle design but not all.

Depending on the attribute that a vehicle designer wants to study, the simulator motion platform requirement varies. For instance, if the aim is to evaluate the vehicle ride attribute on road asphalts of different quality that create perceivable changes of vertical vibrations, the simulator could have a small translational motion envelope but high bandwidth to capture the differences. Of course, a simulator of large motion envelop but small bandwidth cannot capture the high frequency vehicle vibrations. Ideally a motion platform with both large motion envelope and high bandwidth could be employed for most of the vehicle design evaluations, however there is always a trade-off between the weight of the simulator (payload) and its bandwidth, and of course the pricing, as described in Chapter 3.

9.1.3 Comparison of low and high friction effects

In regard to the motion cueing assessments between the low and high friction road conditions, there have been separate main aims of MCA and RH comparisons in each of the experiments. In addition to a common aim of MP size effect which was evaluated between the similar MP sizes in both road friction conditions. Similar MPC algorithm was used in both low and high friction experiments, while the vehicle motion scaling was linear and nonlinear respectively.

To be able to compare the road friction effect on the evaluations the mutual aim of the effect of MP size is elaborated in this section. The subjective evaluations of perception of realism (fidelity) showed, in the low-friction condition in the LHT task, drivers preferred the medium to large MPs, whereas in the high-friction condition in

the GSP task they preferred the medium MP size; both of the driving tasks were similar in terms of presence of large vehicle motions. A reason for the preference of medium MP over the large in GSP task could be due to incoherence between the visual and vestibular cues in the large MP size. However, the nonlinear scaling makes it difficult to conclude.

The increase of MP size in the low-friction condition in the LHT task reduced values of the aggregated performance metrics such as number of failures, speed variation, and lateral position deviation, and increased the lap time, reflecting improved performance. The time series and driver model metrics such as steering reversal rate, and driver model gain, decreased with the increase of MP size, reflecting a more relaxed style of driving and improved performance.

The increase of MP size in the high-friction condition in the GSP task reduced values of the aggregated performance metrics such as speed variation, and lateral position deviation, and increased the lap time, reflecting improved performance. The time series metrics not significantly changed. The driver model gain parameter decreased, indicative of a more relaxed style of driving and improved performance with the increase of MP size.

Comparing the drivers' performance in both low and high friction experiments, despite the differences it is concludable that increase of MP size has quite a similar effect and have improved their performances when the driving tasks are of similar motion demand.

The evaluation in the low road friction level by nature is more of a complex situation for drivers compared to high friction, and the mental workload is higher which might affect their performance. In other words, there are more uncertainties and variations available to drivers' preferences and performance in low friction testing. The experiment designs of both low/high friction studies are transferable to each other. Although it is expected to obtain similar results in case of using same experiment design and drivers in a swapped road friction condition, due to higher mental workload in low friction drivers' preferences and performance might vary slightly e.g. they may prefer the larger MP size in GSP with low friction condition.

Furthermore, the experiments evaluated in this thesis had two different first aims, and their common aim (about the effect of MP size) was always a second factor. There were major differences between the studies, including the driving tasks, test vehicles and drivers, which brings a high degree of variability to the evaluations and makes it difficult to capture the effects of road friction level. Notwithstanding the differences, similar significant effects were observed on drivers' performance, such

as improved performance with the increase of MP size in both low and high friction conditions.

To merely study the effect of the road friction level on drivers' preferences and performance, it is recommended to design a similar repeated measure experiment where the road friction level is the only independent variable. This will increase the appearance of the effect of manipulation on the road friction level. Use same driving task, test vehicle and drivers in both low and high road friction conditions, to minimise the variability. Moreover, the subjective and objective measurement metrics could be selected among the ones employed in the experiments described in Chapter 5 and 6, to capture the desired qualities.

9.1.4 **Optimisation of motion cueing algorithm and motion platform**

The tuning process of the MCAs in the experiments was based on optimisations or merely trial and errors. Emphasises on the significant effect of the MCA parameters on the motion cueing in the literature and observations during the experiment design, motivated for more detailed exploration of these effects. In Chapter 7 the classic and MPC model parameters were reviewed and their variations effects were measured in the time and frequency domain. The optimal settings that minimise the motion errors, were determined. The frequency analysis of the MPC algorithm was unique and it has never been reported before. These findings could be used as general rules for parameter selection of the MCAs of similar structure.

The guidelines for the optimal settings in each of the MCAs were used for optimisations of the simulator MP translational motion workspace e.g. sliding rail size. In Chapter 8, the available information about the motion cueing fidelities was gathered from the literature and defined fidelity criteria. The optimal setting of the MCAs, in addition to a multi-layered optimisation method was employed to define the required MP workspace to meet the fidelity criteria. The analyses were in the time and frequency domain using the classic MCA, and the lateral motion of the vehicle considered by means of a large data set of recordings from professional drivers in the low-friction experiment.

The tilting and its constraints played a major role in the required MP workspace to compensate. Two possible tilt parameter sets were selected based on the review of the literature about commonly used settings, and human perception thresholds which drove a minimum and maximum MP workspace requirement. The method was tested for the two vehicle testing manoeuvres. For the Land Rover handling track a rail size range of 7 (± 3.5) to 20 (± 10) meters of MP lateral workspace was required to meet the fidelity corridor. For the slalom, this range was between 2 (± 1)

to 3 (± 1.5) meters. Another possible scenario is to fix the MP workspace to certain values and address the tilt settings, to compensate for the remainder of motion. This might help to reduce the MP workspace size, although it will result in higher tilt degree, angular velocity and acceleration, which needs further studies since it may not be desirable on the part of the drivers.

Zeeb (2010) explained that for slalom and lane change manoeuvres with no motion scaling, a lateral motion workspace of ± 4 metres is required with an acceleration limit of 1g. The presented optimisation method could be used for the other translational and yaw rotation DoF of the vehicle motion, where there is always relatively large motion available. Few suggestions were provided, including that the roll and pitch of vehicle are usually in small magnitudes below 5 degrees, same is true for the heave motion of the vehicle which is in range of 16 cm on a flat surface, both could be represented directly by a normal hexapod.

Moreover, to bring the chance of frequency domain comparison between the classic and MPC algorithms for the first time, a sinusoids signal input of different frequencies and amplitude of 2.5 m/s^2 was used in the similar workspace optimisation method. The aim was to find out if the MPC algorithm exploits the MP workspace better than classic, and makes any reduction to the required MP size. It was found that to the same input motion, using optimal settings for both of the MCAs, and meeting the fidelity criteria in the frequency domain the MPC requires slightly less ± 14 metres than classic ± 16 metres to achieve a same level of motion cueing fidelity. It shows using the MPC with optimal tuning it is possible to achieve the same level of fidelity using slightly smaller MP workspace size.

9.2 Contributions to knowledge

The main contributions of this thesis can be summarised as follows:

The subjective perception of drivers between the motion cueing algorithms (MCA) is found to be a function of the vehicle motion in a manoeuvre. The model predictive control algorithm (MPC) was preferred by drivers over the classic one in a large demanding manoeuvre with vehicle motion of a variety of frequencies. Drivers' performance was worsened, and higher steering control activity was observed in MPC compared to classic, demonstrating the incongruity between the subjective preferences and objective performance. In a small demanding manoeuvre with nearly a single frequency, no significant difference was observed on the drivers' preference and their performance, although the effect sizes showed preferences of the classic over MPC.

The differences between the vehicle ride heights (RH) were subjectively distinguishable by the drivers in the simulator, where they found standard and low RH more appropriate for the vehicle in terms of the steering and handling qualities of the vehicle. Drivers' performance was found to be worse in the standard and low RH, and steering control activity was the highest in low vehicle RH in all motion platform sizes and road sections. This also shows the incongruity between the subjective preferences and objective performance; it might hypothetically be originated from the racing style of professional drivers that a preferable vehicle configuration has resulted in their higher speed variability, lateral position deviations and steering control activity i.e. worse performance.

The effects of motion platform (MP) workspace size was found to be dependent on the driving task and road friction level. In low-friction condition, the increase of MP size was preferred/undesirable in the large/small motion demanding manoeuvre. Drivers' performance improved/worsened, and the steering control activity reduced/unchanged in large/small motion demanding manoeuvres. In high-friction large motion demanding manoeuvre medium size was preferred in terms of overall realism. For most of the handling and steering quality attributes in the higher RH the larger MP was selected as more appropriate, and vice versa. Drivers' performance improvement was observed, and implications of reduction of steering control activity.

A tuning method was introduced for optimisation of the MPC and classic algorithms in both time and frequency domains. A conservative motion cueing fidelity criterion was defined based on the review of literature and data obtained from the experiments. A multi-layered optimisation method was developed that uses the optimal setting of the MCA, to address the MP translational workspace size to meet the fidelity criteria, applicable for various manoeuvres. It was found that to the same input motion using the MPC it is possible to achieve the same level of fidelity using slightly smaller MP workspace size.

The main aims in this thesis were to study the effects of motion cueing, and design of a vehicle in simulator. Subsequently, the assessments were based on the perception and performance of professional drivers who typically evaluate the vehicle designs and often have higher standards. Thus, the presented conclusions are more applicable to the vehicle design process. It is well worth to conduct a similar experiment(s) and model optimisations with normal drivers and compare its outcomes. Availability of a higher number of normal drivers will help to draw more solid conclusions on differences between MCAs, vehicle RHs, and preferences of MP workspace size. It is possible to anticipate observing lower requirements for the simulator motion systems since normal drivers often have lower demands.

9.3 Study Limitations

The major limitation of this study was the number of participants in both of the experiments. Although the participating drivers were all the professionals from related groups of the vehicle evaluation teams in JLR, there was a limitation on the available number of participants. Moreover, commuting times to/from JLR to Leeds and associated risks factors limited efficient available time for the experiments. A higher number of drivers could have strengthened the statistical power in the analysis of data; however, this issue has been tried to be addressed by analysis of the effect sizes.

This thesis was mainly dedicated to considering the effect of the motion cueing in the simulators and its effects on subjective fidelity and exploration of the drivers' performance. However, having real world equivalent data to compare the driver behaviour performance between the real and virtual environment could bring the possibility for further enhancement in the MCA tuning, and optimisation of the MP workspace size from the perceptual level to the behavioural level.

In the described experiments the drivers' perception of self-motion was restricted to the effects of the vestibular motion cues. However, due to visual-vestibular interactions, the visual cues also play an important role. Moreover, the other audio and haptic cues have an influence on drivers' perception and performance that is worth to be investigated. To study the effects of these cues, more restricted driving tasks should be selected to maximise the appearance of the experimental manipulations, and appropriate measurement metrics should be employed.

The introduced optimisation method for tuning of the model predictive control algorithm in the frequency domain requires several hours of offline simulations, it further intensifies in the multi-layered optimisation of the motion platform workspace. Therefore, it was needed to use a fixed set of optimal parameters for the inner-loop to reduce the computational burden.

The introduced optimal tuning of the MCAs and MP workspace size did not consider the vehicle model and MP dynamics. The reason was to reduce the computation burden and unpredicted variability during the optimisations. Considering the dynamics could further optimise the MCA tunings and the MP workspace sizing.

9.4 Potential for future work

The introduced optimal tuning parameters for the MCAs showed the possibility of obtaining a few sets of optimal parameters that minimise the motion errors and

meet the fidelity criteria in the offline analysis. Despite being candidates from offline analysis, further experiments could be conducted to compare them based on drivers' subjective perception and performance.

There are other parameters in the MPC algorithm affecting the motion cueing, those are the prediction and control horizons, fixed or variable look-ahead information. Although the choice of these parameters is more restricted by the computational burden and estimation of reference input, it is worth having a similar offline analysis, and experiments to be able to address their effects and optimal values.

The MP workspace optimisation could be employed as a generalised method for MP workspace sizing for the vehicle motions in any manoeuvre. It is possible to do a similar analysis for the data collected in the high-friction vehicle attribute evaluation experiment.

The analysis of the optimal parameters for MCA and MP workspace size were based on using vehicle lateral motion during manoeuvres. However, the introduced methods are general and could be used for the longitudinal motion of the vehicle and might slightly vary the obtained results.

The MP workspace optimisation considered the vehicle motion data from the performance of professional drivers, which meets the workspace requirement for the vehicle design purpose. Using data collected from normal drivers, same approach could be used to address the workspace size for other applications e.g. research or training.

Further research in time and frequency domain for finding the motion cueing fidelity criteria in all degrees of freedom of vehicle motion is a valuable and essential need in driving simulators since it helps to define the MCA tuning and MP workspace more optimally.

By developing and extending the experimental design and scenario it is possible to address other issues such as the drivers' mental efforts, simulator sickness while evaluating their perception and behaviour.

In the experiments, the effects of the vestibular motion cueing were studied in one UoLDS dynamic driving simulator. Transferability of the similar experiments in another simulator with different/similar visual and vestibular characteristics is a worthwhile future research topic.

References

- AbuAli, N. and Abou-zeid, H. 2016. Driver behavior modeling: Developments and future directions. *International Journal of Vehicular Technology*. p12.
- Advani, S. 1998. *The Kinematic design of flight simulator motion bases*. Ph.D. thesis, Delft University of Technology.
- Advani, S., Hosman, R. and Haeck, N. 2002. Integrated design of a motion cueing algorithm and motion-base mechanism for a wright flyer simulator. In: *AIAA Modeling and Simulation Technologies Conference and Exhibit, Monterey, California*. American Institute of Aeronautics and Astronautics.
- AGARD. 1977. *Dynamic characteristics of flight simulator motion systems*. North Atlantic treaty organization advisory group for aerospace research and development.
- AGARD. 1980. *Fidelity of simulation for pilot training* North Atlantic treaty organization advisory group for aerospace research and development.
- Allen, R.W., Rosenthal, T.J. and Cook, M.L. 2011. A short history of driving simulation. *Handbook of Driving Simulation for Engineering, Medicine, and Psychology*. CRC Press.
- Anon. 2015. *Operational definitions of driving performance measures and statistics*. SAE International.
- Asadi, H., Mohamed, S., Lim, C.P. and Nahavandi, S. 2016. A review on otolith models in human perception. *Behavioural Brain Research*. **309**, pp.67-76.
- Asadi, H., Mohamed, S., Lim, C.P., Nahavandi, S. and Nalivaiko, E. 2017. Semicircular canal modeling in human perception. *Reviews in the Neurosciences*. **28**(5), pp.537-549.
- Asadi, H., Mohamed, S., Rahim Zadeh, D. and Nahavandi, S. 2015. Optimisation of nonlinear motion cueing algorithm based on genetic algorithm. *Vehicle System Dynamics*. **53**(4), pp.526-545.
- Augusto, B. and Loureiro, R. 2009. *Motion cueing in the Chalmers driving simulator-A model predictive control approach*. M.Sc. thesis, Chalmers university of technology.
- Bailey, A.C., Jamson, A.H., Wright, S. and Parkes, A.M. 1999. Recent and future development of the Leeds Driving Simulator. In: *Driving Simulation Conference (DSC), Paris, France*.
- Bemporad, A., Morari, M., Dua, V. and Pistikopoulos, E.N. 2002. The explicit linear quadratic regulator for constrained systems. *Automatica*. **38**(1), pp.3-20.
- Berthoz, A., Bles, W., Bühlhoff, H.H., Grácio, B.C., Feenstra, P., Filliard, N., Hühne, R., Kemeny, A., Mayrhofer, M. and Mulder, M. 2013. Motion scaling for high-performance driving simulators. *IEEE Transactions on Human-Machine Systems*. **43**(3), pp.265-276.
- Bertollini, G.P. and Hogan, R.M. 1999. Applying driving simulation to quantify steering effort preference as a function of vehicle speed. *SAE Technical Paper*.
- Bigler, R.S. 2013. *Automobile driver sensory system modeling*. Ph.D. thesis, University of Cambridge.
- Blana, E. 1996. *Driving simulator validation studies: A literature review* Institute of Transport Studies, University of Leeds
- Boer, E.R. 1996. Tangent point oriented curve negotiation. In: *Conference on Intelligent Vehicles, 19-20 Sept. 1996*, pp.7-12.

- Boer, E.R. 1999. Car following from the driver's perspective. *Transportation Research Part F: Traffic Psychology and Behaviour*. **2**(4), pp.201-206.
- Boer, E.R., Jamson, A.H., Advani, S.K., Horrobin, A.J. and Breda, N. 2014. Are we there yet? An objective mechanism to support the assessment of driving simulator utility. In: *Driving Simulation Conference (DSC), Paris, France*. pp.4-5.
- Boyd, S. and Vandenberghe, L. 2004. *Convex optimization*. Cambridge university press.
- Brandt, T., Dichgans, J. and Koenig, E. 1973. Differential effects of central versus peripheral vision on egocentric and exocentric motion perception. *Experimental Brain Research*. **16**(5), pp.476-491.
- Brems, W., van Doornik, J., de Vries, E. and Wiedemann, J. 2015. Frequency response and latency analysis of a driving simulator for chassis development and vehicle dynamics evaluation. In: *Driving Simulation Conference (DSC), Tübingen, Germany*.
- Bruschetta, M., Cenedese, C. and Beghi, A. 2017. A real-time, mpc-based motion cueing algorithm with look-ahead and driver characterization. *Transportation Research Part F: Traffic Psychology and Behaviour*. **61**, pp.38-52.
- Bulirsch, R., Vögel, M., von Stryk, O., Chucholowski, C. and Wolter, T.-M. 2003. An optimal control approach to real-time vehicle guidance. *Mathematics - Key technology for the future*. Springer, pp.84-102.
- Carsten, O. and Jamson, A.H. 2011. Driving simulators as research tools in traffic psychology. *Handbook of Traffic Psychology*. pp.87-96.
- Chao, J., Shen, J., Chen, W. and Jiang, G. 2014. New signal scaling strategies for return phase training in motion-base spaceflight simulator. *Institution of Mechanical Engineers Part G: Journal of Aerospace Engineering*. **228**(4), pp.483-491.
- Chapron, T. and Colinot, J.-P. 2007. The new PSA Peugeot-Citroën Advanced Driving Simulator Overall design and motion cue algorithm. In: *DSC 2007 North America*.
- Chen, D.C. and Crolla, D.A. 1998. Subjective and objective measures of vehicle handling: drivers & experiments. *Vehicle System Dynamics*. **29**(S1), pp.576-597.
- Chong, L., Abbas, M.M., Medina Flintsch, A. and Higgs, B. 2013. A rule-based neural network approach to model driver naturalistic behavior in traffic. *Transportation Research Part C: Emerging Technologies*. **32**, pp.207-223.
- Clark, A., Sparks, H. and Carmein, J. 2001. Unique features and capabilities of the NADS motion system In: *17th International Technical Conference on the Enhanced Safety of Vehicles*.
- Clark, A.J., Sparks, H.V. and Carmein, J.A. 2001. Unique Features and Capabilities of the NADS Motion System. *SAE International*
- Cohen, J. 1992. A power primer. *Psychol Bull*. **112**(1), pp.155-159.
- Cole, D.J., Pick, A.J. and Odhams, A.M.C. 2006. Predictive and linear quadratic methods for potential application to modelling driver steering control. *Vehicle System Dynamics*. **44**(3), pp.259-284.
- Colombet, F., Dagdelen, M., Reymond, G., Pere, C., Merienne, F. and Kemeny, A. 2008. Motion cueing: What is the impact on the driver's behavior. In: *Driving Simulation Conference (DSC), January Europe, Monaco*. pp.171-181.

- Colombet, F., Fang, Z. and Kemeny, A. 2016. Tilt thresholds for acceleration rendering in driving simulation. *SIMULATION*. **93**(7), pp.595-603.
- Conrad, B. and Schmidt, S. 1969. *The calculation of motion drive signals for piloted flight simulators*. NASA Technical Reports Server (NTRS).
- Conrad, B. and Schmidt, S. 1970. *Motion drive signals for piloted flight simulators*. NASA Technical Reports Server (NTRS).
- Conrad, B., Schmidt, S. and Douvillier, J. 1973. Washout circuit design for multi-degrees-of-freedom moving base simulators. In: *Visual and Motion Simulation Conference, Palo Alto, CA, U.S.A.*: American Institute of Aeronautics and Astronautics.
- Correia Grácio, B.J., Bos, J.E., van Paassen, M.M. and Mulder, M. 2014. Perceptual scaling of visual and inertial cues: effects of field of view, image size, depth cues, and degree of freedom. *Experimental Brain Research*. **232**(2), pp.637-646.
- Correia Grácio, B.J., Pais, A.R.V., van Paassen, M.M., Mulder, M., Kelly, L.C. and Houck, J.A. 2013. Optimal and coherence zone comparison within and between flight simulators. *Journal of Aircraft*. **50**(2), pp.493-507.
- Correia Grácio, B.J., van Paassen, M., Mulder, M. and Wentink, M. 2010. Tuning of the lateral specific force gain based on human motion perception in the desdemona simulator. In: *AIAA Modeling and Simulation Technologies Conference, Toronto, Ontario, Canada*. American Institute of Aeronautics and Astronautics.
- Dagdelen, M., Reymond, G., Kemeny, A., Bordier, M. and Maïki, N. 2004. MPC based motion cueing algorithm: Development and application to the ULTIMATE driving simulator. In: *Driving Simulation Conference (DSC), Paris, France* pp.221-233.
- Dagdelen, M., Reymond, G., Kemeny, A., Bordier, M. and Maïzi, N. 2009. Model-based predictive motion cueing strategy for vehicle driving simulators. *Control Engineering Practice*. **17**(9), pp.995-1003.
- De Winter, J., Van Leeuwen, P. and Happee, R. 2012. Advantages and disadvantages of driving simulators: A discussion. In: *8th International Conference on Methods and Techniques in Behavioral Research, Utrecht, Netherlands*. Citeseer, pp.47-50.
- Donges, E. 1978. A two-level model of driver steering behavior *Human Factors*. **20**(6), pp.691-707.
- Drosdol, J. and Panik, F. 1985. The Daimler-Benz driving simulator a tool for vehicle development *SAE Technical Paper*.
- Edelmann, J., Plöchl, M., Reinalter, W. and Tieber, W. 2007. A passenger car driver model for higher lateral accelerations. *Vehicle System Dynamics*. **45**(12), pp.1117-1129.
- Fang, Z. and Kemeny, A. 2012a. Explicit MPC motion cueing algorithm for real-time driving simulator. In: *7th International Power Electronics and Motion Control Conference (IPEMC), 2-5 June 2012*, pp.874-878.
- Fang, Z. and Kemeny, A. 2012b. Motion cueing algorithms for a real-time automobile driving simulator. In: *Driving Simulation Conference (DSC), Paris, France*. pp.159-174.
- Fang, Z. and Kemeny, A. 2014. Review and prospects of Renault's MPC based motion cueing algorithm for driving simulator. In: *Driving Simulation Conference (DSC), September Paris, France*

- Fang, Z. and Kemeny, A. 2016. An efficient Model Predictive Control-based motion cueing algorithm for the driving simulator. *SIMULATION*. **92**(11), pp.1025-1033.
- Feenstra, P., Van Der Horst, R., Grácio, B.J.C. and Wentink, M. 2010. Effect of simulator motion cuing on steering control performance: Driving simulator study. *Transportation Research Record*. **2185**(1), pp.48-54.
- Fernandez, C. and Goldberg, J.M. 1971. Physiology of peripheral neurons innervating semicircular canals of the squirrel monkey. II. Response to sinusoidal stimulation and dynamics of peripheral vestibular system. *Journal of Neurophysiology*. **34**(4), pp.661-675.
- Fernandez, C. and Goldberg, J.M. 1976. Physiology of peripheral neurons innervating otolith organs of the squirrel monkey. III. Response dynamics. *Journal of Neurophysiology*. **39**(5), pp.996-1008.
- Fetsch, C.R., DeAngelis, G.C. and Angelaki, D.E. 2013. Bridging the gap between theories of sensory cue integration and the physiology of multisensory neurons. *Nature Reviews Neuroscience*. **14**(6), pp.429-442.
- Fetsch, C.R., Turner, A.H., DeAngelis, G.C. and Angelaki, D.E. 2009. Dynamic reweighting of visual and vestibular cues during self-motion perception. *Journal of Neuroscience*. **29**(49), pp.15601-15612.
- Field, A. 2013. *Discovering statistics using IBM SPSS statistics*. sage.
- Fischer, M., Seefried, A. and Seehof, C. 2016. Objective motion cueing test for driving simulators. In: *Driving simulation conference (DSC)*, pp.41-50.
- Fischer, M., Sehammar, H., Ljung Aust, M., Nilsson, M., Lazic, N. and Weiefors, H. 2011. Advanced driving simulators as a tool in early development phases of new active safety functions. In: *3rd International Conference on Road Safety and Simulation, 12/01, Indianapolis, USA*. pp.171-182.
- Fischer, M. and Werneke, J. 2008. The new time-variant motion cueing algorithm for the DLR Dynamic Driving Simulator. In: *Driving Simulation Conference (DSC), January Europe, Monaco*.
- Fisher, D.L., Caird, J., Rizzo, M. and Lee, J.D. 2011. An overview *Handbook of Driving Simulation for Engineering, Medicine, and Psychology*. CRC Press.
- Fisher, R.A. 1992. *Statistical methods for research workers*. New York, NY: Springer New York.
- Freeman, J.S., Watson, G., Papelis, Y.E., Lin, T.C., Tayyab, A., Romano, R.A. and Kuhl, J.G. 1995. The Iowa driving simulator: An implementation and application overview. *SAE Technical Paper*.
- Garrett, N.J.I. and Best, M.C. 2013. Model predictive driving simulator motion cueing algorithm with actuator-based constraints. *Vehicle System Dynamics*. **51**(8), pp.1151-1172.
- Gawthrop, P., Gollee, H. and Loram, I. 2014. Intermittent control in man and machine. *arXiv preprint*.
- Ghazi Zadeh, A., Fahim, A. and El-Gindy, M. 1997. Neural network and fuzzy logic applications to vehicle systems: literature survey. *International Journal of Vehicle Design*. **18**(2), pp.132-193.
- Gibson, J.J. 1950. *The perception of the visual world*. Oxford, England: Houghton Mifflin.
- Gil Gómez, G.L., Nybacka, M., Bakker, E. and Drugge, L. 2015. Findings from subjective evaluations and driver ratings of vehicle dynamics: steering and handling. *Vehicle System Dynamics*. **53**(10), pp.1416-1438.

- Goldfarb, D. and Idnani, A. 1983. A numerically stable dual method for solving strictly convex quadratic programs. *Mathematical Programming*. **27**(1), pp.1-33.
- Gonçalves, J.P. and Ambrósio, J.A. 2005. Road vehicle modeling requirements for optimization of ride and handling. *Multibody System Dynamics*. **13**(1), pp.3-23.
- Gordon, D.A. 1965. Static and dynamic visual fields in human space perception. *Journal of the Optical Society of America*. **55**(10), pp.1296-1303.
- Gordon, T. and Magnuski, N. 2006. Modeling normal driving as a collision avoidance process. In: *8th International Symposium on Advanced Vehicle Control*.
- Grant, P.R., Artz, B., Greenberg, J.D. and Cathey, L. 2001. Motion characteristics of the VIRTTEX motion system In: *Human-Centred Transportation Simulation Conference, University of IOWA*.
- Grant, P.R., Blommer, M., Artz, B. and Greenberg, J. 2009. Analysing classes of motion drive algorithms based on paired comparison techniques. *Vehicle System Dynamics*. **47**(9), pp.1075-1093.
- Grant, P.R., Blommer, M., Cathey, L., Artz, B. and Greenberg, J. 2003. Analyzing classes of motion drive algorithms based on paired comparison techniques. In: *Driving Simulation Conference (DSC), Dearborn, North America*.
- Grant, P.R. and Naseri, A. 2005. Actuator state based adaptive motion drive algorithm. In: *Driving Simulation Conference (DSC), November North America - Orlando*. pp.30-39.
- Grant, P.R. and Reid, L.D. 1997. Motion washout filter tuning: Rules and requirements. *Journal of Aircraft*. **34**(2), pp.145-151.
- Greenberg, J. and Blommer, M. 2011. Physical fidelity of driving simulators. *Handbook of Driving Simulation for Engineering, Medicine, and Psychology*. CRC Press.
- Groen, E.L. and Bles, W. 2004. How to use body tilt for the simulation of linear self motion. *Journal of Vestibular Research*. **14**(5), pp.375-385.
- Groen, E.L., Valenti Clari, M.S.V. and Hosman, R.J.A.W. 2001. Evaluation of perceived motion during a simulated takeoff run. *Journal of Aircraft*. **38**(4), pp.600-606.
- Guo, K. and Guan, H. 1993. Modelling of driver/vehicle directional control system. *Vehicle System Dynamics*. **22**(3-4), pp.141-184.
- Hassan, B. 2014. *A design framework for developing a reconfigurable driving simulator*. Ph.D. thesis, Paderborn, Universität Paderborn.
- Hoffmann, E.R. 1976. Human control of road vehicles. *Vehicle System Dynamics*. **5**(1-2), pp.105-126.
- Hosman, R. 1996. *Pilot's perception in the control of aircraft motions*. Ph.D. thesis, Delft University of Technology.
- Hosman, R. and Advani, S. 2016. Design and evaluation of the objective motion cueing test and criterion. *The Aeronautical Journal*. **120**(1227), pp.873-891.
- Hosman, R., Cardullo, F. and Bos, J. 2011. Visual-Vestibular interaction in motion perception. In: *AIAA Modeling and Simulation Technologies Conference, Portland, Oregon*. American Institute of Aeronautics and Astronautics.
- Hosman, R. and Stassen, H. 1999. Pilot's perception in the control of aircraft motions. *Control Engineering Practice*. **7**(11), pp.1421-1428.

- Hosman, R. and van der Vaart, J. 1978. *Vestibular models and thresholds of motion perception. Results of tests in a flight simulator.* Delft University of Technology.
- Jamson, A.H. 2010. *Motion cueing in driving simulators for research applications.* Ph.D. thesis, University of Leeds.
- Jamson, A.H., Boer, E.R., Advani, S., Cotgrove, T., Bishop, J. and Chappel, P. 2013. *PSI Theme 3 Milestone 2 Deliverable: Assessment of Driving Simulator Verification Plan.* Unpublished.
- Jamson, A.H., Boer, E.R. and Bean, A. 2015. *PSI Theme 3 Milestone 3.0.4 Deliverable: Development of environments to support 3.0 simulator utility data collection.* Unpublished.
- Jamson, A.H., Boer, E.R. and Salter, S. 2014a. *PSI Theme 3 Milestone 3 Deliverable: Toward the Development of a Driving Simulator Standard and Functionality Matrix.* Unpublished.
- Jamson, A.H., Boer, E.R., Salter, S. and Bean, A. 2014b. *PSI Theme 3 Milestones 3.1.2 & 3.2.2 Deliverable: Establishment of test-cases and basis tasks for 3.1 and 3.2 to follow the Common Experimental Approach.* Unpublished.
- Jex, H.R., Magdaleno, R.E. and Junker, A.M. 1978. *Roll tracking effects of G-vector tilt and various types of motion washout.* NASA Technical Reports Server (NTRS).
- Jones, G.M., Barry, W. and Kowalsky, N. 1964. Dynamics of the semicircular canals compared in yaw, pitch and roll. *Aerospace Medicine.* **35**, pp.984-989.
- Käding, W. and Hoffmeyer, F. 1995a. The Advanced Daimler-Benz Driving Simulator. In: SAE International.
- Käding, W. and Hoffmeyer, F. 1995b. The advanced Daimler-Benz driving simulator. *SAE Technical Paper.*
- Kandel, E.R., Schwartz, J.H., Jessell, T.M., Siegelbaum, S.A. and Hudspeth, A.J. 2000. *Principles of neural science.* McGraw-hill New York.
- Kemeny, A. and Panerai, F. 2003. Evaluating perception in driving simulation experiments. *Trends in Cognitive Sciences.* **7**(1), pp.31-37.
- Knapp, J.L.J. 2003. Visual perception of egocentric distance in real and virtual environments. *Virtual and Adaptive Environments.* CRC Press, pp.35-60.
- Kondo, M. 1953. Directional stability (when steering is added). *Journal of the Society of Automotive Engineers of Japan (JSAE).* **7**(5-6), p9.
- Kondo, M. and Ajimine, A. 1968. Driver's sight point and dynamics of the driver-vehicle-system related to it. *SAE Technical Paper.*
- Kurosaki, M. 1978. Optimal washout for control of a moving base simulator. In: *IFAC Proceedings Volumes, January, United Kingdom.* pp.1311-1318.
- Lakerveld, P.R., Damveld, H.J., Pool, D.M., Van der El, K., Van Paassen, M.M. and Mulder, M. 2016. The effects of yaw and sway motion cues in curve driving simulation. *IFAC-PapersOnLine.* **49**(19), pp.500-505.
- Macadam, C.C. 1981. Application of an optimal preview control for simulation of closed-loop automobile driving *IEEE Transactions on Systems, Man, and Cybernetics.* **11**(6), pp.393-399.
- Macadam, C.C. 2003. Understanding and modeling the human driver. *Vehicle System Dynamics.* **40**(1-3), pp.101-134.
- Maciejowski, J.M. 2002. *Predictive control: with constraints.* Pearson education.

- Maran, F. 2013. *Model-based control techniques for automotive applications*. Ph.D. thesis, University of Padova.
- Mark, W., Jelte, B., Eric, G. and Ruud, H. 2006. Development of the motion perception toolbox. In: *AIAA Modeling and Simulation Technologies Conference and Exhibit, Keystone, Colorado*. American Institute of Aeronautics and Astronautics.
- Markkula, G. 2014. Modeling driver control behavior in both routine and near-accident driving. *Human Factors and Ergonomics Society Annual Meeting*. **58**(1), pp.879-883.
- Markkula, G. 2015. *Driver behavior models for evaluating automotive active safety: From neural dynamics to vehicle dynamics*. Ph.D. thesis, Chalmers University of Technology.
- Markkula, G., Benderius, O. and Wahde, M. 2014. Comparing and validating models of driver steering behaviour in collision avoidance and vehicle stabilisation. *Vehicle System Dynamics*. **52**(12), pp.1658-1680.
- Markkula, G., Boer, E., Romano, R. and Merat, N. 2018a. Sustained sensorimotor control as intermittent decisions about prediction errors: computational framework and application to ground vehicle steering. *Biological Cybernetics*. **112**(3), pp.181-207.
- Markkula, G., Boer, E.R., Romano, R., Jamson, A.H., Andrew, T., Horrobin, A. and Bean, A. 2016. *PSI Theme 3 Milestones 3.1.4/3.4.4 Deliverable: Model-Supported Assessment of Simulator Utility for Winter Testing*. Unpublished.
- Markkula, G., Romano, R., Jamson, A.H., Pariota, L., Bean, A. and Boer, E. 2018b. Using driver control models to understand and evaluate behavioural validity of driving simulators. *IEEE Transactions on Human-Machine Systems*. **48**, pp.592-603.
- Markkula, G., Romano, R., Sadraei, E., Jukic, H., Horrobin, A., Tomlinson, A., Jamson, A.H., Giles, O. and Pariota, L. 2017. *PSI Theme 3 Milestone 3.5.6b Assessment of driving simulator utility for driven attributes testing*. Unpublished.
- Markkula, G., Romano, R., Waldram, R., Giles, O., Mole, C.D. and Wilkie, R.M. 2018c. Modelling visual-vestibular integration and behavioural adaptation in the driving simulator. In: *Driving Simulation Conference (DSC), Antibes, France*.
- Markkula, G., Romano, R., Waldram, R., Giles, O., Mole, C.D. and Wilkie, R.M. 2018d. Modelling visual-vestibular integration and behavioural adaptation in the driving simulator. *arXiv preprint*. **1810.12441**.
- MathWorks. 2016a. *Model predictive control QP solver: User's guide*. [Online]. Available from: <https://uk.mathworks.com/help/mpc/ug/qp-solver.html#buj93q0>
- Mayr, R. and Freund, E. 1992. On the design of nonlinear path control in automated vehicle guidance. In: *IEEE/RSJ International Conference on Intelligent Robots and Systems, 7-10 July 1992*, pp.613-620.
- Mayrhofer, M. 2009. *The most modern simulator motion platform, WORKSHOP, E.F.T.S., [Exhibition catalogue]*. Vienna, Austria.
- McRuer, D.T., Allen, R.W., Weir, D.H. and Klein, R.H. 1977. New results in driver steering control models. *Human Factors*. **19**(4), pp.381-397.
- McRuer, D.T. and Graham, D. 1965. *Human pilot dynamics in compensatory systems*. Systems technology.

- Meiry, J.L. 1966. *The vestibular system and human dynamic space orientation*. 1966/11/01 ed. NASA Technical Reports Server (NTRS).
- Meyer, D.E., Abrams, R.A., Kornblum, S., Wright, C.E. and Keith Smith, J. 1988. Optimality in human motor performance: ideal control of rapid aimed movements. *Psychological Review*. **95**(3), p340.
- Mohajer, N., Abdi, H. and Nahavandi, S. 2017. Dynamic response multiobjective optimization of road vehicle ride quality - A computational multibody system approach. *Institution of Mechanical Engineers Part D: Journal of Automobile Engineering*. **231**(2), pp.316-332.
- Mohammadi, A., Asadi, H., Mohamed, S., Nelson, K. and Nahavandi, S. 2018. Optimizing model predictive control horizons using genetic algorithm for motion cueing algorithm. *Expert Systems with Applications*. **92**, pp.73-81.
- Nahon, M.A. and Reid, L.D. 1990. Simulator motion-drive algorithms - A designer's perspective. *Journal of Guidance, Control, and Dynamics*. **13**(2), pp.356-362.
- Nahon, M.A., Reid, L.D. and Kirdeikis, J. 1992. Adaptive simulator motion software with supervisory control. *Journal of Guidance, Control, and Dynamics*. **15**(2), pp.376-383.
- Naseri, H., Nahvi, A. and Salimi Naneh Karan, F. 2015. A new psychological methodology for modeling real-time car following maneuvers. *Travel Behaviour and Society*. **2**(2), pp.124-130.
- Naseri, H., Nahvi, A. and Salimi Naneh Karan, F. 2017. A real-time lane changing and line changing algorithm for driving simulators based on virtual driver behavior. *Journal of Simulation*. **11**(4), pp.357-368.
- Nash, C.J. and Cole, D.J. 2016. Development of a novel model of driver-vehicle steering control incorporating sensory dynamics. *The Dynamics of Vehicles on Roads and Tracks: Proceedings of the 24th International Symposium on Dynamics of Vehicles on Roads and Tracks*.
- Nash, C.J. and Cole, D.J. 2018. Modelling the influence of sensory dynamics on linear and nonlinear driver steering control. *Vehicle System Dynamics*. **56**(5), pp.689-718.
- Nash, C.J. and Cole, D.J. 2019. Identification and validation of a driver steering control model incorporating human sensory dynamics. *Vehicle System Dynamics*. pp.1-23.
- Nash, C.J., Cole, D.J. and Bigler, R.S. 2016. A review of human sensory dynamics for application to models of driver steering and speed control. *Biological Cybernetics*. **110**(2), pp.91-116.
- Nehaoua, L., Mohellebi, H., Amouri, A., Arioui, H., Espie, S. and Kheddar, A. 2008. Design and control of a small-clearance driving simulator *IEEE Transactions on Vehicular Technology*. **57**(2), pp.736-746.
- Neyman, J. and Pearson, E.S. 1933. On the problem of the most efficient tests of statistical hypotheses. *Philosophical Transactions of the Royal Society of London*. **231**, pp.289-337.
- Nieuwenhuizen, F.M. and Bulthoff, H.H. 2013. The MPI cybermotion simulator: a novel research platform to investigate human control behavior. *Journal of Computing Science and Engineering*. **7**(2), pp.122-131.
- Nieuwenhuizen, F.M. and Bülthoff, H.H. 2013. The MPI CyberMotion Simulator: A Novel Research Platform to Investigate Human Control Behavior. *Journal of Computing Science and Engineering*.
- Nordmark, S., Lidstrom, M. and Palmkvist, G. 1984. Moving base driving simulator with wide angle visual system. *SAE Technical Paper*.

- Nybacka, M., He, X., Su, Z., Drugge, L. and Bakker, E. 2014. Links between subjective assessments and objective metrics for steering, and evaluation of driver ratings. *Vehicle System Dynamics*. **52**, pp.31-50.
- Odhams, A.M. and Cole, D.J. 2004. Models of driver speed choice in curves. In: *7th International Symposium on Advanced Vehicle Control*: Citeseer.
- Ormsby, C.C. 1974. *Model of human dynamic orientation*. Ph.D. thesis, Massachusetts Institute of Technology.
- Parrish, R.V., Dieudonne, J.E. and Martin Jr, D.J. 1975. Coordinated adaptive washout for motion simulators. *Journal of Aircraft*. **12**(1), pp.44-50.
- Peters, R.A. 1969. *Dynamics of the vestibular system and their relation to motion perception, spatial disorientation, and illusions*. 1969/01/01 ed. NASA Technical Reports Server (NTRS).
- Plöchl, M. and Edelmann, J. 2007. Driver models in automobile dynamics application. *Vehicle System Dynamics*. **45**(7-8), pp.699-741.
- Plöchl, M. and Lugner, P. 1999. A 3-level driver model and its application to driving simulations. In: *Vehicle System Dynamics Supplement, Pretoria, South africa*.
- Pool, D.M. 2012. *Objective evaluation of flight simulator motion cueing fidelity through a cybernetic approach*. Ph.D. thesis, Delft University of Technology.
- Rauh, J.J. 2003. Virtual development of ride and handling characteristics for advanced passenger cars. *Vehicle System Dynamics*. **40**(1-3), pp.135-155.
- Reid, L.D. 1983. A survey of recent driver steering behavior models suited to accident studies. *Accident Analysis & Prevention*. **15**(1), pp.23-40.
- Reid, L.D. and Nahon, M.A. 1985. *Flight simulation motion-base drive algorithms: Part 1 - developing and testing the equations*. University of Toronto, Institute for Aerospace Studies
- Reid, L.D. and Nahon, M.A. 1986a. *Flight simulation motion-base drive algorithms: Part 2 - selecting the system parameters*. University of Toronto, Institute for Aerospace Studies
- Reid, L.D. and Nahon, M.A. 1986b. *Flight simulation motion-base drive algorithms: Part 3 – pilot evaluations*. University of Toronto, Institute for Aerospace Studies
- Reid, L.D. and Nahon, M.A. 1988. Response of airline pilots to variations in flight simulator motion algorithms. *Journal of Aircraft*. **25**(7), pp.639-646.
- Repa, B.S., Leucht, P.M. and Wierwille, W.W. 1981. *The influence of motion cues on driver-vehicle performance in a simulator*. NASA Technical Reports Server (NTRS).
- Reymond, G., Droulez, J., Berthoz, A. and Kemeny, A. 1999. Contribution of a motion platform to kinesthetic restitution in a driving simulator. In: *Driving Simulation Conference (DSC)*.
- Reymond, G. and Kemeny, A. 2000. Motion Cueing in the Renault Driving Simulator. *Vehicle System Dynamics*. **34**(4), pp.249-259.
- Reymond, G., Kemeny, A., Droulez, J. and Berthoz, A. 2001. Role of lateral acceleration in curve driving: Driver model and experiments on a real vehicle and a driving simulator. *Human factors*. **43**(3), pp.483-495.
- Richalet, J., Rault, A., Testud, J.L. and Papon, J. 1978. Model predictive heuristic control: Applications to industrial processes. *Automatica*. **14**(5), pp.413-428.
- Riemersma, J.B. 1981. Visual control during straight road driving. *Acta Psychol (Amst)*. **48**(1-3), pp.215-225.

- Romano, R. 1999. *Motion control logic for large excursion driving simulators*. Ph.D. thesis, University of Iowa.
- Romano, R. 2003. Non-linear optimal tilt coordination for washout algorithms In: *AIAA Modeling and Simulation Technologies Conference and Exhibit, Austin, Texas*. American Institute of Aeronautics and Astronautics.
- Romano, R., Markkula, G., Boer, E., Jamson, H., Bean, A., Tomlinson, A., Horrobin, A. and Sadraei, E. 2019. An objective assessment of the utility of a driving simulator for low mu testing. *Transportation Research Part F: Traffic Psychology and Behaviour*. **65**, pp.34-45.
- Romano, R., Park, G.D., Paul, V. and Allen, R.W. 2016. Motion cueing evaluation of off-road heavy vehicle handling *SAE Technical Paper*.
- Romano, R., Sadraei, E. and Markkula, G. 2017. Rapid tuning of the classical motion cueing algorithm. In: *Driving Simulation Conference (DSC), Stuttgart, Germany*.
- Rothhämel, M., IJkema, J. and Drugge, L. 2011. A method to find correlations between steering feel and vehicle handling properties using a moving base driving simulator. *Vehicle System Dynamics*. **49**(12), pp.1837-1854.
- Sadraei, E., Romano, R., Advani, S., Jamson, A., Chappell, P., Markkula, G., Bean, A. and Boer, E. 2016. Understanding Cue Utility in Controlled Evasive Driving Manoeuvres: Optimizing Vestibular Cues for Simulator & Human Abilities. *IFAC-PapersOnLine*. **49**(19), pp.414-419.
- Sadraei, E., Romano, R., Jamson, S., Markkula, G. and Jamson, H. 2018. Driving simulator motion base right sizing. In: *Driving Simulation Conference (DSC), Antibes, France*.
- Savona, F., Stratulat, A.M., Diaz, E., Honnet, V., Houze, G., Vars, P., Masfrand, S., Roussarie, V. and Bourdin, C. 2014. The influence of lateral, roll and yaw motion gains on driving performance on an advanced dynamic simulator. In: *6th International Conference on Advances in System Simulation*.
- Schmid, C. and Biegler, L.T. 1994. Quadratic programming methods for reduced hessian SQP. *Computers & Chemical Engineering*. **18**(9), pp.817-832.
- Schroeder, J.A. 1999. *Helicopter flight simulation motion platform requirements*. NASA Technical Reports Server (NTRS).
- Sharp, R.S., Casanova, D. and Symonds, P. 2000. A mathematical model for driver steering control, with design, tuning and performance results. *Vehicle System Dynamics*. **33**(5), pp.289-326.
- Sharp, R.S. and Valtetsiotis, V. 2001. Optimal preview car steering control. *Vehicle System Dynamics*. **35**, pp.101-117.
- Siegler, I., Reymond, G., Kemeny, A. and Berthoz, A. 2001. Sensorimotor integration in a driving simulator: contributions of motion cueing in elementary driving tasks. In: *Driving Simulation Conference (DSC)*, pp.21-32.
- Sinacori, J.B. 1977. *The determination of some requirements for a helicopter flight research simulation facility*. NASA Technical Reports Server (NTRS).
- Sinacori, J.B. 1978. *Piloted aircraft simulation concepts and overview*. NASA Technical Reports Server (NTRS).
- Sivan, R., Ish-Shalom, J. and Huang, J.-K. 1982. An optimal control approach to the design of moving flight simulators. *IEEE Transactions on Systems, Man and Cybernetics*. **12**(6), pp.818-827.

- Slob, J.J. 2008. *State-of-the-Art driving simulators, a literature survey*. Eindhoven University of Technology, Control Systems Technology Group.
- Slob, J.J., Kuijpers, M.R.L., Rosielle, P.C.J.N. and Steinbuch, M. 2009. A new approach to linear motion technology: The wall is the limit. In: *Driving Simulation Conference (DSC), Monaco, Monaco*.
- Steen, J., Damveld, H.J., Happee, R., van Paassen, M.M. and Mulder, M. 2011. A review of visual driver models for system identification purposes. In: *IEEE International Conference on Systems, Man, and Cybernetics, 9-12 Oct. 2011*, pp.2093-2100.
- Steinhausen, W. 1933. Über die Beobachtung der Cupula in den Bogengangampullen des Labyrinths des lebenden Hechts. *Pflügers Archiv European Journal of Physiology*. **232**(1), pp.500-512.
- Stewart, D. 1965. A platform with six degrees of freedom. *Institution of Mechanical Engineers*. **180**(1), pp.371-386.
- Sturgeon, W.R. 1981. Controllers for aircraft motion simulators. *Journal of Guidance, Control, and Dynamics*. **4**(2), pp.184-191.
- Telban, R.J. and Cardullo, F.M. 2005. *Motion cueing algorithm development: Human-centered linear and nonlinear approaches*.
- Telban, R.J., Cardullo, F.M. and Houck, J. 2002. A nonlinear, human-centered approach to motion cueing with a neurocomputing solver In: *AIAA Modeling and Simulation Technologies Conference and Exhibit, Monterey, California*. American Institute of Aeronautics and Astronautics.
- Timings, J. and Cole, D. 2014. Robust lap-time simulation. *Institution of Mechanical Engineers Part D: Journal of Automobile Engineering*. **228**(10), pp.1200-1216.
- Tustin, A. 1947. The nature of the operator's response in manual control, and its implications for controller design. *Journal of the Institution of Electrical Engineers Part II: Automatic Regulators and Servo Mechanisms*. **94**(2), pp.190-206.
- Valente Pais, A.R. 2013. *Perception coherence zones in vehicle simulation* Ph.D. thesis, Delft University of Technology.
- Valente Pais, A.R., Van Paassen, M.M., Mulder, M. and Wentick, M. 2010. Perception coherence zones in flight simulation. *Journal of Aircraft*. **47**(6), pp.2039-2048.
- van der Steen, F.A.M. 1998. *Self-motion perception*. Ph.D. thesis, TU Delft, Delft University of Technology.
- van Egmond, A.A.J., Groen, J.J. and Jongkees, L.B.W. 1949. The mechanics of the semicircular canal. *The Journal of Physiology*. **110**(1-2), pp.1-17.
- Wang, L. 2009. *Model predictive control system design and implementation using MATLAB*. Springer Science & Business Media.
- Wang, Y. and Boyd, S. 2010. Fast model predictive control using online optimization. *IEEE Transactions on Control Systems Technology*. **18**(2), pp.267-278.
- Weir, D.H. and Clark, A.J. 1995. A survey of mid-level driving simulators. *SAE Technical Paper*.
- Weir, D.H. and DiMarco, R.J. 1978. Correlation and evaluation of driver/vehicle directional handling data *SAE Technical Paper*.
- Young, L.R. 1969. Model for vestibular adaptation to horizontal rotation. *Aerospace Medicine*. **40**, pp.1076-1080.

- Young, L.R. and Meiry, J.L. 1968. A revised dynamic otolith model. *Aerospace Medicine*. **39**(6), pp.606-608.
- Zaal, P.M.T., Pool, D.M., Mulder, M. and van Paassen, M.M. 2009. Multimodal pilot control behavior in combined target-following disturbance-rejection tasks. *Journal of Guidance, Control, and Dynamics*. **32**(5), pp.1418-1428.
- Zacharias, G.L. 1978. *Motion cue models for pilot-vehicle analysis*. Bolt Beranek and Newman Inc, Cambridge MA Control Systems Dept.
- Zacharias, G.L. and Young, L.R. 1981. Influence of combined visual and vestibular cues on human perception and control of horizontal rotation. *Experimental Brain Research*. **41**(2), pp.159-171.
- Zadeh, L.A. 1965. Fuzzy sets. *Information and Control*. **8**(3), pp.338-353.
- Zeeb, E. 2010. Daimler's new full-scale, high-dynamic driving simulator-a technical overview. In: *Driving Simulation Conference (DSC), Paris, France*. pp.157-165.

Appendices

A Motion platform characteristics of simulators

Table 0-1. Daimler-Benz driving simulators motion characteristics (Zeeb, 2010)

		Excursion <i>m, deg°</i>	Velocity <i>m/s, deg°/s</i>	Acceleration <i>m/s², deg°/s²</i>
Hexapod	Surge	-1.3/+1.4	?	-9.81/+9.81
	Sway	-1.3/+1.3	?	-9.81/+9.81
	Heave	-1/+1	?	-9.81/+9.81
	Roll	-20/+20	-45/+45	-120/+120
	Pitch	-19/+24	-45/+45	-120/+120
	Yaw	-38/+38	-60/+60	-120/+120
Sliding Rail	Surge or Sway	-7.5/+7.5	-10/+10	-9.81/+9.81

Table 0-2. VTI IV simulator motion characteristics (Fischer et al., 2011)

		Excursion <i>m, deg°</i>	Velocity <i>m/s, deg°/s</i>	Acceleration <i>m/s², deg°/s²</i>
Hexapod	Surge	-0.408/+0.307	-0.8/+0.8	-6.5/+6.5
	Sway	-0.318/+0.318	-0.8/+0.8	-6.0/+6.0
	Heave	-0.264/+0.240	-0.6/+0.6	-6.0/+6.0
	Roll	-16.5/+16.5	-40.0/+40.0	-300/+300
	Pitch	-16.5/+16.5	-40.0/+40.0	-300/+300
	Yaw	-20.5/+20.5	-50.0/+50.0	-300/+300
Sliding Rail	Surge	-2.5/+2.5	-2.0/+2.0	-5.0/+5.0
	Sway	-2.3/+2.3	-3.0/+3.0	-5.0/+5.0

Table 0-3. PSA Peugeot-Citroën motion characteristics (Chapron and Colinot 2007)

		Excursion <i>m, deg°</i>	Velocity <i>m/s, deg°/s</i>	Acceleration <i>m/s², deg°/s²</i>
Hexapod	Surge	-0.408/+0.307	-0.82/+0.82	-6.6/+6.6
	Sway	-0.318/+0.318	-0.82/+0.82	-6.9/+6.9
	Heave	-0.264/+0.240	-0.82/+0.82	-6.2/+6.2
	Roll	-18/+21	-41.3/+41.3	-321/+321
	Pitch	-22/+22	-40.7/+40.7	-321/+321
	Yaw	-23/+23	-53.3/+53.3	-362/+362
Sliding Rail	Surge	-2.61/+2.59	-2.1/+2.1	-5.1/+5.1
	Sway	-2.50/+2.50	-3.1/+3.1	-5.4/+5.4

Table 0-4. NADS1 simulator motion characteristics (Clark, A.J. et al., 2001)

		Excursion <i>m, deg°</i>	Velocity <i>m/s, deg°/s</i>	Acceleration <i>m/s², deg°/s²</i>
Hexapod	Surge	-0.8/+0.8	?	?
	Sway	-0.8/+0.8	?	?
	Heave	-0.6/+0.6	-1.5/+1.5	-9.81/+9.81
	Roll	-25/+25	-45/+45	-120/+120
	Pitch	-25/+25	-45/+45	-120/+120
	Yaw (including turntable)	-390/+390	-60/+60	-120/+120
Sliding Rail	Surge	-9.75/+9.75	-6.1/+6.1	-6.082/+6.082
	Sway	-9.75/+9.75	-6.1/+6.1	-6.082/+6.082

Table 0-5. Toyota Research Driving Simulator (TRDS) motion characteristics (Greenberg and Blommer, 2011)

		Excursion <i>m, deg°</i>	Velocity <i>m/s, deg°/s</i>	Acceleration <i>m/s², deg°/s²</i>
Hexapod	Surge	?	?	?
	Sway	?	?	?
	Heave	?	?	?
	Roll	-25/+25	?	?
	Pitch	-25/+25	?	?
	Yaw (turntable)	-330/+330	?	?
Sliding Rail	Surge	-17.5/+17.5	-6.1/+6.1	-4.9/+4.9
	Sway	-10/+10	-6.1/+6.1	-4.9/+4.9

Table 0-6. DESDEMONA simulator motion characteristics

		Excursion <i>m deg°</i>	Velocity <i>m/s deg°/s</i>	Acceleration <i>m/s² deg°/s²</i>
Six DoF Serial Robot	Heave	-1/+1	-2.2/+2.2	-4.9/+4.9
	Roll	<i>unlimited</i>	-180/+180	-90/+90
	Pitch	<i>unlimited</i>	-180/+180	-90/+90
	Yaw	<i>unlimited</i>	-180/+180	-90/+90
Sliding Rail	Main Arm (Rotational)	<i>unlimited</i>	-155/+155	-45.0/+45.0
	Horizontal (Translational)	-4/+4	-3.2/+3.2	-4.9/+4.9

Table 0-7. MPI CyberMotion simulator motion characteristics (Nieuwenhuizen and Bülthoff, 2013)

		Excursion <i>m, deg°</i>	Velocity <i>m/s, deg°/s</i>	Acceleration <i>m/s², deg°/s²</i>
6 DoF	Axis 1	<i>unlimited</i>	-68/+68	-98/+98
	Axis 2	-128/+48	-57/+57	-70/+70
	Axis 3	-45/+92	-69/+69	-128/+128
	Axis 4	-180/+180	-76/+76	-33/+33
	Axis 5	-58/+58	-76/+76	-95/+95
	Axis 6	-180/+180	-120/+120	-77/+77
Base and Cabin Motion	Actuated Cabin	-0.67/+0.67	-0.5/+0.5	?
	Horizontal (Translational)	-4.9/+4.9	-1.5/+1.5	?

B Assessment of Low-Friction Motion Cueing Experiment Documents

Briefing



PARTICIPANT BRIEFING – MCA STUDY

**** Please acquaint yourself with these instructions, but note that you do not need to memorise any details ****

1.1 Background and Goal of Study

One of the goals of the Programme for Simulation Innovation (PSI) is to answer the questions: “how applicable are driving simulators as virtual prototyping tools?” as well as “what capabilities does the simulator motion system need to have?” The aim is to present drivers in the simulator with an experience as close as possible to the real world. In more detail, the simulator should have a level of fidelity that can evoke sensations and perceptions, and elicit control behaviours from drivers, similar to those in the real world.

This experiment is designed to help us answer those questions in context of low friction vehicle testing, we have prepared various simulator motion configurations that result in different outputs of the motion system and we expect you to make pairwise comparisons between configurations and answer three groups of questions given to you in questionnaire, those are about overall assessment, motion cueing and vehicle assessment. This involves you driving two driving tasks: Slalom and Sweden Land Rover Handling Track (LHT) in the University of Leeds Driving Simulator, both of the tasks are on snow and you will drive a X260 Jaguar car without ABS or SCS. We will collect subjective and objective data and compare your preference on the configurations.

1.2 Experimental sessions

The whole experimental procedure for you will be as below:

1. At the beginning of your session, we first meet in simulator reception office to review this briefing, questionnaire and consent form, then we do familiarization with simulator driving in an urban/rural area, and then familiarization with the slalom and LHT tasks.
2. After familiarisation, the experiment will amount to you driving first the slalom and second LHT driving task a number of times each. In both sections you will be answering the same set of subjective questions; see attached questionnaire.
3. For each of the driving tasks there are three pairs of simulator configurations to be compared.
 - a) One configuration evaluation consists of driving a task twice (2 trials). After finishing the first trial you will stop the car to have a first go at filling up the questionnaire. Then, you do the second trial and complete any questions left unanswered or adjust previous answers.
 - b) Then you’ll drive the second configuration of the pair, and complete the questionnaire same as above.
 - c) Then we move to the second and third pairs of configurations.
4. After completing all evaluations for both driving tasks we’re done. The whole experiment is estimated to take 2 hours of your time.



1.3 Subjective and objective assessments

The subjective evaluation questionnaire is sent to you beforehand with this briefing, however before the start of the experiment we will review it with you to help you understand and remember the questions that we want you to answer. Your responses in the questionnaire are of high value to us in drawing conclusions for our research questions; please do your best when providing your answers.

For each of the driving tasks one shared evaluation form will be used for all three pairwise comparisons. As a result each question is repeated three times in the questionnaire corresponding to three pairs. You make pairwise comparison among configurations within each of the pairs and mark on the ratings, for the first pair you drive please mark the first configuration with the letter A over each rating mark, the second configuration with B, then similarly for second and third pair put crossed with C-D and E-F, as shown in example below. You can further modify the A-B or C-D or E-F positions after completing each of the pairs. Moreover, after driving second and third pairs you can also modify A-B, C-D, E-F of the three pairs relative to each other.

Overall Assessment

1. How realistic was the overall experience in the simulator compared to reality?

For configurations A and B:

Unrealistic	<div style="display: flex; justify-content: space-between; align-items: center;"> <div style="text-align: center;">A ✕</div> <div style="flex-grow: 1; border-bottom: 1px solid black;"></div> <div style="text-align: center;">B ✕</div> </div>	Realistic
-------------	--	-----------

For configurations C and D:

Unrealistic	<div style="display: flex; justify-content: space-between; align-items: center;"> <div style="text-align: center;">D ✕</div> <div style="text-align: center;">C ✕</div> <div style="flex-grow: 1; border-bottom: 1px solid black;"></div> </div>	Realistic
-------------	--	-----------

For configurations E and F:

Unrealistic	<div style="display: flex; justify-content: space-between; align-items: center;"> <div style="text-align: center;">E ✕</div> <div style="text-align: center;">F ✕</div> <div style="flex-grow: 1; border-bottom: 1px solid black;"></div> </div>	Realistic
-------------	--	-----------

Example

1.4 Test drives

In each of the rides drive as you usually would do during a vehicle evaluation and to be able to answer the questions. If you feel any quality of car is not feeling correct you can provide us with comments, in the designated boxes in the questionnaire.

For the Slalom task select second gear and stay close 45 km/h speed. For the LHT task select third gear and adapt speed so that you don't lose control. In both tasks, always



prioritise safe and successful driving as you usually do during evaluations. Moreover please avoid any fast/hard applies on the brake pedal.

Between configuration pairs and driving tasks, the experimenter will ask you to step out of the sim to get fresh air and we prepare the sim for next test case.

1.5 Ethics, safety and confidentiality

As with all our research, this study is subject to the ethical guidelines of the British Psychological Society and the requirements of the Data Protection Act. In particular please note that:

- At no time now, nor in the future, will any information that you provide be published in such a manner that might allow you to be identified as an individual.
- You are free to withdraw from the study at any time without having to give any reason for your decision.

1.6 Thank you very much

We would like to thank you very much for expressing an interest to participate in this research, we hope that you enjoyed your time spent during this study. Your contribution is much appreciated.

Please feel free to attend future project events to hear about the results of the study or alternatively contact Ehsan below in a few months to receive a copy of the milestone report. Finally, if you have any questions, please feel free to ask!

1.7 Contacts

1.7.1 Ehsan Sadraei

PhD Student

University of Leeds Driving Simulator (UoLDS),
Institute for Transport Studies, University of Leeds, LS2 9JT

Office phone: 0113 34 33842

Mobile phone: 07442706329

Email: tses@leeds.ac.uk

1.7.2 Alex Bean

Technical Specialist - Stability Analysis & Virtual Tools, GDEC

Internal: 8712 0412

External: +44 (0) 788 1260412

Email: abean@jaguarlandrover.com

1.7.3 Gustav Markkula

Associate Professor

University of Leeds Driving Simulator (UoLDS),
Institute for Transport Studies, University of Leeds, LS2 9JT

Office phone: 0113 34 39832

Mobile phone: 07402 168480

Email: g.markkula@leeds.ac.uk

Questionnaire

Main experiment

Participant ID:

Driving task: Slalom LHT

In the task you just drove, for each of the configurations after driving one trial, please answer the questions below

- There are three group of questions about overall assessment, motion cuing and vehicle assessment
- For the first pair of configurations put two crosses relatively with A or B on top somewhere along the rating line below, similarly for second and third pair of configurations put C or D and E or F
- After driving second and third pairs of configurations you can modify the answers of all three pairs relative to each other

**Overall
Assessment**

1. How realistic was the overall experience in the simulator compared to reality?

For configurations A and B:

Unrealistic	_____	Realistic
-------------	-------	-----------

For configurations C and D:

Unrealistic	_____	Realistic
-------------	-------	-----------

For configurations E and F:

Unrealistic	_____	Realistic
-------------	-------	-----------

Is there any specific suggestion for improvement? (Please label them for each of the configurations)

--

**Overall
Assessment**

2. Do you think that these simulator configurations would be useful for testing and comparing vehicle designs?

For configurations A and B:

Not Useful	-----	Useful
---------------	-------	--------

For configurations C and D:

Not Useful	-----	Useful
---------------	-------	--------

For configurations E and F:

Not Useful	-----	Useful
---------------	-------	--------

Is there any specific suggestion for improvement? (Please label them for each of the configurations)

**Overall
Assessment**

3. How easy was it to perform the task?

For configurations A and B:



For configurations C and D:



For configurations E and F:



Is there any specific suggestion for improvement? (Please label them for each of the configurations)

Motion Cuing

4. I felt motion in general was

For configurations A and B:



For configurations C and D:



For configurations E and F:



Is there any specific suggestion for improvement? (Please label them for each of the configurations)

Motion Cuing

5. I felt longitudinal acceleration/deceleration and pitch were

For configurations A and B:



For configurations C and D:



For configurations E and F:



Is there any specific suggestion for improvement? (Please label them for each of the configurations)

Motion Cuing

6. I felt lateral acceleration/deceleration and roll were

For configurations A and B:



For configurations C and D:



For configurations E and F:



Is there any specific suggestion for improvement? (Please label them for each of the configurations)

**Vehicle
Assessment**

7. How confident were you in assessing the available grip and the limit of the vehicles ability

For configurations A and B:

Unrealistic	-----	Realistic
-------------	-------	-----------

For configurations C and D:

Unrealistic	-----	Realistic
-------------	-------	-----------

For configurations E and F:

Unrealistic	-----	Realistic
-------------	-------	-----------

Is there any specific suggestion for improvement? (Please label them for each of the configurations)

**Vehicle
Assessment**

8. I felt under/oversteering was

Level of the vehicle's under/oversteer behaviour over a range of corner radii and lateral acceleration

For configurations A and B:



For configurations C and D:



For configurations E and F:



Is there any specific suggestion for improvement? (Please label them for each of the configurations)

**Vehicle
Assessment**

9. I felt time delay of vehicle response was

The delay between steering wheel input and resultant vehicle response

For configurations A and B:



For configurations C and D:



For configurations E and F:



Is there any specific suggestion for improvement? (Please label them for each of the configurations)

Counter balancing table

Order Subject	SLALOM						LHT					
	1	2	3	4	5	6	7	8	9	10	11	12
	MP Size		MP Size		MP Size		MP Size		MP Size		MP Size	
	MCA	MCA	MCA	MCA	MCA	MCA	MCA	MCA	MCA	MCA	MCA	MCA
1	S-M	S-C	M-M	M-C	L-C	L-M	S-C	S-M	M-M	M-C	L-C	L-M
2	S-M	S-C	M-C	M-M	L-C	L-M	S-C	S-M	M-M	M-C	L-M	L-C
3	S-C	S-M	M-M	M-C	L-C	L-M	S-M	S-C	M-M	M-C	L-C	L-M
4	S-M	S-C	M-M	M-C	L-C	L-M	S-M	S-C	M-C	M-M	L-C	L-M
5	L-C	L-M	M-M	M-C	S-M	S-C	L-M	L-C	M-C	M-M	S-C	S-M
6	L-M	L-C	M-C	M-M	S-C	S-M	L-M	L-C	M-M	M-C	S-C	S-M
7	L-M	L-C	M-C	M-M	S-M	S-C	L-M	L-C	M-C	M-M	S-C	S-M
8	L-C	L-M	M-C	M-M	S-M	S-C	L-M	L-C	M-M	M-C	S-C	S-M

MCA tuning parameter values

Classic parameter values, SLM task, the slash are for surge/sway

Parameters		MP size	Small	Medium	Large
Input acceleration scaling			0.2	0.5	0.7
Hexapod Translation	cut-off frequency ω_{hp1} (rad/s)		1.02/1.18	1.51/1.71	1.55/1.84
	cut-off frequency ω_{hp2} (rad/s)		1.75/1.91	2.35/2.62	2.60/2.63
Sliding rail Translation	cut-off frequency ω_{hp1} (rad/s)		0.22/0.16	0.26/0.11	0.31/0.06
	cut-off frequency ω_{hp2} (rad/s)		0.31/0.18	0.35/0.15	0.46/0.09
	cut-off frequency ω_{tp2} (rad/s)		11	11	11
Hexapod Tilt Coordination	cut-off frequency ω_{tp2} (rad/s)		3	3	3

Classic parameter values, LHT task, the slashes are for surge/sway

Parameters		MP size	Small	Medium	Large
Input acceleration scaling			0.15	0.3	0.5
Hexapod Translation	cut-off frequency ω_{hp1} (rad/s)		0.94	1.17	1.68
	cut-off frequency ω_{hp2} (rad/s)		1.61/1.43	2.06/1.83	2.53/2.38
Sliding rail Translation	cut-off frequency ω_{hp1} (rad/s)		0.42/0.36	0.35/0.29	0.26/0.22
	cut-off frequency ω_{hp2} (rad/s)		0.91/0.87	0.73/0.66	0.68/0.59
	cut-off frequency ω_{tp2} (rad/s)		11	11	11
Hexapod Tilt Coordination	cut-off frequency ω_{tp2} (rad/s)		3	3	3

Classic parameter values, yaw channel, the slashes are for SLM/LHT

Parameters		MP size	Small	Medium	Large
Hexapod Rotation	cut-off frequency ω_{hp1} (rad/s)		0.2/0.25	0.2/0.25	0.2/0.25
	cut-off frequency ω_{hp2} (rad/s)		0.5/0.55	0.5/0.55	0.5/0.55

MPC parameter values, SLM task, the slashes are for surge/sway

Parameters		MP size	Small	Medium	Large
Input acceleration scaling			0.2	0.5	0.7
Prediction Horizon			1.6/0.83 s	1.6/0.83 s	1.6/0.83 s
Control Horizon			0.16 s	0.16 s	0.16 s
Hexapod Translation	Acceleration tracking weight, w_{h1}		0	0	0
	Velocity tracking weight, w_{h2}		0.7/0.8	1.1/1.2	1.2/1.3
	Position tracking weight, w_{h3}		0.5/0.6	0.9/1	1/1.1
Sliding rail Translation	Acceleration tracking weight, w_{r1}		0	0	0
	Velocity tracking weight, w_{r2}		0.35	0.35	0.35
	Position tracking weight, w_{r3}		0.25	0.25	0.25
Hexapod Tilt Coordination	Acceleration tracking weight, w_{t1}		0.3	0.3	0.3
	Position tracking weight, w_{t2}		0.1	0.1	0.1
Other	Hexapod+Rail+Tilt summation acceleration tracking weight, w_a		1.5	2	2.5

MPC paramter values, LHT task, the slashes are for surge/sway

Parameters		MP size	Small	Medium	Large
Input acceleration scaling			0.15	0.3	0.5
Prediction Horizon			2 s	2 s	2 s
Control Horizon			0.16 s	0.16 s	0.16 s
Hexapod Translation	Acceleration tracking weight, w_{h1}		0	0	0
	Velocity tracking weight, w_{h2}		0.7/0.8	1/1.1	1.2/1.3
	Position tracking weight, w_{h3}		0.5/0.6	0.9/1	1/1.1
Sliding rail Translation	Acceleration tracking weight, w_{r1}		0	0	0
	Velocity tracking weight, w_{r2}		0.4	0.35	0.35
	Position tracking weight, w_{r3}		0.3	0.25	0.25
Hexapod Tilt Coordination	Acceleration tracking weight, w_{t1}		0.3	0.3	0.3
	Position tracking weight, w_{t2}		0.1	0.1	0.1
Other	Hexapod+Rail+Tilt summation acceleration tracking weight, w_a		1.5	2	2.5

MPC paramter values, yaw channel, the slashes are for SLM/LHT tasks

Parameters		MP size	Small	Medium	Large
Prediction Horizon			0.41 s	0.41 s	0.41 s
Control Horizon			0.16 s	0.16 s	0.16 s
Hexapod Rotation	Velocity tracking weight, w_{h1}		1	1	1
	Position tracking weight, w_{h2}		0.6/0.7	0.6/0.7	0.6/0.7

C Assessment of High-Friction Motion Cueing Experiment Documents

Briefing



PARTICIPANT BRIEFING – DRIVEN ATTRIBUTES EVALUATION (VET) STUDY

** Please acquaint yourself with these instructions, but note that you do not need to memorise any details; the researcher leading the experiment will repeat the instructions to you before you start driving, and will be happy to answer any questions you may have**

1.1 Background

One of the goals of the Programme for Simulation Innovation (PSI) is to answer the questions: “how applicable are driving simulators as virtual prototyping tools?” as well as “what capabilities does the simulator motion system need to have?” The aim is to present drivers in the simulator with an experience as close as possible to the real world. In more detail, the simulator should evoke sensations and perceptions, and elicit control behaviours from drivers, similar to those in the real world. In this study we aim to answer these questions specifically in the context of driven attributes testing of the type carried out by JLR’s vehicle evaluation team (VET).

As you know, we have planned two sets of experiments. The first experiment, carried out last October, involved driving on the real Gosport Lane. This experiment involves driving on a virtual version of the Gosport Lane in the University of Leeds Driving Simulator (UoLDS). You will be seated in the simulator’s physical cockpit of a Jaguar S-type, but the simulated vehicle that you will be driving and evaluating is, just as in October, an L560 Range Rover. You will be driving in three sessions, and the motion characteristics of the simulator will be different between the three sessions. Within each session you subjectively evaluate three different air suspension configurations, just like you did on the real Gosport Lane, by driving the car back and forth on Gosport Lane. Thus the whole simulator experiment will cover a total of nine drives back and forth on Gosport Lane (three times more than on the real Gosport Lane). We will analyse subjective and objective data for each air suspension configuration in each simulator session, and will make comparisons between the configurations and sessions as well as between the real/virtual environments, to answer the questions introduced above.

1.2 Experimental procedure

The whole experimental procedure is described below:

- At the beginning of the experiment, we will meet in the UoLDS reception to review this briefing, questionnaires and consent form; then I will explain to you the safety procedures of the UoLDS.
- Then you will undertake a familiarisation drive to acquaint yourself with the UoLDS, the simulated Gosport Lane and the simulated L560.
- Explanation of the safety procedures and familiarisation drive take 15 minutes.



- After familiarisation, in each trial you will be driving once back and forth on the Gosport Lane to evaluate the driven attributes, bearing in mind the subjective questions to be answered for each air suspension configuration; see attached questionnaire.
- As mentioned, there are three different air suspension configurations to evaluate in each session.
- One evaluation of one suspension configuration consists of driving Gosport Lane back and forth once. In each of the trials after half of the trial (i.e. driving the road in one direction) you will stop to have first go at filling up the questionnaire. Then, after driving back in the other direction, you will answer the questions you were not able to answer in the first half.
- Each driving session lasts about 40 min.
- After each driving session you will be given a short questionnaire related to motion discomfort and realism of the simulation.
- Between driving sessions you will have a pause of about 30 minutes, while the other driver is in the simulator. You will be provided internet access during the pause.
- There will be a break for lunch after both drivers have finished the first session.
- The whole experiment is estimated to take six hours of your time.

1.3 Subjective and objective assessments

The subjective evaluation questionnaire is sent to you beforehand with this briefing, however before the start of the experiment we will review it with you to help you understand and remember the questions that we want you to answer. Your responses in the questionnaire are of high value to us in drawing conclusions for our research questions; please do your best when providing your answers.

One questionnaire will be used for rating all of the three air suspension configurations in all three sessions, so that you can evaluate the configurations **relative** to each other. In the first session, please mark the first configuration you drive with the letter A on the upper (green) rating line, the second with B, and the third with C. In the second session, mark the first configuration with D on the middle (pink) rating line, and so on. The researchers will stay in contact with you all the time and remind you which is the current configuration and where to place the marks.

If for some questions you do not perceive a noticeable difference between the air suspension configurations, please nevertheless provide ratings, which can be on top of each other. You can also add comments in writing.



1.4 Test drives

In each of the air suspension configurations, the driving task is a go and return drive in Gosport Lane. The Gosport lane includes a few corners and one longer straight. Throughout, drive as you usually would do during a vehicle prototype driving attributes evaluations, and so as to be able to answer the questions. However on straight line task please try to keep constant speed and apply few sinusoid steering input, for the evaluation purpose and also we explicitly want those objective data.

Please stay close to the speed limit of 60 mph when possible, but always prioritise safe and successful driving as you usually do during evaluations.

Between drives, there will be a brief pause to let the researchers reload the simulator scenario and for you to complete the questionnaire for the driven configuration.

1.5 Ethics, safety and confidentiality

As with all our research, this study is subject to the ethical guidelines of the British Psychological Society and the requirements of the Data Protection Act. In particular please note that:

- At no time now, nor in the future, will any information that you provide be published in such a manner that might allow you to be identified as an individual.
- You are free to withdraw from the study at any time without having to give any reason for your decision.

1.6 Thank you very much

We would like to thank you very much for expressing an interest in this work, your participation both on the real and today on the virtual Gosport Lane and we hope that you enjoyed your time spent during this study. Your contribution is much appreciated.

Please feel free to attend future project events to hear about the results of the study or alternatively contact John or Hrvoje below in a few months to receive a copy of the milestone report. Finally, if you have any questions, please feel free to ask!

1.7 Contacts

1.7.1 Hrvoje Jukic

Research Assistant
 University of Leeds Driving Simulator (UoLDS)
 Institute for Transport Studies
 University of Leeds, LS2 9JT

Questionnaire

Simulator experiment


Participant ID:

After half a trial of each air suspension configuration, please compare them in terms of ride, steering and handling feel by putting marked crosses on the rating lines following the questions below. For the three air suspension configurations in the **first** session (marks **A, B** and **C**) put the marked crosses on the first rating line, similarly for the three air suspension configurations in the **second** session (marks **D, E** and **F**) and **third** session (marks **G, H** and **I**) put the marked crosses on the second and third rating line respectively. You can put similar answers on top of each other.


Ride

Primary Ride – These are low frequency vertical movements of the vehicle. Evaluate large amplitude (large and obvious, continuous road undulations) that cause suspension movement over a moderate range, up to the whole range of suspension travel.


➤ Session 1 (A, B, C)

Constrained, Trapped		Free, Floaty
Appropriate for this vehicle		

➤ Session 2 (D, E, F)


Constrained, Trapped		Free, Floaty
Appropriate for this vehicle		

➤ Session 3 (G, H, I)


Constrained, Trapped		Free, Floaty
Appropriate for this vehicle		

Secondary Ride – Vertical vibrations that are caused by the road texture and various road disturbances on flat (smooth and coarse) and/or rough roads. They are felt by the driver or passengers through the seat back and cushion, steering wheel, floor pan, etc.


➤ Session 1 (A, B, C)

Crashy, Agitated, Tactile		Settled, Controlled, Calm
Appropriate for this vehicle		

➤ Session 2 (D, E, F)

Crashy, Agitated, Tactile		Settled, Controlled, Calm
Appropriate for this vehicle		

➤ Session 3 (G, H, I)

Crashy, Agitated, Tactile		Settled, Controlled, Calm
Appropriate for this vehicle		

Other comments about ride feeling. If referring to specific session or configuration, please indicate which one(s).

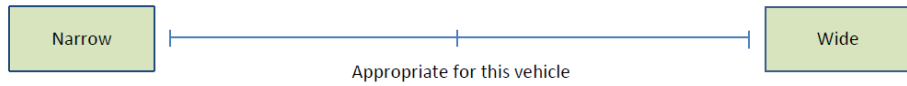
Steering

Straight Ahead and Cornering Controllability

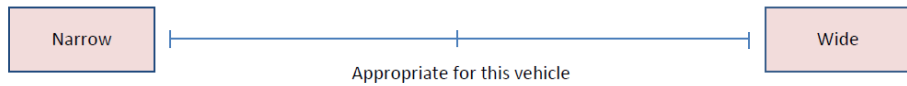
Controllability refers to the steering properties around the straight ahead and cornering tasks and how these characteristics work together to allow the driver precise and confident steering control. These properties are the vehicle reactions and torque feedback to small steering corrections that are required to keep the vehicle travelling in a straight path, as well as when turning the vehicle into a corner i.e. the steering adjustments required to keep the vehicle on the intended curvature. It also includes the steering properties that help the driver return to straight-ahead when exiting a corner.

Window on High Speed (over 30 mph) – The steering angle range where there seems to be no motion response.

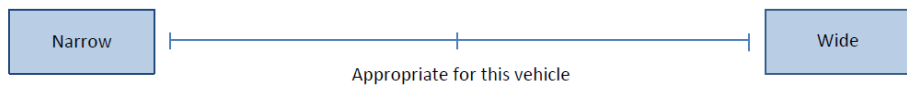
➤ Session 1 (A, B, C)



➤ Session 2 (D, E, F)

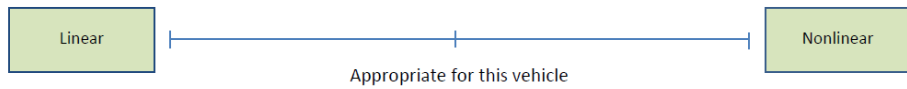


➤ Session 3 (G, H, I)

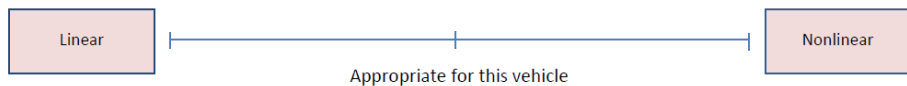


Gain Linearity Away From Centre – The ability of the vehicle to maintain a constant level of response gain.

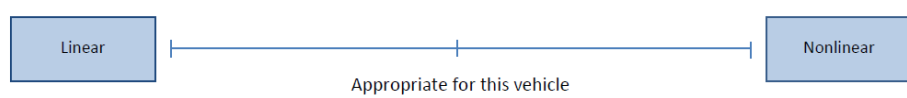
➤ Session 1 (A, B, C)



➤ Session 2 (D, E, F)

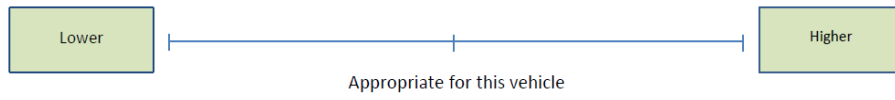


➤ Session 3 (G, H, I)

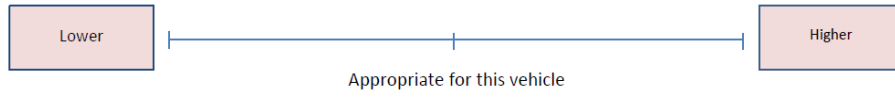


Efforts at Low Speed – General level of steering torque / forces for controlling the vehicle.

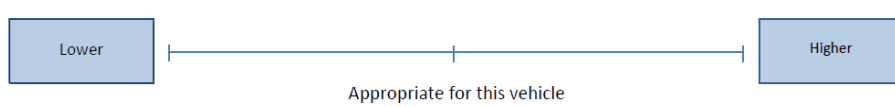
➤ Session 1 (A, B, C)



➤ Session 2 (D, E, F)

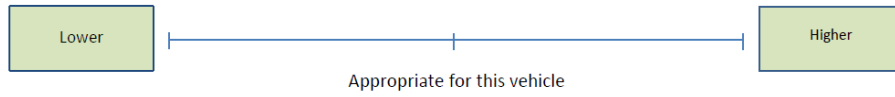


➤ Session 3 (G, H, I)

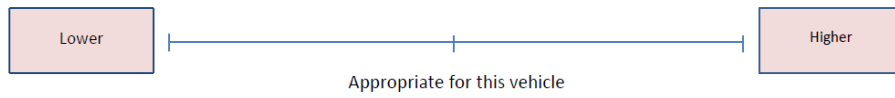


Efforts at High Speed – General level of steering torque / forces for controlling the vehicle.

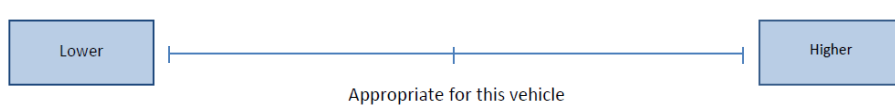
➤ Session 1 (A, B, C)



➤ Session 2 (D, E, F)

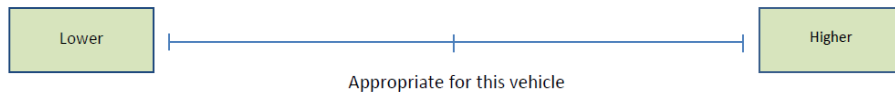


➤ Session 3 (G, H, I)

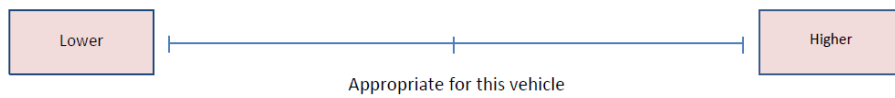


Efforts Mid-Corner – General level of steering torque / forces for controlling the vehicle.

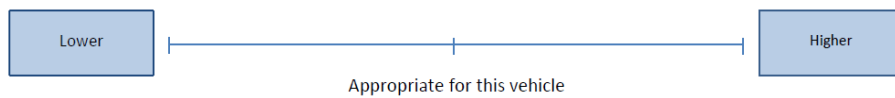
➤ Session 1 (A, B, C)



➤ Session 2 (D, E, F)



➤ Session 3 (G, H, I)



Other comments about steering feeling. If referring to specific session or configuration, please indicate which one(s).

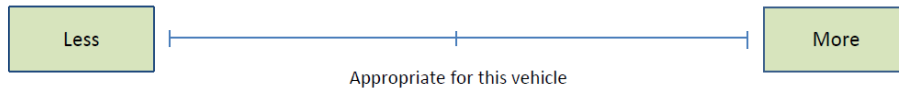
Handling

Straight Ahead and Cornering Stability

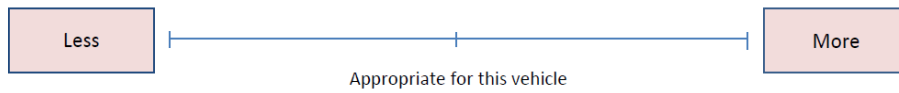
Stability describes the ability of the vehicle to deliver a consistent, comfortable and predictable behaviour during straight line or negotiating a cornering manoeuvre. In addition to steady-state conditions, it also includes the vehicle's ability to accelerate & decelerate without extraneous roll, pitch, yawing and lateral motions.

Pitch (Longitudinal) Acceleration/Deceleration (Lift Squat) – Acceleration pitch/lift Squat describes the degree of vehicle pitch during acceleration/deceleration phases of manoeuvre.

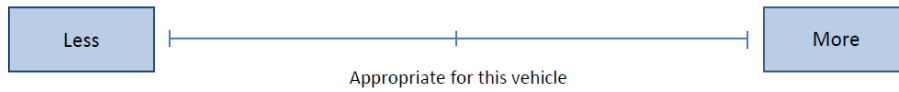
➤ Session 1 (A, B, C)



➤ Session 2 (D, E, F)



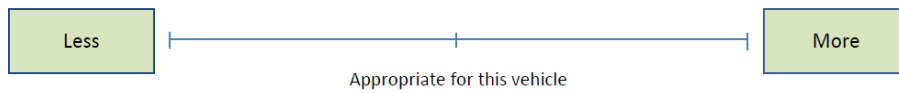
➤ Session 3 (G, H, I)



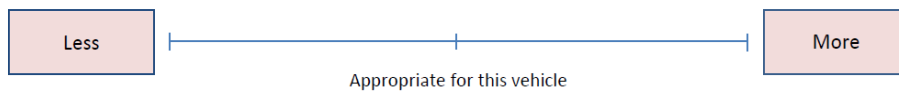
Roll (Lateral) Acceleration/Deceleration – Acceleration roll describes the degree of vehicle roll during acceleration/deceleration in cornering phases of manoeuvre

- **Transient** - The degree of vehicle roll during small corrective steering inputs.

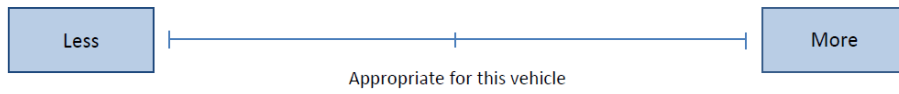
➤ Session 1 (A, B, C)



➤ Session 2 (D, E, F)

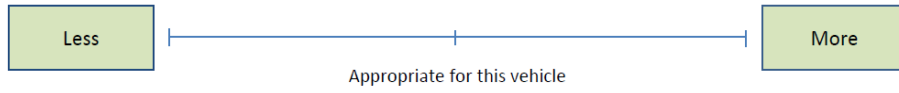


➤ Session 3 (G, H, I)

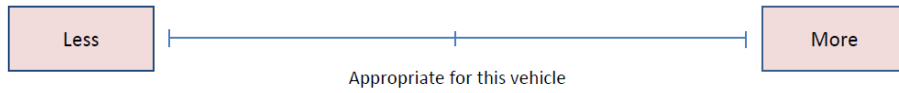


- **Steady State** - The degree of vehicle roll for fixed-level acceleration during cornering.

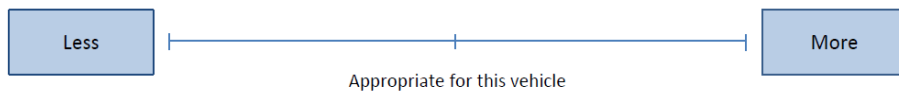
➤ Session 1 (A, B, C)



➤ Session 2 (D, E, F)

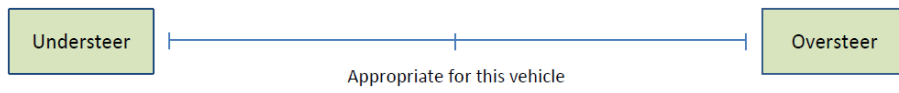


➤ Session 3 (G, H, I)

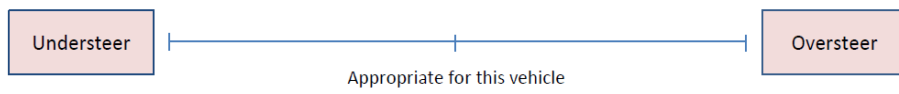


Under/Oversteering – Level of the vehicle's under/oversteer behaviour over a range of corner radii and lateral acceleration while cornering

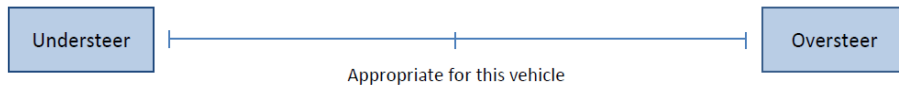
➤ Session 1 (A, B, C)



➤ Session 2 (D, E, F)



➤ Session 3 (G, H, I)



Other comments about handling feeling. If referring to specific session or configuration, please indicate which one(s).

Realism assessment

Participant ID:

For the simulator session you just drove, please answer the questions below

- There are two groups of questions about (i) overall assessment and (ii) motion cuing.
- For each of the three sessions put a cross marked with 1, 2 or 3 along the rating line below. You can assign multiple numbers to the same cross if you wish to indicate no perceived difference between simulator sessions.
- After driving the second and third sessions you can modify the answers of all three sessions relative to each other.

Overall Assessment

1. How realistic was the overall experience in the simulator compared to reality?

For sessions 1, 2 and 3:

Unrealistic	-----	Realistic
-------------	-------	-----------

Any specific suggestions for improvement? (If referring to specific sessions, please indicate which ones.)

2. Do you think that a driving simulator, in the configuration you just experienced, would be useful for testing and comparing vehicle driven attributes?

For sessions 1, 2 and 3:

Not Useful	-----	Useful
---------------	-------	--------

Any specific suggestions for improvement? (If referring to specific sessions, please indicate which ones.)

3. How easy was it to perform the driving task?

For sessions 1, 2 and 3:

Difficult	-----	Easy
-----------	-------	------

Any specific suggestions for improvement? (If referring to specific sessions, please indicate which ones.)

Motion Cuing

4. I felt motion in general was

For sessions 1, 2 and 3:

Unrealistic	—————	Realistic
-------------	-------	-----------

Any specific suggestions for improvement? (If referring to specific sessions, please indicate which ones.)

5. I felt longitudinal acceleration/deceleration and pitch were

For sessions 1, 2 and 3:

Unrealistic	—————	Realistic
-------------	-------	-----------

Any specific suggestions for improvement? (If referring to specific sessions, please indicate which ones.)

6. I felt lateral acceleration/deceleration and roll were

For sessions 1, 2 and 3:

Unrealistic	-----	Realistic
-------------	-------	-----------

Any specific suggestions for improvement? (If referring to specific sessions, please indicate which ones.)

7. I felt time delay of vehicle response was*The delay between steering wheel input and resultant vehicle response*

For sessions 1, 2 and 3:

Unrealistic	-----	Realistic
-------------	-------	-----------

Any specific suggestions for improvement? (If referring to specific sessions, please indicate which ones.)

Counter balancing table

Order Subject	Gosport Lane								
	1	2	3	4	5	6	7	8	9
	MP Size			MP Size			MP Size		
	Height	Height	Height	Height	Height	Height	Height	Height	Height
1	M-L	M-H	M-M	S-H	S-M	S-L	L-L	L-M	L-H
2	L-H	L-M	L-L	M-L	M-M	M-H	S-L	S-H	S-M
3	S-M	S-H	S-L	L-L	L-H	L-M	M-M	M-H	M-L
4	L-M	L-L	L-H	M-M	M-H	M-L	S-H	S-L	S-M
5	L-H	L-L	L-M	M-M	M-L	M-H	S-L	S-M	S-H
6	M-H	M-L	M-M	S-M	S-L	S-H	L-M	L-H	L-L

MCA tuning parameter values

MPC paramter values, GSP task, the slash are for surge/sway

Parameters		MP size	Small	Medium	Large
Prediction Horizon			1.2 s	1.2 s	1.2 s
Control Horizon			0.16 s	0.16 s	0.16 s
Hexapod Translation	Acceleration tracking weight, w_{h1}		0	0	0
	Velocity tracking weight, w_{h2}		1.4	1.4	1.4
	Position tracking weight, w_{h3}		1.2	1.2	1.2
Sliding rail Translation	Acceleration tracking weight, w_{r1}		0	0	0
	Velocity tracking weight, w_{r2}		0.6	0.35	0.35
	Position tracking weight, w_{r3}		0.55	0.25	0.25
Hexapod Tilt Coordination	Acceleration tracking weight, w_{t1}		0.3	0.3	0.3
	Position tracking weight, w_{t2}		0.1	0.1	0.1
Other	Hexapod+Rail+Tilt summation acceleration tracking weight, w_a		1	1.5	2

MPC parameter values, GSP task, for Heave/Yaw channel

Parameters		MP size	Small	Medium	Large
Prediction Horizon			1.2 s	1.2 s	1.2 s
Control Horizon			0.16 s	0.16 s	0.16 s
Hexapod Rotation	Velocity tracking weight, w_{h1}		1.5	1.5	1.5
	Position tracking weight, w_{h2}		0.7	0.7	0.7
Hexapod Translation	Acceleration tracking weight, w_{h1}		1.5	1.5	1.5
	Velocity tracking weight, w_{h2}		0.5	0.5	0.5
	Position tracking weight, w_{h3}		0.3	0.3	0.3

D List of tilt settings used throughout the thesis

	Chapter	Maximum		
		Tilt Angle $\theta_{max} (deg)$	Tilt Angular Velocity $\dot{\theta}_{max} (deg/s)$	Tilt Angular Acceleration $\ddot{\theta}_{max} (deg/s^2)$
Experiment 1	5	6	4	4
Experiment 2	6	6	4	4
Tuning of MCA parameters	7	6	4.3	23.5
			3.22	13.14
Workspace optimisation of MP	8	6	2.5/4.3	8/23.5
			3	10